



CO-TUTELLE THESE DE DOCTORAT DE

L'UNIVERSITE DE RENNES 1
COMUE UNIVERSITE BRETAGNE LOIRE

ECOLE DOCTORALE N° 596
Matière Molécules et Matériaux
Spécialité : Chimie Inorganique

NIKOLAEV INSTITUTE OF INORGANIC CHEMISTRY (NIIC)
Novosibirsk, Russia

Par

Viktoria Muravieva

**Briques moléculaires à clusters hétérométalliques chalcogénées
{Re_{6-x}Mo_xSe₈} x = 1-3 : cristallographie, structures électroniques et
propriétés redox**

Thèse présentée et soutenue à Novosibirsk, le 27 novembre 2019
Unité de recherche : Institut des Sciences Chimiques de Rennes – UMR CNRS 6226
Nikolaev Institute of Inorganic Chemistry, Novosibirsk

Rapporteurs avant soutenance :

Emmanuel CADOT
Professeur, Université de Versailles

Sylvie FERLAY
Professeur, Université de Strasbourg

Composition du Jury :

Emmanuel CADOT
Professeur, Université de Versailles / rapporteur

Vladimir FEDIN
Professeur, NIIC de Novosibirsk / examinateur

Stéphane CORDIER
Directeur de recherches CNRS, Université de Rennes 1 /
Directeur de thèse

Nikolay NAUMOV
Professeur, NIIC de Novosibirsk/ Co-directeur de thèse

Maxim SOKOLOV
Professeur, Novosibirsk State University / examinateur

Galina ROMANENKO
Researcher, International Tomography Center, Novosibirsk /
examinatrice

Membres invités:

Pierric LEMOINE
Chargé de Recherches CNRS, Université de Rennes 1

Carmelo PRESTIPINO
Chargé de Recherche CNRS, Université de Rennes 1

Contents

| | |
|--|----|
| Résumé détaillé de la thèse | 5 |
| The list of Acronyms | 23 |
| The list of compounds obtained | 25 |
| 1. Literature Review | 27 |
| 1.1 Introduction..... | 27 |
| 1.2 Cluster chemistry nomenclature..... | 30 |
| 1.3 The structure of heterometallic cluster compounds..... | 31 |
| 1.3.1 Triangular cluster complexes | 31 |
| 1.3.2 Tetrahedral cluster complexes | 33 |
| 1.3.3 Octahedral cluster complexes | 40 |
| 1.4 Preparation of heterometallic cluster compounds..... | 47 |
| 1.4.1 High-temperature synthesis..... | 47 |
| 1.4.2 Preparation in solution | 49 |
| 1.5 Reactivity of heterometallic clusters..... | 52 |
| 1.5.1 Reactions with the modification of the metal core atoms..... | 52 |
| 1.5.2 Ligand exchange reactions..... | 53 |
| 1.5.3 Reactions with metal cations with the formation of coordination polymers | 55 |
| 1.6 Electronic structure of heterometallic cluster complexes $[M_{4-x}M'_xQ_8L_n]$ and $[M_{6-x}M'_xQ_8L_6]$ | 57 |
| 1.6.1 Triangular clusters $[M_3Q_4L_n]$ | 57 |
| 1.6.2 Tetrahedral cluster complexes $[M_4Q_4L_n]$ | 58 |
| 1.6.3 Octahedral cluster complexes $[M_6L^i_8L^a_6]$ and $[M_6L^i_{12}L^a_6]$ | 61 |
| 1.7 Redox properties of the heterometallic cluster complexes..... | 62 |
| 1.7.1 Triangular cluster complexes $[M_3Q_4L_n]$ | 62 |
| 1.7.2 Tetrahedral cluster complexes $[M_4Q_4L_n]$ | 63 |
| 1.7.3 Octahedral cluster complexes $[M_6Q_8L_6]$ | 64 |
| 2. Experimental part | 66 |

| | |
|---|-----------|
| 2.1 Materials and methods..... | 66 |
| 2.2 Preparation protocols..... | 69 |
| 2.2.1 The solution-melt preparation of polymeric phase $K_6[Re_3Mo_3Se_8(CN)^{a-}_{2/2}(CN)^a_4]$ and its depolymerization to the soluble salts: $Cat_n[Re_3Mo_3Se_8(CN)_6]$, $Cat = K, Cs, Ph_4P^+$ | 69 |
| 2.2.2 The solution-melt preparation of $K_6[Re_{3.6}Mo_{2.4}Se_8(CN)^{a-a}_{2/2}(CN)^a_4]$ and $K_5[Re_5MoSe_8(CN)_6] \cdot 11H_2O$ | 72 |
| 2.2.3 Methatesis reaction for preparation of $(n-Bu_4N)_4[Re_5MoSe_8(CN)_6]$ | 72 |
| 2.2.4 Depolymerization of the polymer $K_6[Re_{3.6}Mo_{2.4}Se_8(CN)^{a-a}_{2/2}(CN)^a_4]$ with the formation of soluble salts $Cat_n[Re_{3.6}Mo_{2.4}Se_8(CN)_6]$, $Cat = K, Ph_4P^+$ | 73 |
| 2.2.5 Separation of cluster anions $[Re_4Mo_2Se_8(CN)_6]^{n-}$ and $[Re_3Mo_3Se_8(CN)_6]^{n-}$ and their isolation as salts $Cat_n[Re_{6-x}Mo_xSe_8(CN)_6]$, $Cat = K, n-Bu_4N^+$ | 74 |
| 2.2.6 Preparation of coordination polymers from $[Re_3Mo_3Se_8(CN)_6]^{5-}$ cyanocluster and transition metal ammine complexes | 76 |
| 2.2.7 The ligand exchange reactions of $[Re_3Mo_3Se_8(CN)_6]^{5-}$ and $[Re_4Mo_2Se_8(CN)_6]^{4-}$: formation of $[Re_{6-x}Mo_xSe_8L_6]$, $L = tbp, Ph_3P$ | 78 |
| 3. Results and Discussion..... | 80 |
| 3.1 Preparation of heterometallic cluster complexes $[Re_3Mo_3Se_8(CN)_6]^{n-}$, $[Re_4Mo_2Se_8(CN)_6]^{n-}$ and $[Re_5MoSe_8(CN)_6]^{n-}$ ($n = 4, 5$) as species with well-defined composition..... | 80 |
| 3.1.1 Synthetic route from solid state polymer $K_6[Re_3Mo_3Se_8(CN)^{a-a}_{2/2}(CN)^a_4]$ to soluble species and their mass-spectrometry investigation | 80 |
| 3.1.2 The separation of the cluster anions $[Re_4Mo_2Se_8(CN)_6]^{n-}$ and $[Re_3Mo_3Se_8(CN)_6]^{n-}$ from the mixture and their isolation as salts $Cat_n[Re_{6-x}Mo_xSe_8(CN)_6]$, $Cat = K, n-Bu_4N^+$ | 86 |
| 3.2 Structural features and isomerism of the $\{Re_{6-x}Mo_x\}$ ($x = 1-3$) metal cores in the solid state using SC XRD data..... | 89 |
| 3.3 Investigation of the isomeric composition of the clusters $[Re_3Mo_3Se_8(CN)_6]^{5-}$ and $[Re_4Mo_2Se_8(CN)_6]^{4-}$ in solution..... | 91 |
| 3.4 Quantum chemical calculations for heterometallic cluster anions $[Re_{6-x}Mo_xSe_8(CN)_6]^{n-}$ | 92 |

| | |
|---|------------|
| 3.5 X-ray absorption spectroscopy analysis of the local geometry of the metal core in $[\text{Re}_3\text{Mo}_3\text{Se}_8(\text{CN})_6]^{5-}$ and $[\text{Re}_4\text{Mo}_2\text{Se}_8(\text{CN})_6]^{4-}$ clusters..... | 97 |
| 3.6 The electrochemical study of the cyanoclusters $[\text{Re}_{6-x}\text{Mo}_x\text{Se}_8(\text{CN})_6]^{4-}$ ($x = 1, 2$ and 3) in solution..... | 100 |
| 3.7 UV-Vis spectroscopic investigation of heterometallic anions $[\text{Re}_{6-x}\text{Mo}_x\text{Se}_8(\text{CN})_6]^{n-}$ ($x = 1, 2$, and 3) in solution..... | 102 |
| 3.8 The study of interaction of the heterometallic cyanocluster $[\text{Re}_3\text{Mo}_3\text{Se}_8(\text{CN})_6]^{5-}$ with transition metals ammine complexes and the formation of coordination polymers..... | 105 |
| 3.9 The apical ligand exchange reactions of the clusters $[\text{Re}_3\text{Mo}_3\text{Se}_8(\text{CN})_6]^{5-}$ and $[\text{Re}_4\text{Mo}_2\text{Se}_8(\text{CN})_6]^{4-}$: formation of the complexes $[\text{Re}_{6-x}\text{Mo}_x\text{Se}_8\text{L}_6]$ $\text{L} = \text{tbp}, \text{PPh}_3$ | 113 |
| 3.10 Principal outcome..... | 115 |
| 3.11 Conclusion..... | 116 |
| 4. Detailed description of the crystal structure of heterometallic Re/Mo cluster compounds | 118 |
| 4.1 Crystal structures of the polymeric phases: $\text{K}_6[\text{Re}_3\text{Mo}_3\text{Se}_8(\text{CN})^{a-a}_{2/2}(\text{CN})^a_4]$ and $\text{K}_6[\text{Re}_{3.6}\text{Mo}_{2.4}\text{Se}_8(\text{CN})^{a-a}_{2/2}(\text{CN})^a_4]$ | 118 |
| 4.2 Crystal structures of molecular complexes $\text{Cat}_5[\text{Re}_3\text{Mo}_3\text{Se}_8(\text{CN})_6]$ ($\text{Cat} = \text{K}, \text{Cs}$) and $(\text{Ph}_4\text{P})_4[\text{Re}_3\text{Mo}_3\text{Se}_8(\text{CN})_6] \cdot 2\text{CH}_3\text{CN}$ | 120 |
| 4.3 Crystal structures of tetrabutylammonium salts of heterometallic clusters with different metal ratio $(\text{n-Bu}_4\text{N})_4[\text{Re}_{6-x}\text{Mo}_x\text{Se}_8(\text{CN})_6]$ $x = 1, 2$ and 3 | 123 |
| 4.4 Crystal structures of coordination polymers based on $[\text{Re}_3\text{Mo}_3\text{Se}_8(\text{CN})_6]^{5-}$ cyanocluster and metal ammine complexes of Cd^{2+} , Ni^{2+} and Co^{2+} | 125 |
| 4.5 Crystal structures of heterometallic clusters with apical organic ligands $[\text{Re}_{6-x}\text{Mo}_x\text{Se}_8\text{L}_6]$ $\text{L} = \text{tbp}, \text{Ph}_3\text{P}$ | 130 |
| Acknowledgements..... | 137 |
| 5. Supplementary | 138 |
| 6. Copies of the accepted and published articles related to the PhD manuscript.... | 151 |
| References | 198 |

Résumé détaillé de la thèse

Les complexes à clusters octaédriques de molybdène et de rhénium sont les composés les plus étudiés de tous les composés à clusters. Dans cette famille, il existe une très grande diversité structurale: des polymères à structures en chaînes, en couches ou bien en réseaux 3D jusqu'aux structures moléculaires basées sur des complexes isolés les uns des autres. Au cours des deux dernières décennies, beaucoup de travaux de recherche ont été orientés non seulement vers la synthèse et l'étude de nouveaux complexes à clusters moléculaires, mais aussi vers l'élaboration de composés supramoléculaires et de matériaux fonctionnels à partir de clusters. Cet intérêt est lié au fait que les complexes moléculaires à clusters ont un ensemble de propriétés uniques. Elles ont pour origine principale la présence de liaisons entre les métaux qui permettent la délocalisation des électrons de valence sur tout le cluster. Les composés à base de clusters octaédriques présentent des propriétés de photoluminescence dans une fenêtre optique très large dans le rouge profond/proche infrarouge, des transitions rédox réversibles sans changement de géométrie ou encore du magnétisme. Les composés à base de clusters octaédriques de rhénium ont une radio-opacité élevée en raison de la concentration locale élevée d'atomes d'éléments lourds. On connaît aussi des clusters qui présentent des propriétés catalytiques dans les réactions de photoréduction du CO_2 en méthanol et de photodégradation de la rhodamine B. La géométrie rigide, la haute stabilité et les propriétés physico-chimiques des clusters octaédriques décrits ci-dessus en font des briques de construction prometteuses pour la conception de matériaux fonctionnels de différents types. Des approches ont été développées pour modifier l'environnement du cluster par ses ligands afin d'élargir les possibilités d'utilisation de ces briques fonctionnelles de construction dans le domaine de la chimie des matériaux.

Les propriétés des clusters octaédriques étudiés ont pour origine non seulement la nature des atomes métalliques qui constituent le cluster, mais aussi la nature des ligands auquel il est lié et leur position autour du cluster (coiffante ou bien terminale). Un changement dans la composition du cluster en utilisant deux types de métaux pour former des clusters

hétérométalliques peut constituer un excellent outil pour modifier en douceur mais de façon notable les propriétés physicochimiques des composés à clusters afin d'obtenir de nouvelles caractéristiques physico-chimiques. La combinaison d'atomes de rhénium et de molybdène, deux éléments 5d et 4d respectivement caractérisés par des nombres d'électrons de valence différents, pour former un même cluster est une idée pertinente que nous avons explorée. Les chimies et les techniques de préparation des clusters de molybdène et celles des clusters de rhénium, bien connues mais différentes, sont maîtrisées.

Les clusters hétérométalliques octaédriques sont très peu étudiés en comparaison par exemple aux clusters hétérométalliques de la famille des cubanes. Les quelques exemples de la littérature sont les suivants :

- Les 'pseudo-binaires' hétérométalliques de la famille des phases de Chevrel, *e.g.* $M_{6-x}M'_xQ_8$ ($M = \text{Re}$, $M' = \text{Mo}$, $Q = \text{S}$, Se , $x = 2$; $Q = \text{Te}$, $x = 4$; $M = \text{Re}$, $M' = \text{Mo}$, $Q = \text{Se}$, $x = 1.5$; $M = \text{Mo}$, $M' = \text{Ru}$, $Q = \text{Te}$, $x = 0.5, 1, 1.5$; $M = \text{Mo}$, $M' = \text{Rh}$, $Q = \text{Te}$, $x = 0.5$; $M = \text{Nb}$, $M' = \text{Ru}$, $Q = \text{Te}$, $x = 2.83 - 3.5$).
- Les sels solubles contenant les complexes $[\text{Re}_{6-x}\text{Os}_x\text{Se}_8\text{L}_6]$ ($x = 1, 2, 3$; $\text{L} = \text{Cl}$, PEt_3 , OH); $[\text{Mo}_5\text{NbI}_8\text{L}_6]$ ($\text{L} = \text{Cl}$, CN , H_2O , OH); $[\text{Mo}_{6-x}\text{W}_x\text{Cl}_8\text{L}_6]$ ($\text{L} = \text{Cl}$, F).
- Les deux composés $\text{Cs}_5[\text{Re}_{\approx 4.5}\text{Mo}_{\approx 1.5}\text{S}_8(\text{CN})_6]$ et $\text{CaK}_4[\text{Re}_3\text{Mo}_3\text{S}_8(\text{CN})_6]$, sont les deux seuls exemples de sels à clusters mixtes Re/Mo.

Les clusters octaédriques de molybdène et de rhénium sont formés par chimie du solide à haute température. Dans les conditions de synthèses, l'utilisation de ces deux métaux pour former des clusters mixtes conduit à la formation d'impuretés comme cela a déjà été démontré pour les pseudo-binaires de type phase de Chevrel. C'est la raison pour laquelle, les propriétés physiques de ces dernières n'ont toujours pas été reportées dans la littérature. Un défi de cette chimie des clusters octaédriques hétéronucléaires Mo/Re consiste donc à trouver des méthodes de synthèse de nouvelles phases en grandes quantités et le cas échéant de rechercher les méthodes de purification et de séparation les plus pertinentes.

Les techniques de préparation utilisées pour les sulfures à clusters ont été appliquées dans la présente étude à la préparation de complexes de sélénures à clusters hétérométalliques. La chimie des sélénures à clusters $\{\text{Re}_{6-x}\text{Mo}_x\text{Se}_8\}$ semble être plus favorable à l'optimisation de procédures de synthèse afin de préparer des clusters hétérométalliques bien définis en termes de composition et d'isomères. Après avoir présenté les protocoles de synthèses optimisés, nous exposerons l'influence du rapport Mo/Re (ou encore la valeur de x en considérant le cluster $\{\text{Re}_{6-x}\text{Mo}_x\text{Se}_8\}$) sur les propriétés du cluster qui en résultent.

Contenu du manuscrit

Le premier chapitre est divisé en six parties et il est consacré à la recherche bibliographique dans le domaine de la synthèse, de la cristallographie et des propriétés des complexes hétérométalliques à clusters de métaux de transition riches en électrons.

- Les concepts de base utilisés dans la chimie des clusters pour décrire leurs structures et leurs comptes électroniques (ex. : nucléarité, ligands inners / apicaux, le nombre d'électrons de valence) sont brièvement abordés dans la première section d'introduction.
- La deuxième partie de l'introduction porte sur une revue issue de la littérature consacrée aux caractéristiques structurales des complexes et des structures basées sur des clusters hétérométalliques trinucéaires, tétranucéaires et hexanucéaires. La géométrie du cluster métallique et les types d'environnement impliquant les ligands inners et apicaux sont décrits pour des structures à complexes isolés ou bien pour des structures polymériques.
- La troisième partie de la revue de littérature est consacrée à la description de méthodes connues pour la préparation de complexes à clusters hétérométalliques. Les méthodes considérées sont divisées en deux catégories : les synthèses à haute température et les synthèses en solution.
- La quatrième partie de la revue bibliographique est consacrée à la réactivité des clusters hétérométalliques. Les réactions avec une modification i) du nombre

d'atomes formant le complexe à cluster, ii) de la nature des ligands environnant les clusters hétérométalliques ainsi que iii) de leur interaction avec les cations de métaux de transition pour former des polymères de coordination de différentes topologies, ont été considérées.

- La cinquième partie est consacrée aux caractéristiques spécifiques de la structure électronique des complexes à clusters hétérométalliques et de leurs analogues homo-métalliques.
- Dans la sixième partie, les propriétés d'oxydo-réduction des clusters hétérométalliques sont comparées à leurs analogues homométalliques. Sur la base de l'analyse des données publiées, il a été montré que la substitution hétérométallique avait un effet important sur la structure électronique des complexes à clusters et sur leurs propriétés. Les complexes à clusters hétérométalliques présentent souvent une activité rédox élevée par rapport à leurs analogues homométalliques. Les principales difficultés de l'étude expérimentale des clusters hétérométalliques sont mises en évidence.

Le deuxième chapitre de la thèse est consacré à la description des méthodes de préparation de sélénures à clusters hétérométalliques $\{\text{Re}_{6-x}\text{Mo}_x\text{Se}_8\}$ ($x = 1, 2, 3$) : réactifs de départ et produits utilisés, équipement et méthodologie. Les résultats des analyses des composés obtenus par EDS, DRX, spectrométrie de masse, spectroscopie d'absorption des rayons X (EXAFS), analyse par CHN élémentaire, RMN, spectroscopie IR sont présentés.

Dans le troisième chapitre de la thèse, les résultats de la recherche sont discutés en détail. Les principaux résultats de la présente étude sont brièvement présentés ci-dessous.

1. Description des structures cristallines des composés étudiés

Dans le présent travail, plus de 20 nouveaux composés basés sur des complexes de sélénures à clusters hétérométalliques $\{\text{Re}_{6-x}\text{Mo}_x\text{Se}_8\}$ ($x = 1, 2$ et 3 ,) ont été préparés : des solides polymériques, des cyanures moléculaires avec des contre-ions organiques et inorganiques, des polymères de coordination avec diverses topologies et des complexes

neutres contenant des dérivés de phosphine et de pyridine en tant que ligands apicaux. Les structures de 19 composés ont été étudiées à partir des données de diffraction des rayons X sur monocristal. Les structures obtenues mettent en évidence que les clusters hétérométalliques ont une topologie semblable à celles des clusters homométalliques connus de type $[M_6Q_8L_6]$. Les atomes de rhénium et de molybdène forment le cluster octaédrique $\{Re_{6-x}Mo_x\}$. Les ligands inners de sélénure sont coordonnés selon un mode μ_3 - à chaque face de l'octaèdre $\{Re_{6-x}Mo_x\}$, formant le cœur de cluster noté $\{Re_{6-x}Mo_xSe_8\}$. Chaque atome de métal est en outre coordonné par un ligand apical, le cyanure dans la plupart des structures (Figure 1). Les atomes de rhénium et de molybdène dans toutes les structures obtenues sont distribués de manière aléatoire sur les positions définissant l'octaèdre métallique. Le désordre ou plutôt le désordre orientationnel des clusters rend difficile l'étude de la géométrie locale et des phénomènes d'isométrie.

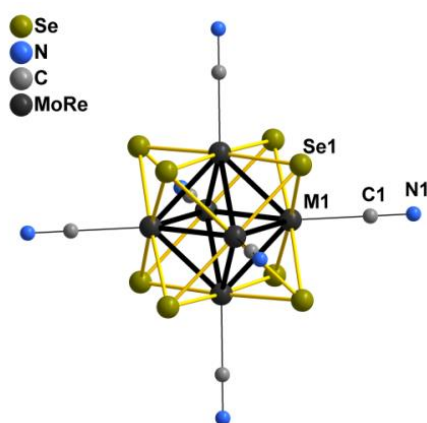


Figure 1 : Structure de l'anion à cluster $[Re_{6-x}Mo_xSe_8(CN)_6]^{n-}$.

2. Dépendance de la réaction de formation de phase en fonction de la température

La réaction à haute température entre les binaires $MoSe_2$ et $ReSe_2$ dans un bain fondu de cyanure de potassium pour une plage de températures allant de 630 à 800 °C en ampoule de silice conduit à la formation de cristaux octaédriques de la phase polymérique $K_6[Re_{6-x}Mo_xSe_8(CN)^{a-a}_{2/2}(CN)^a_4]$. Cette dernière est caractérisée par une structure basée sur des chaînes polymériques, les clusters sont liés les uns aux autres par l'intermédiaire

de ligands cyanure (Figure 2). Le rapport des métaux Mo/Re dépend de la température de réaction. x passe de 3 à 2,4 pour une augmentation de la température de synthèse de 630 à 800 °C. La préparation à 630 °C conduit à la formation d'une phase majoritaire à clusters $\{\text{Re}_3\text{Mo}_3\text{Se}_8\}$ et de phases secondaires contenant des clusters $\{\text{Re}_2\text{Mo}_4\text{Se}_8\}$ et $\{\text{Re}_4\text{Mo}_2\text{Se}_8\}$.

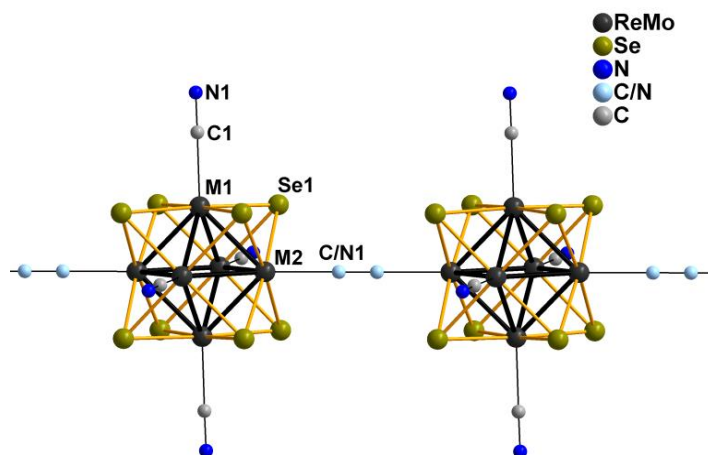


Figure 2 : Représentation d'une partie de la chaîne polymérique $[\text{Re}_{6-x}\text{Mo}_x\text{Se}_8(\mu\text{-CN})_{2/2}(\text{CN})_4]_{\infty}^{6-}$.

Le chauffage de la phase polymérique $\text{K}_6[\text{Re}_{6-x}\text{Mo}_x\text{Se}_8(\text{CN})^{a-a}_{2/2}(\text{CN})^a_4]$ dans de l'eau en présence d'oxygène et de petites quantités de cyanure de potassium entraîne la destruction de la structure polymérique et la formation de complexes moléculaires solubles $[\text{Re}_{6-x}\text{Mo}_x\text{Se}_8(\text{CN})_6]^{n-}$, où les six groupes cyano sont situés en position terminales. La dépolymérisation ne modifie pas la composition du cœur du cluster $\{\text{Re}_{6-x}\text{Mo}_x\text{Se}_8\}$. La réaction de dépolymérisation permet donc d'obtenir des clusters anioniques moléculaires. L'étude par spectrométrie de masse de la composition des produits de dépolymérisation a montré qu'une augmentation de la température de synthèse du polymère entraînait une augmentation de la quantité de la phase à clusters $\{\text{Re}_4\text{Mo}_2\text{Se}_8\}$ et une diminution de la quantité de la phase à clusters $\{\text{Re}_2\text{Mo}_4\text{Se}_8\}$ (Figure 3). La réaction de dépolymérisation oxydante en solution du précurseur $\text{K}_6[\text{Re}_{3,6}\text{Mo}_{2,4}\text{Se}_8(\mu\text{-CN})(\text{CN})_4]$ obtenu à 800°C conduit à la formation d'une solution aqueuse contenant un mélange d'anions à clusters $[\text{Re}_3\text{Mo}_3\text{Se}_8(\text{CN})_6]^{5-}$ et $[\text{Re}_4\text{Mo}_2\text{Se}_8(\text{CN})_6]^{5-}$.

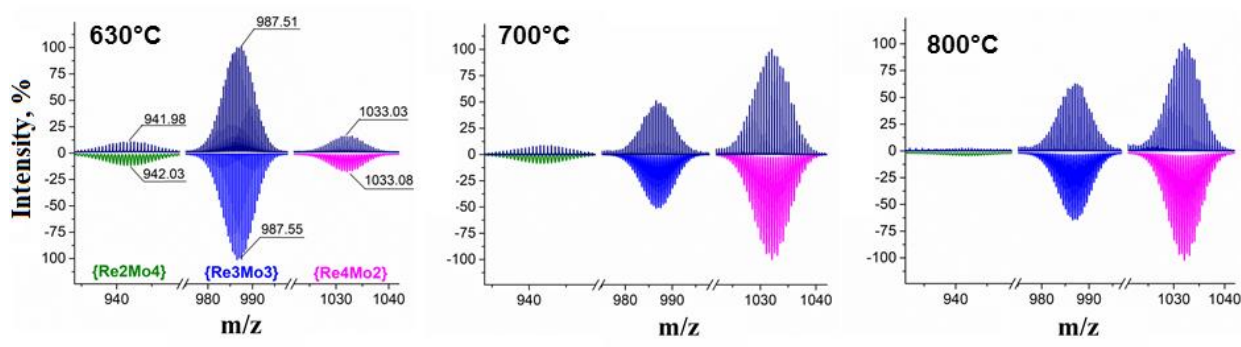


Figure 3 : Fragments de spectres de masse d'ions négatifs de sels $(\text{Ph}_4\text{P})_4[\text{Re}_{6-x}\text{Mo}_x\text{Se}(\text{CN})_6]$ dans CH_3CN / DMF . La température de réaction de la préparation du polymère est indiquée dans le coin supérieur gauche de chaque spectre.

Il a été constaté expérimentalement que lorsqu'un excès de bromure de tétrabutylammonium est ajouté à une solution aqueuse contenant un mélange d'anions à clusters $[\text{Re}_3\text{Mo}_3\text{Se}_8(\text{CN})_6]^{5-}$ et $[\text{Re}_4\text{Mo}_2\text{Se}_8(\text{CN})_6]^{5-}$ en présence d'oxygène, l'anion $[\text{Re}_4\text{Mo}_2\text{Se}_8(\text{CN})_6]^{5-}$ subit une oxydation et précipite sous forme de sel $(\text{n-Bu}_4\text{N})_4[\text{Re}_4\text{Mo}_2\text{Se}_8(\text{CN})_6]$. Le spectre de masse d'une solution du sel obtenu ne met en évidence que les adduits de l'anion $[\text{Re}_4\text{Mo}_2\text{Se}_8(\text{CN})_6]^{4-}$ avec des cations tétrabutylammonium. Au cours des expériences, il a été montré que la précipitation complète se produit dans une plage de pH allant de 7 à 9. Le cluster anionique $[\text{Re}_3\text{Mo}_3\text{Se}_8(\text{CN})_6]^{5-}$ dans ces conditions expérimentales reste en solution et peut à nouveau être isolé par précipitation en phase solide sous la forme de sels $(\text{n-Bu}_4\text{N})_4[\text{Re}_3\text{Mo}_3\text{Se}_8(\text{CN})_6]$ ou $\text{K}_5[\text{Re}_3\text{Mo}_3\text{Se}_8(\text{CN})_6]$.

L'interaction des diséléniures de molybdène et de rhénium avec du cyanure de potassium à 800°C en présence du polymère $\text{K}_6[\text{Re}_{3,6}\text{Mo}_{2,4}\text{Se}_8(\mu\text{-CN})(\text{CN})_4]$ conduit à la formation du complexe moléculaire $\text{K}_5[\text{Re}_5\text{MoSe}_8(\text{CN})_6]$ contenant l'anion cluster $[\text{Re}_5\text{MoSe}_8(\text{CN})_6]^{5-}$. Le sel résultant est facilement solubilisé dans l'eau et se sépare facilement des cristaux de polymère. L'anion à cluster $[\text{Re}_5\text{MoSe}_8(\text{CN})_6]^{5-}$ de la solution résultante a été isolé par précipitation sous forme solide dans le sel $(\text{n-Bu}_4\text{N})_4[\text{Re}_5\text{MoSe}_8(\text{CN})_6]$. L'analyse par spectrométrie de masse et l'analyse élémentaire du sel obtenu n'ont pas révélé la présence d'impuretés de complexes à clusters avec une composition différente. La possibilité de faire varier la composition et les proportions des produits obtenus dans les précurseurs de départ en fonction de la

température et le fait que les propriétés d'oxydo-réduction en solution sont différentes pour chaque valeur de x pour les complexes $[\text{Re}_{6-x}\text{Mo}_x\text{Se}_8(\text{CN})_6]^{n-}$ ont permis d'isoler sélectivement les anions hétérométalliques $[\text{Re}_5\text{MoSe}_8(\text{CN})_6]^{n-}$, $[\text{Re}_4\text{Mo}_2\text{Se}_8(\text{CN})_6]^{n-}$ et $[\text{Re}_3\text{Mo}_3\text{Se}_8(\text{CN})_6]^{n-}$ ($n = 4, 5$) sous la forme de composés définis.

3. Caractéristiques structurales et isomériques du cluster $\{\text{Re}_{6-x}\text{Mo}_x\}$ à l'état solide

Une analyse des distances interatomiques dans les structures des composés contenant les clusters $\{\text{Re}_3\text{Mo}_3\text{Se}_8\}$ montre que les distances moyennes M-M dépendent faiblement du nombre d'électrons de valence du cluster. Dans toutes les structures étudiées, le cluster est faiblement distordu, la différence entre les liaisons longues et les liaisons courtes métal-métal est inférieure à 0,04 Å. Dans le cas des clusters hétérométalliques $\{\text{Re}_3\text{Mo}_3\}$, $\{\text{Re}_4\text{Mo}_2\}$, l'isomérisation est possible (Figure 4).

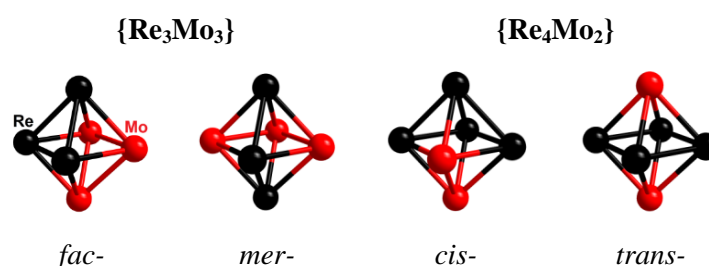


Figure 4 : Isomérisation des clusters $\{\text{Re}_3\text{Mo}_3\}$ et $\{\text{Re}_4\text{Mo}_2\}$.

La symétrie locale du cluster imposée par le groupe d'espace de la structure cristalline et celle du groupe ponctuelle réelle des isomères $\{\text{Re}_3\text{Mo}_3\}$ et $\{\text{Re}_4\text{Mo}_2\}$ ne coïncident généralement pas. Par conséquent, les anions hétérométalliques contenant divers isomères du cluster sont orientationnellement désordonnés sur plusieurs positions dans le cristal. La diffraction des rayons X donne accès à des modèles avec des positions moyennes et donc à des distances interatomiques moyennées. Ces modèles sont caractérisés par une distorsion légère, voire inexistante, du cluster métallique. L'occupation aléatoire des positions des atomes de rhénium et de molybdène dans le cluster a été observée dans toutes les structures des composés étudiés.

4. Etude de la composition isomérique en solution

L'analyse de la composition isomérique des clusters hétérométalliques n'est pas possible à l'état solide. Elle est rendue possible grâce aux réactions de dépolymérisation qui donnent des espèces solubles. Les analyses RMN ^{77}Se ont été effectuées pour les composés diamagnétiques $\text{K}_5[\text{Re}_3\text{Mo}_3\text{Se}_8(\text{CN})_6]$ et $(\text{n-Bu}_4\text{N})_4[\text{Re}_4\text{Mo}_2\text{Se}_8(\text{CN})_6]$ contenant les complexes à 22 électrons par cluster, $[\text{Re}_3\text{Mo}_3\text{Se}_8(\text{CN})_6]^{5-}$ et $[\text{Re}_4\text{Mo}_2\text{Se}_8(\text{CN})_6]^{4-}$, respectivement. Les données RMN ^{77}Se indiquent que le cluster $\{\text{Re}_3\text{Mo}_3\text{Se}_8\}$ existe sous la forme d'un isomère unique, mer- $\{\text{Re}_3\text{Mo}_3\text{Se}_8\}$, tandis que dans les conditions expérimentales utilisées, le cluster $\{\text{Re}_4\text{Mo}_3\text{Se}_8\}$ existe sous la forme des isomères cis et trans dans un rapport cis:trans proche de 2:1.

5. Calculs quantiques des anions hétérométalliques de cyanoclusters $[\text{Re}_{6-x}\text{Mo}_x\text{Se}_8(\text{CN})_6]^{n-}$

Le calcul DFT sur les motifs isolés a été appliqué afin d'analyser l'effet de la substitution d'atomes de rhénium par des atomes de molybdène sur la structure électronique et la géométrie optimisée des complexes. Le diagramme des orbitales moléculaires (OM) de l'isomère mer de l'anion $[\text{Re}_3\text{Mo}_3\text{Se}_8(\text{CN})_6]^{7-}$ ($x = 3$) pour un nombre d'électrons de valences de 24 est présenté sur la Figure 6. Ce nombre de 24 correspond à une saturation électronique de tous les niveaux liants. Ainsi, le diagramme d'OM contient un bloc d'orbitales liantes occupées et un bloc d'orbitales anti-liantes inoccupées plus hautes en énergies. Notons que les niveaux HOMO et HOMO-1 se situent quasiment à la même énergie et sont séparés par un pseudo-gap d'environ 0,8 V des autres orbitales liantes. La séparation énergétique entre les niveaux HOMO et HOMO-1 du bloc des orbitales anti-liantes est d'environ 1,6 eV. Les diagrammes d'OM des autres anions hétérométalliques $[\text{Re}_{6-x}\text{Mo}_x\text{Se}_8(\text{CN})_6]^{n-}$ ($x \neq 3$) ont un arrangement similaire des niveaux d'énergie à celui que nous venons de décrire pour $[\text{Re}_3\text{Mo}_3\text{Se}_8(\text{CN})_6]^{5-}$.

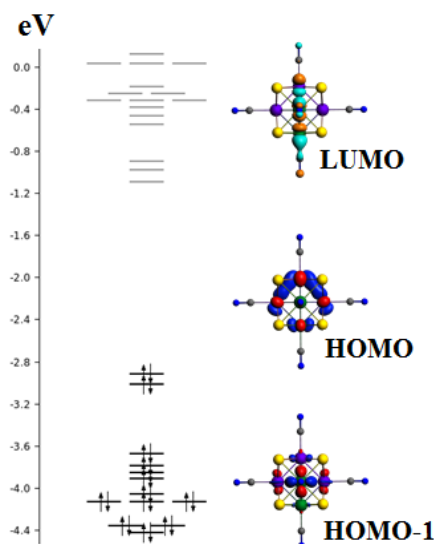


Figure 6 : Diagramme d'orbitales moléculaires pour l'isomère mer de $[\text{Re}_3\text{Mo}_3\text{Se}_8(\text{CN})_6]^{7-}$.

L'analyse de la géométrie optimisée des anions hétérométalliques obtenue par ces calculs quantiques a montré que la dépopulation des orbitales liantes conduit à une modification de l'énergie de l'orbitale HOMO-1, accompagnée d'une distorsion importante du cluster. La Figure 7 représente l'évolution des distances moyennes Re-Re, Re-Mo et Mo-Mo pour un nombre d'électrons de valences par cluster allant de 21 à 24 pour les isomères mer et fac du cluster anionique $[\text{Re}_3\text{Mo}_3\text{Se}_8(\text{CN})_6]^{n-}$.

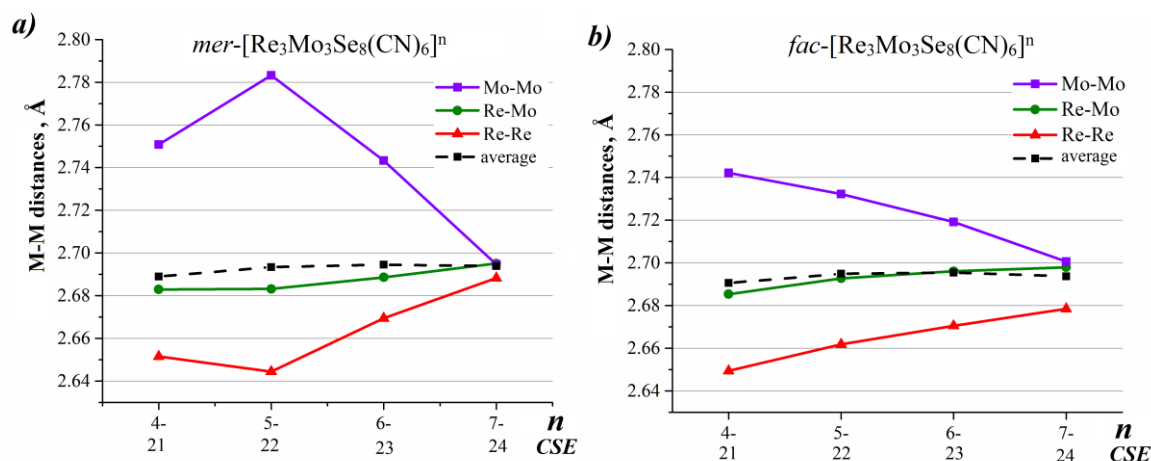


Figure 7 : Evolution des distances M-M –pour les isomères mer- (a) et fac (b) du cluster anionique $[\text{Re}_3\text{Mo}_3\text{Se}_8(\text{CN})_6]^{n-}$.

Les calculs théoriques des géométries optimisées obtenues par calcul DFT mettent en évidence une distorsion importante pour les clusters hétérométalliques pauvres en

électrons. Pour confirmer expérimentalement la distorsion, nous avons analysé nos composés par spectroscopie d'absorption des rayons X (EXAFS), qui permet d'accéder aux géométries locales réelles.

6. Etudes par spectroscopie d'absorption des rayons X (EXAFS : Extended X-Ray Absorption Fine Structure)

Les clusters les plus déformés d'après les calculs quantique sont les clusters à 22 électrons de valence dans les composés $K_5[Re_3Mo_3Se_8(CN)_6] \cdot 11H_2O$ et $(n-Bu_4N)_4[Re_4Mo_2Se_8(CN)_6]$. Ils ont été choisis pour l'analyse des distances interatomiques par spectroscopie d'absorption des rayons X. Les courbes calculées après affinement concordent bien avec les données expérimentales (Figure 8). Les distances Re-Re obtenues par EXAFS sont plus courtes que les distances moyennes M-M, et les distances Mo-Mo sont sensiblement plus longues en cohérence avec les résultats des calculs de DFT.

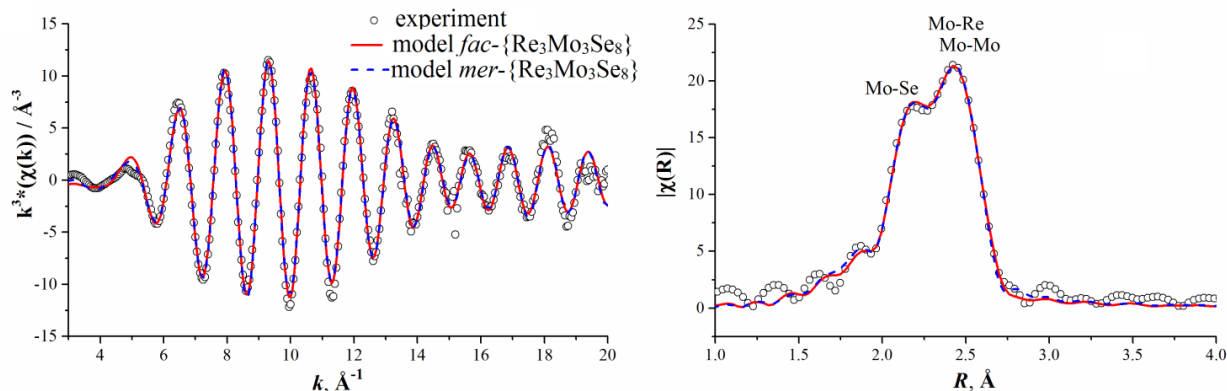


Figure 8 : Signaux EXAFS des modèles mer et fac de $K_5[Re_3Mo_3Se_8(CN)_6] \cdot 11H_2O$ et spectre expérimental au seuil Mo K $\chi(k) k^3 \cdot \chi(k)$ (figures de gauche) et transformées de Fourier correspondantes (figures de droite). Les courbes des modèles obtenues à partir de l'ajustement de courbes (espace d'ajustement - k) sont données sous forme de lignes.

Les données EXAFS et les calculs quantiques montrent que les clusters $\{Re_3Mo_3\}$ et $\{Re_4Mo_2\}$ dans les anions sont fortement déformés. L'évaluation de cette distorsion ne peut pas être déterminée à partir des analyses par diffraction des rayons X sur

monocristal car la symétrie locale du cluster ne coïncide pas avec la symétrie ponctuelle des groupes d'espace dans lesquels ces composés cristallisent. Nous avons montré ici, l'efficacité d'une étude combinant calculs quantiques et spectroscopie d'absorption des rayons X pour déterminer la géométrie locale des clusters hétérométalliques.

7. Etude des propriétés d'oxydo-réduction

L'activité redox des clusters est actuellement mise à profit dans la chimie des matériaux polymères et donne des perspectives dans des domaines tels que l'électrocatalyse, l'électro-détection, le stockage de l'énergie ou bien encore les dispositifs électrochromiques. Les complexes à clusters en raison de leurs caractéristiques géométriques, de leur stabilité et de la possibilité de les fonctionnaliser à façon sont des briques moléculaires prometteuses pour l'élaboration de matériaux hybrides.

Les clusters hétérométalliques présentent souvent une activité redox élevée par rapport à leurs analogues homométalliques. Les propriétés redox des complexes hétérométalliques obtenus sous forme de sels $(n\text{-Bu}_4\text{N})_4[\text{Re}_{6-x}\text{Mo}_x\text{Se}_8(\text{CN})_6]$ ($x = 1, 2, 3$) ont été étudiées par voltamétrie cyclique (Figure 9). Le remplacement successif d'atomes de rhénium par des atomes de molybdène dans les complexes à clusters $[\text{Re}_{6-x}\text{Mo}_x\text{Se}_8(\text{CN})_6]^{n-}$ conduit à une augmentation de la charge n des anions et ceci pour un même nombre d'électrons de valence. Ces modifications s'accompagnent de transitions redox supplémentaires par rapport au cluster homométallique $[\text{Re}_6\text{Se}_8(\text{CN})_6]^{4-}$. Les complexes hétérométalliques à forte teneur en molybdène sont caractérisés par plusieurs transitions redox réversibles dans une fenêtre étroite de potentiel. Les valeurs des potentiels électrochimiques des anions à clusters hétérométalliques $[\text{Re}_{6-x}\text{Mo}_x\text{Se}_8(\text{CN})_6]^{n-}$ se situent entre les valeurs connues des clusters homométalliques du rhénium et celles des clusters hexacyanés de molybdène. Le décalage des potentiels d'oxydation par rapport aux analogues du rhénium vers la région des valeurs négatives conduit à la stabilisation des états déficitaires en électrons des anions hétérométalliques.

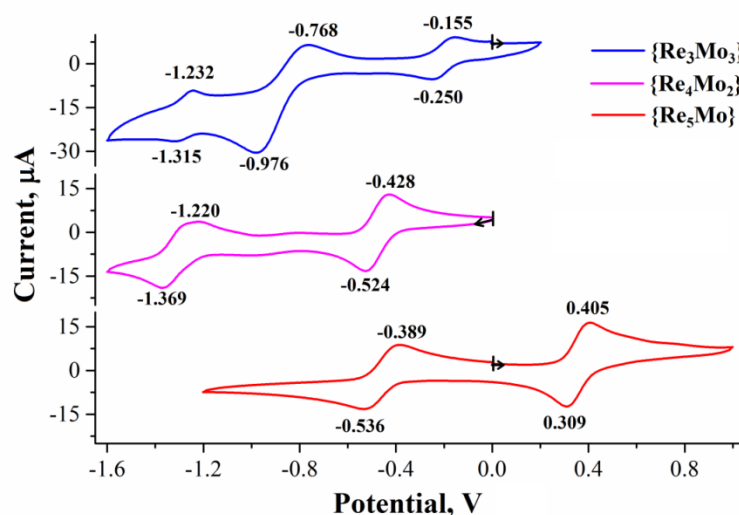










Figure 9 : Courbes CV pour $[\text{Re}_{6-x}\text{Mo}_x\text{Se}_8(\text{CN})_6]^{n-}$ ($x = 1, 2, 3$) dans de l'acétonitrile (électrode de référence - Ag / AgCl), vitesse de balayage 0,2 V / s.

8. Analyses par spectroscopie d'absorption UV/visible

Les spectres d'absorption des anions à clusters hétérométalliques $[\text{Re}_{6-x}\text{Mo}_x\text{Se}_8(\text{CN})_6]^{n-}$ ($x = 1, 2, 3$) en solution sont représentés sur la Figure 10. Leur allure change progressivement en fonction de x et de la charge n . Les spectres d'absorption des complexes hétérométalliques dans la région du visible changent considérablement en lien avec la modification de la structure électronique du cluster ; ce qui se traduit par des changements de couleur (Tableau 1).

Tableau 1 : Récapitulatif de l'évolution des couleurs des solutions à clusters anioniques $[\text{Re}_{6-x}\text{Mo}_x\text{Se}_8(\text{CN})_6]^{n-}$ en fonction de la charge n et du nombre d'électrons de valence par cluster.

| | $[\text{Re}_3\text{Mo}_3\text{Se}_8(\text{CN})]^{n-}$ | | | $[\text{Re}_4\text{Mo}_2\text{Se}_8(\text{CN})]^{n-}$ | | | $[\text{Re}_5\text{MoSe}_8(\text{CN})]^{n-}$ | |
|-------------------------------|---|---|---|---|---|---|---|---|
| Charge anionique | 4- | 5- | 6- | 4- | 5- | 6- | 4- | 5- |
| Nbre électrons de valence | 21 | 22 | 23 | 22 | 23 | 24 | 23 | 24 |
| Image de la solution d'anions |  |  |  |  |  |  |  |  |

Les spectres UV-Vis des complexes déficitaires en électrons (nombre d'électrons de valence < 24) contiennent de larges bandes d'absorption faiblement intenses dans le proche infrarouge. Ces bandes sont absentes dans les spectres d'absorption des anions saturés en électrons (nombre d'électrons de valence = 24).

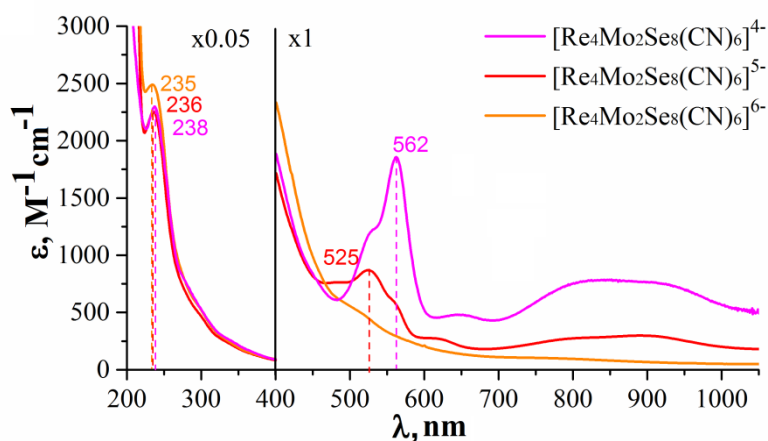


Figure 10 : Spectres d'absorption électronique pour les solutions de clusters anioniques $[\text{Re}_4\text{Mo}_2\text{Se}_8(\text{CN})_6]^{n-}$ ($n = 4 - 6$).

Les bandes d'absorption dans la région UV pour les complexes à clusters $[\text{Re}_{6-x}\text{Mo}_x\text{Se}_8(\text{CN})_6]^{n-}$ sont caractérisées par une forte absorbance. La position de leurs maxima dépend de la composition et de la charge du complexe à cluster. Ces bandes correspondent probablement à un grand nombre de transitions des orbitales liantes à caractère métallique vers des orbitales non liantes inoccupées. Notons que pour une composition donnée, à chaque nombre d'électron de valence correspond une couleur différente. Cette propriété fait donc de cette famille de composés à clusters anioniques $[\text{Re}_{6-x}\text{Mo}_x\text{Se}_8(\text{CN})_6]^{n-}$, des briques fonctionnelles adaptées pour la réalisation de dispositifs électro-chromiques.

9. Interaction des cyanoclusters hétérométalliques avec des complexes amoniaqués de métaux de transition

Comme la plupart des cyano-complexes de métaux de transition, les cyanoclusters lorsqu'ils sont associés à des cations de métaux de transition forment des composés peu

solubles caractérisés par des structures polymériques avec un grand nombre de contacts M-CN-M'. La chimie des polymères de coordination cyanocluster montre une grande variété de types de structures aux caractéristiques prometteuses. Le nouveau complexe hétérométallique $[\text{Re}_3\text{Mo}_3\text{Se}_8(\text{CN})_6]^{5-}$ est caractérisé par une charge 5-. Cette charge est rarement stabilisée dans la chimie des clusters hexacyanés. La possibilité de stabiliser une telle charge ouvre la possibilité d'élaborer de nouveaux composés avec des topologies jamais rencontrées auparavant parmi les polymères de coordination rapportés dans la littérature. Dans ce travail, la méthode de contre-diffusion de solutions a été utilisée pour obtenir des monocristaux de polymère de coordination. Il a été constaté que l'interaction d'une solution aqueuse d'ammoniaque de sels cobalt (II) ou de nickel (II) avec une solution aqueuse de $\text{K}_5[\text{Re}_3\text{Mo}_3\text{Se}_8(\text{CN})_6]$ conduit à la formation de polymères de coordination isostructuraux de formule $[\text{M}(\text{NH}_3)_6]_4[\{\text{M}(\text{NH}_3)_2\}\{\text{Re}_3\text{Mo}_3\text{Se}_8(\text{CN})_6\}_2] \cdot 15\text{H}_2\text{O}$ (M = Co, Ni) avec une structure en couches. Une étude de l'interaction d'une solution aqueuse du sel $\text{K}_5[\text{Re}_3\text{Mo}_3\text{Se}_8(\text{CN})_6]$ avec des solutions aqueuses d'ammoniaque de sels de cadmium (II) a montré que la composition et la structure des composés résultants dépendaient de la nature des anions autre que les complexes à clusters présents dans la solution. En effet, lorsque de l'acétate de cadmium est utilisé dans la réaction, il se forme des cristaux du composé polymérique à chaîne $\{[\text{Cd}(\text{NH}_3)_5]_2[(\text{Cd}(\text{NH}_3)_4]_3[\text{Re}_3\text{Mo}_3\text{Se}_8(\text{CN})_6]_2\} \cdot 5\text{H}_2\text{O}$. Un excès d'anions chlorures dans la réaction conduit à la formation du composé $\{[\text{Cd}(\text{NH}_3)_4]_3\text{Re}_3\text{Mo}_3\text{Se}_8(\text{CN})_6\}\text{Cl}$, avec une structure tridimensionnelle. Les homologues $\{[\text{Cd}(\text{NH}_3)_4]_3\text{Re}_3\text{Mo}_3\text{Se}_8(\text{CN})_6\}\text{X}$ (X = Br, I) ont également été obtenus en utilisant respectivement un excès d'ions bromures et iodures. Cette série de composés cristallise dans le groupe d'espace *R*-3. Les structures sont basées sur l'interpénétration de deux réseaux primitifs qui se correspondent par une translation (2/3, 1/3, 1/3). Chaque réseau est formé de complexes $[\text{Cd}(\text{NH}_3)_4]^{2+}$ qui relie entre eux les complexes $[\text{Re}_3\text{Mo}_3\text{Se}_8(\text{CN})_6]^{5-}$. La composition est de 3 complexes cationiques $[\text{Cd}(\text{NH}_3)_4]^{2+}$ pour un complexe anionique $[\text{Re}_3\text{Mo}_3\text{Se}_8(\text{CN})_6]^{5-}$. Ainsi, un atome halogène supplémentaire complète la charge du complexe à cluster pour contrebalancer la charge des 3 complexes cationiques. Au-delà d'assurer la neutralité, cet atome halogène supplémentaire stabilise l'édifice structurale par des liaisons hydrogène

entre les atomes d'hydrogène des molécules d'ammoniac coordonnées aux cations cadmium (Figure 11).

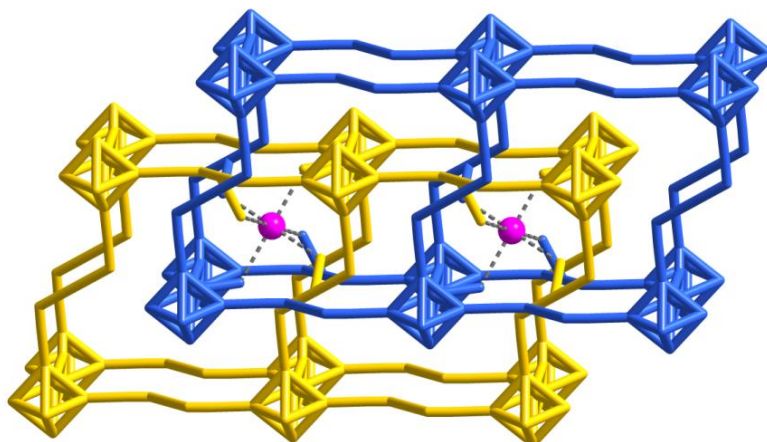


Figure 11 : Représentation schématique des réseaux interpénétrés formés des cations $[\text{Cd}(\text{NH}_3)_4]^{2+}$ et des anions $[\text{Re}_3\text{Mo}_3\text{Se}_8(\text{CN})_6]^{5-}$ dans $\{[\text{Cd}(\text{NH}_3)_4]_3\text{Re}_3\text{Mo}_3\text{Se}_8(\text{CN})_6\}\text{Cl}$. Les atomes d'azote des molécules d'ammoniaque, les atomes de sélénium et d'hydrogène sont omis pour plus de clarté. Les deux réseaux sont représentés en jaune et en bleu, les anions chlorures en rose.

Les composés obtenus $\{[\text{Cd}(\text{NH}_3)_4]_3\text{Re}_3\text{Mo}_3\text{Se}_8(\text{CN})_6\}\text{X}$ subissent une oxydation réversible lors d'un recuit à l'air ; ce qui conduit à une amorphisation partielle de l'échantillon. L'exposition des d'échantillons recuits dans de l'ammoniaque ou de la vapeur d'hydrazine entraîne la réduction du complexe à clusters, accompagnée du rétablissement de la cristallinité de l'échantillon. Les modifications de la couleur des échantillons solides lors de l'oxydation et de la réduction sont les mêmes que celles qui sont observées en solution après oxydation du complexe de départ puis réduction de la forme oxydée (Figure 12).

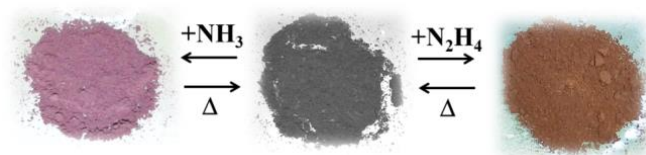


Figure 12 : Images illustrant les changements de couleur de l'échantillon recuit du composé $\{[\text{Cd}(\text{NH}_3)_4]_3\text{Re}_3\text{Mo}_3\text{Se}_8(\text{CN})_6\}\text{I}$ après exposition sous vapeurs d'ammoniac et d'hydrazine.

L'oxydation/réduction réversible de l'anion dans la structure du polymère s'effectue sans provoquer la destruction du réseau ; ce qui est un phénomène rare dans la chimie des polymères de coordination.

10. Réaction d'échange des ligands cyanures par des ligands dérivés des pyridines et des phosphines

Des complexes hétérométalliques à clusters $\{\text{Re}_{6-x}\text{Mo}_x\text{Q}_8\}$ ($\text{Q} = \text{S}, \text{Se}$) sont formés dans un bain fondu de cyanure de potassium et ont été obtenus uniquement avec des ligands cyanure. À ce jour, il n'existe aucun exemple de substitution de ligands cyanure dans des complexes à clusters homométalliques octaédriques. Cela est un facteur limitant l'intégration de ces nouveaux clusters hétérométalliques dans des matériaux hybrides ou bien pour la fonctionnalisation de surfaces en vue d'applications potentielles. Nous avons montré que les clusters hétérométalliques $\{\text{Re}_{6-x}\text{Mo}_x\text{Q}_8\}$ présentent une réactivité accrue. En particulier les groupements cyanures sont facilement échangeables en solution. Ceci permet la fonctionnalisation de tous les sites métalliques par des ligands organiques en position apicale. Après optimisation des conditions expérimentales, les ligands cyanure dans les complexes hétérométalliques à cluster $[\text{Re}_3\text{Mo}_3\text{Se}_8(\text{CN})_6]^{5-}$ et $[\text{Re}_4\text{Mo}_2\text{Se}_8(\text{CN})_6]^{4-}$ ont été substitués par des ligands dérivés de la pyridine et des phosphines par voie solvothermale. Des composés basés sur des motifs neutres $[\text{Re}_3\text{Mo}_3\text{Se}_8(\text{tbp})_6]$ et $[\text{Re}_4\text{Mo}_2\text{Se}_8\text{L}_6]$ ($\text{L} = \text{terbutypyridin}, \text{PPh}_3$) ont été synthétisés et caractérisés.

Conclusion

La chimie des clusters est un domaine de recherche en plein essor en raison des potentialités d'applications allant de la santé à la production verte d'énergie. Dans ce cadre, ces travaux portaient sur les synthèses, les déterminations structurales et les caractérisations de nouveaux composés à clusters hétérométalliques de molybdène et de rhénium. Il a été démontré que la "substitution" des atomes métallique d'un cluster $\{\text{Re}_6\}$ par des atomes de molybdène pour former un cluster $\{\text{Re}_{6-x}\text{Mo}_x\}$ est un outil efficace

pour i) modifier et contrôler les propriétés physico-chimiques du cluster et ii) générer de nouvelles propriétés et de nouvelles structures. Avant cette étude, seuls quelques travaux consacrés principalement à la synthèse et aux études structurales de composés hétérométalliques octaédriques étaient rapportées dans la littérature. La principale difficulté qui a limité le développement de ce champ de recherche était la formation simultanée et la co-cristallisation de plusieurs clusters hétérométalliques avec des rapports Mo/Re différents ou bien pour un même rapport, de plusieurs isomères. Ce problème a été résolu dans ce travail en utilisant la séparation post-synthétique basée sur les différences des comportements redox et de solubilité des chalcogénures à clusters hétérométalliques. Cela a permis d'étudier individuellement les structures, les caractéristiques spectroscopiques et les propriétés redox de clusters bien définis dans les complexes de type $[\text{Re}_{6-x}\text{Mo}_x\text{Se}_8(\text{CN})_6]^{n-}$ ($x = 1, 2, 3$). Ces travaux fournissent une série de clusters Re/Mo capables de plusieurs transitions électrochimiques dans une fenêtre étroite de potentiels, accompagnées d'une modification de leur spectre optique. Ils pourront par exemple être utilisés pour la réalisation de capteurs ou de dispositifs électrochromiques.

Au cours de ce travail, ont été déterminés les effets stériques et électroniques qui permettent d'expliquer les propriétés physiques des clusters hétérométalliques. Pour cela nous avons utilisé des approches combinant expériences (i.e. diffraction des rayons X, spectroscopies d'absorption des rayons X, RMN, UV-visible) et théorie avec les calculs des géométries optimisées et des structures électroniques. L'ensemble des approches mise en œuvre pour étudier les clusters octaédriques $\{\text{Re}_{6-x}\text{Mo}_x\text{Se}_8\}$ pourra être étendue à l'étude d'autres systèmes produisant des clusters hétérométalliques de compositions et de nucléarités différentes.

The list of acronyms:

edt : 1,2-ethanedithiolate anion $[\text{C}_2\text{H}_4\text{S}_2]^{2-}$
Cp : cyclopentadienyl anion C_5H_5^-
Cp^{*} : pentamethylcyclopentadienyl anion C_5Me_5^-
Cp' : methylcyclopentadienyl anion $\text{C}_5\text{H}_4\text{Me}^-$
Cp^{Et} : ethyltetramethylcyclopentadienyl anion $\text{C}_5\text{EtMe}_4^-$
Cp[#] = Cp, Cp', Cp^{*}
Hnta : 2,2',2''-nitrilotriacetate anion $[\text{N}(\text{CH}_2\text{CO}_2\text{H})(\text{CH}_2\text{CO}_2)_2]^{2-}$
dmpe : 1,2-bis(dimethylphosphino)ethane $\text{Ph}_2\text{P}(\text{CH}_2)_2\text{PPh}_2$
dppm : bis(diphenylphosphino)methane $\text{Ph}_2\text{PCH}_2\text{PPh}_2$
Tp : Tris(pyrazolyl)hydroborate (1-) $[\text{HB}(\text{C}_3\text{N}_2\text{H}_3)_3]^-$
dtc : diethyldithiocarbamate
pts⁻ : p-toluenesulfonate
Me₆tren : tris[2-(dimethylamino)ethyl]amine
py : pyridine
tbp : 4-tert-butylpyridine
cys : cysteine
cod : 1,5-cyclooctadiene
DMF : N,N-dimethylformamide
DMSO : dimethyl sulfoxide
THF : tetrahydrofuran
CSE : Cluster Skeletal Electron
MO : Molecular Orbital
HOMO : Highest Occupied Molecular Orbital
LUMO : Lowest Unoccupied Molecular Orbital
CV : Cyclic Voltammetry
EPR : Electron Paramagnetic Resonance
NMR : Nuclear Magnetic Resonance
SC XRD : Single Crystal X-ray Diffraction
PXRD : Powder X-ray Diffraction

EDS : Energy-Dispersive X-ray Spectroscopy

IR : Infrared

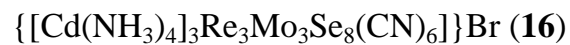
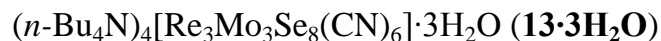
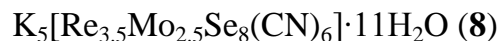
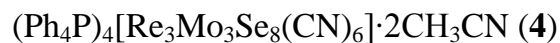
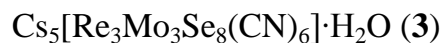
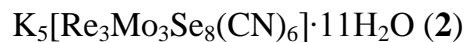
UV-Vis : Ultraviolet–Visible

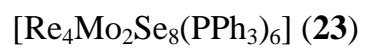
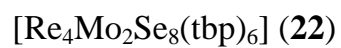
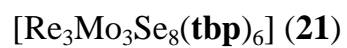
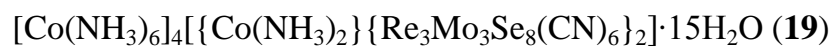
EXAFS : Extended X-ray Absorption Fine Structure

DFT : Density Functional Theory

COSMO : Conductor like Screening Model

The list of compounds obtained:





Chapter 1: Literature Review

1.1 Introduction

Relevance of the topic. Transition metals in low oxidation states are intent to the formation of metal-metal bonds. Compounds containing bonds mentioned are called “cluster” compounds [1]. The chemistry of transition metal cluster compounds is currently an intensively developing field of coordination chemistry, attracting more and more research groups. One of the most actively studied types of cluster compounds are the octahedral cluster complexes of molybdenum, tungsten, and rhenium. The study of compounds concerned is conducted in research groups around the world. Among octahedral cluster complexes, compounds of various structural motifs are found: from chain-like polymers, layered, or 3D network structures, to molecular cluster complexes [2-4]. The study of octahedral cluster compounds with a polymeric structure, for example, Chevrel [5] or Bronger phases [6], took place at the early stage of the development of chemistry of cluster compounds. Over the past two decades, the focus of research has shifted toward the synthesis and study of molecular cluster complexes, as well as supramolecular compounds and functional materials based on them. This is due to the fact that molecular cluster complexes possess a set of promising properties due to structural features of the cluster core, such as photoluminescence, reversible redox transitions without changing the geometry of the cluster complex, magnetism [7, 8]. Compounds based on octahedral rhenium cluster complexes exhibit high radiopacity due to the high local concentration of heavy element atoms [9]. Cluster complexes are known that exhibit catalytic properties in the reactions of photoreduction of CO₂ to methanol and photodegradation of rhodamine B [10, 11]. Rigid geometry, high stability and predictable chemical properties of octahedral complexes in the presence of the physicochemical features discussed above make them promising building blocks for the design of functional materials of various types. Developed approaches to the modification of the ligand environment expand the possibilities for the use of cluster building blocks in the field of chemistry of functional materials.

The properties of the cluster complexes under consideration are due to the nature of the atoms that compose the cluster core and, in particular, the nature of the metal atoms. A change in the composition of the core leading to heterometallic cluster complexes can serve as an excellent tool for changing the physicochemical properties of cluster compounds and introducing new characteristics that are not typical for homometallic analogues.

The degree of development of the research topic. Despite the fact that heterometallic cluster complexes are actively studied and the prospects for their use, for example, in catalysis, are obvious [12-14], octahedral heterometallic clusters are investigated scarcely. Although the Chevrel heterometallic polymer phases $M_{6-x}M'_xQ_8$ ($M = \text{Re}$, $M' = \text{Mo}$, $Q = \text{S}$, Se , $x = 2$; $Q = \text{Te}$, $x = 4$ [15]; $M = \text{Re}$, $M' = \text{Mo}$, $Q = \text{Se}$, $x = 1.5$ [16]; $M = \text{Mo}$, $M' = \text{Ru}$, $Q = \text{Te}$, $x = 0.5, 1, 1.5$ [17-19]; $M = \text{Mo}$, $M' = \text{Rh}$, $Q = \text{Te}$, $x = 0.5$ [17]; $M = \text{Nb}$, $M' = \text{Ru}$, $Q = \text{Te}$, $x = 2.83 - 3.5$ [20]) have been known for a long time, the study of molecular octahedral heterometallic cluster complexes is limited to several publications. Earlier, soluble heterometallic complexes $[\text{Re}_{6-x}\text{Os}_x\text{Se}_8\text{L}_6]$ ($x = 1, 2, 3$ $\text{L} = \text{Cl}$, PEt_3 , OH [21, 22]); $[\text{Mo}_5\text{NbI}_8\text{L}_6]$ ($\text{L} = \text{Cl}$, CN , H_2O , OH [23, 24]); $[\text{Mo}_{6-x}\text{W}_x\text{Cl}_8\text{L}_6]$ ($\text{L} = \text{Cl}$, F [25, 26]); $\text{K}_6[\text{Re}_3\text{Mo}_3\text{S}_8(\text{CN})^{a-a}_{2/2}(\text{CN})^a_4]$ [27] were obtained. It is important to note that a detailed study of the effect of substitution of core metal atoms on the properties of octahedral cluster complexes was hardly carried out before the beginning of this work. This is largely due to the lack of methods for producing such compounds in the form of individual phases, free from impurities of other heterometallic and homometallic clusters.

The classical Werner theory for many years served as the main theoretical basis for the coordination chemistry of transition metals [28]. The discovery of polynuclear coordination compounds with atypical short $M - M$ contacts required a change in classical concepts. The beginning of a new field of coordination chemistry of transition metals was marked by the use by Cotton in 1964 of the concept of “cluster” for polynuclear metal complexes containing $M - M$ bonds in their structure [1]. At the moment, the chemistry of cluster compounds is actively developing and contains many structural types of compounds with prospects for use in various fields of material science.

Among the cluster complexes, a special group of the so-called high-valence or inorganic clusters is distinguished, from which the active development of the entire cluster branch of coordination chemistry has begun. The formal separation of cluster complexes into groups of high and low-valence cluster complexes was proposed by Cotton, based on the average oxidation state of the metal atoms of the cluster complex. High-valence cluster complexes include complexes with oxidation states of metals $+2 - +4$, low-valence complexes $-1 - +1$. Despite the fact that such a separation can be rather arbitrary, typical representatives of various groups show significant differences in the ligand environment of the cluster core, metal – metal bond lengths, and preference for certain transition metal groups [29].

High-valence cluster complexes include mainly chalcogenide and halide cluster complexes known for transition metals of 4–10 groups. A lot of works are found in the literature, covering preparation techniques, studying the structure and properties of various high-valence cluster complexes [2-4, 13, 30]. Basically, the ongoing research (with the exception of cubane clusters) is focused on the study of the properties of cluster complexes containing only one type of metal in the cluster core. Nevertheless, examples of cluster compounds with two (or even more) types of metal atoms - heterometallic clusters exist in different structural types of high-valence cluster complexes. The metal atoms of the metal core make a significant contribution to the frontier molecular orbitals of the cluster complex, which determine the basic properties of the cluster; therefore, the substitution of metal-core atoms with atoms of another metal can be a tool that allows one to directly influence the properties of the cluster complex.


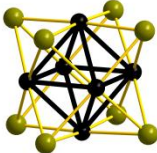
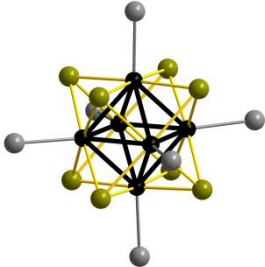
Heterometallic cluster compounds are scarcely studied in comparison with homometallic analogues of high-valence cluster complexes due to experimental difficulties in the substitution of metal core atoms and the subsequent characterization of the obtained compounds. The most significant examples of substitution and subsequent study of the properties of heterometallic clusters exist only among the tetranuclear high-valence cluster complexes. Substitution in other classes is mainly scattered, the structure and properties of the resulting heterometallic clusters are often insufficiently examined.

This literature review is mainly devoted to the systematization of existing literature data on the structural features and properties of heterometallic high-valence cluster complexes of transition metals, as well as the study of the comparison of existing examples of substitution among high-valence cluster complexes of different nuclearity. Below structural features, preparation techniques, electronic structure, and properties of heterometallic high-valence transition metal cluster complexes will be considered.

1.2 Cluster chemistry nomenclature

The terminology used in the literature to describe the structure of cluster complexes is described here. The term nuclearity indicates the number of metal atoms of a cluster complex. Metal atoms are connected to each other by means $M - M$ bonds forming the metal core $\{M_n\}$, which is additionally stabilized by interaction with the ligand environment. Based on the nomenclature introduced by Schäfer and Schnering [31] for octahedral complexes (in this review, it will be used for all cluster complexes), internal (inner - *i*) and external ligands (outer - *a*) are separated. Internal ligands are usually coordinated by the bridging type, combining several atoms of the metal core. The metal core and internal ligands form the cluster core $\{M_nL_k^i\}$. External ligands additionally coordinate the metal atoms of the metal core forming the cluster complex $[M_nL_k^iL_p^a]$. In the Table 1, the terminology used is illustrated by the example of an octahedral cluster compound with the general formula $A_n[M_6L_8^iL_6^a]$.

Table 1.1: Cluster nomenclature using compound with common formula $A_n[M_6L_8^iL_6^a]$ as example

| Term | metal core $\{M_6\}$ | cluster core $\{M_6L_8^i\}$ | cluster complex $[M_6L_8^iL_6^a]^{n-}$ |
|-----------|---|---|---|
| Structure |  |  |  |

An important characteristic of a high-valence cluster complex is the number of cluster skeletal electrons (CSE), electrons involved in the formation of metal-metal bonds.

Knowing the stoichiometry of the cluster complex and the ligand charge, a simple calculation allows one to estimate this number:

$$CSE = n + l + z$$

- n is the total number of valence electrons of the metal atoms of the metal core;
- l is the total charge of the ligands of the cluster;
- z is the charge of the cluster complex;

For a cluster complex, a change in the number of CSEs can lead to a change in the optical, magnetic, and other physicochemical properties.

1.3 The structure of heterometallic cluster compounds

High-valence homometallic cluster complexes exhibit a variety of types of structures, including cluster complexes of various nuclearity (from trinuclear in $\text{Mo}_3\text{S}_7\text{Br}_4$ to 36 in $\text{Rb}_{10}\text{Mo}_{36}\text{S}_{38}$) and the diverse ligand environment of the metal core [2, 4]. Heterometallic clusters are less distributed and occur mostly among trinuclear $\{\text{M}_3\}$, tetranuclear $\{\text{M}_4\}$ and hexanuclear $\{\text{M}_6\}$ clusters, demonstrating only some of the variants of coordination of internal ligands known for homometallic clusters.

1.3.1 Triangular cluster complexes

Examples of heterometallic trinuclear cluster complexes are few in number and are limited to triangular clusters with two stable variants of the structure of the cluster core: $\{\text{M}_3(\mu_3\text{-L}^i)(\mu_2\text{-L}^i)_3\}$ and $\{\text{M}_3(\mu_3\text{-L}^i)_2\}$. A typical structure of cluster complexes based on the $\{\text{M}_3(\mu_3\text{-L}^i)(\mu_2\text{-L}^i)_3\}$ and $\{\text{M}_3(\mu_3\text{-L}^i)_2\}$ core is shown in Figure 1.1. Metal atoms in the resulting complexes are connected into a triangular metal core $\{\text{M}_3\}$. In the case of $\{\text{M}_3\text{L}_4^i\}$, one internal ligand (L^i) is coordinated to the metal core of type μ_3 , the remaining internal ligands are coordinated to the edges of the triangle of μ_2 type, in the case of $\{\text{M}_3\text{L}_2^i\}$ the internal ligands are coordinated in the μ_3 type on both sides of the triangular metal core. The metal atoms are additionally coordinated by the apical ligands (L^a), from 1 to 4 apical ligands per metal atom.

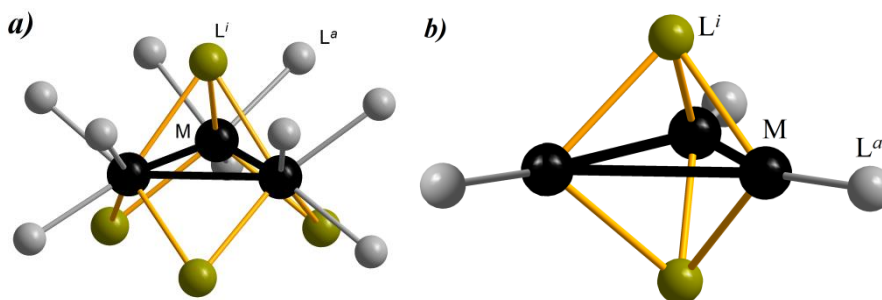


Figure 1.1: The structure of triangular cluster complexes $[M_3L_4L^a_9]$ (a) and $[M_3L_2L^a_3]$ (b).

The lengths of the M – M, M – M' bonds and the number of CSEs for known examples of heterometallic triangular cluster complexes in comparison with their homometallic analogues are given in the Table 1.2.

Table 1.2: CSE value and average M-M, M-M' (Å) bond distances for heterometallic triangular clusters and their homometallic analogues (standard error is given in brackets)

| | CSE | M–M | M–M' | Reference |
|---|-----|-----------------------|----------|-----------|
| <i>Homometallic {M₃Sⁱ₂}</i> | | | | |
| [Cp [*] ₂ Ru ₂ S ₂ Ru(CO) ₂ (PPh ₃)] | 16 | 2.841 | – | [33] |
| [Cp [*] ₃ Rh ₃ S ₂] ²⁺ | 18 | 2.830 | – | [34] |
| [Cp [*] ₃ Ir ₃ S ₂] ²⁺ | 18 | 2.832 | – | [34] |
| <i>Heterometallic {M₂M'Lⁱ₂}</i> | | | | |
| [(Cp [*] Ru) ₂ (μ ₂ -H)(μ ₃ -S) ₂ (RhCl ₂ (PPh ₃))] | 16 | 2.77[2] | 2.707(3) | [35] |
| [(Cp [*] Ir) ₂ {Mo(CO) ₂ (MeCN) ₂ }(μ ₃ -S) ₂] ²⁺ | 16 | 2.7965(4) | 2.88[3] | [36] |
| <i>Homometallic {M₃Sⁱ₄}</i> | | | | |
| [Mo ₃ S ₄ (H ₂ O) ₉] ⁴⁺ | 6 | 2.732(7) | – | [37] |
| [W ₃ S ₄ (H ₂ O) ₉] ⁴⁺ | 6 | 2.723(15) | – | |
| <i>Heterometallic {M₂M'Sⁱ₄}</i> | | | | |
| [Mo ₂ S ₄ (edt) ₂ (Cu(PPh ₃))]⁻ | 12 | 2.858[8] | 2.77[3] | [38] |
| [W ₂ S ₄ (edt) ₂ (Cu(PPh ₃))]⁻ | 12 | 2.848[6] | 2.75[2] | [38] |
| [MoW ₂ S ₄ (H ₂ O) ₉] ⁴⁺ | 6 | 2.723(6) ^a | | [32] |
| [Mo ₂ WS ₄ (H ₂ O) ₉] ⁴⁺ | 6 | 2.728(6) ^a | | |

| | | |
|--|---|------------------------|
| $[\text{MoW}_2\text{S}_4(\text{Hnta})_3]^{2-}$ | 6 | 2.749(19) ^c |
| $[\text{Mo}_2\text{WS}_4(\text{Hnta})_3]^{2-}$ | 6 | 2.754(20) ^c |

^{a,c}Mo and W are disordered between common positions of metal core, average M–M bond distance is given; ^bHNTA = $[\text{N}(\text{CH}_2\text{CO}_2\text{H})(\text{CH}_2\text{CO}_2)_2]^{2-}$

In the case where the apical ligand environment of M and M' is the same, the metal atoms are randomly distributed over common positions ($[\text{MoW}_2\text{S}_4(\text{H}_2\text{O})_9]^{4+}$ and others [32]). The different coordination environment of the metal atoms M and M' leads to the ordering of metal atoms in the structures.

The heterometallic cluster $[(\text{Cp}^*\text{Ru})_2(\mu_2\text{-H})(\mu_3\text{-S})_2(\text{RhCl}_2(\text{PPh}_3))]$ and its homometallic analogue $[\text{Cp}^*_2\text{Ru}_2\text{S}_2\text{Ru}(\text{CO})_2(\text{PPh}_3)]$ contain the same number CSE. Moreover, the Ru – Ru bond length for the $[(\text{Cp}^*\text{Ru})_2(\mu_2\text{-H})(\mu_3\text{-S})_2(\text{RhCl}_2(\text{PPh}_3))]$ cluster complex is much shorter than the bond lengths in the homometallic complex $[\text{Cp}^*_2\text{Ru}_2\text{S}_2\text{Ru}(\text{CO})_2(\text{PPh}_3)]$. The average Rh – Ru bond length is also shorter than the known Ru – Ru and Rh – Rh distances for homometallic triangular clusters. Among heterometallic clusters with $\{\text{M}_3\text{L}_4^i\}$ core, complexes containing both molybdenum and tungsten contain the same number of CSEs in comparison with homometallic molybdenum and tungsten triangular clusters. The average metal – metal bond lengths for such heterometallic clusters are close to the known distances for $[\text{Mo}_3\text{S}_4(\text{H}_2\text{O})_9]^{4+}$ and $[\text{W}_3\text{S}_4(\text{H}_2\text{O})_9]^{4+}$.

1.3.2 Tetrahedral cluster complexes

Heterometallic tetranuclear cluster complexes are presented in the literature mainly as tetrahedral cluster complexes with $\{\text{M}_4(\mu_3\text{-L})_4^i\}$ core. A typical structure of such cluster complexes is shown in Figure 1.2. Cluster complexes have tetrahedral metal core $\{\text{M}_4\}$. The internal ligands are coordinated by the μ_3 -type to each face of the tetrahedron. Each metal atom can additionally coordinate from 1 to 3 apical ligands. Metal atoms and internal ligands together form a distorted cube; therefore, cluster complexes of this structure are often called “cubane” clusters in the literature.

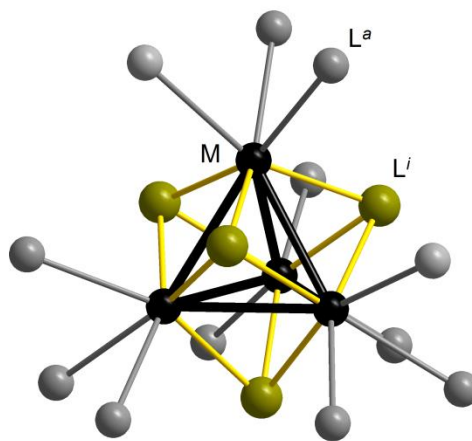


Figure 1.2: The structure of the tetrahedral cluster complex $[M_4L_4^iL_{12}^a]$.

Polymer compounds containing tetrahedral clusters. Compounds belonging to this class can be described by the general formula $[M_4L_4^iL_{12/3}^{a-a}]_{\infty\infty\infty}$ in Schäfer's notation and exhibit cubic spinel-type structures. The family of isostructural phases includes two main types of compounds: AM_4Q_8 and $M_4Q_4X_4$. Heterometallic cluster compounds of both types were obtained: $GaM_{4-x}M'Q_8$ $M = Nb$ $M' = Mo$ $Q = Se$ $x = 0 - 4$ [39]; $M = Nb$ $M' = Ta$ $Q = Se$ $x = 0 - 4$ [40]; $M = Ta$ $M' = Mo$ $Q = Se$ $x = 0 - 4$ [39]; $M = V$ $M' = Mo$ $Q = S$ $x = 0 - 4$ [41]; $M = V$ $M' = Cr$ $Q = Se$ $x = 0 - 4$ [42]; $AMo_2Re_2S_8$ $A = Fe, Co, Ni, Zn$ [43]; $M_{4-x}M'Q_4X_4$ $M = Nb$, $M' = Mo$, $Q = S$, $X = I$ $x = 0 - 4$ [39]; $M = Nb$, $M' = Mo$, $Q = Se$, $X = I$ $x = 0 - 3$ [39]; $M = Re$ $M' = Mo$ $Q = S$ $X = Te$ $x = 0, 1, 2$ [44, 45] (Table 1.3). The structure of compounds AM_4Q_8 will be considered using $GaMo_4S_8$ as an example [46]. This compound consists from fragments of $[Mo_4S_4^iS_{12}^a]$ condensed through sulfide ligands. The formula in Schäfer's notation for $GaMo_4S_8$ is $Ga[Mo_4S_4^iS_{12/3}^{a-a}]$. The structure of the compound is shown in Figure 1.3. $[GaS_4]^{5-}$ tetrahedra and $\{Mo_4S_4\}^{5+}$ cluster cores are located in a cubic cell according to the NaCl type (Figure 1.3 a). The structure of $Nb_4Se_4I_4$ [47] (in Schäfer's notation $[Nb_4Se_4^iI_{12/3}^{a-a}]$) is similar to $GaMoS_8$. I_4 tetrahedra and $\{Nb_4Se_4\}$ cores alternate in a cubic cell. The structure of most heterometallic analogs of $GaMo_4S_8$ and $Nb_4Se_4I_4$ phases was determined using powder diffraction data.

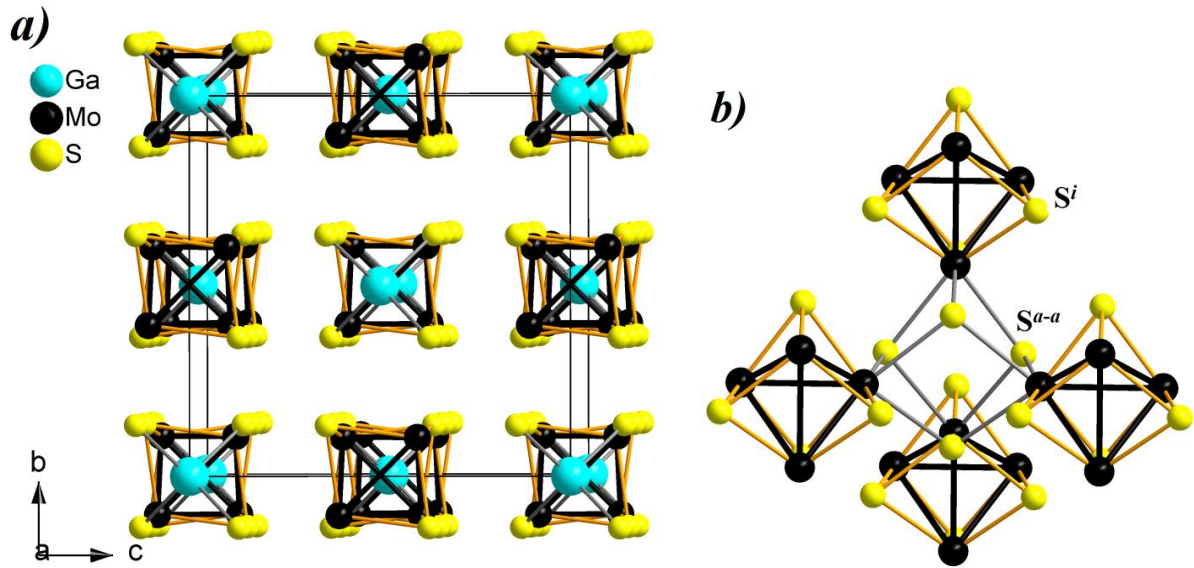


Figure 1.3: The structure of $\text{Ga}[\text{Mo}_4\text{S}_4\text{S}^i\text{S}^{a-a}_{12/3}]$: lattice packing by spinel-type, Mo-S^a bonds are omitted for clarity (a); cluster core condensation into a polymeric framework (b).

Table 1.3: Heterometallic cluster polymers $\text{AM}_{4-x}\text{M}'\text{Q}_8$ and $\text{M}_{4-x}\text{M}'\text{Q}_4\text{X}_4$

| Composition | Reference |
|---|-----------|
| $\text{GaNb}_{4-x}\text{Mo}_x\text{Se}_8$ $x = 0 - 4$ | [39] |
| $\text{GaNb}_{4-x}\text{Ta}_x\text{Se}_8$ $x = 0 - 4$ | [40] |
| $\text{GaTa}_{4-x}\text{Mo}_x\text{Se}_8$ $x = 0 - 4$ | [39] |
| $\text{GaV}_{4-x}\text{Mo}_x\text{S}_8$ ($0 \leq x \leq 4$) | [41] |
| $\text{GaV}_{4-x}\text{Cr}_x\text{Se}_8$ $x = 0 - 4$ | [42] |
| $\text{AMo}_2\text{Re}_2\text{S}_8$ A = Fe, Co, Ni, Zn | [43] |
| $\text{Nb}_{4-x}\text{Mo}_x\text{S}_4\text{I}_4$ $x = 0 - 4$ | [39] |
| $\text{Nb}_{4-x}\text{Mo}_x\text{Se}_4\text{I}_4$ $x = 0 - 4$ | [39] |
| $\text{Re}_{4-x}\text{Mo}_x\text{S}_4\text{Te}_4$ $x = 0, 1, 2$ | [44-45] |

Compounds containing molecular tetrahedral clusters. A large number of heterometallic tetrahedral clusters of non-polymer structure were obtained. This section mainly refers to heterometallic clusters with the core $\{\text{M}_3\text{M}'\text{S}_4^i\}$ where M = Mo, M' = Cr - Cu, Ru - Ag,

W, Os - Pt; $M = W$ $M' = Fe, Co, Ni, Pd, Pt$ [12, 14, 48-51]. Clusters with selenide core $\{M_3M'Se_4^i\}$ are known for $M = Mo$ and W , $M' = Ni, Pd, Co, Cu$ [52-57]. There are examples of heterometallic cubane clusters with the $\{M_3M'S_4^i\}$ core, for other metals, $M = Re$, $M' = Co$ [58], $M = Fe$, $M' = Nb, Ta$ [59, 60], $M = Cr$, $M' = Co, Fe$ [61, 62]. There are less known clusters with the core $\{M_2M'_2S_4^i\}$ $M = Mo$, $M' = Fe, Co, Ni, Cu$; $M = W$, $M' = Fe, Co, Cu$; $M = Nb$, $M' = Cu$; $M = V$, $M' = Fe, Co$ [12, 63-65]. Water molecules, halide, rhodanide ions, CO molecules, as well as various organic molecules $L = \mathbf{Cp}$ (Cp - cyclopentadienyl), Cp^* , PR_3 and others can serve as apical ligands of tetrahedral heterometallic clusters. The ligand environment of the metal of tetrahedral cluster complexes can be octahedral, tetrahedral, or, in some cases, in the form of a square pyramid (Figure 1.4).

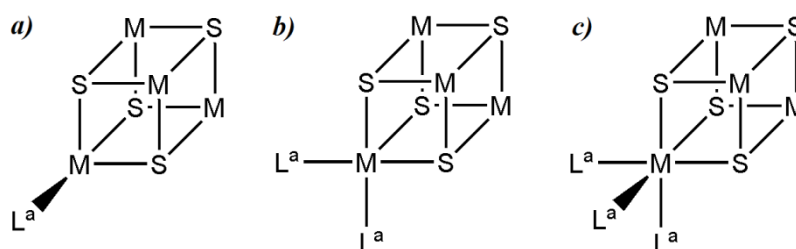


Figure 1.4: Possible ligand environment types of metal atom in tetrahedral cluster complexes $[M_4S_4L_n]$, tetrahedral (a), square pyramidal (b), octahedral (c).

The ligand environment of the metal atoms M and M' in heterometallic cluster complexes, in general, is different. The most common octahedral ligand environment for the metal atom M is octahedral and tetrahedral for M' . Examples of the structure of heterometallic cluster complexes with coordination environment of this type are shown in Figure 1.5. Other combinations are less common. The lengths of the $M - M$, $M - M'$ bonds and the number of CSEs of various sulfide heterometallic tetrahedral clusters and their homometallic analogues with an indication of the type of ligand environment of metal atoms are given in Table 1.4. The different ligand environment on the metal atoms M and M' leads to the ordering of metal atoms in the structures of the compounds. In the case when the metal atoms of the heterometallic cluster have the same ligand environment, the metal atoms in the structures are randomly distributed within common positions. For example, $[W_3MoS_4(H_2O)_{12}]^{5+}$ [66].

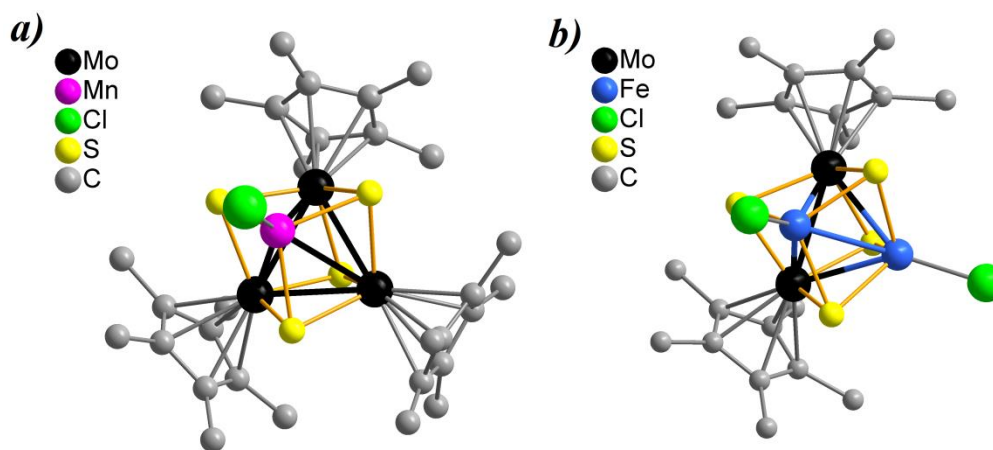


Figure 1.5: The structure of cluster complexes $[\text{Mo}_3\text{MnS}_4\text{Cp}^*_3\text{Cl}]$ (a) $[\text{Mo}_2\text{Fe}_2\text{S}_4\text{Cp}^*_2\text{Cl}_2]$ (b).

Cluster complexes with the cores $\{\text{M}_3\text{M}'\text{Q}_8\}$ ($\text{M} = \text{Mo}, \text{W}$ and $\text{Q} = \text{S}, \text{Se}$) in some cases form dimers in which the cores are condensed through a common edge or vertex (Figure 1.6).

Dimers with a common edge are found for $\text{M}' = \text{Co}, \text{Ni}, \text{Cu}, \text{Pd}$ $[\{\text{Mo}_3\text{CoS}_2\text{S}^{i-i}_{4/2}(\text{H}_2\text{O})_9\}_2]^{8+}$ [81], $[\{\text{W}_3\text{NiQ}_2\text{Q}^{i-i}_{4/2}(\text{H}_2\text{O})_9\}_2]^{8+}$ ($\text{Q} = \text{S}, \text{Se}$) [56, 82], $[\{\text{W}_3\text{PdQ}_2\text{Q}^{i-i}_{4/2}(\text{H}_2\text{O})_9\}_2]^{8+}$ ($\text{Q} = \text{Se}$) [53], $[\{\text{Mo}_3\text{PdQ}_2\text{Q}^{i-i}_{4/2}(\text{H}_2\text{O})_9\}_2]^{8+}$ ($\text{Q} = \text{Se}$) [83], $[\{\text{Mo}_3\text{CuS}_2\text{S}^{i-i}_{4/2}(\text{H}_2\text{O})_9\}_2]^{8+}$ [84]. Vertex condensation is characteristic of complexes, where M' is a p -element, which will not be considered here. The homometallic cluster complex $[\{\text{Mo}_3\text{S}_4(\text{H}_2\text{O})_9\}\text{Mo}\{\text{Mo}_3\text{S}_4(\text{H}_2\text{O})_9\}]^{8+}$ ($\text{M}' = \text{Mo}$) is the only example of condensation of the cores through the vertex in the case when M' is a transition metal [85]. $[\text{M}_2\text{M}'_2\text{S}_4^i]$ clusters do not form dimeric structures.

Table 1.4: CSE number and average M-M, M-M' and M'-M' (Å) bond distances for selected sulfide heterometallic cubane clusters and homometallic analogues (the ligand environment of metal atoms is indicated, standard error is given in brackets)

| | CSE | M-M | M-M' | M'-M' | Reference |
|--|-----|-----------|------|-------|-----------|
| <i>Homometallic $\{\text{M}_4\text{S}_4\}$ M – octahedral</i> | | | | | |
| $[\text{V}_4\text{S}_4\text{Cp}^{*4}]$ | 8 | 2.868(2) | – | – | [67] |
| $[\text{Cr}_4\text{S}_4\text{Cp}'_4]$ | 12 | 2.82-2.85 | – | – | [68] |
| $[\text{Mo}_4\text{S}_4(\text{CN})_{12}]^{6-}$ | 10 | 2.831(3) | – | – | [69] |
| $[\text{W}_4\text{S}_4(\text{CN})_{12}]^{6-}$ | 10 | 2.845(1) | – | – | |

| | | | | | |
|---|---------|-------------|----------------------|---|------|
| $[\text{Re}_4\text{S}_4(\text{CN})_{12}]^{4-}$ | 12 | 2.764(3) | – | – | [70] |
| <i>Homometallic $\{\text{M}_4\text{S}_4\}$ M – tetrahedral</i> | | | | | |
| $[\text{Fe}_4\text{S}_4(\text{N}\{\text{SiMe}_3\}_2)_4]$ | 20 | 2.91(5) | – | – | [71] |
| <i>$\{\text{M}_3\text{M}'\text{S}_4\}$ M – octahedral, M' – octahedral</i> | | | | | |
| $[\text{Mo}_3\text{VCp}^*_3\text{S}_4]_2(\mu\text{-Cl})_3$ | 14 – 15 | 2.9299 | 2.78(1) | – | [48] |
| $[\text{W}_3\text{MoS}_4(\text{H}_2\text{O})_{12}]^{5+}$ | 11 | | 2.81(3) ^b | | [66] |
| <i>$\{\text{M}_3\text{M}'\text{S}_4\}$ M – octahedral, M' – tetrahedral</i> | | | | | |
| $[\text{Cr}_3\text{CoS}_4\text{Cp}_3(\text{CO})]$ | 16 | 2.810-2.824 | 2.649-2.666 | – | [61] |
| $[\text{Cr}_3\text{FeS}_4\text{Cp}_3(\text{O}_2\text{C}_2\text{Me}_3)]$ | 14 | 2.828-2.848 | 2.721-2.787 | – | [62] |
| $[\text{Mo}_3\text{CrS}_4\text{Cp}^*_3\text{Cl}]$ | 14 | 2.8873 | 2.88(2) | – | [48] |
| $[\text{Mo}_3\text{MnS}_4\text{Cp}^*_3\text{Cl}]$ | 15 | 2.8397 | 2.94(4) | – | [48] |
| $[\text{Mo}_3\text{FeS}_4(\text{H}_2\text{O})_{10}]^{4+}$ | 14 | 2.767[7] | 2.671[11] | – | [72] |
| $[\text{Mo}_3\text{CoS}_4\text{Cp}'_3(\text{CO})]$ | 16 | 2.838[11] | 2.745[11] | – | [73] |
| $[\text{Mo}_3\text{NiS}_4(\text{H}_2\text{O})_{10}]^{4+}$ | 16 | 2.755[10] | 2.640[9] | – | [74] |
| $[\text{Mo}_3\text{CuS}_4(\text{dmpe}^c)_3\text{Cl}_4]^+$ | 16 | 2.782[1] | 2.823[8] | – | [75] |
| $[\text{Cp}'_3\text{Mo}_3\text{S}_4\text{Pd}(\text{PPh}_3)]^+$ | 16 | 2.836(8) | 2.864(8) | – | [50] |
| $[\text{Cp}'_3\text{Mo}_3\text{S}_4\text{Pt}(\text{PPh}_3)]^+$ | 16 | 2.837(8) | 2.861(8) | – | [50] |
| $[\text{W}_3\text{NiS}_4\text{Cp}'_3(\text{PPh}_3)]$ | 16 | 2.809[1] | 2.733[9] | – | [76] |
| $[\text{W}_3\text{CuS}_4(\text{dmpe})_3\text{Br}_4]^+$ | 16 | 2.780[2] | 2.884[7] | – | [75] |
| $[\text{Cp}'_3\text{W}_3\text{S}_4\text{Pd}(\text{PPh}_3)]^+$ | 16 | 2.805(8) | 2.91(1) | – | [51] |
| $[\text{Cp}'_3\text{W}_3\text{S}_4\text{Pt}(\text{PPh}_3)]^+$ | 16 | 2.824(4) | 2.895(4) | – | [51] |
| $[\text{Re}_3\text{CoS}_4\text{Cl}_6(\text{PMe}_2\text{Ph})_4]$ | 16 | 2.770(5) | 2.600(5) | – | [58] |
| <i>$\{\text{M}_3\text{M}'\text{S}_4\}$ M – octahedral, M' – square prism</i> | | | | | |
| $[\text{Cp}'_3\text{Mo}_3\text{S}_4\text{Ru}(\text{CO})_2]^+$ | 14 | 2.84(2) | 2.94(4) | – | [49] |
| $[\text{Cp}'_3\text{Mo}_3\text{S}_4\text{RhCl}(\text{PPh}_3)]^+$ | 14 | 2.83(2) | 2.92(4) | – | |
| <i>$\{\text{M}_3\text{M}'\text{S}_4\}$ M – tetrahedral, M' – octahedral</i> | | | | | |
| $[(\text{Tp}^d)\text{VFe}_3\text{S}_4(\text{CN})_3]^{2-}$ | 19 | 2.650(7) | 2.74(1) | – | [59] |

| | | | | | |
|--|----|-------------|-------------|----------|------|
| $[\text{NbFe}_3\text{S}_4\text{Cl}_3(\text{dppm}^e)\text{CH}_3\text{CN}]^{2-}$ | 20 | 2.71(2) | 2.75(1) | – | [60] |
| $[\text{MoFe}_3\text{S}_4\text{Cl}_4(\text{dmpe})]^-$ | 19 | 2.703-2.732 | 2.724-2.767 | – | [77] |
| $[\text{TaFe}_3\text{S}_4\text{Cl}_3(\text{dppm})\text{CH}_3\text{CN}]^{2-}$ | 20 | 2.71(3) | 2.74(2) | – | [60] |
| $\{M_2M'_2S_4\}$ <i>M</i> – octahedral, <i>M'</i> – tetrahedral <i>e</i> | | | | | |
| $[\text{V}_2\text{Fe}_2\text{S}_4(\text{MeCp})_2(\text{NO})_2]$ | 18 | 2.957 | 2.590 | 2.738 | [63] |
| $[\text{V}_2\text{Co}_2\text{S}_4(\text{MeCp})_2(\text{NO})_2]$ | 20 | 2.926 | 2.735 | 2.738 | [64] |
| $[\text{Nb}_2\text{Cu}_2\text{S}_4\text{Cl}_2(\text{PMe}_3)_6]$ | 20 | 2.931(1) | 2.87(3) | 2.881(1) | [65] |
| $[\text{Mo}_2\text{Fe}_2\text{S}_4\text{Cp}^*_2\text{Cl}_2]$ | 16 | 2.8219(7) | 2.757[4] | 2.791(1) | [78] |
| $[\text{Mo}_2\text{Co}_2\text{S}_4\text{Cp}^{\text{Et}f}_2\text{Cl}_2]$ | 18 | 2.804(1) | 2.756[5] | 2.955(2) | [79] |
| $[\text{W}_2\text{Fe}_2\text{S}_4\text{Cp}^*_2(\text{NO})_2]$ | 20 | 2.8198(9) | 2.766[4] | 2.735(3) | [80] |

^aCp' – methylcyclopentadienyl; ^bMo and W are disordered between common positions of the metal core average M–M bond distance is given; ^cdmpe – 1,2- bis(dimethylphosphino)ethane; ^dTp – tris(pyrazolyl)hydroborate (1-); ^edppm – bis(diphenylphosphino)methane; ^fCp^{Et} – ethyltetramethylcyclopentadienyl.

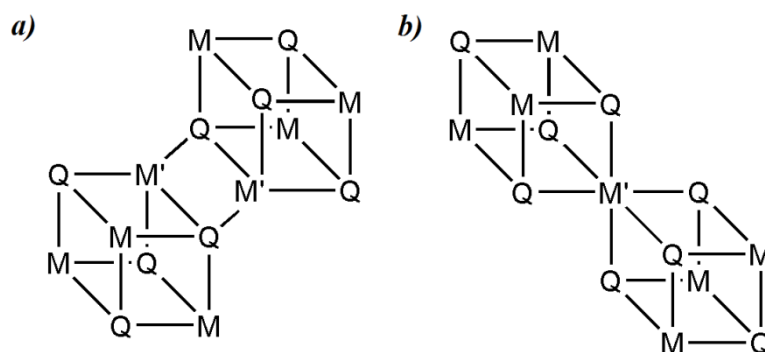


Figure 1.6: Simplified view of the structure of condensed tetrahedral clusters: $\{M_3M'Q_2Q_{4/2}\}_2$ with edge condensation (a); $[\{M_3Q_4\}M'\{M_3Q_4\}]$, vertex condensation, apical ligand are omitted for clarity (b).

It is worth noting that, for $[M_2M'_2S_4]$ cluster complexes with an octahedral environment *M* and a tetrahedral *M'* containing 22 CSEs, the metal cores have no tetrahedral structure. In this case, *M'* – *M'* bonds are not formed, and the metal core is in the shape of a butterfly (Figure 1.7). The Table 1.5 shows the average bond lengths *M* – *M*, *M* – *M'* and the distances *M'*... *M'* for cluster complexes $[M_2M'_2S_4]$, in which the metal cores $\{M_2M'_2\}$ have the shape of a butterfly.

Table 1.5: Average bond distances M–M, M–M' and M'–M' (Å) for heterometallic clusters $[M_2M'_2S_4]$, containing 22 CSE, with butterfly-shape metal core $\{M_2M'_2\}$

| | CSE | M–M | M–M' | M'···M' | Reference |
|--|-----|-----------|----------|----------|-----------|
| $[V_2Ni_2S_4(MeCp)_2(NO)_2]$ | 22 | 2.871 | 2.8 | 3.022 | [64] |
| $[V_2Cu_2S_4(OC_4H_8dte^a)_2(PhS)_2]^{2-}$ | 22 | 2.787(4) | 2.78(1) | 3.338(3) | [86] |
| $[Mo_2Co_2S_4Cp^{Et}_2(NO)_2]$ | 22 | 2.8135(6) | 2.766[4] | 3.116(1) | [80] |
| $[Mo_2Ni_2S_4Cp'_2(CO)_2]$ | 22 | 2.829(1) | 2.722[2] | 2.960(1) | [87] |
| $[Mo_2Cu_2S_4Cp^*_2Cl_2]$ | 22 | 2.865(1) | 2.788[9] | 3.058(3) | [88] |
| $[W_2Co_2S_4Cp^*_2(NO)_2]$ | 22 | 2.7984(5) | 2.780[4] | 3.131(1) | [80] |
| $[W_2Cu_2S_4(SCN)_8]^{4-}$ | 22 | 2.845(2) | 2.76[3] | 2.999(4) | [89] |

^adte – diethyldithiocarbamate

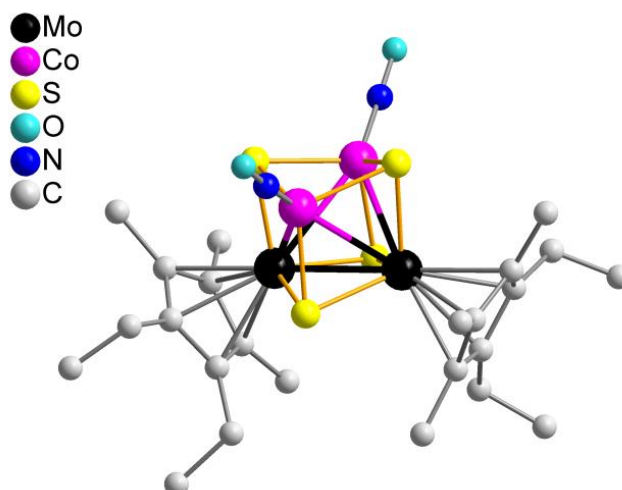


Figure 1.7: The structure of $[Mo_2Co_2S_4Cp^{Et}_2(NO)_2]$ with butterfly $\{Mo_2Co_2\}$ metal core.

1.3.3 Octahedral cluster complexes

Hexanuclear high-valence heterometallic cluster complexes are presented in the literature in general as octahedral clusters. Octahedral cluster complexes demonstrate two stable types of coordination of internal ligands - $\{M_6(\mu_3-L)_8\}$ and $\{M_6(\mu_2-L)_{12}\}$. Metal atoms of cluster complexes form an octahedral metal core $\{M_6\}$. In the first case, the internal ligands are coordinated by the μ_3 type to each face of the octahedron. In the case of

$\{M_6(\mu_2-L^i)_{12}\}$, the internal ligands are coordinated along the edges of the metal core. Each metal atom is additionally coordinated by the apical ligand. The structure of the $[M_6L_8^iL_6^a]$ and $[M_6L_{12}^iL_6^a]$ cluster complexes is shown in Figure 1.8.

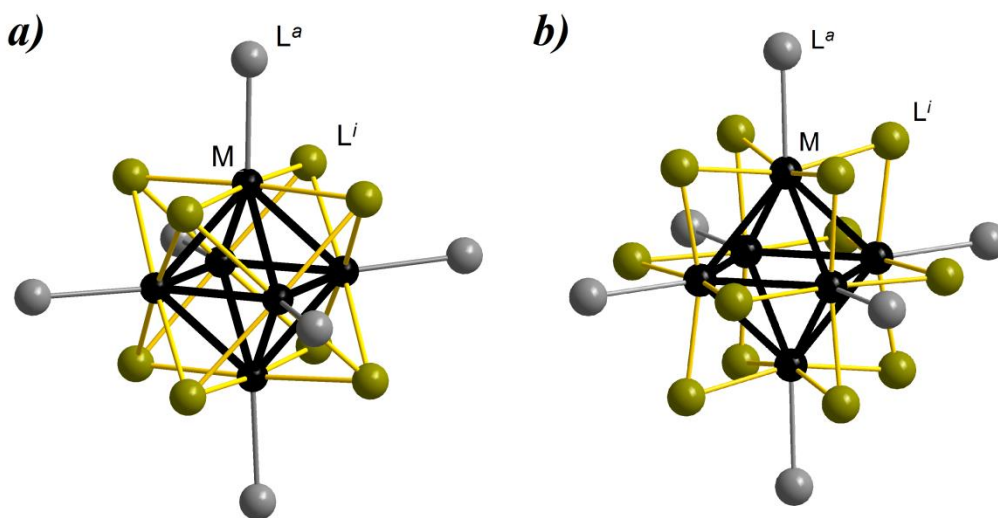


Figure 1.8: The structure of octahedral cluster complexes: $[M_6L_8^iL_6^a]$ (a) and $[M_6L_{12}^iL_6^a]$ (b).

Triangular and tetrahedral heterometallic cluster complexes do not demonstrate isomerism of the metal core, due to the small number of metal atoms. In the case of heterometallic octahedral cluster complexes, the metal cores of the composition $\{M_3M'_3\}$ and $\{M_4M'_2\}$ can exist in the form of two geometric isomers each, *mer*-, *fac*- $\{M_3M'_3\}$ and *cis*-, *trans*- $\{M_4M'_2\}$.

The number of heterometallic octahedral cluster complexes is scarce. This class of compounds includes heterometallic analogs of Chevrel phases $M_{6-x}M'_xQ_8$ $M = \text{Re}$ $M' = \text{Mo}$ $Q = \text{S, Se}$ $x = 2$, $Q = \text{Te}$ $x = 4$ [15] $M = \text{Re}$ $M' = \text{Mo}$ $Q = \text{Se}$ $x = 1.5$ [16]; $M = \text{Mo}$ $M' = \text{Ru}$ $Q = \text{Te}$ $x = 0.5, 1, 1.5$ [17-19] $M = \text{Mo}$, $M' = \text{Rh}$ $Q = \text{Te}$ $x = 0.5$ [17] $M = \text{Nb}$ $M' = \text{Ru}$ $Q = \text{Te}$ $x = 2.83 - 3.5$ [20], chalcogenide clusters with the cores $\{\text{Re}_{6-x}\text{Os}_x\text{Q}_8^i\}$ $Q = \text{S, Se}$ [21, 90], halogenide clusters $\{\text{Ta}_{6-x}\text{M}_x\text{Cl}_{12}^i\}$ $M = \text{Mo, Nb}$; $\{\text{Mo}_{6-x}\text{M}_x\text{X}_8^i\}$ $M = \text{W}$ $X = \text{Cl, Nb}$ $X = \text{I}$ [23, 91]. The structural features of these compounds will be considered in more detail below.

Chevrel phases. Chevrel phases represent a large group of isotypical polymeric compounds based on cluster complexes of the type $[M_6L_8^iL_6^a]$ [92-95]. The compound formula in Schäfer's notation is $\text{Mo}_6\text{L}_2^i\text{L}_{6/2}^{i-a}\text{L}_{6/2}^{a-i}$. The structure of Chevrel phases can be de-

scribed as condensed cubic fragments $\{M_6L_8^i\}$, which are linked by bridging chalcogenide ligands. The structure of Mo_6Se_8 is shown in Figure 1.9. Each $\{M_6L_8^i\}$ cube can receive up to 4 electrons, changing its electronic state from 20 to 24 cluster skeletal electrons, inclusive. In this case, the three-dimensional polymer structure has channels wherein metal ions can be intercalated when doping the initial phase $\{M_6L_8^i\}$.

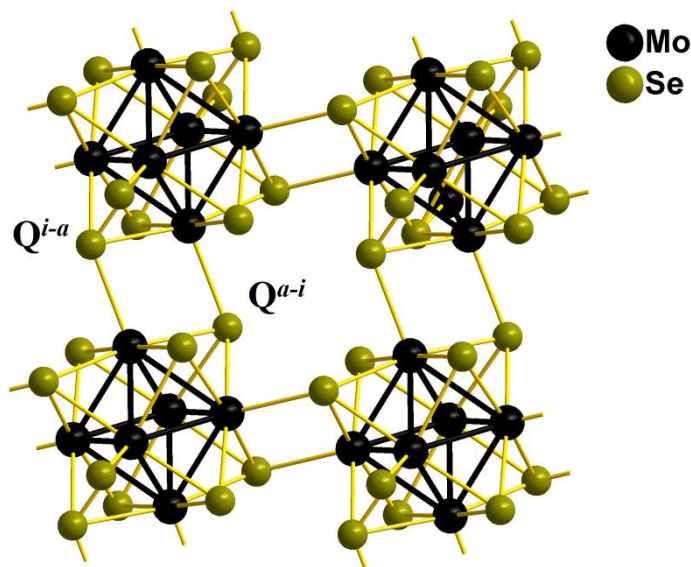


Figure 1.9: The structure of Chevrel phase Mo_6Se_8 .

The examples of heterometallic analogs of Chevrel phases $M_{6-x}M'_xQ_8$ are listed in the Table 1.6. Heterometallic Chevrel phases are isostructural to their homometallic analogues. These phases occur as solid solutions with Mo (or Ru) atoms being partially substituted by other transition metal atoms. Non-isovalent substitution leads to a change in the number of cluster skeletal electrons. The homometallic phases Mo_6Q_8 $Q = S, Se, Te$ contain 20 electrons and are electron-deficient. Whereas their heterometallic analogues, for example, $Mo_4Ru_2Q_8$ $Q = Se, Te$ or $Mo_2Re_4Q_8$ ($Q = S, Se$) contain 24 CSEs. The resulting compositions exhibit semiconductor properties in contrast to the unsubstituted Chevrel phases. This fact is related to the reduction of the HOMO-LUMO gap upon non-isovalent substitution. For Chevrel phases with the electron count from 22 to 24, superconductivity was discovered at low temperatures. Optimum properties have been found for $PbMo_6S_8$ containing 22 CSEs [97].

Table 1.6: The list of heterometallic Chevrel phases

| The formula | Reference |
|--|-----------|
| $\text{Mo}_2\text{Re}_4\text{S}_{8-x}\text{Se}_x$ ($0 \leq x \leq 8$) | [15, 96] |
| $\text{Mo}_2\text{Re}_4\text{Se}_{8-x}\text{Te}_x$ ($0 \leq x \leq 1.2$) | [15] |
| $\text{Mo}_4\text{Re}_2\text{Te}_8$ | [15] |
| $\text{Mo}_{1.5}\text{Re}_{4.5}\text{Se}_8$ | [16] |
| $\text{Mo}_4\text{Ru}_2\text{Q}_8$ ($\text{Q} = \text{Se}, \text{Te}$) | [16, 19] |
| $\text{Mo}_{6-x}\text{Ru}_x\text{Te}_8$ ($x = 0.5, 1.0, 1.5$) | [17-19] |
| $\text{Mo}_{5.5}\text{Rh}_{0.5}\text{Te}_8$ | [17] |
| $\text{Mo}_{4.66}\text{Rh}_{1.33}\text{Te}_8$ | [19] |
| $\text{Nb}_x\text{Ru}_{6-x}\text{Te}_8$ ($2.83 \leq x \leq 3.50$) | [20] |

Rhenium-osmium chalcogenide cluster compounds. $\text{Cs}_3\text{Re}_5\text{OsS}_{11}$, the formula in Schäfer's notation is $\text{Cs}_3[\text{Re}_5\text{OsS}_8^i\text{S}_{6/2}^{a-a}]$. This compound has a polymeric structure. Structural units $[\text{Re}_5\text{OsS}_8\text{S}_6]$ are condensed via apical sulfur ligands. The binding motif of the polymer structure of the compound is shown in Figure 1.10. The atoms of the metal core are randomly distributed between common positions. The resulting heterometallic compound has 24 cluster skeletal electrons. [90] The non-isovalent substitution of the rhenium atom by the osmium atom leads to the charge of the anionic part of the structure is 3-. A homometallic analogue of this structure containing a rhenium cluster: $\text{Li}_4\text{Re}_6\text{S}_{11}$ also contains 24 CSE, however, in this case, the anionic part of the structure is charged 4- [98].

The compound $\text{Re}_4\text{Os}_2\text{Se}_8\text{Cl}_4$ also has a polymeric nature. The formula in Schäfer's notation is $[\text{Re}_8\text{Os}_4\text{Se}_{14}^i\text{Se}_{2/2}^{i-a}\text{Se}_{2/2}^{a-i}\text{Cl}_6^a\text{Cl}_{4/2}^{a-a}]$. The structural units $[\text{Re}_4\text{Os}_2\text{Se}_8\text{Cl}_6]$ are condensed into polymer chains using selenide ligands. Further linking of the polymeric chains into the polymer layers is implemented *via* apical chloride ligands. The structure of the polymer layer fragment is shown in Figure 1.11. The rhenium and osmium atoms are randomly distributed between common positions of metal core in the structure [21].

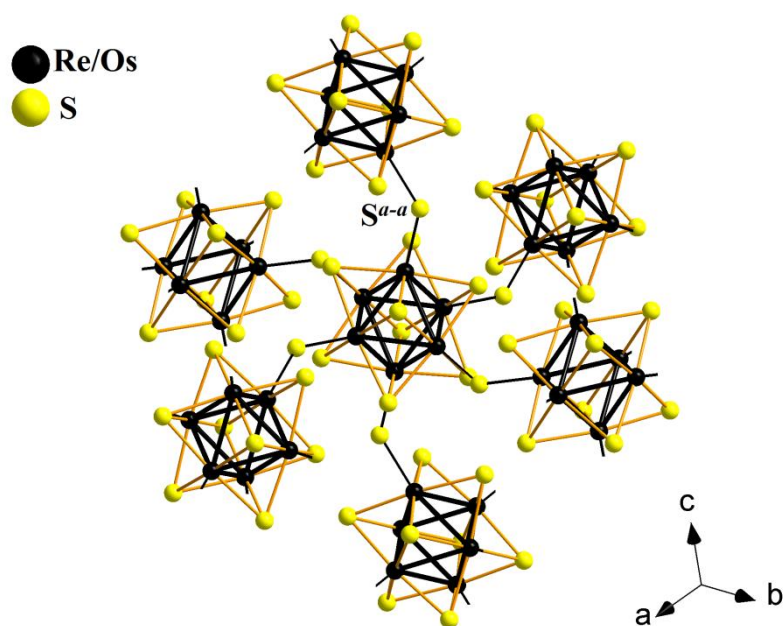


Figure 1.10: The binding motif of the polymer structure of the compound $\text{Cs}_3\text{Re}_5\text{OsS}_{11}$.

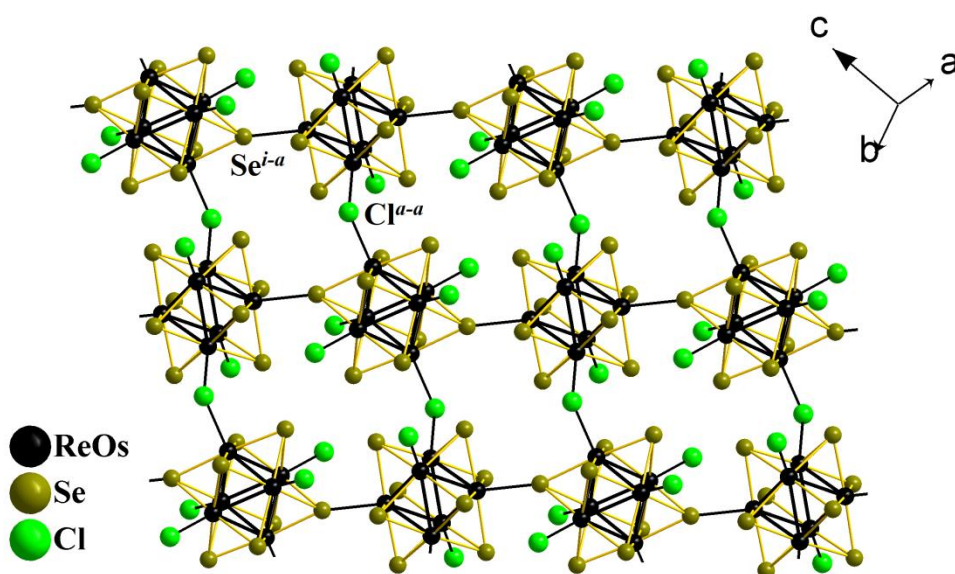


Figure 1.11: The structure of the polymeric layer fragment of the compound $\text{Re}_4\text{Os}_2\text{Se}_8\text{Cl}_4$.

Anions $[\text{Re}_4\text{Os}_2\text{Se}_8\text{Cl}_6]^{2-}$ and $[\text{Re}_5\text{OsSe}_8\text{Cl}_6]^{3-}$ were obtained separately in the salts $\text{Kat}_3[\text{Re}_5\text{OsSe}_8\text{Cl}_6]$ and $\text{Kat}_2[\text{Re}_4\text{Os}_2\text{Se}_8\text{Cl}_6]$ $\text{Kat} = \text{Cs}^+, \text{Bu}_4\text{N}^+$. The iso-charged cluster anions $[\text{Re}_3\text{Os}_3\text{Se}_8\text{Cl}_6]^-$ and $[\text{Re}_4\text{Os}_2\text{Se}_7\text{Cl}_7]^-$ co-crystallize in the compound $\text{K}_2[\text{Re}_3\text{Os}_3\text{Se}_8\text{Cl}_6][\text{Re}_4\text{Os}_2\text{Se}_7\text{Cl}_7]$. The metal atoms of the cluster core of the compounds

are randomly distributed on common positions in the structure. The resulting cluster complexes contain 24 CSEs and differ from homometallic analogs in the charge of the cluster anion. The presence in a solution containing anions $[\text{Re}_4\text{Os}_2\text{Se}_8(\text{PEt}_3)_6]^{2-}$ of a mixture of *trans*- and *cis*-isomers of the anion, containing the corresponding isomeric metal core, was confirmed by NMR (nuclear magnetic resonance spectroscopy) on a ^{31}P nucleus. The *trans*-isomer was isolated as the product of the incomplete substitution $[\text{Re}_4\text{Os}_2\text{Se}_8(\text{PEt}_3)_2\text{Cl}_4]$ (Figure 1.12). The compound presents two types of the isomerism: isomerism of metal core atoms and apical ligand environment, with following notation *trans, trans*- $[\text{Re}_4\text{Os}_2\text{Se}_8(\text{PEt}_3)_2\text{Cl}_4]$ [21].

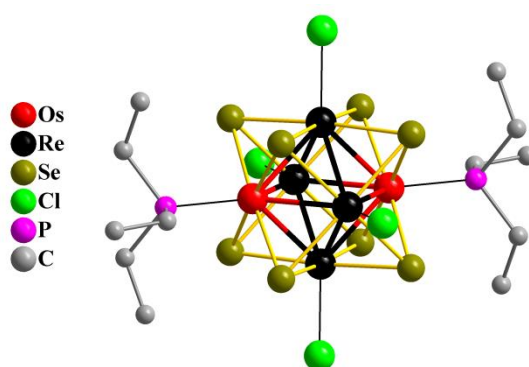


Figure 1.12: The structure of *trans,trans*- $[\text{Re}_4\text{Os}_2\text{Se}_8(\text{PEt}_3)_2\text{Cl}_4]$.

Halide clusters. Soluble salts of cluster anions having 6 apical hydroxo-groups, $\text{K}_3[\text{Mo}_5\text{NbI}_8(\text{OH})_6]^3-$, 6 cyano-groups $(\text{Pr}_4\text{N})_3[\text{Mo}_5\text{NbI}_8(\text{CN})_6]^3-$, and also the neutral complex $[\text{Mo}_5\text{NbI}_8(\text{H}_2\text{O})_6]$ and mixed ligand $[\text{Mo}_5\text{NbI}_8(\text{H}_2\text{O})_3(\text{OH})_3] \cdot 2\text{H}_2\text{O}$, $\text{K}[\text{Mo}_5\text{NbI}_8(\text{H}_2\text{O})_2\text{Cl}_4]$ complexes were obtained. The structure of these cluster complexes was determined by SC XRD on the contrary to other halide clusters mentioned below. The molybdenum and niobium atoms in the structures of the compounds are randomly distributed. The resulting cluster complexes contain 24 CSEs and the charge of the $[\text{Mo}_5\text{NbI}_8(\text{OH})_6]^{3-}$ anion differs by one from the 24-electron homometallic analogue $[\text{Mo}_6\text{I}_8\text{I}_6]^{2-}$ [23].

Halogen heterometallic clusters with $\{\text{Ta}_{6-x}\text{M}_x\text{Cl}_{12}\}$ $x = 1, 2$ cores were obtained. Cluster anions of the composition $[\text{Ta}_5\text{MoCl}_{12}\text{Cl}_6]^{2-}$ and $[\text{Ta}_4\text{Mo}_2\text{Cl}_{12}\text{Cl}_6]^{2-}$ were obtained in the form of salts with $n\text{-Et}_4\text{N}^+$ cations [99]. A series of heterometallic cluster anions of the composition $[\text{Nb}_n\text{Ta}_{6-n}\text{Cl}_{12}\text{F}_6]^{4-}$ ($n = 0 - 6$) was obtained in the form of salts with

sodium cations [100]. The cluster anions $[\text{Mo}_{6-x}\text{W}_x\text{Cl}_8\text{X}_6]^{2-}$ ($x = 0 - 6$) $\text{X} = \text{Cl}$ [25] $\text{X} = \text{F}$ [26] were obtained as salts with $n\text{-Bu}_4\text{N}^+$ cations ($\text{X} = \text{F}$). The structure of $[\text{Mo}_{6-x}\text{W}_x\text{Cl}_8\text{X}_6]^{2-}$ anions in the solution was determined by ^{19}F NMR.

Table 1.7: Average bond distances obtained from SC XRD for electron precise clusters with heterometallic cores $\{\text{M}_{6-x}\text{M}'_x\text{L}_8\}$ and homometallic analogues

| Compound | ne ⁻ | M-M | M-L ⁱ | Reference |
|---|-----------------|---|---|-----------|
| <i>Homometallic {Mo₆I₈} and {Nb₆I₈}</i> | | | | |
| Cs ₂ Mo ₆ I ₈ I ₆ | 24 | 2.679 | 2.779 | [101] |
| (PPN) ₂ Mo ₆ I ₈ Cl ₆ | 24 | 2.671 | 2.781 | [102] |
| <i>Homometallic {Re₆Qⁱ₈}</i> | | | | |
| Li ₄ Re ₆ S ₁₁ | 24 | 2.617 | 2.412 | [98] |
| Re ₆ S ₆ Cl ₆ | 24 | 2.614(3) | 2.506(9) | [103] |
| Tl ₅ Re ₆ Se ₈ Cl ₇ | 24 | 2.614(5) | 2.523(3) | [104] |
| [Re ₆ Se ₈ (PEt ₃) ₆] ²⁺ | | 2.646(2) | 2.516(8) | [105] |
| <i>Heterometallic {Mo₅NbI₈}</i> | | | | |
| (Pr ₄ N) ₃ [Mo ₅ NbI ₈ (CN) ₆] | 24 | 2.7011(10) | 2.7932(5) | [23] |
| [Mo ₅ NbI ₈ (OH) ₃ (H ₂ O) ₃]·2H ₂ O | 24 | 2.6762 | 2.8095 | |
| K[Mo ₅ NbI ₈ (H ₂ O) ₂ Cl ₄] | 24 | 2.6726 | 2.801 | |
| <i>Heterometallic {Re_{6-x}Os_xQⁱ₈}</i> | | | | |
| Cs ₃ Re ₅ OsS ₁₁ | 24 | 2.617 | 2.415 | [90] |
| Re ₄ Os ₂ Se ₈ Cl ₄ | 24 | 2.633(11) | 2.515(11) | [21] |
| Cs ₃ Re ₅ OsSe ₈ Cl ₆ ·2H ₂ O | 24 | 2.624(5) | 2.518(8) | [21] |
| Cs ₂ Re ₄ Os ₂ Se ₈ Cl ₆ | 24 | 2.623(8) | 2.509(10) | |
| [Re ₅ OsSe ₈ (PEt ₃) ₆] ³⁺ | 24 | 2.645(6) | 2.509(8) | |
| [Re ₄ Os ₂ Se ₈ (PEt ₃) ₆] ⁴⁺ | 24 | 2.648(10) | 2.506(6) | |
| <i>trans,trans</i> -[Re ₄ Os ₂ Se ₈ (PEt ₃) ₂ Cl ₄] | 24 | 2.616(1) ^a 2.640(3) ^b | 2.514(8) ^c 2.489(5) ^d | |

^aRe-Re; ^bRe-Os; ^cRe-Se; ^dOs-Se

According to the results of X-ray diffraction studies, heterometallic substitution has weak effect on the average lengths of the M – M and M – Se bonds compared to isoelectronic homometallic analogues (Table 1.7). The ligand environment of metal atoms of heterometallic cluster complexes is the same, with the exception *trans, trans*- $[\text{Re}_4\text{Os}_2\text{Se}_8(\text{PEt}_3)_2\text{Cl}_4]$ [21], leading to the random distribution of the metal atoms.

1.4 Preparation of heterometallic cluster compounds

In this section, the reactions that lead to the formation of a cluster core will be considered. Reactions with a change in the number of atoms of the metal core, ligand substitution, and interaction with metal salts will be considered in the section "reactivity". Most examples of synthetic methods for preparation of heterometallic cluster complexes with insignificant changes repeat the existing approaches for the synthesis of homometallic clusters described, for example, in a review of Fedorov et al. [2]. The methods for producing high-valence heterometallic cluster compounds can be roughly divided into two groups: high-temperature synthesis and synthesis from solution. Triangular heterometallic cluster complexes are obtained from solution. Tetrahedral heterometallic clusters are obtained both under high-temperature synthesis conditions and in solutions. The formation of an octahedral metal core is carried out in most cases under conditions of high-temperature synthesis. The well-known examples of the preparation of heterometallic cluster compounds will be considered in more detail below.

1.4.1 High-temperature synthesis

High-temperature reactions to obtain cluster compounds are usually carried out in the evacuated and sealed silica ampoules. This method is based on the assumption that if the phase is thermodynamically stable under certain experimental conditions, then it can be obtained from various starting compounds taken in the required stoichiometry. Simple elements and their combinations, *e.g.* metal halides or chalcogenides, can be used as the starting compounds for the synthesis of chalcogenide clusters. This method allows one to obtain thermodynamically stable phases for a given ratio of metals in the cluster core.

Clusters $\{M_4\}$. Using the high-temperature synthesis method, a series of isotypic polymer compounds with the spinel structure were obtained, namely $\text{GaM}_{4-x}\text{M}'\text{Se}_8$, where $\text{M} = \text{Nb}$ $\text{M}' = \text{Mo}$ $x = 0 - 4$ [39]; $\text{M} = \text{Nb}$ $\text{M}' = \text{Ta}$ $x = 0 - 4$ [40]; $\text{M} = \text{Ta}$ $\text{M}' = \text{Mo}$ $x = 0 - 4$ [39]; $\text{M} = \text{V}$ $\text{M}' = \text{Mo}$ $x = 0 - 4$ [41]; $\text{M} = \text{V}$ $\text{M}' = \text{Cr}$ $x = 0 - 4$ [42]; and $\text{AMo}_2\text{Re}_2\text{S}_8$ where $\text{A} = \text{Fe}, \text{Co}, \text{Ni}$ [43]; $\text{M}_{4-x}\text{M}'\text{Q}_4\text{X}_4$ $\text{M} = \text{Nb}$, $\text{M}' = \text{Mo}$, $\text{Q} = \text{S}$, $\text{X} = \text{I}$ $x = 0 - 4$ [39]; $\text{M} = \text{Nb}$, $\text{M}' = \text{Mo}$, $\text{Q} = \text{Se}$, $\text{X} = \text{I}$ $x = 0 - 3$ [39]; $\text{M} = \text{Re}$ $\text{M}' = \text{Mo}$ $\text{Q} = \text{S}$ $\text{X} = \text{Te}$ $x = 0, 1$,

2, 3 [44, 45]. The general formula for the polymer framework for all mentioned phases is $[M_4Q_4X^{a-a}_{12/3}]_{\infty}$. Reactions are carried out from stoichiometric mixtures of simple substances when heated to a temperature of about 800-1000°C.

Clusters $\{M_6\}$. A series of heterometallic analogs of Chevrel phases $M_{6-x}M'_xQ_8$ $M = \text{Re}$ $M' = \text{Mo}$ $Q = \text{S, Se}$ $x = 2$, $Q = \text{Te}$ $x = 4$ [15] $M = \text{Re}$ $M' = \text{Mo}$ $Q = \text{Se}$ $x = 1.5$ [16]; $M = \text{Mo}$ $M' = \text{Ru}$ $Q = \text{Te}$ $x = 0.5, 1, 1.5$ [17-19] $M = \text{Mo}$, $M' = \text{Rh}$ $Q = \text{Te}$ $x = 0.5$ [17] $M = \text{Nb}$ $M' = \text{Ru}$ $Q = \text{Te}$ $x = 2.83 - 3.5$ [20] was obtained from stoichiometric amounts of simple elements in evacuated and sealed silica ampoule heated at 1150-1200° C during several days. The composition of the metal core is determined by the stoichiometry of the metal reagents. The reaction of stoichiometric amounts of Re, Os, Se, and binary ReCl_5 at 850°C leads to the formation of a heterometallic polymer phase $\text{Re}_4\text{Os}_2\text{Se}_8\text{Cl}_4$ [106]. In the presence of stoichiometric amounts of CsCl or KCl, the compounds $\text{Cs}_3\text{Re}_5\text{OsSe}_8\text{Cl}_6$, $\text{Cs}_2\text{Re}_4\text{Os}_2\text{Se}_8\text{Cl}_6$ and $\text{K}_2[\text{Re}_3\text{Os}_3\text{Se}_8\text{Cl}_6][\text{Re}_4\text{Os}_2\text{Se}_7\text{Cl}_7]$ containing heterometallic anions $[\text{Re}_{6-x}\text{Os}_x\text{Se}_8\text{Cl}_6]^{x-4}$ $x = 1, 2, 3$ are formed [106]. The $\text{Cs}_3\text{Re}_5\text{OsS}_{11}$ compound was obtained at a temperature of 850°C by the reaction of stoichiometric amounts of metal powders and cesium carbonate in a stream of hydrogen and sulfur vapor [90].

One of the known methods for the synthesis of cyanocluster compounds is the high-temperature reaction of binary chalcogenides and metal chalcogen halides with an excess of potassium cyanide. This method allows one to obtain cyanoclusters of transition metals of various nuclearity. For example, the reaction of binary tellurides of niobium, tantalum and tungsten with potassium cyanide at 340 - 460°C leads to the formation of tetrahedral cyanoclusters $[\text{M}_4\text{Te}_4(\text{CN})_{12}]^{n-}$ $M = \text{W}$ [107] and $[\text{M}_4\text{OTe}_4(\text{CN})_{12}]^{n-}$ $M = \text{Nb, Ta}$ [108, 109]. The interaction of various molybdenum selenides with KCN at 650°C leads to the formation of octahedral cyanoclusters $\text{K}_6[\text{Mo}_6\text{Se}_8(\text{CN})^{a-a}_{2/2}(\text{CN})^a_4]$ [110] and $\text{K}_7[\text{Mo}_6\text{Se}_8(\text{CN})_6]$ [111]. Rhenium chalcogenides, interacting with KCN under various conditions, form either the octahedral cluster polymers $\text{K}_4[\text{Re}_6\text{S}_{10}(\text{CN})_2]$ and $\text{K}_4[\text{Re}_6\text{Se}_{10}(\text{CN})_4]$ [112] or the molecular twelvenuclear cluster $[\text{Re}_{12}\text{S}_{17}\text{C}(\text{CN})_6]^{8-/6-}$ [113]. Also, it is interesting to note, that the interaction of triangular and tetrahedral cluster complexes with potassium cyanide can lead to the transformation of metal core into higher nuclearity ones. For example, the interaction of triangular cluster compounds

$M_3Q_7X_4$ ($M = Mo$ $Q = Te$ $X = I$; $M = W$ $Q = S, Se$ $X = Br$) with KCN at 400°C leads to the formation of tetrahedral clusters $[M_4Q_4(CN)_{12}]^{n-}$ ($M = Mo$ $Q = Te$, $M = W$ $Q = S, Se$) [107]. Before the beginning of this study, there were several examples that showed that the reaction with KCN is also suitable for the preparation of heterometallic cluster complexes. For example, the reaction of heterometallic tetrahedral $Re_{4-x}Mo_xS_4Te_4$ clusters ($x = 0.67, 1, 1.33, \text{ and } 2$) with an excess of potassium cyanide leads to the formation of heterometallic octahedral cluster compounds $Cs_5[Re_{6-x}Mo_xS_8(CN)_6] \cdot 2H_2O$ ($x \sim 1.5$), containing a mixture of heterometallic anions $[Re_5MoS_8(CN)_6]^{5-}$ and $[Re_4Mo_2S_8(CN)_6]^{5-}$ [114]. The presence of rhenium and molybdenum sulfides in the reaction mixture during interaction with KCN at a temperature of 750°C led to the formation of a heterometallic cluster polymer $K_6[Re_3Mo_3S_8(CN)^{a-}_{2/2}(CN)^a_4]$ [27].

The number of heterometallic halide clusters known to date is scarce. The cluster polymer $Mo_{6-x}Nb_xI_{11}$ $x \approx 1,3$ isostructural to Nb_6I_{11} was obtained by the reaction of stoichiometric amounts of simple substances at 650°C [23]. Chloride cluster complexes $[Mo_{6-x}W_xCl_{14}]^{2-}$ $x = 0 - 6$ [25] and $[Ta_{6-x}Mo_xCl_{18}]^{2-}$ $x = 1, 2$ [99] can be obtained using metal chlorides, aluminum powder, and a mixture of $AlCl_3/NaCl$ as a melt when heated at 550 and 320°C, respectively. Cluster complexes with $\{Nb_{6-x}TaCl_{12}\}^{2+}$ $x = 0 - 6$ core are formed upon the interaction of $TaCl_5$, Nb in NaCl at 720–820°C [100].

1.4.2 Preparation in solution

The second group of methods for the synthesis of heterometallic cluster complexes combines reactions carried out in solutions at room temperature or under moderate heating. The reduction of chalcogen-containing metal compounds in solution leads to the formation of cluster complexes. Accordingly, chalcogenide triangular or tetrahedral cluster complexes were obtained. For example, upon the reduction of NH_4MS_4 , $M = Mo, W$ in the $NaBH_4$ solution, the complexes $[Mo_4S_4(H_2O)_{12}]^{5+}$ and $[W_3S_4(H_2O)_9]^{4+}$ [115] are formed. Another way to obtain cluster complexes is the reaction of reduction condensation of binuclear complexes or triangular clusters. For example, the reaction of the $[Mo_2O_2S_2(H_2O)_4]^{2+}$ dimer complex with $NaBH_4$ in an HCl solution leads to the formation of the $[Mo_4S_4(H_2O)_{12}]^{5+}$ tetrahedral cluster [116]. The triangular cluster $[Mo_3S_4(Et_2PS_2)_4]$

reacts with molybdenum carbonyl in toluene upon boiling to form the tetrahedral cluster $[\text{Mo}_4\text{S}_4(\text{Et}_2\text{PS}_2)_6]$ [117]. This method is also widely used to obtain heterometallic complexes. Binuclear complexes $\{\text{M}_2\}$ or trinuclear metal cluster compounds ($\{\text{M}_3\}$) in solutions react under reduction conditions with a source of another metal, thereby forming heterometallic cluster complexes with heterometallic cores $\{\text{M}_2\text{M}'_2\text{Q}_4\}$ and $\{\text{M}_3\text{M}'\text{Q}_4\}$ [12].

Clusters $\{\text{M}_3\}$. The triangular heterometallic cluster complexes $[\text{Mo}_2\text{WS}_4(\text{H}_2\text{O})_9]^{4+}$ and $[\text{MoW}_2\text{S}_4(\text{H}_2\text{O})_9]^{4+}$ can be obtained by the interaction of equimolar amounts of $[\text{NH}_4]_2[\text{WS}_4]$ and the binuclear complex $\text{Na}_2[\text{Mo}_2\text{O}_2\text{S}_2(\text{cys})_2] \cdot 4\text{H}_2\text{O}$ (cys is cysteine) with NaBH_4 in an aqueous solution [32]. $[\text{M}_2\text{S}_4(\text{edt})_2(\text{Cu}(\text{PPh}_3))]^-$ $\text{M} = \text{Mo}, \text{W}$ clusters are formed upon the interaction of the copper complex $[\text{Cu}(\text{PPh}_3)_2(\text{S}_2\text{P}(\text{OCH}_2\text{CH}_3)_2)]$ and the binuclear molybdenum complex $\text{Et}_4\text{N}[\text{Mo}_2\text{S}_4(\text{edt})_2]$ in CH_2Cl_2 [38]. The heterometallic clusters $[(\text{Cp}^*\text{Ru})_2(\mu_2\text{-H})(\mu_3\text{-S})_2(\text{RhCl}_2(\text{PPh}_3))]^-$ and $[(\text{Cp}^*\text{Ir})_2\{\text{Mo}(\text{CO})_2(\text{MeCN})_2\}(\mu_3\text{-S})_2]^{2+}$ can be obtained similarly in the reaction of the binuclear complexes $[\text{Ru}_2(\text{SH})_2\text{Cl}_2(\text{Cp}^*)_2]$ and $[\text{Ir}_2(\text{SH})_2\text{Cl}_2(\text{Cp}^*)_2]$ with the complexes $\text{RhCl}(\text{PPh}_3)_3$ and $[\text{Mo}(\text{C}_6\text{H}_5\text{CH}_3)(\text{CO})_3]$, respectively [35, 36].

Clusters $\{\text{M}_4\}$. A 2003 review by Rosa Llusar and Santiago Uriel summarizes synthetic approaches to the production of tetrahedral clusters based on heterometallic cores $\{\text{M}_3\text{M}'\text{S}_4\}$ and $\{\text{M}_2\text{M}'_2\text{S}_4\}$, where $\text{M} = \text{Mo}, \text{W}$ $\text{M}' =$ transition metals of the 4th period [12]. In general, $\{\text{M}_2\text{M}'_2\text{S}_4\}$ clusters can be obtained in two ways: by the reaction of binuclear metal complexes with two equivalents of mononuclear compounds M' or with binuclear complexes containing the $\{\text{M}'_2\}$ fragment. A diagram describing the methods for producing $\{\text{M}_2\text{M}'_2\text{S}_4\}$ clusters is shown in Figure 1.13.

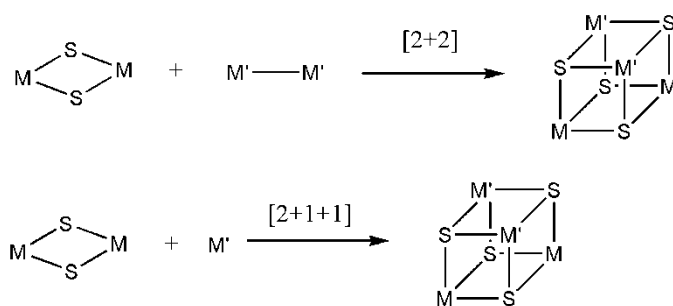


Figure 1.13: The preparation scheme of clusters $\{\text{M}_2\text{M}'_2\text{S}_4\}$ [12].

Depending on the coordination environment of metal atoms in the starting cluster based complexes, various variants of the coordination environment of metals in a tetrahedral heterometallic complex can be obtained. Interaction of $[\text{Mo}_2(\mu_2\text{-S})_4\text{Cp}^\#_2]$ ($\text{Cp}^\# = \text{Cp}, \text{Cp}', \text{Cp}^*$) with $[\text{CrCp}(\text{CO})_2]$, $[\text{Co}_2(\text{CO})_8]$, two equivalents of CuCl , $[\text{Fe}(\text{NO})_2(\text{CO})_2]$ in organic solvents leads to the formation of the corresponding heterometallic tetrahedral clusters $[\text{Mo}_2\text{M}'_2\text{S}_4(\text{Cp}^\#)_2\text{L}_2]$ $\text{M}' = \text{Cr L} = \text{CO}$ [118], $\text{M}' = \text{Co L} = \text{CO}$ [119] $\text{M}' = \text{Fe L} = \text{NO}$ [80] $\text{M}' = \text{Cu L} = \text{Cl}$ [88]. The interaction of $[\text{W}_2(\mu_2\text{-S})_4\text{Cp}_2]$ with $[\text{Co}_2(\text{CO})_8]$, $[\text{Fe}(\text{NO})_2(\text{CO})_2]$ leads to the formation of $[\text{W}_2\text{M}'_2\text{S}_4(\text{Cp}^\#)_2\text{L}_2]$ ($\text{M}' = \text{Co L} = \text{NO}$, $\text{M}' = \text{Fe L} = \text{NO}$ [80]). The interaction of $[\text{Mo}_2(\mu_2\text{-S})_2\text{S}_2(\text{dtc})_2]$ and $[\text{Mo}_2(\mu_2\text{-S})_2\text{S}_2(\text{edt})_2]^{2-}$ with $\text{Co}_2(\text{CO})_8$ leads to the formation of heterometallic tetrahedral clusters $[\text{M}_2\text{Co}_2\text{S}_4(\text{dtc})_2(\text{CH}_3\text{CN})_2(\text{CO})_2]$ $\text{M} = \text{Mo}, \text{W}$ [120, 121]. The copper-containing compounds $[\text{Mo}_2\text{Cu}_2\text{S}_4(\text{edt})_2(\text{PPh}_3)_2]$ are obtained by the reaction of $[\text{Mo}_2(\mu_2\text{-S})_2\text{S}_2(\text{edt})_2]^{2-}$ with $[\text{Cu}(\text{PPh}_3)_3\text{Cl}]$ in an inert atmosphere [122]. The tungsten heterocluster $[\text{W}_2\text{Cu}_2\text{S}_4(\text{edt})_2(\text{PPh}_3)_2]$ can be a result of a similar reaction of $[\text{W}_2(\mu_2\text{-S})_2\text{S}_2(\text{edt})_2]^{2-}$ with CuCl_2 in the presence of PPh_3 [122].

The $\{\text{M}_3\text{M}'\text{S}_4\}$ clusters can be obtained by the interaction of triangular homometallic clusters $\{\text{M}_3\}$ with the metal source M' (Figure 1.14).

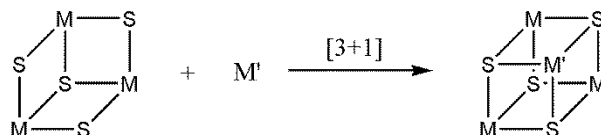


Figure 1.14: The preparation scheme of clusters $\{\text{M}_3\text{M}'\text{S}_4\}$ [12].

Cluster complexes $[\text{Mo}_3\text{M}'\text{S}_4(\text{H}_2\text{O})_{10}]^{4+}$ were obtained for transition metals $\text{M}' = \text{Fe}, \text{Co}, \text{Ni}, \text{Cu}$. The interaction of the initial homometallic complex $[\text{Mo}_3\text{S}_4(\text{H}_2\text{O})_9]^{4-}$ with metals in an acidic medium leads to the formation of $[\text{Mo}_3\text{M}'\text{S}_4(\text{H}_2\text{O})_{10}]^{4+}$ $\text{M}' = \text{Fe}$ [123], Co [81], Ni [74], Cu [84]. Similarly, selenide analogs of the $[\text{Mo}_3\text{NiSe}_4(\text{H}_2\text{O})_{10}]^{4+}$ [55] molybdenum-nickel cluster and $[\text{Mo}_{3-x}\text{W}_x\text{NiSe}_4(\text{H}_2\text{O})_{10}]^{4+}$ $x = 0\text{--}3$ trimetallic clusters can be obtained [82]. Complexes with $\{\text{Mo}_3\text{M}'\text{S}_4\}$ cores having an even number of CSEs crystallize from acidic solutions in the form of isolated cluster complexes $([\text{Mo}_3\text{M}'\text{S}_4(\text{H}_2\text{O})_{10}](\text{pts})_4 \cdot 7\text{H}_2\text{O})$ $\text{M}' = \text{Fe}, \text{Co}$ ($\text{pts} - p\text{-toluenesulfonate}$). In the case of

cluster complexes with odd SCEs, the dimeric structures $[\{\text{Mo}_3\text{M}'\text{S}_4(\text{H}_2\text{O})_9\}_2](\text{pts})_8 \cdot n\text{H}_2\text{O}$ ($\text{M} = \text{Co}$, CSE = 18; $\text{M} = \text{Cu}$, CSE = 20) are formed. The heterometallic cluster complexes $[\text{M}_3\text{M}'\text{S}_4\text{Cp}^\#_3\text{L}_3]$ $\text{M} = \text{Mo}$, W with cyclopentadienyl ligands were obtained by the reaction of $[\text{M}_3\text{S}_4\text{Cp}^\#_3]^+$ with $[\text{Cr}(\text{CO})_3(\text{CH}_3\text{CN})_3]$, $[\text{Ni}(\text{cod})_2]$ (cod - 1,5-cyclooctadiene) with the formation of $[\text{M}_3\text{CrS}_4\text{Cp}_3(\text{CO})_3][\text{pts}]$ $\text{M} = \text{Mo}$ [124], $[\text{M}_3\text{NiS}_4\text{Cp}'_3][\text{pts}]$ $\text{M} = \text{Mo}$, W [50, 76]. Copper-containing heteroclusters $[\text{M}_3\text{CuS}_4((\text{EtO})_2\text{PS}_2)_3(\mu_2\text{-O}_2\text{CR})\text{L}]$ ($\text{R} = \text{CH}_3$, CF_3 , CCl_3 ; $\text{L} = \text{DMF}$ - dimethylformamide, DMSO - dimethyl sulfoxide, py - pyridine, CH_3CN) can be obtained by reaction of $[\text{M}_3\text{S}_4\{(\text{EtO})_2\text{PS}_2\}_3(\mu_2\text{-(EtO)}_2\text{PS}_2)(\text{H}_2\text{O})]$ and CuI in various organic solvents in the presence of RCOOEt [125-127]. Interaction of $[\text{Mo}_3\text{Q}_4(\text{dmpe})_3\text{X}_3][\text{PF}_6]$ and $[\text{W}_3\text{S}_4\text{X}_3(\text{dmpe})_3][\text{PF}_6]$ in **THF** (tetrahydrofuran) with CuX $\text{X} = \text{halogen}$ or with $[\text{Cu}(\text{CH}_3\text{CN})_4][\text{PF}_6]$ in the presence of an $n\text{-Bu}_4\text{NX}$ salt gives $[\text{M}_3\text{CuQ}_4(\text{dmpe})_3\text{X}_4][\text{PF}_6]$ $\text{Q} = \text{S}$ $\text{M} = \text{Mo}$, $\text{X} = \text{Cl}$; $\text{M} = \text{Mo}$, W $\text{X} = \text{Br}$ [75] $\text{Q} = \text{Se}$ $\text{M} = \text{Mo}$, $\text{X} = \text{Cl}$; $\text{M} = \text{Mo}$, W $\text{X} = \text{Br}$ [54].

Clusters $\{\text{M}_6\}$. The synthesis of the octahedral cluster $[\text{Mo}_6\text{S}_8(\text{PET}_3)_6]$ can be carried out using reductive condensation in solution from triangular cluster precursors $[\text{Mo}_3\text{S}_4\text{Cl}_4(\text{PET}_3)(\text{MeOH})]$ using magnesium metal in **THF** is known in the literature [128].

1.5 Reactivity of heterometallic clusters

Reactions in which heterometallic high-valence cluster complexes are involved can be conditionally divided into three groups. The first group includes reactions with the change of the metal core atoms. The second group includes ligand substitution reactions, the third group contains reactions of anionic cyanocomplexes with metal cations with the formation of polymeric structures.

1.5.1 Reactions with the modification of the metal core atoms

Clusters $\{\text{M}_3\}$. Various triangular cluster complexes $[\text{M}_3\text{Q}_4\text{L}_n]$ $\text{M} = \text{Mo}$, W ; $\text{Q} = \text{S}$, Se ; $\text{L} = \text{Cp}$, H_2O undergo reductive addition reactions of the metal atom M' to form a tetrahedral

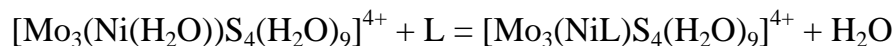
cluster $[M_3M'Q_4L_n]$ $M = Mo$ $M' = Ni, Co, Fe, Cr, Cu, Pd, Pt, Ir, Rh, Hg, Mn, W$ [12, 14, 48, 51]. Detailed examples were described above in the preparation section.

Clusters $\{M_4\}$. Only one example of the transmetallation reaction of heterometallic cluster complexes $[M_3M'Q_8L_n]$, which allows to replace the M' atoms with atoms of another metal is known. The interaction of the cationic complex $[Mo_3M'S_4(H_2O)_{10}]^{4+}$ ($M' = Fe, Ni$) with the Cu^{2+} copper cation leads to the formation of the copper cluster complex $[Mo_3CuS_4(H_2O)_{10}]^{4+}$ and the release of metal ions M'^{2+} [129].

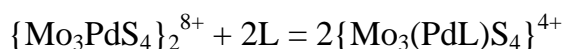
1.5.2 Ligand exchange reactions

Clusters $\{M_3Q_4\}$. Coordinated water molecules in the $[M_3S_4(H_2O)_9]$ $M = Mo, W$ complexes can be replaced by thiocyanates, carboxylates, amine derivatives, and others [2]. It was shown that the substitution of water for thiocyanate in the mixed metal cluster complexes $[Mo_2WS_4(H_2O)_9]^{4+}$ and $[MoW_2S_4(H_2O)_9]^{4+}$ proceeds faster on molybdenum atoms than on tungsten ones [130].

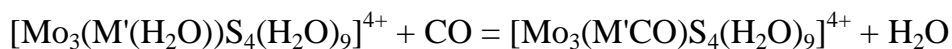
Clusters $\{M_4Q_4\}$. In the heterometallic aqua complexes of tetrahedral cluster complexes $[M_3M'S_4(H_2O)_{10}]$, the apical ligands of the heteroatom M' are easier to undergo substitution reactions than the apical ligands of M . This allows selective ligand substitution at one vertex of the tetrahedron [129]. For example, water molecules coordinated to nickel atoms in the $[Mo_3NiS_4(H_2O)_{10}]^{4+}$ cluster complex are replaced by various ligands L ($L = Cl^-, Br^-, I^-, SCN^-, CO$, water-soluble phosphine derivatives) [131], according to the reaction:



The reaction of the dimeric palladium cluster complex $\{Mo_3PdS_4\}_2^{8+}$, with various ligands $L = CO, P(C_6H_4SO_3)_3^{3-}, Cl^-, Br^-, NCS^-$ leads to the formation of an isolated cluster $\{Mo_3(PdL)S_4\}^{4+}$ [132]:



Also known are the processes of substitution of a water molecule coordinated to M' for the $[\text{Mo}_3\text{M}'\text{S}_4(\text{H}_2\text{O})_{10}]^{4+}$ M' = Co, Ni, Pd complexes upon interaction with CO in aqueous solutions [55]:



The replacement of aqua ligand with chloride is also known for the copper complex $[\text{Mo}_3\text{CuS}_4(\text{H}_2\text{O})_{10}]^{4+}$ [133].

Clusters $\{M_6Q_8\}$. Substitution of apical halide ligands for octahedral cluster complexes has been studied in sufficient detail. Apical halide ligands can be substituted using several approaches. The interaction of the halide cluster complexes of rhenium $[\text{Re}_6\text{Q}_8\text{X}_6]^{4-}$ and molybdenum $[\text{Mo}_6\text{X}_8\text{X}_6]^{n-}$ with various silver salts AgL leads to precipitation of insoluble silver halide AgX during the reaction and the formation of substituted complexes $[\text{Re}_6\text{Q}_8\text{L}_6]$ and $[\text{Mo}_6\text{X}_8\text{L}_6]$ [105, 134-138]. Heating of rhenium halide clusters $[\text{Re}_6\text{Q}_8\text{X}_6]^{n-}$ (Q = S, Se) with organic ligands leads to the formation of a substituted $[\text{Re}_6\text{Q}_8\text{L}_6]$ cluster complex [139-146]. The interaction of rhenium cluster polymers with the formula $[\text{Re}_6\text{Q}_4^i\text{Q}^{i-a}_{4/2}\text{Q}^{a-i}_{4/2}\text{Br}^a_2]$ (Q = S, Se) with a melt of alkali metal cyanide or hydroxide leads to the destruction of the polymer structure and the replacement of halide ligands by cyano and hydroxo groups, respectively, with the formation of $[\text{Re}_6\text{Q}_8\text{L}_6]^{4-}$ L = CN [147] OH [148]. The addition of HX X = Cl, Br acids in the presence of CsX salts to the solution of the hydroxo complex leads to the reverse substitution of apical hydroxo groups for the halide [148]. And the interaction of the hydroxo-complex with a solution of potassium cyanide leads to the formation of a mixed ligand cyano-hydroxo complex $[\text{Re}_6\text{Se}_8(\text{CN})_4(\text{OH})_2]^{4-}$ [149]. Some of the considered reaction examples are also applicable to heterometallic octahedral halide cluster complexes.

Heating of $[\text{Re}_5\text{OsSe}_8\text{Cl}_6]^{3-}$ and $[\text{Re}_4\text{Os}_2\text{Se}_8\text{Cl}_6]^{2-}$ in a mixture of NaCN and NaNO_3 leads to the formation of $[\text{Re}_5\text{OsSe}_8(\text{CN})_6]^{3-}$ and $[\text{Re}_4\text{Os}_2\text{Se}_8(\text{CN})_6]^{2-}$ cyano-complexes [106]. The interaction of the salts of $[\text{Re}_5\text{OsSe}_8\text{Cl}_6]^{3-}$ and $[\text{Re}_4\text{Os}_2\text{Se}_8\text{Cl}_6]^{2-}$ anions with PET_3 in DMF upon heating leads to the formation of fully substituted cationic complexes $[\text{Re}_5\text{OsSe}_8(\text{PET}_3)_6]^{3+}$ and $[\text{Re}_4\text{Os}_2\text{Se}_8(\text{PET}_3)_6]^{4+}$. In the case of $[\text{Re}_4\text{Os}_2\text{Se}_8\text{Cl}_6]^{2-}$, the product of incomplete substitution, the neutral complex *trans,trans*- $[\text{Re}_4\text{Os}_2\text{Se}_8(\text{PET}_3)_2\text{Cl}_4]$

was also isolated. It is important to note that this complex is a product of the selective replacement of ligands on osmium atoms leading to the ordering of the positions of metal atoms in the structure of the compound due to the difference in the ligand environment of rhenium and osmium atoms, that made it possible to determine the heterometallic metal core as the trans- $\{\text{Re}_4\text{Os}_2\}$ isomer [21]. Heating of the polymer $[\text{Mo}_5\text{NbI}_8^i\text{I}^{a-a}_{6/3}]$ in an aqueous solution of KCN or KOH in the atmosphere of argon leads to depolymerization and the formation of molecular complexes $[\text{Mo}_5\text{NbI}_8^i(\text{CN})_6]^{3-}$ and $[\text{Mo}_5\text{NbI}_8^i(\text{OH})_6]^{3-}$, respectively. The reaction of the hydroxo complex with sulfuric acid leads to the formation of a mixed ligand neutral complex $[\text{Mo}_5\text{NbI}_8^i(\text{H}_2\text{O})_3(\text{OH})_3]$. The reaction with hydrochloric acid leads to the formation of a mixed ligand complex $[\text{Mo}_5\text{NbI}_8^i(\text{H}_2\text{O})_2\text{Cl}_4]^-$ [23]. Water molecules in $[\text{Mo}_5\text{NbI}_8^i(\text{H}_2\text{O})_2\text{Cl}_4]$ can be completely replaced by chlorine ions by the reaction of $[\text{Mo}_5\text{NbI}_8^i(\text{H}_2\text{O})_2\text{Cl}_4]$ with Ph_4PCl in acetonitrile [24].

1.5.3 Reactions with metal cations with the formation of coordination polymers

Cluster cyanocomplexes are stable in aqueous and organic solutions and provide convenient building blocks for the design of new cluster compounds. Cyanoclusters have a rigid topology for the arrangement of cyanide ligands, high resistance to hydrolysis, and substitution of cyanide ligands. By analogy with mononuclear transition metal cyanocomplexes, cyanoclusters can coordinate to cations of transition, post-transition metals with the formation of insoluble precipitates containing a large number of $\text{M}-\text{XN}-\text{M}'$ bonds [150-152]. A study of the interactions of octahedral cyanoclusters of various metals showed that, depending on the reaction conditions, the charges of the cluster anion and the metal cation, structures of various topologies, compounds of a molecular, chain-like, layered or framework structure can form. The structures of coordination polymers of different topologies, based on $[\text{Re}_6\text{Q}_8(\text{CN})_6]^{4-/3-}$ $\text{Q} = \text{S}, \text{Se}$ cluster complexes and transition metal cations M^{2+} are shown in Figure 1.15 b – d. The identical arrangement of cyanide ligands, whenever coordination of inner ligands is presented (edge-bridged or face-capped), permits the formation of the structures of the same topology. The most numerous stable structural type among coordination polymers based on octahedral cyanoclusters are structures of Prussian blue type. Compounds of this type have a six-connected

framework in which the anion is bonded to six metal cations *via* bridging cyanides (Figure 1.15 a, b). This structural type is found among the cluster anions $[\text{Mo}_6\text{Se}_8(\text{CN})_6]^{7-}$ [153], $[\text{Nb}_6\text{Cl}_9\text{O}_3(\text{CN})_6]^{5-}$ [154], $[\text{M}_6\text{Cl}_{12}(\text{CN})_6]^{4-}$ $\text{M} = \text{Nb}, \text{Ta}$ [155], $[\text{Re}_6\text{Q}_8(\text{CN})_6]^{3-/4-}$ $\text{Q} = \text{S}, \text{Se}$ [156] $[\text{Re}_6\text{Te}_8(\text{CN})_6]^{3-}$ [157].

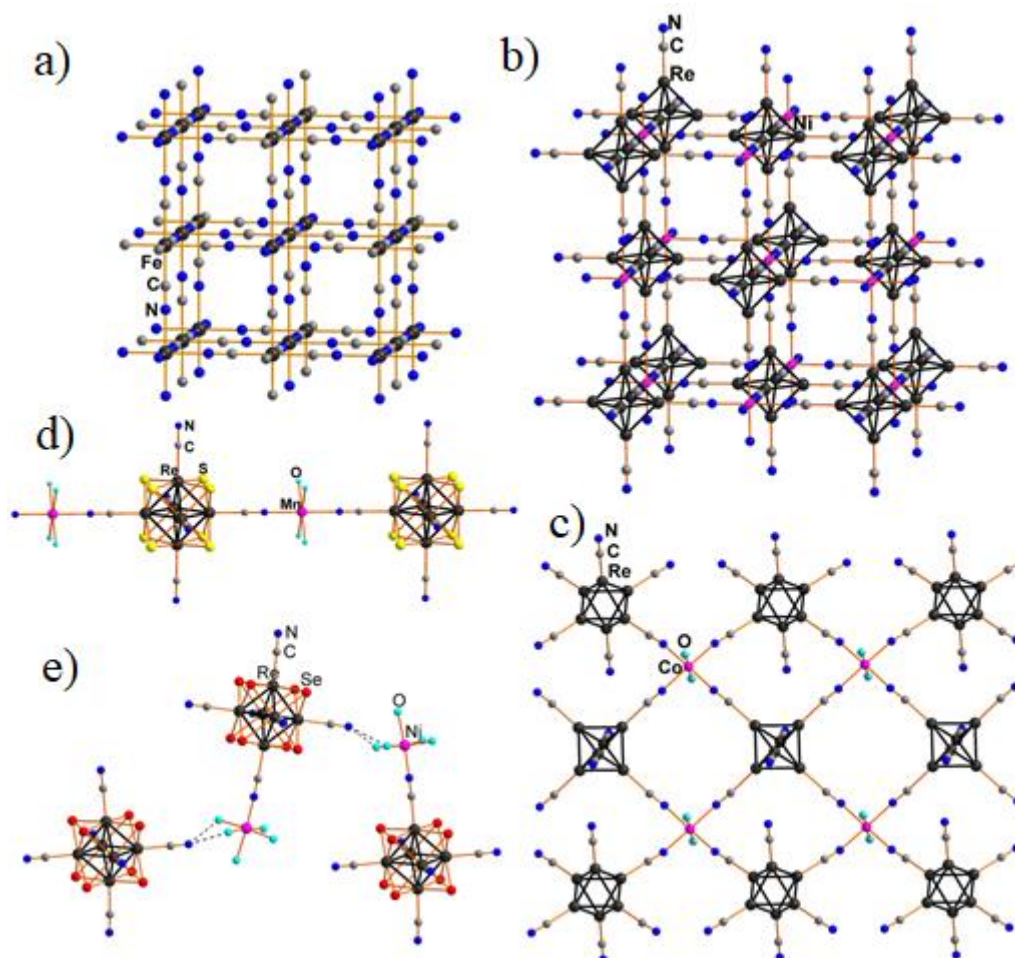


Figure 1.15: The structure of Prussian Blue [158] (a); the fragments of the structure of coordination polymers based on $[\text{Re}_6\text{Q}_8(\text{CN})_6]^{4-/3-}$ clusters and transition metal cations with different topology: 3D-framework $\text{Ni}_3[\text{Re}_6\text{Se}_8(\text{CN})_6]_2 \cdot 33\text{H}_2\text{O}$ [156] (b); layered $\text{Cs}_2\text{Co}(\text{H}_2\text{O})_2[\text{Re}_6\text{S}_8(\text{CN})_6]_2$ [159] (c); chain-like $(\text{Pr}_4\text{N})_2\text{Mn}(\text{H}_2\text{O})_5[\text{Re}_6\text{S}_8(\text{CN})_6] \cdot \text{H}_2\text{O}$ [160] (d); molecular $(\text{nBu}_4\text{N})_2\text{Ni}(\text{H}_2\text{O})_5[\text{Re}_6\text{Se}_8(\text{CN})_6] \cdot 2\text{H}_2\text{O}$ [161] (e).

Heterometallic cluster anions with apical cyanide ligands can also react with salts of transition and post-transition metals. For example, the interaction of the heterometallic anion $[\text{Re}_5\text{OsSe}_8(\text{CN})_6]^{3-}$ with nickel cations leads to the formation of the polymeric structure $\text{Ni}_3[\text{Re}_5\text{OsSe}_8(\text{CN})_6]_2 \cdot n\text{H}_2\text{O}$ [106], similar to $\text{Ni}_3[\text{Re}_6\text{Se}_8(\text{CN})_6]_2 \cdot 33\text{H}_2\text{O}$ [156]. The reaction of the cluster anions $[\text{Re}_4\text{Os}_2\text{Se}_8(\text{CN})_6]^{3-}$ and $[\text{Re}_5\text{OsSe}_8(\text{CN})_6]^{3-}$ with the copper

complex $[(\mathbf{Me}_6\mathbf{tren})\text{Cu}(\text{CF}_3\text{SO}_3)]^+$ ($\mathbf{Me}_6\mathbf{tren}$ - tris(2-(dimethylamino)ethyl)amine)) leads to the formation of molecular structures $\{\text{Re}_{6-x}\text{Os}_x\text{Se}_8[\text{CNCu}(\mathbf{Me}_6\mathbf{tren})]_6\}^{9+}$ $x = 1, 2$ [106]. The interaction of the previously obtained heterometallic cluster anion $[\text{Re}_3\text{Mo}_3\text{S}_8(\text{CN})_6]^{6-}$ with cadmium and zinc amine complexes also led to the formation of structures of Prussian blue type $[\text{Cd}(\text{NH}_3)_4]_2\{\text{Cd}[\text{Re}_3\text{Mo}_3\text{S}_8(\text{CN})_6]\} \cdot 1.5\text{H}_2\text{O}$ and $[\text{Zn}(\text{NH}_3)_4]_2\{\text{Zn}[\text{Re}_3\text{Mo}_3\text{S}_8(\text{CN})_6]\} \cdot 2\text{H}_2\text{O}$ [162, 163].

1.6 Electronic structure of heterometallic cluster complexes $[\text{M}_{4-x}\text{M}'_x\text{Q}_8\text{L}_n]$ and $[\text{M}_{6-x}\text{M}'_x\text{Q}_8\text{L}_6]$

A feature of the electronic structure of cluster complexes is that the atoms of the cluster nucleus, especially metals, are rigidly bonded to each other and form a common system of molecular levels, which determines the properties of the cluster anion. Substitution of metal atoms in the metal core has a significant effect on the electronic structure of the complex. The electronic structure of triangular, tetrahedral, and octahedral high-valence cluster complexes and the effect of heterometallic substitution on the electronic structure will be considered below.

1.6.1 Triangular clusters $[\text{M}_3\text{Q}_4\text{L}_n]$

Among the triangular cluster complexes, the most studied are cluster complexes with $\{\text{M}_3\text{Q}_4\}$ core. The diagram of molecular orbitals (MOs) for homometallic triangular clusters with the cores $\{\text{M}_3\text{Q}_4\}$ $\text{M} = \text{Mo}, \text{W}$ $\text{Q} = \text{S}, \text{Se}$ for geometry with C_{3v} symmetry is shown in Figure 1.16.

The resulting diagram consists of three bonding orbitals, one non-bonding and five anti-bonding orbitals [164]. The most stable state for such clusters is the filling of three bonding orbitals, which corresponds to the full connectivity of the metal core. The energy gap between the orbitals $1e$ and $2a_1$ does not allow the formation of cluster complexes with CSE 7 and 8 [165]. However, such complexes (and even with CSE 9) can be obtained by electrochemical reduction of a cluster complex [13]. It should be noted that the heterometallic cluster complexes $[\text{MoW}_2\text{S}_4(\text{H}_2\text{O})_9]^{4+}$, $[\text{Mo}_2\text{WS}_4(\text{H}_2\text{O})_9]^{4+}$ and $[\text{MoW}_2\text{S}_4(\text{Hnta})_3]^{2-}$,

$[\text{Mo}_2\text{WS}_4(\text{Hnta})_3]^{2-}$ similarly to the homometallic cluster complexes of molybdenum and tungsten have 6 CSEs in a stable state (Table 1.2).

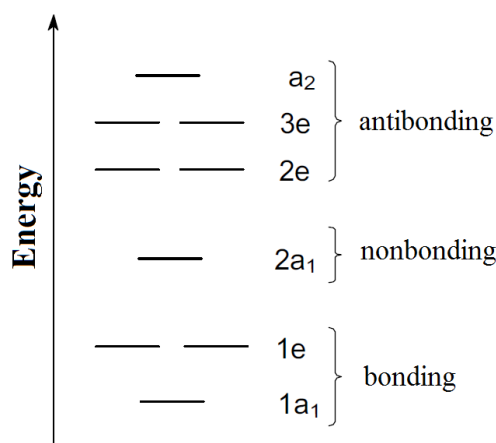


Figure 1.16. Qualitative MO diagram for triangular cluster complexes $[\text{M}_3\text{Q}_4\text{L}_9]$ $\text{M} = \text{Mo}, \text{W}$ $\text{Q} = \text{S}, \text{Se}$ with C_{3v} symmetry taken from [164], corresponding to levels of near frontier region which have strong metal-metal character.

1.6.2 Tetrahedral cluster complexes $[\text{M}_4\text{Q}_4\text{L}_n]$

The electronic structure of homometallic tetrahedral cluster complexes $[\text{M}_4\text{Q}_4\text{L}_{12}]$ was studied in detail in the works of Susanna Harris [166]. Metal atoms in tetrahedral cluster complexes with $\{\text{M}_4\text{Q}_4\}$ core have the same coordination of internal chalcogenide ligands, and the number of apical ligands can be different. To construct high-quality diagrams of molecular orbitals, an approach is used in which the interaction of metal fragments $[\text{ML}_n]$ with a certain geometry of the ligand environment is considered. The cluster is considered as a product of the interaction of such fragments (metal fragment orbital approach). Qualitative schemes of molecular orbitals for tetrahedral cluster complexes with different types of ligand environment are shown in Figure 1.17. The most common type of ligand environment $[\text{M}_4\text{Q}_4\text{L}_{12}]$ is found for metal atoms in octahedral ligand environment. The qualitative diagram of molecular orbitals for cluster complexes of this type contains six bonding, six non-bonding, and eight antibonding molecular orbitals (Figure 1.17 a). Cluster complexes of this type with a fully connected metal core should have 12 CSEs; an increase in the number of CSEs occurs due to the filling of non-bonding molecular orbitals. Non-bonding orbitals are located quite high, and homometallic cluster com-

plexes of this type with CSEs more than 12 are usually not found. When the number of CSEs decreases below 12, the clusters have incomplete metal-core bonding and a difference appears between the metal – metal bond lengths [166]. Another type of ligand environment, which is also quite common, is $[M_4Q_4L_4]$, where metal atoms have a tetrahedral environment. The electronic structure of such cluster complexes strongly depends on the type of apical ligands. In this case, the structure of complexes in which apical ligands have a π -acceptor nature will be considered. The qualitative scheme of molecular orbitals for cluster complexes of this type contains 8 non-bonding, 6 bonding and 6 antibonding orbitals (Figure 1.17 b). The filling of eight non-bonding and six bonding orbitals in this case is necessary for the full connectivity of the metal core [166].

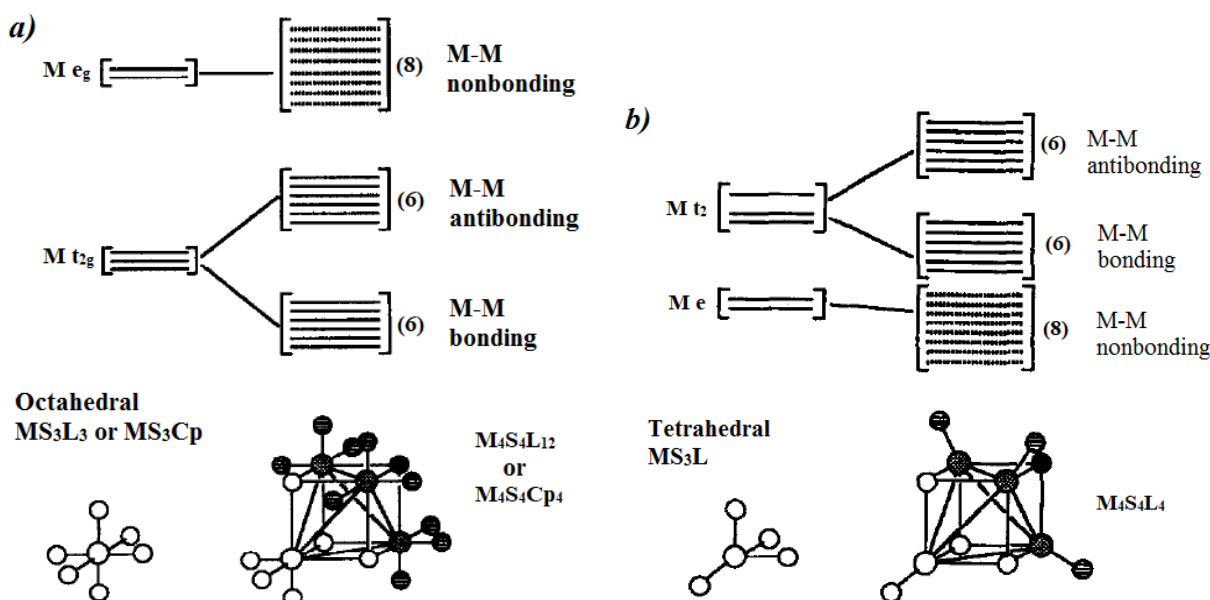


Figure 1.17: Qualitative MO diagrams for cluster complexes $[M_4Q_4L_{12}]$ (a) and $[M_4Q_4L_4]$ (b) taken from [166], corresponding to levels of near frontier region which have strong metal-metal character.

The case of heterometallic tetrahedral cluster complexes is more complicated, since the geometry of the ligand environment of metals of different types can be different. The final heterometallic clusters are considered as the products of the interaction of the fragments $[ML_n]$ and $[M'L'_m]$, where M and M' belong to transition metal row, L and L' are ligands associated with the metal center. As mentioned earlier, the most typical cases are the complexes $[M_2M'_2Q_4L_6L'_2]$ and $[M_3M'Q_4L_9L']$, where M has an octahedral environment and M' a tetrahedral environment. Molecular orbital diagrams for the heterometallic

cluster complex $[\text{Mo}_3\text{NiS}_4(\text{H}_2\text{O})_9(\text{CO})]^{4+}$ are shown in Figure 1.18. The choice of metals M and M' can affect the relative position of the orbitals of the initial fragments $[\text{ML}_n]$ and $[\text{M}'\text{L}'_m]$ with respect to each other. This affects the difference between the HOMO (higher occupied molecular orbital) and LUMO (lower unoccupied molecular orbital), and can also affect the strength of the metal-metal bond [167].

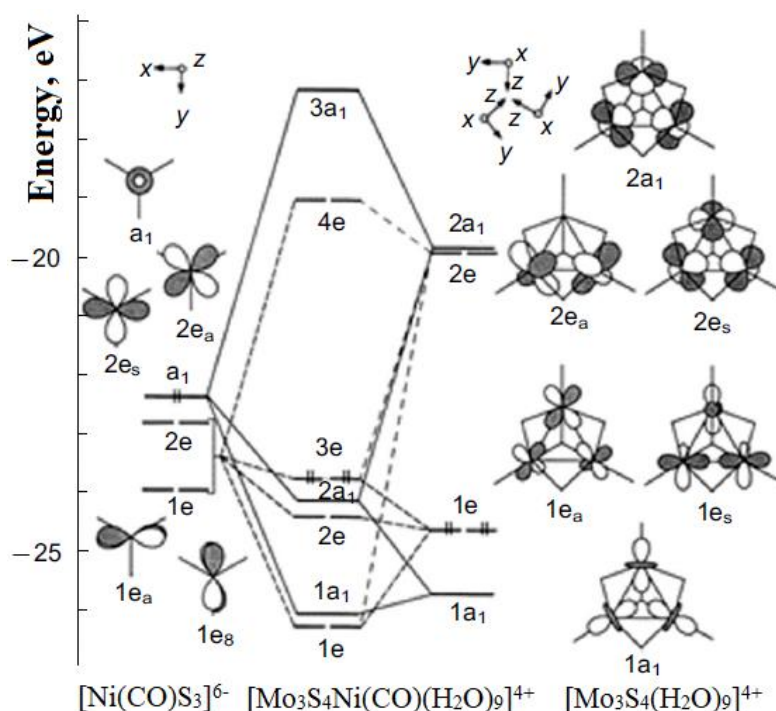


Figure 1.18. The MO diagram for heterometallic cluster complex $[\text{Mo}_3\text{NiS}_4(\text{H}_2\text{O})_9(\text{CO})]^{4+}$ (16 CSEs) taken from [167], corresponding to levels of near frontier region which have strong metal-metal character.

The full connectivity of the metal core for the $[\text{M}_3\text{M}'\text{Q}_4\text{L}_9\text{L}']$ clusters correspond to 16 CSEs. A similar combination of the ligand environment for $\{\text{M}_2\text{M}'_2\text{S}_4\}$ corresponds to 10 bonding orbitals, respectively, 20 CSEs correspond to the maximum connectivity of the metal core. If, however, with a given ligand environment, the CSE number > 20 , then the metal core no longer have a tetrahedral structure, because of induced cleavage of some M – M bonds (Table 1.5, Figure 1.7).

1.6.3 Octahedral cluster complexes $[M_6L^i_8L^a_6]$ and $[M_6L^i_{12}L^a_6]$

Qualitative schemes of molecular orbitals for the octahedral high-valence cluster complexes $[M_6L^i_8L^a_6]$ and $[M_6L^i_{12}L^a_6]$ are shown in Figure 1.19. The final cluster is considered as the product of the interaction of fragments $[ML_5]$ with the geometry of a square pyramid of C_{4v} symmetry. The full connectivity of the octahedral metal core $[M_6L^i_8L^a_6]$ corresponds to the filling of a bonding block of 12 orbitals. This corresponds to the presence of 24 cluster skeletal electrons or 12 M – M two-electron bonds in the octahedral metal core $\{M_6\}$. In the $[M_6L^i_{12}L^a_6]$ clusters, the presence of 16 CSEs is typical for the complete connectivity of the metal core.

The electronic structure of the anions $[Re_{6-x}Os_xSe_8L_6]^{n-}$ $x = 1$, $L = Cl$ [21] $x = 1, 2$ $L = OH$ [22] was studied by DFT calculations. Based on the obtained data, the authors conclude that an increase in the number of osmium atoms in the core leads to a noticeable decrease in the difference in the energy between HOMO and LUMO levels, which affect the optical properties of the cluster core (Figure 1.20) [22].

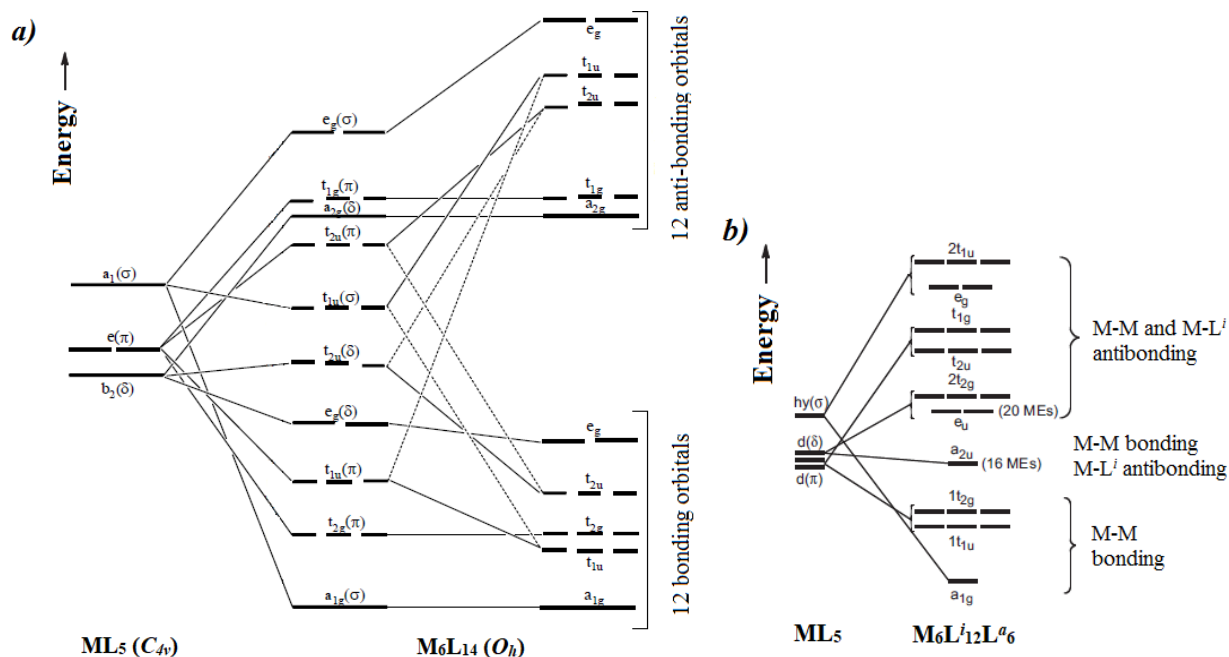


Figure 1.19: Qualitative scheme MO for octahedral cluster complexes: $[M_6L^i_8L^a_6]$ [168] (a) $[M_6L^i_{12}L^a_6]$ [169] (b), corresponding to levels of near frontier region which have strong metal-metal character.

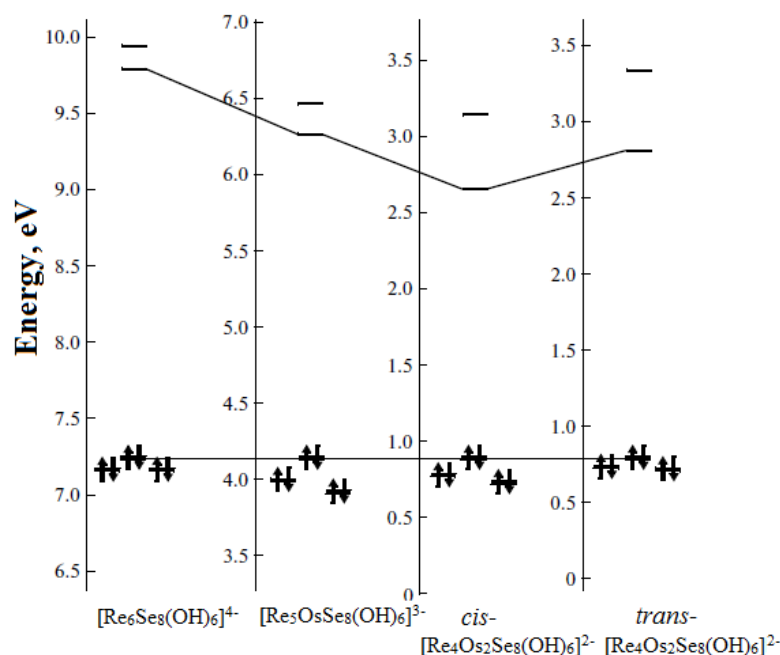


Figure 1.20: MO diagrams for 24-electron cluster anions $[\text{Re}_{6-x}\text{Os}_x\text{Se}_8(\text{OH})_6]^{x-4}$ [22], corresponding to levels of near frontier region which have strong metal-metal character.

1.7 Redox properties of the heterometallic cluster complexes

The effect of heterometallic substitution on the properties of a high valence cluster complex can be observed when comparing the redox properties of a heterometallic cluster and its homometallic analogues.

1.7.1 Triangular cluster complexes $[\text{M}_3\text{Q}_4\text{L}_n]$

The redox properties of triangular heterometallic molybdenum-tungsten cluster complexes $\{\text{Mo}_{3-x}\text{W}_x\text{S}_4\}$ $x = 1, 2, 3$ were studied by the cyclic voltammetry method. Homometallic triangular sulfide clusters $\{\text{M}_3\text{S}_4\}$ exhibit three reversible redox transitions. With an increase in the number of tungsten atoms in a triangular cluster, there is a shift of the reduction potentials to a more negative region. This effect can be observed in Table 1.8. The number of transitions does not change.

Table 1.8: Redox potentials (E vs NHE) for $[\text{Mo}_{3-x}\text{W}_x\text{S}_4(\text{Hnta})_3]^{2+}$ $x = 0-3$ (taken from [14])

| Cluster complex | E _{1/2} / B | | |
|--|----------------------|-------|-------|
| | I | II | III |
| $[\text{Mo}_3\text{S}_4(\text{Hnta})_3]^{2+}$ | -0.42 | -0.86 | -1.17 |
| $[\text{Mo}_2\text{WS}_4(\text{Hnta})_3]^{2+}$ | -0.51 | -1.00 | -1.44 |
| $[\text{MoW}_2\text{S}_4(\text{Hnta})_3]^{2+}$ | -0.62 | -1.18 | -1.56 |
| $[\text{W}_3\text{S}_4(\text{Hnta})_3]^{2+}$ | -0.90 | -1.19 | -1.66 |

1.7.2 Tetrahedral cluster complexes $[\text{M}_4\text{Q}_4\text{L}_n]$

Using the example of $[\text{Mo}_{4-x}\text{M}'_x\text{S}_4(\text{H}_2\text{O})_{12}]^{5+}$ tetrahedral cluster complexes ($x = 0-3$), it was shown that the substitution of the molybdenum atom by the isoelectronic tungsten atom leads only to a decrease in the potentials of redox transitions, without changing of their number (Table 1.9).

Table 1.9: Redox potentials (E vs NHE) for $[\text{Mo}_{4-x}\text{W}_x\text{S}_4(\text{H}_2\text{O})_{12}]^{5+}$ $x = 0 - 3$ (taken from [14])

| Cluster complex | E / mV | |
|---|--------|------|
| | I | II |
| $[\text{Mo}_4\text{S}_4(\text{H}_2\text{O})_{12}]^{5+}$ | 860 | 210 |
| $[\text{Mo}_3\text{WS}_4(\text{H}_2\text{O})_{12}]^{5+}$ | 673 | 6 |
| $[\text{Mo}_2\text{W}_2\text{S}_4(\text{H}_2\text{O})_{12}]^{5+}$ | 422 | -248 |
| $[\text{MoW}_3\text{S}_4(\text{H}_2\text{O})_{12}]^{5+}$ | 258 | -395 |

The effect of non-isovalent substitution on the redox properties of the cluster complex has a more complex character. The many values of redox potentials measured by the CV method for various sulfide cluster complexes of tungsten and molybdenum indicate that the reduction potentials can not only shift, but the number of observed transitions can also change [12, 13, 48]. Some reduction potentials for heterometallic tetrahedral clusters illustrating this conclusion are given in Table 1.10.

Table 1.10: Redox potentials (V) for tetrahedral heterometallic molybdenum and tungsten cluster complexes $\{M_3M'Q_4\}$ (taken from [13])

| Cluster complex | Redox potentials vs Ag/AgCl | | | |
|--------------------------------------|-----------------------------|-------|-------|----|
| | I | II | III | IV |
| $[Cp'_3Mo_3S_4Ni(PPh_3)]^+$ | -1.20 | +0.80 | +1.40 | – |
| $[Cp'_3W_3S_4Pt(PPh_3)]^+$ | -1.40 | +0.57 | +0.98 | – |
| $[Mo_3FeS_4(H_2O)_{10}]^{4+}$ | -0.91 | -1.47 | -1.72 | – |
| $[Mo_3NiS_4(H_2O)_{10}]^{4+}$ | -0.91 | -1.48 | -1.72 | – |
| $[Mo_3CoS_4Cl(dmpe)_3Cl_3]^+$ | -0.10 | -0.91 | – | – |
| $[Mo_3CuS_4Cl(dmpe)_3Cl_3]^+$ | -0.81 | -1.19 | – | – |
| $[Mo_3FeS_4Cl(dmpe)_3Cl_3]^+$ | +0.26 | +1.06 | – | – |
| $[Mo_3Se_4CoCl(dmpe)_3Cl_3]^+$ | -0.15 | – | – | – |
| $[Mo_3CuS_4SCN(H_2O)_3(C_2O_4)_3]^+$ | -0.35 | – | – | – |

1.7.3 Octahedral cluster complexes $[M_6Q_8L_6]$

The redox properties of octahedral heterometallic cluster complexes have been studied scarcely. The only suitable example is the study of cluster complexes $[Re_6-xOs_xSe_8(PEt_3)_6]$ [21] (Figure 1.21). A study of the electrochemical behavior of the complexes $[Re_6Se_8(PEt_3)_6]$, $[Re_5OsSe_8(PEt_3)_6]$ and $[Re_4Os_2Se_8(PEt_3)_6]$ showed that non-isovalent heterometallic substitution leads to a shift in the potentials of redox transitions, and a change in their number. The value of the reduction potential of clusters with 24 CSE decreases with an increase in the number of osmium atoms in the cluster core. This decrease in potential made it possible to obtain the first 25 CSEs cluster complexes: $Na(Bu_4N)_3[Re_5OsSe_8(CN)_6]$ and $(PPh_4)_2(CoCp_2)[Re_4Os_2Se(CN)_6]$, containing $[Re_5OsSe_8(CN)_6]^{4-}$ and $[Re_4Os_2Se(CN)_6]^{3-}$ anions, respectively [106].

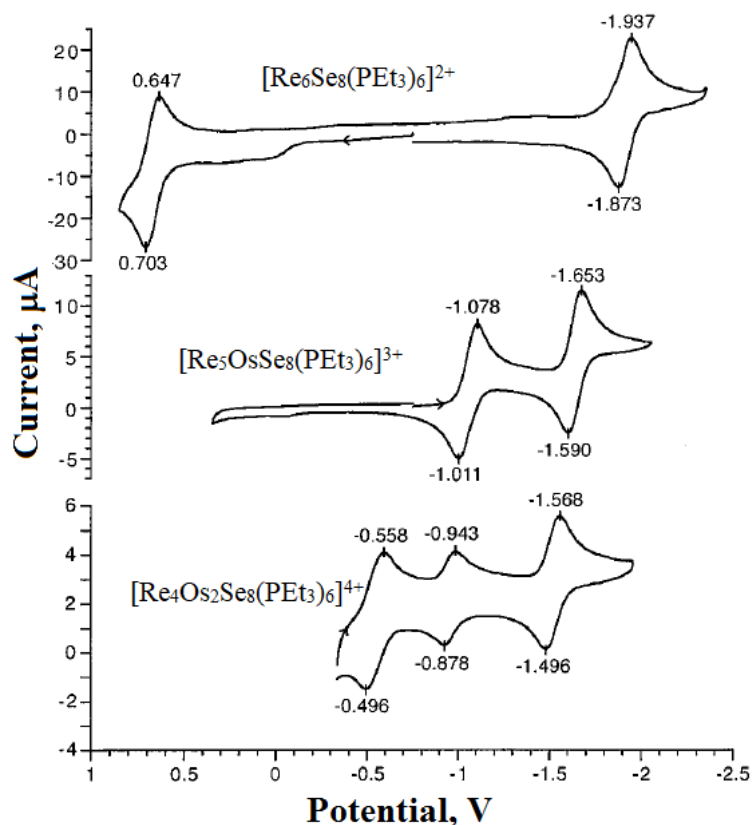


Figure 1.21: Cyclic voltammograms for cluster complexes $[\text{Re}_{6-x}\text{Se}_8(\text{PEt}_3)_6]^{2+x}$, $x = 0-2$ (taken from [21]).

* * *

An analysis of the published data shows that heterometallic substitution has a significant effect on the electronic structure of cluster complexes and their properties. On the other hand, the study of heterometallic cluster complexes is a more difficult task compared to homometallic ones, since several products with different metal ratios can form under synthesis conditions. Tetrahedral cluster complexes are the most studied of the considered heterometallic cluster complexes. The reason for this, in our opinion, is the dissolution method of synthesis, which allows one to obtain mixed-ligand cluster complexes in which the coordination environment of metals M and M' is different. The preparation of heterometallic octahedral cluster complexes is carried out by high-temperature synthesis, which leads to the formation of a mixture of isomers and cluster complexes with different metal ratios and the same ligand environment, which complicates the isolation of individual heterometallic cluster compounds.

Chapter 2: Experimental part

2.1 Materials and methods

Powders of metals were previously annealed in a stream of hydrogen at a temperature of 900 ° C. Selenium in granules had a purity of 99.999%, metal halides - 98-99%, potassium cyanide - 96%, potassium thiocyanate - 99%, cadmium acetate - 99%, iodine crystals - 99.8%, Bu_4NClO_4 -> 99.0%, Ph_4PBr and $\text{n-Bu}_4\text{NBr}$ - 98%, 4-tert-butylpyridine - 96% and triphenylphosphine - 99%. Reagents were used without further purification. The solvents used: acetone, acetonitrile, dichloromethane, DMF, THF, pentane, ethanol were qualified as pure and were used without further purification. Dissolved oxygen from distilled water was removed by prolonged boiling in a stream of argon. Ultrasonic treatment was performed using a Sapphire 5.7 ultrasonic bath. MoSe_2 and ReSe_2 were obtained by the reaction of powders of metallic rhenium and molybdenum with selenium in stoichiometric amounts in evacuated and sealed ampoules, which were heated at 600-800°C during 48 hours. The phase purity of the obtained samples of compounds was confirmed by powder XRD analysis. In the case of samples unstable in air with the loss of crystallinity, the analysis of powder XRD analysis was not carried out.

X-ray diffraction studies were carried out using automatic diffractometers: Bruker X8 APEX CCD, Agilent Xcalibur CCD AtlasS2, APEX II Bruker AXS and D8Venture Bruker AXS. In all cases, Mo $\text{K}\alpha$ radiation ($\lambda = 0.71073 \text{ \AA}$) was used. The primary data, including cell parameters, Miller indices, and intensities of the measured reflections, were processed using software supplied with a diffractometer on which a single crystal was taken. The absorption was calculated using the SADABS program [170]. The structures were solved by the direct method and refined by full-matrix least squares by F^2 using the SHELXL-2014 program in the anisotropic model (with the exception of hydrogen atoms) [171]. The contribution of disordered solvent molecules for structures **19**, **21–22** was estimated using the SQUEEZE procedure of the PLATON program [172]. Hydrogen atoms of water molecules were not localized. Hydrogen atoms of organic ligands were

geometrically localized. The metal positions in the resulting structures of the heterometallic cluster complexes were occupied together by rhenium and molybdenum atoms. The ratio of metals in the positions was specified independently under the assumption that each of the positions was fully occupied. Crystallographic data and characteristics of diffraction experiments including CCDC numbers of published structural data are gathered in Table S1 – S6 in the Supplementary. Cif-files have been deposited at the Cambridge Crystallographic Data. Copies of this information may be obtained free of charge from the CCDC, 12 Union Road, Cambridge CB2 1 EZ, UK (fax: +44 1223 336033; <http://www.ccdc.cam.ac.uk/conts/retrieving.html>) The selected interatomic distances for the resulting structures in comparison with homometallic analogues are given in Table 4.1 and 4.2 in Chapter 4.

Powder Diffraction. Powder X-ray diffraction patterns were recorded using Philips PW1820 / 1710 and Bruker Advanced D8 diffractometers with copper radiation (Cu K α 1 1.54060 Å). Theoretical diffraction patterns were calculated using PowderCell 2.4 software [173]. The diffraction patterns for compounds **2–4**, **6**, **15**, **16**, and **18** are shown in Figure S1 – S3 in the Supplementary.

Chemical analysis. Elemental (C, H, N, S) analysis was performed using a Thermo Electron Microanalyser Flash EA1112 CHNS / O analyzer. The ratio of the heavy elements in the obtained samples was estimated using energy dispersive analysis using a Hitachi TM-3000 electron microscope with a Bruker Nano EDS analyzer and a JEOL JSM-7100F scanning microscope with an EDS analyzer Oxford Instruments AZtecEnergy.

Infrared Spectroscopy. The IR spectra of samples in the form of KBr pellets were recorded using a Bruker Scimitar FTS 2000 spectrometer in the range 4000–375 cm⁻¹.

Spectroscopy of electron paramagnetic resonance. The EPR spectra at 77 K were recorded using a Bruker EMX EPR spectrometer.

Mass spectrometry. High resolution mass spectra with electrospray ionization were obtained using Bruker maXis 4G ESI-q-TOF and Thermo Scientific Q Exactive mass spectrometers. Signals for negatively charged ions were measured in the range of 300–3000 m / z (injection of the solution at a rate of 0.18 ml/h, voltage + 2500 V, atomizer pressure

2 bar, dry gas flow 6 l/min, gas temperature 200°C. Acetonitrile, dichloromethane were used as solvents.

Nuclear magnetic resonance spectroscopy. ^{77}Se NMR spectra of solutions of the obtained compounds were recorded at room temperature using a 400 MHz BRUKER Avance III NMR spectrometer.

Electronic absorption spectra of solutions of the obtained compounds in the range of 200-1100 nm were recorded on spectrophotometers Analytik Jena Specord 205, Agilent Carry 60 and Perkin Elmer Lambda 35.

X-ray absorption spectroscopy. X-ray absorption measurements for samples of heterometallic cluster complexes and standards were carried out at room temperature in the transmission mode with radiation energies for Mo (K-absorption edge, 20 keV) for Re (L_3 absorption edge, 10.535 keV) synchrotron radiation source SAMBA synchrotron center Soleil in France [174]. The measurements were performed in the continuous scanning mode monitoring the incident and passing beams using Oxford ionization chambers [175]. During the measurement, a standard sample (molybdenum and rhenium foil) was simultaneously measured with the residual photons of the second ionization chamber for energy calibration. The calculated amount of the sample was ground in a mortar, mixed with cellulose and pressed into a tablet. The signal was processed using the standard procedure: subtracting the background, normalizing the absorption edge, extracting the EXAFS $\chi(k)$ signal and its Fourier transform, which provides a map in the real space of the distribution of distances R around the absorbing atom. The Demeter software package was used to process and refine data [176]. The initial theoretical functions were obtained on the basis of crystallographic data on the arrangement of atoms. The occupancies of the metal atoms sites were changed in order to obtain the arrangement of a particular isomer of the metal core. The final parameters obtained by refining the experimental data for compounds **10** and **12** are given in Tables S7, S8 in the Supplementary.

Quantum chemical calculations. Quantum-chemical calculations for the complexes $[\text{Re}_3\text{Mo}_3\text{Se}_8(\text{CN})_6]^{n-}$, $[\text{Re}_4\text{Mo}_2\text{Se}_8(\text{CN})_6]^{n-}$ and $[\text{Re}_5\text{MoSe}_8(\text{CN})_6]^{n-}$ were performed in frames of the density functional theory (DFT) using programs ADF2017 [177-179]. The

geometrical parameters for cluster anions were optimized using the PW92 + revPBE functional [180, 181]. In the calculations, the ZORA/TZ2P basis was used taking into account the relativistic effect of zero order [182, 183]. The effects of the water environment were taken into account using the COSMO (Conductor like Screening Model) model [184]. The MO diagrams and the typical structure of HOMO, HOMO-1, and LUMO for the cluster complexes $[\text{Re}_5\text{MoSe}_8(\text{CN})_6]^{n-}$ ($n = 3 - 5$) and $[\text{Re}_4\text{Mo}_2\text{Se}_8(\text{CN})_6]^{n-}$ ($n = 4 - 6$) are given in Figures S4 – S6 in the Supplementary.

Cyclic voltammetry. Cyclic voltammograms were recorded using Metrohm Computrace 797 VA and Elins P-20X8 analyzers using a standard three-electrode circuit (the working electrode is glassy carbon, the auxiliary electrode is platinum, and the reference electrode is silver chloride, 3.5 M KCl). The studies were carried out in solutions with concentrations of $2-3 \times 10^{-3}$ M of the test substance in DMF or acetonitrile. 0.1 M Bu_4NClO_4 solution was used as electrolytes. All measurements were carried out in an argon atmosphere.

Thermogravimetric analysis. Thermogravimetric analysis of the samples was carried out using NETZSCH TG 209 F1 Iris in a helium flow (30 ml/min) with a heating rate of $10^\circ\text{C}/\text{min}$.

Diffuse reflectance spectra. To record the diffuse reflectance spectra of solid samples, a 3101 PC UV / VIS / NIR spectrometer was used.

2.2 Preparation protocols

2.2.1 The solution-melt preparation of polymeric phase $\text{K}_6[\text{Re}_3\text{Mo}_3\text{Se}_8(\text{CN})^{a-a}_{2/2}(\text{CN})^a_4]$ and its depolymerization to the soluble salts: $\text{Cat}_n[\text{Re}_3\text{Mo}_3\text{Se}_8(\text{CN})_6]$, $\text{Cat} = \text{K}, \text{Cs}, \text{Ph}_4\text{P}^+$

$\text{K}_5[\text{Re}_3\text{Mo}_3\text{Se}_8(\text{CN})_{2/2}(\text{CN})_4]$ (I). A mixture of stoichiometric amounts of MoSe_2 (0.900 g, 3.54 mmol), ReSe_2 (1.220 g, 3.54 mmol) and excess KCN (2.032 g, 31.21 mmol) was thoroughly grounded and placed in a quartz ampoule, which was subsequently evacuated and sealed. The ampoule with reagents was heated at 630°C during 14 days. After cooling slowly to room temperature, the ampoule was opened. The obtained melt containing

the octahedral crystals of compound **1** was washed on a glass filter using degassed water in a flow of argon. An admixture of unreacted rhenium and molybdenum diselenides was removed by ultrasonic treatment in ethanol and subsequent decantation of the suspension. The obtained crystals were dried in a dynamic vacuum. Yield of **1**: 1.560 g (72%). The yield of product **1** can be improved up to 90% by increasing the exposure under heating up to 4 weeks. Crystals for single crystal X-ray diffraction analysis were taken directly from the reaction mixture. Compound **1** is sensitive to atmospheric oxygen and moisture. Recording the powder diffraction pattern in air leads to a gradual decomposition of the sample and an evolution of the diffraction pattern. The diffraction of satisfactory quality pattern was obtained for crystals grounded in mineral oil. The ratio of heavy elements according to the results of energy dispersive spectroscopy for crystals **1** found: K: Mo: Re: Se = 5.9: 2.9: 3.1: 8.4, calcd.: K : Mo : Re : Se = 6.0 : 3.0 : 3.0 : 8.0. Calculated for $C_5N_5Se_8K_6Mo_3Re_3$: C 3.26, N 3.80, found: C 3.31, N 3.37%. IR (KBr): $\nu = 2072, 2093\text{ cm}^{-1}$ ($C\equiv N$).

$K_5[Re_3Mo_3Se_8(CN)_6]\cdot 11H_2O$ (**2**). The crystals of compound **1** (0.500 g, 0.27 mmol) were placed in an aqueous KCN solution (0.050 g, 0.77 mmol; 10 ml) and intensively stirred in air under mild heating for several hours. The resulting intensely colored solution was filtered and evaporated in vacuo to a volume of 3 ml. Then, 3 ml of ethanol was added to the resulting solution until a precipitate of compound **2** formed. The precipitate was separated by centrifugation, washed with ethanol and dried in air. Yield of **2**: 0.355 g (71%). Crystals of compound **2** suitable for X-ray diffraction studies were obtained by slow diffusion of ethanol vapor into a concentrated aqueous solution of compound **2** (100 mg/ml). The ratio of heavy elements according to the EDS analysis for crystals **2** found: K: Mo: Re: Se = 4.8: 2.9: 3.1: 8.1, calcd.: K : Mo : Re : Se = 5.0 : 3.0 : 3.0 : 8.0. Calculated for $C_6N_6K_5Se_8Mo_3Re_3(H_2O)_5$: C 3.75, H 0.52, N 4.38; C 3.78, H 0.54, N 4.02% were found. IR (KBr): $\nu = 3570, 1614$ (O–H); 2093 cm^{-1} ($C\equiv N$). UV-Vis (H_2O): λ_{max} (ϵ) = 236 (46970), 550 (1487); 613 nm ($735\text{ mol}^{-1}\cdot\text{dm}^3\cdot\text{cm}^{-1}$).

$Cs_5[Re_3Mo_3Se_8(CN)_6]\cdot H_2O$ (**3**). Compound **2** (0.500 g, 0.26 mmol) was dissolved in 5 ml of water and CsCl (0.500 g, 2.97 mmol) was added. The resulting solution was evaporated to a volume of about 2 ml and slowly cooled. The microcrystalline powder obtained

after cooling was filtered, washed with alcohol and dried in air. Yield of **3**: 0.513 g (82%). Crystals suitable for single crystal X-ray diffraction analysis were obtained by diffusion of an aqueous solution of compound **2** (15 mg/ml) into a more concentrated solution of CsCl (150 mg / ml) in a thin tube with the neck. The ratio of heavy elements according to the EDS for crystals **3** found: Cs: Mo: Re: Se = 5.1: 2.9: 3.1: 8.5, calcd.: Cs : Mo : Re : Se = 5.0 : 3.0 : 3.0 : 8.0. Calculated for $C_6N_6Cs_5Se_8Mo_3Re_3(H_2O)_4$: C 3.04, H 0.34, N 3.54; Found: C 2.91, H 0.32, N 3.38%. IR (KBr): $\nu = 3432, 1606$ (O – H), 2095 cm^{-1} ($C\equiv N$).

$(Ph_4P)_4[Re_3Mo_3Se_8(CN)_6]\cdot 2CH_3CN$ (**4**). 100 mg (0.05 mmol) of compound **2** was dissolved in 10 ml of water. Then, an aqueous solution of Ph_4PBr (0.140 g, 0.3 mmol; 15 ml) was added dropwise with stirring to the resulting solution until a precipitate formed. The resulting precipitate was separated by centrifugation, washed with water and dissolved in acetonitrile. The resulting solution was left in the air for several hours. The intensely stained stock solution was discolored, and dark blue crystals formed on the walls and bottom of the beaker. After precipitation, the mother liquor was decanted and the crystals were dried in air. Yield **4**: 116 mg (76%). Compound **4** in air quickly loses solvate acetonitrile molecules, which lead to amorphization of the sample. Grinding the crystals of the compound in mineral oil allowed to slow down the amorphization process and record a diffraction pattern of satisfactory quality. The ratio of heavy elements according to the EDS for crystals **4** found: Re: Mo: Se: P = 2.8: 3.2: 7.7: 3.8, calcd.: Re: Mo: Se: P = 3.0 : 3.0 : 8.0 : 4.0. Calculated for $C_{106}H_{86}Mo_3N_8P_4Re_3Se_8$: C 41.42, H 2.82, N 3.65; Found: C 41.61, H 2.55, N 3.71%. ESI-MS (-, CH_3CN/DMF) calculated $(Ph_4P)[Re_3Mo_3Se_8(CN)_6]^{2-}$ 987.55, found 987.51 (100%); $(Ph_4P)_2[Re_3Mo_3Se_8(CN)_6]^{2-}$ 1156.12, found 1156.07 (69%); $(Ph_4P)[Re_4Mo_2Se_8(CN)_6]^{2-}$ 1033.08, found 1033.03 (15%); $(Ph_4P)[Re_2Mo_4Se_8(CN)_6]^{2-}$ 942.03, found 941.98, 10%; $(Ph_4P)_2[Re_4Mo_2Se_8(CN)_6]^{2-}$ 1201.65, found 1201.59 (9%); $(Ph_4P)_2[Re_2Mo_4Se_8(CN)_6]^{2-}$ 1112.61, found 1112.55 (7%). IR (KBr): $\nu = 2091\text{ cm}^{-1}$ ($C\equiv N$); 1436, 1107, 995, 754, 721, 691, 526 (absorption bands for Ph_4P^+). UV-Vis (DMF): λ_{max} (ϵ) = 567 nm ($2360\text{ mol}^{-1}\cdot\text{dm}^3\cdot\text{cm}^{-1}$), 666 (748), 820 (738), 922 (776).

2.2.2 The solution-melt preparation of $K_6[Re_{3.6}Mo_{2.4}Se_8(CN)^{a-a}_{2/2}(CN)^a_4]$ and $K_5[Re_5MoSe_8(CN)_6] \cdot 11H_2O$

$K_6[Re_{3.6}Mo_{2.4}Se_8(CN)^{a-a}_{2/2}(CN)^a_4]$ (**5**). Compound **5** was obtained according to the procedure described for **1** at 800°C. Amount of reagents used: MoSe₂ (1.777 g, 7.00 mmol), ReSe₂ (2.409 g, 7.00 mmol), KCN (4.023 g, 61.92 mmol). The ampoule with reagents was heated for 14 days. After cooling, the ampoule was opened and the resulting product was washed with degassed water. The solution after washing turned orange-red and contained compound **6**. The obtained crystals of compound **5** were purified from MoSe₂ impurities by ultrasonic treatment in ethanol. Yield of **5**: 2.750 g. Crystals **5** isostructural to compound **1** were obtained. The ratio of heavy elements for crystals **5** according to the EDS found: K: Mo: Re: Se = 5.9: 3.6: 2.4: 8.4, calcd. K: Mo: Re: Se = 6.0 : 3.6 : 2.4 : 8.0.

$K_5[Re_5MoSe_8(CN)_6] \cdot 11H_2O$ (**6**). An aqueous solution from previous step was evaporated to a volume of 3 ml and slowly cooled, which led to the formation of a fine crystalline powder on the walls of the glass. The resulting precipitate was filtered, washed with ethanol and dried in air. Yield of **6**: 700 mg. Powder diffraction data showed that compound **6** is isostructural to **2**. The ratio of heavy elements according to the EDS for sample **6** found: K: Mo: Re: Se 6.3: 1.0: 5.0: 8.1, calcd. K: Mo: Re: Se = 5.0 : 1.0 : 5.0 : 8.0. IR (KBr): $\nu = 2095\text{ cm}^{-1}$ (C≡N). UV-Vis (H₂O): λ_{max} (ϵ) = 230 nm (50840 mol⁻¹·dm³·cm⁻¹), 477 (454).

2.2.3 Methatesis reaction for preparation of $(n\text{-Bu}_4\text{N})_4[Re_5MoSe_8(CN)_6]$

$(n\text{-Bu}_4\text{N})_4[Re_5MoSe_8(CN)_6]$ (**7**). 80 mg of compound **6** was dissolved in water and an aqueous solution of tetrabutylammonium bromide (150 mg in 10 ml) was added dropwise. An aqueous solution of 0.1 M HCl was added dropwise to the resulting solution until a precipitate formed. After the solution was completely bleached, the solution was decanted, the precipitate was washed with water, separated by centrifugation, dried in air and recrystallized from acetone. Yield of **7**: 75 mg (74%). Crystals suitable for single crystal X-ray diffraction were obtained by diffusion of pentane vapor into solution **7** in acetone. The ratio of heavy elements according to the EDS for crystals of **7** found: Re: Mo: Se = 4.9: 1.1: 7.4, calcd. Re: Mo: Se 5.0 : 1.0 : 8.0. Calculated for

$C_{70}H_{144}N_{10}Se_8MoRe_5$: C 30.03 H 5.19 N 5.01, C 30.01 H 5.11 N 4.95% was found. ESI-MS: (–, CH_2Cl_2): calculated on $((n-Bu)_4N)_2[Re_5MoSe_8(CN)_6]^{2-}$ 1150.32, found 1150.30 (100%); $((n-Bu)_4N)[Re_5MoSe_8(CN)_6]^{2-}$ 1029.16, found 1029.16 (65%); $[Re_5MoSe_8(CN)_6]^{3-}$ 605.34, found 605.36 (18%). IR (KBr): $\nu = 2108\text{ cm}^{-1}$ (CN), 2958, 2872, 1629, 1485, 1381, 1150, 883, 739 (absorption bands for $(CH_3(CH_2)_3)_4N^+$). UV-Vis (CH_3CN) λ_{max} (ϵ): 232 nm ($48560\text{ M}^{-1}\text{cm}^{-1}$), 464 (724), 518 (573), 562 (894), 665 (193), 957 (411).

2.2.4 Depolymerization of the polymer $K_6[Re_{3.6}Mo_{2.4}Se_8(CN)_6]^{a-}_{2/2}(CN)_4$ with the formation of soluble salts $Cat_n[Re_{3.6}Mo_{2.4}Se_8(CN)_6]$, Cat = K, Ph_4P^+

$K_5[Re_{3.6}Mo_{2.4}Se_8(CN)_6] \cdot 11H_2O$ (**8**). 2.600 g (1.35 mmol) of **5**, KCN (0.300 g, 4.62 mmol) was dissolved in 30 ml of water during stirring in air. The solution was evaporated to a volume of 10 ml and 30 ml of ethanol was added causing precipitation of **8**. Yield of **8**: 2.460 g (91%). The PXRD results showed that compound **8** is isostructural to **2**. The ratio of heavy elements according to the EDS for sample **8** found: K: Mo: Re: Se = 4.8: 2.4: 3.6: 8.1, calcd. 5.0 : 2.4 : 3.6: 8.0.

$(Ph_4P)_4[Re_{3.6}Mo_{2.4}Se_8(CN)_6] \cdot 2CH_3CN$ (**9**). Compound **9** was prepared analogously to **4**. Salt **8** (135 mg, 0.06 mmol) was dissolved in 10 ml of water and an aqueous solution of Ph_4PBr (200 mg, 0.48 mmol; 15 ml) was added. Yield of **9**: 180 mg (89%). The PXRD results showed that compound **9** is isostructural to **4**. The ratio of heavy elements according to the EDS for crystals **9** found: P: Re: Mo: Se = 4.3: 3.6: 2.4: 7.7, calcd. 4.0 : 3.6 : 2.4 : 8.0. ESI-MS: (–, CH_2Cl_2) m/z for $\{(Ph_4P)[Re_3Mo_3Se_8(CN)_6]\}^{2-}$ 987.054, found 987.037 (63%); for $\{(Ph_4P)[Re_4Mo_2Se_8(CN)_6]\}^{2-}$ 1032.077, found 1032.062 (100%); for $\{(Ph_4P)_2[Re_3Mo_3Se_8(CN)_6]\}^{2-}$ 1156.119, found 1156.103 (62%); for $\{(Ph_4P)_2[Re_4Mo_2Se_8(CN)_6]\}^{2-}$ 1201.642, found 1201.628 (98%). UV-Vis (DMF): λ_{max} (ϵ) = 564 nm ($2300\text{ mol}^{-1} \cdot \text{dm}^3 \cdot \text{cm}^{-1}$), 613 (986), 666 (682), 831 (821), 934 (830).

2.2.5 Separation of cluster anions $[\text{Re}_4\text{Mo}_2\text{Se}_8(\text{CN})_6]^{\text{n-}}$ and $[\text{Re}_3\text{Mo}_3\text{Se}_8(\text{CN})_6]^{\text{n-}}$ and their isolation as salts $\text{Cat}_n[\text{Re}_{6-x}\text{Mo}_x\text{Se}_8(\text{CN})_6]$, $\text{Cat} = \text{K}, \text{n-Bu}_4\text{N}^+$

$(\text{n-Bu}_4\text{N})_4[\text{Re}_4\text{Mo}_2\text{Se}_8(\text{CN})_6]$ (**10**). Compound **8** (2.000 g, 0.96 mmol) was dissolved in 20 ml of water. An aqueous solution of $\text{n-Bu}_4\text{NBr}$ (1.750 g, 5.45 mmol; 10 ml) was added dropwise to the resulting solution while stirring. When the reaction mixture is stirred for one hour, precipitation of **10** occurs, accompanied by an increase in the pH of the solution. The resulting precipitate was separated by filtration, washed with water, dried in air and recrystallized from acetonitrile. Yield of **10**: 1.206 g (93%). Crystals suitable for single crystal X-ray diffraction analysis were obtained by diffusion of THF vapor into acetonitrile solution of **10**. The ratio of heavy elements according to the EDS for crystals **10** found: Re: Mo: Se 3.9: 2.1: 8.3, calcd. 4.0 : 2.0 : 8.0. Calculated for $\text{C}_{70}\text{H}_{144}\text{N}_{10}\text{Se}_8\text{Mo}_2\text{Re}_4$: C 31.20 H 5.39 N 5.20, found C 30.86 H 5.41 N 5.03%. ESI-MS: ($^-$, CH_2Cl_2): calculated for $((\text{n-Bu})_4\text{N})_2[\text{Re}_4\text{Mo}_2\text{Se}_8(\text{CN})_5]^{2-}$ 1104.80, found 1104.79 (100%); $((\text{n-Bu})_4\text{N})[\text{Re}_4\text{Mo}_2\text{Se}_8(\text{CN})_6]^{2-}$ 983.65, found 983.64 (52%); $((\text{n-Bu})_4\text{N})[\text{Re}_4\text{Mo}_2\text{Se}_8(\text{CN})_5]^{2-}$ 970.65, found 970.64 (48%); $\{((\text{n-Bu})_4\text{N})_3[\text{Re}_4\text{Mo}_2\text{Se}_8(\text{CN})_6](\text{CH}_3\text{CO})\}^{2-}$ 1247.45, found 1247.42 (30%); $\{((\text{n-Bu})_4\text{N})_3[\text{Re}_4\text{Mo}_2\text{Se}_8(\text{CN})_6]\text{N}\}^{2-}$ 1232.94, found 1232.91 (20%). ^{77}Se NMR $[\text{D}_6]$ acetone, δ : 14 ppm, 297, 322, 495. IR (KBr): $\nu = 2106 \text{ cm}^{-1}$ (CN), 2962, 2871, 1627, 1481, 1381, 1151, 883 (absorption bands for $(\text{CH}_3(\text{CH}_2)_3)_4\text{N}^+$). UV-Vis (CH_3CN) λ_{max} (ϵ): 237 nm ($45960 \text{ M}^{-1}\text{cm}^{-1}$), 531 (1223), 562 (1856), 821 (780), 913 (759).

$\text{K}_4[\text{Re}_4\text{Mo}_2\text{Se}_8(\text{CN})_6]$ (**11**). 1 g (0.37 mmol) of compound **10** was dissolved in 30 ml of acetonitrile and a solution of KSCN in acetonitrile (500 mg, 2.57 mmol; 20 ml) was added dropwise. The precipitate was separated by decantation, washed several times with acetonitrile and dried in air. Yield of **11**: 650 mg (93%). The resulting sample was amorphous under PXRD. The ratio of heavy elements according to the EDS for **11** found: K: Re: Mo: Se = 3.7: 3.8: 2.2: 8.2, calcd. 4.0 : 4.0 : 2.0 : 8.0. UV-Vis (H_2O) λ_{max} (ϵ): 236 ($40394 \text{ M}^{-1}\text{cm}^{-1}$), 524 nm ($994 \text{ M}^{-1}\text{cm}^{-1}$), 564 (1587), 641 (473), 790 (666), 914 (624).

$\text{K}_5[\text{Re}_3\text{Mo}_3\text{Se}_8(\text{CN})_6] \cdot 11\text{H}_2\text{O}$ (**12**). The aqueous solution remained after the precipitation of **10** in the previous preparation steps was extracted with CH_2Cl_2 . The organic layer was

separated using a separatory funnel and evaporated. The product was dissolved in acetonitrile, a KSCN acetonitrile solution (300 mg, 3.1 mmol; 20 ml) was added dropwise, which caused an immediate precipitation. The resulting precipitate was separated by centrifugation, washed with acetonitrile, and then dried in air. Yield of **12**: 950 mg (97%). According to PXRD data, compound **12** is isostructural to **2**. The ratio of heavy elements according to the EDS for **12** found: K: Re: Mo: Se = 5.3: 3.0: 3.0: 8.2, calcd. 5.0 : 3.0 : 3.0 : 8.0. ^{77}Se NMR [D_2] water, δ : 172 ppm, 365. UV-Vis 238 nm, 548, 611, 785.

(n-Bu₄N)₄[Re₃Mo₃Se₈(CN)₆] (13) and (n-Bu₄N)₄[Re₃Mo₃Se₈(CN)₆]·3H₂O (13·3H₂O). 80 mg (0.04 mmol) of compound **12** was dissolved in water and an aqueous solution of n-Bu₄NBr (170 mg, 0.53 mmol; 5 ml) was added. Then, the obtained product was extracted in CH₂Cl₂. The organic layer was separated using a separatory funnel. The resulting solution had a bright vinous color. A small amount of a iodine solution in CH₂Cl₂ was added dropwise to the resulting solution until the color of the solution became dark blue. The process was monitored by thin layer chromatography. After a complete color change of the solution, the solvent was evaporated until a blue crystalline powder formed. The resulting powder was washed with water, dried in air and recrystallized from acetone. Yield 45 mg (43%). Crystals suitable for single crystal XRD were obtained by diffusion of pentane vapor into a solution of product in acetone. Two types of crystals were found: **13** and **13·3H₂O**, containing solvate water molecules. Compound **13** is isostructural to compounds **10** and **7**. The PXRD analysis showed the presence of two phases corresponding to those obtained from SC XRD data. Upon recrystallization of the dried powder, a single-phase sample of **13** is formed. The ratio of heavy elements for crystals **13** found: Re: Mo: Se = 3.0: 3.0: 7.4, calcd. 3.0 : 3.0 : 8.0. Calculated for C₇₀H₁₄₄N₁₀Se₈Mo₃Re₃ C 32.28 H 5.57 N 5.38, found C 31.75 H 5.46 N 5.24. ESI-MS: (-, CH₂Cl₂) calculated for {((n-Bu)₄N)₂[Re₃Mo₃Se₈(CN)₆]}²⁻ 1059.27 found 1059.26 (100%); {((n-Bu)₄N)[Re₃Mo₃Se₈(CN)₆]}²⁻ 938.11 found 938.13 (86%); {((n-Bu)₄N)₃[Re₃Mo₃Se₈(CN)₅]}¹⁻ 2362.83 found 2362.80 (30%); [Re₃Mo₃Se₈(CN)₅]³⁻ 544.66 found 544.65 (29%). IR (KBr): ν = 2106 cm⁻¹ (CN), 2961, 2874, 1632, 1483, 1381, 1151, 883 (absorption bands for (CH₃(CH₂)₃)₄N⁺). UV-Vis (CH₃CN) λ_{max} (ϵ): 244 nm (33960 M⁻¹cm⁻¹), 563 (1904), 608 (1329), 663 (757), 903 (592).

2.2.6 Preparation of coordination polymers from $[\text{Re}_3\text{Mo}_3\text{Se}_8(\text{CN})_6]^{5-}$ cyanocluster and transition metal ammine complexes

$\{[\text{Cd}(\text{NH}_3)_5]_2(\text{Cd}(\text{NH}_3)_4)_3[\text{Re}_3\text{Mo}_3\text{Se}_8(\text{CN})_6]_2\} \cdot 5\text{H}_2\text{O}$ (**14**). Crystals of compound **14** were obtained by layering an aqueous ammonia solution (12%, 2 ml) of cadmium acetate (8 mg, 0.034 mmol) in an aqueous ammonia solution (6%, 2 ml) of compound **2** (8 mg, 0.004 mmol) in a thin tube with a neck. The rod-shaped crystals of compound **14** were formed on the walls of the tube within a few days. Crystals for SC XRD were taken directly from the reaction mixture. The resulting crystals turned out to be unstable in air and rapidly lost crystallinity. The registration of the diffraction pattern was impossible due to the amorphization of the sample. The ratio of heavy elements according to the EDS for crystals **14** found: Cd: Re: Mo: Se = 2.6: 3.1: 2.9: 7.5, calcd. 2.5 : 3.0 : 3.0 : 8.0. IR (KBr): $\nu = \nu$ (N–H) 3532 cm^{-1} , 3329, 3246 ν (C \equiv N) 2083; δ_d (NH₃) 1732, 1591, 1466; δ_s (NH₃) 1200; ρ_r (NH₃) 582; ν (M–N) 390.

$\{[\text{Cd}(\text{NH}_3)_4]_3\text{Re}_3\text{Mo}_3\text{Se}_8(\text{CN})_6\}$ Cl (**15**). An aqueous ammonia solution (25%, 4 ml) of cadmium acetate (25 mg, 0.108 mmol) was mixed with an aqueous solution of compound **2** (80 mg, 0.039 mmol) and KCl (120 mg, 1.624 mmol) in 7 ml of water. Then the solution was left in the air for several hours, and a fine crystalline precipitate **15** formed. The solution over the precipitate was decanted, the precipitate was washed with water, ethanol and dried in air. Yield of **15**: 43 mg (50%). Single crystals of compound **15** were obtained by layering two solutions in a thin tube, similarly to the synthesis of compound **14**, instead of cadmium acetate, cadmium chloride (6 mg, 0.033 mmol) was used. Within a few days, two types of crystals formed on the walls of the tube: rod-shaped crystals of compound **14** and prismatic crystals of compound **15**. Prismatic crystals for SC XRD were taken directly from the reaction mixture. The ratio of heavy elements according to the EDS results for crystals **15** found: Cd: Re: Mo: Se: Cl = 3.1: 3.2: 2.8: 8.3: 0.9, calcd. 3.0 : 3.0 : 3.0 : 8.0 : 1.0. IR (KBr): $\nu = \nu$ (N–H) 3555 cm^{-1} , 3435, 3331, 3254, 3152; ν (C \equiv N) 2083; δ_d (NH₃) 1639, 1585; δ_s (NH₃) 1190, 1150; ρ_r (NH₃) 579; ν (M–N) 384.

$\{[\text{Cd}(\text{NH}_3)_4]_3\text{Re}_3\text{Mo}_3\text{Se}_8(\text{CN})_6\}$ Br (**16**). Compound **16** was obtained analogously to **15**. Instead of KCl, KBr (120 mg, 1.018 mmol) was used. Yield of **16**: 63 mg (72%). Crystals of compound **16** were obtained similarly to crystals of **15**; instead of cadmium chloride,

an aqueous ammonia solution (12%, 2 ml) of cadmium acetate (8 mg, 0.035 mmol) and KBr (20 mg, 0.169 mmol) were used. Prismatic crystals formed on the walls of the tube for several days. The ratio of heavy elements according to the EDS results for crystals **16** found: Cd: Re: Mo: Se: Br = 3.3: 2.8: 3.2: 8.5: 1.0, calcd. 3.0 : 3.0 : 3.0 : 8.0 : 1.0. IR (KBr): $\nu = \nu$ (N–H) 3560 cm^{-1} , 3427, 3331, 3146; ν (C \equiv N) 2083; δ_d (NH₃) 1585; δ_s (NH₃) 1186, 1146; ρ_r (NH₃) 577; ν (M–N) 386.

$\{[Cd(NH_3)_4]_3Re_3Mo_3Se_8(CN)_6\}$ **I** (**17**). Compound **17** was obtained analogously to **15**; instead of potassium chloride, potassium iodide (150 mg, 0.904 mmol) was used. Yield of **17**: 68 mg (76%). Crystals of compound **17** were obtained analogously to **15**; instead of a solution of cadmium chloride, an aqueous ammonia solution (12%, 2 ml) of cadmium acetate (8 mg, 0.035 mmol) and KI (18 mg, 0.109 mmol) were used. Prismatic crystals of compound **17** grew on the walls of the tube for several days. The ratio of heavy elements by means of EDS for crystals **17** found: Cd: Re: Mo: Se: I = 2.7: 3.2: 2.8: 8.3: 0.8, calcd. 3.0 : 3.0 : 3.0 : 8.0 : 1.0. IR (KBr): $\nu = \nu$ (N–H) 3570 cm^{-1} , 3335, 3250, 3148; ν (C \equiv N) 2087; δ_d (NH₃) 1584; δ_s (NH₃) 1180, 1148; ρ_r (NH₃) 571; ν (M–N) 384.

$\{[Cd(NH_3)_4]_2[Cd(NH_3)_3(NCS)]Re_3Mo_3Se_8(CN)_6\}$ (**18**). Compound **18** was obtained analogously to **15**; instead of potassium chloride, potassium thiocyanate (100 mg, 1.032 mmol) was used. Yield of **18**: 68 mg (76%). Crystals of compound **18** were obtained similarly to crystals **15**; instead of a solution of cadmium chloride, an aqueous ammonia solution (12%, 2 ml) of cadmium acetate (8 mg, 0.035 mmol) and KSCN (11 mg, 0.109 mmol) were used. Prismatic crystals of compound **18** grew on the walls of the tube for several days. The ratio of heavy elements according to EDS for crystals **18** found: Cd: Re: Mo: Se: S = 3.3: 3.1: 2.9: 8.6: 1.1, calcd. 3.0 : 3.0 : 3.0 : 8.0 : 1.0. IR (KBr): $\nu = \nu$ (N–H) 3570 cm^{-1} , 3341, 3256; ν (C \equiv N) 2091; δ_d (NH₃) 1585; δ_s (NH₃) 1193; ρ_r (NH₃) 582; ν (M–N) 386.

$[Co(NH_3)_6]_4[\{Co(NH_3)_2\}\{Re_3Mo_3Se_8(CN)_6\}_2] \cdot 15H_2O$ (**19**). 2 ml of an aqueous ammonia solution containing 7.0 mg CoCl₂·6H₂O (0.03 mmol) with an ammonia concentration of 12% (wt.%) Was layered on 2 ml of an aqueous ammonia solution of compound **2** (12.0 mg, 0.006 mmol) (6 wt.% of ammonia) in a thin glass tube with a neck. The tube was tightly closed and left for a week at room temperature. During this time, crystals of com-

pound **19** grew on the walls of the tube. Crystals for single crystal X-ray diffraction studies were taken directly from the reaction mixture. The ratio of heavy elements according to EDS for compound **19** found: Co: Re: Mo: Se = 2.6: 3.1: 2.9: 8.3, calcd. 2.5 : 3.0 : 3.0 : 8.0. Registration of the diffraction pattern was not possible due to the amorphization of the sample.

$[Ni(NH_3)_6]_4[\{Ni(NH_3)_2\} \{Re_3Mo_3Se_8(CN)_6\}_2] \cdot 15H_2O$ (**20**). Compound **20** was obtained analogously to **19**, using an aqueous ammonia solution containing 8.0 mg of $NiCl_2 \cdot 6H_2O$ (0.03 mmol). Crystals for single crystal X-ray diffraction studies were taken from the reaction mixture. The ratio of heavy elements according to EDS for compound **20** found: Ni: Re: Mo: Se = 2.7: 3.1: 2.9: 8.2, calcd. 2.5 : 3.0 : 3.0 : 8.0. The registration of the diffraction pattern was impossible due to the amorphization of the sample.

2.2.7 The ligand exchange reactions of $[Re_3Mo_3Se_8(CN)_6]^{5-}$ and $[Re_4Mo_2Se_8(CN)_6]^{4-}$: formation of $[Re_{6-x}Mo_xSe_8L_6]$, L = *tbp*, Ph_3P

$[Re_3Mo_3Se_8(tbp)_6]$ (**21**). The solvothermal reaction of compound **2** (60 mg, 0.030 mmol) and 4-*tert*-butylpyridine (300 μ l, 2.222 mmol) in 2 ml of a mixture of water and acetonitrile (1:3 by volume) at 160°C for 96 hours led to the formation of dark rod-shaped crystals. The crystals were washed on a glass filter with water and acetonitrile and dried in air. Yield of **21**: 40 mg (59%). The registration of the diffraction pattern was impossible due to the amorphization of the sample. The ratio of heavy elements according to EDS for crystals **21** found: Re: Mo: Se: S = 3.1: 2.9: 8.3, calcd. 3.0 : 3.0 : 8.0. Calculated for $C_{54}H_{78}Mo_3N_6Re_3Se_8$ C 28.33 H 3.43 N 3.67, found C 27.17 H 3.43 N 3.56. IR (KBr): ν = [py] 3068 cm^{-1} 3037, 1611, 1494, 1274, 1200 1226m 1067, 1019, 847, 825, 748, 725 [t-Bu] 2962, 2901, 2868, 1413, 1365, 567.

$[Re_4Mo_2Se_8(tbp)_6]$ (**22**). Compound **22** was obtained analogously to **21**; in this case, compound **11** (63 mg, 0.033 mmol) was used as a cluster-containing reagent. Yield of **22**: 38 mg (50%). The registration of the powder diffraction pattern was impossible due to the amorphization of the sample. The ratio of heavy elements according to EDS for crystals **22** found: Re: Mo: Se = 3.8: 2.2: 7.9, calcd. 4.0 : 2.0 : 8.0. Calculated for $C_{54}H_{78}Mo_2N_6Re_4Se_8$ C 27.25 H 3.30 N 3.53, found C 26.93 H 2.92 N 3.61. IR (KBr): ν =

[py] 3069 cm⁻¹ 3040, 1612, 1493, 1274, 1226, 1200, 1068, 1021, 845, 826, 749, 723 [t-Bu] 2962, 2902, 2867, 1413, 1365, 1328, 568.

[Re₄Mo₂Se₈(PPh₃)₆] (**23**). 63 mg (0.033 mmol) of compound **11** was dissolved in 2 ml of water, then a solution of PPh₃ (120 mg, 0.458 mmol) in 3 ml of DMF was added. The resulting mixture was heated in a reactor at 160°C for 4 days. The obtained crystals of compound **23** were washed with water, DMF and ethanol, and dried in air. Yield of **23**: 40 mg (35%). The registration of the powder diffraction pattern was impossible due to the amorphization of the sample. The ratio of heavy elements according to EDS for crystals **23** found: Re: Mo: Se: P = 3.8: 2.2: 7.5: 6.0, calcd. 4.0 : 2.0 : 8.0 : 6.0. Calculated for C₁₀₈H₉₀P₆Se₈Mo₂Re₄ C 41.28 H 2.89, found C 40.94 H 2.83. IR (KBr): ν = [PPh₃] 3048 cm⁻¹, 1479, 1431, 1088, 847, 741, 700, 519.

Chapter 3: Results and Discussion

3.1 Preparation of heterometallic cluster complexes $[\text{Re}_3\text{Mo}_3\text{Se}_8(\text{CN})_6]^{n-}$, $[\text{Re}_4\text{Mo}_2\text{Se}_8(\text{CN})_6]^{n-}$ and $[\text{Re}_5\text{MoSe}_8(\text{CN})_6]^{n-}$ ($n = 4, 5$) as species with well-defined composition

3.1.1 Synthetic route from solid state polymer $\text{K}_6[\text{Re}_3\text{Mo}_3\text{Se}_8(\text{CN})^{a-a}_{2/2}(\text{CN})^a_4]$ to soluble species and their mass-spectrometry investigation

The reaction of a mixture of molybdenum and rhenium selenides with an excess of potassium cyanide at 630°C leads to the formation of octahedral crystals of compound $\text{K}_6[\text{Re}_3\text{Mo}_3\text{Se}_8(\text{CN})^{a-a}_{2/2}(\text{CN})^a_4]$ (**1**) (Figure 3.1). A yield higher than 90% was obtained with an experiment lasting about four weeks.

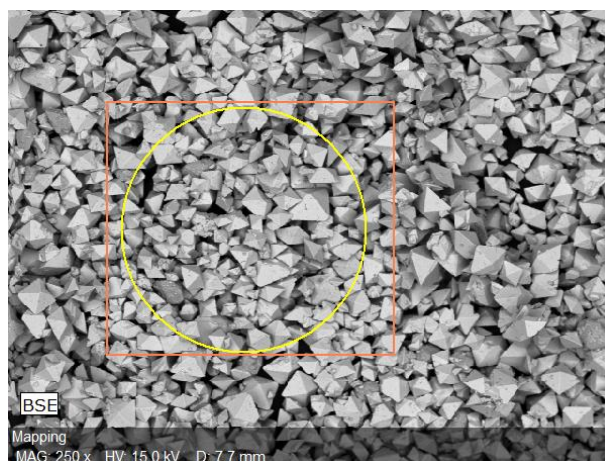
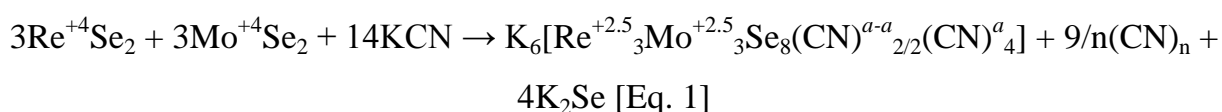


Figure 3.1: The photo image of the crystals of compound $\text{K}_6[\text{Re}_3\text{Mo}_3\text{Se}_8(\text{CN})^{a-a}_{2/2}(\text{CN})^a_4]$ (**1**).

During the interaction of metal diselenides with KCN, the formation of compound **1** occurs according to the expected reaction equation:



The reducing agent is a cyanide ion, which forms gaseous cyanogen (CN)₂ or an amorphous solid paracyanogen (CN)_n [185]. According to SC X-ray diffraction data, compound **1** has a chain-like polymeric structure. The crystals of polymer **1** are stable under an inert atmosphere and do not dissolve in oxygen-free water. Exposure to oxygen in air leads to the destruction of the polymer structure, which is accompanied by an evolution of the powder diffraction pattern of the sample (Figure 3.2).

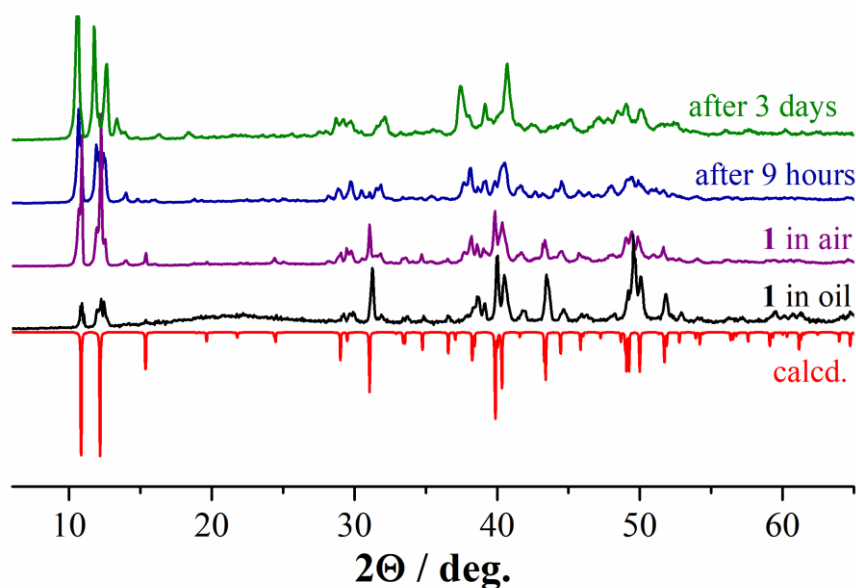
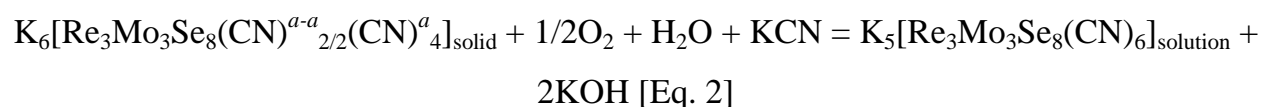


Figure 3.2: Powder XRD patterns for the sample of the compound **1** under exposure in air.

Compound **1** dissolves in air in an aqueous KCN solution giving a vinous solution. After evaporation of the solution and precipitation with ethanol, the compound K₅[Re₃Mo₃Se₈(CN)₆]·11H₂O (**2**) was isolated. According to X-ray diffraction data, the obtained compound is an ionic salt of the cluster anion [Re₃Mo₃Se₈(CN)₆]⁵⁻ and has high solubility in water. The dissolution of the polymer is accompanied by a two-electron oxidation of the cluster core, according to the equation:



The precipitation of tetraphenylphosphonium salt of [Re₃Mo₃Se₈(CN)₆]⁵⁻ and subsequent crystallization of the product from acetonitrile leads to one-electron oxidation of the cluster with the formation of salt (Ph₄P)₄[Re₃Mo₃Se₈(CN)₆]·2CH₃CN (**4**), according to the equations:

1. $\text{K}_5[\text{Re}_3\text{Mo}_3\text{Se}_8(\text{CN})_6]_{\text{solution}} + 5\text{Ph}_4\text{PBr} = (\text{Ph}_4\text{P})_5[\text{Re}_3\text{Mo}_3\text{Se}_8(\text{CN})_6]\downarrow + 5\text{KBr}$ [Eq. 3a]
2. $(\text{Ph}_4\text{P})_5[\text{Re}_3\text{Mo}_3\text{Se}_8(\text{CN})_6] + 1/4\text{O}_2 + 1/2\text{H}_2\text{O} = (\text{Ph}_4\text{P})_4[\text{Re}_3\text{Mo}_3\text{Se}_8(\text{CN})_6] + \text{Ph}_4\text{POH}$ [Eq. 3b]

The simplified reaction scheme describing the preparation of heterometallic clusters starting from chain polymeric phase to soluble molecular complexes is depicted in Figure 3.3. The crystal structure features of polymer $\text{K}_6[\text{Re}_3\text{Mo}_3\text{Se}_8(\text{CN})^{a-a}_{2/2}(\text{CN})^a_4]$ (**1**) and products of its depolymerization, salts **2-4** are discussed in details below in the Sections 4.1 and 4.2 of Chapter 4, respectively.

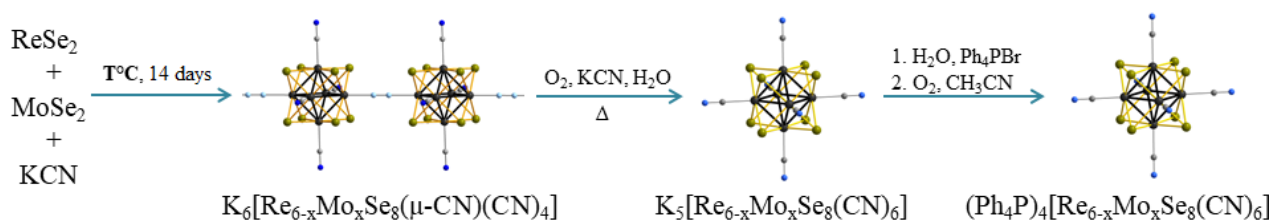


Figure 3.3: The simplified reaction scheme of the preparation of heterometallic clusters ($x = 3$, $T = 630^\circ\text{C}$).

Compound **4**, containing a cluster with 21 CSEs is characterized by a paramagnetic signal with a g -factor of 2.430 in the EPR spectrum (Figure 3.4 a). The obtained value of the g -factor is close to the previously published values for the homometallic cluster compounds of rhenium $[\text{Re}_6\text{Q}_8\text{L}_6]^{3-}$ ($\text{Q} = \text{S}, \text{Se}, \text{Te}$; $\text{L} = \text{CN}, \text{Cl}, \text{Br}$; $g = 2.44\text{--}2.56$) [186, 187]. Oxidation is accompanied by a change in the UV-Vis spectra and the color of the solution. Electronic absorption spectra and photographs of dilute solutions of compounds **2** and **4** are shown in Figure 3.4 b.

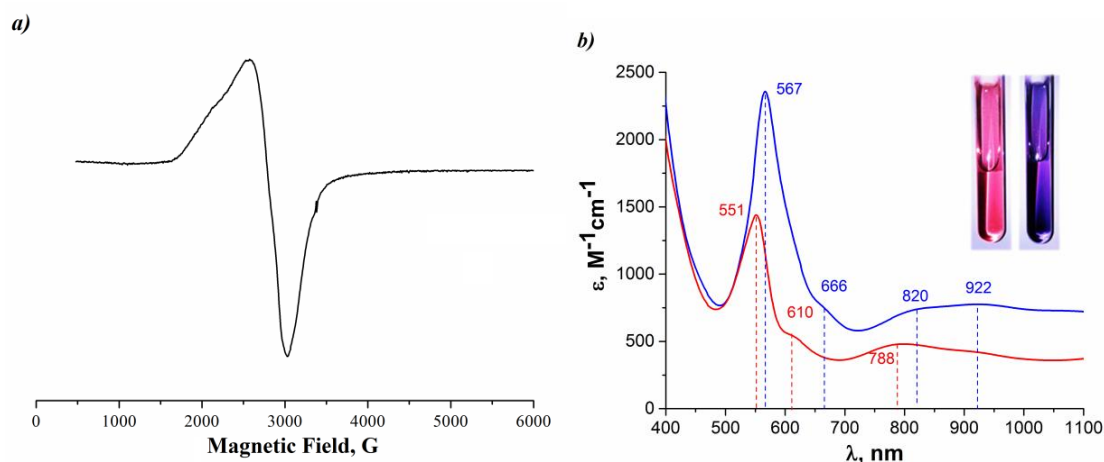


Figure 3.4: The EPR spectra for crystals of the compound **4** at 77K ($g = 2.430$) (a) UV-Vis spectra for the solution of **2** in water (red line) and **4** in DMF (blue line) (b).

The negative ion mass spectrum of a solution of compound $(\text{Ph}_4\text{P})_4[\text{Re}_3\text{Mo}_3\text{Se}_8(\text{CN})_6]$ (**4**) in a DMF/ CH_3CN mixture contains a large number of signals corresponding to adducts of cluster anions with tetraphenylphosphonium cations (Figure 3.5).

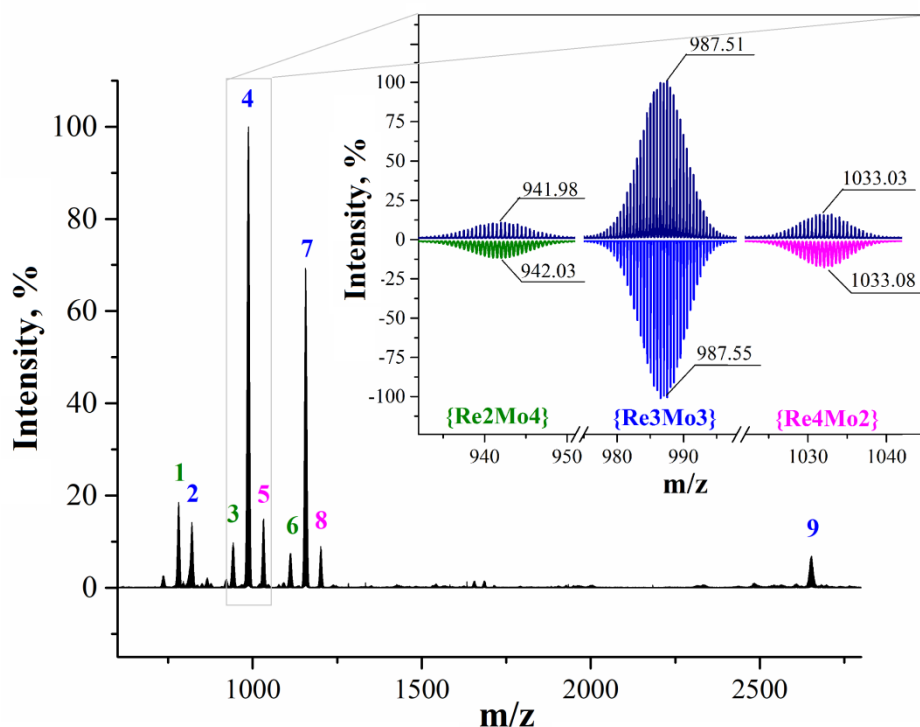


Figure 3.5: Common view of the mass-spectra of negative ions of compound **4** in a mixture of DMF/ CH_3CN . (1 – $\{\text{H}[\text{Re}_2\text{Mo}_4\text{Se}_8(\text{CN})_6]\}^{2-}$, 2 – $\{\text{H}[\text{Re}_3\text{Mo}_3\text{Se}_8(\text{CN})_6]\}^{2-}$, 3 – $\{(\text{Ph}_4\text{P})[\text{Re}_2\text{Mo}_4\text{Se}_8(\text{CN})_6]\}^{2-}$, 4 – $\{(\text{Ph}_4\text{P})[\text{Re}_3\text{Mo}_3\text{Se}_8(\text{CN})_6]\}^{2-}$, 5 – $\{(\text{Ph}_4\text{P})[\text{Re}_4\text{Mo}_2\text{Se}_8(\text{CN})_6]\}^{2-}$, 6 – $\{(\text{Ph}_4\text{P})_2[\text{Re}_2\text{Mo}_4\text{Se}_8(\text{CN})_6]\}^{2-}$, 7 – $\{(\text{Ph}_4\text{P})_2[\text{Re}_3\text{Mo}_3\text{Se}_8(\text{CN})_6]\}^{2-}$, 8 – $\{(\text{Ph}_4\text{P})_2[\text{Re}_4\text{Mo}_2\text{Se}_8(\text{CN})_6]\}^{2-}$, 9 – $\{(\text{Ph}_4\text{P})_3[\text{Re}_3\text{Mo}_3\text{Se}_8(\text{CN})_6]\}^{1-}$). Upper right corner – enlarged fragment of the spectra with calculated isotopic distribution of the corresponded signals.

In the process of ionization, one-electron oxidation of cluster anions partially occurs; therefore, some signals correspond to cluster anions with a 3- charge. The most intense signals relate to the anion of the composition $[\text{Re}_3\text{Mo}_3\text{Se}_8(\text{CN})_6]^{4-/3-}$. An enlarged fragment of the mass spectrum in Figure 3.5 evidences the signal with the highest intensity that corresponds to the adduct $\{(\text{Ph}_4\text{P})[\text{Re}_3\text{Mo}_3\text{Se}_8(\text{CN})_6]\}^{2-}$. It also contains signals of lower intensity corresponding to adducts of the composition $\{(\text{Ph}_4\text{P})[\text{Re}_4\text{Mo}_2\text{Se}_8(\text{CN})_6]\}^{2-}$ and $\{(\text{Ph}_4\text{P})[\text{Re}_2\text{Mo}_4\text{Se}_8(\text{CN})_6]\}^{2-}$. The distance between single signals in the distribution for adducts (except 9) is 0.5 Da, which corresponds to an adduct charge of 2–. The results of mass spectrometry show that, despite the fact that the ratio of Re / Mo in compound **4**

according to the results of EDS and SC XRD is close to 1/1, solution of **4** contains a mixture of cluster anions $[\text{Re}_{6-x}\text{Mo}_x\text{Se}_8(\text{CN})_6]^{4-}$ with different composition of the core, $x = 2, 3, 4$. According to estimation made on the basis of signal intensities in the mass spectrum, the content of $[\text{Re}_4\text{Mo}_2\text{Se}_8(\text{CN})_6]^{4-}$ and $[\text{Re}_2\text{Mo}_4\text{Se}_8(\text{CN})_6]^{4-}$ anions in the sample is about 10 and 15%, respectively.

According to XRD data, compounds **1–4** were single-phase. Based on the available information on their actual composition, it can be concluded that these phases are solid solutions in which cluster anions having the same charge but different core composition co-crystallize. The $[\text{Re}_2\text{Mo}_4\text{Se}_8(\text{CN})_6]^{4-}$ and $[\text{Re}_4\text{Mo}_2\text{Se}_8(\text{CN})_6]^{4-}$ anions contain an even number of electrons and are diamagnetic; therefore, paramagnetic signal of **4** belongs to the cluster anion $[\text{Re}_3\text{Mo}_3\text{Se}_8(\text{CN})_6]^{4-}$ (Table 3.1).

Table 3.1: The CSEs numbers of heterometallic anions $[\text{Re}_{6-x}\text{Mo}_x\text{Se}_8(\text{CN})_6]^{4-}$ $x = 2, 3, 4$

| Anion | $[\text{Re}_2\text{Mo}_4\text{Se}_8(\text{CN})_6]^{4-}$ | $[\text{Re}_3\text{Mo}_3\text{Se}_8(\text{CN})_6]^{4-}$ | $[\text{Re}_4\text{Mo}_2\text{Se}_8(\text{CN})_6]^{4-}$ |
|-------------|---|---|---|
| CSEs number | 20 | 21 | 22 |

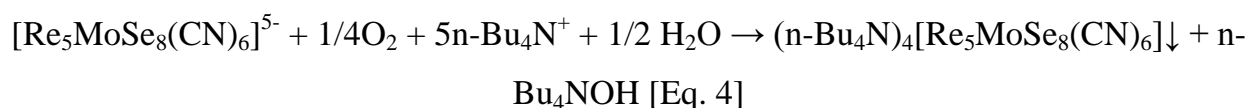
The octahedral cluster core is formed at the stage of high-temperature synthesis and does not collapse under mild conditions. This statement is supported by close Re / Mo ratios according to the EDS results of polymer **1** and its oxidation products in solution reactions (compounds **2–4**).

Experiments were conducted to investigate the influence of the conditions of the solution-melt synthesis stage on the ratio of rhenium and molybdenum in the resulting products. According to EDS and high resolution mass spectrometry, a change in the ratio of MoSe_2 and ReSe_2 in the initial load does not significantly affect the composition of the polymer and its oxidation products in solution. Otherwise, an increase in the temperature of preparation from 630°C to 800°C leads to the increase of the rhenium content in the resulting crystals of the polymeric phase $\text{K}_6[\text{Re}_{6-x}\text{Mo}_x\text{Se}_8(\text{CN})^{a-a}_{2/2}(\text{CN})^a_4]$. It reaches a maximum in $\text{K}_6[\text{Re}_{3.6}\text{Mo}_{2.4}\text{Se}_8(\text{CN})^{a-a}_{2/2}(\text{CN})^a_4]$ (**5**) obtained at 800°C. In this case, a certain amount of unreacted MoSe_2 remained in the reaction mixture. The detailed comparison of the interatomic distances and metal site occupancy factors of

$\text{K}_6[\text{Re}_3\text{Mo}_3\text{Se}_8(\text{CN})^{a-a}_{2/2}(\text{CN})^a_4]$ (**1**) and $\text{K}_6[\text{Re}_{3.6}\text{Mo}_{2.4}\text{Se}_8(\text{CN})^{a-a}_{2/2}(\text{CN})^a_4]$ (**5**) can be found below in the Section 4.1 in Chapter 4.

Another cluster product is formed during the reaction at 800°C in addition to polymer $\text{K}_6[\text{Re}_{3.6}\text{Mo}_{2.4}\text{Se}_8(\text{CN})^{a-a}_{2/2}(\text{CN})^a_4]$ (**5**). This product can be easily separated from the crystals of polymer **5** by washing with degassed water, giving orange solution. Upon evaporation of the solution, a salt $\text{K}_5[\text{Re}_5\text{MoSe}_8(\text{CN})_6]$ (**6**) was isolated. Compound **6** contains rhenium and molybdenum in a ratio of 5/1 according to the results of EDS. According to X-ray powder diffraction data, salt **6** is isostructural to salt **2** (Figure S2 in the Supplementary).

When an excess of $n\text{-Bu}_4\text{NBr}$ is added to the $\text{K}_5[\text{Re}_5\text{MoSe}_8(\text{CN})_6]$ aqueous solution in air, the cluster is oxidized with atmospheric oxygen and precipitates as $(n\text{-Bu}_4\text{N})_4[\text{Re}_5\text{MoSe}_8(\text{CN})_6]$ (**7**), according to equation:



Mass spectrometric analysis of the solution of compound **7** revealed the presence of adducts of the $[\text{Re}_5\text{MoSe}_8(\text{CN})_6]^{4-}$ anion with tetrabutylammonium cations (Figure 3.6 a). No adducts of cluster anions of a different composition were found. The powder pattern of the sample of compound **7** is shown in Figure 3.6 b.

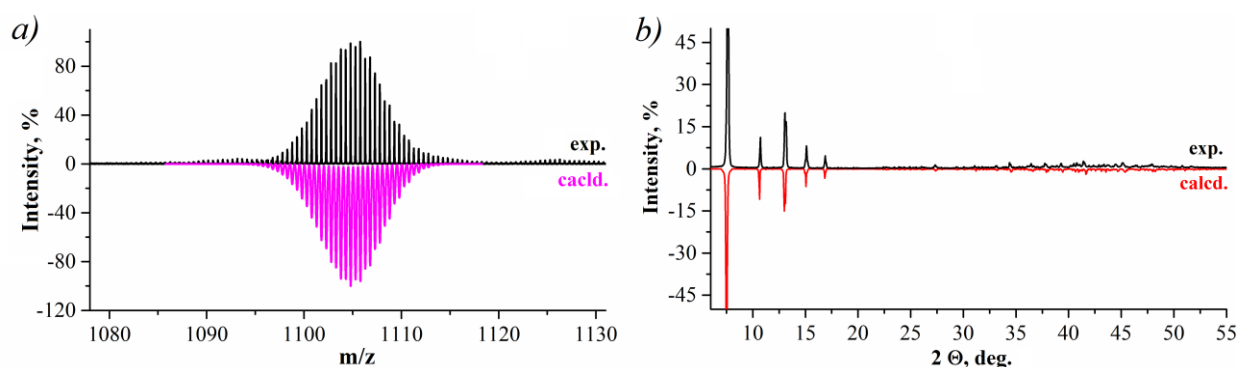


Figure 3.6: The fragment of the mass-spectra of negative ions of the compound **7** in CH_2Cl_2 in comparison with theoretical isotopic distribution, the signal corresponds to the adduct $\{(\text{Bu}_4\text{N})_2[\text{Re}_5\text{MoSe}_8(\text{CN})_6]\}^{2-}$ (a); powder XRD pattern for compound **7** (recorded, black vs calculated, red) (b).

$\text{K}_6[\text{Re}_{6-x}\text{Mo}_x\text{Se}_8(\text{CN})^{a-a}_{2/2}(\text{CN})^a_4]$ polymers obtained at 700 and 800°C were subjected to oxidative depolymerization and cation exchange reactions, according to the scheme in Figure 3.3, leading to the formation of tetraphenylphosphonium salts $(\text{Ph}_4\text{P})_4[\text{Re}_{6-x}\text{Mo}_x\text{Se}_8(\text{CN})_6]\cdot 2\text{CH}_3\text{CN}$ ($x \approx 2.4\text{--}2.5$), isostructural to compound **4**. The ratio of cluster anions with different core compositions in solutions of the salts was studied by high resolution mass spectrometry (Figure 3.7). It was shown that an increase in the temperature of the solution–melt synthesis leads to an increase in the content of the cluster with the $\{\text{Re}_4\text{Mo}_2\text{Se}_8\}$ core and a decrease in the content of the cluster with the $\{\text{Re}_2\text{Mo}_4\text{Se}_8\}$ core.

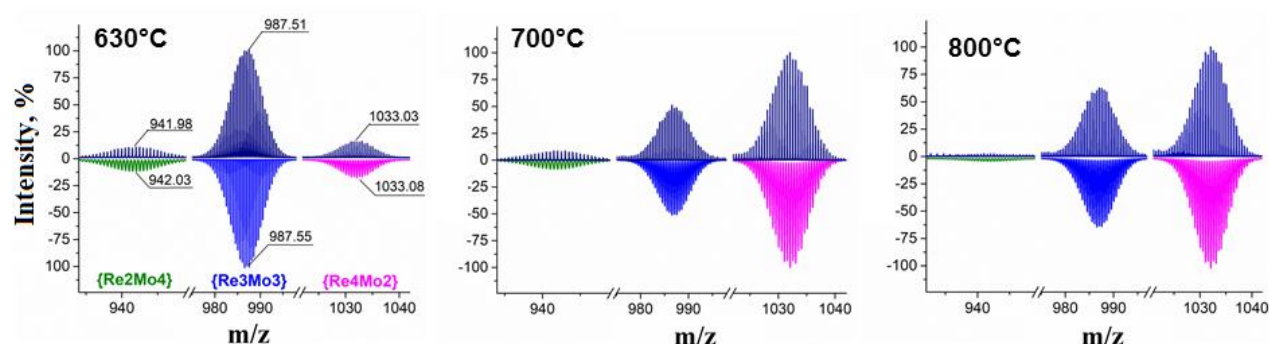


Figure 3.7: The fragments of mass spectra of negative ions of salts $(\text{Ph}_4\text{P})_4[\text{Re}_{6-x}\text{Mo}_x\text{Se}_8(\text{CN})_6]$ in $\text{CH}_3\text{CN}/\text{DMF}$. The temperature of the high temperature stage is indicated in the upper left part of the picture.

Thus, the ionic salts $\text{K}_5[\text{Re}_{3.6}\text{Mo}_{2.4}\text{Se}_8(\text{CN})_6]$ (**8**) and $(\text{Ph}_4\text{P})_4[\text{Re}_{3.6}\text{Mo}_{2.4}\text{Se}_8(\text{CN})_6]\cdot 2\text{CH}_3\text{CN}$ (**9**) (obtained from polymer **5** as described in Figure 3.3) contain the cluster anions $[\text{Re}_4\text{Mo}_2\text{Se}_8(\text{CN})_6]^{n-}$ and $[\text{Re}_3\text{Mo}_3\text{Se}_8(\text{CN})_6]^{n-}$. Compound **8** was further used to isolate these anions as individual compounds.

3.1.2 The separation of the cluster anions $[\text{Re}_4\text{Mo}_2\text{Se}_8(\text{CN})_6]^{n-}$ and $[\text{Re}_3\text{Mo}_3\text{Se}_8(\text{CN})_6]^{n-}$ from the mixture and their isolation as salts $\text{Cat}_n[\text{Re}_{6-x}\text{Mo}_x\text{Se}_8(\text{CN})_6]$, $\text{Cat} = \text{K}, \text{n-Bu}_4\text{N}^+$

It was found experimentally that when an excess of tetrabutylammonium bromide is added in air to an aqueous solution of $\text{K}_5[\text{Re}_{3.6}\text{Mo}_{2.4}\text{Se}_8(\text{CN})_6]$ (**8**), the salt $(\text{n-Bu}_4\text{N})_4[\text{Re}_4\text{Mo}_2\text{Se}_8(\text{CN})_6]$ (**10**) is precipitated from the solution. The mass spectrum of the solution of the obtained salt in CH_2Cl_2 contains adducts of the $[\text{Re}_4\text{Mo}_2\text{Se}_8(\text{CN})_6]^{4-}$ cluster anion with tetrabutylammonium cations (Figure 3.8 a). No adducts of other anion-

ic complexes were found. According to powder XRD data, the resulting product is single-phase (Figure 3.8 b).

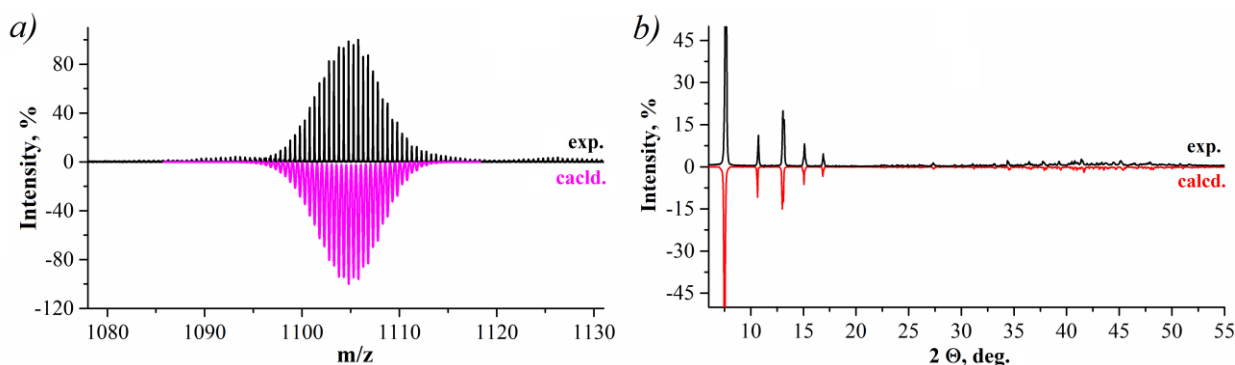
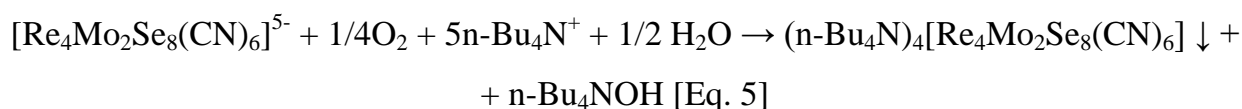


Figure 3.8: The fragment of the mass spectra of negative ions of the compound **10** in CH_2Cl_2 , the signal corresponds to the adduct $\{(\text{Bu}_4\text{N})_2[\text{Re}_4\text{Mo}_2\text{Se}_8(\text{CN})_6]\}^{2-}$ (a); powder XRD pattern for **10** (recorded, black vs calculated, red) (b).

Compound **10** is the ionic salt of the cluster anion $[\text{Re}_4\text{Mo}_2\text{Se}_8(\text{CN})_6]^{4-}$ and $n\text{-Bu}_4\text{N}^+$ cations. A change in the charge of the cluster anion from 5^- for a mixture of cluster anions in the initial solution to 4^- indicates an one-electron oxidation reaction. It was found that the pH of the solution after precipitation of salt **10** increases. The expected reaction proceeds according to the equation:



The evolution of this reaction depends on the pH of the solution. During the experiments, it was shown that the complete precipitation of the $[\text{Re}_4\text{Mo}_2\text{Se}_8(\text{CN})_6]^{4-}$ cluster occurs in the pH range of 7–9. The cluster anion $[\text{Re}_3\text{Mo}_3\text{Se}_8(\text{CN})_6]^{5-}$ under these experimental conditions remains in solution (Figure 3.9).

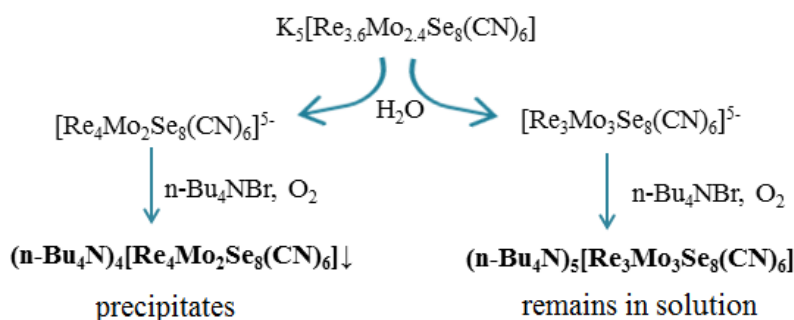
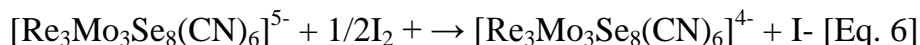


Figure 3.9: The scheme of separation of a mixture of heterometallic cluster anions to individual clusters.

The $[\text{Re}_3\text{Mo}_3\text{Se}_8(\text{CN})_6]^{5-}$ cluster complex was isolated from the solution by extraction into dichloromethane followed by the oxidation with I_2 . One-electron oxidation of the cluster anion $[\text{Re}_3\text{Mo}_3\text{Se}_8(\text{CN})_6]^{5-}$ with iodine solution leads to the formation of the anion $[\text{Re}_3\text{Mo}_3\text{Se}_8(\text{CN})_6]^{4-}$, according to the reaction:



One-electron oxidation of the cluster anion is accompanied by a change in the color of the solution (Figure 3.10). The oxidation process was monitored by UV-Vis spectra.

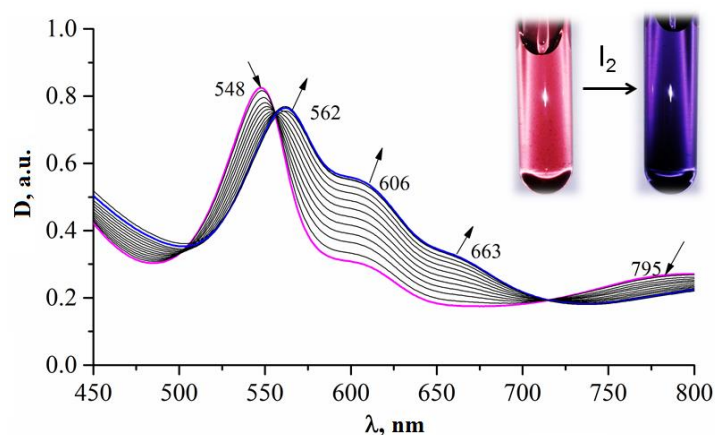


Figure 3.10: UV-Vis spectra for $[\text{Re}_3\text{Mo}_3\text{Se}_8(\text{CN})_6]^{5-/4-}$ while titration by iodine solution in CH_3CN .

Upon evaporation of the solution containing the $[\text{Re}_3\text{Mo}_3\text{Se}_8(\text{CN})_6]^{4-}$ cluster, a dark powder of a mixture of the compounds $(\text{n-Bu}_4\text{N})_4[\text{Re}_3\text{Mo}_3\text{Se}_8(\text{CN})_6]$ (**13**) and $(\text{n-Bu}_4\text{N})_4[\text{Re}_3\text{Mo}_3\text{Se}_8(\text{CN})_6] \cdot 3\text{H}_2\text{O}$ (**13·3H₂O**) was obtained. Recrystallization from acetone made it possible to obtain a single-phase product containing only compound **13** (Figure 3.11 a). A mass spectrometric study of solution of **13** confirmed the presence of only adducts of the $[\text{Re}_3\text{Mo}_3\text{Se}_8(\text{CN})_6]^{4-}$ cluster anion with tetrabutylammonium cations and the absence of anions with a different metal ratio (Figure 3.11 b). Compounds **7**, **10** and **13** are isostructural. Their crystal structures features, including metal site occupancies factors and interatomic bond distances are discussed in details below in the Section 4.3 in Chapter 4.

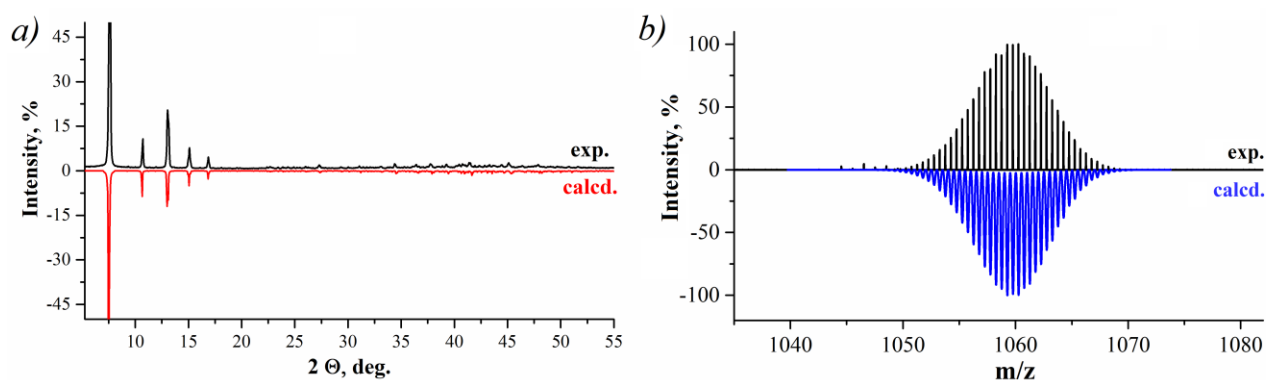


Figure 3.11: Powder XRD pattern for **13** (recorded, black vs calculated, red) (a) The fragment of the mass spectra of negative ions of the compound **13** in CH_2Cl_2 , the signal corresponds to the adduct $\{(\text{Bu}_4\text{N})_2[\text{Re}_3\text{Mo}_3\text{Se}_8(\text{CN})_6]\}^{2-}$ (b).

Thus, a change in the conditions of the high-temperature reaction and differences in the redox properties of cluster complexes with different Re/Mo ratio allowed us to obtain heterometallic cluster complexes $[\text{Re}_5\text{MoSe}_8(\text{CN})_6]^{4-}$, $[\text{Re}_4\text{Mo}_2\text{Se}_8(\text{CN})_6]^{4-}$ and $[\text{Re}_3\text{Mo}_3\text{Se}_8(\text{CN})_6]^{4-}$ in the form of defined compounds.

3.2 Structural features and isomerism of the $\{\text{Re}_{6-x}\text{Mo}_x\}$ ($x = 1-3$) metal cores in the solid state using SC XRD data

Detailed description of the crystal structures including the asymmetric unit composition, position point symmetry and coordination environment of significant structure moieties of heterometallic compounds obtained in present study can be found below in the Chapter 4. The analysis of interatomic distances in the structures of compounds **1–4**, **13** containing $\{\text{Re}_3\text{Mo}_3\text{Se}_8\}$ core shows that the average M – M distances are weakly dependent on the number of CSEs (Table 4.1 in Chapter 4). The difference between the average bond lengths in polymer **1** containing a 24-electron core $\{\text{Re}_3\text{Mo}_3\text{Se}_8\}$ and salt **2** with a 22-electron core $\{\text{Re}_3\text{Mo}_3\text{Se}_8\}$ is about 0.018 Å. The difference between the bond lengths in **2** and salts **4** and **13** (21 CSE) is only 0.005-0.006 Å (Table 4.1 in Chapter 4).

Moreover, in all the structures studied, the cluster is slightly distorted, the difference between the longest and the shortest metal-metal bonds is less than 0.04 Å. Similarly, the difference between the longest and shortest M – M distances in the cores $\{\text{Re}_4\text{Mo}_2\text{Se}_8\}$ and $\{\text{Re}_5\text{MoSe}_8\}$ cores, respectively, is 0.04 and 0.02 Å (Table 4.1 in Chapter 4, com-

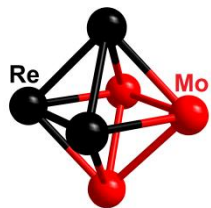
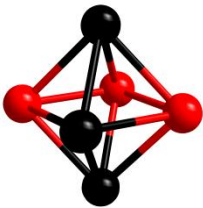
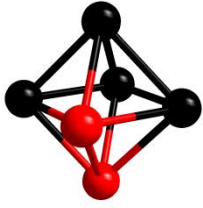
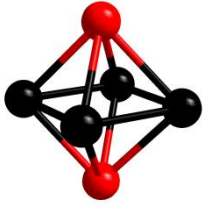
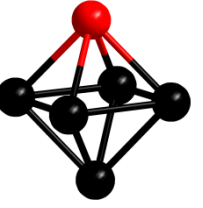
pounds **10** and **7**). According to SC X-ray diffraction data the $\{\text{Re}_{6-x}\text{Mo}_x\}$ metal cores ($x = 1-3$) in heterometallic cluster complexes are quite regular or only slightly distorted octahedra.

It is known that a change in the number of cluster skeletal electrons in the core has different effects on interatomic distances. Thus, the lengths of Re – Re bonds in chalcogenide octahedral clusters are insensitive to changes in the number of CSEs. For example, the Re – Re distances in the $[\text{Re}_6\text{Se}_8(\text{CN})_6]^{n-}$ cluster complex remain almost the same when the CSE changes from 24 to 23 (2.633 Å in $\text{K}_4[\text{Re}_6\text{Se}_8(\text{CN})_6] \cdot 3.5\text{H}_2\text{O}$ [147] and 2.633 Å in $(\text{Ph}_4\text{P})_2\text{H}[\text{Re}_6\text{Se}_8(\text{CN})_6] \cdot 8\text{H}_2\text{O}$ [188]). Mo – Mo distances in $[\text{Mo}_6\text{Se}_8(\text{CN})_6]^{n-}$ clusters with 20 and 21 CSE (2.711 Å in $(\text{Me}_4\text{N})_4\text{K}_2[\text{Mo}_6\text{Se}_8(\text{CN})_6] \cdot 10\text{H}_2\text{O}$ and 2.700 Å in $\text{K}_7[\text{Mo}_6\text{Se}_8(\text{CN})_6] \cdot 8\text{H}_2\text{O}$ [111]) are also very close. On the other hand, niobium halide cluster complexes show a stronger dependence of the Nb – Nb bond lengths on the electronic state of the cluster. The average Nb – Nb distances increase from 2.910 Å in $\text{K}_4[\text{Nb}_6\text{Cl}^i_{12}\text{Cl}^a_6]$ (16 CSE) to 2.967 Å in $(\text{Me}_4\text{N})_3[\text{Nb}_6\text{Cl}^i_{12}\text{Cl}^a_6]$ (15 CSE) and up to 3.02 Å in $(\text{Me}_4\text{N})_2[\text{Nb}_6\text{Cl}^i_{12}\text{Cl}^a_6]$ (14 CSE [189], that is, a decrease in the number of CSEs per electron leads to a change in the Nb – Nb lengths by approximately 0.05 Å.

It should be noted that the case of heterometallic cluster complexes is more complicated, since isomerism is possible for heterometallic core (with the exception of the metal core composition $\{\text{M}_5\text{M}'\}$). The possible arrangement of metal atoms in the heterometallic core $\{\text{Re}_3\text{Mo}_3\}$, $\{\text{Re}_4\text{Mo}_2\}$ and $\{\text{Re}_5\text{Mo}\}$ with the highest possible point symmetry group of the metal core are shown in Table 3.2. It is important to note that the symmetry of the cluster anion in the crystal structure and the point symmetry group of the $\{\text{Re}_3\text{Mo}_3\}$ and $\{\text{Re}_4\text{Mo}_2\}$ isomers generally do not coincide. Therefore, heterometallic anions containing various isomers of the metal core should be randomly distributed over several possible orientations in the crystal structure of the compounds, which leads to an averaged interatomic distances and low distortion of the metal core. The joint occupancy of metal positions by rhenium and molybdenum atoms in the metal core in all structures studied confirms this assumption.

As a result, the question of the local geometry of the heterometallic metal core and the presence of the geometric isomers $\{\text{Re}_3\text{Mo}_3\}$ and $\{\text{Re}_4\text{Mo}_2\}$ in the compounds under study remain open.

Table 3.2: Possible geometries of the heterometallic metal cores $\{\text{Re}_{6-x}\text{Mo}_x\}$ ($x = 1-3$) and their point group symmetry.

| $\{\text{Re}_3\text{Mo}_3\}$ | | $\{\text{Re}_4\text{Mo}_2\}$ | | $\{\text{Re}_5\text{Mo}\}$ |
|---|---|---|--|---|
|  |  |  |  |  |
| <i>fac-</i> | <i>mer-</i> | <i>cis-</i> | <i>trans-</i> | |
| C_{3v} | C_{2v} | C_{2v} | D_{4h} | C_{4v} |

3.3 Investigation of the isomeric composition of the clusters $[\text{Re}_3\text{Mo}_3\text{Se}_8(\text{CN})_6]^{5-}$ and $[\text{Re}_4\text{Mo}_2\text{Se}_8(\text{CN})_6]^{4-}$ in solution

The analysis of the isomeric composition was carried out by ^{77}Se NMR in solutions of salts of cluster complexes: **12** containing a 22-diamagnetic cluster electron anion $[\text{Re}_3\text{Mo}_3\text{Se}_8(\text{CN})_6]^{5-}$ and compound **10** containing a 22-electron anion $[\text{Re}_4\text{Mo}_2\text{Se}_8(\text{CN})_6]^{4-}$ (Figure 3.12). Examination of the theoretical correlation of ^{77}Se signals for possible isomers of the $\{\text{Re}_3\text{Mo}_3\text{Se}_8\}$ core (Table 3.3) shows that the ^{77}Se NMR spectrum of the *fac*-isomer should contain 4 signals, with a relative intensity ratio of 1:3:3:1, the *mer*-isomer should give only two signals of the same intensity. The experimental NMR spectrum of compound **12** contains two signals at 172 and 365 ppm with close values of the integrated intensities, which were assigned to the *mer*-isomer of the $\{\text{Re}_3\text{Mo}_3\text{Se}_8\}$ core. The *cis*-isomer of the $\{\text{Re}_4\text{Mo}_2\text{Se}_8\}$ core should show 3 signals with relative intensities of 1:2:1, the selenium atoms of the *trans*-isomer are chemically equivalent, therefore, only one signal should be presented in the NMR spectrum. The experimental spectrum of compound **10** contains 4 signals, which indicates the presence of a mixture of two isomers. Based on the ratio of integrated intensities, the signals at 14, 297

and 195 ppm were assigned to the *cis*-isomer of the core $\{\text{Re}_4\text{Mo}_2\text{Se}_8\}$, and the signal 322 ppm to the *trans*-isomer of the core $\{\text{Re}_4\text{Mo}_2\text{Se}_8\}$. An assessment of the integral signal intensities showed that the content of the *cis*-isomer in the obtained solution was approximately two times higher than the *trans*-isomer.

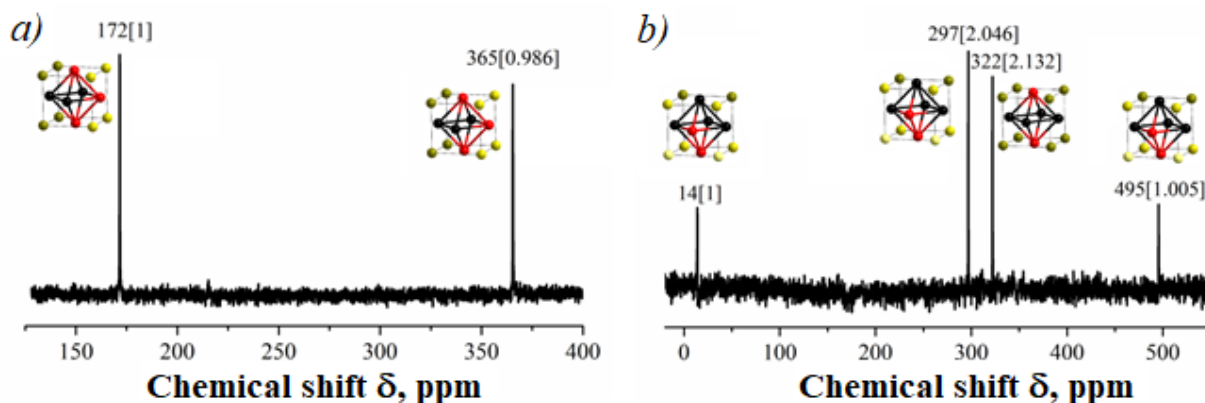


Figure 3.12: ^{77}Se NMR spectra for **12** in D_2O (a) and **10** in CD_3COCD_3 (b).

Table 3.3: Calculated ^{77}Se NMR signal ratio for $\{\text{Re}_3\text{Mo}_3\text{Se}_8\}$ and $\{\text{Re}_4\text{Mo}_2\text{Se}_8\}$ cores. Chemically equivalent selenium atoms are shown in different yellow shade.

| <i>fac</i> - $\{\text{Re}_3\text{Mo}_3\text{Se}_8\}$ | <i>mer</i> - $\{\text{Re}_3\text{Mo}_3\text{Se}_8\}$ | <i>cis</i> - $\{\text{Re}_4\text{Mo}_2\text{Se}_8\}$ | <i>trans</i> - $\{\text{Re}_4\text{Mo}_2\text{Se}_8\}$ |
|--|--|--|--|
| | | | |
| 1:3:3:1 | 4:4 | 2:4:2 | 8 |

Thus, NMR data favor the hypothesis that the $\{\text{Re}_3\text{Mo}_3\text{Se}_8\}$ core exists in the form of a single isomer - *mer*- $\{\text{Re}_3\text{Mo}_3\text{Se}_8\}$, while the $\{\text{Re}_4\text{Mo}_2\text{Se}_8\}$ core exist as both *cis*- and *trans*-isomers under experimental conditions.

3.4 Quantum chemical calculations for heterometallic cluster anions $[\text{Re}_{6-x}\text{Mo}_x\text{Se}_8(\text{CN})_6]^{n-}$

To analyze the geometry and electronic structure of heterometallic cluster complexes, quantum chemical calculations in frames of the density functional theory were used. The

geometry of cluster anions has been optimized in C_1 symmetry. The electronic structure of heterometallic clusters using the *mer*-isomer of the $[\text{Re}_3\text{Mo}_3\text{Se}_8(\text{CN})_6]^{7-}$ anion as an example will be considered. Molecular orbital diagrams for the *mer*-isomer of the $[\text{Re}_3\text{Mo}_3\text{Se}_8(\text{CN})_6]^{7-}$ anion contain a block of occupied bonding orbitals and a block of free antibonding orbitals located higher (Figure 3.13). Two bonding MO (HOMO and HOMO-1) are located above the other bonding orbitals. It leads to the formation of two energy gaps: the first separates the frontier orbitals (HOMO from LUMO) and is about 1.6 eV, the second separates the HOMO and HOMO-1 orbitals from the underlying occupied orbitals to about ≈ 0.8 eV. The MO diagram for the *fac*-isomer $[\text{Re}_3\text{Mo}_3\text{Se}_8(\text{CN})_6]^{7-}$ is similar to that considered above for the *mer*-isomer. The MO diagrams for the $[\text{Re}_4\text{Mo}_2\text{Se}_8(\text{CN})_6]^{n-}$ and $[\text{Re}_5\text{MoSe}_8(\text{CN})_6]^{n-}$ clusters have similar character to $[\text{Re}_3\text{Mo}_3\text{Se}_8(\text{CN})_6]^{7-}$ ones and are shown in Figures S4, S5 in the Supplementary.

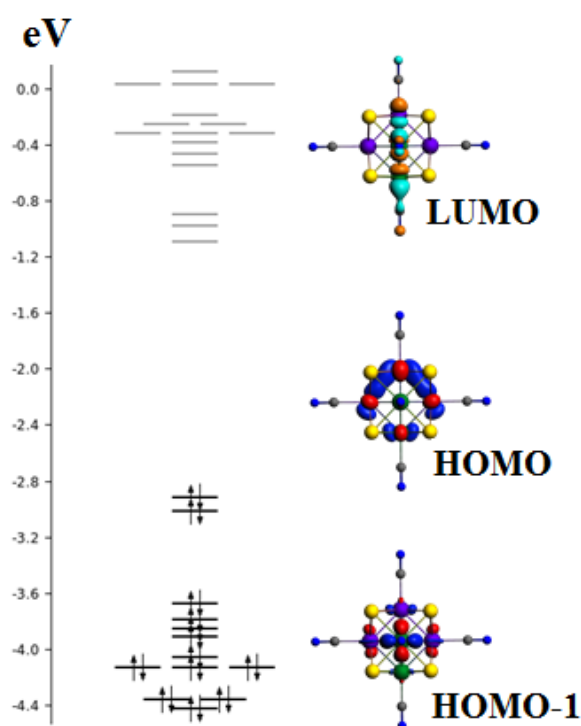


Figure 3.13: The MO diagram for *mer*-isomer of $[\text{Re}_3\text{Mo}_3\text{Se}_8(\text{CN})_6]^{7-}$.

Comparison of the formation energies of the isomers showed that the *mer*-isomer is more stable (the difference in the formation energies is small and amounts to about 2–3 kcal/mol depending on the charge of the cluster complex). An analysis of the composi-

tion of the HOMO and HOMO-1 showed that the largest contribution to the MO is made by the molybdenum atomic orbitals.

The cluster anion $[\text{Re}_3\text{Mo}_3\text{Se}_8(\text{CN})_6]^{7-}$ contains 24 CSE. MO diagrams were calculated for heterometallic cluster anions with different number of CSEs and accordingly, different charges. Figure 3.14 shows the change in the MO diagrams for the *mer*-isomer of the $[\text{Re}_3\text{Mo}_3\text{Se}_8(\text{CN})_6]^{7-}$ during the electron removal. When the first electron is removed, the degenerate HOMO and HOMO-1 orbitals separate, the HOMO-1 orbital goes down in energy (red arrow), and the position of the HOMO orbital remains practically unchanged (blue arrow). For the 22-electron cluster, the largest change in the energy of the HOMO-1 orbital is observed.

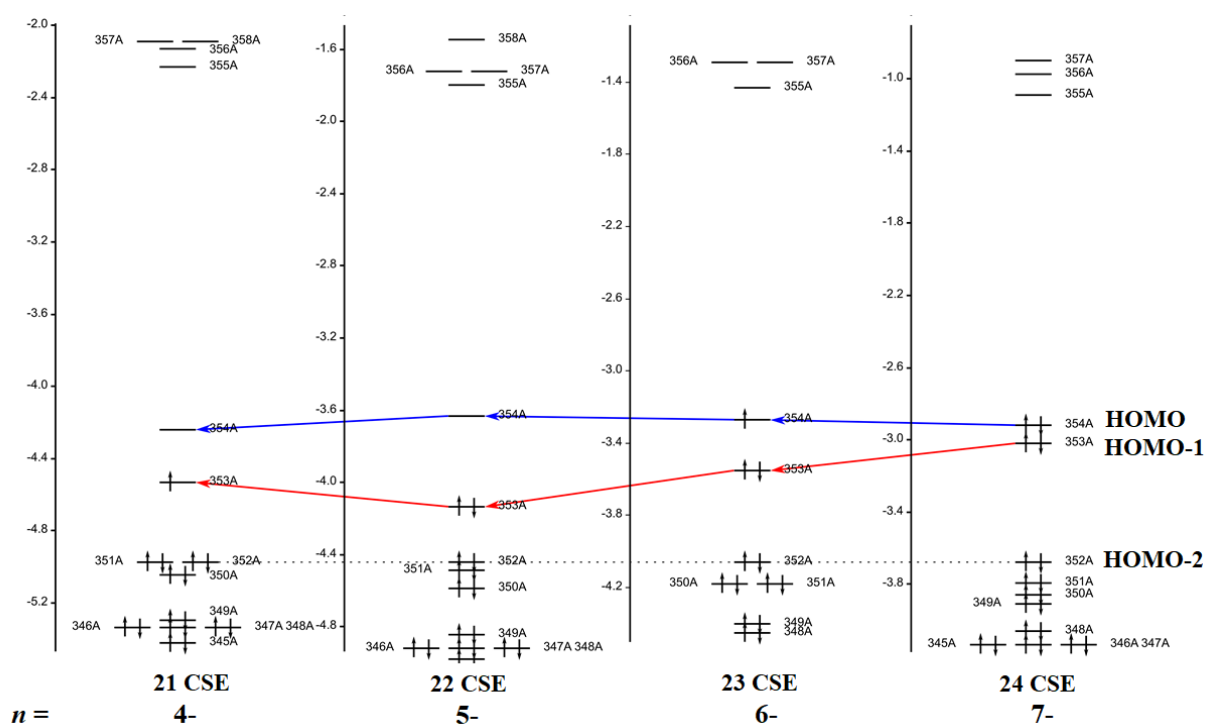


Figure 3.14: The evolution of MO diagrams for *mer*-isomer of $[\text{Re}_3\text{Mo}_3\text{Se}_8(\text{CN})_6]^{n-}$ with electron removal. The diagrams are shifted in energy in order that HOMO-2 level is located at the same energy.

Such a change in the electronic structure is accompanied by a change in the optimized geometry of the cluster anion. The 24-electron metal core $\{\text{Re}_3\text{Mo}_3\}$ is an almost perfect octahedron, the M-M bond lengths are almost equal. The removal of electrons leads to a change in bond lengths. The significant shortening of Re-Re distances and an extension of Mo-Mo distances in the metal core is observed according to the optimized geometries. Figure 3.15 shows the calculated average Re-Re, Re-Mo, Mo-Mo distances of the cluster

anions of $mer\text{-}[\text{Re}_3\text{Mo}_3\text{Se}_8(\text{CN})_6]^{n-}$ and $fac\text{-}[\text{Re}_3\text{Mo}_3\text{Se}_8(\text{CN})_6]^{n-}$ containing different numbers of CSEs. The distortion of the metal core observed theoretically is much larger than one found from structural data. The difference between the largest and smallest metal-metal distances is maximal for the *mer*-isomer containing 22-electron per cluster and equal to 0.139 Å.

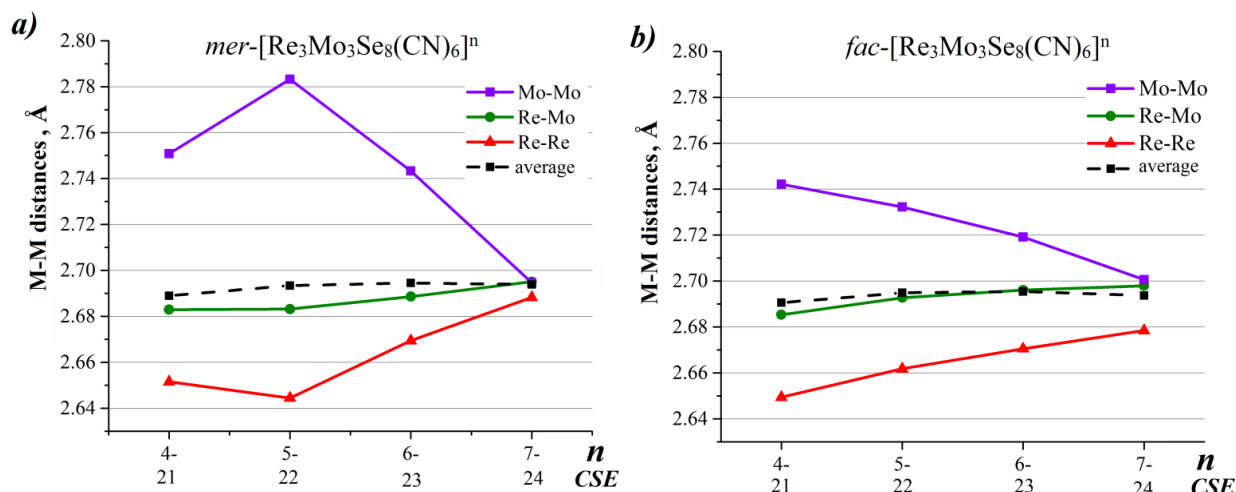


Figure 3.15: The M-M distances for *mer*- (a) and *fac*-isomers (b) of cluster $[\text{Re}_3\text{Mo}_3\text{Se}_8(\text{CN})_6]^{n-}$.

The geometry of the cluster anions of $cis\text{-}[\text{Re}_4\text{Mo}_2\text{Se}_8(\text{CN})_6]^{n-}$ and $trans\text{-}[\text{Re}_4\text{Mo}_2\text{Se}_8(\text{CN})_6]^{n-}$ changes in a similar way with a decrease in the number of CSEs. The metal core in the *trans*- $[\text{Re}_4\text{Mo}_2\text{Se}_8(\text{CN})_6]^{6-}$ anion containing 24 CSEs has the geometry of an almost perfect octahedron. The *cis*-isomer is also only slightly distorted. The removal of two electrons from the orbitals of these anions leads to a strong distortion of the metal core (Figure 3.16).

The distortion of the $[\text{Re}_5\text{MoSe}_8(\text{CN})_6]^{n-}$ cluster upon electron removal is similar to the distortion of the *trans*-isomer $[\text{Re}_4\text{Mo}_2\text{Se}_8(\text{CN})_6]^{n-}$. The metallocluster of anions containing 23 and 24 CSEs are slightly distorted, while the 22-electron anion shows a noticeable difference in metal-metal distances in the cluster core (Figure 3.17). It should be noted that the 22-electron cluster anion $[\text{Re}_5\text{MoSe}_8(\text{CN})_6]^{3-}$ has not yet been experimentally obtained.

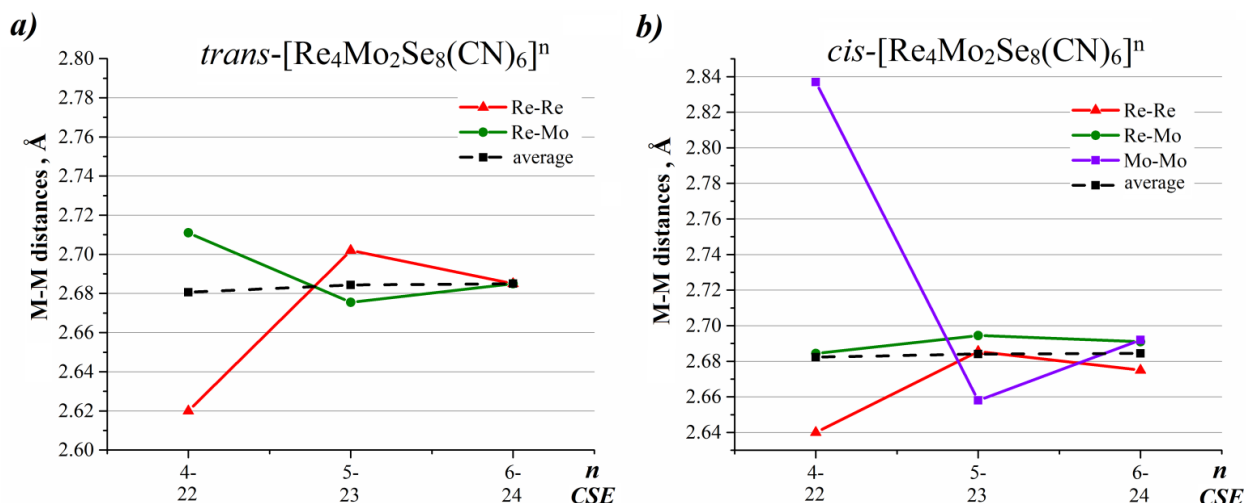


Figure 3.16: The M-M distances for *trans*- (a) and *cis*-isomers (b) of the cluster [Re₄Mo₂Se₈(CN)₆]ⁿ.

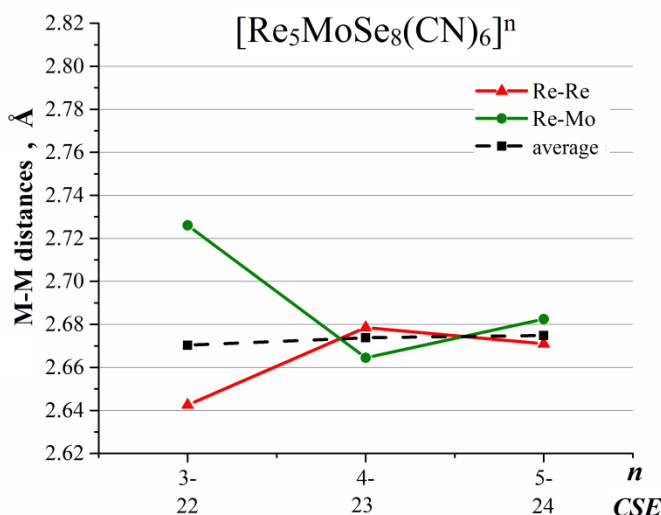


Figure 3.17: The M-M distances for the cluster [Re₅MoSe₈(CN)₆]ⁿ.

As mentioned above, the crystallographic data for heterometallic cluster complexes based on heterometallic {Re₃Mo₃Se₈} cores allow localizing only averaged positions of metals and does not allow determination of the real position of metal atoms in heterometallic cluster complexes. An analysis of the geometry of heterometallic anions by the method of quantum chemical calculations showed that the removal of electrons from the orbitals of the heterometallic cluster anions leads to a change in the energy of the HOMO-1 orbital, accompanied by a significant distortion of the metal core. To experimentally confirm the distortion, the X-ray absorption spectroscopy method was used, which allows us to determine the local environment of metal atoms in the structure of the heterometallic cluster.

3.5 X-ray absorption spectroscopy analysis of the local geometry of the metal core in $[\text{Re}_3\text{Mo}_3\text{Se}_8(\text{CN})_6]^{5-}$ and $[\text{Re}_4\text{Mo}_2\text{Se}_8(\text{CN})_6]^{4-}$ clusters

Cluster complexes with the most distorted metal core (according to quantum chemical calculations) $\text{K}_5[\text{Re}_3\text{Mo}_3\text{Se}_8(\text{CN})_6] \cdot 11\text{H}_2\text{O}$ (**12**) and $(\text{n-Bu}_4\text{N})_4[\text{Re}_4\text{Mo}_2\text{Se}_8(\text{CN})_6]$ (**10**) containing 22 CSEs were chosen for analysis of the local core geometry by means of X-ray absorption spectroscopy. The analysis of the local environment of molybdenum and rhenium atoms in the heterometallic metallocluster for complexes **12** and **10** was carried out using the EXAFS method. The signals $k^3 \cdot \chi(k)$ for the K absorption edge of Mo and the L_3 absorption edge of Re are shown in Figures 3.18 and 3.19 (left). The amplitudes for the corresponding Fourier transform of the EXAFS signal were calculated in the k interval 3 - 20 \AA^{-1} (Mo) and 3 - 17.9 \AA^{-1} (Re for **12**) and 3 - 18.8 \AA^{-1} (Re for **10**), using a window of 1 - 4 \AA . The Fourier transforms of the EXAFS signal for samples **12** and **10** are shown in Figures 3.18 and 3.19 (right). The experimental data were refined using the standard EXAFS equation [190]. Refinement was carried out using the Artemis program based on the IFEFFIT package [176]. Structural models for the $\{\text{Re}_3\text{Mo}_3\text{Se}_8\}$ and $\{\text{Re}_4\text{Mo}_2\text{Se}_8\}$ cores were obtained from crystallographic data. The atom coordinates in the single unit cell of the structures of corresponding compounds **12** and **10** were extracted and metal site occupancy factors were modified to contain ordered isomeric distribution. The simplified single cell model for *mer*-isomer of $[\text{Re}_3\text{Mo}_3\text{Se}_8(\text{CN})_6]^{5-}$ is shown in Figure S7 in Supplementary. The local environment around Mo and Re atoms were then extracted from the prepared structural models up to the sphere of 8 \AA radius. The phase and amplitude were calculated using the FEFF-6 code [191]. The final refinement parameters are given in Table S7, S8 in the Supplementary.

The model functions obtained after refinement are in good agreement with experimental data. Models for different core isomers showed similar results. It was not possible to determine unambiguously from the obtained data the type of core isomerism.

The M–M interatomic distances obtained for the cluster anions $[\text{Re}_3\text{Mo}_3\text{Se}_8(\text{CN})_6]^{5-}$ and $[\text{Re}_4\text{Mo}_2\text{Se}_8(\text{CN})_6]^{4-}$ by the EXAFS method are given in Table 3.4 and 3.5. It can be seen

that in both cases the Re-Re distances are shorter than the average M-M distances, and the Mo-Mo distances are noticeably longer. A comparison of the M – M interatomic distances obtained by EXAFS and DFT showed that in both cases a similar distortion of the metal core is observed: elongation of Mo – Mo bonds and shortening of Re – Re bonds.

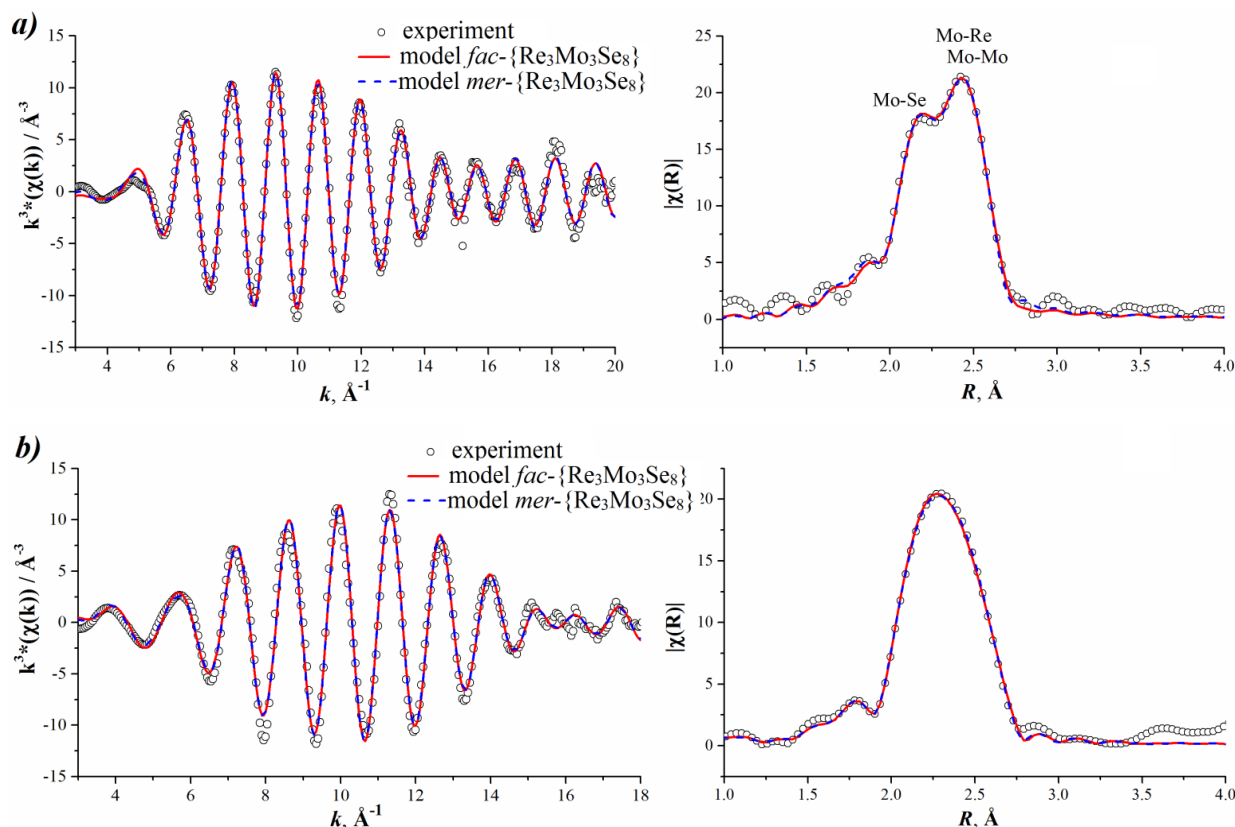


Figure 3.18: EXAFS signals for the sample of **12** for Mo K-edge (a) and Re L₃-edge (b), experimental $k^3 \cdot \chi(k)$ spectra (left figures), corresponded Fourier transform (right figures). The model curves obtained from fitting (fitting space – k) are given as lines.

It was shown that the interatomic M – M distances in the $[\text{Re}_3\text{Mo}_3\text{Se}_8(\text{CN})_6]^{5-}$ and $[\text{Re}_4\text{Mo}_2\text{Se}_8(\text{CN})_6]^{4-}$ anions determined theoretically by quantum chemical calculations and experimentally from EXAFS spectra are consistent. Both approaches show that the metalloclusters $\{\text{Re}_3\text{Mo}_3\}$ and $\{\text{Re}_4\text{Mo}_2\}$ in the anions are strongly distorted. The obtained distortion cannot be determined from structural data obtained by X-ray diffraction, since the diffraction data contain the averaged positions of the metal atoms and therefore, the averaged interatomic distances.

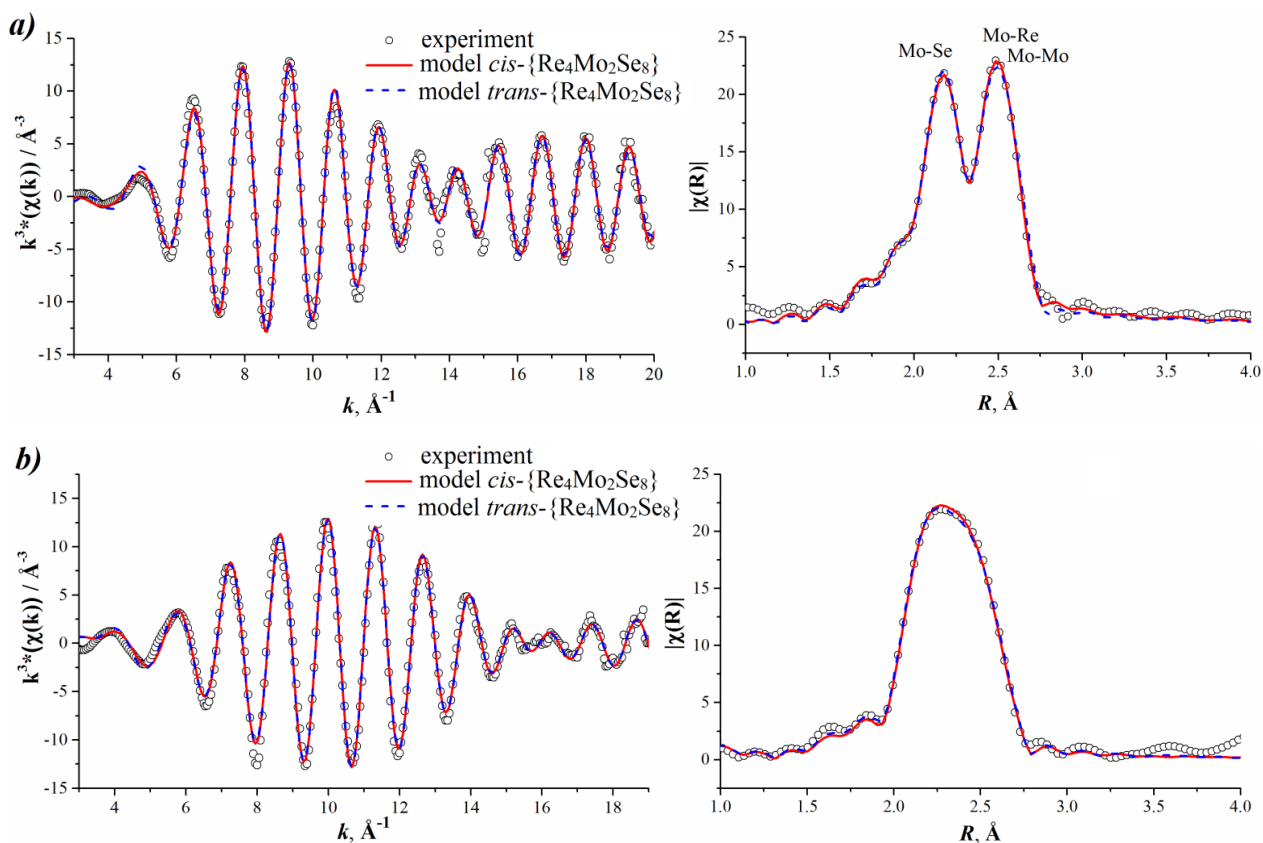


Figure 3.19: EXAFS signals for the sample of **10** for Mo K-edge (a) and Re L₃-edge (b), experimental $k^3 \cdot \chi(k)$ spectra (left figures), corresponded Fourier transform (right figures). The model curves obtained from fitting (fitting space – k) are given as lines.

Table 3.4: The comparison of the interatomic M-M (Å) distances for 22-electronic anion $[\text{Re}_3\text{Mo}_3\text{Se}_8(\text{CN})_6]^{5-}$ obtained by means of EXAFS, SC XRD and DFT calculations

| | <i>mer</i> - $[\text{Re}_3\text{Mo}_3\text{Se}_8(\text{CN})_6]^{5-}$ | | SC XRD [192] |
|--------------------|--|-----------|-----------------|
| | EXAFS | DFT [192] | |
| $R_{\text{Mo-Mo}}$ | 2.776 | <2.783> | — |
| $R_{\text{Mo-Re}}$ | 2.688 | <2.683> | — |
| $R_{\text{Re-Re}}$ | 2.634 | <2.645> | — |
| $R_{\text{M-M}}$ | <2.693> | <2.693> | 2.6494(9) |

Table 3.5: The comparison of the interatomic M-M (Å) distances for 22-electronic anion $[\text{Re}_4\text{Mo}_2\text{Se}_8(\text{CN})_6]^{4-}$ obtained by means of EXAFS, SC XRD and DFT calculations

| | <i>cis</i> - $[\text{Re}_4\text{Mo}_2\text{Se}_8(\text{CN})_6]^{4-}$ | | <i>trans</i> - $[\text{Re}_4\text{Mo}_2\text{Se}_8(\text{CN})_6]^{4-}$ | | SC XRD |
|--------------------|--|---------|--|---------|-------------|
| | EXAFS | DFT | EXAFS | DFT | |
| $R_{\text{Mo-Mo}}$ | 2.784 | 2.837 | – | – | – |
| $R_{\text{Mo-Re}}$ | 2.678 | <2.685> | 2.671 | <2.711> | – |
| $R_{\text{Re-Re}}$ | 2.629 | <2.648> | 2.636 | <2.620> | – |
| $R_{\text{M-M}}$ | <2.667> | <2.682> | <2.659> | <2.681> | <2.646(14)> |

3.6 The electrochemical study of the cyanoclusters $[\text{Re}_{6-x}\text{Mo}_x\text{Se}_8(\text{CN})_6]^{4-}$ ($x = 1, 2$ and 3) in solution

The redox properties of the obtained heterometallic cluster complexes $(\text{n-Bu}_4\text{N})_4[\text{Re}_{6-x}\text{Mo}_x\text{Se}_8(\text{CN})_6]$ ($x = 1, 2$ and 3) were studied by the cyclic voltammetry method (Figure 3.20). The voltammogram for the $[\text{Re}_5\text{MoSe}_8(\text{CN})_6]^{n-}$ cluster in the electrochemical window of acetonitrile contains two electrochemical transitions (Figure 3.20, red line). The areas of the cathodic and anodic peaks of the obtained transitions are close, however, the ΔE of the processes are 0.147 and 0.096 V, respectively, which indicates the quasi-reversible nature of electrochemical reactions. Common characteristic value of ΔE for one-electron reversible redox transition is usually observed as 0.059 V. Despite this fact for many cluster complexes, including the homometallic clusters $[\text{Mo}_6\text{Se}_8(\text{CN})_6]^{n-}$ ($\Delta E = 0.9 - 0.134$ V) [193] and $[\text{Re}_6\text{Se}_8(\text{CN})_6]^{n-}$ ($\Delta E = 0.11$ V), significantly larger ΔE values are observed. This may occur due to a slow change in the geometry of cluster complexes in comparison with the rate of the electrochemical reaction. The transition potential located to the right from the zero in the cyclic voltammogram of $[\text{Re}_5\text{MoSe}_8(\text{CN})_6]^{n-}$ was assigned to one-electron oxidation of $[\text{Re}_5\text{MoSe}_8(\text{CN})_6]^{4-}$ (23 CSEs) \leftrightarrow $[\text{Re}_5\text{MoSe}_8(\text{CN})_6]^{3-}$ (22 CSEs). The transition left from the zero potential, respectively, relates to the reduction of $[\text{Re}_5\text{MoSe}_8(\text{CN})_6]^{4-}$ (23 CSEs) \leftrightarrow $[\text{Re}_5\text{MoSe}_8(\text{CN})_6]^{5-}$ (24 CSE). The values of the half-wave potentials $E_{1/2}$ for all transitions under consideration are given in Table 3.6.

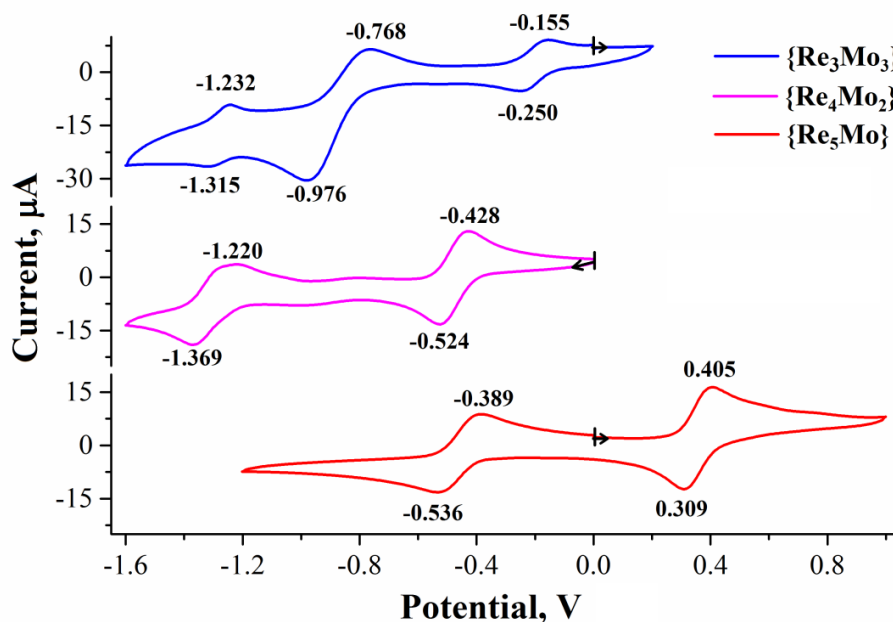


Figure 3.20: CV curves for $[\text{Re}_{6-x}\text{Mo}_x\text{Se}_8(\text{CN})_6]^{n-}$ $x = 1, 2, 3$ in acetonitrile (reference electrode – Ag/AgCl), scan speed 0.2 V/sec.

Voltammograms for the cluster complexes $[\text{Re}_3\text{Mo}_3\text{Se}_8(\text{CN})_6]^{n-}$ and $[\text{Re}_4\text{Mo}_2\text{Se}_8(\text{CN})_6]^{n-}$ were considered similarly. The assignment of the obtained transitions and the values of $E_{1/2}$ are given in Table 3.6. Noticeable difference between the cathode and anode currents was found for the transition of the $[\text{Re}_3\text{Mo}_3\text{Se}_8(\text{CN})_6]^{n-}$ cluster complex with a value of $E_{1/2} = -0.870$ V. It can be seen that the intensities of the currents of this transition substantially exceed the currents of the neighboring transitions of this cluster anion. This may indicate the presence of associated chemical process for this electrochemical reaction influencing the CV curve behavior.

The successive replacement of rhenium atoms with molybdenum atoms in the cluster core of the $[\text{Re}_{6-x}\text{Mo}_x\text{Se}_8(\text{CN})_6]^{n-}$ cyanocomplexes leads to an increase in the charge of isoelectronic anions and the appearance of additional (compared to $[\text{Re}_6\text{Se}_8(\text{CN})_6]^{4-}$) redox transitions. Heterometallic cluster complexes with high molybdenum content are electrochemically active capable of several redox transition in the narrow window of potential. The values of the electrochemical potentials $E_{1/2}$ of heterometallic cluster anions $[\text{Re}_{6-x}\text{Mo}_x\text{Se}_8(\text{CN})_6]^{n-}$ are located between the known values for homometallic rhenium and molybdenum cyanoclusters. The shift of the oxidation potentials in comparison with

rhodium analogues to the region of negative values leads to stabilization of the electron-deficient states (21, 22, 23 CSE) of heterometallic anions.

Table 3.6: $E_{1/2}$ potentials (V) from CV data for $\{M_6Se_8\}$ ($M = Re, Mo$) clusters, potentials are normalized according to the Ag/AgCl/3.5 M KCl electrode. The charges of the cluster anions corresponded to the redox transition are given in brackets

| Anion (solvent)\ CSE number | 20/21 | 21/22 | 22/23 | 23/24 |
|---|-------------------|-------------------|-------------------|-------------------|
| $[Re_6Se_8(CN)_6]^{(n-1)-/n-}$ (CH ₃ CN) [194] | – | – | – | 0.125 (3-/4-) |
| $[Re_5MoSe_8(CN)_6]^{(n-1)-/n-}$ (CH ₃ CN) | | | 0.357 (3-/4-) | -0.462 (4-/5-) |
| $[Re_4Mo_2Se_8(CN)_6]^{(n-1)-/n-}$ (CH ₃ CN) | – | – | -0.476 (4-/5-) | -1.294 (5-/6-) |
| $[Re_3Mo_3Se_8(CN)_6]^{(n-1)-/n-}$ (CH ₃ CN) | – | -0.202 (4-/5-) | -0.870 (5-/6-) | -1.270 (6-/7-) |
| $[Re_3Mo_3Se_8(CN)_6]^{(n-1)-/n-}$ (DMF) [192] | – | -0.325 (4-/5-) | -0.818 (5-/6-) | -1.410 (6-/7-) |
| $[Mo_6Se_8(CN)_6]^{(n-1)-/n-}$ (H ₂ O) [193] | -0.647 (6-/7-) | -1.081 (7-/8-) | -1.574 (8-/9-) | – |

3.7 UV-Vis spectroscopic investigation of heterometallic anions $[Re_{6-x}Mo_xSe_8(CN)_6]^{n-}$ ($x = 1, 2$, and 3) in solution

Electronic absorption spectra of the salts of heterometallic cluster anions $[Re_{6-x}Mo_xSe_8(CN)_6]^{n-}$ ($x = 1, 2$, and 3) with different charges were detected in aqueous solutions and acetonitrile (Figure 3.21). The $[Re_3Mo_3Se_8(CN)_6]^{6-}$ and $[Re_4Mo_2Se_8(CN)_6]^{6-}$ anions were obtained by reducing the potassium salts $K_5[Re_{6-x}Mo_xSe_8(CN)_6]$ with an excess of $NaBH_4$ in an aqueous solution. According to spectra obtained, the cluster anion $[Re_5MoSe_8(CN)_6]^{5-}$ is not subjected to reduction in aqueous $NaBH_4$ solution.

The spectra of $[Re_{6-x}Mo_xSe_8(CN)_6]^{n-}$ heterometallic cluster anions ($x = 1, 2$ and 3) contain absorption bands in the UV region with high extinction values of $35000 - 50000 \text{ M}^{-1}\text{cm}^{-1}$. The position of the maximum of the absorption band in the UV region weakly depends on the composition of the cluster core. It is known that for the $[Re_6Se_8(CN)_6]^{4-}$ cluster, this maximum is located at 230 nm [195]. It shifts to a longer wavelength region with an increase in the number of molybdenum atoms in the cluster core (232 nm for

$[\text{Re}_5\text{MoSe}_8(\text{CN})_6]^{4-}$, 238 nm for $[\text{Re}_4\text{Mo}_2\text{Se}_8(\text{CN})_6]^{4-}$ and 244 nm for $[\text{Re}_3\text{Mo}_3\text{Se}_8(\text{CN})_6]^{4-}$). The position of this maximum depends weakly on the anion charge (238 nm for $[\text{Re}_4\text{Mo}_2\text{Se}_8(\text{CN})_6]^{4-} \rightarrow 236$ nm for $[\text{Re}_4\text{Mo}_2\text{Se}_8(\text{CN})_6]^{5-} \rightarrow 235$ nm $[\text{Re}_4\text{Mo}_2\text{Se}_8(\text{CN})_6]^{6-}$). Since the absorption bands in the UV region have high extinction, and the position of the maxima weakly depends on the composition and charge state of the cluster, these bands probably correspond to a large number of transitions from the underlying bonding orbitals to unoccupied anti-bonding orbitals.

The absorption spectra of heterometallic cluster anions in the visible region of the spectrum contain characteristic absorption bands, the number, position and extinction coefficient of which depend on the core composition and charge state of the cluster complex. The maxima of the characteristic absorption bands are red-shifted with the decreasing of the cluster anion charge leading to the solution color change. *E.g.* the UV-Vis spectrum of $[\text{Re}_3\text{Mo}_3\text{Se}_8(\text{CN})_6]^{4-}$ cluster anion represents the band with the maximum located at 563 nm, one-electron reduction leads to the shift of the maximum to 548 nm for $[\text{Re}_3\text{Mo}_3\text{Se}_8(\text{CN})_6]^{5-}$ and then to 518 nm for $[\text{Re}_3\text{Mo}_3\text{Se}_8(\text{CN})_6]^{6-}$. A similar red-shift is observed for the rhenium cluster anion (605 nm for $[\text{Re}_6\text{Se}_8(\text{CN})_6]^{3-} \rightarrow 440$ nm for $[\text{Re}_6\text{Se}_8(\text{CN})_6]^{4-}$ [195]).

The color of the solution of anions of different compositions correlates with the number of CSEs: solutions of $[\text{Re}_4\text{Mo}_2\text{Se}_8(\text{CN})_6]^{6-}$ and $[\text{Re}_5\text{MoSe}_8(\text{CN})_6]^{5-}$ anions containing 24 CSEs are yellow, 23-electron anions $[\text{Re}_3\text{Mo}_3\text{Se}_8(\text{CN})_6]^{6-}$, $[\text{Re}_4\text{Mo}_2\text{Se}_8(\text{CN})_6]^{5-}$ and $[\text{Re}_5\text{MoSe}_8(\text{CN})_6]^{4-}$ are orange, 22-electron anions $[\text{Re}_3\text{Mo}_3\text{Se}_8(\text{CN})_6]^{5-}$ and $[\text{Re}_4\text{Mo}_2\text{Se}_8(\text{CN})_6]^{4-}$ are pink, and the cluster anion $[\text{Re}_3\text{Mo}_3\text{Se}_8(\text{CN})_6]^{4-}$, containing 21 CSCs, is blue (Table 3.7).

In the near IR region (700 - 1000 nm) in the spectra of electron-deficient cluster complexes, *i.e.* $[\text{Re}_3\text{Mo}_3\text{Se}_8(\text{CN})_6]^{4-/5-/6-}$ (21/22/23 CSEs), $[\text{Re}_4\text{Mo}_2\text{Se}_8(\text{CN})_6]^{4-/5-}$ (22/23 CSEs) and $[\text{Re}_5\text{MoSe}_8(\text{CN})_6]^{4-}$ (23 CSEs), wide absorption bands with low extinction are observed. This observation is also characteristic for the 23-electron homometallic cluster $[\text{Re}_6\text{Se}_8(\text{CN})_6]^{3-}$ [195]. UV-Vis absorption spectra of 24-electron cluster complexes do not contain absorption bands in the near infrared region. It can be assumed that these ab-

sorption bands correspond to electronic transitions to unoccupied HOMO orbitals from the underlying occupied orbitals.

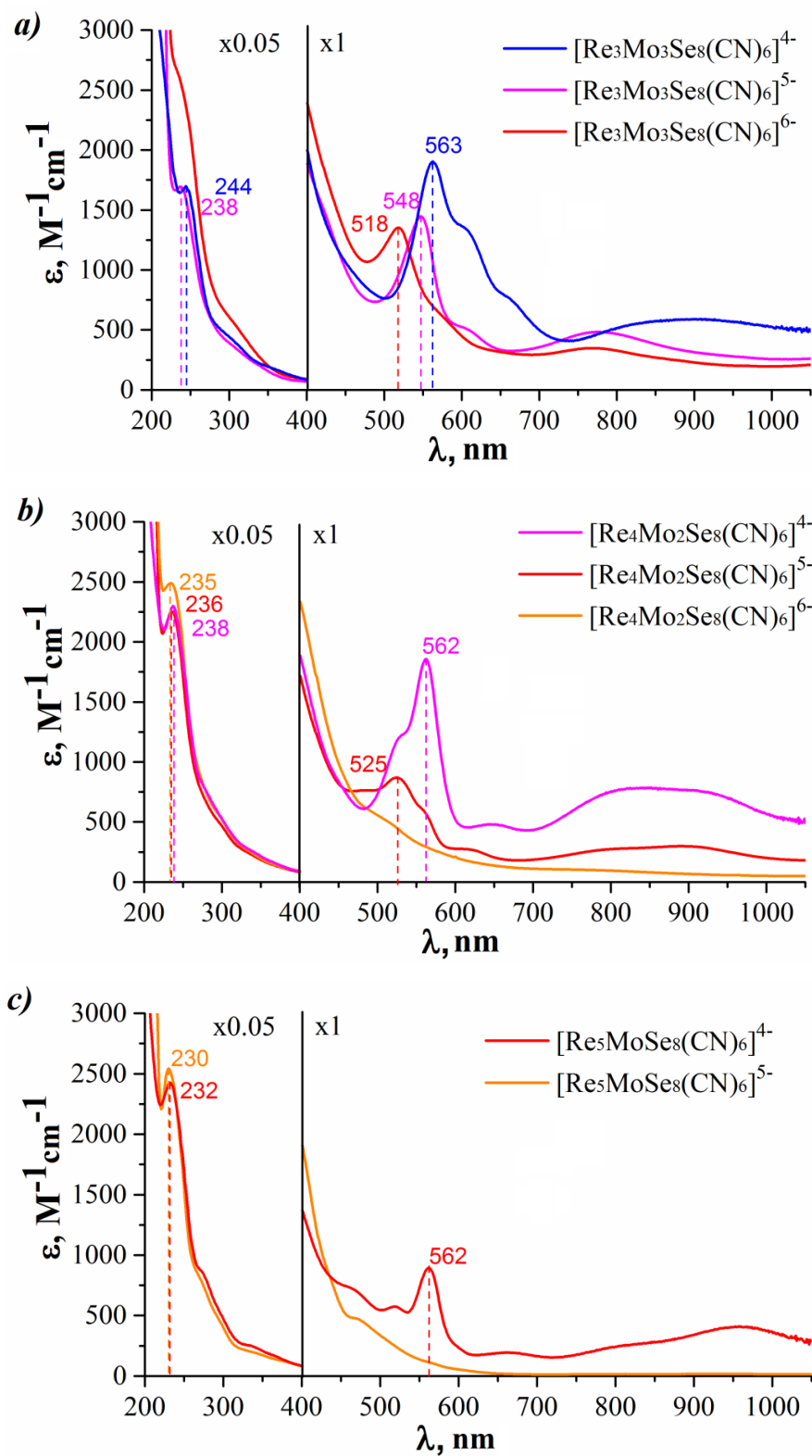










Figure 3.21: Electronic absorption spectra for the solutions of the cluster anions: $[\text{Re}_3\text{Mo}_3\text{Se}_8(\text{CN})_6]^{n-}$ ($n = 4 - 6$) (a); $[\text{Re}_4\text{Mo}_2\text{Se}_8(\text{CN})_6]^{n-}$ ($n = 4 - 6$) (b); $[\text{Re}_5\text{MoSe}_8(\text{CN})_6]^{n-}$ ($n = 4, 5$) (c).

Table 3.7: The anion charge, CSE number and the solution color of the heterometallic cluster anions $[\text{Re}_{6-x}\text{Mo}_x\text{Se}_8(\text{CN})_6]^{n-}$

| | $[\text{Re}_3\text{Mo}_3\text{Se}_8(\text{CN})]^{n-}$ | | | $[\text{Re}_4\text{Mo}_2\text{Se}_8(\text{CN})]^{n-}$ | | | $[\text{Re}_5\text{MoSe}_8(\text{CN})]^{n-}$ | |
|----------------|---|---|---|---|--|---|---|---|
| Anion charge | 4- | 5- | 6- | 4- | 5- | 6- | 4- | 5- |
| CSE number | 21 | 22 | 23 | 22 | 23 | 24 | 23 | 24 |
| Solution color |  |  |  |  |  |  |  |  |

Redox transitions of the heterometallic cluster anions lead to the noticeable shift of the absorption maxima in visible region and correspondingly to a remarkable color change of the cluster anion. The solution color correlates with a number of CSEs in the heterometallic cluster core.

3.8 The study of interaction of the heterometallic cyanocluster $[\text{Re}_3\text{Mo}_3\text{Se}_8(\text{CN})_6]^{5-}$ with transition metals ammine complexes and the formation of coordination polymers

The literature review examines examples of the interaction of octahedral cyanoclusters with cations of transition and post-transition metals with the formation of polymer compounds. The charge of the octahedral cyanocluster, generally, has a strong influence on the type of connectivity and the dimension of the resulting coordination polymers. The closest example to the cluster complexes studied in this work is the interaction of the sulfur heterometallic cluster anion $[\text{Re}_3\text{Mo}_3\text{S}_8(\text{CN})_6]^{6-}$ with cadmium and zinc ammine complexes, and compounds with the structure of Prussian blue type are formed [162, 163].

The selenide anion $[\text{Re}_3\text{Mo}_3\text{Se}_8(\text{CN})_6]^{5-}$ obtained is stable in water solution with a charge of 5-, this charge is quite rare among cyanocluster anions and may lead to the formation of compounds with a different framework structure. Therefore, the interaction of salts of the $[\text{Re}_3\text{Mo}_3\text{Se}_8(\text{CN})_6]^{5-}$ cyanocluster with transition metal ammine complexes were in-

vestigated in order to determine the effect of the anion charge on the structure of coordination polymers.

Like most cyanometallates, $[\text{Re}_3\text{Mo}_3\text{Se}_8(\text{CN})_6]^{5-}$ anions rapidly form insoluble precipitates with transition metal cations. In this work, the method of counter diffusion of solutions was used to slow the reaction and obtain single crystals of the polymeric product. It was found that the interaction of an aqueous ammonia solution of cobalt (II) and nickel (II) salts with an aqueous solution of $\text{K}_5[\text{Re}_3\text{Mo}_3\text{Se}_8(\text{CN})_6] \cdot 11\text{H}_2\text{O}$ leads to the formation of isostructural coordination polymers with a layered structure and the formula $[\text{M}(\text{NH}_3)_6]_4[\{\text{M}(\text{NH}_3)_2\}\{\text{Re}_3\text{Mo}_3\text{Se}_8(\text{CN})_6\}_2] \cdot 15\text{H}_2\text{O}$ ($\text{M} = \text{Co}$ (**19**), Ni (**20**)). The obtained compounds turned out to be unstable in air. They quickly lose coordinated ammonia molecules and solvate water molecules with the formation of an amorphous product.

The polymer layers $[\{\text{M}(\text{NH}_3)_2\}\{\text{Re}_3\text{Mo}_3\text{Se}_8(\text{CN})_6\}_2]^{8-}_{\infty}$ in structures **19** and **20** are four-connected square net with *sql* topology. The structure of the polymer layer is shown in Figure 3.22.

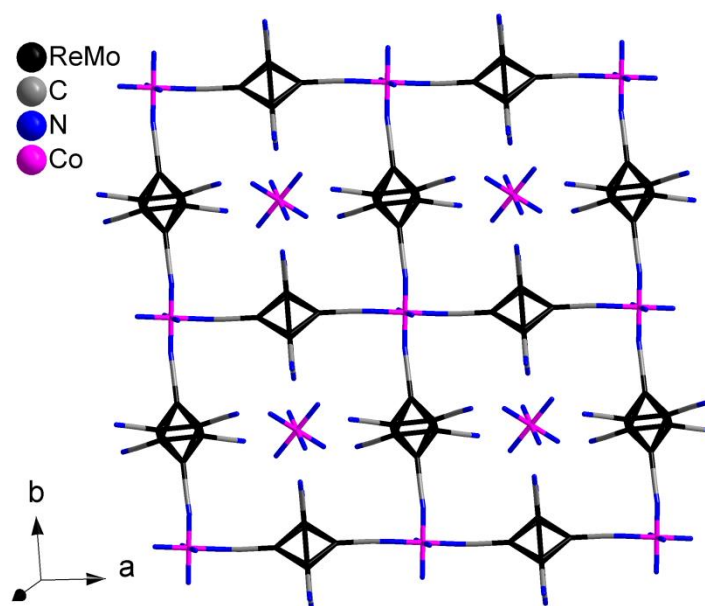


Figure 3.22: The fragment of the structure of the polymeric layer $[\{\text{Co}(\text{NH}_3)_2\}\{\text{Re}_3\text{Mo}_3\text{Se}_8(\text{CN})_6\}_2]^{8-}_{\infty}$ in the structure **19**.

Layered compounds are found among coordination polymers based on rhenium homometallic cluster complexes. For example, compounds of the composition $\text{Cs}_2\text{M}[\text{Re}_6\text{S}_8(\text{CN})_6] \cdot 2\text{H}_2\text{O}$ ($\text{M} = \text{Mn}, \text{Fe}, \text{Co}, \text{Cd}$) are formed by layers

$[\{M(H_2O)_2\}\{Re_6Se_8(CN)_6\}]^{2-}_{\infty\infty}$, where the cluster anion and metal cation form four-connected nodes of a square net [159]. The layered structure of the *hcb* topology was found for the compound $[\{Mn(H_2O)_3\}_2\{Re_6Se_8(CN)_6\}]\cdot 3.3H_2O$, where two manganese cations form a node of a three-connected network of the composition $[\{Mn(H_2O)_3\}_4\{Re_6Se_8(CN)_6\}_3]^{4-}_{\infty\infty}$ [196]. The layered structure is also characteristic of the compound based on $[Re_6Se_8(CN)_6]^{4-}$ and trimethylstannane cations $[SnMe_3]^+$. For example, in the compounds $[(SnMe_2)_4(\mu_3-O)_2(\mu_2-OH)_2(H_2O)_2][\{SnMe_3\}_2\{Re_6Se_8(CN)_6\}]$ and $[(Me_3Sn)_3(OH)_2][\{Me_3Sn\}_3\{Re_6Se_8(CN)_6\}]_3$, the cluster complex forms four-connected nodes of the polymer layer [197, 198]

Studying the interaction of an aqueous solution of the cluster complex $K_5[Re_3Mo_3Se_8(CN)_6]$ with aqueous ammonia solutions of cadmium (II) salts showed that the composition and structure of the resulting compounds depends on the nature of the anion of the cadmium (II) salt. In the case of cadmium acetate, crystals of the compound $[\{Cd(NH_3)_5\}_2\{Cd(NH_3)_4\}_3[Re_3Mo_3Se_8(CN)_6]_2]\cdot 5H_2O$ (**14**) with a chain-like structure are formed. The polymer chains are formed by cluster anions and cadmium $[Cd(NH_3)_4]^{2+}$ ammino complexes coordinated to the anion cyano groups located in the *cis*-position. This type of coordination leads to the formation of a curved polymeric chain (Figure 3.23). Crystals of **14** also turned out to be unstable, rapidly losing crystallinity in air.

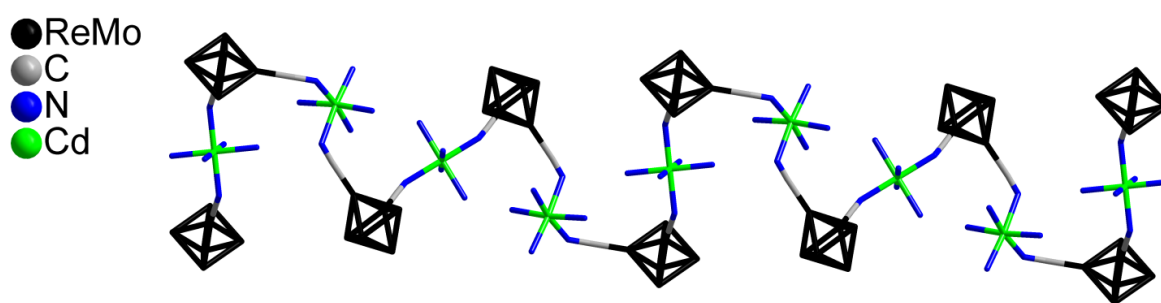


Figure 3.23: The simplified structure of the polymeric chain in the structure **14**, hydrogen, selenium atoms, terminal cyano-groups and $[Cd(NH_3)_n]^{2+}$ groups are omitted for clarity.

The use of the cadmium (II) chloride in the reaction led to the formation of two types of crystals: lamellar crystals of compound **14** and prismatic crystals of the compound $[\{Cd(NH_3)_4\}_3Re_3Mo_3Se_8(CN)_6]Cl$ (**15**). The addition of excess of potassium chloride to the aqueous ammonia solution of cadmium acetate led to the predominant formation of

compound **15**. Using other potassium halides, the isostructural **15** compounds $\{[\text{Cd}(\text{NH}_3)_4]_3[\text{Re}_3\text{Mo}_3\text{Se}_8(\text{CN})_6]\}\text{Br}$ (**16**) and $\{[\text{Cd}(\text{NH}_3)_4]_3[\text{Re}_3\text{Mo}_3\text{Se}_8(\text{CN})_6]\}\text{I}$ (**17**) are formed. The use of potassium thiocyanate led to the formation of the compound $\{[\text{Cd}(\text{NH}_3)_4]_2[\text{Cd}(\text{NH}_3)_3(\text{NCS})][\text{Re}_3\text{Mo}_3\text{Se}_8(\text{CN})_6]\}$ (**18**). The structural features of compound **18** and asymmetric unit composition, close environment of cationic and anionic nodes of all prepared coordination polymers are given in details below in the Section 4.4 of Chapter 4.

Compounds **15-17** have a 3 dimensional framework structure. The cluster anion acts as a six-connected node, cadmium aminocomplexes form the edges of the framework (Figure 3.24). The network in structures **15-17** are twice interpenetrating and are interconnected by a translation vector with coordinates $(2/3, 1/3, 1/3)$. The interaction between the two frameworks is carried out by hydrogen bonds between the hydrogen atoms of the ammonia molecules coordinated to the cadmium cations and the halide anion (Figure 3.25).

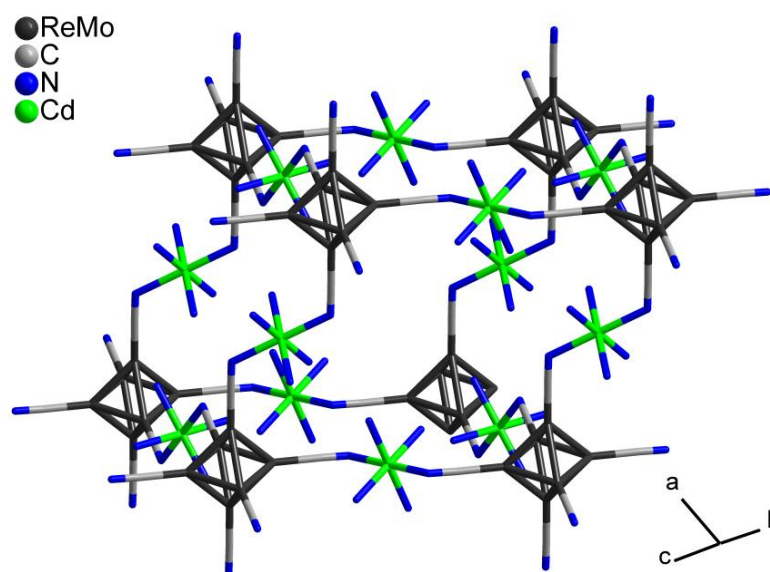


Figure 3.24: The simplified structure of the fragment of the network in **15**, hydrogen and selenium atoms are omitted for clarity.

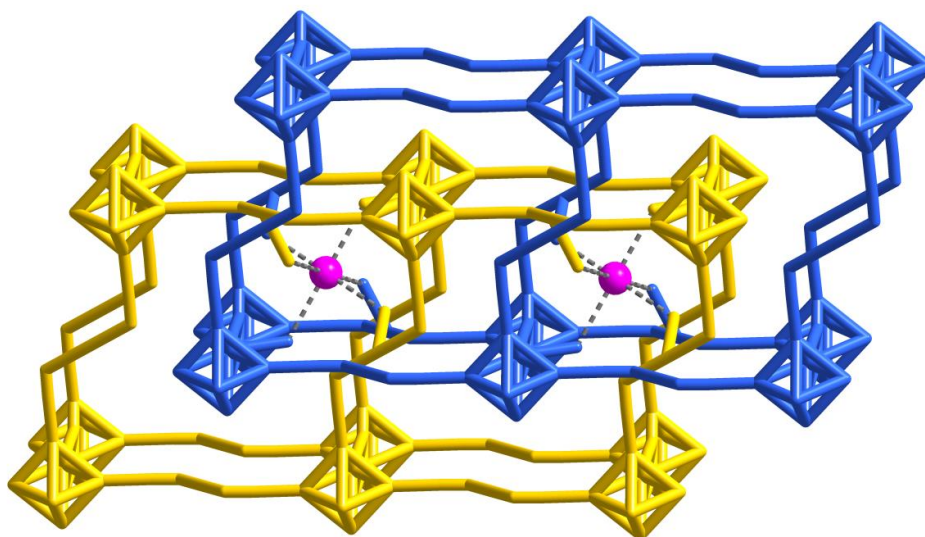


Figure 3.25: The simplified structure of the interpenetrated frameworks in the structure **15**, of nitrogen atoms of apical ammonia groups, selenium and hydrogen atoms are omitted for clarity. Different networks are shown in yellow and blue colors, chloride anions are given in pink color.

The $\text{N} \cdots \text{X}$ distances in structure **15–17** are 3.334(6) Å ($\text{X} = \text{Cl}$), 3.468(3) Å ($\text{X} = \text{Br}$), 3.641(6) Å ($\text{X} = \text{I}$). The obtained distances are consistent with those known in the literature for compounds with the hydrogen bond $\text{NH} \cdots \text{X}$ [199]. The distance between the donor and the acceptor of the hydrogen bond increases with increasing radius of the halide anion ($R = 1.81$ Å, 1.96 Å, and 2.20 Å for the chloride, bromide, and iodide anions, respectively [200]). The size of the halide anion also affects the unit cell parameters of structural compounds **15–17**. The crystal structure parameter increases from 15.0363(8) Å to 15.3596(15) Å upon transition from the chloride anion to the iodide anion, and parameter c changes slightly (Table S4, S5 in the Supplementary).

Interpenetrating frameworks of a similar topology are known for mononuclear cyanometallates $\text{Rb}[\text{Cd}\{\text{Ag}(\text{CN})_2\}_3]$ [201]. Among cluster complexes, similar structures are known for $[\text{SnMe}_3]_3[\text{Re}_6\text{S}_8(\text{CN})_6]$ [202] and $[\text{M}(\text{H}_2\text{O})_4]_3[\text{W}_6\text{S}_8(\text{CN})_6] \cdot x\text{H}_2\text{O}$ ($x \approx 23$; $\text{M} = \text{Mn}, \text{Fe}, \text{Co}$) [203]. The networks in these structures are not charged and do not contain additional ions that compensate the charge.

Compounds **15–18** can be obtained in preparative amounts by mixing solutions of the cluster salt and a solution containing cadmium acetate and excess potassium halide at

high ammonia contents. During the slow evaporation of ammonia, fine crystalline powders of **15–18** precipitate, which are stable in air and do not lose crystallinity rapidly.

Some properties of solid samples of compounds using compound **17** as an example will be considered. Thermogravimetric analysis of **17** showed that the removal of ammonia molecules proceeds smoothly in the temperature range 80–280°C (Figure 3.26).

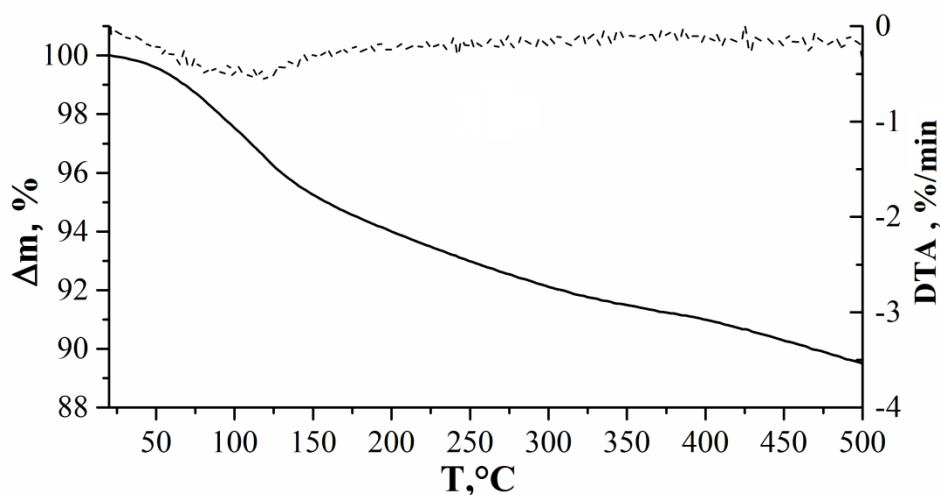


Figure 3.26: The TGA curves for the crystals of compound **17**.

It turned out that the obtained compounds lose some of the ammonia molecules upon annealing in air, the sample is partially amorphized and the remaining reflections shift to the region of large 2θ angles, which is associated with a decrease in the unit cell parameters. When the annealed sample is kept under ammonia vapor, the position of the reflections returns to the initial values. The exposure of the annealed samples in hydrazine vapor also leads to the restoration of crystallinity (Figure 3.27).

The diffuse reflection spectra in the Kubelka–Munk coordinates for the samples after annealing and exposure under ammonia and hydrazine vapor demonstrate the shift of the characteristic bands in the visible spectral region (Figure 3.28). The maxima of the absorption bands in the visible region of the spectrum correspond to similar absorption maxima in the absorption spectra for the cluster anions $[\text{Re}_3\text{Mo}_3\text{Se}_8(\text{CN})_6]^{n-}$ with different charges n in solutions (Table 3.8). The color change of the solid sample of **17** upon annealing and exposure under reductive nitrogen-containing vapor was assigned to the

redox transformations of the cluster anion embedded in the framework structure of the coordination polymer (Figure 3.29).

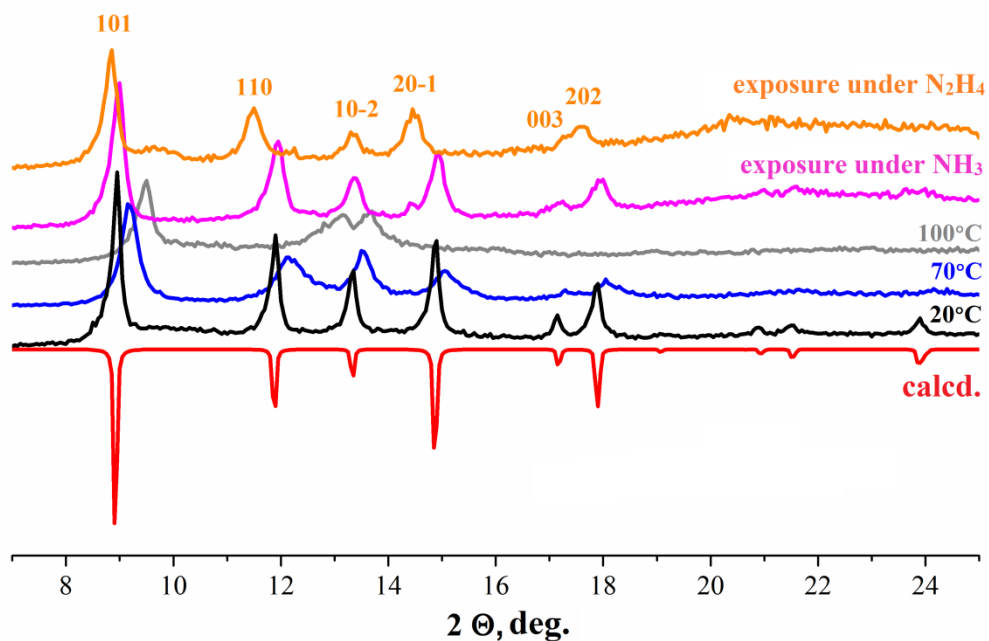


Figure 3.27: Powder XRD patterns for the samples of compound $\{[\text{Cd}(\text{NH}_3)_4]_3\text{Re}_3\text{Mo}_3\text{Se}_8(\text{CN})_6\}\text{I}$ (**17**) after the heating under different temperatures and exposure under ammonia and hydrazine vapor.

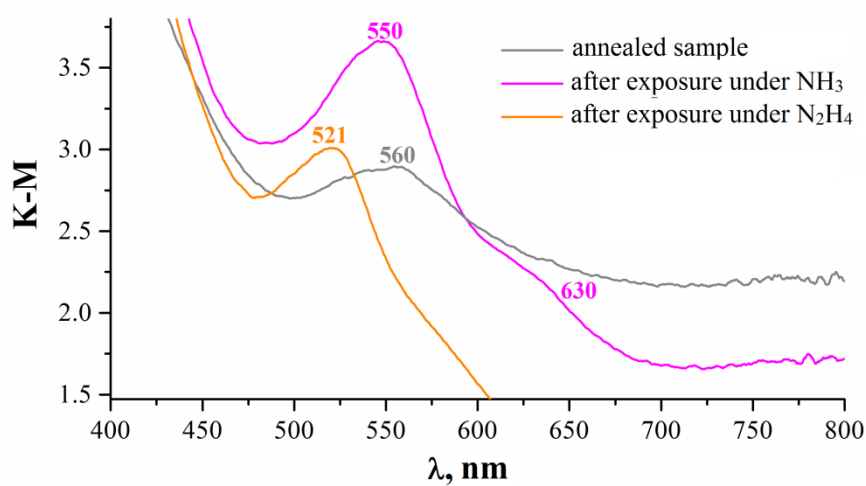


Figure 3.28: The diffuse reflectance spectra for the samples of compound **17** in the visible region.

Table 3.8: The values of the maxima of the characteristic bands in the diffuse reflectance spectra of the solid samples of **17** and absorption spectra of the cluster anions $[\text{Re}_3\text{Mo}_3\text{Se}_8(\text{CN})_6]^{n-}$ with different charge n in solution

| | Annealed sample | After exposure under NH_3 | After exposure under N_2H_4 |
|--------------|---|---|---|
| Band maximum | 560 nm | 550 nm | 521 nm |
| | $[\text{Re}_3\text{Mo}_3\text{Se}_8(\text{CN})_6]^{4-}$ in solution | $[\text{Re}_3\text{Mo}_3\text{Se}_8(\text{CN})_6]^{5-}$ in solution | $[\text{Re}_3\text{Mo}_3\text{Se}_8(\text{CN})_6]^{6-}$ in solution |
| Band maximum | 563 nm | 548 nm | 518 nm |

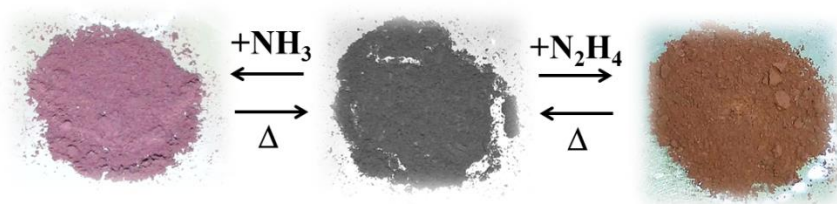


Figure 3.29: The color change of the annealed sample of compound **17** after exposure under the ammonia and hydrazine vapor.

According to the results of the study, it was shown that the charge of the cluster anion in solution affects the structure of the formed compounds. The interaction of the $[\text{Re}_3\text{Mo}_3\text{S}_8(\text{CN})_6]^{6-}$ and $[\text{Re}_3\text{Mo}_3\text{Se}_8(\text{CN})_6]^{5-}$ anions, which have the same geometry but different charge, with the cadmium ammino complex, in the first case provides a network structure of the Prussian blue type, in the second, a coordination polymer of chain-like topology. The presence of halide anions in the reaction mixture leads to a radical change in the preferred coordination polymer topology. The formation of a large number of hydrogen bonds between the hydrogen atoms of the amino groups and the halide anions stabilizes the formation of three-dimensional self-interpenetrated frameworks. The reversible oxidation/reduction of the anion in the polymeric structure is carried out without its decomposition, which is a rare phenomenon in the chemistry of coordination polymers. The transitions cause the remarkable color change of solid samples. These properties could be relevant to the design of chemical sensor materials.

3.9 The apical ligand exchange reactions of the clusters $[\text{Re}_3\text{Mo}_3\text{Se}_8(\text{CN})_6]^{5-}$ and $[\text{Re}_4\text{Mo}_2\text{Se}_8(\text{CN})_6]^{4-}$: formation of the complexes $[\text{Re}_{6-x}\text{Mo}_x\text{Se}_8\text{L}_6]$ $\text{L} = \text{tbp}, \text{PPh}_3$

As noted in the literature review, octahedral cluster complexes with apical halide ligands are convenient reagents for ligand substitution reactions. Heterometallic cluster complexes with $\{\text{Re}_{6-x}\text{Mo}_x\text{Q}_8\}$ $\text{Q} = \text{S}, \text{Se}$ core are formed in a potassium cyanide melt and were obtained only with cyanide ligands. There were no examples of substitution of cyanide ligands in high-valence octahedral cluster complexes before the beginning of the present study, which significantly limited their possible usage. On the other hand, examples of substitution of cyanide ligands for mononuclear transition metal complexes are known [204-206], evidencing that substitution considered is possible in principle.

Various approaches to substitution were studied and it was found that substitution of cyanide ligands in $[\text{Re}_{6-x}\text{Mo}_x\text{Se}_8(\text{CN})_6]^{n-}$ ($x = 3, 4$) cluster complexes is possible under solvothermal conditions. The interaction of the cluster salts $\text{K}_5[\text{Re}_3\text{Mo}_3\text{Se}_8(\text{CN})_6]$ and $\text{K}_4[\text{Re}_4\text{Mo}_2\text{Se}_8(\text{CN})_6]$ with 4-tert-butylpyridine in a water-acetonitrile mixture when heated to 160°C leads to the formation of crystals of compounds $[\text{Re}_3\text{Mo}_3\text{Se}_8(\text{tbp})_6]$ (**21**) and $[\text{Re}_4\text{Mo}_2\text{Se}_8(\text{tbp})_6]$ (**22**), respectively. A successful reaction requires a large excess of tert-butylpyridine and a mixture of water-acetonitrile, in a ratio of 1/1. During the reaction, all six cyanide groups are substituted and neutral complexes are formed. The initial salts of the clusters contain 22 CSE, while the substitution products contain 23 and 24 CSE, respectively, which means that the reduction of cluster complexes occurs during the reaction. The EPR spectrum of the paramagnetic complex $[\text{Re}_3\text{Mo}_3\text{Se}_8(\text{tbp})_6]$ (**21**) ($g = 2.299$) is shown in Figure 3.30.

A similar reaction occurs when the $\text{K}_4[\text{Re}_4\text{Mo}_2\text{Se}_8(\text{CN})_6]$ salt interacts with triphenylphosphine in a water-DMF mixture when heated to 160°C . Complete substitution of cyano groups leads to the formation of a neutral complex $[\text{Re}_4\text{Mo}_2\text{Se}_8(\text{PPh}_3)_6]$ (**23**). The crystal structure of the obtained neutral complexes is discussed in details below in the Section 4.5 of Chapter 4.

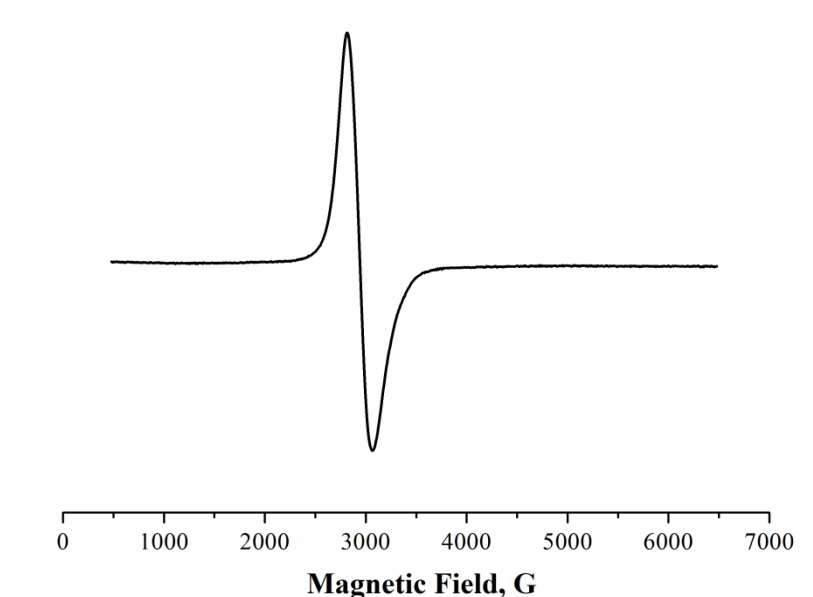


Figure 3.30: The EPR spectra of compound **21** at 77K.

Thus, the substitution of cyanide ligands in the heterometallic cluster complexes $[\text{Re}_3\text{Mo}_3\text{Se}_8(\text{CN})_6]^{5-}$ and $[\text{Re}_4\text{Mo}_2\text{Se}_8(\text{CN})_6]^{4-}$ was successfully carried out under conditions of solvothermal synthesis, which opens up the possibility of obtaining new complexes with heterometallic core and further development of chemistry of such complexes.

3.10 Principal outcome

1. It was found that the high-temperature reaction of ReSe_2 and MoSe_2 in a potassium cyanide melt leads to the formation of a phase of composition $\text{K}_6[\text{Re}_{6-x}\text{Mo}_x\text{Se}_8(\text{CN})]^{a-} {}_{2/2}(\text{CN})^a_4]$ ($x = 2.4, 3$), containing the cluster cores $\{\text{Re}_4\text{Mo}_2\text{Se}_8\}$, $\{\text{Re}_3\text{Mo}_3\text{Se}_8\}$ and $\{\text{Re}_2\text{Mo}_4\text{Se}_8\}$. With an increase in the synthesis temperature from 630 to 800°C, the content of the $\{\text{Re}_4\text{Mo}_2\text{Se}_8\}$ core increases, while $\{\text{Re}_2\text{Mo}_4\text{Se}_8\}$ decreases.
2. Experimental conditions for the separation of the cluster anions $[\text{Re}_5\text{MoSe}_8(\text{CN})_6]^{4-}$, $[\text{Re}_4\text{Mo}_2\text{Se}_8(\text{CN})_6]^{4-}$ and $[\text{Re}_3\text{Mo}_3\text{Se}_8(\text{CN})_6]^{4-}$ and the isolation of these anions individually in $(\text{Bu}_4\text{N})_4[\text{Re}_{6-x}\text{Mo}_x\text{Se}_8(\text{CN})_6]$ ($x = 1 - 3$) were found. This separation is based on the difference in the redox properties of the anions and the different solubility of their salts.
3. According to the data of X-ray diffraction analysis, DFT quantum chemical calculations and X-ray absorption spectroscopy, the average M – M distances in the metal core practically do not depend on the number of cluster skeletal electrons, while the Mo – Mo bond lengths in the metal core increase with decreasing number of CSEs. Meanwhile, Re – Re bond lengths decrease, accompanied by a significant distortion of the metal core.
4. It was shown that an increase in the number of molybdenum atoms in the $[\text{Re}_{6-x}\text{Mo}_x\text{Se}_8(\text{CN})_6]^{n-}$ anions ($x = 1-3$, $n = 4-6$) leads to a decrease in the electrochemical potentials and a change in the optical absorption spectra. A decrease in the number of cluster skeletal electrons in anions causes a red-shift in the absorption bands in the visible region towards larger wavelengths.
5. It was found that the $[\text{Re}_3\text{Mo}_3\text{Se}_8(\text{CN})_6]^{5-}$ cyanocomplex reacts with the amino complexes of transition metals with the formation of coordination polymers of various structures. The interaction of this anion with the cadmium (II) ammine complex in the presence of halide ions leads to the formation of isostructural compounds $\{[\text{Cd}(\text{NH}_3)_4]_3\text{Re}_3\text{Mo}_3\text{Se}_8(\text{CN})_6\}\text{X}$ ($\text{X} = \text{Cl}, \text{Br}, \text{I}$) containing three-dimensional covalently connected frameworks. These compounds are capable of reversible oxidation and re-

duction with a change in the charge state of the $[\text{Re}_3\text{Mo}_3\text{Se}_8(\text{CN})_6]^{5-}$ anion without decomposition of the polymeric framework.

6. It was shown that, under solvothermal conditions, pyridine and phosphine ligands replace the cyano groups of the cluster anions $[\text{Re}_3\text{Mo}_3\text{Se}_8(\text{CN})_6]^{5-}$ and $[\text{Re}_4\text{Mo}_2\text{Se}_8(\text{CN})_6]^{4-}$ with the formation of neutral complexes $[\text{Re}_3\text{Mo}_3\text{Se}_8(\text{tbp})_6]$ and $[\text{Re}_4\text{Mo}_2\text{Se}_8\text{L}_6]$, $\text{L} = \text{tbp}$, PPh_3 , which opens up the possibility of obtaining new complexes with heterometallic core and the further development of the chemistry of such complexes.

3.11 Conclusion

This work was carried out in the field of an actively developing area of cluster coordination chemistry, namely the chemistry of octahedral cluster complexes. Given the structural features of cluster complexes, the approach of mixing different type of metal atoms in a cluster core seems to be a promising tool for modifying the physicochemical properties of clusters. Prior to the start of this study, only a few examples of works devoted mainly to the synthesis and study of the structure of heterometallic compounds were presented in the literature. The main difficulty hampering the further development of this direction was the formation and co-crystallization of several heterometallic cluster complexes of different metal ratios. The methods for isolating such heterometallic cluster complexes in molecular salts with well-defined composition have not been previously reported in the literature. The problem of separation was successfully solved in the present work using heterometallic Re / Mo clusters as an example. This provided the opportunity to study the structure, spectroscopic characteristics and redox properties individually for each heterometallic cluster complexes of the series $[\text{Re}_{6-x}\text{Mo}_x\text{Se}_8(\text{CN})_6]^{n-}$ ($x = 1, 2$ and 3).

The developed approaches for the preparation and separation are general and can be used to study the reactions of high-temperature synthesis of other heterometallic octahedral cluster complexes and to obtain a wide range of heterometallic compounds of transition metals. It is planned to further develop approaches for the joint use of X-ray diffraction, EXAFS and NMR spectroscopy, geometry and electronic structure calculations to study the structure and composition of heterometallic cluster compounds. This study opened a series of Re / Mo

clusters capable of several successive electrochemical transitions in a narrow potential window, accompanied by a change in the optical spectrum of the cluster complex. Clusters with such reversible color-changing transitions are of interest in the field of electrochemically active materials and can be used to create sensors.

Chapter 4: Detailed description of the crystal structure of heterometallic Re/Mo cluster compounds

4.1 Crystal structures of the polymeric phases: $K_6[Re_3Mo_3Se_8(CN)^{a-a}_{2/2}(CN)^a_4]$ and $K_6[Re_{3.6}Mo_{2.4}Se_8(CN)^{a-a}_{2/2}(CN)^a_4]$

Compounds $K_6[Re_3Mo_3Se_8(CN)^{a-a}_{2/2}(CN)^a_4]$ (**1**) and $K_6[Re_{3.6}Mo_{2.4}Se_8(CN)^{a-a}_{2/2}(CN)^a_4]$ (**5**) are isostructural. The structure of the compounds will be considered using compound **1** as an example. Compound **1** crystallizes in tetragonal space group $I4/m$. An asymmetric unit of the structure contains two metal atoms sites M1 and M2, randomly occupied by rhenium and molybdenum atoms, a selenium atom, two potassium atoms, a carbon and nitrogen atom belonging to the apical cyanide group, and also the C/N1 position of bridged cyanide. M1, one of the potassium atoms and the cyanide atoms of the apical fragment are located in a special position on the plane of symmetry m with coordinates $(x, y, 0)$. M2 and C/N1 of the bridge cyanide are located on the fourth-order symmetry axis with coordinates $(0, 0, z)$. The second potassium atom is located in a position with -4 symmetry, with coordinates $(0, 1/2, 1/4)$. The selenium atom is located in a general position. From the crystallographic data, both bridged cyanide atoms are equivalent and are connected by a symmetry element (mirror plane m). The C/N1 position of the independent fragment was refined with an equal occupancy (0.5 / 0.5) of carbon and nitrogen atoms. Some differences were revealed in the ratios of rhenium and molybdenum in the indicated M1 and M2 sites. M2 located directly on the axis of symmetry contains more molybdenum (0.7 Mo) than the basal position M1 (0.4 Mo).

The cluster core $\{Re_3Mo_3Se_8\}$ demonstrate a typical structure of the octahedral chalcogenide cluster $\{M_6Q_8\}$. The molybdenum and rhenium atoms are randomly distributed in

the octahedral metal core $\{\text{Re}_3\text{Mo}_3\}$. The selenium atoms are coordinated by the μ_3 type to each face of the octahedron. Cluster cores are arranged according to linear chains through bridging cyanide ligands that bind two metal atoms (M2) of two different cluster cores. The basal metal atoms (M1) are additionally coordinated by apical cyanide ligands. The structure of the polymeric chain $[\text{Re}_3\text{Mo}_3\text{Se}_8(\text{CN})^{a-a}_{2/2}(\text{CN})^a_4]_\infty^{6-}$ and the unit cell of **1** are shown in Figure 4.1. The polymeric chains are located along the $00l$ direction of the structure at the vertices and in the center of the face AB, the potassium ions are located in the cavities between the chains.

The octahedral metal core $\{\text{Re}_3\text{Mo}_3\}$ in structure **1** is slightly distorted following a tetragonal elongation (Figure 4.2). Distortion lowers the ideal point symmetry of the O_h octahedron to D_{4h} . The distorted octahedron contains two types of bond lengths: longer M1 – M2 bonds between apical (M2) and basal (M1) metal atoms (2.6755 (7) Å) and shorter M1 – M1 bonds between basal atoms (2.6518 (7) Å). The average bond lengths M-M, M-Se and M-C for compound **1** are given in Table 4.1. The average metal-metal bond lengths range between the known lengths for the cyanide homometallic analogues $\text{K}_4[\text{Re}_6\text{Se}_8(\text{CN})_6] \cdot 3.5\text{H}_2\text{O}$ [147] and $\text{K}_6[\text{Mo}_6\text{Se}_8(\text{CN})^{a-a}_{2/2}(\text{CN})^a_4]$ [110] (2.633 and 2.703 Å, respectively). The distances M-Se and M-C follow a similar pattern. The C – N distances in the structures of homo- and heterometallic cyanoclusters are almost identical.

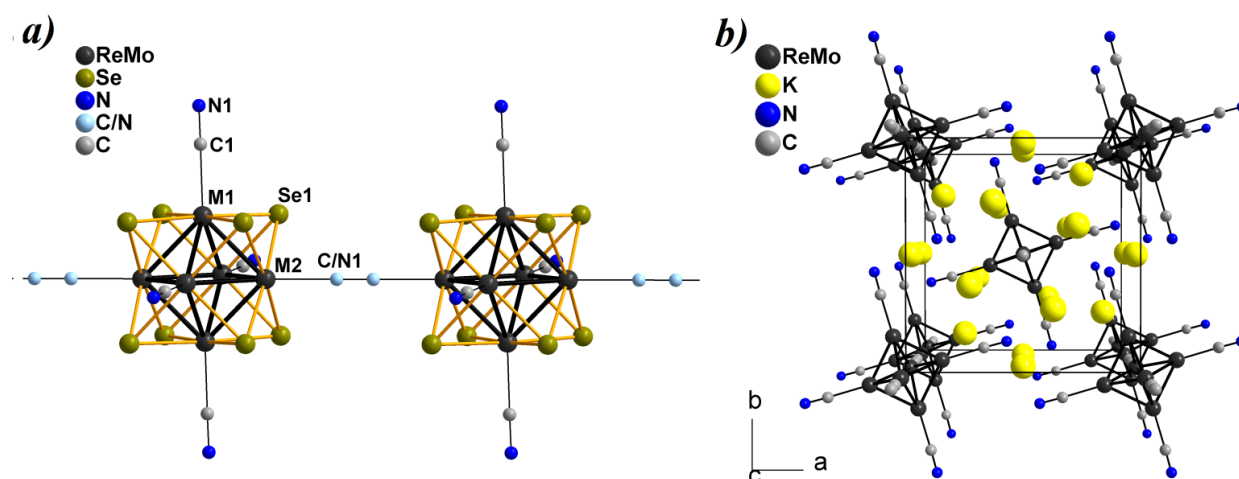


Figure 4.1: The structure of compound **1**: the fragment of the polymeric chain $[\text{Re}_3\text{Mo}_3\text{Se}_8(\mu\text{-CN})_{2/2}(\text{CN})_4]_\infty^{6-}$ (a) unit cell in the structure **1**, selenium atoms are omitted for clarity (b).

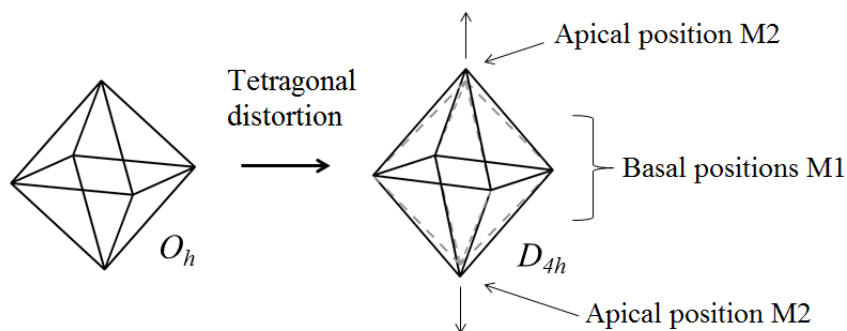


Figure 4.2: The distortion type of the metal core in the structure **1**.

The unit cell parameters of structures **1** and **5** differ slightly (Table S1 and S2 in the Supplementary). M1 and M2 in structure **5** have higher rhenium content compared to those of structure **1** (rhenium content in the positions is 0.70 and 0.35, respectively). The average lengths of M – M bonds in structure **5** are slightly lower than those observed in structure **1** (Table 4.1).

4.2 Crystal structures of molecular complexes $\text{Cat}_5[\text{Re}_3\text{Mo}_3\text{Se}_8(\text{CN})_6]$ (Cat = K, Cs) and $(\text{Ph}_4\text{P})_4[\text{Re}_3\text{Mo}_3\text{Se}_8(\text{CN})_6] \cdot 2\text{CH}_3\text{CN}$

$K_5[\text{Re}_3\text{Mo}_3\text{Se}_8(\text{CN})_6] \cdot 11\text{H}_2\text{O}$ (**2**). Compound **2** crystallizes in cubic space group $Fm-3m$. The asymmetric unit of the highly symmetric structure **2** contains one metal position M1, selenium, carbon, and nitrogen atoms belonging to cluster anion and potassium atoms located on two independent positions as well as oxygen atoms of solvate water molecules located in three independent positions. All atoms are located in special positions of the structure. The site occupancy of the M1 by rhenium and molybdenum atoms was refined to be 0.5 / 0.5. Similarly, the refined site occupancies of potassium positions give the first potassium position with a full occupancy and the second one with statistical occupancy (potassium content 0.1667). Two oxygen positions of solvate water molecules had statistical occupancy of 0.5, the third was fully occupied.

Due to its high symmetry, the metal core in structure **2** is an ideal octahedron with O_h symmetry. The resulting structure **2** contains isolated cluster anions $[\text{Re}_3\text{Mo}_3\text{Se}_8(\text{CN})_6]^{5-}$. Cya-

nide ligands coordinated in apical position. Cluster anions are packed into a bulk structure using ionic interactions between the nitrogen atom of the cyanide ligand and potassium cations. Structure **2** is similar to the structure of Prussian blue, and analogous to the salt of the molybdenum cluster complex $K_7[Mo_6Se_8(CN)_6] \cdot 8H_2O$ [111]. Potassium cation and cyanide ligands of the cluster in structure **2** have an ionic contact with a $K \cdots N$ distance of 2.684 Å. In the cavities of the structure there are positions with statistical occupancy of the remaining potassium ions and solvate water molecules. The structure of the cluster anion $[Re_3Mo_3Se_8(CN)_6]^{5-}$ and the fragment of crystal packing of the structure **2** are shown in Figure 4.3. The distances M-M, M-Se, M-C in structure **2** are slightly smaller than those obtained for structure **1** (Table 4.1).

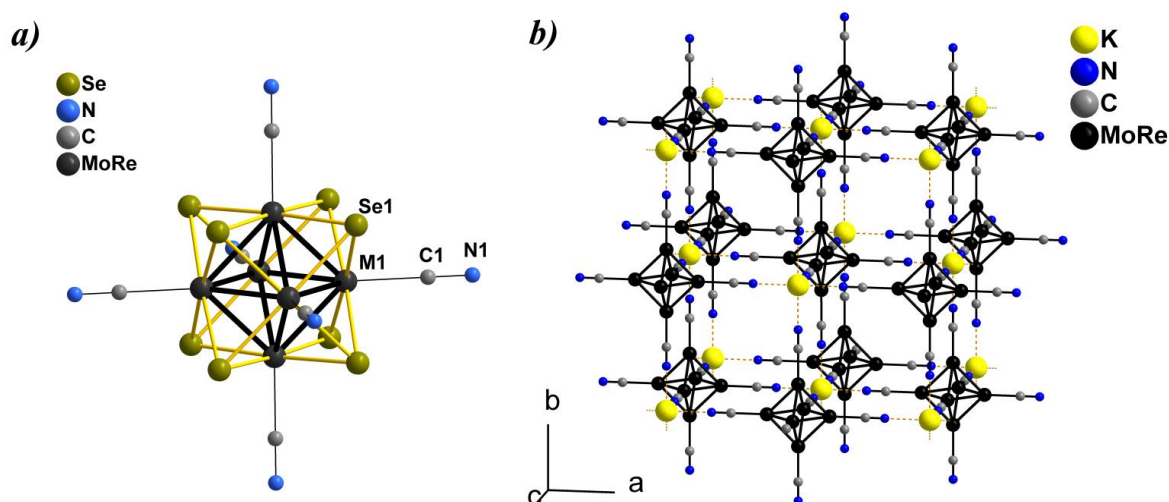


Figure 4.3: The structure of the compound **2**: cluster anion $[Re_3Mo_3Se_8(CN)_6]^{5-}$ (a) the fragment of crystal packing, selenium atoms, partially occupied potassium positions and solvate water molecules are omitted for clarity (b).

$Cs_5[Re_3Mo_3Se_8(CN)_6] \cdot H_2O$ (**3**). Compound **3** crystallizes in trigonal space group $P-3c1$. The asymmetric unit of the structure contains one metal position M1, two selenium atoms, one carbon and nitrogen atom. It also comprises cesium atoms statistically distributed between five independent positions and an oxygen atom located in one statistically occupied position. One of the selenium atoms, the cesium atom Cs1 and the oxygen atom are located in special positions on the 3-fold symmetry axes with coordinates $(0, 0, z)$, $(1/3, -1/3, z)$ and $(1/3, 2/3, z)$. The remaining atoms are located in general positions. The Mo/Re occupancies of the M1 were refined as 0.5 / 0.5.

Structure **3** contains cluster anions $[\text{Re}_3\text{Mo}_3\text{Se}_8(\text{CN})_6]^{5-}$, the structure of which is similar to that considered above. Cluster anions and cesium cations form a bulk packing due to weak ionic interactions of selenium atoms and nitrogen atoms of the cyanide groups of the cluster with cesium cations. The resulting structure contains $\{\text{Cs}_3[\text{Re}_3\text{Mo}_3\text{Se}_8(\text{CN})_6]\}^{2-\infty}$ layers (cesium atoms are located in a special position with full occupancy), the structure of which is shown in Figure 4.4. The distances between cesium cations and selenium and nitrogen atoms of the cluster anion in the layer are 3.81 Å and 3.38 Å, respectively. Remaining cesium atoms are located in the interlayer space statistically distributed between four independent positions.

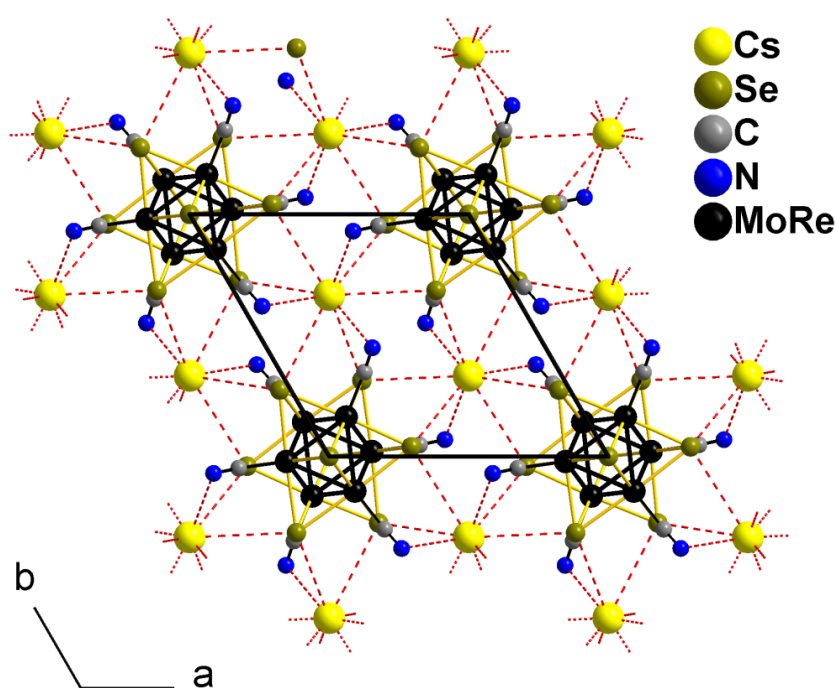


Figure 4.4: The fragment of the layer $\{\text{Cs}_3[\text{Re}_3\text{Mo}_3\text{Se}_8(\text{CN})_6]\}^{2-\infty}$ in the structure **3**.

$(\text{Ph}_4\text{P})_4[\text{Re}_3\text{Mo}_3\text{Se}_8(\text{CN})_6] \cdot 2\text{CH}_3\text{CN}$ (**4**). The resulting compound crystallizes in triclinic space group $P-1$. The asymmetric unit of the structure contains three metal positions M1, M2 and M3, four selenium atoms, three carbon atoms, and three nitrogen atoms of cyanide groups. It also contains two independent tetraphenylphosphonium cations and a solvate acetonitrile molecule. All atoms are located in general positions. The Re / Mo ratio on the M1, M2 and M3 positions were refined independently. The obtained position populations were close to 0.5 / 0.5 and were fixed at these values. Hydrogen atoms of phenyl groups were refined in geometrically calculated positions. The packing of struc-

ture **4** contains tetraphenylphosphonium cations Ph_4P^+ and cluster anions $[\text{Re}_3\text{Mo}_3\text{Se}_8(\text{CN})_6]^{4-}$ in small cavities between which solvate acetonitrile molecules are located. Cluster anions are located in the center of the unit cell (Figure 4.5). The average distances M-M, M-Se, M-C are close to those obtained for structures **2** and **3** (Table 4.1).

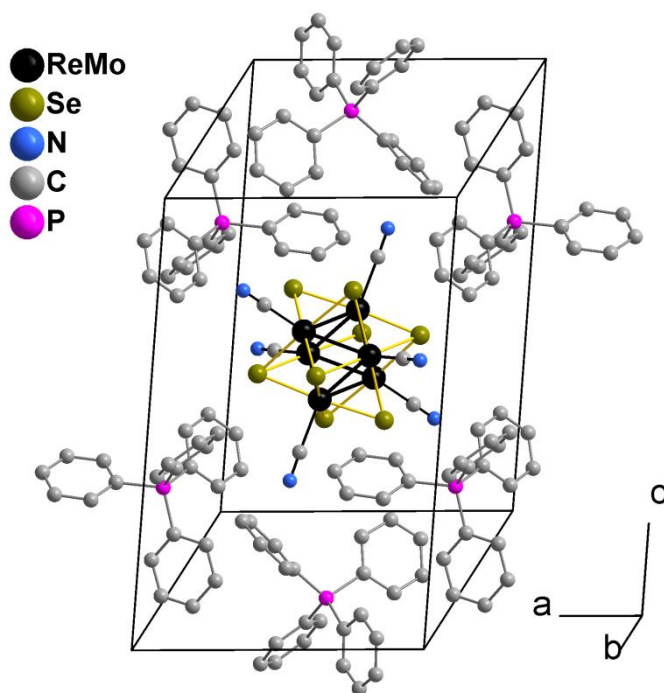


Figure 4.5: The unit cell of the structure **4**, solvate acetonitrile molecules are omitted for clarity.

4.3 Crystal structures of tetrabutylammonium salts of heterometallic clusters with different metal ratio $(n\text{-Bu}_4\text{N})_4[\text{Re}_{6-x}\text{Mo}_x\text{Se}_8(\text{CN})_6]$ $x = 1, 2$ and 3

Tetrabutylammonium salts $(n\text{-Bu}_4\text{N})_4[\text{Re}_5\text{MoSe}_8(\text{CN})_6]$ (**7**), $(n\text{-Bu}_4\text{N})_4[\text{Re}_4\text{Mo}_2\text{Se}_8(\text{CN})_6]$ (**10**) and $(n\text{-Bu}_4\text{N})_4[\text{Re}_3\text{Mo}_3\text{Se}_8(\text{CN})_6]$ (**13**) have a similar structure. The structure of these compounds will be considered using compound **10** as an example. The compound crystallizes in orthorhombic space group *Pbca*. The asymmetric unit of the structure contains 3 positions of the metal M1, M2 and M3, 4 atoms of selenium, 3 carbon and nitrogen atoms of cyanide groups. The cationic part contains two crystallographically independent tetrabutylammonium cations. All atoms are located in general positions. As a result of the refinement, the Re / Mo ratio in M1, M2 and M3 were: 0.727 / 0.273, 0.683 / 0.317 and

0.59 / 0.41, respectively. The total rhenium / molybdenum ratio in the resulting structure is 4/2 and is in good agreement with the EDS results.

The cluster anions $[\text{Re}_4\text{Mo}_2\text{Se}_8(\text{CN})_6]^{4-}$ have a geometry similar to that considered above. Anions are located at the vertices and centers of the faces of the unit cell. Tetrabutylammonium cations are located in the cavities between the anions. The structure does not contain the cavities with solvent molecules. The unit cell of **10** is shown in Figure 4.6.

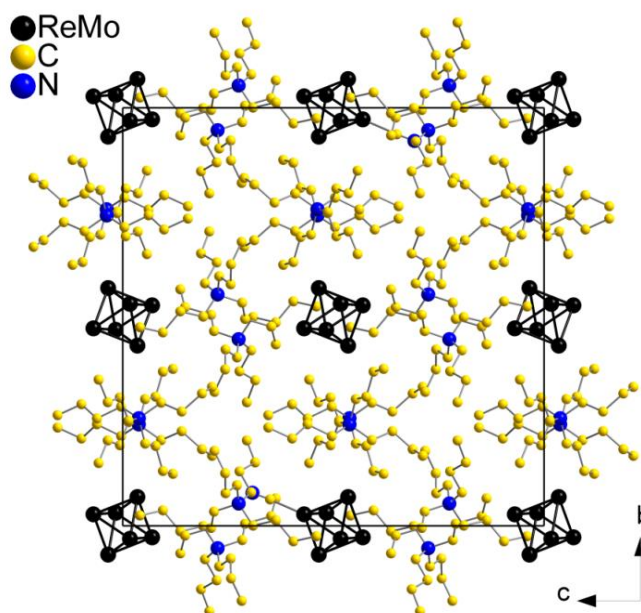


Figure 4.6: The structure of the unit cell of **10**, hydrogen, selenium atoms and cyanide ligands are omitted for clarity.

The unit cell parameters change only slightly with a change in the composition of the metal core (Tables S2, S3 in the Supplementary). The rhenium/molybdenum ratio in the M1, M2 and M3 positions with independent refinement for structure **7** was 0.854 / 0.146, 0.859 / 0.141 and 0.806 / 0.194. The total Re / Mo ratio in structure **7** is 5/1, which is in good agreement with the data of elemental analysis. The metal ratio for structure **13** was 0.546 / 0.454, 0.555 / 0.445 and 0.413 / 0.587, which leads to a total metal ratio of 3/3, which is consistent with EDS data. The average lengths of M – M bonds increase with an increase in the molybdenum content in the cluster core of the compound. The shortest bonds are observed for compound **7** (2.640 Å), and the longest bonds are observed in structure **13** (2.656 Å). M – Se bond lengths show similar behavior. The M – C distances for the structures obtained are almost the same. The distances M – M, M – Se, M – C for

structure **13** are close to related distances in structure **4**, which mainly contains the cluster anion $[\text{Re}_3\text{Mo}_3\text{Se}_8(\text{CN})_6]^{4-}$.

The selected interatomic distances M-M and M-L for structures **7**, **10** and **13** are given in Table 4.1. The obtained distances range between the known values for rhenium and molybdenum selenide clusters $\text{K}_6[\text{Mo}_6\text{Se}_8(\text{CN})^{a-a}_{2/2}(\text{CN})^a_4]$, $\text{K}_7[\text{Mo}_6\text{Se}_8(\text{CN})_6] \cdot 8\text{H}_2\text{O}$, $(\text{Me}_4\text{N})_4\text{K}_2[\text{Mo}_6\text{Se}_8(\text{CN})_6] \cdot 10\text{H}_2\text{O}$ and $\text{K}_4[\text{Re}_6\text{Se}_8(\text{CN})_6] \cdot 3.5\text{H}_2\text{O}$, $(\text{Me}_4\text{N})_4[\text{Re}_6\text{Se}_8(\text{CN})_6] \cdot 3.33\text{H}_2\text{O}$ (Table 4.1). The interatomic distances for compounds with the $\{\text{Re}_3\text{Mo}_3\text{S}_8\}$ core are lower than those obtained for compounds based on the $\{\text{Re}_3\text{Mo}_3\text{Se}_8\}$ core (Table 4.1). This is probably due to the smaller size of the sulfide cluster.

$(n\text{-Bu}_4\text{N})_4[\text{Re}_3\text{Mo}_3\text{Se}_8(\text{CN})_6] \cdot 3\text{H}_2\text{O}$ (**13·3H₂O**). Compound **13·3H₂O** crystallizes in the monoclinic space group $P2_1/c$. The asymmetric unit of the structure contains three metal positions M1, M2 and M3, four selenium atoms and three carbon and nitrogen atoms of cyanide groups, as well as two tetrabutylammonium cations and two positions of oxygen atoms. All atoms are in general positions. The ratio of rhenium and molybdenum atoms obtained as a result of refinement is consistent with the elemental analysis for **13·3H₂O** crystals. Solvate water molecules are located in the cavities between tetrabutylammonium cations and cluster anions. The interatomic distances in the cluster anion of the structure are close to those obtained for structure **13** (Table 4.1).

4.4 Crystal structures of coordination polymers based on $[\text{Re}_3\text{Mo}_3\text{Se}_8(\text{CN})_6]^{5-}$ cyanocluster and metal ammine complexes of Cd^{2+} , Ni^{2+} and Co^{2+}

$\{[\text{Cd}(\text{NH}_3)_5]_2[\text{Cd}(\text{NH}_3)_4]_3[\text{Re}_3\text{Mo}_3\text{Se}_8(\text{CN})_6]_2\} \cdot 5\text{H}_2\text{O}$ (**14**). Compound **14** crystallizes in the monoclinic space group $P-1$. The asymmetric unit of the structure contains two cluster anions $[\text{Re}_3\text{Mo}_3\text{Se}_8(\text{CN})_6]^{5-}$ and 6 cadmium atoms Cd1 – Cd6. Atoms belonging to cluster anions are located in general positions. The total occupancy of all metal positions leads to a Re-Mo ratio in the cluster core of 1/1. The asymmetric unit of the structure is shown in Figure 4.7. The cadmium atoms Cd1, Cd3 are located in special position with

the point symmetry -1 . The remaining cadmium atoms are located in general positions. Cluster complexes in the resulting structure **14** are linked into polymer chains by means bridging groups $[\text{Cd}(\text{NH}_3)_4]^{2+}$. The simplified structure of the polymer chain is shown in Figure 4.8. The cadmium atoms of $[\text{Cd}(\text{NH}_3)_4]^{2+}$ adopt two nitrogen atoms of cluster cyanogroups gaining octahedral environment $[\text{Cd}(\text{NH}_3)_4(\text{NC})_2]$. The environment of the Cd2 and Cd3 atoms are the *trans*- $[\text{Cd}(\text{NH}_3)_4(\text{NC})_2]$ octahedron, and Cd1 is the *cis*- $[\text{Cd}(\text{NH}_3)_4(\text{NC})_2]$ octahedron.

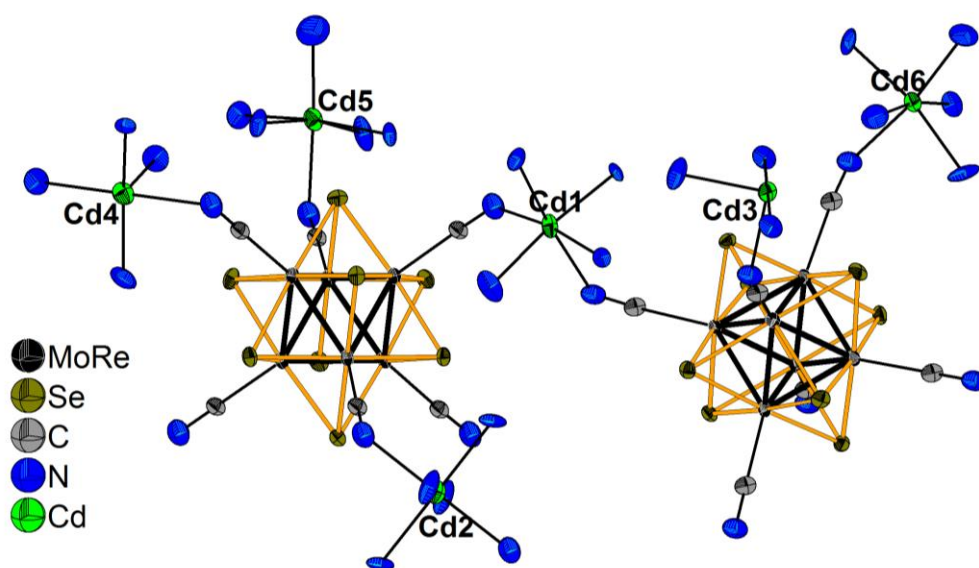


Figure 4.7: The asymmetric unit of the structure **14**, thermal ellipsoids are shown in 50% of probability.

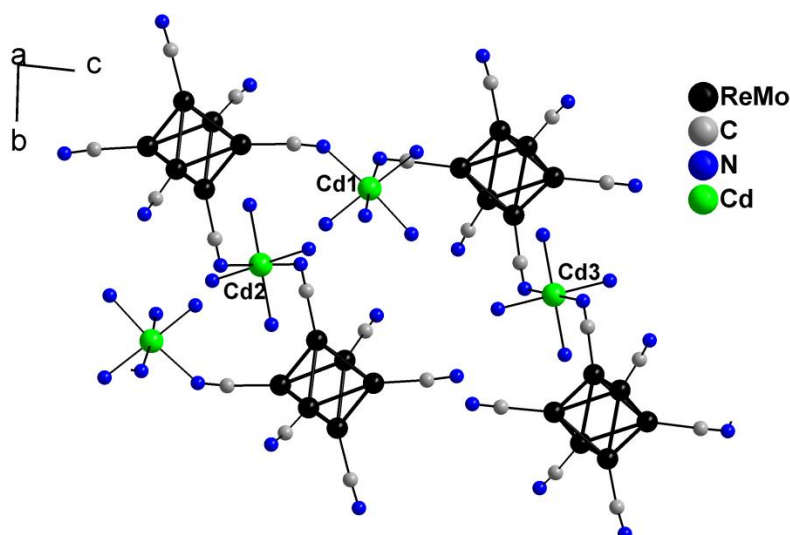


Figure 4.8: The fragment of the polymeric chain in the structure **14**. Hydrogen, selenium atoms and terminal groups $[\text{Cd}(\text{NH}_3)_n]^{2+}$ are omitted for clarity.

$\{[Cd(NH_3)_4]_3Re_3Mo_3Se_8(CN)_6\}X$, with $X = Cl$ (**15**), Br (**16**), I (**17**). Compounds **15-17** are isostructural. The structure of the compounds will be considered using compound **15** as an example. The compound crystallizes in trigonal space group $R\bar{3}$. The asymmetric unit of the structure contains two metal atoms M1 and M2, two selenium atoms, carbon and nitrogen atom of a cyanide group, a cadmium atom, two nitrogen atoms of ammonia molecules and a chlorine atom. The chlorine atom is located in a special position with $\bar{3}$ point symmetry. The atoms Se1 and Cd1 are also located in special positions with symmetry 3 and $\bar{1}$, respectively. The remaining atoms are located in general positions. The Re/Mo ratio in the resulting structure was refined to 1/1.

Compound **15** has a framework structure. The polymeric framework is formed by cluster anions and $[Cd(NH_3)_4]^{2+}$ groups. The cluster anion acts as a six-connected node. Cadmium cations bind two nitrogen atoms of cluster cyanogroups and form the edges of the framework. The coordination environment of cadmium ions is octahedral *trans*- $[Cd(NH_3)_4(NC)_2]$. The coordination environment of anions and cations in the polymeric structure is shown in Figure 4.9. The detailed description of the polymeric framework is given in the Results and Discussion part. Cell parameters of structures **16** and **17** differ slightly from those of **15**, due to the larger radii of the halide anion.

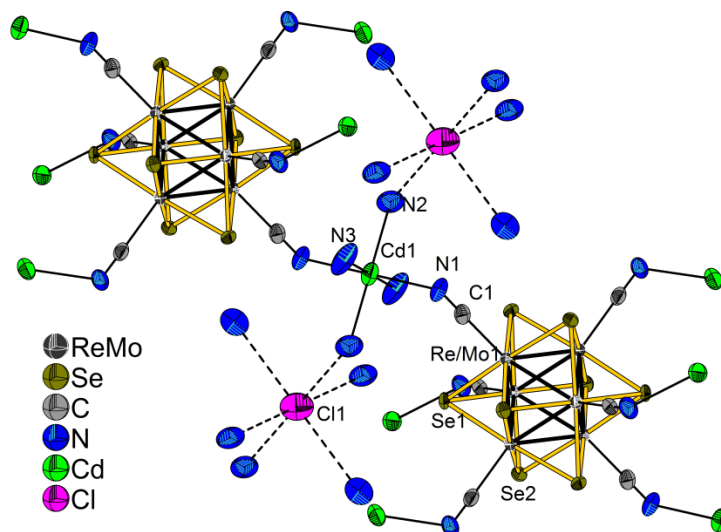


Figure 4.9: Coordination environment of cationic and anionic nodes in the structure **15**. Thermal ellipsoids are given in 75% of probability.

$\{[Cd(NH_3)_4]_2[Cd(NH_3)_3(NCS)]Re_3Mo_3Se_8(CN)_6\}$ (**18**). Compound **18** also crystallizes in trigonal space group $R\bar{3}$, and has an analogous structure of the framework. The asymmetric unit of the structure contains two metal atoms M1 and M2, two selenium atoms, carbon and nitrogen atom of a cyanide group, a cadmium atom, two positions of nitrogen atoms of ammonia molecules, as well as a sulfur, carbon and nitrogen atoms of the thiocyanate anion. The main difference between structure **18** and structures **15–17** discussed above is observed in the coordination environment of cadmium ions and the arrangement of the thiocyanate anion. The sulfur atom is located in special position with a $\bar{3}$ symmetry, similarly to the chlorine atom in the structure of the compound **15**. The carbon atom and the nitrogen atom of the thiocyanate anion are statistically distributed between six equivalent positions each, located on the octahedron around the sulfur atom at a distance of 1.64 Å and 2.773 Å, respectively. The occupancy of each position is 0.167. The sulfur atom is surrounded by five nitrogen atoms of the ammonia molecules, statistically distributed between six general positions with occupancy of 0.833 each, located on the octahedron around the sulfur atom at a distance of 3.493 Å (Figure 4.10 a). The ligand environment of the cadmium atom is shown in Figure 4.10 b.

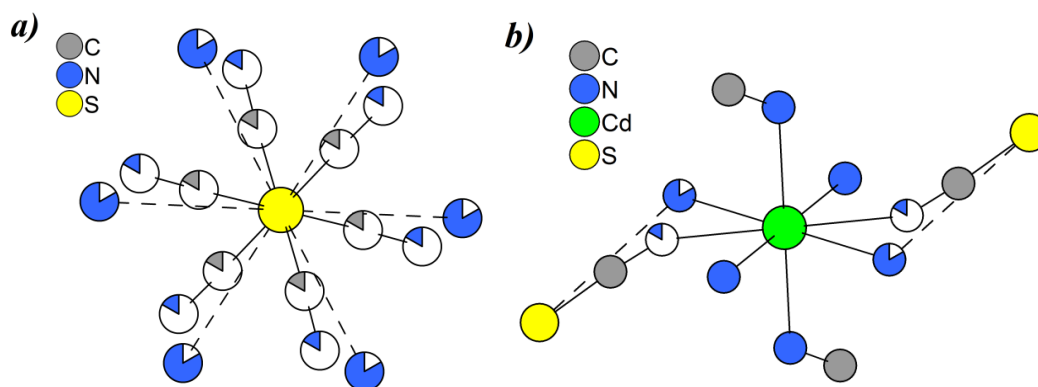


Figure 4.10: Coordination environment of the atoms in the structure **18**: environment of the sulfur atoms (a) and cadmium atoms (b), the size of the colored part corresponds to the occupancy of the site.

The Cd – N interatomic distances for structures **14–18** exceed the previously obtained values for the coordination polymer $[Cd(NH_3)_4]_2\{Cd[Re_3Mo_3S_8(CN)_6]\} \cdot 1.5H_2O$ based on a sulfide cluster (Table 4.2), due to the smaller size of the sulfide cluster anion.

$[M(NH_3)_6]_4[\{M(NH_3)_2\}\{Re_3Mo_3Se_8(CN)_6\}_2] \cdot 15H_2O$ $M = Co$ (**19**), Ni (**20**). Compounds **19** and **20** are isostructural. The structure of the compounds obtained will be considered using compound **19** as an example. This compound crystallizes in triclinic space group $P-1$. The asymmetric unit of the cell contains six metal positions M1 to M6, eight selenium atoms Se1 – Se8, six carbon and nitrogen atoms of cyanogroups belonging to two crystallographically independent cluster anions. The atoms M1 – M3, Se1-Se4, C1-C3, and N1-N3 belong to one cluster anion, M4-M6, Se5-Se8, C4-C6, N4-N6 to the second cluster anion, respectively. Atoms corresponding to cluster anions are located in general positions. The geometric centers of the anions coincide with the centers of inversion with the coordinates (0 0 0) and (0.5 0.5 0). Cluster anions are located at the vertices and in the center of the face C of the unit cell. The cationic part is represented by five independent cobalt positions: Co1 – Co5. The cobalt atoms are located in special positions with a symmetry of -1 .

Compound **19** has a layered structure. The layers are formed by cluster anions and cobalt cations. The Co1 atom coordinates four nitrogen atoms of the cyanogroups of the cluster, which are located in the plane at an angle of 45° relative to each other (Figure 4.11 a). The coordination environment of the Co1 atom is the $trans-[Co(NH_3)_2(NC)_4]^{2-}$ octahedron (Figure 4.11 d). The cobalt atoms Co2 - Co5 are located in the octahedral environment of ammonia molecules and form isolated cationic complexes $[Co(NH_3)_6]^{2+}$ (Figure 4.11 c). These complexes are located inside the layer cells and in the interlayer space, compensating the excess of negative charge of the polymeric layer (Figure 4.11 a, b). The interatomic distances for the resulting structures are given in Tables 4.1 and 4.2.

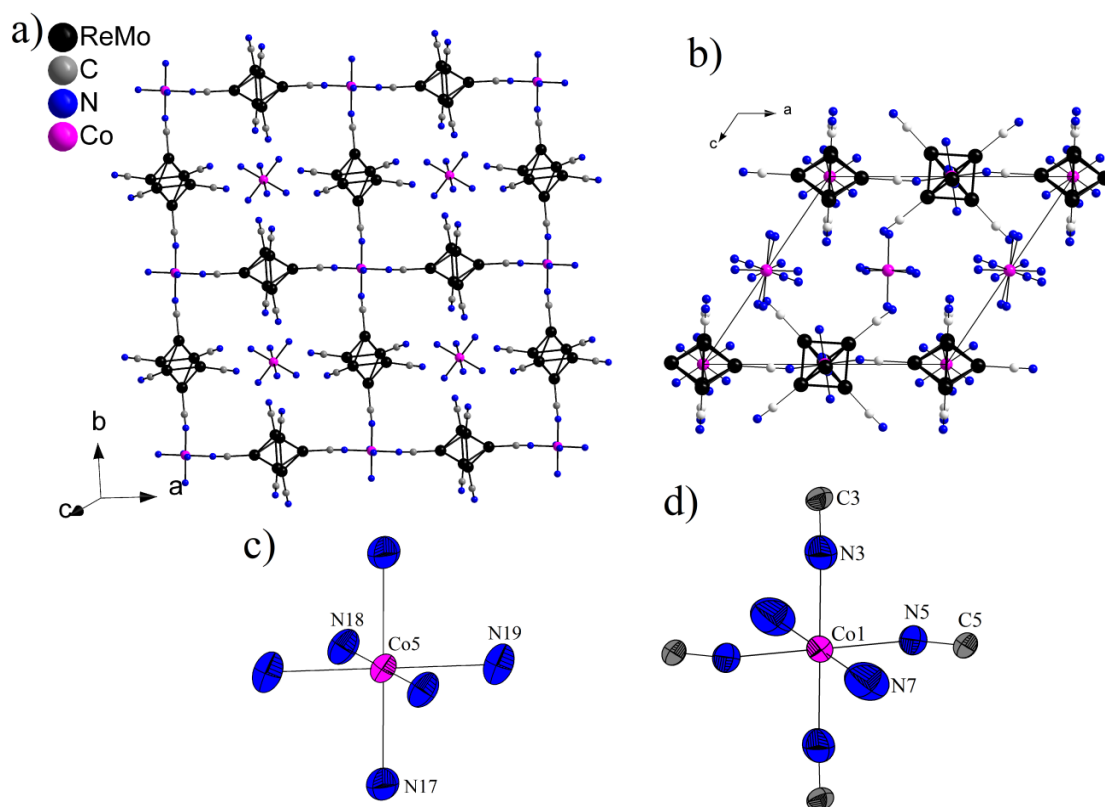


Figure 4.11: The structure of the compound **19**: the fragment of the polymeric layer $[\{\text{Co}(\text{NH}_3)_2\}\{\text{Re}_3\text{Mo}_3\text{Se}_8(\text{CN})_6\}_2]_{\infty}^{8-}$ (a); the unit cell of the structure (b); coordination environment of the Co5 atom (c); coordination environment of the Co1 atom (d). Selenium, hydrogen atoms and solvate water molecules are omitted for clarity.

4.5 Crystal structures of heterometallic clusters with apical organic ligands $[\text{Re}_{6-x}\text{Mo}_x\text{Se}_8\text{L}_6]$ $\text{L} = \text{tbp}, \text{Ph}_3\text{P}$

$[\text{Re}_{6-x}\text{Mo}_x\text{Se}_8(\text{tbp})_6]$ ($x = 3$ (**21**), $x = 2$ (**22**)). Compounds **21** and **22** have a similar structure. The structure of the compounds obtained will be considered using compound **21** as an example. Cluster complex **21** crystallizes in the triclinic space group $P\bar{1}$. The independent part of the structure contains six metal atoms, eight selenium atoms, six tert-butylpyridine ligands. The total occupancies of metal positions correspond to 3/3 Re/Mo ratio agreeing well with the results of EDS. The $[\text{Re}_3\text{Mo}_3\text{Se}_8(\text{tbp})_6]$ neutral cluster complexes are packed into a bulk structure; there are small cavities between the complexes filled with the electron density of disordered solvent molecules. According to the residual electronic density removed by SQUEEZE procedure, the compound contains about eight solvate acetonitrile molecules. The structure of the $[\text{Re}_3\text{Mo}_3\text{Se}_8(\text{tbp})_6]$ cluster complex is

shown in Figure 4.12. The interatomic distances for the resulting structures are given in Table 4.1.

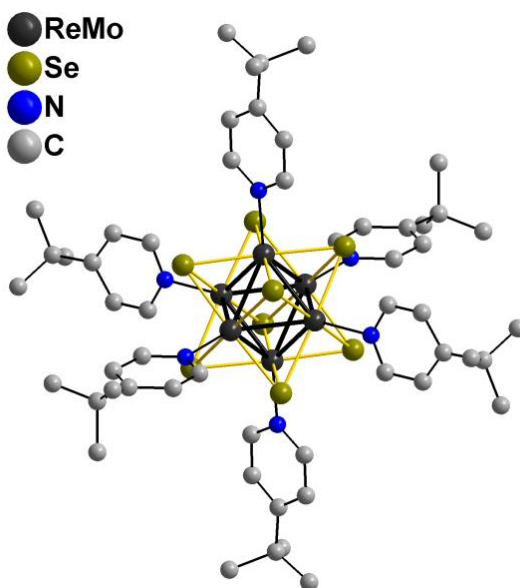


Figure 4.12: The structure of the complex $[\text{Re}_3\text{Mo}_3\text{Se}_8(\text{tbp})_6]$ (**21**).

$[\text{Re}_4\text{Mo}_2\text{Se}_8(\text{PPh}_3)_6]$ (**23**). Compound **23** crystallizes in triclinic space group *P*-1. The asymmetric part of the structure contains six metal atoms, eight selenium atoms, six triphenylphosphine ligands. The total occupancies of metal positions is correlated by EDS results. The neutral cluster complexes $[\text{Re}_4\text{Mo}_2\text{Se}_8(\text{PPh}_3)_6]$ in structure **23** are closely packed, the structure does not contain cavities. The structure of cluster complex **23** is shown in Figure 4.13.

M-M bond distances within the heterometallic cluster complexes $[\text{Re}_{6-x}\text{Mo}_x\text{Se}_8\text{L}_6]$ ($x = 3$ $\text{L} = \text{tbp}$, $x = 4$ $\text{L} = \text{tbp}$, PPh_3) with organic ligands are between the known values for the homometallic cluster complexes of rhenium and molybdenum with a similar ligand environment: *trans*- $[\text{Re}_6\text{Se}_8(\text{PPh}_3)_4\text{Cl}_2]$, $(\text{SbF}_6)_2[\text{Re}_6\text{Se}_8(\text{py})_6]$ and $[\text{Mo}_6\text{Se}_8(\text{PPh}_3)_6] \cdot 2\text{H}_2\text{O}$, $[\text{Mo}_6\text{S}_8(\text{tbp})_6]$ (Table 4.1). Metal-ligand bond lengths also follow this tendency.

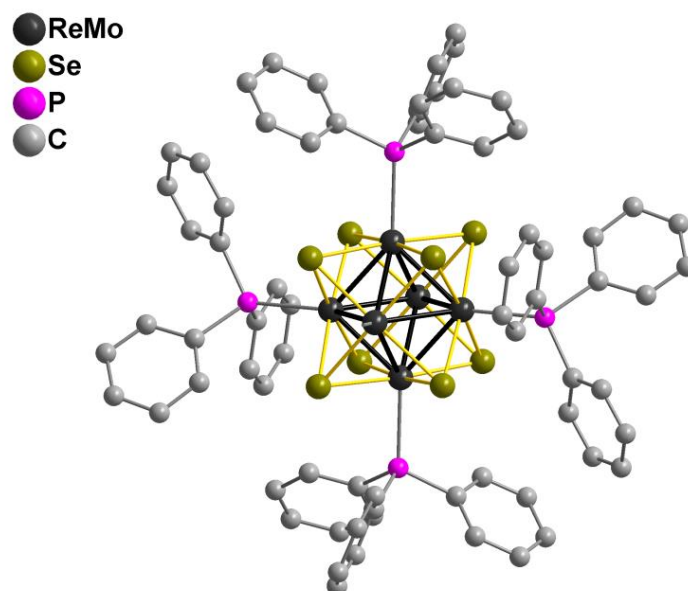


Figure 4.13: The structure of the cluster complex $[\text{Re}_4\text{Mo}_2\text{Se}_8(\text{PPh}_3)_6]$ (**23**), two PPh_3 ligands are omitted for clarity.

Table 4.1: Interatomic distances (\AA , <average>) M–M, M–L for heterometallic cluster complexes with the cores $\{\text{Re}_{6-x}\text{Mo}_x\text{Q}_8\}$ Q = S, Se in comparison with homometallic analogues

| | M–M | M–Q ⁱ | M–L ^a | Reference |
|---|--|--|---|-----------------|
| Homometallic clusters with the cores $\{\text{M}_6\text{Se}_8\}$ M = Mo, Re | | | | |
| $\text{K}_6[\text{Mo}_6\text{Se}_8(\text{CN})^{a-a}_{2/2}(\text{CN})^a_4]$ | 2.6711(4)–2.7193(4) <2.703(4)> | 2.5683(3)–2.5873(3) <2.5763(3)> | 2.204(3) | [110] |
| $\text{K}_7[\text{Mo}_6\text{Se}_8(\text{CN})_6] \cdot 8\text{H}_2\text{O}$ | 2.700(3) | 2.562(3) | 2.17(2) | [111] |
| $(\text{Me}_4\text{N})_4\text{K}_2[\text{Mo}_6\text{Se}_8(\text{CN})_6] \cdot 10\text{H}_2\text{O}$ | 2.700(2) – 2.721(2) <2.711(2)> | 2.568(2) – 2.584(2) <2.573(5)> | 2.19(2) – 2.21(1) <2.20(2)> | [111] |
| $\text{K}_4[\text{Re}_6\text{Se}_8(\text{CN})_6] \cdot 3.5\text{H}_2\text{O}$ | 2.624(1) – 2.642(1) <2.633(1)> | 2.516(2) – 2.538(2) <2.526(2)> | 2.09(2) – 2.12(2) <2.11> | [147] |
| $(\text{Me}_4\text{N})_4[\text{Re}_6\text{Se}_8(\text{CN})_6] \cdot 3.33\text{H}_2\text{O}$ | 2.622(2) – 2.638(2) <2.633(2)> | 2.520(3) – 2.550(3) <2.533(3)> | 2.06(2) – 2.14(2) <2.09(2)> | [207] |
| Heterometallic clusters with the cores $\{\text{Re}_{6-x}\text{Mo}_x\text{Q}_8\}$ | | | | |
| $\text{CaK}_4[\text{Re}_3\text{Mo}_3\text{S}_8(\text{CN})_6] \cdot 8\text{H}_2\text{O}$ | 2.6273(8) | 2.439(2) | 2.173(13) | [27] |
| $\text{K}_6[\text{Re}_3\text{Mo}_3\text{S}_8(\text{CN})^{a-a}_{2/2}(\text{CN})^a_4]$ | 2.6323(3) – 2.6399(3) <2.637(4)> | 2.4344(8) – 2.4544(8) <2.444(8)> | 2.209(6) $\mu\text{-C}_\text{N}$, 2.157(5) | [27] |
| $\text{K}_6[\text{Re}_3\text{Mo}_3\text{Se}_8(\text{CN})^{a-a}_{2/2}(\text{CN})^a_4]$ (1) | 2.6518(7)–2.6755(7) <2.667(8)> | 2.5476(8)–2.5633(7) <2.56(2)> | 2.15(1) $\mu\text{-C}_\text{N}$ 2.20(1) | [192] |
| $\text{K}_6[\text{Re}_{3.6}\text{Mo}_{2.4}\text{Se}_8(\text{CN})^{a-a}_{2/2}(\text{CN})^a_4]$ (5) | 2.6481(7) – 2.6663(6) <2.660(9)> | 2.5442(7) – 2.5653(7) <2.554(9)> | 2.15(1) $\mu\text{-C}_\text{N}$ 2.22(1) | present work |
| $\text{K}_5[\text{Re}_3\text{Mo}_3\text{Se}_8(\text{CN})_6] \cdot 11\text{H}_2\text{O}$ (2) | 2.6494(9) | 2.5464(9) | 2.14(2) | [192] |
| $\text{Cs}_5[\text{Re}_3\text{Mo}_3\text{Se}_8(\text{CN})_6] \cdot \text{H}_2\text{O}$ (3) | 2.6451(9)–2.6459(9) <2.645(11)> | 2.541(1)–2.549(1) <2.54(3)> | 2.157(11) | [192] |
| $(\text{Ph}_4\text{P})_4[\text{Re}_3\text{Mo}_3\text{Se}_8(\text{CN})_6] \cdot 2\text{CH}_3\text{CN}$ (4) | 2.6407(2)–2.6619(2) <2.654(2)> | 2.5197(3)–2.5463(3) <2.539(7)> | 2.164(3)–2.171(3) <2.17(2)> | [192] |
| $(\text{n-Bu}_4\text{N})_4[\text{Re}_3\text{Mo}_3\text{Se}_8(\text{CN})_6]$ (13) | 2.6417(10) – 2.6697(10) <2.656(9)> | 2.5294(15) – 2.5559(15) <2.542(8)> | 2.142(14) – 2.188(15) <2.16(2)> | present work |

| | | | | |
|---|--------------------------------------|--|------------------------------------|-----------------|
| (n-Bu ₄ N) ₄ [Re ₃ Mo ₃ Se ₈ (CN) ₆]·3H ₂ O (13·3H ₂ O) | 2.6354(4) – 2.6703(4) <2.656(11)> | 2.5245(7) – 2.5616(7) <2.541(11)> | 2.152(6) – 2.176(6) <2.16(1)> | present work |
| (n-Bu ₄ N) ₄ [Re ₄ Mo ₂ Se ₈ (CN) ₆] (10) | 2.6274(6) – 2.6659(6) <2.646(14)> | 2.5233(10) – 2.5575(10) <2.540(9)> | 2.143(10) – 2.195(11) <2.16(2)> | present work |
| (n-Bu ₄ N) ₄ [Re ₅ MoSe ₈ (CN) ₆] (7) | 2.6296(5) – 2.6481(5) <2.640(7)> | 2.5163(9) – 2.5401(9) <2.529(7)> | 2.13(1) – 2.12(1) <2.12(1)> | present work |
| Coordination polymers based on heterometallic cluster cyanocomplexes [Re_{6-x}Mo_xQ₈(CN)₆]ⁿ⁻ | | | | |
| [Zn(NH ₃) ₄] ₈ [Zn{Re ₃ Mo ₃ S ₈ (CN) ₆ }] ₃ ·9H ₂ O | 2.6230(8), 2.6248(10) | 2.427(3), 2.439(2) | 2.145(14), 2.17(3) | [162] |
| [Zn(NH ₃) ₄] ₂ [Zn{Re ₃ Mo ₃ S ₈ (CN) ₆ }]·2H ₂ O | 2.6374(17) | 2.426(4) | 2.23(3) | [162] |
| [Cd(NH ₃) ₄] ₂ {Cd[Re ₃ Mo ₃ S ₈ (CN) ₆]}·1.5H ₂ O | 2.6357(8) | 2.427(2) | 2.144(13) | [163] |
| {[Cd(NH ₃) ₅] ₂ (Cd(NH ₃) ₄) ₃ [Re ₃ Mo ₃ Se ₈ (CN) ₆] ₂ }·5H ₂ O (14) | 2.631(1)–2.684(1) <2.654> | 2.527(2)–2.564(2) / <2.547> | 2.10(2)–2.20(2) <2.14> | [208] |
| {[Cd(NH ₃) ₄] ₃ Re ₃ Mo ₃ Se ₈ (CN) ₆ }Cl (15) | 2.6465(5)–2.6498(5) <2.648> | 2.5439(7)–2.5475(9) <2.545> | 2.146(6) | [208] |
| {[Cd(NH ₃) ₄] ₃ Re ₃ Mo ₃ Se ₈ (CN) ₆ }Br (16) | 2.6480(3)–2.6531(3) <2.651> | 2.5475(3)–2.5537(4) <2.550> | 2.152(2) | [208] |
| {[Cd(NH ₃) ₄] ₃ Re ₃ Mo ₃ Se ₈ (CN) ₆ }I (17) | 2.6459(5)–2.6529(5) <2.650> | 2.5439(6)–2.5507(7) <2.547> | 2.147(6) | [208] |
| {[Cd(NH ₃) ₄] ₂ [Cd(NH ₃) ₃ (NCS)]Re ₃ Mo ₃ Se ₈ (CN) ₆ } (18) | 2.6421(9) – 2.6461(9) <2.644> | 2.5451(12) – 2.5506(14) <2.548> | 2.135(11) | present work |
| [Co(NH ₃) ₆] ₄ {[Co(NH ₃) ₂]{Re ₃ Mo ₃ Se ₈ (CN) ₆ }] ₂ ·15H ₂ O (19) | 2.6240(7) – 2.6802(7) <2.6511> | 2.5311(10) – 2.5629(9) <2.549> | 2.149(10) - 2.178(9) <2.16> | [209] |
| [Ni(NH ₃) ₆] ₄ {[Ni(NH ₃) ₂]{Re ₃ Mo ₃ Se ₈ (CN) ₆ }] ₂ ·15H ₂ O (20) | 2.6224(4) – 2.6664(4) <2.6465> | 2.5308(6) – 2.5649(6) <2.5495> | 2.142(6) – 2.169(6) <2.156> | [209] |
| Cluster complexes with organic ligands | | | | |
| <i>trans</i> -[Re ₆ Se ₈ (PPh ₃) ₄ Cl ₂] | 2.6294(6)–2.6574(6) | 2.507(1)–2.538(1) | 2.522(3)–2.526(3) (Re-P) | [142] |
| (SbF ₆) ₂ [Re ₆ Se ₈ (py) ₆] | 2.6126(7) – 2.6293(8) | 2.5102(14) – | 2.180(11) – 2.214(12) | [210] |

| | | | | |
|--|---------------------------------------|---------------------------------------|---|-----------------|
| | 2.622(5) | 2.5288(15) 2.520(5) | 2.197(14) | |
| [Mo ₆ Se ₈ (PPh ₃) ₆]·2H ₂ O | 2.7018(8) – 2.7275(8) 2.715(7) | 2.5292(9)–2.5876(9) 2.559(14) | 2.579(2) – 2.621(2) 2.600(19) | [211] |
| [Mo ₆ Se ₈ (tbp) ₆] | 2.6492(6)–2.6575(6) 2.655(4) | 2.4381(13)–2.4601(15) 2.450(6) | 2.266(4), 2.276(4), 2.280(4), 2.274(6) | [212] |
| [Re ₃ Mo ₃ Se ₈ (tbp) ₆] (21) | 2.6316(6) – 2.6561(7) <2.640> | 2.5356(10) – 2.5570(10) <2.547> | 2.223(8) – 2.261(8) <2.245> | [213] |
| [Re ₄ Mo ₂ Se ₈ (tbp) ₆] (22) | 2.6247(14) – 2.6391(15) <2.632> | 2.539(2) – 2.556(2) <2.547> | 2.21(2) – 2.24(2) <2.23> | present work |
| [Re ₄ Mo ₂ Se ₈ (PPh ₃) ₆] (23) | 2.6716(4) – 2.6909(4) <2.683> | 2.4994(6) – 2.5565(7) <2.531> | 2.5024(16) – 2.5350(15) <2.515> | present work |

Table 4.2: Interatomic distances TM – N (Å, <average>) in coordination polymers based on heterometallic cluster cyanocomplexes $[\text{Re}_{6-x}\text{Mo}_x\text{Q}_8(\text{CN})_6]^{n-}$

| | TM-N _C | TM-N _{H3} | Reference |
|--|--------------------------------|---|--------------|
| $[\text{Zn}(\text{NH}_3)_4]_8[\text{Zn}\{\text{Re}_3\text{Mo}_3\text{S}_8(\text{CN})_6\}_3] \cdot 9\text{H}_2\text{O}$ | 2.35(3) | 1.994(10), 2.04(2) | [162] |
| $[\text{Zn}(\text{NH}_3)_4]_2[\text{Zn}\{\text{Re}_3\text{Mo}_3\text{S}_8(\text{CN})_6\}] \cdot 2\text{H}_2\text{O}$ | 2.194(19) | 2.16(3) | [162] |
| $[\text{Cd}(\text{NH}_3)_4]_2\{\text{Cd}[\text{Re}_3\text{Mo}_3\text{S}_8(\text{CN})_6]\} \cdot 1.5\text{H}_2\text{O}$ | 2.339(12) | 2.265(12) | [163] |
| $[\text{Co}(\text{NH}_3)_6]_4[\{\text{Co}(\text{NH}_3)_2\}\{\text{Re}_3\text{Mo}_3\text{Se}_8(\text{CN})_6\}_2] \cdot 15\text{H}_2\text{O}$ (19) | 2.119(11) - 2.144(9) <2.13> | 2.127(10) - 2.188(8) <2.17> | [209] |
| $[\text{Ni}(\text{NH}_3)_6]_4[\{\text{Ni}(\text{NH}_3)_2\}\{\text{Re}_3\text{Mo}_3\text{Se}_8(\text{CN})_6\}_2] \cdot 15\text{H}_2\text{O}$ (20) | 2.088(4) - 2.109(4) <2.098> | 2.094(5) – 2.157(5) <2.135> | [209] |
| $\{[\text{Cd}(\text{NH}_3)_5]_2(\text{Cd}(\text{NH}_3)_4)_3[\text{Re}_3\text{Mo}_3\text{Se}_8(\text{CN})_6]_2\} \cdot 5\text{H}_2\text{O}$ (14) | 2.37(2)–2.52(2) <2.43> | 2.27(2)–2.47(2) <2.36> | [208] |
| $\{[\text{Cd}(\text{NH}_3)_4]_3\text{Re}_3\text{Mo}_3\text{Se}_8(\text{CN})_6\}\text{Cl}$ (15) | 2.418(6) | 2.323(7)–2.326(6) <2.325> | [208] |
| $\{[\text{Cd}(\text{NH}_3)_4]_3\text{Re}_3\text{Mo}_3\text{Se}_8(\text{CN})_6\}\text{Br}$ (16) | 2.419(3) | 2.310(3)–2.347(3) <2.328> | [208] |
| $\{[\text{Cd}(\text{NH}_3)_4]_3\text{Re}_3\text{Mo}_3\text{Se}_8(\text{CN})_6\}\text{I}$ (17) | 2.411(5) | 2.301(6)–2.344(6) <2.323> | [208] |
| $\{[\text{Cd}(\text{NH}_3)_4]_2[\text{Cd}(\text{NH}_3)_3(\text{NCS})]\text{Re}_3\text{Mo}_3\text{Se}_8(\text{CN})_6\}$ (18) | 2.419(12) | 2.316(17) – 2.318(14) <2.317> 2.46(9) N _{SC} | present work |

Acknowledgements

The author sincerely thanks the scientific supervisors Prof. Naumov N.G. and Dr. Cordier S. for support, advice and help during performance of the work. The author expresses special gratitude to Dr. Gayfulin Y.M. and Dr. Pomelova T.A., Dr.Sc. Vasilyeva I.G. and Dr.Sc. Bakovets V.V. for the help with the manuscript. The author thanks the members of the laboratory of synthesis and growth single crystals of compounds of rare earth elements of Nikolaev Institute of Inorganic Chemistry of the Siberian Branch of the Russian Academy of Sciences (NIIC SB RAS) and the team "Chimie du Solide et Matériaux" of Institut des Sciences Chimiques de Rennes (ISCR), as well as Dr. Ryzhikov M.R. (NIIC SB RAS, Novosibirsk) for quantum chemical calculations; Dr. Yansole V.V. (International Tomography Center - ITC, Novosibirsk) and Jehan P. (Centre Régional de Mesures Physiques de l'Ouest - CRMPO, Rennes) for mass spectrometry analysis; Dr. Pirayazev D.A. (NIIC SB RAS, Novosibirsk), Dr. Samsonenko D.G. (NIIC SB RAS, Novosibirsk), Dr. Lemoine P. and Dr. Dorset V. from the CDIFX (Centre de DIFfractométrie X, ISCR, Rennes) for crystallographic measurements; Dr. Kuchumov B.M. (NIIC SB RAS, Novosibirsk), Gouttefangeas F. and Loic J. (Centre de Microscopie Electronique à Balayage – CMEBA, Rennes) for EDS; Dr. Prestipino C. (ICSR, Rennes) for EXAFS measurements; Dr. Orione C. (ICSR, Rennes) for NMR; Dr. Plyusnin P.E. (NIIC SB RAS, Novosibirsk) for the results of TGA; Dr. Guizhoarn T. (ICSR, Rennes) for EPR spectra; Yushina I.V. (NIIC SB RAS, Novosibirsk) for reflection spectra; Alferova N.I. (NIIC SB RAS, Novosibirsk) for IR spectra; Escadelias M. (ICSR, Rennes) for CHN analysis. The author acknowledges the French synchrotron center SOLEIL for the access to the Spectroscopy Applied to Material Based on Absorption (SAMBA) beamline. And also special thanks are given to the French Embassy for providing scholarships for studying in co-tutelle PhD program between University of Rennes 1 and NIIC SB RAS. The author also thanks the international research project CLUSPOM between France and Russia.

Chapter 5: Supplementary

Summary of single-crystal data collections and structure refinement conditions

Table S1

| Compound | 1 | 2 | 3 |
|---|--|--|--|
| CCDC number | 1558003 | 1558004 | 1558005 |
| Chemical formula | C ₄ K ₆ Mo ₂ N ₆ Re ₄ Se ₈ | C ₆ K ₅ Mo ₃ N ₆ O ₁₁ Re ₃ Se ₈ | C ₆ Cs ₅ Mo ₃ N ₆ ORe ₃ Se ₈ |
| Molecular weight, g/mol | 1935.06 | 2005.72 | 2314.77 |
| Space group | <i>I4/m</i> | <i>Fm</i> $\bar{3}$ <i>m</i> | <i>P</i> $\bar{3}$ <i>c1</i> |
| <i>a</i> , Å | 11.5322(2) | 15.7344(2) | 9.9219(2) |
| <i>b</i> , Å | 11.5322(2) | 15.7344(2) | 9.9219(2) |
| <i>c</i> , Å | 9.3666(4) | 15.7344(2) | 19.6531(5) |
| α , ° | 90 | 90 | 90 |
| β , ° | 90 | 90 | 90 |
| γ , ° | 90 | 90 | 120 |
| Z; V, Å ³ | 2; 1245.68(6) | 4; 3895.4(2) | 2; 1675.53(8) |
| Crystal size, mm | 0.05×0.05×0.05 | 0.16×0.16×0.12 | 0.19×0.19×0.17 |
| $\rho_{\text{calcd.}}$, g·cm ⁻³ | 4.913 | 3.420 | 4.588 |
| μ , mm ⁻¹ | 28.681 | 18.275 | 25.938 |
| θ range, ° | 4.51 – 32.03 | 3.66 – 28.97 | 4.11 – 29.53 |
| <i>h</i> _min, <i>h</i> _max | -10 ≤ <i>h</i> ≤ 16 | -14 ≤ <i>h</i> ≤ 20 | -13 ≤ <i>h</i> ≤ 12 |
| <i>k</i> _min, <i>k</i> _max | -13 ≤ <i>k</i> ≤ 16 | -11 ≤ <i>k</i> ≤ 19 | -12 ≤ <i>k</i> ≤ 12 |
| <i>l</i> _min, <i>l</i> _max | -12 ≤ <i>l</i> ≤ 9 | -21 ≤ <i>l</i> ≤ 14 | -27 ≤ <i>l</i> ≤ 26 |
| Reflections collected/unique, <i>R</i> _{int} | 2094/872, 0.0217 | 3008/287, 0.0141 | 8229/1448, 0.0406 |
| Reflections (<i>I</i> > 2σ(<i>I</i>)) | 785 | 274 | 1352 |
| GoF | 1.201 | 1.384 | 1.292 |
| <i>R</i> (<i>I</i> > 2σ(<i>I</i>)) | <i>R</i> _I = 0.0362, <i>R</i> _{w2} = 0.0802 | <i>R</i> _I = 0.0245, <i>R</i> _{w2} = 0.0794 | <i>R</i> _I = 0.0462, <i>R</i> _{w2} = 0.0922 |
| Largest difference peak and hole, e·Å ⁻³ | 2.07, -1.38 | 1.05, -0.80 | 1.57, -1.91 |

Table S2

| Compound | 4 | 5 | 7 |
|---|---------------------------------------|---------------------------------------|---------------------------------------|
| CCDC number | 1558006 | 1938377 | – |
| Chemical formula | $C_{106}H_{86}Mo_3N_8P_4Re_3Se_8$ | $C_5K_6Mo_{2.40}N_5Re_{3.60}Se_8$ | $C_{70}H_{144}Mo_1N_{10}Re_5Se_8$ |
| Molecular weight, g/mol | 3073.80 | 1887.93 | 2787.95 |
| Space group | $P\bar{1}$ | $I4/m$ | $Pbca$ |
| a , Å | 12.3663(3) | 11.5438(14) | 23.2636(15) |
| b , Å | 13.1230(3) | 11.5438(14) | 16.6604(11) |
| c , Å | 16.9407(4) | 9.3453(12) | 23.6093(16) |
| α , ° | 110.0425(8) | 90 | 90 |
| β , ° | 95.9443(9) | 90 | 90 |
| γ , ° | 101.6537(8) | 90 | 90 |
| Z ; V , Å ³ | 1; 2484.45(10) | 2; 1245.3 | 4; 9150.5(10) |
| Crystal size, mm | 0.08×0.05×0.04 | 0.100×0.060×0.030 | 0.450×0.340×0.210 |
| $\rho_{\text{calcd.}}$, g·cm ⁻³ | 2.054 | 5.035 | 2.024 |
| μ , mm ⁻¹ | 7.054 | 30.865 | 9.988 |
| θ range, ° | 1.71 – 32.65 | 2.495 – 27.462 | 2.993 – 27.484 |
| h_{min} , h_{max} | $-17 \leq h \leq 17$ | $-14 \leq h \leq 14$ | $-30 \leq h \leq 29$ |
| k_{min} , k_{max} | $-14 \leq k \leq 19$ | $-11 \leq k \leq 14$ | $-21 \leq k \leq 21$ |
| l_{min} , l_{max} | $-24 \leq l \leq 24$ | $-12 \leq l \leq 12$ | $-30 \leq l \leq 30$ |
| Reflections collected/unique, R_{int} | 36510/14100, 0.0291 | 2953/750, 0.0255 | 72401/10435, 0.1011 |
| Reflections ($I > 2\sigma(I)$) | 11603 | 686 | 8198 |
| GoF | 1.028 | 1.112 | 1.091 |
| $R(I > 2\sigma(I))$ | $R_I = 0.0254$, $R_{w2} = 0.0521$ | $R_I = 0.0243$, $R_{w2} = 0.0585$ | $R_I = 0.0528$, $R_{w2} = 0.1295$ |
| Largest difference peak and hole, e·Å ⁻³ | 1.01, -1.32 | 1.128, -1.365 | 3.836, -3.775 |

Table S3

| Compound | 10 | 13 | 13·3H₂O |
|---|--|--|---|
| CCDC number | 1938375 | 1938011 | 1938376 |
| Chemical formula | C ₇₀ H ₁₄₄ Mo ₂ N ₁₀ Re ₄ Se ₈ | C ₇₀ H ₁₄₄ Mo ₃ N ₁₀ Re ₃ Se ₈ | C ₇₀ H ₁₄₄ Mo ₃ N ₁₀ O ₃ Re ₃ Se ₈ |
| Molecular weight, g/mol | 2694.30 | 2606.53 | 2652.04 |
| Space group | <i>Pbca</i> | <i>Pbca</i> | <i>P2₁/c</i> |
| <i>a</i> , Å | 23.3309(11) | 23.344(3) | 13.5315(5) |
| <i>b</i> , Å | 16.6427(7) | 16.654(2) | 16.9193(6) |
| <i>c</i> , Å | 23.6615(12) | 23.654(3) | 20.9974(9) |
| α , ° | 90 | 90 | 90 |
| β , ° | 90 | 90 | 103.122(2) |
| γ , ° | 90 | 90 | 90 |
| Z; V, Å ³ | 4; 9187.5(7) | 4; 9196.1(2) | 2; 4681.7(3) |
| Crystal size, mm | 0.210×0.150×0.030 | 0.550×0.500×0.350 | 0.120× 0.070× 0.050 |
| $\rho_{\text{calcd.}}$, g·cm ⁻³ | 1.948 | 1.883 | 1.881 |
| μ , mm ⁻¹ | 8.724 | 7.569 | 7.406 |
| θ range, ° | 2.988 – 27.480 | 2.989 – 27.484 | 2.912 – 27.538 |
| <i>h</i> _min, <i>h</i> _max | -30 ≤ <i>h</i> ≤ 30 | -30 ≤ <i>h</i> ≤ 30 | -17 ≤ <i>h</i> ≤ 17 |
| <i>k</i> _min, <i>k</i> _max | -21 ≤ <i>k</i> ≤ 16 | -21 ≤ <i>k</i> ≤ 21 | -21 ≤ <i>k</i> ≤ 19 |
| <i>l</i> _min, <i>l</i> _max | -30 ≤ <i>l</i> ≤ 30 | -30 ≤ <i>l</i> ≤ 30 | -27 ≤ <i>l</i> ≤ 27 |
| Reflections collected/unique, <i>R</i> _{int} | 54595/10518, 0.0867 | 82967/10361, 0.1093 | 62801/10740, 0.0860 |
| Reflections (<i>I</i> > 2 σ (<i>I</i>)) | 7286, 0.0867 | 7721, 0.1093 | 7513, 0.0860 |
| GoF | 1.119 | 1.200 | 1.054 |
| <i>R</i> (<i>I</i> > 2 σ (<i>I</i>)) | <i>R</i> _I = 0.0486 <i>R</i> _{w2} = 0.1144 | <i>R</i> _I = 0.0903 <i>R</i> _{w2} = 0.1600 | <i>R</i> _I = 0.0344 <i>R</i> _{w2} = 0.0667 |
| Largest difference peak and hole, e·Å ⁻³ | 2.773, -2.490 | 2.730, - 2.331 | 1.670, - 1.215 |

Table S4

| Compound | 14 | 15 | 16 |
|---|--|---|---|
| CCDC number | 1824886 | 1824887 | 1824888 |
| Chemical formula | $\text{C}_{12}\text{Cd}_5\text{H}_{76}\text{Mo}_6\text{N}_{34}\text{O}_5\text{Re}_6\text{Se}_{16}$ | $\text{C}_6\text{Cd}_3\text{Cl}_1\text{H}_{36}\text{Mo}_3\text{N}_{18}\text{Re}_3\text{Se}_8$ | $\text{C}_6\text{Br}_1\text{Cd}_3\text{H}_{36}\text{Mo}_3\text{N}_{18}\text{Re}_3\text{Se}_8$ |
| Molecular weight, g/mol | 4295.26 | 2211.28 | 2255.74 |
| Space group | <i>P</i> -1 | <i>R</i> -3 | <i>R</i> -3 |
| <i>a</i> , Å | 10.2664(8) | 15.0363(8) | 15.2258(10) |
| <i>b</i> , Å | 17.7456(11) | - | 15.2258(10) |
| <i>c</i> , Å | 22.3759(14) | 15.3935(9) | 15.3834(11) |
| α , ° | 85.142(4) | 90 | 90 |
| β , ° | 86.718(4) | 90 | 90 |
| γ , ° | 88.258(4) | 120 | 120 |
| <i>Z</i> ; <i>V</i> , Å ³ | 2; 4053.9(5) | 3; 3014.0(4) | 3; 3088.5(5) |
| Crystal size, mm | 0.16×0.06×0.04 | 0.06×0.05×0.04 | 0.18×0.10×0.09 |
| $\rho_{\text{calcd.}}$, g·cm ⁻³ | 3.519 | 3.655 | 3.638 |
| μ , mm ⁻¹ | 18.317 | 18.796 | 19.249 |
| θ range, ° | 2.949 - 27.510 | 3.074 – 27.479 | 3.066 – 27.484 |
| <i>h</i> _min, <i>h</i> _max | -13 ≤ <i>h</i> ≤ 13 | -19 ≤ <i>h</i> ≤ 19 | -19 ≤ <i>h</i> ≤ 19 |
| <i>k</i> _min, <i>k</i> _max | -13 ≤ <i>k</i> ≤ 22 | -19 ≤ <i>k</i> ≤ 19 | -19 ≤ <i>k</i> ≤ 19 |
| <i>l</i> _min, <i>l</i> _max | -29 ≤ <i>l</i> ≤ 29 | -17 ≤ <i>l</i> ≤ 19 | -19 ≤ <i>l</i> ≤ 19 |
| Reflections collected/unique, <i>R</i> _{int} | 31877/17950, 0.0662 | 6288/1533, 0.0329 | 14709/1571, 0.0422 |
| Reflections (<i>I</i> > 2σ(<i>I</i>)) | 9447 | 1302 | 1440 |
| GoF | 0.964 | 1.088 | 1.109 |
| <i>R</i> (<i>I</i> > 2σ(<i>I</i>)) | <i>R</i> _I = 0.0620 <i>R</i> _{w2} = 0.1149 | <i>R</i> _I = 0.0271 <i>R</i> _{w2} = 0.0672 | <i>R</i> _I = 0.0148 <i>R</i> _{w2} = 0.0340 |
| Largest difference peak and hole, e·Å ⁻³ | 2.448, -2.851 | 1.362, -1.617 | 0.507, -0.890 |

Table S5

| Compound | 17 | 18 | 19 |
|---|---|---|---|
| CCDC number | 1824889 | – | CSD 434766 |
| Chemical formula | $C_6Cd_3H_{36}I_1Mo_3N_{18}Re_3Se_8$ | $C_7H_{33}Cd_3Mo_3N_{18}Re_3S_1Se_8$ | $C_{12}H_{78}Co_5Mo_6N_{38}Re_6Se_{16}$ |
| Space group | <i>R</i> -3 | <i>R</i> -3 | $P\bar{1}$ |
| Molecular weight, g/mol | 2302.73 | 2213.56 | 4005.97 |
| <i>a</i> , Å | 15.3596(14) | 15.0783(15) | 14.5327(10) |
| <i>b</i> , Å | 15.3596(14) | 15.0783(15) | 14.5343(9) |
| <i>c</i> , Å | 15.3897(13) | 15.4665(16) | 14.9987(10) |
| α , ° | 90 | 90 | 115.259(3) |
| β , ° | 90 | 90 | 118.858(3) |
| γ , ° | 120 | 120 | 92.755(3) |
| Z; V, Å ³ | 3; 3144.3(6) | 3; 3045.3(7) | 1; 2376.8(3) |
| Crystal size, mm | 0.20×0.17×0.14 | 0.220×0.210×0.200 | 0.095×0.065×0.035 |
| $\rho_{\text{calcd.}}$, g·cm ⁻³ | 3.648 | 3.621 | 2.799 |
| μ , mm ⁻¹ | 18.691 | 18.492 | 15.371 |
| θ range, ° | 3.058 – 27.483 | 2.702 – 36.370 | 2.998 - 27.522 |
| <i>h</i> _min, <i>h</i> _max | -19 ≤ <i>h</i> ≤ 19 | -22 ≤ <i>h</i> ≤ 24 | -18 ≤ <i>h</i> ≤ 18 |
| <i>k</i> _min, <i>k</i> _max | -19 ≤ <i>k</i> ≤ 19 | -25 ≤ <i>k</i> ≤ 24 | -18 ≤ <i>k</i> ≤ 18 |
| <i>l</i> _min, <i>l</i> _max | -19 ≤ <i>l</i> ≤ 19 | -25 ≤ <i>l</i> ≤ 25 | -19 ≤ <i>l</i> ≤ 19 |
| Reflections collected/unique, <i>R</i> _{int} | 12940/1609, 0.0416 | 36185/3211, 0.0871 | 29256/10904, 0.0370 |
| Reflections (<i>I</i> >2σ(<i>I</i>)) | 1488 | 2467 | 8401 |
| GoF | 1.077 | 1.212 | 1.036 |
| <i>R</i> (<i>I</i> >2σ(<i>I</i>)) | <i>R</i> ₁ = 0.0277 <i>wR</i> ₂ = 0.0724 | <i>R</i> ₁ = 0.0555 <i>wR</i> ₂ = 0.1542 | <i>R</i> ₁ = 0.0389 <i>wR</i> ₂ = 0.0888 |
| Largest difference peak and hole, e·Å ⁻³ | 1.876, -2.650 | 3.179, -2.633 | 1.661, -2.912 |

Table S6

| Compound | 20 | 21 | 23 |
|---|--|--|---|
| CCDC number | CSD 434765 | 1896176 | – |
| Chemical formula | C ₁₂ H ₇₈ Mo ₆ N ₃₈ Ni ₅ O ₁₅ Re ₆ Se ₁₆ | C ₅₆ H ₈₁ Mo ₃ N ₇ Re ₃ Se ₈ | C ₁₀₈ H ₉₀ Mo _{2.1} P ₆ Re _{3.9} Se ₈ |
| Molecular weight, g/mol | 4244.87 | 2330.37 | 3132.50 |
| Space group | <i>P</i> $\bar{1}$ | <i>P</i> $\bar{1}$ | <i>P</i> $\bar{1}$ |
| <i>a</i> , Å | 14.5884(11) | 14.431(2) | 14.0237(14) |
| <i>b</i> , Å | 14.6083(10) | 15.681(2) | 15.9342(15) |
| <i>c</i> , Å | 14.9941(11) | 18.758(2) | 24.156(2) |
| α , ° | 115.186(3) | 105.580(5) | 84.965(4) |
| β , ° | 118.526(3) | 103.786(5) | 84.351(4) |
| γ , ° | 92.364(3) | 98.813(5) | 64.848(3) |
| Z; V, Å ³ | 1, 2417.5(3) | 2, 3862.3(8) | 2, 4856.0(8) |
| Crystal size, mm | 0.080×0.050×0.030 | 0.60×0.19×0.17 | 0.200×0.050×0.040 |
| $\rho_{\text{calcd.}}$, g·cm ⁻³ | 2.916 | 2.004 | 2.142 |
| μ , mm ⁻¹ | 15.248 | 8.959 | 8.245 |
| θ range, ° | 2.965 – 27.508 | 2.930 – 27.483 | 2.152 – 32.722 |
| <i>h</i> _min, <i>h</i> _max | -18 ≤ <i>h</i> ≤ 18 | -18 ≤ <i>h</i> ≤ 18 | -21 ≤ <i>h</i> ≤ 21 |
| <i>k</i> _min, <i>k</i> _max | -18 ≤ <i>k</i> ≤ 18 | -20 ≤ <i>k</i> ≤ 20 | -19 ≤ <i>k</i> ≤ 24 |
| <i>l</i> _min, <i>l</i> _max | -19 ≤ <i>l</i> ≤ 19 | -24 ≤ <i>l</i> ≤ 24 | -36 ≤ <i>l</i> ≤ 36 |
| Reflections collected/unique, <i>R</i> _{int} | 57212/11084, 0.0502 | 70201/17687, 0.0652 | 186910/34478, 0.0559 |
| Reflections (<i>I</i> > 2σ(<i>I</i>)) | 8871 | 12717 | 25666 |
| GoF | 1.036 | 1.037 | 1.059 |
| <i>R</i> (<i>I</i> > 2σ(<i>I</i>)) | <i>R</i> _I = 0.0253 <i>wR</i> ₂ = 0.0465 | <i>R</i> _I = 0.0503 <i>wR</i> ₂ = 0.1126 | <i>R</i> _I = 0.0463 <i>wR</i> ₂ = 0.1093 |
| Largest difference peak and hole, e·Å ⁻³ | 1.799, -0.946 | 2.857, -2.924 | 2.879, -2.640 |

Resulting variables for a simultaneous fit of experimental EXAFS spectra at Mo K-edge and Re L₃-edge

Table S7

| | model <i>cis</i> -{Re ₄ Mo ₂ } | model <i>trans</i> -{Re ₄ Mo ₂ } |
|------------------------------------|--|--|
| Fitting range, Å ⁻¹ | 3 – 18.8 (Re) 3 – 20 (Mo) | 3 – 18.8 (Re) 3 – 20 (Mo) |
| Reduced χ^2 | 87750856.8 | 83384877.0 |
| R-factor | 0.033 | 0.036 |
| Number of variables | 18 | 16 |
| $\Delta E_0(Mo)$, eV | 0(3) | 0(2) |
| <i>ampMo</i> | 0.9(2) | 0.9(1) |
| $\Delta E_0(Re)$, eV | 8(2) | 8(2) |
| <i>ampRe</i> | 0.9(1) | 1.0(1) |
| σ^2_{Mo-C} , Å ² | 0.002(4) | 0.003(5) |
| σ^2_{Mo-Se} | 0.0045(9) | 0.0037(6) |
| σ^2_{Mo-Mo} | 0.001(1) | – |
| σ^2_{Mo-Re} | 0.005(3) | 0.0037(4) |
| σ^2_{Re-C} | 0.002(2) | 0.002(2) |
| σ^2_{Re-Se} | 0.0031(6) | 0.0038(6) |
| σ^2_{Re-Re} | 0.0031(4) | 0.0027(4) |
| R_{Mo-C} , Å | 2.157(2) | 2.167(3) |
| R_{Mo-Se} | 2.537(5) | 2.539(4) |
| R_{Mo-Mo} | 2.784(1) | – |
| R_{Mo-Re} | 2.678(5) | 2.671(4) |
| R_{Re-C} | 2.112(2) | 2.113(2) |
| R_{Re-Se} | 2.520(3) | 2.531(4) |
| R_{Re-Re} | 2.629(3) | 2.636(3) |
| $N(Mo)_{Mo}$ | 1 | - |
| $N(Mo)_{Re}$ | 3 | 4 |
| $N(Mo)_{Se}$ | 4 | 4 |
| $N(Mo)_C$ | 1 | 1 |
| $N(Re)_{Mo}$ | 1.5 | 2 |
| $N(Re)_{Re}$ | 2.5 | 2 |
| $N(Re)_{Se}$ | 4 | 4 |
| $N(Re)_C$ | 1 | 1 |

Table S8

| | model <i>mer</i>-{Re₃Mo₃} |
|------------------------------------|--|
| Fitting range, Å ⁻¹ | 3 – 17.9 (Re) 3 – 20 (Mo) |
| Reduced χ^2 | 96719716.6 |
| <i>R</i> -factor | 0.033 |
| Number of variables | 18 |
| $\Delta E_0(Mo)$, eV | 4(3) |
| <i>ampMo</i> | 0.9(2) |
| $\Delta E_0(Re)$, eV | 10(3) |
| <i>ampRe</i> | 0.9(3) |
| σ^2_{Mo-C} , Å ² | 0.001(3) |
| σ^2_{Mo-Se} | 0.005(2) |
| σ^2_{Mo-Mo} | 0.001(1) |
| σ^2_{Mo-Re} | 0.007(4) |
| σ^2_{Re-C} | 0.001(2) |
| σ^2_{Re-Se} | 0.004(1) |
| σ^2_{Re-Re} | 0.002(1) |
| R_{Mo-C} , Å | 2.164(1) |
| R_{Mo-Se} | 2.551(5) |
| R_{Mo-Mo} | 2.776(1) |
| R_{Mo-Re} | 2.688(7) |
| R_{Re-C} | 2.106(1) |
| R_{Re-Se} | 2.528(4) |
| R_{Re-Re} | 2.634(2) |
| $N(Mo)_{Mo}$ | 1.33 |
| $N(Mo)_{Re}$ | 2.67 |
| $N(Mo)_{Se}$ | 4 |
| $N(Mo)_C$ | 1 |
| $N(Re)_{Mo}$ | 2.67 |
| $N(Re)_{Re}$ | 1.33 |
| $N(Re)_{Se}$ | 4 |
| $N(Re)_C$ | 1 |

Powder XRD patterns

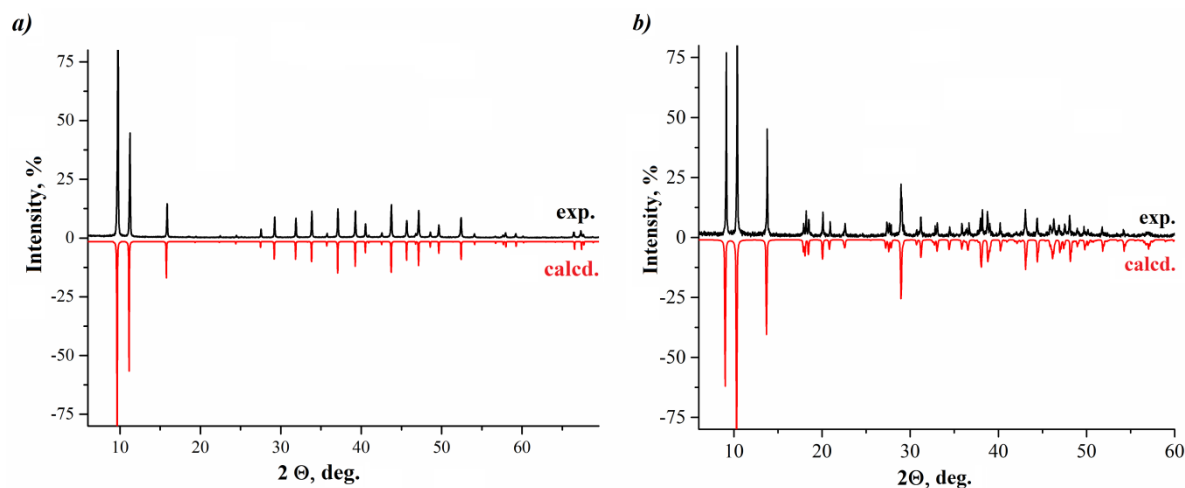


Figure S1: Powder XRD patterns for compound 2 (a) and 3 (b) experimental black lines vs calculated red.

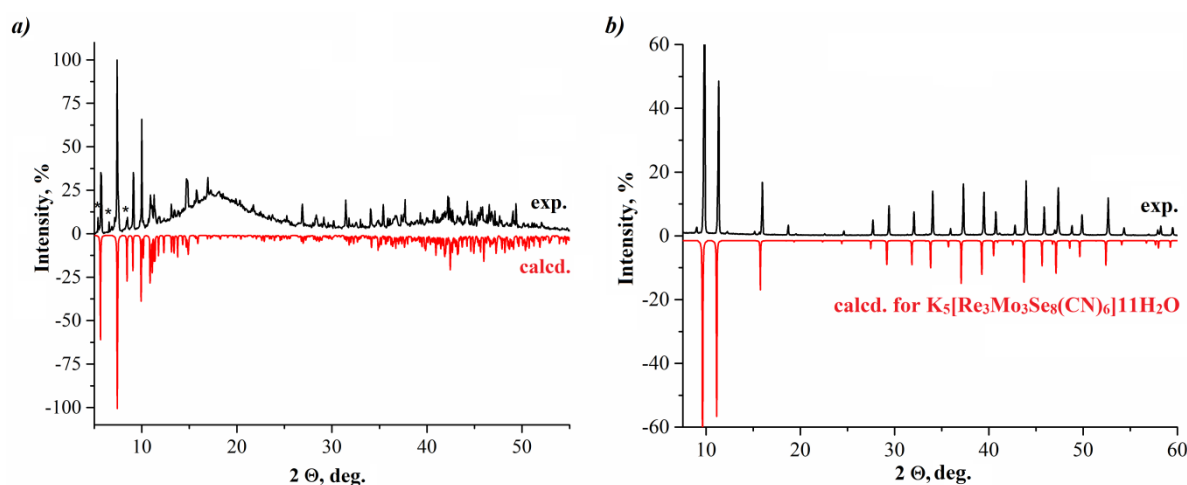


Figure S2: Powder XRD patterns for compound 4 (* - desolvation product) (a) and 6 (b), experimental black lines vs calculated red.

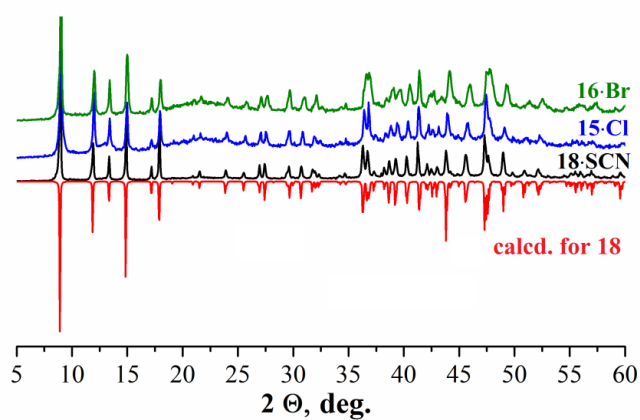


Figure S3: Powder XRD patterns for compounds 15, 16 и 18, experimental black, blue and green lines vs calculated red.

Quantum chemical calculation data, MO diagrams and MO pictures.

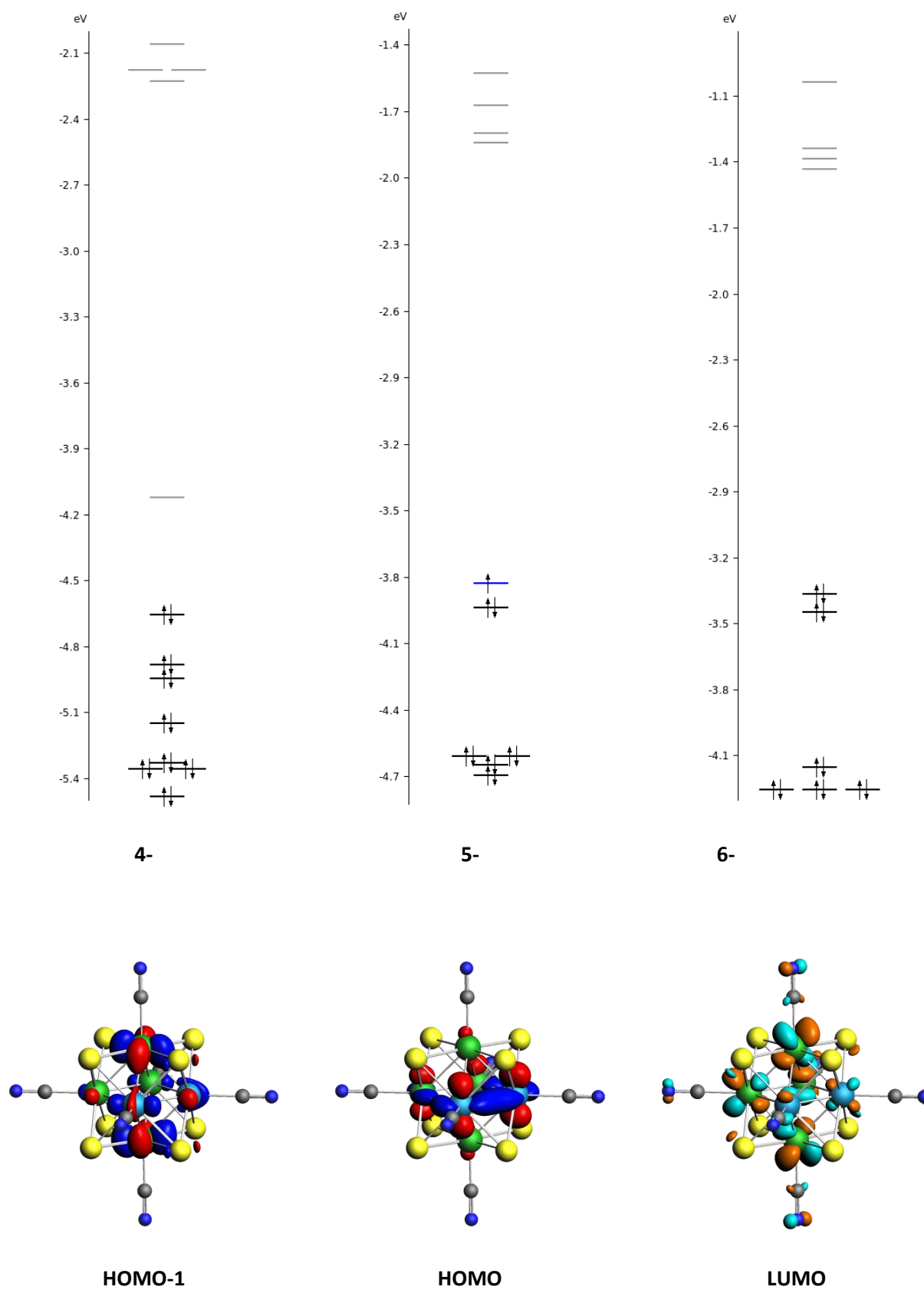


Figure S4. MO diagrams and MO picture $cis-[Re_4Mo_2Se_8(CN)_6]^{3-}$.

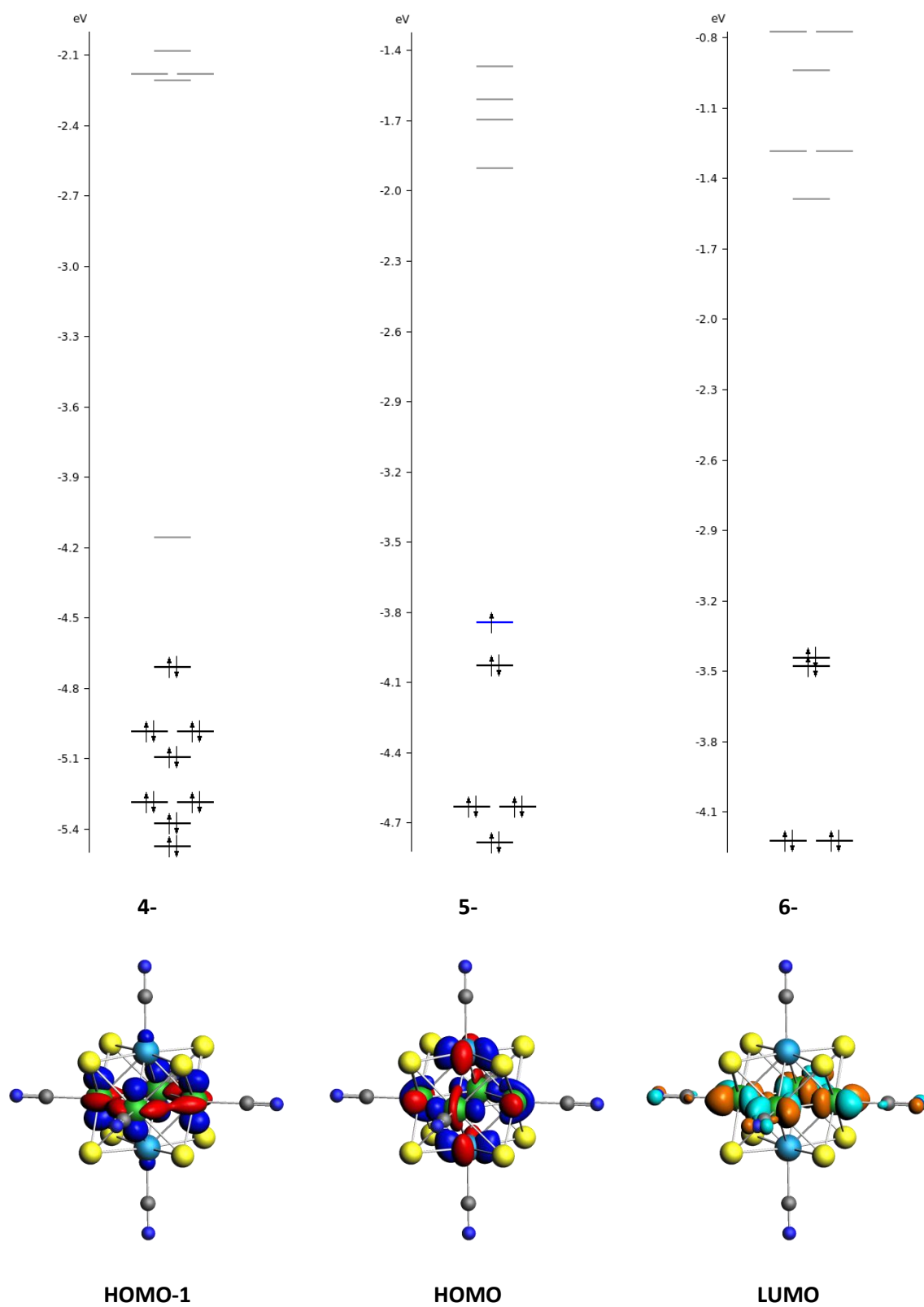


Figure S5. MO diagrams and MO picture for $trans-[Re_4Mo_2Se_8(CN)_6]^{n-}$.

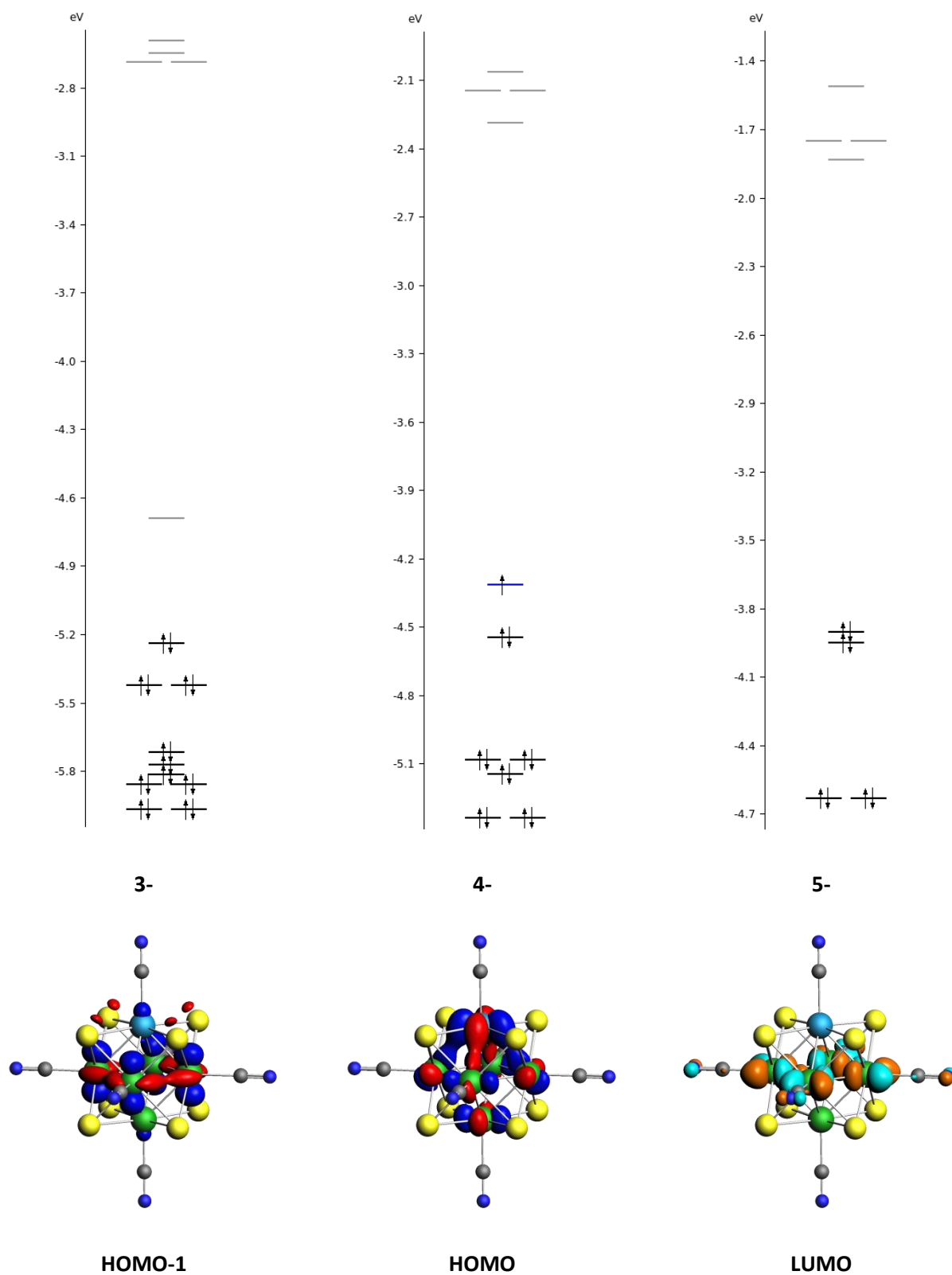


Figure S6. MO diagrams and MO picture for $[\text{Re}_5\text{MoSe}_8(\text{CN})_6]^{n-}$.

EXAFS structural modeling

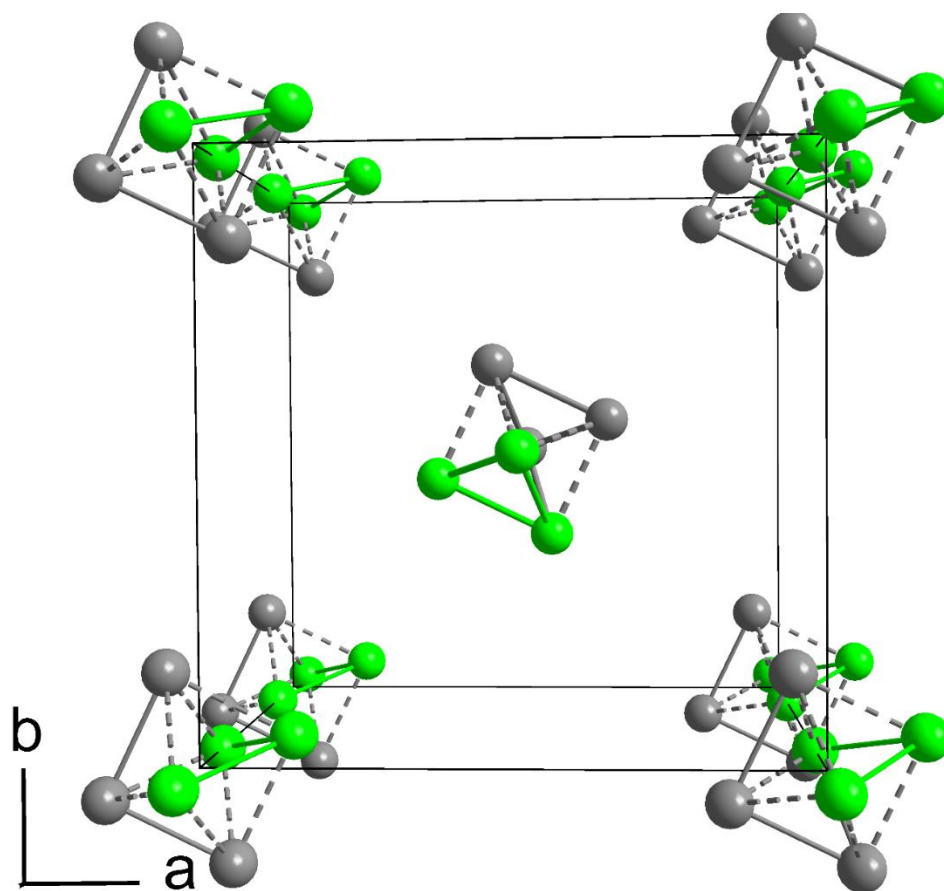


Figure S7: Simplified single-cell structural model containing *mer*-isomer of the $\{\text{Re}_3\text{Mo}_3\}$ metal core. All atoms excluding rhenium(grey) and molybdenum(green) are omitted for clarity.

6. Copies of the accepted and published articles related to the PhD manuscript

CHEMISTRY

A European Journal

A Journal of



Accepted Article

Title: Tailoring heterometallic cluster functional building blocks: synthesis, separation, structural and DFT studies of $[\text{Re}_6\text{-xMoxSe}_8(\text{CN})_6]_n$ -

Authors: V.K. Muravieva, Y.M. Gayfulin, C. Prestipino, P. Lemoine, M.R. Ryzhikov, V.V. Yanshole, S. Cordier, and Nikolay Gennadievich Naumov

This manuscript has been accepted after peer review and appears as an Accepted Article online prior to editing, proofing, and formal publication of the final Version of Record (VoR). This work is currently citable by using the Digital Object Identifier (DOI) given below. The VoR will be published online in Early View as soon as possible and may be different to this Accepted Article as a result of editing. Readers should obtain the VoR from the journal website shown below when it is published to ensure accuracy of information. The authors are responsible for the content of this Accepted Article.

To be cited as: *Chem. Eur. J.* 10.1002/chem.201903321

Link to VoR: <http://dx.doi.org/10.1002/chem.201903321>

Supported by
ACES

WILEY-VCH

Tailoring heterometallic cluster functional building blocks: synthesis, separation, structural and DFT studies of $[\text{Re}_{6-x}\text{Mo}_x\text{Se}_8(\text{CN})_6]^{n-}$

V.K. Muravieva,^[a,b] Y.M. Gayfulin,^[a] C. Prestipino,^[b] P. Lemoine,^[b] M.R. Ryzhikov,^[a,c]
V.V. Yanshole,^[c,d] S. Cordier^{*[b]} and N.G. Naumov^{*[a,c]}

Abstract: Influence of the metal core composition and geometry on the structure, spectroscopic properties and redox potentials was investigated for the first time for heterometallic (Re/Mo)₆ octahedral clusters. The discrete anionic clusters $[\text{Re}_{6-x}\text{Mo}_x\text{Se}_8(\text{CN})_6]^{n-}$ ($x = 2, 3$; $n = 4, 5$) were obtained as individual salts. Their isomeric composition and bond lengths distribution were inspected using a combination of single-crystal X-ray structure analysis, NMR, EXAFS and DFT calculations.

Octahedral cluster chalcogenides $\{\text{M}_6\text{Q}_8\}$ ($\text{M} = \text{Mo}, \text{W}, \text{Tc}, \text{Re}, \text{Q} = \text{S}, \text{Se}, \text{Te}$) represent an important class of inorganic compounds containing metal-metal bonds. Their structures are based on rigid M_6Q_8 core composed of the metal octahedron M_6 coordinated by the face-capped chalcogenide ligands. The M_6Q_8 moiety is additionally coordinated by apical ligands subjected to soft chemical modification. Rhenium and molybdenum clusters of this type were intensively investigated over the last decades due to the rich chemistry, structural diversity and functional properties in the solid state and in solution. Most prominent examples are: superconductivity of solid-state phases based on $[\text{Mo}_6\text{Q}_8]$ (Chevrel phases),^[1] photoluminescence of discrete rhenium clusters $[\text{Re}_6\text{Q}_8\text{L}_6]^n$,^[2] radiopacity,^[3] and redox chemistry.^[4] Numerous theoretical investigations showed that frontier molecular orbitals of the cluster core consist of the atomic orbitals of all metal atoms and (to a less extent) inner ligands.^[5] Consequently, the cluster core can be considered as a chemically stable "superatom", whose composition and geometry determines the electronic structure and drives physicochemical properties of compounds.^[6] Since the orbitals of each metal atom make a decisive contribution to the electronic structure of the whole cluster complex, the intrinsic properties of cluster

compounds significantly depend on the nature of metals forming metalocluster.

One of the most intriguing and poorly explored possibilities that cluster complexes provide is the ability to gradually "substitute" a different number of metal atoms in a cluster core for atoms of another type, thus obtaining heterometallic cluster-based superatoms. This approach is the only practical way to investigate a gradual change in the properties of clusters at a fundamental level of structure-properties correlations during the transition from $\{\text{M}_6\text{Q}_8\}$ to $\{\text{M}'_6\text{Q}_8\}$ cores. The main difficulty of this approach is that chalcogenide clusters are synthesized by a high-temperature synthesis, and the post-synthetic modification of the octahedral metal core is unachievable without its reassembling. This feature emphasizes the importance and the need of development of experimental procedures for synthesis and separation of cluster compounds based on heterometallic cores.

The modulation of the cluster valence electron (CVE) count by a metal substitution was first applied in heterometallic Chevrel phases in 1978 with the preparation of $[\text{Mo}_2\text{Re}_4\text{Q}_8]$ ($\text{Q} = \text{S}, \text{Se}$) compounds.^[7] The aforementioned study was then followed by the preparation and investigation of other substituted Chevrel phases: $\{\text{Mo}_{6-x}\text{M}_x\text{Q}_8\}$ ($\text{M} = \text{Re}, \text{Q} = \text{Te}, x = 2$; $\text{M} = \text{Ru}, \text{Q} = \text{Te}, 0 \leq x \leq 2$; $\text{Q} = \text{Se}, x = 2$; $\text{M} = \text{Rh}, \text{Q} = \text{Te}, x = 0.5, 1.33$).^[8] In contrast with polymeric phases of constant composition, the first attempt to synthesize the discrete chalcogenide clusters based on Re/Mo heterometallic cores by a high-temperature synthesis has resulted in the formation of water-soluble salts $\text{Cs}_5[\text{Re}_{6-x}\text{Mo}_x\text{Se}_8(\text{CN})_6] \cdot n\text{H}_2\text{O}$, $x = 1.64$ or 1.79 .^[9] Our recent study has revealed that the formation of cluster cores with different ratio of metals in the melt of KCN occurs even at the optimized reaction temperature.^[10]

Herein, we report the first detailed study of the discrete anionic clusters $[\text{Re}_4\text{Mo}_2\text{Se}_8(\text{CN})_6]^{7-}$ and $[\text{Re}_3\text{Mo}_3\text{Se}_8(\text{CN})_6]^{7-}$ as individual species. A practical method for their separation from reaction mixtures was developed. Isomerism and cluster distortion of metal cores in the solid state and in solution were investigated using a combination of single-crystal X-ray structure analysis, NMR, EXAFS and DFT calculations. In addition, spectroscopic properties and redox potentials of the heterometallic clusters were elucidated and found to be strongly correlated with the metal core composition.

The reaction between MoSe_2 and ReSe_2 in KCN melt at high temperature results in the formation of the polymeric phase $\text{K}_6[\text{Re}_{6-x}\text{Mo}_x\text{Se}_8(\mu\text{-CN})(\text{CN})_4]$ with variable composition. This phase crystallizes in tetragonal space group $I4/m$ and displays polymeric structure based on 1D chains composed of cluster

[a] V.K. Muravieva, Y.M. Gayfulin, M.R. Ryzhikov and N.G. Naumov
Nikolaev Institute of Inorganic Chemistry SB RAS,
630090, 3, Acad. Lavrentiev ave., Novosibirsk, Russia
E-mail: naumov@niic.nsc.ru

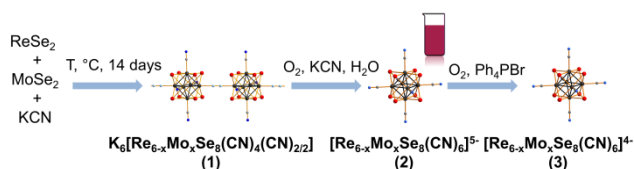
[b] V.K. Muravieva, C. Prestipino, P. Lemoine, S. Cordier
Univ Rennes, CNRS, ISCR (Institut des Sciences Chimiques de
Rennes) UMR 6226, F-35000, France

[c] M.R. Ryzhikov, V.V. Yanshole, N.G. Naumov
Novosibirsk State University
2, Pirogova str., Novosibirsk, 630090, Russia

[d] V.V. Yanshole
International Tomography Center SB RAS
3A, Institutskaya str., Novosibirsk, 630090, Russia

Supporting information for this article is given via a link at the end of the document.

fragments $[\text{Re}_{6-x}\text{Mo}_x\text{Se}_8(\text{CN})_4]$ linked by $\mu\text{-CN}$ groups in *trans*-position. It can be “depolymerized” by dissolution of the crude melt in H_2O in the presence of atmospheric O_2 . This reaction is accompanied by oxidation yielding, after recrystallization, the ionic salts $\text{K}_6[\text{Re}_{6-x}\text{Mo}_x\text{Se}_8(\text{CN})_6] \cdot n\text{H}_2\text{O}$ containing exactly the same Re/Mo ratio as initial polymer. Further metathesis reactions and recrystallization from CH_3CN in air lead to formation of salts $(\text{Ph}_4\text{P})_4[\text{Re}_{6-x}\text{Mo}_x\text{Se}_8(\text{CN})_6]$ according to the Scheme 1:



Scheme 1. A general way for preparation of soluble clusters from polymer phases $\text{K}_6[\text{Re}_{6-x}\text{Mo}_x\text{Se}_8(\mu\text{-CN})(\text{CN})_4]$ $x = 2.4\text{--}3$.

It was found previously that reaction at 630°C resulted in formation of the polymeric phase with $x = 3$.^[10] Here we report that the increase of the synthesis temperature up to 800°C led to formation of isostructural polymeric phase with x varied from 2.4 to 3.0. A non-integer metal ratio in the obtained compounds indicates that these salts are composed of mixture of several discrete cluster anions, probably, $[\text{Re}_2\text{Mo}_4\text{Se}_8(\text{CN})_6]^{n-}$, $[\text{Re}_3\text{Mo}_3\text{Se}_8(\text{CN})_6]^{n-}$ and $[\text{Re}_4\text{Mo}_2\text{Se}_8(\text{CN})_6]^{n-}$. To prove this assumption, several samples of the polymeric phase $\text{K}_6[\text{Re}_{6-x}\text{Mo}_x\text{Se}_8(\mu\text{-CN})(\text{CN})_4]$ were synthesized at different temperatures and transformed to the soluble salts with Ph_4P^+ . The $\text{CH}_3\text{CN}/\text{DMF}$ solutions of these salts were investigated using a high-resolution electrospray mass-spectrometry. It was found that the polymer prepared at 630°C yielded the salt composed of $[\text{Re}_3\text{Mo}_3\text{Se}_8(\text{CN})_6]^{4-}$ anion with minor amount of $[\text{Re}_4\text{Mo}_2\text{Se}_8(\text{CN})_6]^{4-}$ and $[\text{Re}_2\text{Mo}_4\text{Se}_8(\text{CN})_6]^{4-}$ anions (Figure 1, a, Figure S4). The increase of the temperature up to 700°C and 800°C led to significant increase of the fraction of $[\text{Re}_4\text{Mo}_2\text{Se}_8(\text{CN})_6]^{4-}$ anion (Figure 1, b, c, Figures S5, S6). It is worth noting that the $\text{ReSe}_2/\text{MoSe}_2$ ratio in the pre-loaded reaction mixture does not affect the composition of the resulting cluster phase.

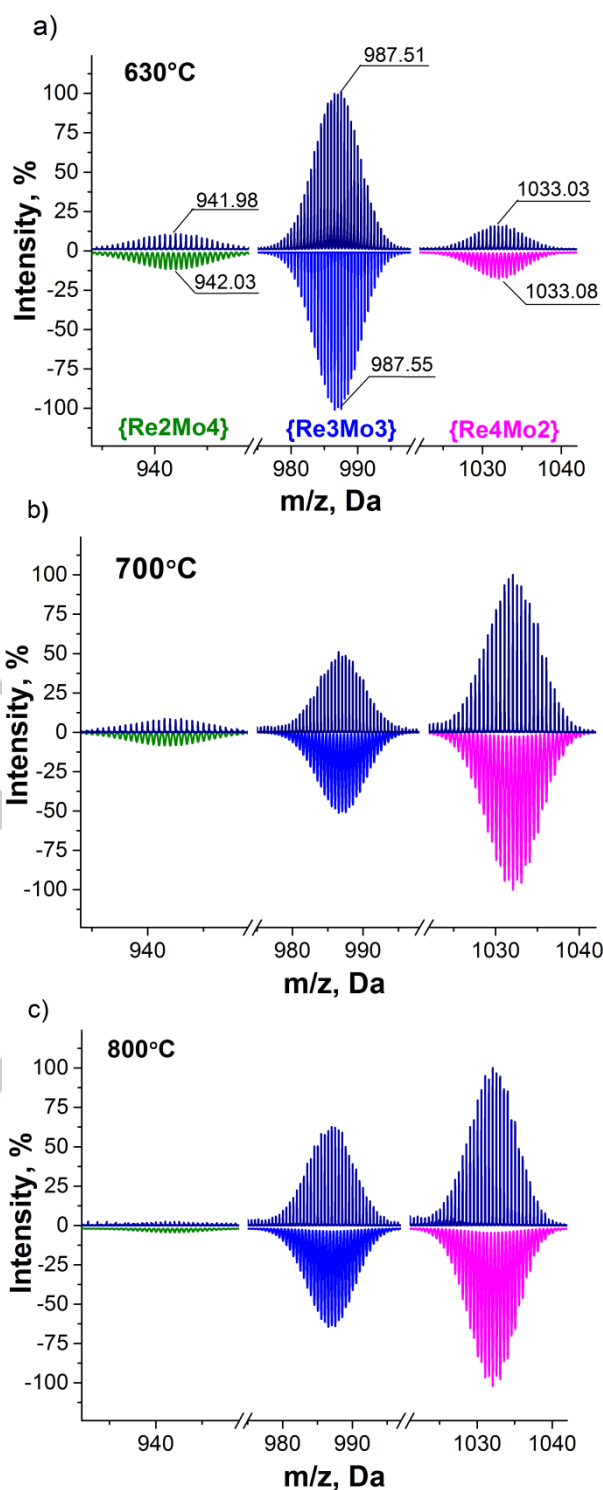


Figure 1. ESI-MS spectra in negative mode of $(\text{Ph}_4\text{P})_4[\text{Re}_{6-x}\text{Mo}_x\text{Se}_8(\text{CN})_6]$ salts prepared from $\text{K}_6[\text{Re}_{6-x}\text{Mo}_x\text{Se}_8(\mu\text{-CN})(\text{CN})_4]$ synthesized at different reaction temperatures (top) and their calculated spectra (bottom). Signals corresponds to the adducts $\{(\text{Ph}_4\text{P})[\text{Re}_2\text{Mo}_4\text{Se}_8(\text{CN})_6]\}^{2-}$ ($m/z_{\text{calcd}} = 942.031$ Da), $\{(\text{Ph}_4\text{P})[\text{Re}_3\text{Mo}_3\text{Se}_8(\text{CN})_6]\}^{2-}$ ($m/z_{\text{calcd}} = 987.554$ Da) and $\{(\text{Ph}_4\text{P})[\text{Re}_4\text{Mo}_2\text{Se}_8(\text{CN})_6]\}^{2-}$ ($m/z_{\text{calcd}} = 1033.077$ Da, left to right, correspondingly).

The phase $K_6[Re_3.6Mo_{2.4}Se_8(\mu-CN)(CN)_4]$ (**1**) synthesized at 800°C was structurally characterized (Tables S1 and S2 in Supplementary) and was used as precursor for the preparation of compounds $K_5[Re_3.6Mo_{2.4}Se_8(CN)_6] \cdot 11H_2O$ (**2**) and $(Ph_4P)_4[Re_3.6Mo_{2.4}Se_8(CN)_6] \cdot CH_3CN$ (**3**) as summarized in Scheme 1. Salts **2** and **3** contain comparable quantities of cluster anions $[Re_4Mo_2Se_8(CN)_6]^{5-}$ and $[Re_3Mo_3Se_8(CN)_6]^{7-}$.

We have found an easy and convenient method of separation of cluster anions $[Re_3Mo_3Se_8(CN)_6]^{5-}$ and $[Re_4Mo_2Se_8(CN)_6]^{5-}$ based on the difference of redox properties of these clusters. A crucial stage in the separation procedure is the addition of aqueous solution of *n*-Bu₄NBr to the aqueous solution of **2** during stirring in air. Anion $[Re_4Mo_2Se_8(CN)_6]^{5-}$ was found to be unstable toward oxidation in these conditions and this led to the precipitation of the salt $(n-Bu_4N)_4[Re_4Mo_2Se_8(CN)_6]$ (**4**) as individual phase containing the anion $[Re_4Mo_2Se_8(CN)_6]^{4-}$ (22 CVE) only. The remaining colored mother solution contains the $[Re_3Mo_3Se_8(CN)_6]^{5-}$ anion, and further precipitation was not observed even after long exposure of the solution in air or addition of large excess of *n*-Bu₄NBr. The extraction of $[Re_3Mo_3Se_8(CN)_6]^{5-}$ from aqueous solution by CH₂Cl₂ was successful. Crystallization of the highly charged anion $[Re_3Mo_3Se_8(CN)_6]^{5-}$ in organic solution was not achieved. One electron oxidation of $[Re_3Mo_3Se_8(CN)_6]^{5-}$ was performed in order to reduce the charge of the cluster anion (Figure 2). Then diffusion of Et₂O vapor into solution with oxidized cluster led to formation of crystalline salt $(n-Bu_4N)_4[Re_3Mo_3Se_8(CN)_6]$ (**5**) containing the anion $[Re_3Mo_3Se_8(CN)_6]^{4-}$ (21 CVE). Mass-spectrometry investigations confirm the selectivity of separation. The mass spectra of **5** in CH₂Cl₂ demonstrates the presence of $[Re_3Mo_3Se_8(CN)_6]^{4-}$ anion adducts only (Figure S8). The ESI-MS spectra of **4** in acetone demonstrates the signals for adducts of $[Re_4Mo_2Se_8(CN)_6]^{4-}$ without noticeable admixtures of $[Re_3Mo_3Se_8(CN)_6]^{4-}$ (Figure S7). $[Re_3Mo_3Se_8(CN)_6]^{5-}$ anion can be also isolated from organic media as water soluble salt $K_5[Re_3Mo_3Se_8(CN)_6] \cdot 11H_2O$ (**6**) by means of metathesis reaction with KSCN.

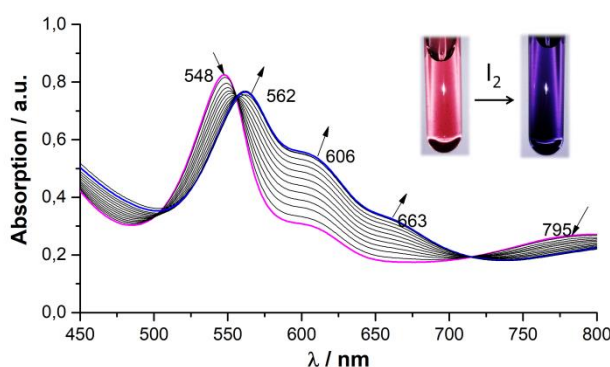


Figure 2. Evolution of UV-Vis spectra of $[Re_3Mo_3Se_8(CN)_6]^{5-/4-}$ anions (compound **5**) in DMF solution during redox titration by iodine solution. Purple line corresponds to the $[Re_3Mo_3Se_8(CN)_6]^{5-}$ anion, blue line – to the $[Re_3Mo_3Se_8(CN)_6]^{4-}$ one.

One can see that the selective one-electron oxidation of $[Re_4Mo_2Se_8(CN)_6]^{5-}$ anion by air oxygen and the formation of insoluble salt **4** in water are the driving forces of the separation process. Examination of redox properties of $[Re_4Mo_2Se_8(CN)_6]^{4-}$ anion in electrochemical conditions displayed two quasi-reversible redox waves characterized by $E_{1/2}$ values of -0.476 V and -1.294 V vs Ag/AgCl (Figure 3, Table 1). These processes correspond to the reduction of $[Re_4Mo_2Se_8(CN)_6]^{4-}$ cluster with 22 CVE and consequent formation of $[Re_4Mo_2Se_8(CN)_6]^{5-}$ anion with 23 CVE and $[Re_4Mo_2Se_8(CN)_6]^{6-}$ anion with 24 CVE, respectively. CV curve of $[Re_3Mo_3Se_8(CN)_6]^{5-}$ anion (compound **5** in CH₃CN, Figure S10) showed three successive steps of reduction forming $[Re_3Mo_3Se_8(CN)_6]^{5-/6-/7-}$ anions (22, 23 and 24 CVE, respectively). Half-wave potentials of these processes in CH₃CN were -0.202 V, -0.870 V and -1.270 V, respectively. It is important to note that the increase of Mo content within the cluster core causes significant negative shift of potential corresponding to oxidation process from 24 to 23 CVE and to the appearance of further oxidation from 23 to 22 and from 22 to 21 CVE redox pairs (Table 1). Therefore, a non-isovalent substitution of metal atoms in the cluster core is a powerful tool for tuning of the redox properties of cluster compounds. The difference of electrochemical potentials of $[Re_3Mo_3Se_8(CN)_6]^{5-}$ and $[Re_4Mo_2Se_8(CN)_6]^{5-}$ anions (Table 1) allowed the selective oxidation of the latter. Complete oxidation of $[Re_4Mo_2Se_8(CN)_6]^{5-}$ anion and precipitation of **4** occur at pH 7-9, while $[Re_3Mo_3Se_8(CN)_6]^{5-}$ anion remains in solution.

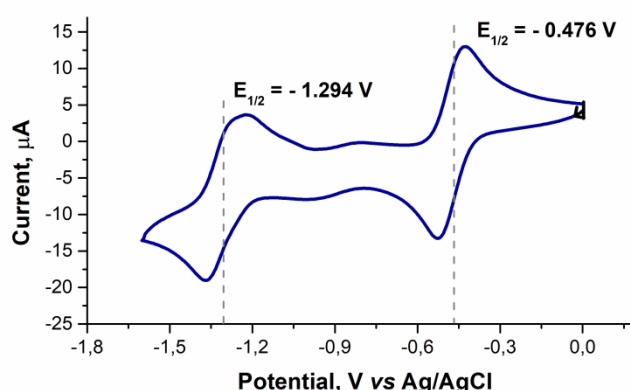


Figure 3. Cyclic voltammogram of **4** in CH₃CN under Ar, 25 mV·sec⁻¹ scan rate.

Table 1. Redox data for {M₆Se₈}-type clusters (M = Re, Mo; potentials are normalized vs Ag/AgCl/3.5 M KCl electrode). Redox pair charges are in brackets.

| Anion | 20/21 | 21/22 | 22/23 | 23/24 |
|------------------------|-------|-------|----------|----------|
| $[Re_6Se_8(CN)_6]$ | – | – | – | 0.125 |
| $(CH_3CN)^{[4]}$ | | | | (3-/4-) |
| $[Re_4Mo_2Se_8(CN)_6]$ | – | – | -0.476 | -1.294 |
| (CH_3CN) | | | (4-/5-) | (5-/6-) |

| | | | | |
|---|-------------------|-------------------|---|-------------------|
| $[\text{Re}_3\text{Mo}_3\text{Se}_8(\text{CN})_6]$ (CH_3CN) | – | -0.202 (4-/5-) | -0.870 (5-/6-) | -1.270 (6-/7-) |
| $[\text{Re}_3\text{Mo}_3\text{Se}_8(\text{CN})_6]$ (DMF) ^[10] | – | -0.325 (4-/5-) | -0.818 (E _{pc}) (5-/6-) | -1.410 (6-/7-) |
| $[\text{Mo}_6\text{Se}_8(\text{CN})_6]$ (H_2O) ^[11] | -0.647 (6-/7-) | -1.081 (7-/8-) | -1.574 (8-/9-) | – |

It is obvious, that $\{\text{Re}_3\text{Mo}_3\text{Se}_8\}$ and $\{\text{Re}_4\text{Mo}_2\text{Se}_8\}$ cores can also exist in two isomeric forms each (Figure 4). According to our crystallographic data, high symmetry of the lattice results in shared occupancy of Re and Mo atoms in metal sites, that does not allow to distinguish these forms due to their co-crystallization and orientational disorder. In order to shed light on the isomeric composition of obtained clusters, ^{77}Se NMR spectra of diamagnetic 22 CVE cluster salts **4** and **6** were recorded in acetone and H_2O , respectively.

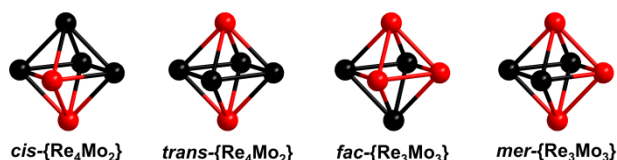


Figure 4. Isomerism of the octahedral metal cores $\{\text{Re}_3\text{Mo}_3\}$ and $\{\text{Re}_4\text{Mo}_2\}$.

The $\{\text{Re}_3\text{Mo}_3\text{Se}_8\}$ cluster can exist as *mer*- $\{\text{Re}_3\text{Mo}_3\text{Se}_8\}$ isomer of C_{2v} symmetry comprising two types of chemically non-equivalent selenium atoms in the ratio of 4:4, or *fac*- $\{\text{Re}_3\text{Mo}_3\text{Se}_8\}$ of C_{3v} symmetry exhibiting four non-equivalent selenium atoms in the ratio of 1:3:3:1. The ^{77}Se NMR spectrum of **6** contains two signals at 172 and 365 ppm with close integral intensities (Figure 5a). This finding should be attributed to the existence of *mer*- $\{\text{Re}_3\text{Mo}_3\text{Se}_8\}$ isomer only.

Similar consideration of the $\{\text{Re}_4\text{Mo}_2\text{Se}_8\}$ isomers leads to three different types of selenium atoms giving NMR signals with 2:4:2 theoretical intensities for *cis*- $\{\text{Re}_4\text{Mo}_2\text{Se}_8\}$ isomer and only one signal for *trans*- $\{\text{Re}_4\text{Mo}_2\text{Se}_8\}$ isomer. ^{77}Se NMR spectrum of **4** demonstrated four signals at 14, 297, 322 and 495 ppm (Figure 5b) indicating the mixture of both *cis*- and *trans*- isomers. The content of *cis*- $\{\text{Re}_4\text{Mo}_2\text{Se}_8\}$ was estimated as about twice higher than *trans*- $\{\text{Re}_4\text{Mo}_2\text{Se}_8\}$. The results of NMR spectroscopy demonstrated that high temperature synthesis likely lead to the formation of only *mer*-isomer in case of $\{\text{Re}_3\text{Mo}_3\text{Se}_8\}$ and both *cis*- and *trans*- isomers in case of $\{\text{Re}_4\text{Mo}_2\text{Se}_8\}$ cluster, with 1:2 ratio in the polymeric phase $\text{K}_6[\text{Re}_{3.6}\text{Mo}_{2.4}\text{Se}_8(\mu\text{-CN})(\text{CN})_4]$ (**1**) and products of its metathesis.

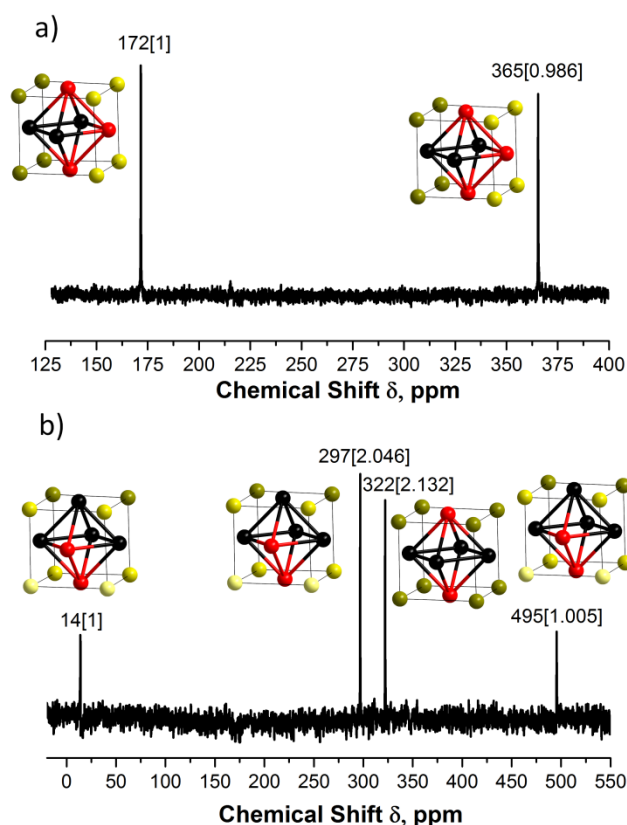


Figure 5. ^{77}Se NMR spectra for a) **6** in D_2O b) **4** in CD_3COCD_3 , integrated intensities are shown in brackets.

To analyze the optimized geometry and electronic structure of novel heterometallic-cores $\{\text{Re}_4\text{Mo}_2\}$, DFT calculations were performed for both *cis*- and *trans*- isomers of $[\text{Re}_4\text{Mo}_2\text{Se}_8(\text{CN})_6]^{n-}$ anion ($n = 4-6$, CVE count from 22 to 24). Molecular orbital (MO) diagrams for $[\text{Re}_4\text{Mo}_2\text{Se}_8(\text{CN})_6]^{n-}$ isomers are shown in Figure 6. Orbitals of 24 CVE clusters have mixed bonding-antibonding character relative to metal-metal interactions below Fermi energy level (HOMO, HOMO-1 and etc.) and anti-bonding above the Fermi energy level (LUMO, LUMO+1 and etc.). The HOMO and HOMO-1 are composed mostly of rhenium and molybdenum atomic orbitals with some contribution of selenium atomic orbitals (about 25%). The MO disposition demonstrates the presence of relatively large HOMO-LUMO gap of ~2 eV and smaller gap of 0.6-0.7 eV between HOMO-1 and HOMO-2 (for 23 and 24 CVE cluster anions).

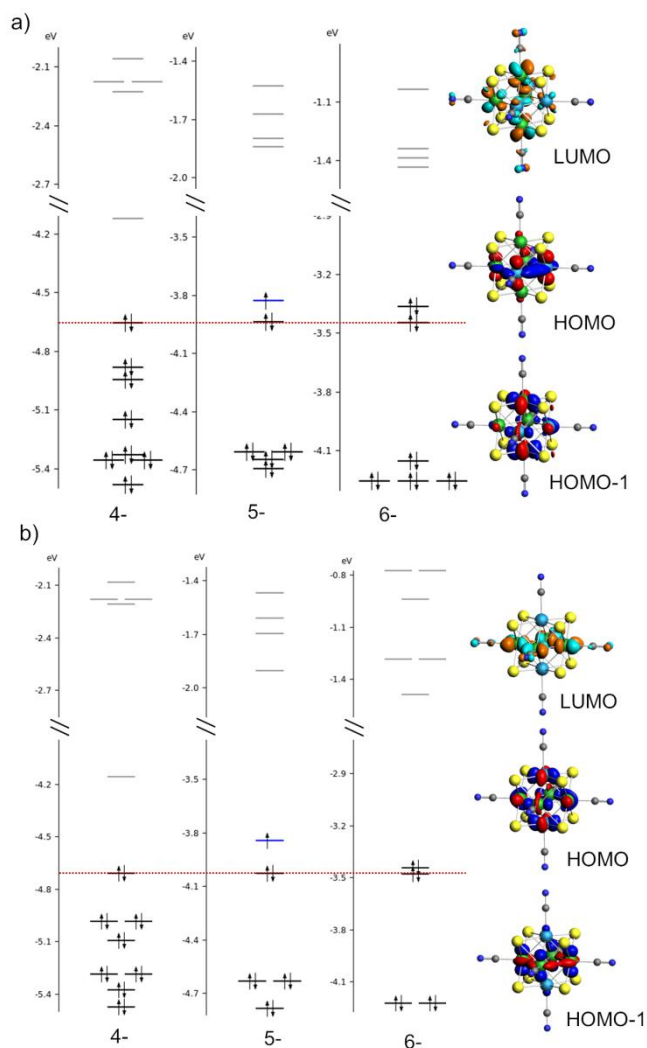


Figure 6. Molecular orbital diagrams of *cis*- (a) and *trans*- (b) isomers of $[\text{Re}_4\text{Mo}_2\text{Se}_8(\text{CN})_6]^{n-}$ ($n = 4-6$ from left to right). On the insets: typical view of the HOMO-1, HOMO and LUMO for $[\text{Re}_4\text{Mo}_2\text{Se}_8(\text{CN})_6]^{4-}$ anion. The diagrams are lined on the HOMO-1 level.

The calculated mean M–M distances for isomers of $[\text{Re}_4\text{Mo}_2\text{Se}_8(\text{CN})_6]^{4-}$ anion are listed in Table 2. The attentive analysis of optimized geometries reveals that both *cis*- and *trans*- isomers of 24 CVE $\{\text{Re}_4\text{Mo}_2\}$ cores are barely distorted, with close metal-metal distances. Removal of two valence electrons from HOMO level causes strong distortion of metal cores in both *cis*- and *trans*- isomers (Figure 7a). The octahedral distortion leads to the loss of the O_h symmetry by axial distortion to D_{4h} -symmetrized *trans*-isomer. Elongation of the metal bond in the case of *cis*- $[\text{Re}_4\text{Mo}_2\text{Se}_8(\text{CN})_6]^{4-}$ anion leads to C_{2v} point symmetry (Figure 7b). The difference between the shortest and the largest M–M bonds of 22-electron $[\text{Re}_4\text{Mo}_2\text{Se}_8(\text{CN})_6]^{4-}$ anion has the remarkable values of 0.197 and 0.091 Å for *cis*- and *trans*-isomer, respectively. In both cases the distortion is provided by the preference of molybdenum to form longer and rhenium – shorter distances with the surrounding atoms (Table

2). Mo–Se and Re–Se distances are close and do not show the similar consistency as metal distances (Table S5). It is worth noting that average M–M bond distances are practically equal for both isomers and all CVE counts (Figure 7a), and are close to the data of single-crystal X-Ray structural analysis.

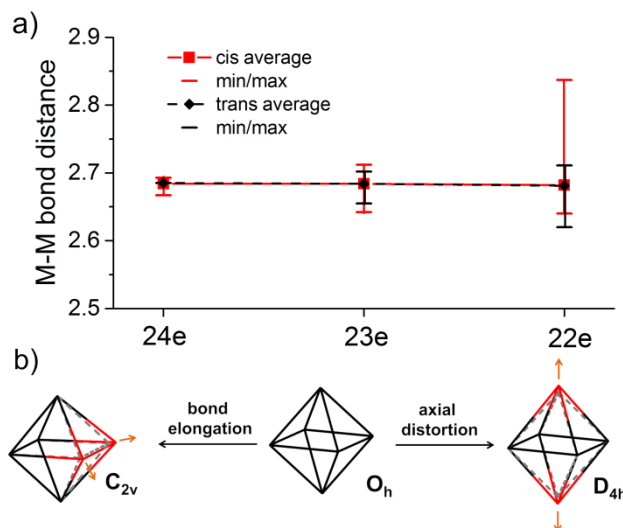


Figure 7. a) analysis of the DFT optimized geometries of the anions $[\text{Re}_4\text{Mo}_2\text{Se}_8(\text{CN})_6]^{n-}$ $n = 6$ - (24 electrons), 5- (23e), 4- (22e) b) octahedral distortion in 22-electron $\{\text{Re}_4\text{Mo}_2\}$ metal cores.

Table 2. The comparison of the M–M distances and octahedron diagonals (R_d) for 22-electron $\{\text{Re}_4\text{Mo}_2\}$ metal core obtained by theoretical and experimental techniques.

| | <i>cis</i> - $\{\text{Re}_4\text{Mo}_2\}$ | | <i>trans</i> - $\{\text{Re}_4\text{Mo}_2\}$ | | SC XRD |
|--------------------|---|-----------|---|-----------|-------------|
| | EXAFS model | DFT model | EXAFS model | DFT model | |
| $R_{\text{Mo-Mo}}$ | 2.784 | 2.837 | – | – | – |
| $R_{\text{Mo-Re}}$ | 2.678 | <2.685> | 2.671 | <2.711> | – |
| $R_{\text{Re-Re}}$ | 2.629 | <2.648> | 2.636 | <2.620> | – |
| $R_{\text{M-M}}$ | <2.667> | <2.682> | <2.659> | <2.681> | <2.646(14)> |

To evaluate the real geometry of $\{\text{Re}_4\text{Mo}_2\}$ and $\{\text{Re}_3\text{Mo}_3\}$ cluster cores, Extended X-Ray Absorption Fine Structure (EXAFS) measurements were carried out on Mo K-edge and Re L₃-edge for solids $(n\text{-Bu}_4\text{N})_4[\text{Re}_4\text{Mo}_2\text{Se}_8(\text{CN})_6]$ (**4**) and $\text{K}_5[\text{Re}_3\text{Mo}_3\text{Se}_8(\text{CN})_6] \cdot 11\text{H}_2\text{O}$ (**6**) both having 22 CVE, which have the most significant distortion of metal core according to DFT calculations. The experimental data obtained for Re and Mo have been simultaneously fitted by the model containing pure isomeric atom arrangement. The final theoretical functions for both isomers in the case of $\{\text{Re}_4\text{Mo}_2\}$ agree well with the experimental spectra (Figure 8, Figure S12). The final fitting parameters can

be found in Table S3. The resulted metal-metal distances obtained by the fitting of the EXAFS spectra and respective octahedron distortion were found to follow the same trend as DFT optimized geometries (Table 2). Both fits revealed visibly enlarged Mo-Mo and shortened Re-Re distances comparing to crystallographic data of **4**.

Fitting of the data obtained for $K_5[Re_3Mo_3Se_8(CN)_6] \cdot 11H_2O$ (**6**) salt reveals that, although only slightly smaller reliability factors, the *mer*-isomer model presents a set of final parameters more consistent than *fac*-one (see σ^2 Mo-Mo Table S4 ; Figure S11) in agreement with the results of NMR spectroscopy. DFT optimized geometry for $[Re_3Mo_3Se_8(CN)_6]^{5-}$ discussed in our previous study^[10] and geometry resulted from EXAFS fitting in present work were found to correlate similarly as it was found for $[Re_4Mo_2Se_8(CN)_6]^{4-}$ also comprising elongated Mo-Mo and shortened Re-Re distances (Table S6).

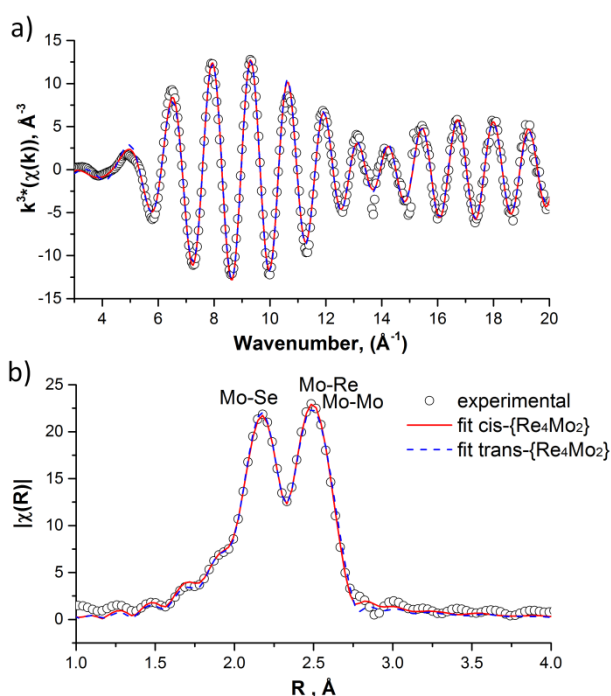


Figure 8. a) EXAFS measurements for the compound **4** (weighted by k^3) Mo K-edge, b) Fourier transform magnitudes. Model fits (fitting space – k) are reported as lines.

In this work we have carried out for the first time the detailed analysis of the structure of heterometallic cluster complexes $[Re_4Mo_2Se_8(CN)_6]^{7-}$ and $[Re_3Mo_3Se_8(CN)_6]^{7-}$. The data obtained by the use of X-Ray structural analysis and EXAFS agree well with the DFT calculations demonstrating significant distortion of metal octahedron upon electron removal, which however, keeps the average M–M distances at the similar values. ^{77}Se NMR measurements in solution have shown that the $[Re_3Mo_3Se_8(CN)_6]^{7-}$ anions contain the *mer*- $\{Re_3Mo_3Se_8\}$ isomer only while the $[Re_4Mo_2Se_8(CN)_6]^{7-}$ anions exist as the mixture of both *cis*- and *trans*- isomers of $\{Re_4Mo_2Se_8\}$ core. This investigation has become possible by the development of the

synthetic method for separation and further characterization of $[Re_4Mo_2Se_8(CN)_6]^{7-}$ and $[Re_3Mo_3Se_8(CN)_6]^{7-}$ anions in individual phases from the solid solution $K_6[Re_{6-x}Mo_xSe_8(\mu-CN)(CN)_4]$ formed in high temperature synthesis due to the difference in redox behavior of anions with different Re/Mo ratio. Thus, it was shown that the substitution of metal atoms in cluster core and the variation in the ratio of metals is a powerful tool for changing the electronic structure and, as a consequence, the redox properties, UV-Vis spectra and color of octahedral cluster solutions and crystals. The discovered possibility to isolate these redox-active anions pave the way for the further engineering of cluster building blocks and new cluster materials with tailored physico-structural properties through ligand exchange reactions and formation of cluster solids by assembling of cluster building blocks via covalent and supramolecular interactions.

Acknowledgements

The research was supported by the Ministry of Science and Education of the Russian Federation. Authors are greatly acknowledged to French Synchrotron SOLEIL for the opportunity to use SAMBA XAS beamline. V. Muravieva thanks French Embassy for providing the scholarship for co-tutelle PhD program between France and Russia. The authors are acknowledged to International Associate Laboratory N° 1144 CLUSPOM between France and Russia. The authors thank the "Centre de Diffractométrie X" (CDIFX) of the Institute of Chemical Science of Rennes for single-crystal X-ray diffraction facilities. The authors also thank V. Dorcet for crystallographic data, Ph. Jehan for mass-spectrometry and C. Orione for NMR.

Keywords: cluster compounds • heterometallic complexes • EXAFS • structure • electronic structure

- [1] a) H. D. Yoo, I. Shterenberg, Y. Gofer, G. Gershinsky, N. Pour, D. Aurbach, *Energy Environ. Sci.* **2013**, 6, 2265-2279; b) L. Mei, J. T. Xu, Z. X. Wei, H. K. Liu, Y. T. Li, J. M. Ma, S. X. Dou, *Small* **2017**, 13.
- [2] S. Cordier, Y. Molard, K. A. Brylev, Y. V. Mironov, F. Grasset, B. Fabre, N. G. Naumov, *J. Clust. Sci.* **2014**, 26, 53-81.
- [3] A. A. Krasilnikova, M. A. Shestopalov, K. A. Brylev, I. A. Kirilova, O. P. Khripko, K. E. Zubareva, Y. I. Khripko, V. T. Podorognaya, L. V. Shestopalova, V. E. Fedorov, Y. V. Mironov, *J. Inorg. Biochem.* **2015**, 144, 13-17.
- [4] J.-C. P. Gabriel, K. Boubekour, S. Uriel, P. Batail, *Chem. Rev.* **2001**, 101, 2037-2066.
- [5] a) V. I. Baranovski, D. V. Korolkov, *Polyhedron* **2004**, 23, 1519-1526; b) A. Deluzet, H. Duclaud, P. Sautet, S. A. Borshch, *Inorg. Chem.* **2002**, 41, 2537-2542; c) T. G. Gray, *Chem. - Eur. J.* **2009**, 15, 2581-2593; d) T. G. Gray, C. M. Rudzinski, E. E. Meyer, R. H. Holm, D. G. Nocera, *J. Am. Chem. Soc.* **2003**, 125, 4755-4770.
- [6] a) A. Pinkard, A. M. Champsaur, X. Roy, *Account. Chem. Res.* **2018**, 51, 919-929; b) E. V. Alexandrov, A. V. Virovets, V. A. Blatov, E. V. Peresypkina, *Chem. Rev.* **2015**, 115, 12286-12319.
- [7] A. Perrin, M. Sergent, O. Fischer, *Mater. Res. Bull.* **1978**, 13, 259-264.
- [8] a) A. Perrin, R. Chevrel, M. Sergent, O. Fischer, *J. Solid State Chem.* **1980**, 33, 43-47; b) W. Honle, H. D. Flack, K. Yvon, *J. Solid State Chem.* **1983**, 49, 157-165; c) F. J. Berry, C. D. Gibbs, *Dalton Trans.* **1991**, 57-59; d) F. J. Berry, C. D. Gibbs, C. Greaves, *J. Solid State Chem.* **1991**, 92, 148-153.
- [9] N. G. Naumov, K. A. Brylev, Y. V. Mironov, A. V. Virovets, D. Fenske, V. E. Fedorov, *Polyhedron* **2004**, 23, 599-603.

[10] V. K. Muravieva, Y. M. Gayfulin, M. R. Ryzhikov, I. N. Novozhilov, D. G. Samsonenko, D. A. Piryazev, V. V. Yanshole, N. G. Naumov, *Dalton Trans.* **2018**, 47, 3366-3377.

[11]

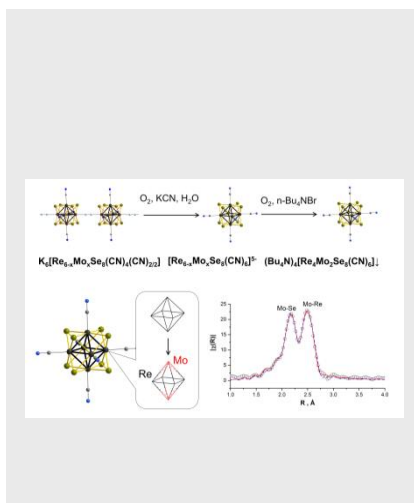
C. Magliocchi, X. Xie, T. Hughbanks, *Inorg. Chem.* **2004**, 43, 1902-1911.

Entry for the Table of Contents (Please choose one layout)

Layout 1:

COMMUNICATION

Excision reaction of polymeric phase $K_6[Re_{3.6}Mo_{2.4}Se_8(m-CN)(CN)_4]$ and selective oxidation afford the individual heterometallic redox-active $[Re_4Mo_2Se_8(CN)_6]^{n-}$ and $[Re_3Mo_3Se_8(CN)_6]^{n-}$ cyanoclusters. Electron deficient anions demonstrate significant metal core distortion determined by EXAFS and DFT calculations.



V.K. Muravieva, Y.M. Gayfulin, C. Prestipino, P. Lemoine, M.R. Ryzhikov, V.V. Yanshole, S. Cordier, N.G. Naumov*

Page No. – Page No.

Tailoring heterometallic cluster functional building blocks: synthesis, separation, structural and DFT studies of $[Re_{6-x}Mo_xSe_8(CN)_6]^{n-}$

Layout 2:

COMMUNICATION

((Insert TOC Graphic here))

Author(s), Corresponding Author(s)*

Page No. – Page No.

Title

Text for Table of Contents

PAPER

[View Article Online](#)
[View Journal](#) | [View Issue](#)Cite this: *Dalton Trans.*, 2018, **47**, 3366

Mixed-metal clusters with a {Re₃Mo₃Se₈} core: from a polymeric solid to soluble species with multiple redox transitions†

Viktoria K. Muravieva,^{a,b} Yakov M. Gayfulin,^a Maxim R. Ryzhikov,^{a,c} Igor N. Novozhilov,^a Denis G. Samsonenko,^{a,c} Dmitry A. Piryazev,^{a,c} Vadim V. Yanshole^{c,d} and Nikolay G. Naumov^{a,c}

Cluster compounds based on a new {Re₃Mo₃Se₈}ⁿ core were obtained and studied. The polymeric solid K₆[Re₃Mo₃Se₈(CN)₄(CN)_{2/2}] (**1**) containing 24 cluster valence electrons (CVE) was isolated as a result of high-temperature reaction. Water-soluble salts K₅[Re₃Mo₃Se₈(CN)₆]·11H₂O (**2**) and Cs₅[Re₃Mo₃Se₈(CN)₆]·H₂O (**3**) were prepared from compound **1**. Crystal structures of the diamagnetic compounds **2** and **3** contain a cluster anion [Re₃Mo₃Se₈(CN)₆]^{5−} with a 22-electronic core {Re₃Mo₃Se₈}⁺. Metathesis reaction followed by recrystallization from CH₃CN yielded paramagnetic salt (Ph₄P)₄[Re₃Mo₃Se₈(CN)₆]·2CH₃CN (**4**) containing the {Re₃Mo₃Se₈}²⁺ core with 21 CVE. Cyclic voltammetry of the solution of **4** displayed three quasi-reversible waves with *E*_{1/2} = −0.325, −0.818 and −1.410 V vs. Ag/AgCl electrode indicating the presence of [Re₃Mo₃Se₈(CN)₆]^{4−/5−/6−/7−} transitions. Electronic structure calculations showed that both *mer*- and *fac*-isomers of [Re₃Mo₃Se₈(CN)₆]^{n−} clusters undergo great distortion when the number of CVE decreases.

Received 22nd September 2017,
Accepted 24th January 2018

DOI: 10.1039/c7dt03571c

rsc.li/dalton

Introduction

Rhenium and molybdenum octahedral chalcogenide cluster complexes are the typical examples of transition metal high-valence clusters.¹ Their structures are composed of an M₆ octahedron, each face of which is coordinated by bridging a chalcogenide ligand (inner ligands), forming the {M₆Q₈}ⁿ cluster core. The metal atoms are connected with covalent bonds, composing a joint electron system with a specific number of cluster valence electrons (CVE) depending on the metal composition and charge. Each metal atom is additionally coordinated by an apical ligand L, giving the resulting formula of [M₆Q₈L₆]ⁿ for a discrete molecular cluster fragment. The compounds based on octahedral clusters have been intensively studied during the last few decades due to the promising structural features and physicochemical properties of the

cluster core. Among the latter one can consider intense red luminescence,² magnetism³ and highly effective X-ray contrast properties.⁴ Also, the cluster core is usually able to undergo reversible redox transitions proceeded without a significant change in the cluster geometry.^{2c,3d,5} Well-developed apical ligand exchange chemistry along with chemical stability and rigid geometry of the cluster core allows the designing of unique hybrid materials, *e.g.* liquid crystal phases,⁶ polymeric matrixes with immobilized clusters⁷ and cluster-coated surfaces.⁸ Discrete [M₆Q₈L₆]^{n−} structural units were found to be promising building blocks for the bottom-up design of different types of supramolecular arrays *e.g.* coordination polymers and extended molecular solids.⁹

Physical and chemical properties of the cluster core are driven by the electronic structure, or more precisely, mutual location and energy of frontier orbitals. The previous electronic structure calculations demonstrated that d-orbitals of metal atoms make a significant contribution to octahedral cluster frontier orbitals.^{2a,10} Therefore, the insertion of a non-isovalent metal atom into a cluster core has been set forth as a promising way to modify the electronic structure of cluster units and consequently intrinsic physical properties of the resulting compounds in comparison with homometallic species. All synthetic routes to compounds with {M₆Q₈} cluster cores require high-temperature synthesis from simple starting materials,^{5a,11} with the exception of the low-temperature prepa-

^aNikolaev Institute of Inorganic Chemistry SB RAS, 3, Acad. Lavrentiev ave., Novosibirsk, 630090, Russia. E-mail: naumov@niic.nsc.ru^bInstitut des Sciences Chimiques de Rennes, Université de Rennes 1, UMR 6226 URI-CNRS, Campus de Beaulieu, Rennes, 35042, France^cNovosibirsk State University, 2, Pirogova str., Novosibirsk, 630090, Russia^dInternational Tomography Center SB RAS, 3A, Institutskaya str., Novosibirsk, 630090, Russia

† Electronic supplementary information (ESI) available. CCDC 1558003–1558006. For ESI and crystallographic data in CIF or other electronic format see DOI: 10.1039/c7dt03571c

ration of $[\text{Mo}_6\text{S}_8(\text{PET}_3)_6]$ by a reductive condensation of $[\text{Mo}_3\text{S}_4\text{Cl}_4(\text{PET})_4]$ moieties.¹²

As a result, the preparation of mixed-metal cluster compounds may face difficulties corresponding to the formation of minor cluster products with different core metal ratios and isomerisms of the equally composed clusters. Due to this, there are limited examples of known mixed-metal rhenium-based clusters, and especially a narrow range of practically available cluster cores is the major problem in their solution chemistry. There are some examples of solids containing heterometallic chalcogenide cluster cores in the literature: $\{\text{Mo}_{6-x}\text{M}_x\text{Q}_8\}$ ($\text{M} = \text{Re}$, $\text{Q} = \text{S}$, Se , $x = 4$, $\text{Q} = \text{Te}$, $x = 2, 4$; $\text{M} = \text{Ru}$, $\text{Q} = \text{Se}$, Te , $0 \leq x \leq 2$; $\text{M} = \text{Rh}$, $\text{Q} = \text{Te}$, $x = 0.5, 1.33$) and $\{\text{Mo}_2\text{Re}_4\text{S}_{8-x}\text{Se}_x\}$ $0 \leq x \leq 8$, $\{\text{Mo}_2\text{Re}_4\text{Se}_{8-x}\text{Te}_x\}$ $0 \leq x \leq 1.2$.¹³ An extensive solid state and solution chemistry was reported for heterometallic $\{\text{M}_6\text{Q}_8\}$ -type clusters with $\{\text{Re}_{6-x}\text{Os}_x\text{Se}_8\}$ ($x = 1-3$) cores.¹⁴ The isolated molecular octahedral clusters of Re and Mo with composition $\text{Cs}_5[\text{Re}_{6-x}\text{Mo}_x\text{S}_8(\text{CN})_6] \cdot 2\text{H}_2\text{O}$ ($x = 1-2$) were prepared as a mixture with $x \approx 1.7$ by reaction of the tetrahedral cluster $\text{Re}_4\text{Mo}_x\text{S}_4\text{Te}_4$ with KCN.¹⁵ Finally, the preparation of heterometallic clusters with the $\{\text{Re}_3\text{Mo}_3\text{S}_8\}^n$ core and their accessibility for solution ligand-exchange chemistry were recently published.¹⁶

Here we report synthetic procedures and a detailed experimental and theoretical study of mixed-metal octahedral clusters based on the novel $\{\text{Re}_3\text{Mo}_3\text{Se}_8\}^n$ core ($n = -1, +1$ and $+2$). Cluster species were prepared from an equimolar mixture of metal selenides and KCN by a high temperature route giving a polymeric mixed-metal compound. Soluble salts of $[\text{Re}_3\text{Mo}_3\text{Se}_8(\text{CN})_6]^{5-/4-}$ cluster anions were obtained using depolymerization reaction. The crystallographic study, redox property investigation and electronic structure calculation of mixed-metal octahedral clusters based on the $\{\text{Re}_3\text{Mo}_3\text{Se}_8\}^n$ core are presented in this work.

Results and discussion

Synthesis

The reactions of binary transition metal chalcogenides including MQ_2 ($\text{M} = \text{Re}$, Mo ; $\text{Q} = \text{S}$, Se) with molten cyanides at high temperatures are known to form transition metal clusters of $\{\text{M}_6\text{Q}_8\}$ -type.^{6a,17-19} These processes involve the reduction of the transition metal atom M^{4+} of chalcogenide by CN^- anions. Cyanide ions, as suggested, have been oxidized and transformed to a gaseous cyanogen $(\text{CN})_2$ or amorphous solid paracyanogen $(\text{CN})_n$.²⁰ It is especially valuable that the practically simple method for obtaining cluster compounds in the melt of cyanides was found to be applicable for the synthesis of several different cluster cores. For example, this method was applied for the preparation of homometallic clusters of Re and Mo, namely $\text{K}_6[\text{Mo}_6\text{Se}_8(\text{CN})_5]$,^{6a} $\text{Cs}_4[\text{Re}_6\text{S}_9(\text{CN})_4]$,¹⁷ $\text{K}_4[\text{Re}_6\text{S}_{10}(\text{CN})_2]$,¹⁸ $\text{K}_4[\text{Re}_6\text{Se}_{10}(\text{CN})_4]$ ¹⁸ and $\text{K}_8[\text{Re}_{12}\text{CS}_{17}(\text{CN})_6]$.¹⁹ The adaptation of the method for obtaining heterometallic clusters took a lot of effort because of the formation of numerous byproducts in the reaction mixture. Recently, the reaction of an equimolar mixture of MS_2 ($\text{M} = \text{Re}$, Mo) with KCN was

applied for the preparation of mixed-metal clusters based on $\{\text{Re}_3\text{Mo}_3\text{S}_8\}^n$ cores.¹⁶ In this work, we have successfully used this technique to obtain heterometallic cluster compounds with the $\{\text{Re}_3\text{Mo}_3\text{Se}_8\}^n$ core. Preliminary experiments revealed that the reaction between ReSe_2 , MoSe_2 and KCN leads to the formation of a complex product containing molecular and polymeric cluster species with a mixture of $\{\text{Re}_{6-x}\text{Mo}_x\text{Se}_8\}$ ($x = 0-4$) cluster cores. The product ratio was found to depend strongly on the preparation temperature. Decreasing the temperature to 630°C allowed us to shift the reaction equilibrium to the preferential formation of $\{\text{Re}_3\text{Mo}_3\}$ -based clusters. Treating the equimolar mixture of ReSe_2 and MoSe_2 with an excess of KCN at 630°C in a sealed silica ampoule led to the formation of black octahedral crystals of compound $\text{K}_6[\text{Re}_3\text{Mo}_3\text{Se}_8(\text{CN})_5]$ (**1**). The diamagnetic behavior of compound **1** correlates with an even number of CVE in the $\{\text{Re}_3\text{Mo}_3\text{Se}_8\}^-$ core (24 CVE). The IR spectrum of compound **1** demonstrates two characteristic bands related to $\nu(\text{CN})$ vibrations with the maxima at 2072 and 2093 cm^{-1} . Presumably, the absorbance band with a lower wavenumber could be assigned to apical cyanide vibrations in the equatorial plane, while the latter band corresponds to the bridging cyanides. The corresponding shift of the absorption band of $\text{C}\equiv\text{N}$ vibration is well-documented in the case of bridging CN^- ligands in polymeric cyanometalates.²¹ Terminal M-CN complexes generally exhibit sharp, intense bands between 2000 and 2200 cm^{-1} , which shift by up to $50-100\text{ cm}^{-1}$ to higher frequencies upon additional ligation at the N atom. This assignment also correlates with the reported properties of rhenium cluster coordination polymers with the composition $(\text{Pr}_4\text{N})_2\text{M}(\text{H}_2\text{O})_4[\text{Re}_6\text{S}_8(\text{CN})_6]$ ($\text{M} = \text{Mn}$, Ni). They demonstrate the shift of the vibration band maximum of bridging CN^- by $30-50\text{ cm}^{-1}$ toward higher values compared with the terminal cyanide group in $\text{Cs}_3\text{K}[\text{Re}_6\text{S}_8(\text{CN})_6] \cdot 2\text{H}_2\text{O}$.²²

Compound **1** is insoluble in H_2O or other solvents because of the polymeric structure. Nevertheless, it can be solubilized by gentle heating in aqueous KCN forming a pink solution. The reduction of the solution volume and the addition of ethanol resulted in the precipitation of $\text{K}_5[\text{Re}_3\text{Mo}_3\text{Se}_8(\text{CN})_6] \cdot 11\text{H}_2\text{O}$ (**2**). The diffusion of ethanol into an aqueous solution of **2** allowed us to obtain crystals suitable for X-ray structural analysis. The compound was found to crystallize in the cubic space group $Fm\bar{3}m$. Energy dispersive spectrometry (EDS) analysis performed on powder and single crystals displayed the atomic ratio $\text{K}:\text{Mo}:\text{Re}:\text{Se} = 4.8:2.8:3.2:8.1$. Mixing of the aqueous solutions of **2** and CsCl causes the precipitation of dark-brown powder of compound $\text{Cs}_5[\text{Re}_3\text{Mo}_3\text{Se}_8(\text{CN})_6] \cdot \text{H}_2\text{O}$ (**3**) which crystallizes in the $P\bar{3}c1$ space group. Compounds **2** and **3** are ionic salts and demonstrate the framework crystal structures based on $[\text{Re}_3\text{Mo}_3\text{Se}_8(\text{CN})_6]^{5-}$ cluster anions (Fig. 1) and alkali cations.

As one can notice, the solubilization of polymeric compound **1** is accompanied by two-electron oxidation of the cluster core $\{\text{Re}_3\text{Mo}_3\text{Se}_8\}^-$ to $\{\text{Re}_3\text{Mo}_3\text{Se}_8\}^+$. The diamagnetic behavior of the $\{\text{Re}_3\text{Mo}_3\text{Se}_8\}^+$ core with 22 CVE was confirmed by EPR measurements of **2** and **3**. The 24- and 23-electron

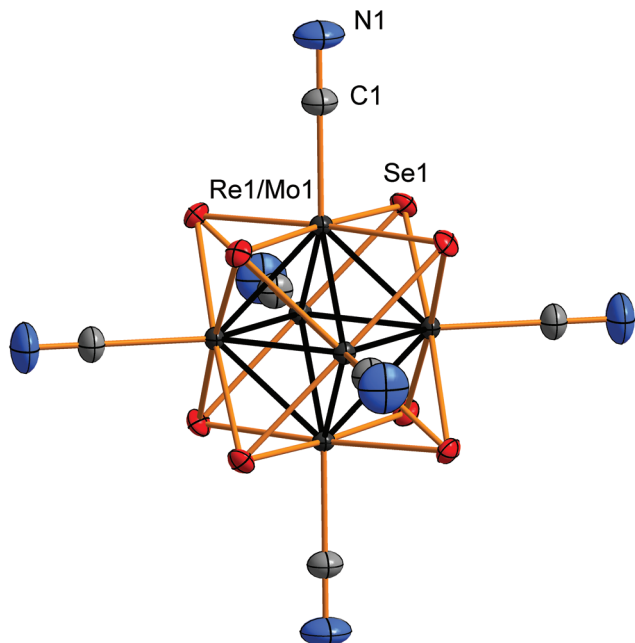


Fig. 1 Structure of cluster anion $[\text{Re}_3\text{Mo}_3\text{Se}_8(\text{CN})_6]^{5-}$ in **2**, and thermal ellipsoids of 50% probability.

forms of the cluster anion $[\text{Re}_3\text{Mo}_3\text{Se}_8(\text{CN})_6]^{7-/6-}$ were not isolated during the solubilization of **1** indicating the vulnerability of forms with a large CVE number toward air oxygen. In contrast to the compound **1**, only one characteristic band of $\nu(\text{CN})$ vibrations was found in the IR spectra of both compounds **2** and **3** with the maxima at 2093 and 2095 cm^{-1} , respectively.

The UV-Vis spectrum of compound **2** in aqueous solution (Fig. 2) reveals absorption bands in the visible region with maxima at 550 and 610 nm to be characteristic of $[\text{Re}_3\text{Mo}_3\text{Se}_8(\text{CN})_6]^{5-}$ cluster anions. The metathesis reaction between aqueous solutions of **2** and Ph_4PBr led to the immedi-

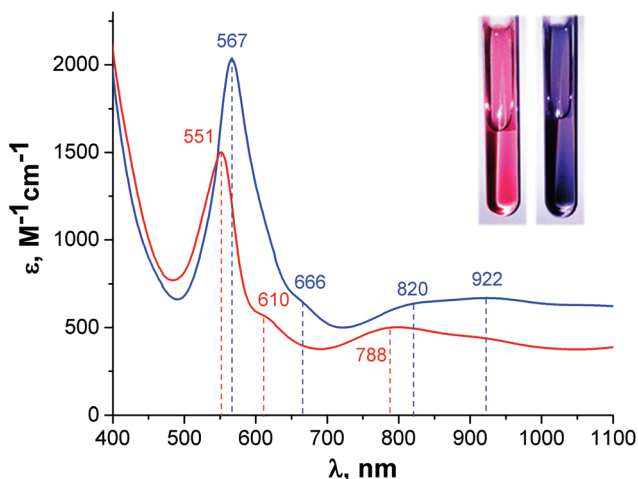


Fig. 2 The UV-Vis spectra for aqueous solution of **2** in H_2O (red) and **4** in DMF (blue). Inset: The photographic images of the solutions of **2** in H_2O (left) and **4** in DMF (right).

ate precipitation of pink powder accompanied by the complete solution bleaching. The amorphous precipitate has the composition $(\text{Ph}_4\text{P})_5[\text{Re}_3\text{Mo}_3\text{Se}_8(\text{CN})_6]$ according to elemental analysis results. Freshly prepared, it dissolves readily in CH_3CN and DMF forming pink solutions demonstrating the aforementioned characteristic absorption bands in UV-Vis spectra (550, 610 nm). The solution in CH_3CN is stable under an inert atmosphere, but disposition in air results in the precipitation of the blue crystalline powder of $(\text{Ph}_4\text{P})_4[\text{Re}_3\text{Mo}_3\text{Se}_8(\text{CN})_6] \cdot 2\text{CH}_3\text{CN}$ (**4**) accompanied by solution bleaching. Compound **4** is highly soluble in DMF. The DMF solution of **4** is characterized by UV-Vis spectroscopy demonstrating an absorption band with 567 nm maximum (Fig. 2, blue curve). The single absorption band of the CN^- ligand in **4** appears at 2091 cm^{-1} , which is close to those for **2** and **3**.

Thus, the rapid oxidation of the $\{\text{Re}_3\text{Mo}_3\text{Se}_8\}^+$ (22 CVE) cluster core to the $\{\text{Re}_3\text{Mo}_3\text{Se}_8\}^{2+}$ one with 21 CVE occurs in organic solvents. The suggested paramagnetic behavior of **4** was confirmed by EPR measurements. The broad paramagnetic signal with a value of g -factor equal to 2.430 was found (Fig. S1†). The g -value is close to previously reported ones for hexanuclear rhenium cluster anions $[\text{Re}_6\text{Q}_8\text{L}_6]^{3-}$ ($\text{Q} = \text{S}, \text{Se}, \text{Te}$; $\text{L} = \text{CN}, \text{Cl}, \text{Br}$; $g = 2.44\text{--}2.56$).^{3b,23} The outcome of the above data evidences that the $\{\text{Re}_3\text{Mo}_3\text{Se}_8\}^n$ cluster core can exist in (at least) three electronic states with n equal to 1−, 1+ and 2+ corresponding to 24, 22 and 21 CVE. Thereby, we suppose that $\{\text{Re}_3\text{Mo}_3\text{Se}_8\}$ -based clusters are one of the most electrochemically active among all known octahedral chalcogenide clusters. In prospect, it opens a way of designing the magnetically, optically and catalytically active cluster-based materials.

Crystal structures

Structure of $\text{K}_6[\text{Re}_3\text{Mo}_3\text{Se}_8(\text{CN})_5]$ (1**).** Compound **1** crystallizes in the tetragonal space group $I4/m$ and displays a polymeric structure based on 1D chains $[\text{Re}_3\text{Mo}_3\text{Se}_8(\text{CN})_4(\text{CN})_{2/2}]^{6-}_{\infty}$ lying along the c -axis (Fig. 3). The chains are composed of cluster fragments linked to each other by $\mu\text{-CN}$ groups in the *trans*-position, similarly to the reported structures of $\text{K}_6[\text{Mo}_6\text{Se}_8(\text{CN})_5]$ and $\text{K}_6[\text{Re}_3\text{Mo}_3\text{Se}_8(\text{CN})_5]$ solids.^{6a,16} Due to the high symmetry, the asymmetric unit contains only two mixed

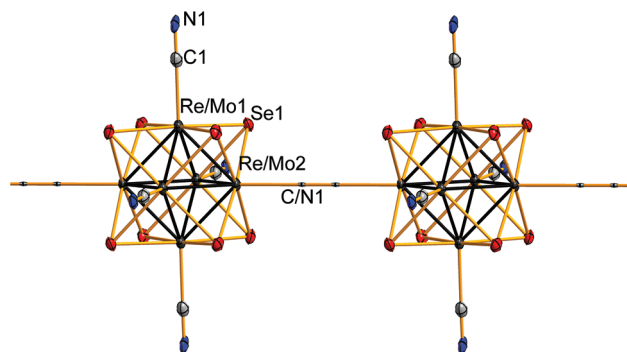


Fig. 3 Fragment of polymeric chain $[\text{Re}_3\text{Mo}_3\text{Se}_8(\text{CN})_4(\text{CN})_{2/2}]^{6-}_{\infty}$ in **1**, and thermal ellipsoids of 75% probability are shown.

positions of Re/Mo atoms. The average M–M distance in the metal core is equal to 2.667(8) Å lying almost midway between those for {Re₆} and {Mo₆} 24-e cluster cores in K₄[Re₆Se₈(CN)₆] \cdot 3.5H₂O²⁴ and Mg₂Mo₆Se₈²⁵ (2.633 and 2.697 Å, respectively). M–Se distances follow the same tendency (Table 1).

The structure of **1** comprises the slightly distorted octahedron M₆. This distortion breaks the O_h symmetry of the ideal octahedral unit to the D_{4h} one. It can be described as the elongation of the octahedron along the *c*-axis of the structure. Two types of M–M bond lengths are presented: eight longer bonds between apical and basal metal atoms; and four shorter bonds between only basal ones (2.6755(7) Å and 2.6518(7) Å, respectively). Two possible isomers of the mixed-metal octahedron may be presented in the structure of **1**: *fac*-isomer with C_{3v} symmetry and *mer*-isomer with C_{2v} symmetry (Fig. 4). One can notice that the symmetry of two isomers of the {Re₃Mo₃} metalocluster is lower than the point group symmetry of the crystal. To fit the lattice symmetry the isomers must be disordered between all possible orientations of two isomers relative to the *c*-axis of the structure (Fig. S2 and S3†). Apparently, an average structure does not allow us to analyze real Re–Re, Re–Mo, and Mo–Mo bond lengths. The evaluated Re/Mo site occupancy factors demonstrate the site preference of molybdenum atoms to be placed in the 4-fold axis positions of the distorted octahedron, making more contribution to the formation of polymeric chains (S.O.F for Re1(8 h/m.) – 0.60, Re2(4e/4.) – 0.30).

Structure of K₅[Re₃Mo₃Se₈(CN)₆] \cdot 10H₂O (2**).** The compound crystallizes in a highly symmetrical cubic space group *Fm* $\bar{3}$ *m*. The crystal structure is composed of the cluster anions [Re₃Mo₃Se₈(CN)₆]^{5–} (22 CVE) forming a Prussian blue-type framework by means of ionic contacts between cluster CN-ligands and K⁺ cations at a K–N distance of 2.684 Å (Fig. 5). Other K⁺ cations and solvate H₂O molecules bonded by a net of hydrogen bonds were found in the framework pores. Note that the asymmetric unit of the [Re₃Mo₃Se₈(CN)₆]^{5–} cluster anion contains only one position of the metal atom located at

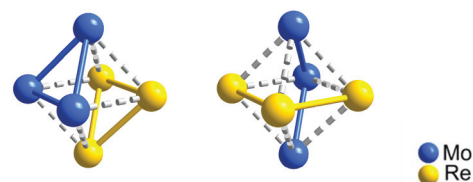


Fig. 4 The isomerism of octahedral metalocluster {Re₃Mo₃}, *fac*-(Re₃Mo₃) (left) and *mer*-(Re₃Mo₃) (right).

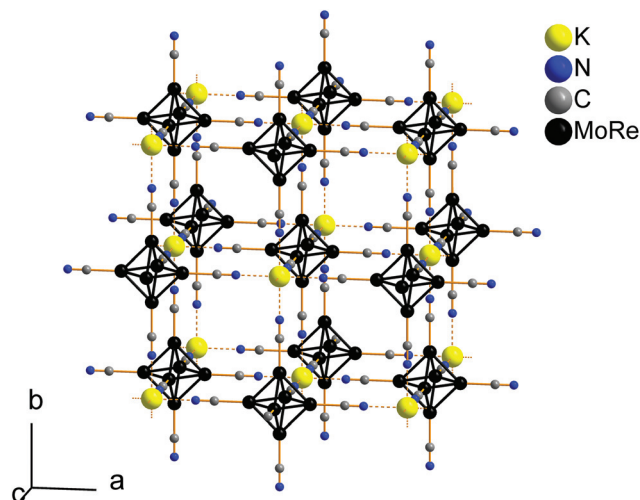


Fig. 5 Fragment of crystal packing in **2**. Selenium atoms, extra-framework cations and solvate H₂O molecules are omitted for clarity.

the 4*m*.*m* symmetry site, forming an ideal octahedron with the M–M distance equal to 2.6494(9) Å.

Structure of Cs₅[Re₃Mo₃Se₈(CN)₆] \cdot H₂O (3**).** The crystals suitable for single crystal X-ray analysis were obtained during the slow diffusion of aqueous solutions of **2** and CsCl. The compound crystallizes in the trigonal *P* $\bar{3}$ *c*1 space group. The crystal structure represents the layers based on ionic contacts of

Table 1 Selected interatomic distances (Å) in compounds **1**–**4**

| | 1 | | 2 | |
|------|---------------------|----------|-------|-----------|
| | Range | Average | Range | Average |
| M–M | 2.6518(7)–2.6755(7) | 2.667(8) | — | 2.6494(9) |
| M–Se | 2.5476(8)–2.5633(7) | 2.56(2) | — | 2.5464(9) |
| M–C | 2.15(1)–2.20(1) | 2.17(2) | — | 2.14(2) |
| C–N | 1.15(3)–1.16(1) | 1.153(2) | — | 1.18(2) |

| | 3 | | 4 | |
|------|---------------------|-----------|---------------------|----------|
| | Range | Average | Range | Average |
| M–M | 2.6451(9)–2.6459(9) | 2.645(11) | 2.6407(2)–2.6619(2) | 2.654(2) |
| M–Se | 2.541(1)–2.549(1) | 2.54(3) | 2.5197(3)–2.5463(3) | 2.539(7) |
| M–C | — | 2.157(11) | 2.164(3)–2.171(3) | 2.17(2) |
| C–N | — | 1.16(2) | 1.151(4)–1.154(4) | 1.15(2) |

$[\text{Re}_3\text{Mo}_3\text{Se}_8(\text{CN})_6]^{5-}$ anions and Cs^+ cations (Fig. S4†). More Cs^+ cations and solvate H_2O molecules are disordered in the interlayer space. The asymmetric unit contains two positions of metal atoms. The average M–M distance in the metal core for compound 3 is equal to 2.645(11) Å, being in agreement with that for compound 2.

Structure of $(\text{Ph}_4\text{P})_4[\text{Re}_3\text{Mo}_3\text{Se}_8(\text{CN})_6]\cdot 2\text{CH}_3\text{CN}$ (4). The crystal structure of compound 4 consists of closely packed $[\text{Re}_3\text{Mo}_3\text{Se}_8(\text{CN})_5]^{4-}$ cluster anions and Ph_4P^+ cations with solvate CH_3CN molecules located in the voids between voluminous cations and anions (Fig. S5†). Having a low-symmetry triclinic space group $P\bar{1}$, there are three independent metal positions in the asymmetric unit of the structure. The average M–M distance in the $[\text{Re}_3\text{Mo}_3\text{Se}_8(\text{CN})_5]^{4-}$ anion (21 CVE) is 2.654(2) Å. The comparison of average M–M and M–Se distances in compounds 1–4 shows that the tendency of change in bond lengths along with varying CVE does not show linear behavior.

According to ESI mass spectrometry, the DMF/ CH_3CN solution of 4 clearly contains minor amounts of $[\text{Re}_4\text{Mo}_2\text{Se}_8(\text{CN})_6]^{4-}$ and $[\text{Re}_2\text{Mo}_4(\text{CN})_6]^{4-}$ anions. These anions have the same charge and geometry as $[\text{Re}_3\text{Mo}_3\text{Se}_8(\text{CN})_5]^{4-}$ anions. Consequently, they occupy common atomic positions with $[\text{Re}_3\text{Mo}_3\text{Se}_8(\text{CN})_5]^{4-}$ cluster anions in the structure of 4 forming a solid solution that cannot be distinguished by means of single crystal and powder X-ray diffraction analysis. Nevertheless, the $\{\text{Re}_3\text{Mo}_3\}$ -based cluster is the major component, which defines M–M distances and phase properties.

Mass spectrometry

The EDS of solid state phases of compounds 1–4 showed small but important deviations in the Re:Mo ratio indicating the presence of several cluster forms. In order to determine them, high-resolution ESI-MS analysis was performed using a DMF/ CH_3CN solution of 4. Mass spectra revealed six cluster-related signals in 930–1050 and 1100–1220 m/z ranges in the negative detection mode, which can be symbolically divided into two intensive “triplets” of isotopic patterns (Fig. 6). The distance of 0.5 m/z between isotope signals in all patterns indicates the charge of all ions obtained to be -2 . The central and most intense isotopic patterns in both “triplets” are perfectly matched with the calculated ones for associates of target cluster anions $[\text{Re}_3\text{Mo}_3\text{Se}_8(\text{CN})_6]^{n-}$ ($n = 4$ and 3) with Ph_4P^+ cations. The signal from the central isotopic pattern in the 930–1050 m/z range was assigned to the $[\text{Re}_3\text{Mo}_3\text{Se}_8(\text{CN})_6]^{3-}$ adduct with one Ph_4P^+ cation, namely $(\text{Ph}_4\text{P})[\text{Re}_3\text{Mo}_3\text{Se}_8(\text{CN})_6]^{2-}$ ($m/z = 987.51$, 100%). The “satellite” isotopic distribution patterns in the first triplet were assigned to $(\text{Ph}_4\text{P})[\text{Re}_2\text{Mo}_4\text{Se}_8(\text{CN})_6]^{2-}$ ($m/z = 941.98$, 10%) and $(\text{Ph}_4\text{P})[\text{Re}_4\text{Mo}_2\text{Se}_8(\text{CN})_6]^{2-}$ ($m/z = 1033.03$, 15%) adducts. The detection of the $(\text{Ph}_4\text{P})[\text{Re}_3\text{Mo}_3\text{Se}_8(\text{CN})_6]^{2-}$ form suggests that further oxidation of the $\{\text{Re}_3\text{Mo}_3\text{Se}_8\}$ cluster core has occurred during the ionization process. The second triplet in the 1100–1220 m/z range represents the isotopic distribution pattern for four-charged clusters with two Ph_4P^+ cations: $(\text{Ph}_4\text{P})_2[\text{Re}_2\text{Mo}_4\text{Se}_8(\text{CN})_6]^{2-}$ ($m/z = 1112.55$, 7%), $(\text{Ph}_4\text{P})_2[\text{Re}_3\text{Mo}_3\text{Se}_8(\text{CN})_6]^{2-}$ ($m/z = 1156.07$, 69%), and

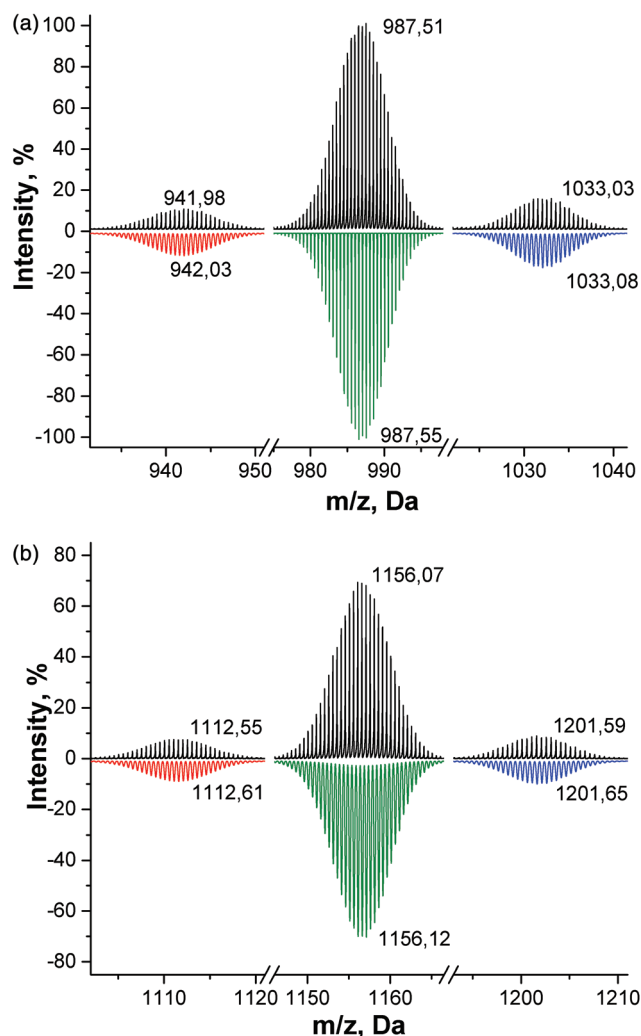


Fig. 6 Selected isotopic distribution patterns for 3-adducts (a) and 2-adducts (b) in ESI-MS of 4 in DMF/ CH_3CN . Observed spectra (black) are shown vs. calculated ones for corresponding adducts of $[\text{Re}_2\text{Mo}_4\text{Se}_8(\text{CN})_6]^{n-}$, $[\text{Re}_3\text{Mo}_3\text{Se}_8(\text{CN})_6]^{n-}$ and $[\text{Re}_4\text{Mo}_2\text{Se}_8(\text{CN})_6]^{n-}$ anions (red, green and blue, respectively).

$(\text{Ph}_4\text{P})_2[\text{Re}_4\text{Mo}_2\text{Se}_8(\text{CN})_6]^{2-}$ ($m/z = 1201.59$, 9%). Thus, mass-spectrometry directly demonstrated the presence of admixtures based on $\{\text{Re}_2\text{Mo}_4\}$ and $\{\text{Re}_4\text{Mo}_2\}$ heterometallic cores formed under the high-temperature conditions together with the main product containing the $\{\text{Re}_3\text{Mo}_3\}$ core. It is worth noting that this result was obtained after long-term optimization of preparation conditions. The preparation of the reaction mixture with a higher target product content was not achieved in any experiments. Otherwise, a low content of admixture clusters in 1–4 allowed us to explore optical, magnetic and other physical properties of the target compound without significant mismatching.

DFT calculations

Analysis of the interatomic distances in the crystal structures of the $\{\text{Re}_3\text{Mo}_3\text{Se}_8\}$ -based clusters 1–4 revealed that average

metal-metal bond lengths are weakly sensitive to the CVE number (Table 2). Notably, the M-M average distance in 24 CVE cluster $[\text{Re}_3\text{Mo}_3\text{Se}_8(\text{CN})_5]^{6-}$ in the structure of compound **1** is only 0.022 or 0.018 Å longer compared to the structures of 22 CVE cluster $[\text{Re}_3\text{Mo}_3\text{Se}_8(\text{CN})_6]^{5-}$ in the structures of compounds **2** and **3**. Also, the differences in average M-M distances are insignificant for the 22 CVE cluster in the structures of **2** and **3** and the 21 CVE cluster in the structure of **4**. The corresponding differences are of 0.004–0.005 Å, respectively. The $\{\text{Re}_3\text{Mo}_3\}$ metallocluster in all considered structures forms practically an ideal octahedron. However, the X-ray diffraction data reflect only the averaged atomic coordinates in consideration of all possible relative positions of two isomers of $[\text{Re}_3\text{Mo}_3\text{Se}_8(\text{CN})_6]^{n-}$ anions and, hence, give the limited information for the analysis of metal-metal bonding within the cluster core.

It is known that different kinds of clusters demonstrate different influences of the CVE number on the M-M average distance. Rhenium chalcogenide clusters $\text{Re}_6\text{Q}_8\text{L}_6$, Q = S, Se, Te, L = CN, Cl, Br, I are non-sensitive to a CVE value. For example, average Re-Re distances in the $[\text{Re}_6\text{Se}_8(\text{CN})_6]^{n-}$ clusters keep practically the same values when the CVE changes from 24 to 23 (2.633 Å in $\text{K}_4[\text{Re}_6\text{Se}_8(\text{CN})_6] \cdot 3.5 \text{H}_2\text{O}$ and 2.633 Å in $(\text{Ph}_4\text{P})_2\text{H}[\text{Re}_6\text{Se}_8(\text{CN})_6] \cdot 8\text{H}_2\text{O}$).²⁶ The same phenomenon occurs for the cyanide molybdenum cluster $[\text{Mo}_6\text{Se}_8(\text{CN})_6]^{n-}$. Mo-Mo distances are close in the structures containing 20 or 21 CVE (2.711 Å in $(\text{Me}_4\text{N})_4\text{K}_2[\text{Mo}_6\text{Se}_8(\text{CN})_6] \cdot 10\text{H}_2\text{O}$ and 2.700 Å in $\text{K}_7[\text{Mo}_6\text{Se}_8(\text{CN})_6] \cdot 8\text{H}_2\text{O}$).^{3a,27} However, halide niobium clusters with $\{\text{Nb}_6\text{X}_{12}\}$ cores existing with a number of valence electrons from 14 to 16 demonstrate a stronger influence of CVE on Nb-Nb distances. Particularly in the case of X = Cl the average Nb-Nb distance elongates from 2.910 Å in $\text{K}_4[\text{Nb}_6\text{Cl}_{12}\text{Cl}^{\text{a}}_6]$ (16 CVE) through 2.967 Å in $(\text{Me}_4\text{N})_3[\text{Nb}_6\text{Cl}_{12}\text{Cl}^{\text{a}}_6]$ (15 CVE) to 3.02 Å in $(\text{Me}_4\text{N})_2[\text{Nb}_6\text{Cl}_{12}\text{Cl}^{\text{a}}_6]$ (14 CVE), *i.e.* the removal of one cluster valence electron causes the increase of average Nb-Nb distances to about 0.05 Å.²⁸

The case of mixed-metal cluster compounds with the $\{\text{Re}_3\text{Mo}_3\text{Se}_8\}$ cluster core is more complicated due to the existence of two isomers of the cluster core, namely *fac*- with C_{3v} symmetry and *mer*- with C_{2v} symmetry (Fig. 4). The orientational disorder of the isomers causes Re/Mo sites to be mixed in all observed structures. To analyze the electronic structure

and geometry of mixed-metal clusters with different CVE, DFT calculations of $[\text{Re}_3\text{Mo}_3\text{Se}_8(\text{CN})_6]^{n-}$ ($n = 4-7$, CVE count from 21 to 24) were performed for both *fac*- and *mer*-isomers of the $\{\text{Re}_3\text{Mo}_3\}$ metallocluster. The molecular orbital (MO) diagrams for different isomers are shown in Fig. 7. Below the Fermi energy level one can see the block of orbitals with a mixed bonding-antibonding character, and above the Fermi energy level there are antibonding orbital blocks. The MO disposition for both isomers of heterometallic $[\text{Re}_3\text{Mo}_3\text{Se}_8(\text{CN})_6]^{n-}$ differs from homometallic $[\text{Re}_6\text{Se}_8(\text{CN})_6]^{n-}$ ones by the presence of a gap between 353A and 352A orbitals (HOMO-1 and HOMO-2 for 24e cluster anions). The value of this energy gap is about 0.4 eV. Both orbitals are of bonding nature.

The 354A and 353A (HOMO and HOMO-1 for 24e cluster anion) orbitals are composed mostly of molybdenum atomic orbitals with minor contribution from rhenium and selenium. As one can see, the consequent electron removal leads to 353A orbital lowering. In this case, the 354A orbital remains nearly without change (insignificant decreasing during 24-23-22 CVE variation and increasing with 22-21 CVE change).

The calculated M-M distances are listed in Table 2. The attentive analysis of calculated distances revealed that both *mer*- and *fac*-isomers of the 24 CVE $\{\text{Re}_3\text{Mo}_3\}$ core are barely distorted, with similar average Re-Re, Re-Mo and Mo-Mo bond lengths. The *mer*-isomer demonstrated the average Re-Re bond length value to be only 0.007 Å shorter compared to the average Mo-Re and Mo-Mo bonds. Also the Re-Re average bond length in the *fac*-isomer is 0.023 shorter than that of Mo-Mo and Mo-Re bonds. A significant spatial distortion of the cluster core is observed during stepwise electron removal in the *fac*-isomer. The Mo-Mo average distance elongates by 0.041 Å accompanied by shortening of Re-Mo and Re-Re bonds (Fig. 8). Shortening of Re-Re bonds in the *fac*-isomer is by 0.029 Å. The *fac*-isomer of the 22 CVE cluster is the most distorted with the difference between the largest and smallest M-M distances having the relatively large value of 0.197 Å, which is not typical of octahedral transition metal clusters. The *mer*-isomer demonstrated similar behavior, with the large difference between the shortest and largest M-M bonds being 0.139 Å. Such elongation seems to correspond to the significant contribution of the molybdenum d-orbitals to 354a and 353a orbitals. The large difference between the shortest and

Table 2 Calculated M-M distances (Å) in *fac*- and *mer*-isomers of the metallocluster in $[\text{Re}_3\text{Mo}_3\text{Se}_8(\text{CN})_6]^{n-}$ anions

| Isomer | <i>n</i> | Mo-Mo | | Re-Mo | | Re-Re | | M-M Average |
|--------------|----------|---------------|-----------|---------------|-----------|---------------|-----------|-------------|
| | | Range | Average | Range | Average | Range | Average | |
| <i>fac</i> - | 7- | 2.7003–2.7007 | 2.7006(2) | 2.6977–2.6981 | 2.6979(1) | 2.6782–2.6790 | 2.6785(4) | 2.6937 |
| | 6- | 2.6902–2.7757 | 2.72(4) | 2.6782–2.7198 | 2.70(2) | 2.6630–2.6854 | 2.67(1) | 2.6954 |
| | 5- | 2.6756–2.8437 | 2.73(8) | 2.6582–2.7353 | 2.69(3) | 2.6471–2.6909 | 2.66(2) | 2.6949 |
| | 4- | 2.7103–2.8053 | 2.74(4) | 2.6674–2.7030 | 2.69(1) | 2.6435–2.6609 | 2.649(8) | 2.6905 |
| <i>mer</i> - | 7- | 2.6946–2.6947 | 2.6947(1) | 2.6874–2.7030 | 2.695(6) | 2.6882–2.6883 | 2.6883(1) | 2.6939 |
| | 6- | — | 2.7433 | 2.6810–2.7021 | 2.689(9) | — | 2.6694 | 2.6945 |
| | 5- | 2.7831–2.7833 | 2.7832(1) | 2.6639–2.7139 | 2.68(2) | 2.6444–2.6445 | 2.6445(1) | 2.6934 |
| | 4- | — | 2.7508 | 2.6798–2.6892 | 2.683(4) | 2.6514–2.6516 | 2.6515(1) | 2.6890 |

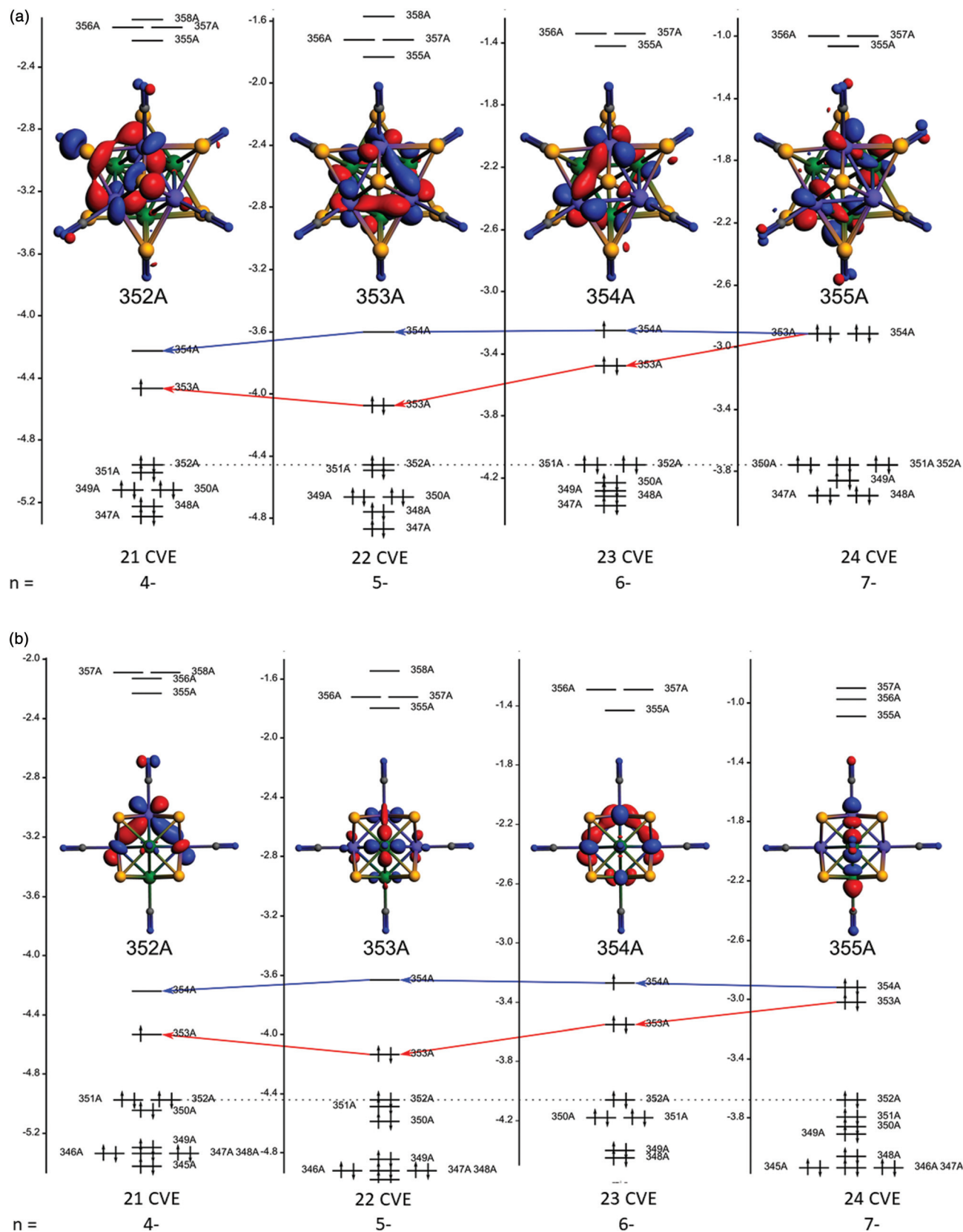


Fig. 7 Molecular orbital diagrams of *fac-* (a) and *mer-* (b) isomers of $[\text{Re}_3\text{Mo}_3\text{Se}_8(\text{CN})_6]^{n-}$ ($n = 4-7$ from left to right). Insets: Typical view of the 355A, 354A, 353A, and 352A orbitals for $[\text{Re}_3\text{Mo}_3\text{Se}_8(\text{CN})_6]^{5-}$ anion. MO diagrams are aligned with respect to 352A orbital energy.

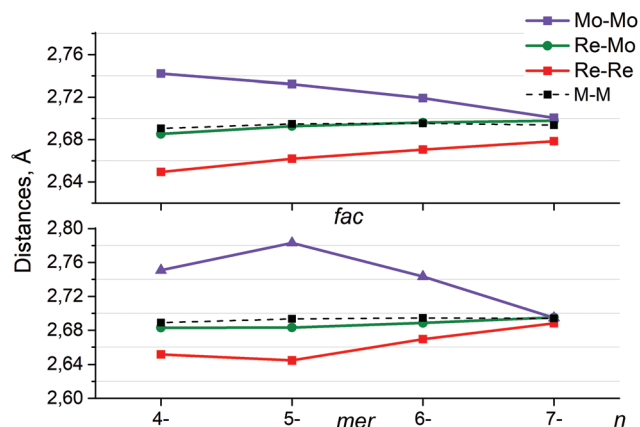


Fig. 8 Calculated average Mo–Mo, Re–Mo, Re–Re and M–M distances in the *fac*-isomer (up) and *mer*-isomer (down) of the metallocluster in $[\text{Re}_3\text{Mo}_3\text{Se}_8(\text{CN})_6]^{n-}$ anions depending on the charge n .

largest M–M bonds represents significant octahedron distortion. However, scarce M–M bond distribution intervals according to structural data for compounds 1–4 correlate with the presence of orientational disorder of $\{\text{Re}_3\text{Mo}_3\}$ isomers masking the real cluster core distortion in obtained structures.

The average M–M distances for the *fac*-isomer of the $[\text{Re}_3\text{Mo}_3\text{Se}_8(\text{CN})_6]^{n-}$ cluster anion increase slightly when the CVE number varies from 21 to 23 (Table 2, Fig. 8). Specifically, the value of 2.6905 Å in the 21 CVE cluster increases to 2.6949 Å (22 CVE) and 2.6954 Å (23 CVE) and finally decreases to 2.6937 Å in the 24 CVE cluster. The *mer*-isomer distances follow the same tendency (2.6890 Å for 21 CVE, 2.6934 Å for 22 CVE, 2.6945 Å for 23 CVE and 2.6939 Å for 24 CVE). One can notice that average M–M distances obtained from DFT calculations for both isomers are close and the calculated values match well with the structural data. A general trend to the slight elongation of calculated distances may be due to the used water environment in calculation approximation.

Electrochemical properties

The redox properties of **4** were investigated in DMF solution using cyclic voltammetry vs. Ag/AgCl electrode. The voltammogram demonstrates two quasi-reversible redox couples with $E_{1/2}$ at -1.410 and -0.325 V and $\Delta E = 100$ and 110 mV, respectively, and one quasi-reversible reduction wave at $E_{pc} = -0.818$ V (Fig. 9). These couples correspond to the series of one-electron transitions, namely $[\text{Re}_3\text{Mo}_3\text{Se}_8(\text{CN})_6]^{7-/6-}$ (24 \rightarrow 23 CVE), $[\text{Re}_3\text{Mo}_3\text{Se}_8(\text{CN})_6]^{6-/5-}$ (23 \rightarrow 22 CVE) and $[\text{Re}_3\text{Mo}_3\text{Se}_8(\text{CN})_6]^{5-/4-}$ (22 \rightarrow 21 CVE). The observed potentials agree well with the inaccessibility of $[\text{Re}_3\text{Mo}_3\text{Se}_8(\text{CN})_6]^{7-}$ and $[\text{Re}_3\text{Mo}_3\text{Se}_8(\text{CN})_6]^{6-}$ anions in aqueous solutions, as well as with the oxidation of $[\text{Re}_3\text{Mo}_3\text{Se}_8(\text{CN})_6]^{5-}$ anions by air oxygen in CH_3CN or DMF solution. As it can be seen from the literature data, the new mixed-metal clusters display a dramatic decrease in 24/23 CVE redox potential in comparison with the values for the $[\text{Re}_6\text{Se}_8(\text{CN})_6]^{3-/4-}$ cluster (Table 3). On the other hand, the $[\text{Mo}_6\text{Se}_8(\text{CN})_6]^{7-}$ clusters display the lower potentials of 22/21/

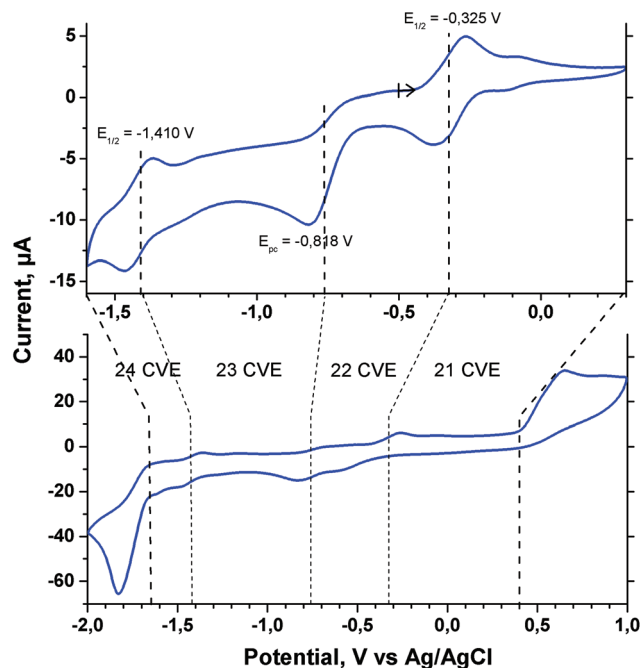


Fig. 9 Cyclic voltammograms of **4** in DMF.

Table 3 Redox data for $\{\text{M}_6\text{Se}_8\}$ -type clusters (M = Re, Mo, potentials are normalized vs. Ag/AgCl/3.5 M KCl electrode)

| CVE count | 20/21 | 21/22 | 22/23 | 23/24 |
|---|----------|----------|------------|----------|
| $[\text{Re}_6\text{Se}_8(\text{CN})_6]^{3-/4-} (\text{CH}_3\text{CN})^{5a}$ | — | — | — | 0.125 |
| $[\text{Re}_3\text{Mo}_3\text{Se}_8(\text{CN})_6]^{4-/5-/-6-/7-}$ (DMF) | — | -0.325 | -0.818 | -1.410 |
| | | | (E_{pc}) | |
| $[\text{Mo}_6\text{Se}_8(\text{CN})_6]^{6-/7-/-8-/9-}$ (H_2O) ²⁷ | -0.647 | -1.081 | -1.574 | — |

20 CVE transitions in comparison with $[\text{Re}_3\text{Mo}_3\text{Se}_8(\text{CN})_6]^{n-}$ ones.²⁷

The cyclic voltammogram is framed in both sides with multi-electron irreversible waves located at $E_{pc} = -1.828$ and $E_{pa} = 0.654$ V. The waves are characterized by sharp deformation of the baseline angle and high intensity. These transitions were attributed to multi-electron irreversible reduction and oxidation of cluster anions, accompanied by irreversible decomposition of the cluster anion. The presence of $\{\text{Re}_4\text{Mo}_2\}$ and $\{\text{Re}_2\text{Mo}_4\}$ byproducts is manifested presumably as two redox couples of negligible intensity at about -0.10 V and -1.25 V.

Conclusion

This research opens the development of a new class of cluster compounds displaying perspective redox properties and intriguing geometry distortion correlated with the CVE number. The heterometallic clusters with $\{\text{Re}_{6-n}\text{Mo}_n\text{Se}_8\}$ cores were synthesized using high-temperature reaction between ReSe_2 ,

MoSe₂ and KCN. The optimization of reaction conditions allowed us to obtain the polymeric compound K₆[Re₃Mo₃Se₈(CN)₅] comprising a {Re₃Mo₃Se₈} based cluster along with minor amounts of {Re₄Mo₂Se₈} and {Re₂Mo₄Se₈} ones. This compound acts as the precursor for soluble salts of discrete cluster anions [Re₃Mo₃Se₈(CN)₆]^{5-/4-}. The new anions have a remarkable redox activity in a narrow electrochemical window. Cyclic voltammetry of the [Re₃Mo₃Se₈(CN)₆]⁴⁻ anion in compound **4** in DMF revealed three waves corresponding to the [Re₃Mo₃Se₈(CN)₆]^{4-/5-/6-/7-} transitions. DFT calculations showed that the removal of electrons from the cluster causes a significant elongation of Mo–Mo bonds and shortening of Re–Re ones resulting in a significant geometric distortion of the {Re₃Mo₃Se₈} core.

Experimental section

Materials and methods. ReSe₂ and MoSe₂ were synthesized by reaction between elementary substances in a stoichiometry ratio in evacuated silica ampoules. The ampoules with reagents were heated at 600 °C for 48 h. Other reagents and solvents were used as purchased.

Elemental analyses were performed with a Thermo Electron Microanalyser Flash EA1112 CHNS/O. Energy dispersive spectroscopy (EDS) was performed on a Hitachi TM-3000 electron microscope equipped with a Bruker Nano EDS analyzer. FT-IR spectra using KBr pellets were recorded on a Bruker Scimitar FTS 2000 spectrometer in the range 4000–375 cm⁻¹. UV-Vis absorption measurements were performed in the wavelength range 400–1100 nm on an Analytik Jena Specord 205 UV-Vis spectrophotometer. EPR spectra were registered using a Bruker EMX EPR-spectrometer.

Electrospray ionization mass spectrometry (ESI-MS) was carried out on a Bruker maXis 4G high-resolution ESI-q-TOF mass spectrometer (negative ion mode, range 300–3000 *m/z*, direct injection with automatic syringe 0.18 ml per hour, voltage +2500 V, nebulizer pressure 2 bar, dry gas 6 L min⁻¹, dry gas temperature 200 °C).

Cyclic voltammetry was carried out on a Metrohm Computrace 797 VA voltammetry analyzer using a three-electrode scheme with GC working, Pt auxiliary and Ag/AgCl/3.5 M KCl reference electrodes. Investigations were carried out for a 2.5 × 10⁻³ M solution of cluster salt **4** in a 0.1 M solution of Bu₄NClO₄ in DMF under an Ar atmosphere. The registered value of *E*_{1/2} for Fe^{0/+} couple was 0.550 V under the same conditions. We were not able to register the potential of Fe^{0/+} couple in the solution of compound **4** probably because of the precipitation of cluster salt with the Fe⁺ cation.

Preparation of K₆[Re₃Mo₃Se₈(CN)₅] (1**).** A mixture of MoSe₂ (0.900 g, 3.54 mmol), ReSe₂ (1.220 g, 3.54 mmol) and KCN (2.032 g, 31.21 mmol) was intimately ground and transferred to a silica ampoule. The ampoule was evacuated, sealed and heated at 630 °C for two weeks, and then the ampoule was slowly cooled to room temperature. The resulting melt contain-

ing black octahedral crystals of **1** was washed with H₂O and purged with argon on a glass filter to remove the excess of KCN. The admixture of unreacted selenides was removed by sonication and decantation in ethanol. The crystals were dried under dynamic vacuum to give 1.560 g of the product. Yield: 72%. The yield can be improved up to 90% increasing the reaction time to 4 weeks. IR (KBr): $\tilde{\nu}$ = 2072, 2093 cm⁻¹ (C≡N); EDS: K:Mo:Re:Se = 5.9:2.7:3.3:8.4; elemental analysis calcd (%) for C₅N₅Se₈K₆Mo₃Re₃: C 3.26, N 3.80; found: C 3.31, N 3.37%. The PXRD analysis of compound **1** is presented in Fig. S6.† Compound **1** is oxygen and moisture sensitive. Grounding the sample and measuring in air leads to the evolution of the powder pattern and formation of a soluble cluster compound. Its treatment with an aqueous solution of KCN produces compound **2**.

Preparation of K₅[Re₃Mo₃Se₈(CN)₆]·11H₂O (2**).** Compound **1** (0.500 g, 0.27 mmol) and KCN (0.050 g, 0.77 mmol) were gently heated and stirred in H₂O (10 ml) in air giving pink solution. The solution was filtered and the volume of the solution was reduced to 3 ml under vacuum, and then 3 ml of ethanol was added causing immediate precipitation. The precipitate was separated by centrifugation, washed with ethanol and dried in air. Yield: 0.355 g (71%). IR (KBr): $\tilde{\nu}$ = 3570, 1614 (O–H); 2093 cm⁻¹ (C≡N); UV-Vis (H₂O): $\lambda_{\max}(\epsilon)$ = 550(1487); 613 nm (735 mol⁻¹ dm³ cm⁻¹); EDS: K:Mo:Re:Se = 4.8:2.8:3.2:8.1; elemental analysis calcd (%) for C₆N₆K₅Se₈Mo₃Re₃·(H₂O)₅: C 3.75, H 0.52, N 4.38; found: C 3.78, H 0.54, N 4.02%. The crystals suitable for single crystal X-ray analysis were obtained during the diffusion of ethanol into the aqueous solution of **2** (100 mg ml⁻¹). The PXRD analysis of compound **2** is presented in Fig. S7.†

Preparation of Cs₅[Re₃Mo₃Se₈(CN)₅]·H₂O (3**).** Compound **2** (0.500 g, 0.26 mmol) and CsCl (0.500 g, 2.97 mmol) were dissolved in H₂O (5 ml). The solution was evaporated to a volume of about 2 ml and slowly cooled. The microcrystalline powder was filtered, washed with ethanol and dried in air. Yield: 0.513 g (82%). IR (KBr): $\tilde{\nu}$ = 3432, 1606 (O–H), 2095 cm⁻¹ (C≡N); EDS: K:Mo:Re:Se = 5.1:3.1:2.9:8.5; elemental analysis calcd (%) for C₆N₆Cs₅Se₈Mo₃Re₃·(H₂O)₄: C 3.04, H 0.34, N 3.54; found: C 2.91, H 0.32, N 3.38%. The crystals suitable for single crystal X-ray analysis were obtained during the slow diffusion of aqueous solutions of **2** (15 mg ml⁻¹) and CsCl (150 mg ml⁻¹) in a thin glass tube. The PXRD analysis of compound **3** is presented in Fig. S8.†

Preparation of (Ph₄P)₄[Re₃Mo₃Se₈(CN)₆]·2CH₃CN (4**).** 0.100 g (0.05 mmol) of compound **2** was dissolved in water (10 ml). 15 ml of aqueous solution of Ph₄PBr (0.140 g, 0.3 mmol) was added causing precipitation. The precipitate was separated by centrifugation, washed with water and dissolved in CH₃CN. The solution was left in air for about 2 hours. Thin dark-blue crystals were precipitated on the bottom of the glass during that time. The supernatant solution was decanted and the crystals were dried in air to yield 116 mg (76%) of the product. IR (KBr): $\tilde{\nu}$ = 2091 (C≡N); all bands related to the Ph₄P⁺ cation are observed; UV-Vis (DMF): $\lambda_{\max}(\epsilon)$ = 567 nm (2360 mol⁻¹ dm³ cm⁻¹). ESI-MS (*m/z*, Da) calcd for (Ph₄P)

Table 4 Selected crystal, collection and refinement data for 1–4

| Compound | 1 | 2 | 3 | 4 |
|---|--|--|--|--|
| Chemical formula | C ₄ K ₆ Mo ₂ N ₆ Re ₄ Se ₈ | C ₆ K ₅ Mo ₃ N ₆ O ₁₁ Re ₃ Se ₈ | C ₆ Cs ₅ Mo ₃ N ₆ ORe ₃ Se ₈ | C ₁₀₆ H ₈₆ Mo ₃ N ₈ P ₄ Re ₃ Se ₈ |
| Formula weight | 1935.06 | 2005.72 | 2314.77 | 3073.80 |
| Space group | <i>I4/m</i> | <i>Fm</i> $\bar{3}$ <i>m</i> | <i>P</i> $\bar{3}$ <i>c</i> 1 | <i>P</i> $\bar{1}$ |
| <i>A</i> [Å] | 11.5322(2) | 15.7344(2) | 9.9219(2) | 12.3663(3) |
| <i>B</i> [Å] | 11.5322(2) | 15.7344(2) | 9.9219(2) | 13.1230(3) |
| <i>C</i> [Å] | 9.3666(4) | 15.7344(2) | 19.6531(5) | 16.9407(4) |
| α [°] | 90 | 90 | 90 | 110.0425(8) |
| β [°] | 90 | 90 | 90 | 95.9443(9) |
| γ [°] | 90 | 90 | 120 | 101.6537(8) |
| <i>V</i> [Å ³] | 1245.68(6) | 3895.4(2) | 1675.53(8) | 2484.45(10) |
| <i>Z</i> | 2 | 4 | 2 | 1 |
| Crystal size [mm ³] | 0.05 × 0.05 × 0.05 | 0.16 × 0.16 × 0.12 | 0.19 × 0.19 × 0.17 | 0.08 × 0.05 × 0.04 |
| λ [Å] | 0.71073 | 0.71073 | 0.71073 | 0.71073 |
| <i>T</i> [K] | 150(2) | 130(2) | 130(2) | 150(2) |
| ρ_{calc} [g cm ^{−3}] | 4.913 | 3.420 | 4.588 | 2.054 |
| μ [cm ^{−1}] | 28.681 | 18.275 | 25.938 | 7.054 |
| 2 θ range [°] | 4.51–32.03 | 3.66–28.97 | 4.11–29.53 | 1.71–32.65 |
| Index range | −10 ≤ <i>h</i> ≤ 16 −13 ≤ <i>k</i> ≤ 16 −12 ≤ <i>l</i> ≤ 9 | −14 ≤ <i>h</i> ≤ 20 −11 ≤ <i>k</i> ≤ 19 −21 ≤ <i>l</i> ≤ 14 | −13 ≤ <i>h</i> ≤ 12 −12 ≤ <i>k</i> ≤ 12 −27 ≤ <i>l</i> ≤ 26 | −17 ≤ <i>h</i> ≤ 17 −14 ≤ <i>k</i> ≤ 19 −24 ≤ <i>l</i> ≤ 24 |
| Reflections collected | 2094 | 3008 | 8229 | 36 510 |
| Unique reflections | 872 | 287 | 1448 | 14 100 |
| Reflections observed (<i>I</i> > 2 σ (<i>I</i>)) | 785 | 274 | 1352 | 11 603 |
| <i>R</i> _{int} | 0.0217 | 0.0141 | 0.0406 | 0.0291 |
| Parameters refined | 42 | 28 | 86 | 596 |
| Restraints | 0 | 6 | 31 | 0 |
| GoF | 1.201 | 1.384 | 1.292 | 1.028 |
| <i>R</i> (<i>I</i> > 2 σ (<i>I</i>)) | 0.0362 | 0.0245 | 0.0462 | 0.0254 |
| <i>R</i> _w (<i>I</i> > 2 σ (<i>I</i>)) | 0.0802 | 0.0794 | 0.0922 | 0.0521 |
| $\Delta\rho_{\text{max}}, \Delta\rho_{\text{min}}$ [e Å ^{−3}] | 2.07, −1.38 | 1.05, −0.80 | 1.57, −1.91 | 1.01, −1.32 |

[Re₃Mo₃Se₈(CN)₆]^{2−}: 987.55, found 987.51; EDS: Re : Mo : Se : P = 2.8 : 3.2 : 7.7 : 3.8; elemental analysis calcd (%) for C₁₀₆H₈₆Mo₃N₈P₄Re₃Se₈: C 41.42, H 2.82, N 3.65; found: C 41.61, H 2.55, N 3.71%. The PXRD analysis of compound 4 is presented in Fig. S9.† Compound 4 readily loses solvate CH₃CN molecules in air causing the amorphization of the sample. Grinding and measuring of the sample in mineral oil allowed the slow degradation.

Single crystal diffraction studies

Diffraction data for 1 and 4 were obtained on a Bruker X8 Apex automatic four-circle diffractometer equipped with a CCD detector (MoK α , graphite monochromator, φ and ω scans). Diffraction data for a single crystal of compounds 2 and 3 were obtained on an Agilent Xcalibur diffractometer equipped with a CCD AtlasS2 detector (MoK α , graphite monochromator, φ scans). Data collection, frame integration, data processing and absorption correction were performed with the use of the APEX2, SAINT, SADABS and CrysAlisPro program packages.²⁹ The structures were solved by direct methods and refined by the full-matrix least squares technique in the anisotropic approximation (except for hydrogen atoms) using the SHELX-2014 software.³⁰ Positions of hydrogen atoms of Ph₄P⁺ cations were calculated geometrically and refined in the riding model. Hydrogen atoms of the water molecules were not located. For the refinement of metal site occupancies Re and Mo atoms were placed in the same positions and fixed using EXYZ and EADP SHELXL commands. The total occupation of

each position was set to 1. Free refinement gave the Re : Mo ratio close to 3 : 3 in all structures.

Complete crystallographic data have been deposited at the Cambridge Crystallographic Data Centre under the CCDC codes 1558003–1558006 for compounds 1–4,† respectively. The crystallographic data and details of the structure refinements are summarized in Table 4. Selected bond distances are given in Table 1.

Computational details

Density functional theory (DFT) calculations were carried out for the [Re₃Mo₃Se₈(CN)₆] cluster anions in *fac*- and *mer*-forms with 4−, 5−, 6− and 7− charge in the ADF2016 program package.³¹ Geometric parameters for the cluster anions were optimized with the PW92 + revPBE density functional³² and all-electron TZ2P basis set.³³ The zero order regular approximation (ZORA) was used in all calculations in this work to take into account the scalar relativistic effects.³⁴ Water environment effects were added with a Conductor like Screening Model (COSMO).³⁵

Conflicts of interest

There are no conflicts to declare.

Acknowledgements

This work was supported by the grant of the Russian Foundation for Basic Research (Project RFBR no. 16-33-00085). The authors greatly acknowledge the LIA CLUSPOM between France and Russia. We thank Federal Agency for Scientific Organizations for funding. We thank Muriel Escadeillas and Thierry Guizouarn from Institut des Sciences Chimiques de Rennes for CHNS analysis and EPR measurements.

References

- (a) V. Y. Fedorov, Y. V. Mironov, N. G. Naumov, M. N. Sokolov and V. P. Fedin, *Usp. Khim.*, 2007, **76**, 571–595; (b) M. N. Sokolov, N. G. Naumov, P. P. Samoylov and V. P. Fedin, in *Compr. Inorg. Chem. II*, ed. K. Poeppelmeier, Elsevier, Amsterdam, 2nd edn, 2013, pp. 271–310.
- (a) T. G. Gray, C. M. Rudzinski, E. E. Meyer, R. H. Holm and D. G. Nocera, *J. Am. Chem. Soc.*, 2003, **125**, 4755–4770; (b) Y. Molard, F. Dorson, K. A. Brylev, M. A. Shestopalov, Y. Le Gal, S. Cordier, Y. V. Mironov, N. Kitamura and C. Perrin, *Chem. – Eur. J.*, 2010, **16**, 5613–5619; (c) T. Yoshimura, C. Suo, K. Tsuge, S. Ishizaka, K. Nozaki, Y. Sasaki, N. Kitamura and A. Shinohara, *Inorg. Chem.*, 2010, **49**, 531–540; (d) M. N. Sokolov, M. A. Mihailov, E. V. Peresypkina, K. A. Brylev, N. Kitamura and V. P. Fedin, *Dalton Trans.*, 2011, **40**, 6375–6377; (e) K. Kirakci, P. Kubát, M. Dušek, K. Fejfarová, V. Šícha, J. Mosinger and K. Lang, *Eur. J. Inorg. Chem.*, 2012, **2012**, 3107–3111; (f) O. A. Efremova, M. A. Shestopalov, N. A. Chirtsova, A. I. Smolentsev, Y. V. Mironov, N. Kitamura, K. A. Brylev and A. J. Sutherland, *Dalton Trans.*, 2014, **43**, 6021–6025; (g) A. A. Ivanov, M. A. Shestopalov, K. A. Brylev, V. K. Khlestkin and Y. V. Mironov, *Polyhedron*, 2014, **81**, 634–638.
- (a) Y. V. Mironov, A. V. Virovets, N. G. Naumov, V. N. Ikorskii and V. E. Fedorov, *Chem. – Eur. J.*, 2000, **6**, 1361–1365; (b) T. V. Larina, V. N. Ikorskii, N. T. Vasenin, V. F. Anufrienko, N. G. Naumov, E. V. Ostanina and V. E. Fedorov, *Russ. J. Coord. Chem.*, 2002, **28**, 554–556; (c) A. Perrin and C. Perrin, *C. R. Chim.*, 2012, **15**, 815–836.
- (a) A. A. Krasilnikova, M. A. Shestopalov, K. A. Brylev, I. A. Kirilova, O. P. Khripko, K. E. Zubareva, Y. I. Khripko, V. T. Podorognaya, L. V. Shestopalova, V. E. Fedorov and Y. V. Mironov, *J. Inorg. Biochem.*, 2015, **144**, 13–17; (b) A. A. Krasilnikova, A. O. Solovieva, A. A. Ivanov, K. E. Trifonova, T. N. Pozmogova, A. R. Tsygankova, A. I. Smolentsev, E. I. Kretov, D. S. Sergeevichev, M. A. Shestopalov, Y. V. Mironov, A. M. Shestopalov, A. F. Poveschenko and L. V. Shestopalova, *Nanomedicine*, 2017, **13**, 755–763.
- (a) J.-C. P. Gabriel, K. Boubekeur, S. Uriel and P. Batail, *Chem. Rev.*, 2001, **101**, 2037–2066; (b) T. G. Gray, *Coord. Chem. Rev.*, 2003, **243**, 213–235; (c) A. Gandubert, K. A. Brylev, T. Thuong Nguyen, N. G. Naumov, N. Kitamura, Y. Molard, R. Gautier and S. Cordier, *Z. Anorg. Allg. Chem.*, 2013, **639**, 1756–1762; (d) S. A. Baudron, A. Deluzet, K. Boubekeur and P. Batail, *Chem. Commun.*, 2002, 2124–2125.
- (a) C. Magliocchi, X. Xie and T. Hughbanks, *Inorg. Chem.*, 2000, **39**, 5000–5001; (b) M. A. Cortes, F. Dorson, M. Prevot, A. Ghoufi, B. Fontaine, F. Goujon, R. Gautier, V. Circu, C. Meriadec, F. Artzner, H. Folliot, S. Cordier and Y. Molard, *Chem. – Eur. J.*, 2014, **20**, 8561; (c) V. Circu, Y. Molard, M. Amela-Cortes, A. Bentaleb, P. Barois, V. Dorcet and S. Cordier, *Angew. Chem., Int. Ed.*, 2015, **54**, 10921; (d) M. Prévôt, M. Amela-Cortes, K. S. Manna, S. Cordier, T. Roisnel, H. Folliot, L. Dupont and Y. Molard, *J. Mater. Chem. C*, 2015, **3**, 5152–5161; (e) Y. Molard, *Acc. Chem. Res.*, 2016, **49**, 1514–1523.
- (a) A. Garreau, F. Massuyeau, S. P. Cordier, Y. Molard, E. Gautron, P. Bertoncini, E. Faulques, J. Wery, B. Humbert, A. Bulou and J.-L. Duvail, *ACS Nano*, 2013, **7**, 2977–2987; (b) M. Amela-Cortes, A. Garreau, S. Cordier, E. Faulques, J.-L. Duvail and Y. Molard, *J. Mater. Chem. C*, 2014, **2**, 1545–1552; (c) M. Amela-Cortes, S. Paofai, S. Cordier, H. Folliot and Y. Molard, *Chem. Commun.*, 2015, **51**, 8177–8180; (d) S. Cordier, F. Grasset, Y. Molard, M. Amela-Cortes, R. Boukherroub, S. Ravaine, M. Mortier, N. Ohashi, N. Saito and H. Haneda, *J. Inorg. Organomet. Polym. Mater.*, 2015, **25**, 189; (e) J. Bignon, N. Huby, M. Amela-Cortes, Y. Molard, A. Garreau, S. Cordier, B. Bêche and J. L. Duvail, *Nanotechnol.*, 2016, **27**, 1; (f) T. Thai Giang, D. Benjamin, G. Fabien, S. Noriko, S. Norio, N. Thi Kim Ngan, T. Kohsei, U. Tetsuo, A.-C. Marian, M. Yann, C. Stéphane and O. Naoki, *Sci. Technol. Adv. Mater.*, 2016, **17**, 443–453.
- (a) S. Cordier, B. Fabre, Y. Molard, A.-B. Fadjie-Djomkam, N. Tournerie, A. Ledneva, N. G. Naumov, A. Moréac, P. Turban, S. Tricot, S. Ababou-Girard and C. Godet, *J. Phys. Chem. C*, 2010, **114**, 18622–18633; (b) D. Dybtsev, C. Serre, B. Schmitz, B. Panella, M. Hirscher, M. Latroche, P. L. Llewellyn, S. Cordier, Y. Molard, M. Haouas, F. Taulelle and G. Férey, *Langmuir*, 2010, **26**, 11283–11290; (c) S. Kumar, O. P. Khatri, S. Cordier, R. Boukherroub and S. L. Jain, *Chemistry*, 2015, **21**, 3488–3494.
- (a) A. V. Virovets, Y. M. Gayfulin, E. V. Peresypkina, Y. V. Mironov and N. G. Naumov, *CrystEngComm*, 2015, **17**, 1477–1482; (b) Y. Kim, V. E. Fedorov and S.-J. Kim, *J. Mater. Chem.*, 2009, **19**, 7178–7190; (c) S. Jin and F. J. DiSalvo, *Chem. Mater.*, 2002, **14**, 3448–3457; (d) M. V. Bennett, L. G. Beauvais, M. P. Shores and J. R. Long, *J. Am. Chem. Soc.*, 2001, **123**, 8022–8032; (e) M. V. Bennett, M. P. Shores, L. G. Beauvais and J. R. Long, *J. Am. Chem. Soc.*, 2000, **122**, 6664–6668; (f) M. P. Shores, L. G. Beauvais and J. R. Long, *Inorg. Chem.*, 1999, **38**, 1648–1649; (g) M. P. Shores, L. G. Beauvais and J. R. Long, *J. Am. Chem. Soc.*, 1999, **121**, 775; (h) N. G. Naumov, A. V. Virovets, M. N. Sokolov, S. B. Artemkina and V. E. Fedorov, *Angew. Chem., Int. Ed.*, 1998, **37**, 1943–1945; (i) L. G. Beauvais, M. P. Shores and

- J. R. Long, *Chem. Mater.*, 1998, **10**, 3783–3786; (j) Z. Zheng and X. Tu, *CrystEngComm*, 2009, **11**, 707–719.
- 10 (a) T. G. Gray, *Chem. – Eur. J.*, 2009, **15**, 2581–2593; (b) V. I. Baranovski and D. V. Korolkov, *Polyhedron*, 2004, **23**, 1519–1526; (c) L. Hernández-Acevedoa and R. Arratia-Pérez, *J. Chil. Chem. Soc.*, 2003, **48**, 125–128; (d) A. Deluzet, H. Duclausaud, P. Sautet and S. A. Borshch, *Inorg. Chem.*, 2002, **41**, 2537–2542; (e) H. Honda, T. Noro, K. Tanaka and E. Miyoshi, *J. Chem. Phys.*, 2001, **114**, 10791–10797.
 - 11 (a) G. Pilet and A. Perrin, *C. R. Chim.*, 2005, **8**, 1728–1742; (b) T. Saito, *Dalton Trans.*, 1999, 97–106.
 - 12 T. Saito, N. Yamamoto, T. Yamagata and H. Imoto, *J. Am. Chem. Soc.*, 1988, **110**, 1646–1647.
 - 13 (a) W. Bronger, C. Koppe, M. Loevenich, D. Schmitz and T. Schuster, *Z. Anorg. Allg. Chem.*, 1997, **623**, 695–698; (b) F. J. Berry, C. D. Gibbs and C. Greaves, *J. Solid State Chem.*, 1991, **92**, 148–153; (c) F. J. Berry and C. D. Gibbs, *Dalton Trans.*, 1991, 57–59; (d) A. Perrin, R. Chevrel, M. Sergent and O. Fischer, *J. Solid State Chem.*, 1980, **33**, 43–47; (e) A. Perrin, M. Sergent and O. Fischer, *Mater. Res. Bull.*, 1978, **13**, 259–264.
 - 14 (a) K. A. Brylev, N. G. Naumov, S. G. Kozlova, M. R. Ryzhikov, S. J. Kim and N. Kitamura, *Russ. J. Coord. Chem.*, 2012, **38**, 183; (b) E. G. Tulsy, N. R. M. Crawford, S. A. Baudron, P. Batail and J. R. Long, *J. Am. Chem. Soc.*, 2003, **125**, 15543–15553; (c) E. G. Tulsy and J. R. Long, *Inorg. Chem.*, 2001, **40**, 6990–7002.
 - 15 N. G. Naumov, K. A. Brylev, Y. V. Mironov, A. V. Virovets, D. Fenske and V. E. Fedorov, *Polyhedron*, 2004, **23**, 599–603.
 - 16 Y. M. Gayfulin, N. G. Naumov, M. R. Rizhikov, A. I. Smolentsev, V. A. Nadolinny and Y. V. Mironov, *Chem. Commun.*, 2013, **49**, 10019.
 - 17 N. G. Naumov, S.-J. Kim, A. V. Virovets, Y. V. Mironov and V. E. Fedorov, *Bull. Korean Chem. Soc.*, 2006, **27**, 635–636.
 - 18 Y. V. Mironov, V. E. Fedorov, C. C. McLauchlan and J. A. Ibers, *Inorg. Chem.*, 2000, **39**, 1809–1811.
 - 19 Y. V. Mironov, N. G. Naumov, S. G. Kozlova, S.-J. Kim and V. E. Fedorov, *Angew. Chem., Int. Ed.*, 2005, **44**, 6867–6871.
 - 20 T. K. Brotherton and J. W. Lynn, *Chem. Rev.*, 1959, **59**, 841–883.
 - 21 M. Shatruk, C. Avendano and K. R. Dunbar, *Prog. Inorg. Chem.*, 2009, **56**, 155–334.
 - 22 N. G. Naumov, S. B. Artemkina, A. V. Virovets and V. E. Fedorov, *J. Solid State Chem.*, 2000, **153**, 195–204.
 - 23 C. Guilbaud, A. Deluzet, B. Domercq, P. Molinie, C. Coulon, K. Boubekeur and P. Batail, *Chem. Commun.*, 1999, 1867–1868.
 - 24 N. G. Naumov, A. V. Virovets, N. V. Podberezskaya and V. E. Fedorov, *J. Struct. Chem.*, 1997, **38**, 857–862.
 - 25 E. Levi, A. Mitelman, O. Isnard, M. Brunelli and D. Aurbach, *Inorg. Chem.*, 2008, **47**, 1975–1983.
 - 26 N. G. Naumov, E. V. Ostanina, A. V. Virovets, M. Schmidtman, A. Müller and V. E. Fedorov, *Russ. Chem. Bull.*, 2002, **51**, 866–871.
 - 27 C. Magliocchi, X. Xie and T. Hughbanks, *Inorg. Chem.*, 2004, **43**, 1902–1911.
 - 28 C. Perrin, S. Ihmaine and M. Sergent, *New J. Chem.*, 1988, **12**, 321–328.
 - 29 (a) APEX2 (Version 1.08), SAINT (Version 7.03), SADABS (Version 2.11), Bruker AXS Inc., Madison, WI, 2004; (b) CrysAlisPro 1.171.38.41, Rigaku Oxford Diffraction, 2015.
 - 30 (a) G. M. Sheldrick, *Acta Crystallogr., Sect. A: Found. Crystallogr.*, 2015, **71**, 3–8; (b) G. M. Sheldrick, *Acta Crystallogr., Sect. C: Struct. Chem.*, 2015, **71**, 3–8.
 - 31 (a) G. te Velde, F. M. Bickelhaupt, E. J. Baerends, C. Fonseca Guerra, S. J. A. van Gisbergen, J. G. Snijders and T. Ziegler, *J. Comput. Chem.*, 2001, **22**, 931–967; (b) C. Fonseca Guerra, G. J. Snijders, G. te Velde and J. E. Baerends, *Theor. Chem. Acc.*, 1998, **99**, 391–403.
 - 32 (a) J. P. Perdew and Y. Wang, *Phys. Rev. B: Condens. Matter Mater. Phys.*, 1992, **45**, 13244–13249; (b) J. P. Perdew, K. Burke and M. Ernzerhof, *Phys. Rev. Lett.*, 1996, **77**, 3865–3868.
 - 33 E. Van Lenthe and E. J. Baerends, *J. Comput. Chem.*, 2003, **24**, 1142–1156.
 - 34 E. van Lenthe, A. Ehlers and E.-J. Baerends, *J. Chem. Phys.*, 1999, **110**, 8943–8953.
 - 35 C. C. Pye and T. Ziegler, *Theor. Chem. Acc.*, 1999, **101**, 396–408.

CrystEngComm

Accepted Manuscript



This article can be cited before page numbers have been issued, to do this please use: V. K. Muravieva, Y. M. Gayfulin, P. Lemoine, S. Cordier and N. G. Naumov, *CrystEngComm*, 2018, DOI: 10.1039/C8CE00527C.

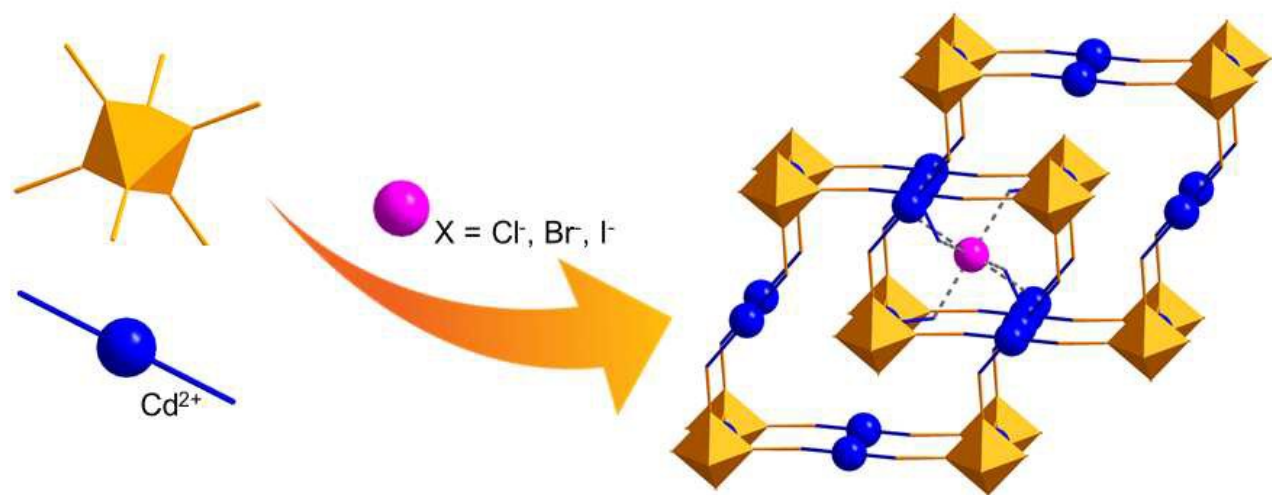


This is an Accepted Manuscript, which has been through the Royal Society of Chemistry peer review process and has been accepted for publication.

Accepted Manuscripts are published online shortly after acceptance, before technical editing, formatting and proof reading. Using this free service, authors can make their results available to the community, in citable form, before we publish the edited article. We will replace this Accepted Manuscript with the edited and formatted Advance Article as soon as it is available.

You can find more information about Accepted Manuscripts in the [author guidelines](#).

Please note that technical editing may introduce minor changes to the text and/or graphics, which may alter content. The journal's standard [Terms & Conditions](#) and the ethical guidelines, outlined in our [author and reviewer resource centre](#), still apply. In no event shall the Royal Society of Chemistry be held responsible for any errors or omissions in this Accepted Manuscript or any consequences arising from the use of any information it contains.



Interpenetrating frameworks $\{[\text{Cd}(\text{NH}_3)_4]_3[\text{Re}_3\text{Mo}_3\text{Se}_8(\text{CN})_6]\}_X$ ($X = \text{Cl}^-, \text{Br}^-, \text{I}^-$) driven by $\text{N-H}\cdots\text{X}$ bonding exhibit remarkable stability and reversible transitions in the solid state.



Journal Name

ARTICLE

Stabilization of interpenetrating cluster-based frameworks promoted by N-H...X hydrogen bonds: synthesis, structures and properties of $\{[\text{Cd}(\text{NH}_3)_4]_3[\text{Re}_3\text{Mo}_3\text{Se}_8(\text{CN})_6]\}\text{X}$ (X = Cl, Br and I)

Received 00th January 20xx,
Accepted 00th January 20xx

DOI: 10.1039/x0xx00000x

www.rsc.org/

Viktoriya K. Muravieva,^{a,b} Yakov M. Gayfulin,^a Pierrick Lemoine,^b Nikolay G. Naumov,^{*a,c} and Stéphane Cordier^b.

Control of the covalent coordination polymer structures using non-covalent interactions is a promising way for obtaining the functional materials by a self-assembly in solution. Here we report the crucial role of the halide anions in formation of the interpenetrating frameworks based on the cluster cyanometalate. It was found that interaction of $[\text{Re}_3\text{Mo}_3\text{Se}_8(\text{CN})_6]^{5-}$ cluster anions and Cd^{2+} cations in aqueous ammonia lead to formation of the 1D polymeric compound $\{[\text{Cd}(\text{NH}_3)_5]_2[\text{Cd}(\text{NH}_3)_4]_3[\text{Re}_3\text{Mo}_3\text{Se}_8(\text{CN})_6]_2\} \cdot 5\text{H}_2\text{O}$ (**1**). The compound **1** is unstable outside the mother liquor due to the rapid loss of the NH_3 and H_2O molecules. Addition of the KX (X = Cl, Br, I) to the reaction mixture led to selective formation of the 3D framework compounds $\{[\text{Cd}(\text{NH}_3)_4]_3[\text{Re}_3\text{Mo}_3\text{Se}_8(\text{CN})_6]\}\text{X}$ (**2-4** for X = Cl, Br, I, respectively) stabilized by the N-H...X hydrogen bonding. Compounds **2-4** demonstrate high thermal stability as well as the ability to reversible loss of ammonia and reversible oxidation in the solid state.

Introduction

Crystalline coordination polymers are the class of attractive materials having potential applications in gas storage and separation, catalysis, drug delivery etc.¹⁻⁹ The primary approach exploited for obtaining the coordination polymers at present time is the self-assembly of organic and/or inorganic building blocks in solution.^{10,11} Due to the numerous possible geometries and different coordination modes of building blocks, the self-assembly of the target crystalline materials from the reagent solution is often complex and unpredictable process. Use of the soluble pre-made building blocks with defined geometries and properties is a relevant approach for the rational design of materials with predetermined structures and properties.^{12,13} The resulting network topologies of coordination architectures prepared by means of the self-assembly in solution are generally influenced by i) geometry of building blocks in solution and their ability to form covalent and non-covalent interactions; ii) size effect of the species involved in the self-assembly reaction and iii) the charge of the

units in reaction solution.

Cyanometalates are the large class of mono- and polynuclear species, which are widely applied as the pre-made building blocks for constructing functional coordination polymers.¹⁴⁻¹⁶ Ambidentate nature of the cyanide ligand is exploited to perform bridging coupling of moieties forming the network structures via coordination of *d*- or *f*-metal cations. The high energy of M–CN–M' interactions usually lead to the formation of robust frameworks with a large number of covalent contacts.

In addition to the strong covalent bonding between the nodes of polymeric architectures, the relatively weak interactions between specific groups may also play a key role in formation of the polymeric structures from solutions. Self-assembly of the supramolecular structures based on weak intermolecular contacts is the popular approach for design of the polymeric arrays.¹⁷⁻²⁰ However, this approach is quite limited in the cyanometalate chemistry because of domination of the strong M–CN–M' covalent interactions over weak dispersive forces.²¹⁻²⁷

Cluster cyanometallates, especially hexanuclear rhenium and molybdenum ones, are widely used as the metallic nodes in order to imply new topologies and intrinsic properties to the polymeric materials.²⁸⁻³⁴ In contrast to the common polynuclear building blocks, the molecular orbitals of clusters are delocalized over all atoms of the cluster core.^{35,36} Accordingly, the intrinsic cluster properties are strongly depended on the nature of core atoms. Applying clusters with unique spectroscopic properties and redox chemistry as the building blocks may lead to predetermined characteristics of

^a Nikolaev Institute of Inorganic Chemistry SB RAS 3, Acad. Lavrentiev ave., Novosibirsk, 630090, Russia.
E-mail: naumov@niic.nsc.ru

^b Univ Rennes, CNRS, ISCR (Institut des Sciences Chimiques de Rennes) - UMR 6226, F-35000, France.

^c Novosibirsk State University, 2, Pirogova str., Novosibirsk, 630090, Russia.

† Electronic Supplementary Information (ESI) available: [General characterization details for **2-4** and crystal data: summary of single-crystal data collections and structure refinement conditions of **1-4**, PXRD data, FT-IR spectra, TGA plots and DRS figures] See DOI: 10.1039/x0xx00000x

the resulting polymeric compound. Specific combination of the charge and geometry for each individual cluster should determine the topology of the cluster-based networks. The non-isovalent "substitution" in the cluster core is an opportunity to influence on the specific characteristics of the cluster, *i.e.* charge, redox behavior and spectroscopic characteristics without significant change of the geometry. For example, the heterometallic cluster $[\text{Re}_3\text{Mo}_3\text{Se}_8(\text{CN})_6]^{6-}$ is able to form common Prussian blue as well as unique "anti-Prussian blue" networks based on Zn^{2+} and Cd^{2+} ammonia complexes.^{37,38} Recently discovered, the $[\text{Re}_3\text{Mo}_3\text{Se}_8(\text{CN})_6]^{n-}$ cluster anion demonstrated rich redox chemistry accompanied by color changes in dependence of the redox state. It shows the stable 5- charge of the mixed-metal cluster anion, which is not known among the analogues $[\text{Re}_6\text{Q}_8(\text{CN})_6]^{4-/3-}$,^{39,40} $[\text{Re}_3\text{Mo}_3\text{S}_8(\text{CN})_6]^{6-}$ ⁴¹ and $[\text{Mo}_6\text{Q}_8(\text{CN})_6]^{7-/6-}$.^{42,43} The unusual cluster charge accompanied by the rich redox chemistry of cluster unit allows us to expect cluster-based networks with promising features.

Here we present a rare example of cyanometalate-based frameworks where the weak dispersive interactions play a key role in formation of the crystal structure. Preparation, structure and reversible phase transition over the crystalline states has been discovered for three new coordination polymers based on the mixed-metal $[\text{Re}_3\text{Mo}_3\text{Se}_8(\text{CN})_6]^{5-}$ cluster anions and Cd^{2+} cations. It was shown that presence of halides in solution favors the formation of the stable interpenetrating frameworks due to the $\text{NH}\cdots\text{X}$ ($\text{X} = \text{Cl}, \text{Br}$ or I) hydrogen bonding.

Experimental

Materials and methods.

The starting $\text{K}_5[\text{Re}_3\text{Mo}_3\text{Se}_8(\text{CN})_6]\cdot 11\text{H}_2\text{O}$ salt was prepared as described.⁴⁴ Other reagents were purchased from commercial sources and used without further purification. IR spectra in KBr pellets were recorded on a Bruker Scimitar FTS 2000 spectrometer in the range 4000–375 cm^{-1} . Energy Dispersive Spectroscopy (EDS) was performed on an electron microscope Hitachi TM-3000 equipped with a Bruker Nano EDS analyzer. Powder X-ray diffraction patterns of the synthesized compounds were recorded using a Philips PW1820/1710 diffractometer (Cu $\text{K}\alpha$ radiation, graphite monochromator, silicon plate was used as an external standard). Simulated patterns were generated by PowderCell 2.4 software.⁴⁵ The thermogravimetric analysis was carried out with a NETZSCH TG 209 F1 Iris Thermo Microbalance in a stream of helium (30 mL min^{-1}) at a heating rate of 10 $^\circ\text{C min}^{-1}$ with the sample masses used of 14.953 mg, 15.891 mg and 10.200 mg for compounds **2**, **3** and **4**, respectively. Diffuse reflectance spectra were registered by means of an UV/VIS/NIR spectrometer Shimadzu 3101 PC.

Synthetic procedures

$\{[\text{Cd}(\text{NH}_3)_5]_2[\text{Cd}(\text{NH}_3)_4]_3[\text{Re}_3\text{Mo}_3\text{Se}_8(\text{CN})_6]_2\}\cdot 5\text{H}_2\text{O}$ (1**).** Single crystals of compound **1** were prepared by layering of a solution of $\text{Cd}(\text{CH}_3\text{COO})_2$ (8 mg, 0.034 mmol) in aqueous ammonia (12%

mass, 2 ml) on a solution of $\text{K}_5[\text{Re}_3\text{Mo}_3\text{Se}_8(\text{CN})_6]\cdot 11\text{H}_2\text{O}$ (8 mg, 0.004 mmol) in aqueous ammonia (6%, 2 ml) in a thin glass tube with a neck. Rod-shaped crystals of compound **1** were found on a tube wall after several days. Single crystals for X-ray diffraction analysis were taken directly from the mother liquor. EDS for **1**: Cd : Re : Mo : Se 2.6 : 3.1 : 2.9 : 7.5. IR for **1**: (cm^{-1}) $\nu(\text{N-H})$ 3532 3329 3246; $\nu(\text{C}\equiv\text{N})$ 2083; $\delta_d(\text{NH}_3)$ 1732 1591 1466; $\delta_s(\text{NH}_3)$ 1200; $\rho_r(\text{NH}_3)$ 582; $\nu(\text{M-N})$ 390.

$\{[\text{Cd}(\text{NH}_3)_4]_3[\text{Re}_3\text{Mo}_3\text{Se}_8(\text{CN})_6]\}\text{Cl}$ (2**).** A solution of $\text{Cd}(\text{CH}_3\text{COO})_2$ (25 mg, 0.108 mmol) in concentrated aqueous ammonia (25%, 4 ml) was mixed with an aqueous solution of $\text{K}_5[\text{Re}_3\text{Mo}_3\text{Se}_8(\text{CN})_6]\cdot 11\text{H}_2\text{O}$ (80 mg, 0.039 mmol) and KCl (120 mg, 1.624 mmol) in 7 ml of H_2O . After precipitation of a crystalline powder, the mother liquor was decanted and the product was washed with water. Then the product was dried in air. Yield: 43 mg (50%). To prepare single crystals of compound **2** a solution of CdCl_2 (6 mg, 0.033 mmol) in 2 ml of aqueous ammonia (12%) was layered on a solution of $\text{K}_5[\text{Re}_3\text{Mo}_3\text{Se}_8(\text{CN})_6]\cdot 11\text{H}_2\text{O}$ (8 mg, 0.004 mmol) in aqueous ammonia (6%, 2 ml) in a thin glass tube with a neck. Two types of crystals were found on the tube wall after several days: purple rod-shaped crystals of the compound **1** and prismatic crystals of the compound **2**. The crystals with prismatic shape were selected directly from the mother liquor for single crystal X-ray diffraction study. EDS for **2** Cd : Re : Mo : Se : Cl 3.1 : 3.2 : 2.8 : 8.3 : 0.9. IR for **2**: (cm^{-1} , Figure S1) $\nu(\text{N-H})$ 3555 3435 3331 3254 3152; $\nu(\text{C}\equiv\text{N})$ 2083; $\delta_d(\text{NH}_3)$ 1639 1585; $\delta_s(\text{NH}_3)$ 1190 1150; $\rho_r(\text{NH}_3)$ 579; $\nu(\text{M-N})$ 384.

$\{[\text{Cd}(\text{NH}_3)_4]_3[\text{Re}_3\text{Mo}_3\text{Se}_8(\text{CN})_6]\}\text{Br}$ (3**).** Compound **3** was obtained using a similar procedure as for compound **2**. KBr (120 mg, 1.018 mmol) was used instead of KCl. Yield: 63 mg (72%). To obtain single crystals of compound **3**, a solution of $\text{Cd}(\text{CH}_3\text{COO})_2$ (8 mg, 0.035 mmol) and KBr (20 mg, 0.169 mmol) in aqueous ammonia (12%, 2 ml of) was layered on a solution of $\text{K}_5[\text{Re}_3\text{Mo}_3\text{Se}_8(\text{CN})_6]\cdot 11\text{H}_2\text{O}$ (6 mg, 0.003 mmol) and KBr (18 mg, 0.153 mmol) in aqueous ammonia (6%, 2 ml) in a thin glass tube with a neck. The tube was tightly closed. Shiny crystals with prismatic shape were found on the tube wall after several days. The crystals for single crystal X-ray diffraction was taken directly from the mother liquor. EDS for **3** Cd : Re : Mo : Se : Br 3.3 : 2.8 : 3.2 8.5 : 1.0. IR for **3** (cm^{-1} , Figure S1) $\nu(\text{N-H})$ 3560 3427 3331 3146; $\nu(\text{C}\equiv\text{N})$ 2083; $\delta_d(\text{NH}_3)$ 1585; $\delta_s(\text{NH}_3)$ 1186 1146; $\rho_r(\text{NH}_3)$ 577; $\nu(\text{M-N})$ 386.

$\{[\text{Cd}(\text{NH}_3)_4]_3[\text{Re}_3\text{Mo}_3\text{Se}_8(\text{CN})_6]\}\text{I}$ (4**).** Compound **4** was obtained using a similar procedure as for compound **2**. KI (150 mg, 0.904 mmol) was used instead of KCl. Yield: 68 mg (76%). To prepare single crystals of compound **4**, a solution of $\text{Cd}(\text{CH}_3\text{COO})_2$ (8 mg, 0.035 mmol) and KI (18 mg, 0.109 mmol) in aqueous ammonia (12%, 2 ml) was layered on a solution of $\text{K}_5[\text{Re}_3\text{Mo}_3\text{Se}_8(\text{CN})_6]\cdot 11\text{H}_2\text{O}$ (6 mg, 0.003 mmol) and KI (16 mg, 0.096 mmol) in aqueous ammonia (6%, 2 ml) in a thin glass tube with a neck. The tube was tightly closed. Shiny crystals with prismatic shape were found on a tube wall after several days. The crystal for single crystal X-ray diffraction was taken directly from the mother liquor. EDS for **4** Cd : Re : Mo : Se : I 2.7 : 3.2 : 2.8 : 8.3 : 0.8. IR (cm^{-1} , Figure S1) for **4** $\nu(\text{N-H})$ 3570

3335 3250 3148; $\nu(\text{C}\equiv\text{N})$ 2087; $\delta_{\text{d}}(\text{NH}_3)$ 1584; $\delta_{\text{s}}(\text{NH}_3)$ 1180 1148; $\rho_{\text{r}}(\text{NH}_3)$ 571; $\nu(\text{M}-\text{N})$ 384.

Phase purity of **2-4** was established by comparing the X-ray powder diffraction pattern of a bulk sample with one simulated from the single-crystal data (Figures S2-S4). EDS data of the compounds **2-4** revealed no significant difference in composition of single crystals and polycrystalline samples **2-4**.

Crystallography

Single crystal X-Ray structural analysis was carried out at 150 K on an APEX II Bruker AXS diffractometer for **1** and on a D8 Venture Bruker AXS diffractometer for **2-4**, using Mo-K α X-ray wavelength ($\lambda = 0.71073$ Å) at the Centre de diffractométrie X de l'Institut des Sciences Chimiques de Rennes. The structures were solved by direct methods using the SIR97 program,⁴⁶ and then refined with full-matrix least-square methods based on F^2 (SHELXL-2014)⁴⁷ using the WinGX software package.⁴⁸ All non-hydrogen atoms were refined with anisotropic atomic displacement parameters. A statistical distribution of

molybdenum and rhenium atoms on their respective crystallographic sites was considered by constraining equivalent atomic coordinates and anisotropic atomic displacement parameters. Preliminary refinements lead to a Mo/Re ratio close to 3/3. Final refinements were conducted considering a Mo/Re ratio of 3/3. It is important to mention that this constraint have no influence on the reliability factors and the largest difference peak and hole. The residual densities observed in the last Fourier difference maps are located near the nitrogen atoms between nitrogen and halogen atoms suggesting that it arises from the H atoms of the NH_3 molecules. Consequently, the structural models of **2-4** were finally refined considering AFIX 137 instruction for hydrogen atoms. The conditions of data collection and structure refinements for compounds **1-4** are gathered in Table S1. Selected interatomic distances are gathered in the Table 1.

Table 1. Selected interatomic distances in Å (range / average) in the structures **1-4**.

| | 1 | 2 | 3 | 4 |
|--------|------------------------------|------------------------------|------------------------------|------------------------------|
| M-M | 2.631(1)–2.684(1) 2.654 | 2.6465(5)–2.6498(5) 2.648 | 2.6480(3)–2.6531(3) 2.651 | 2.6459(5)–2.6529(5) 2.650 |
| M-Se | 2.527(2)–2.564(2) / 2.547 | 2.5439(7)–2.5475(9) 2.545 | 2.5475(3)–2.5537(4) 2.550 | 2.5439(6)–2.5507(7) 2.547 |
| M-C | 2.10(2)–2.20(2) 2.14 | 2.146(6) | 2.152(2) | 2.147(6) |
| Cd-NH3 | 2.27(2)–2.47(2) 2.36 | 2.323(7)–2.326(6) 2.325 | 2.310(3)–2.347(3) 2.328 | 2.301(6)–2.344(6) 2.323 |
| Cd-NC | 2.37(2)–2.52(2) 2.43 | 2.418(6) | 2.419(3) | 2.411(5) |
| N-X | – | 3.334(6) | 3.468(3) | 3.641(6) |

Results and Discussion

$[\text{Re}_3\text{Mo}_3\text{Se}_8(\text{CN})_6]^{5-}$ anion as the pre-made building block.

The octahedral $[\text{Re}_3\text{Mo}_3\text{Se}_8(\text{CN})_6]^{5-}$ anion belongs to a family of transition metal cluster units with cyanide terminal ligands. Due to ambidentate nature of cyanide ligands, these clusters are able to coordinate transition and post-transition metal cations with the formation of the coordination polymers. Advantages of the cluster cyanometalates as pre-made building blocks are their chemical stability and rigid geometry combined with specific intrinsic properties such as red luminescence,⁴⁹ catalytic and photo-catalytic properties⁵⁰ and ability to be reversibly oxidized retaining the geometry of the unit.⁵¹⁻⁵³ Over the past decades, a lot of coordination polymers have been synthesized based on octahedral clusters $[\text{Re}_6\text{Q}_8(\text{CN})_6]^{4-}$ ($\text{Q} = \text{S}, \text{Se}, \text{Te}$),⁵⁴⁻⁵⁷ $[\text{Mo}_6\text{Se}_8(\text{CN})_6]^{n-}$,⁵⁸ $[\text{Mo}_6\text{Br}_6\text{Q}_8(\text{CN})_6]^{n-}$ ($x = 0, 2$; $\text{Q} = \text{S}, \text{Se}$),^{59,60} $[\text{Nb}_6\text{X}_{12}(\text{CN})_6]^{4-}$,^{61,62} and $[\text{W}_6\text{S}_8(\text{CN})_6]^{n-}$.⁶³ The novel $[\text{Re}_3\text{Mo}_3\text{Se}_8(\text{CN})_6]^{5-}$ anion was prepared recently.⁴⁴ It exhibits geometry of the well-known $[\text{M}_6\text{Q}_8\text{L}_6]^{n-}$ type unit. Atoms of rhenium and molybdenum form the octahedral metallocluster $\{\text{Re}_3\text{Mo}_3\}$, which is face-

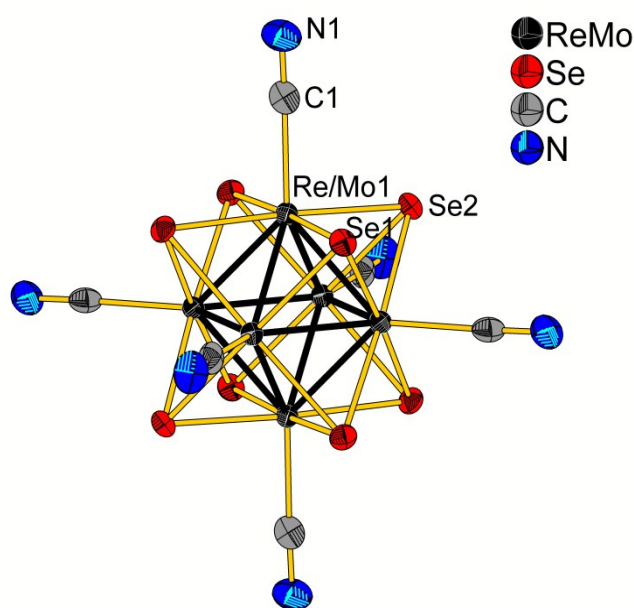


Figure 1. Structure of the cluster anion $[\text{Re}_3\text{Mo}_3\text{Se}_8(\text{CN})_6]^{5-}$ in **2**, ORTEP drawing at the 75% of probability level.

coordinated by μ_3 -Se²⁻ inner ligands. Apical cyanide groups additionally coordinate each metal atom (Figure 1). In comparison with the rhenium homometallic analogue [Re₆Se₈(CN)₆]⁴⁻, the new anion exhibits a higher charge as well as a notable difference in the average M–M distances (2.65 Å compared with 2.63 Å for [Re₆Se₈(CN)₆]⁴⁻³⁹) and electronic structures.³⁶

Another important difference from homometallic clusters is the possible cluster core isomers (*mer*- and *fac*-) with approximately the same total energy according to the DFT calculations.⁴⁴ These isomers may undergo significant distortion accompanied by decrease of the symmetry due to the difference in the Re–Re and Mo–Mo bond lengths. However, the statistical disorder of Re and Mo over all positions of the metal core atoms was found in all known solid-state structures containing the [Re₃Mo₃Se₈(CN)₆]⁵⁻ anion. Compound **1** crystallizes in the low-symmetry *P*-1 (No 2) space group. The asymmetric unit of the structure **1** contains 12 positions of metal atoms of two cluster anions. All Re/Mo positions are randomly occupied, having different site occupancy factors but leading to the average Re/Mo ratio in the asymmetric unit of 6.02(2)/5.98(2), which is represented as 6:6 within experimental errors. Due to their higher crystal structure symmetry (space group *R*-3 No 148), the asymmetric units of compounds **2–4** contain only one mixed cluster metal atom position with the Re/Mo ratio of 3/3. M–M (where M = Re, Mo), M–Se and M–C interatomic distances for compounds **1–4** (Table 1) are in agreement with those previously published for [Re₃Mo₃Se₈(CN)₆]⁵⁻.⁴⁴

Crystal Structure of 1.

The compound **1** displays a polymeric structure based on 1D chains with helicoidal shape (Figure 2). The chains are formed by two independent [Re₃Mo₃Se₈(CN)₆]⁵⁻ cluster anions (named A and B, Figure S5) linked to each other by means of bridging [Cd(NH₃)₄]²⁺ groups following the [–Cd1–A–Cd2–A–Cd1–B–Cd3–B–] sequence. Both A and B cluster anions share two cyanide groups in *cis*-position for formation of the chain. Three (anion B) or four (anion A) of remaining CN-groups are coordinated by the terminal [Cd(NH₃)_n]²⁺ groups (*n* = 4 or 5). In the structure of the chain, two types of bridging [Cd(NH₃)₄]²⁺ fragments are alternating: linear *trans*-[Cd(NH₃)₄(CN)₂] (*i.e.* Cd2 and Cd3 atoms) and *L*-shaped *cis*-[Cd(NH₃)₄(CN)₂] bridges (*i.e.* Cd1 atom). Finally, remaining [Cd(NH₃)_n]²⁺ groups corresponding to Cd4 (*n* = 4) and Cd5 (*n* = 5) atoms are linked to the cluster

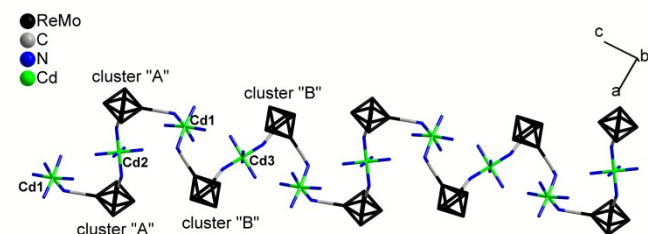


Figure 2. Representation of the chain topology in the structure of **1** in a wire model. Selenium atoms and terminal [Cd(NH₃)_n]²⁺ groups (*n* = 4 or 5) are omitted for clarity.

anions A, while [Cd(NH₃)₅]²⁺ group corresponding to Cd6 (*n* = 5) is linked to the cluster anions B. DOI: 10.1039/C8CE00527C

Crystal Structures of 2–4.

Since the compounds **2–4** are isostructural, overall description of the structure **2** only is given. The cluster anions are linked together by means of bridging *trans*-[Cd(NH₃)₄(CN)₂] nodes forming framework edges (Figure 3). The [Re₃Mo₃Se₈(CN)₆]⁵⁻ cluster units act as six-connected nodes giving the α -polonium related uninodal network (Figure 4). Two identical frameworks are further interpenetrated (Figure 5) with a translation vector of (2/3, 1/3, 1/3). Self-interpenetration of the α -polonium related networks occurs for Rb[Cd{Ag(CN)₂}₃].⁶⁴ According to the classification of interpenetrating 3D networks by Blatov and colleagues,^{65,66} the networks **2–4** belong to the Class *Ia*, which means that identical three-dimensional networks are related by simple translation vector. Cd–N(H₃) and Cd–N(C)

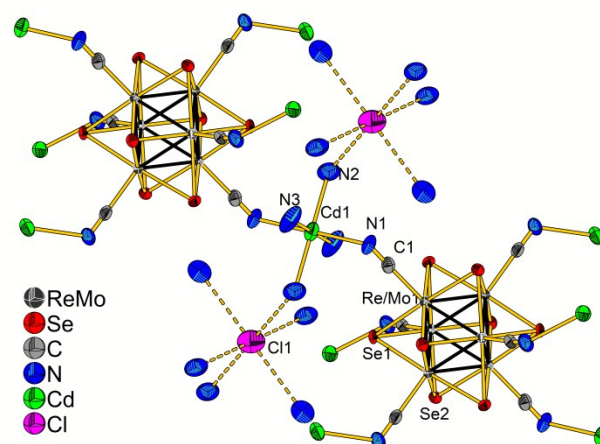


Figure 3. Representation of the bonding of cluster anionic nodes and bridging cationic linkers in **2**. Hydrogen atoms of ammonia molecules are omitted for clarity, ORTEP drawing at the 75% of probability level. Dash lines represent N...Cl contacts. Asymmetric unit atoms are numbered.

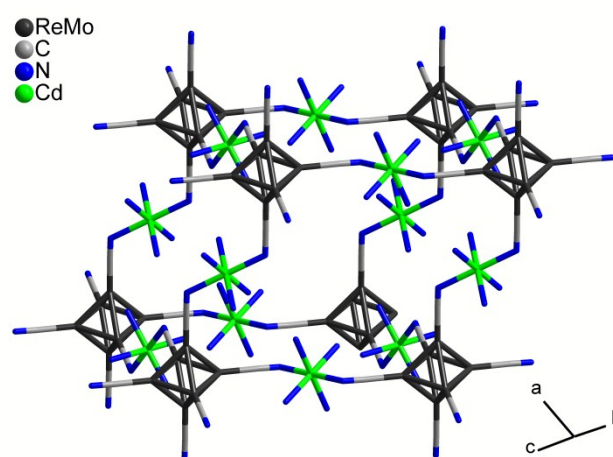


Figure 4. Wire representation of the fragment of the 6-connected network in **2**. Selenium, chlorine and hydrogen atoms are omitted for clarity.

interatomic distances for compounds **2–4** are close to ones for

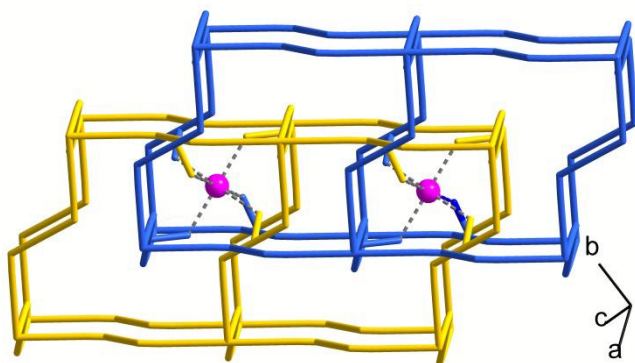


Figure 5. Topology of two-fold interpenetrating α -Po related frameworks in **2** using a wire model. Identical independent frameworks are shown in blue and yellow. The purple balls represent chlorine atoms, dash lines demonstrate N...Cl contacts. Selenium and hydrogen atoms, apical cyanide and extra ammonia groups are omitted for clarity. M_6 clusters are reduced to the dummy atoms in the center of octahedron.

1 (Table 1) and agree well with literature data for cadmium complexes.^{67,68}

Chlorine atoms in the structure of **2** are located in a special position with the point symmetry $\bar{3}$. Six ammonia groups form an ideal octahedron around chlorine atom. The chlorine environment is generated by symmetry operations (inversion center and 3-fold axis) with equal N...Cl distances of 3.334(6) Å (Figure 3 and Table 1) pointing out the $NH_3\cdots Cl$ hydrogen bonding. Six relatively weak $NH_3\cdots Cl$ hydrogen bonds implement the rigid contact of the interpenetrated frameworks as it is shown in Figure 5. The corresponding N...X distances are 3.334(6) Å in **2**, 3.468(3) Å in **3** and 3.641(6) Å in **4**, respectively (Table 1). The experimental N...X distances in the structures of **2–4** are in good agreement with the literature examples of solids with $NH_3\cdots X$ hydrogen bonding.^{69,70} The average known distances of D...A between N(sp²)H₂ donor (D) and X⁻ acceptor (A) of hydrogen bond depend on the radii of halides and are 3.299(6) Å, 3.46(1) Å and 3.66(1) Å for N...Cl, N...Br and N...I, respectively.

Hydrogen bonding between halides and ammonia molecules stabilizes formation of the interpenetrating framework structures **2–4** in competition with chain-like structure of compound **1**. Cell parameters in the crystal structures of **2–4** are influenced by halide size with the parameter *a* increasing significantly from 15.0363(8) Å in **2** to 15.2258(10) Å in **3** and 15.3596(14) Å in **4** (Table S1). This can be attributed to the increase of the ionic radii, which were reported as 1.81 Å, 1.96 Å and 2.20 Å for chloride, bromide and iodide anions, respectively.⁷¹ On the other hand, the *c* parameter does not particularly depend on the halide radius (15.3935(9), 15.3834(11) and 15.3897(13) Å in **2**, **3** and **4**, respectively, Table S1).

Supramolecular architectures in the structures 1–4.

The approach based on molecular tectonics^{72–74} can be useful to clarify the relations between structure and composition in **1–4**. The presented structures can be considered as the combinations of definite tectons with different number and type of possible bonding patterns. The $[Re_3Mo_3Se_8(CN)_6]^{5-}$ anion in structures **1–4** acts as the tecton bearing six strongly

oriented CN-groups with directed lone pairs. The CN sites in compounds mentioned are able to participate in both covalent and non-covalent interactions. The $[Cd(NH_3)_5]^{2+}$ and $[Cd(NH_3)_4]^{2+}$ cadmium-based tectons provide different number of NH_3 sites for non-covalent bonding. Unlike the fixed location of cluster CN-groups, the NH_3 ligands are able to rotate. Finally, the X⁻ anions in the structures **2–4** present the group of spherical tectons with the possibility to participate in large number of non-covalent interactions. Two cluster cyanide groups arranged in *cis*-fashion in **1** are coordinated to cadmium atoms. The binding pattern CN-Cd-NC determines the 1D crystal structure **1** in the absence of X⁻. The cyanide groups not involved into coordination bonding with cadmium interact with hydrogen from NH_3 -groups, forming C-N...H-N synthons. Selected hydrogen bonds are represented in the Figure S6 in the ESI. On the other hand, the same coordination pattern CN-Cd-NC in structures **2–4** involves all cluster interaction sites resulted in formation of the 3D frameworks. Large free volume of the resulting six-connected network (Figure 4) likely makes it unstable without additional bonding. Interpenetration of two identical networks stabilized by means of $NH_3\cdots X$ synthons form the final topology of **2–4**. The CN...HN synthon observed in **1** was also encountered in the structures **2–4**. Selected geometries of the hydrogen bonds presented in the structures **1–4** are listed in Table S2 in the ESI.

Preparation and Thermal Stability.

The compounds **1–4** were synthesized by the self-assembly of $[Re_3Mo_3Se_8(CN)_6]^{5-}$ cluster anions and Cd^{2+} ammonia cations. It was found that using different cadmium salts resulted in formation of different crystalline phases. Compound **1** was obtained in reaction of cluster salt with $Cd(CH_3COO)_2$. Using $CdCl_2$ as the cadmium source in slow crystallization led to formation of the mixture of compounds **1** and **2**. The mixture was observed regardless the reagent stoichiometry and conditions of crystallization. The compound **1** quickly loses ammonia even at room temperature leading to amorphous powder. On the contrary, crystals of **2** having interpenetrating framework structure appeared to be stable in air.

Synthesis of the compounds **2–4** was successfully carried out using the halide source in addition to ammonia solution of cadmium acetate. It was shown that excess of potassium halides in the reaction mixture plays the crucial role on the product composition. For instance, addition of KCl results in the formation of **2**. The addition of KBr and KI led to compounds **3** and **4**, respectively. Note that addition of KF led to obtaining rod-shaped crystals of **1**, which indicate the influence of the ionic radii of the halide on the resulting structure. An X-ray structural analysis showed that halide ions are located in the isolated cavities of the structures **2–4**, and cannot be incorporated into the structures after formation of the framework edges. Therefore, presence of halide ions in the reaction mixture may result in formation of pre-organized supramolecular fragments based on N-H...X hydrogen bonds before the formation of Cd-NC bonds. Inability of the F⁻ anion to form similar frameworks may be explained by its small ionic radii and preferred shorter hydrogen bonding distance.⁷⁵ The

ARTICLE

role of hydrogen bonding in the formation of interpenetrated organic networks is widely known.^{76,77} Some examples of the influence of halides on the crystal structure of the polymeric materials by means of the H...X hydrogen bonds can be found in the literature.⁷⁸⁻⁸⁰ However, most of the examples consider metal-assisted hydrogen bonding (H...X-M). To the best of our knowledge, examples of non-coordinated halide-driven self-assembly of polymeric solids in solution are scarce.⁸¹

The thermal behavior of **2-4** was investigated by thermogravimetric analysis (TG, Figure S7). Heating the crystalline powder samples of **2** and **3** revealed two steps characterized by about 3% (66-67 amu) and 5% (110-113 amu) of mass loss. It corresponds to the loss of 10 ammonia molecules per formula unit (180 amu), which is close to the total amount of 12 NH₃ molecules per formula unit. Maxima of the mass loss rate are located at about 80°C and 175°C, respectively. The remaining ammonia is removed in the wide temperature interval of 180-280°C. The temperatures of ammonia loss are quite typical for cadmium ammine complexes.⁸² The thermal behavior of compound **4** differs from one of **2** and **3**. The TG curve obtained for the crystalline powder sample of **4** revealed continuous mass loss without discrete steps. However, the mass loss for compound **4** occurs at a higher temperature indicating a higher thermal stability of the sample.

The process of partial loss of ammonia molecules was proven to be reversible by powder X-ray diffraction (PXRD) study. Heating the powder sample of **4** under Ar at 100°C for several minutes leads to evolution of the PXRD pattern (Figure 6). As one can see, when temperature increases, the positions of all reflections are gradually moving into the higher angles indicating a decrease of the unit cell parameters in relation with ammonia loss. These shifts are accompanied by the broadening of the peaks, which is a consequence of the

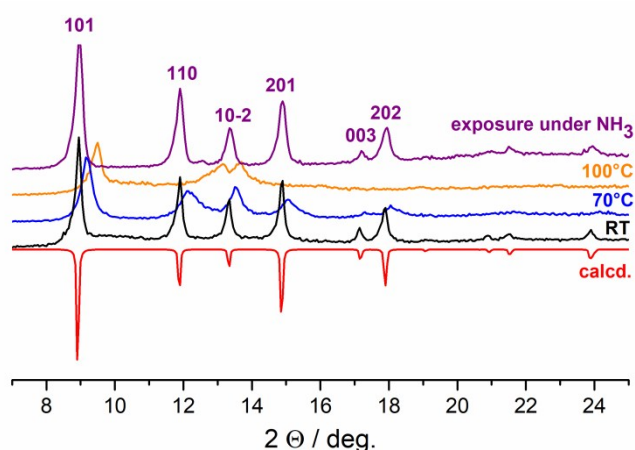


Figure 6. Powder XRD analysis for the sample of **4**. Red line represents the calculated pattern with refined cell parameters $a = 14.90 \text{ \AA}$ and $c = 15.49 \text{ \AA}$; black line was obtained for sample at room temperature; blue and orange lines corresponds to sample heated in Ar for several minutes at 70 and 100°C, respectively. Purple line is for sample after exposure under dry NH₃ vapor.

amorphization of the sample. However, the subsequent exposure of the heated sample of **4** under dry ammonia vapor

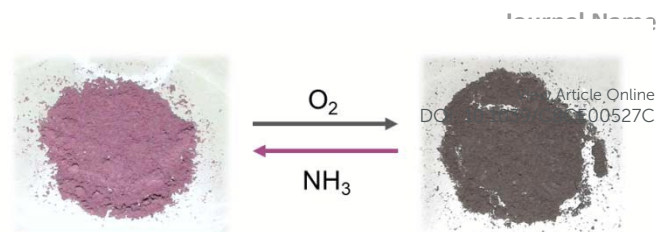


Figure 7. The powder sample of **4** before heating (left) and after heating at 100°C in air for several minutes (right).

for several minutes at room temperature restores the original PXRD pattern. Similar behavior was demonstrated for powder samples of compounds **2** and **3** (Figure S8), while thermal degradation of compound **1** is irreversible. It is worth noting, that only the first step of the ammonia loss is reversible for the compounds **2** and **3**. Heating of the samples at higher temperature and subsequent exposure under dry NH₃ revealed irreversible modification of the powder patterns. The TG data illustrate high structural flexibility of the frameworks **2-4** and open the possible way for post-synthetic modification of framework properties.

Another interesting observation was collected during heating of the powders **2-4** in air at 100°C. It resulted in the dramatic color change of the samples (Figure 7). The color change can be explained by the oxidation of the highly redox active cluster anion from [Re₃Mo₃Se₈(CN)₆]⁵⁻ to [Re₃Mo₃Se₈(CN)₆]⁴⁻ by air oxygen. Corresponding change of the diffuse reflectance spectra (DRS) can be seen in Figure S9 in the ESI. The band characteristic for cluster anion [Re₃Mo₃Se₈(CN)₆]⁵⁻ (550 nm) for initial sample is shifted to higher wavelength after heating of the sample correlating with the UV-Vis spectra data for anions [Re₃Mo₃Se₈(CN)₆]^{5-/4-} in solution. It is in accordance with the corresponding $E_{1/2} = -0.325 \text{ V vs Ag/AgCl}$ in DMF.⁴⁴ Exposure of oxidized sample under NH₃ vapor led to restore the initial structure and color indicating that reduction of the cluster occurs. Note that heating of the sample of **4** under inert atmosphere does not reveal any noticeable color change. Investigation of coordination polymers with switchable oxidation state attract a lot of attention in recent years because of their possible applications as electrochromic devices and electrocatalysts.⁸³ Up to date, only one example of reversible redox transitions was reported for cluster-based coordination polymers.⁸⁴ An existence of reversible redox transitions of the compounds **2-4** indicates that [Re₃Mo₃Se₈(CN)₆]ⁿ⁻ cluster anions are useful as building blocks for construction of redox-active solids.

Conclusions

Here, we report on the synthesis, structural features and properties of four new coordination polymers where the mixed-metal cluster [Re₃Mo₃Se₈(CN)₆]⁵⁻ was firstly used as pre-made building block. Interaction of K₅[Re₃Mo₃Se₈(CN)₆] with Cd(CH₃COO)₂ in aqueous ammonia led to the formation of compound **1** exhibiting 1D helicoidal chain-like structure. Addition of the halide salts KX (X = Cl, Br, I) to the reaction mixture dramatically changes the product composition and leads to the crystallization of **2-4** with interpenetrating three-

dimensional frameworks. The weak N-H...X hydrogen interactions control the formation of the frameworks built on strong covalent M-CN-M' bonds.

It was found that frameworks **2-4** are highly stable and display a set of interesting properties. While crystals of **1** are unstable in air owing to the rapid removal of solvate H₂O and coordinated NH₃ molecules, compounds **2-4** demonstrate the ability to reversible structural transformation as a result of reversible loss of ammonia molecules. Moreover, structural transformations are accompanied by the reversible redox transitions in solid state using the oxidation of cluster unit in air. The transitions cause the remarkable color change of solid samples. These properties could be relevant for the design of chemical sensor materials.

Conflicts of interest

There are no conflicts to declare.

Acknowledgements

The authors thank Russian Foundation for Basic Research for financial support (Project RFBR 17-53-16015). NIIC team thanks Federal Agency for Scientific Organizations for funding. V. Muravieva thanks French Embassy for providing the scholarship for co-tutelle PhD program between France and Russia. The authors are greatly acknowledged to International Associate Laboratory N° 1144 CLUSPOM between France and Russia. The authors also thank the "Centre de Diffractométrie X" (CDIFX) of the Institute of Chemical Science of Rennes for single-crystal X-ray diffraction facilities.

Notes and references

‡ CCDC 1824886–1824889 contain the supplementary crystallographic data for **1-4**. These data can be obtained free of charge via www.ccdc.cam.ac.uk/data_request/cif, or by emailing data_request@ccdc.cam.ac.uk, or by contacting The Cambridge Crystallographic Data Centre, 12 Union Road, Cambridge CB2 1EZ, UK; fax: +44 1223 336033.

- 1 S. Kitagawa, R. Kitaura and S.-I. Noro, *Angew. Chem. Int. Ed.*, 2004, **43**, 2334-2375.
- 2 D. Maspoch, D. Ruiz-Molina and J. Veciana, *Chem. Soc. Rev.*, 2007, **36**, 770-770.
- 3 M. D. Allendorf, C. A. Bauer, R. K. Bhakta and R. J. Houk, *Chem. Soc. Rev.*, 2009, **38**, 1330-1352.
- 4 J. Lee, O. K. Farha, J. Roberts, K. A. Scheidt, S. T. Nguyen and J. T. Hupp, *Chem. Soc. Rev.*, 2009, **38**, 1450-1459.
- 5 J. R. Li, R. J. Kuppler and H. C. Zhou, *Chem. Soc. Rev.*, 2009, **38**, 1477-1504.
- 6 X. Meng, H.-N. Wang, S.-Y. Song and H.-J. Zhang, *Chem. Soc. Rev.*, 2017, **46**, 464-480.
- 7 Z. Xu, L.-L. Han, G.-L. Zhuang, J. Bai, and D. Sun, *Inorg. Chem.*, 2015, **54**, 4737-4743.
- 8 Z.-H. Yan, X.-Y. Li, L.-W. Liu, S.-Q. Yu, X.-P. Wang, and D. Sun, *Inorg. Chem.*, 2016, **55**, 1096-1101.
- 9 H. Wang, J. Xu, D.-S. Zhang, Q. Chen, R.-M. Wen, Z. Chang, and X.-H. Bu, *Angew. Chem. Int. Ed.*, 2015, **54**, 5966-5970.
- 10 R. Chakrabarty, P. S. Mukherjee and P. J. Stang, *Chem. Rev.*, 2011, **111**, 6810-6918.
- 11 T. R. Cook, Y. R. Zheng and P. J. Stang, *Chem. Rev.*, 2013, **113**, 734-777. DOI: 10.1039/C8CE00527C
- 12 D. J. Tranchemontagne, J. L. Mendoza-Cortes, M. O'Keeffe and O. M. Yaghi, *Chem. Soc. Rev.*, 2009, **38**, 1257-1283.
- 13 J. J. Perry IV, J. A. Perman and M. J. Zaworotko, *Chem. Soc. Rev.*, 2008, **38**, 1400-1417.
- 14 X. Y. Wang, C. Avendano and K. R. Dunbar, *Chem. Soc. Rev.*, 2011, **40**, 3213-3238.
- 15 P. Dechambenoit and J. R. Long, *Chem. Soc. Rev.*, 2011, **40**, 3249-3265.
- 16 D. Kundu, E. Talaie, V. Duffort and L. F. Nazar, *Angew. Chem. Int. Ed.*, 2015, **54**, 3431-3448.
- 17 C. A. Schalley, A. Lutzen and M. Albrecht, *Chem. Eur. J.*, 2004, **10**, 1072-1080.
- 18 J. D. Crowley, S. M. Goldup, A. L. Lee, D. A. Leigh and R. T. McBurney, *Chem. Soc. Rev.*, 2009, **38**, 1530-1541.
- 19 G. R. Desiraju, *J. Am. Chem. Soc.*, 2013, **135**, 9952-9967.
- 20 E. Busseron, Y. Ruff, E. Moulin and N. Giuseppone, *Nanoscale*, 2013, **5**, 7098-7140.
- 21 S. Kitagawa and K. Uemura, *Chem. Soc. Rev.*, 2005, **34**, 109-119.
- 22 L. Applegarth, A. E. Goeta and J. W. Steed, *Chem. Commun.*, 2005, 2405-2406.
- 23 J. Pansanel, A. Jouaiti, S. Ferlay, M. Wais Hosseini, J.-M. Planeix and N. Kyritsakas, *New J. Chem.*, 2006, **30**, 71-76.
- 24 K. Uemura, K. Saito, S. Kitagawa and H. Kita, *J. Am. Chem. Soc.*, 2006, **128**, 16122-16130.
- 25 M. S. Tarasenko, E. O. Golenkov, N. G. Naumov, N. K. Moroz and V. E. Fedorov, *Chem. Commun.*, 2009, 2655-2657.
- 26 S. Ferlay and M. W. Hosseini, in *Functional Supramolecular Architectures: For Organic Electronics and Nanotechnology*, eds. P. Samorì and F. Cacialli, Wiley-VCH: Weinheim, 2014, vol. 1, ch. 7, pp. 195-232.
- 27 I. Cvrtila and V. Stilinović, *Cryst. Growth Des.*, 2017, **17**, 6793-6800.
- 28 N. G. Naumov, A. V. Virovets and V. E. Fedorov, *J. Struct. Chem.*, 2000, **41**, 499-520.
- 29 M. V. Bennett, L. G. Beauvais, M. P. Shores and J. R. Long, *J. Am. Chem. Soc.*, 2001, **123**, 8022-8032.
- 30 V. E. Fedorov, N. G. Naumov, Y. V. Mironov, A. V. Virovets, S. B. Artemkina, K. A. Brylev, S. S. Yarovoi, O. A. Efremova and U.-H. Peak, *J. Struct. Chem.*, 2002, **43**, 669-684.
- 31 M. Shatruk, C. Avendano and K. R. Dunbar, in *Progr. Inorg. Chem.*, ed. K. D. Karlin, John Wiley & Sons, Inc., 2009, vol. 56, ch. 3, pp. 155-334.
- 32 Y. Kim, V. E. Fedorov and S.-J. Kim, *J. Mater. Chem.*, 2009, **19**, 7178.
- 33 S. Cordier, Y. Molard, K. A. Brylev, Y. V. Mironov, F. Grasset, B. Fabre and N. G. Naumov, *J. Clust. Sci.*, 2014, **26**, 53-81.
- 34 E. V. Alexandrov, A. V. Virovets, V. A. Blatov and E. V. Peresypkina, *Chem. Rev.*, 2015, **115**, 12286-12319.
- 35 T. G. Gray, C. M. Rudzinski, E. E. Meyer, R. H. Holm and D. G. Nocera, *J. Am. Chem. Soc.*, 2003, **125**, 4755-4770.
- 36 S. G. Kozlova, S. P. Gabuda, K. A. Brylev, Yu. V. Mironov, and V. E. Fedorov, *J. Phys. Chem. A*, 2004, **108**, 10565-10567.
- 37 Y. M. Gayfulin, D. A. Pirayev, Yu. V. Mironov and N. G. Naumov, *Russ. J. Coord. Chem.*, 2017, **43**, 364-367.
- 38 A. V. Virovets, Y. M. Gayfulin, E. V. Peresypkina, Y. V. Mironov and N. G. Naumov, *CrystEngComm*, 2015, **17**, 1477-1482.
- 39 N. G. Naumov, A. V. Virovets, N. V. Podberezskaya and V. E. Fedorov, *J. Struct. Chem.*, 1997, **38**, 857-862.
- 40 A. Slougui, Yu. V. Mironov, A. Perrin, and V. E. Fedorov, *Croat. Chem. Acta*, 1995, **68**, 885-890.
- 41 Y. M. Gayfulin, N. G. Naumov, M. R. Rizhikov, A. I. Smolentsev, V. A. Nadolinny and Y. V. Mironov, *Chem. Commun.*, 2013, **49**, 10019-10021.
- 42 Y. V. Mironov, A. V. Virovets, N. G. Naumov, V. N. Ikorskii and V. E. Fedorov, *Chem. Eur. J.*, 2000, **8**, 1361-1365.

- 43 K. A. Brylev, A. V. Virovets, N. G. Naumov, Y. V. Mironov, D. Fenske and V. E. Fedorov, *Russ. Chem. Bull.*, 2001, **50**, 1140-1143.
- 44 V. K. Muravieva, Y. M. Gayfulin, M. R. Ryzhikov, I. N. Novozhilov, D. G. Samsonenko, D. A. Piryazev, V. Yanshole and N. G. Naumov, *Dalton Trans.*, 2018, **47**, 3366-3377.
- 45 W. Kraus and G. Nolze, *J. Appl. Cryst.*, 1996, **29**, 301-303.
- 46 A. Altomare, M. C. Burla, M. Camalli, G. L. Cascarano, C. Giacovazzo, A. Guagliardi, A. G. G. Moliterni, G. Polidori and R. Spagnac, *J. Appl. Cryst.*, 1999, **32**, 115-119.
- 47 G. M. Sheldrick, *Acta Crystallogr. C*, 2015, **71**, 3-8.
- 48 L. J. Farrugia, *J. Appl. Cryst.*, 2012, **45**, 849-854.
- 49 T. Yoshimura, S. Ishizaka, Y. Sasaki, H.-B. Kim, N. Kitamura, N. G. Naumov, M. N. Sokolov, V. E. Fedorov and *Chem. Lett.*, 1999, **28**, 1121-1122.
- 50 P. Kumar, N. G. Naumov, R. Boukherroub and S. L. Jain, *Appl. Catal., A*, 2015, **499**, 32-38.
- 51 Y. V. Mironov, A. V. Virovets, N. G. Naumov, V. N. Ikorskii and V. E. Fedorov, *Chem. Eur. J.*, 2000, **8**, 1361-1365.
- 52 J.-C. P. Gabriel, K. Boubekeur, S. Uriel and P. Batail, *Chem. Rev.*, 2001, **101**, 2037-2066.
- 53 C. Magliocchi, X. Xie and T. Hughbanks, *Inorg. Chem.*, 2004, **43**, 1902-1911.
- 54 N. G. Naumov, A. V. Virovets, M. N. Sokolov, S. B. Artemkina and V. E. Fedorov, *Angew. Chem. Int. Ed.*, 1998, **37**, 1943-1945.
- 55 L. G. Beauvais, M. P. Shores and J. R. Long, *J. Am. Chem. Soc.*, 2000, **122**, 2763-2772.
- 56 N. G. Naumov, D. V. Soldatov, J. A. Ripmeester, S. B. Artemkina and V. E. Fedorov, *Chem. Commun.*, 2001, 571-572.
- 57 Y. Kim, S.-M. Park, W. Nam and S.-J. Kim, *Chem. Commun.*, 2001, 1470-1471.
- 58 K. A. Brylev, N. G. Naumov, A. V. Virovets, S.-J. Kim and V. E. Fedorov, *J. Clust. Sci.*, 2008, **20**, 165-176.
- 59 S. Cordier, N. G. Naumov, D. Salloum, F. Paul and C. Perrin, *Inorg. Chem.*, 2004, **43**, 219-226.
- 60 G. Daigre, K. Costuas, M. S. Tarasenko, A. Y. Ledneva, N. G. Naumov, P. Lemoine, T. Guizouarn, Y. Molard, M. Amela-Cortes, N. Audebrand and S. Cordier, *Dalton Trans.*, 2018, **47**, 1122-1130.
- 61 B. B. Yan, H. J. Zhou and A. Lachgar, *Inorg Chem*, 2003, **42**, 8818-8822.
- 62 N. G. Naumov, S. Cordier and C. Perrin, *Solid State Sci.*, 2005, **7**, 1517-1521.
- 63 S. Jin and F. J. DiSalvo, *Chem. Mater.*, 2002, **14**, 3448-3457.
- 64 B. F. Hoskins, R. Robson, N. V. Y. Scarlett, *J. Chem. Soc. Chem. Commun.*, 1994, 2025 - 2026.
- 65 V. A. Blatov, L. Carlucci, G. Ciani, D. M. Proserpio, *Cryst. Eng. Comm.* 2004, **6**, 377 - 395.
- 66 I. A. Baburin, V. A. Blatov, L. Carlucci, G. Ciani, D. M. Proserpio, *J. Solid State Chem.* 2005, **178**, 2452-2474.
- 67 K. F. Tebbe, M. Plewa, *Z. Anorg. Allg. Chem.* 1982, **489**, 111-125.
- 68 S. Nishikiori, T. Iwamoto, *J. Struct. Chem.* 1999, **40**, 750-756.
- 69 T. Steiner, *Angew. Chem. Int. Ed.*, 2002, **41**, 48-76.
- 70 A. Kovacs and Z. Varga, *Coord. Chem. Rev.*, 2006, **250**, 710-727.
- 71 R. D. Shannon, *Acta Cryst.*, 1976, **A32**, 751-767.
- 72 D. Braga, G. R. Desiraju, J. S. Miller, A. G. Orpen, S. L. Price, *CrystEngComm*, 2002, **4**, 500-509.
- 73 M. W. Hosseini, *CrystEngComm*, 2004, **6**, 318-322.
- 74 D. Braga, L. Brammer, N. R. Champness, *CrystEngComm*, 2005, **7**, 1-19.
- 75 L. Brammer, E. A. Bruton and P. Sherwood, *Cryst. Growth Des.*, 2001, **1**, 277-290.
- 76 I. A. Baburin, V. A. Blatov, L. Carlucci, G. Ciani, and D. M. Proserpio, *Cryst. Growth Des.*, 2008, **8**, 519-537.
- 77 L.-L. Han, Z.-H. Li, J.-S. Chen, X.-P. Wang, and D. Sun, *Cryst. Growth Des.*, 2014, **14**, 1221-1226. DOI: 10.1039/C8CE00527C
- 78 B.-C. Tzeng, B.-S. Chen, S.-Y. Lee, W.-H. Liu, G.-H. Lee and S.-M. Peng, *New J. Chem.*, 2005, **29**, 1254-1257.
- 79 P. M. Chhetri, X.-K. Yang and J.-D. Chen, *Cryst. Growth Des.*, 2017, **17**, 4801-4809.
- 80 Y. M. Lee, S. J. Hong, H. J. Kim, S. H. Lee, H. Kwak, C. Kim, S.-J. Kim and Y. Kim, *Inorg. Chem. Commun.*, 2007, **10**, 287-291.
- 81 B. K. Park, S. H. Lee, E. Y. Lee, H. Kwak, Y. M. Lee, Y. J. Lee, J. Y. Jun, C. Kim, S.-J. Kim and Y. Kim, *J. Mol. Struct.*, 2008, **890**, 123-129.
- 82 E. Mikuli, M. Liszka and M. Molenda, *J. Therm. Anal. Calorim.*, 2007, **89**, 573-578.
- 83 D. M. D'Alessandro, *Chem. Commun.*, 2016, **52**, 8957-8971.
- 84 Y. M. Litvinova, Y. M. Gayfulin, K. A. Kovalenko, D. G. Samsonenko, J. Leusen, I. V. Korolkov, V. P. Fedin, Y. V. Mironov, *Inorg. Chem.* 2018, **57**, 2072-2084.



A Journal of



Accepted Article

Title: Apical cyanide ligands substitution in heterometallic clusters
[Re₃Mo₃Q₈(CN)₆]_n- (Q = S, Se)

Authors: Viktoria K. Muravieva, Yakov M. Gayfulin, Tatiana I. Lappi,
Vincent Dorcet, Taisiya S. Sukhikh, Pierric Lemoine, Maxim
R. Ryzhikov, Yuri V. Mironov, Stéphane Cordier, and Nikolay
Gennadievich Naumov

This manuscript has been accepted after peer review and appears as an Accepted Article online prior to editing, proofing, and formal publication of the final Version of Record (VoR). This work is currently citable by using the Digital Object Identifier (DOI) given below. The VoR will be published online in Early View as soon as possible and may be different to this Accepted Article as a result of editing. Readers should obtain the VoR from the journal website shown below when it is published to ensure accuracy of information. The authors are responsible for the content of this Accepted Article.

To be cited as: *Eur. J. Inorg. Chem.* 10.1002/ejic.201900198

Link to VoR: <http://dx.doi.org/10.1002/ejic.201900198>

WILEY-VCH

Apical cyanide ligands substitution in heterometallic clusters [Re₃Mo₃Q₈(CN)₆]ⁿ⁻ (Q = S, Se)

Viktoria K. Muravieva,^[a, b] Yakov M. Gayfulin,^[a] Tatiana I. Lappi,^[a, c] Vincent Dorcet,^[b] Taisiya S. Sukhikh,^[a, c] Pierric Lemoine,^[b] Maxim R. Ryzhikov,^[a, c] Yuri V. Mironov,^[a, c] Stéphane Cordier,^[b] Nikolay G. Naumov*^[a, c]

Abstract: A number of transition metal cluster compounds can be obtained only in the melt of inorganic cyanides and, therefore, contain terminal cyanide ligands. Substitution of these ligands, which is often necessary to change the physicochemical properties of the clusters, is an urgent problem because of their low reactivity in substitution reactions. In this work, a synthetic approach has been developed for the substitution of CN-ligands in the heterometallic cluster anions [Re₃Mo₃Q₈(CN)₆]ⁿ⁻ (Q = S, n = 6; Q = Se, n = 5) by the 4-*tert*-butylpyridine (TBP) molecules. Two new compounds, namely [Re₃Mo₃S₈(TBP)₆] (1) and [Re₃Mo₃Se₈(TBP)₆] (2), were obtained with high yields and crystallized in solvothermal conditions. It has been shown that the compounds 1 and 2 are based on the paramagnetic cluster cores {Re₃Mo₃Q₈}⁰ containing 23 cluster valence electrons (CVE). Geometry of the new compounds has been investigated using the X-Ray structural analysis. The electronic structure has been analyzed using the DFT calculations showing large distortion of M₆ cluster core.

Introduction

Octahedral rhenium and molybdenum cluster complexes have been intensively studied over the past decades due to their versatility: a number of the useful chemical and physical properties, e.g. adjustable solubility, rich redox chemistry, red to NIR luminescence and radiopacity.^[1] Properties of these compounds may be varied in a wide range depending strongly on the nature of apical ligands. Obtaining of the desired set of properties of the cluster compound (e.g. for construction of

functional materials) requires the detailed study of the chemical approaches to the modification of the ligand environment. An outstanding feature of the rhenium and molybdenum octahedral clusters is the possibility to be prepared by a high-temperature synthesis, which results in the formation of the compounds with relatively labile halide apical ligands.^[2] It was shown that various molecules and ions could substitute halide apical ligands by the use of several synthetic approaches, e.g. removal of the halide in reaction with Ag(I) salts^[3] or ligand exchange in the molten organic compounds.^[4]

While the homonuclear hexacyano clusters of molybdenum and rhenium are being known since a long time, the heterometallic octahedral chalcogenide cluster complexes based on {Re₃Mo₃Q₈} (Q = S, Se) cores have been prepared only recently.^[5] The investigation of these clusters is of great interest because the heterometallic substitution within the cluster core is a useful tool for tuning the cluster charge, redox potentials and chemical properties. However, further study of the reactivity of the novel cluster complexes is hampered by the fact that they can be obtained only in the high-temperature melt of inorganic cyanides. Therefore, they contain the strongly coordinated apical cyanide ligands at the preparation stage. Ambidentate nature of the cyanide is widely exploited for the design of cluster-based coordination polymers with a number of transition, post transition and rare earth metal cations.^[6] However, cyanide cluster complexes are generally inert toward the ligand exchange reactions. There is a lack of literature examples of the apical cyanide ligand exchange in the chemistry of transition metal clusters despite of numerous examples in the chemistry of mononuclear cyanometallates.^[7] In that frame, development of a convenient method for substitution of the apical cyanide ligands is important for further application of the heterometallic structural units in material design.

The present work deals with the cyanide exchange reactions in the mixed-metal rhenium-molybdenum clusters. We have found that substitution of the cyanide ligands for 4-*tert*-butylpyridine (TBP) is possible under solvothermal conditions. During the reaction, two new neutral complexes with general formula [Re₃Mo₃Q₈(TBP)₆] (Q = S, Se) were obtained. The preparation, the geometric and electronic structures of the novel compounds are discussed.

- [a] V. K. Muravieva, PhD Y. M. Gayfulin, T. I. Lappi, PhD T. S. Sukhikh, PhD M. R. Ryzhikov, Dr. Sci. Y. V. Mironov, Dr. Sci. N. G. Naumov
Nikolaev Institute of Inorganic Chemistry SB RAS
3, Acad. Lavrentiev ave., Novosibirsk, 630090 (Russian Federation)
naumov@niic.nsc.ru
- [b] V. K. Muravieva, PhD V. Dorcet, PhD P. Lemoine, PhD S. Cordier,
Institut des Sciences Chimiques de Rennes, Université de Rennes
1, UMR 6226 UR1-CNRS
Campus de Beaulieu, Rennes, 35042 (France)
- [c] T. I. Lappi, PhD T. S. Sukhikh, PhD M. R. Ryzhikov, Dr. Sci. Y. V. Mironov, Dr. Sci. N. G. Naumov
Novosibirsk State University
2, Pirogova str., Novosibirsk, 630090 (Russian Federation)

Supporting information for this article is given via a link at the end of the document.

Results and Discussion

Preparation and Structure. As it was mentioned above, substitution chemistry of coordinated cyanides is quite developed for mononuclear cyanometallates.^[7a] At the same time, the cyanide cluster complexes of rhenium and molybdenum are kinetically inert toward the ligand exchange. Our first attempts to replace the terminal cyanides of the $[\text{Re}_3\text{Mo}_3\text{Q}_8(\text{CN})_6]^{1-}$ cluster anions showed that the salts of these anions are insoluble in 4-*tert*-butylpyridine and other pyridine derivatives and hence inert in reactions with them up to 200–220°C. The use of these neat solvents did not lead to the reaction and formation of cluster products containing the pyridine ligands. To make this reaction possible, we examined mixtures of solvents in which the reaction equilibrium shifts to the right due to the increase of solubility of the starting material and formation of insoluble products. In the conditions described in Experimental Section, the crystalline compounds **1** and **2** were obtained using a mixture of TBP, acetonitrile and water at 160°C. It was also found that the reaction of $\text{CaK}_4[\text{Re}_3\text{Mo}_3\text{S}_8(\text{CN})_6] \cdot 8\text{H}_2\text{O}$ and $\text{K}_5[\text{Re}_3\text{Mo}_3\text{Se}_8(\text{CN})_6] \cdot 11\text{H}_2\text{O}$ with TBP proceeds only in high excess of the latter. Note that the starting cluster anion $[\text{Re}_3\text{Mo}_3\text{S}_8(\text{CN})_6]^{6-}$ contains 23 cluster valence electrons (CVE) while the $[\text{Re}_3\text{Mo}_3\text{Se}_8(\text{CN})_6]^{5-}$ anion contains 22 CVE. Nevertheless, products **1** and **2** are both paramagnetic and contain the $\{\text{Re}_3\text{Mo}_3\text{Q}_8\}^0$ cores with 23 CVE. Therefore, the reduction of the $\{\text{Re}_3\text{Mo}_3\text{Se}_8\}^+$ cluster core takes place during the ligand exchange reaction forming the neutral complexes in both cases. EPR spectra of polycrystalline samples of compounds **1** and **2** demonstrate broad signals with *g*-values of 2.245 and 2.299, respectively (Figure 1); those are substantially higher than the conventional electron spin *g*-factor. Similar broad signals were observed in numerous rhenium and molybdenum octahedral clusters with *g* = 2.44–2.56 for $[\text{Re}_6\text{Q}_8\text{L}_6]^{3-}$ (Q = S, Se, Te; L = CN, Cl)^[8] and 2.289 for $\text{K}_6\text{Mo}_6\text{Se}_8(\text{CN})_5$.^[9]

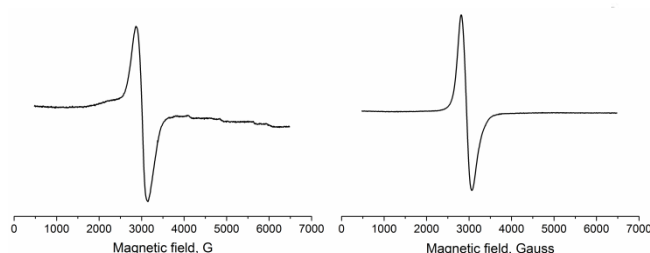


Figure 1 EPR spectra for **1** (left) and **2** (right) measured at 77K.

The compounds **1** and **2** crystallize in the tetragonal space group $P4_2/n$ and the triclinic space group $P-1$, respectively. The structures represent crystal packings of the cluster units $[\text{Re}_3\text{Mo}_3\text{S}_8(\text{TBP})_6]$ and $[\text{Re}_3\text{Mo}_3\text{Se}_8(\text{TBP})_6]$ (Figure 2). While the metallic core in the fragment $\{\text{Re}_3\text{Mo}_3\text{S}_8\}$ is a nearly perfect octahedron (the M–M distances vary in the range of 2.6078(6) – 2.6157(6) Å), the structure of **2** comprises the slightly distorted

octahedrons M_6 of two crystallographically non-equivalent cluster complexes. This distortion is caused by the notable difference in lengths of eight bonds between the apical and the basal metal atoms and four bonds between the basal metal atoms only. The M–M bond lengths vary from 2.6316(6) to 2.6561(7) Å. Note that the two possible isomers of the mixed-metal octahedron may be presented, namely a *fac*-isomer with C_{3v} symmetry and a *mer*-isomer with C_{2v} symmetry. One can notice that the symmetry of the isomers of the $\{\text{Re}_3\text{Mo}_3\}$ metallocluster is different than the point group symmetry of the crystals of **1** and **2**. To fit the lattice symmetry, the isomers must be disordered between possible orientations. Apparently, the average structures do not allow us to analyze the real Re–Re, Re–Mo, Mo–Mo bond lengths in the crystal structures and to compare them with the DFT calculations.

The average M–M distances of 2.612 Å in **1** and 2.640 Å in **2** lie between the respective values reported for the 23 CVE $\{\text{Re}_6\text{Q}_8\}^{3+}$ core in $(\text{Ph}_4\text{P})_2(\text{H})[\text{Re}_6\text{Se}_8(\text{CN})_6] \cdot 8\text{H}_2\text{O}$ and $(\text{Ph}_4\text{P})_3[\text{Re}_6\text{S}_8(\text{CN})_6]$ ^[10] and $\{\text{Mo}_6\text{Q}_8\}$ cores in $\text{La}_{0.94}\text{Mo}_6\text{Se}_8$ ^[11] and HoMo_6S_8 .^[12] The same tendency can be found for the corresponding M–Q distances. Each M_6 octahedron is coordinated with eight Q ligands and six TBP ligands via the nitrogen atoms of the pyridine rings. The average M–N distances are slightly longer than the typical Re–N distances found in the octahedral rhenium clusters with the terminal TBP or pyridine ligands.^[4h, 13] They are close to the Mo–N distances found in the compounds $[\text{Mo}_6\text{S}_8(\text{py})_6]$ and $[\text{Mo}_6\text{S}_8(\text{TBP})_6]$.^[14] Presence of the voluminous *tert*-butyl group in the aromatic rings prevents the formation of π – π stacking between the terminal ligands of the nearby clusters. However, the structure **1** present the close packing of the cluster units without any solvent-accessible voids. On the contrary, the structure **2** contains the large cavities filled by the electron density originating from disordered solvate CH_3CN molecules. This difference of structure packings may be caused by the different volumes of S- and Se-containing cluster units. According to the electron count found by the SQUEEZE procedure, the structure **2** contains about 8 extra CH_3CN molecules. Solvate molecules in **2** can be easily removed during the experimental procedures, and the elemental analysis did not show the presence of CH_3CN molecules in the dried sample of compound **2**.

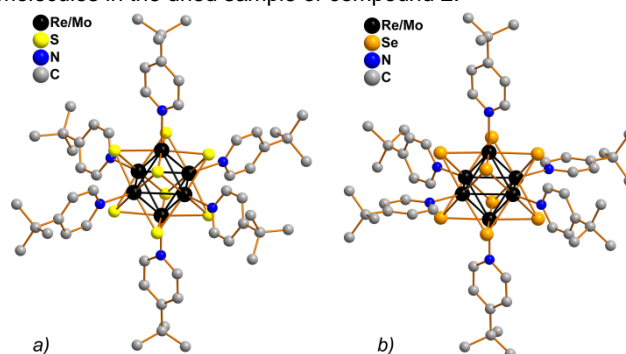


Figure 2. Ball-and-stick representation of the cluster complexes $[\text{Re}_3\text{Mo}_3\text{S}_8(\text{TBP})_6]$ (a) and $[\text{Re}_3\text{Mo}_3\text{Se}_8(\text{TBP})_6]$ (b) in the structures of compounds **1** and **2**, respectively. Hydrogen atoms are not shown. Disordered *tert*-butyl groups are shown in one orientation for clarity.

The compound **1** is insoluble in common solvents, while the compound **2** dissolves in CH_2Cl_2 forming the dark-brown solution. Cyclic voltammetry showed that the compound **2** has a quasi-reversible one-electron oxidation process ($\Delta E = 0.16$ V) with $E_{1/2} = 0.027$ V vs Ag/AgCl electrode. This process corresponds to the formation of the $[\text{Re}_3\text{Mo}_3\text{Se}_8(\text{TBP})_6]^+$ cluster with 22 CVE. The reduction of the compound **2** was detected as the irreversible process with E_{pc} at about -1.26 V vs Ag/AgCl electrode. The irreversibility indicates, most probably, a decomposition of the cluster during its reduction. Our attempts to carry out the chemical oxidation or reduction of the $[\text{Re}_3\text{Mo}_3\text{Se}_8(\text{TBP})_6]$ cluster led to the irreversible chemical transformations giving the unidentified products.

DFT calculations.

Molecular orbital (MO) diagrams for the *fac*- and *mer*- isomers of the $[\text{Re}_3\text{Mo}_3\text{Q}_8(\text{py})_6]$ ($\text{Q} = \text{S}, \text{Se}$) clusters calculated with C_1 symmetry are similar in the near frontier orbital region (Figure 3). In the region from -6.0 eV to -4.4 eV the MOs are primarily localized on atomic orbitals (AO) of the $\{\text{M}_6\text{Q}_8\}$ core atoms with minor contribution from AO of the terminal ligands. HOMO and HOMO-1 have similar energies with 0.2 eV splitting and separated from HOMO-2 by ~ 0.8 eV gap. LUMO separated from HOMO and HOMO-1 by ~ 1.1 eV. Thus in all $[\text{Re}_3\text{Mo}_3\text{Q}_8(\text{py})_6]$ clusters the MOs are characterized by the bi-gap structure. LUMO and orbitals up to ~ -1.2 eV are primarily localized on AO of the py ligand atoms with minor contribution from the AO of the metal atoms. HOMO, HOMO-1 and HOMO-2 are primarily localized on the AO of the $\{\text{M}_6\text{Q}_8\}$ core atoms. The dominant contributions in HOMO, HOMO-1 and HOMO-2 come from AO of the Mo atoms, the exceptions are HOMO-1 in the *mer*-isomers of both sulfide and selenide clusters (Table 1, Figure 4). Figure S1 in Supplementary presents isosurfaces and energies of molecular orbitals in the near frontier orbital region for LUMO, HOMO and lower lying molecular orbitals. Energy analysis shows that the *mer*-isomers are slightly more stable than the *fac*-isomers ($\Delta E = 0.1$ eV).

The known homometallic Re_6 clusters with the pyridine derivatives, namely, *trans*- $[\text{Re}_6\text{S}_8\text{Cl}_4(\text{ppy})_2]^{2-}$ ($\text{ppy} = 4$ -phenylpyridine) and *trans*- $[\text{Re}_6\text{S}_8\text{Cl}_4(\text{bpy})_2]^{2-}$ ($\text{bpy} = 4,4'$ -bipyridine), have considerably larger HOMO-LUMO gap of about 3.6 eV in comparison with the $[\text{Re}_3\text{Mo}_3\text{Q}_8(\text{py})_6]$ ($\text{Q} = \text{S}, \text{Se}$) clusters.^[15] Similar to the $[\text{Re}_3\text{Mo}_3\text{Q}_8(\text{py})_6]$ clusters, HOMO and HOMO-1 in these $\{\text{Re}_6\}$ complexes are mainly metal-centered and split by a small gap. LUMO in *trans*- $[\text{Re}_6\text{S}_8\text{Cl}_4(\text{ppy})_2]^{2-}$ is localized on the bpy ligands, while in *trans*- $[\text{Re}_6\text{S}_8\text{Cl}_4(\text{bpy})_2]^{2-}$ it is localized on the $\{\text{Re}_6\}$ core. Interestingly, the bi-gap structure of the $[\text{Re}_3\text{Mo}_3\text{Q}_8(\text{py})_6]$ clusters was not observed in the case of the homometallic species.

Optimized geometries for the *mer*-isomers of the clusters are quite far from octahedral, however, the $\{\text{Re}_3\text{Mo}_3\}$ core have almost perfect C_{2v} symmetry, which is the highest possible symmetry for such spatial distribution of the atoms (Figure 5). Geometry of the *mer*-isomer of the $\{\text{Re}_3\text{Mo}_3\}$ core can be represented as the asymmetric rhombic bipyramid with the Re–Mo–Re–Mo rhomb on the base, molybdenum and rhenium atoms as the apexes of the bigger and smaller pyramids (Mo–

M_{rhomb} distances are longer than Re– M_{rhomb} distances), respectively.

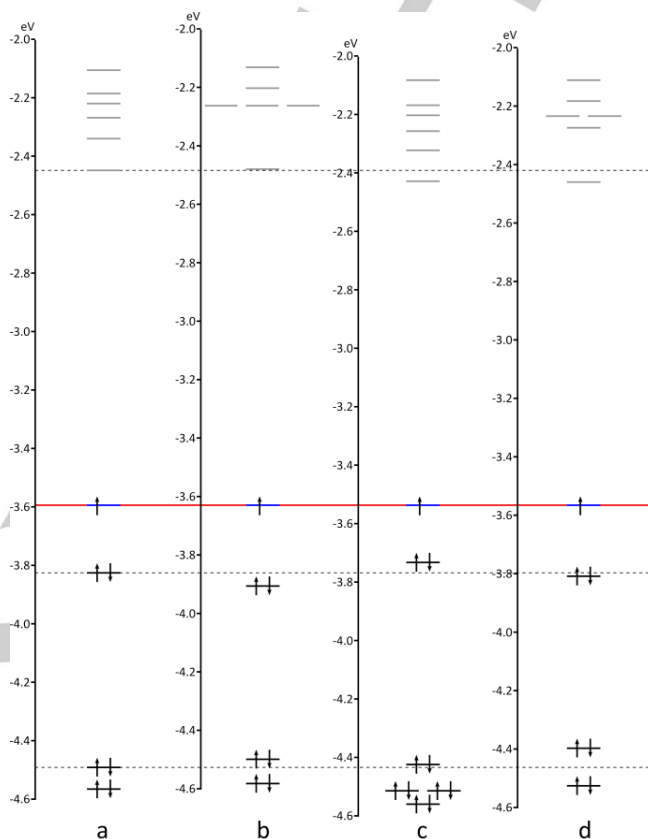


Figure 3. The energy levels diagram in the near frontier orbital region for *fac*- and *mer*- isomers of the $[\text{Re}_3\text{Mo}_3\text{Q}_8(\text{py})_6]$ clusters. a – *fac*- $[\text{Re}_3\text{Mo}_3\text{S}_8(\text{py})_6]$, b – *mer*- $[\text{Re}_3\text{Mo}_3\text{S}_8(\text{py})_6]$, c – *fac*- $[\text{Re}_3\text{Mo}_3\text{Se}_8(\text{py})_6]$, d – *mer*- $[\text{Re}_3\text{Mo}_3\text{Se}_8(\text{py})_6]$.

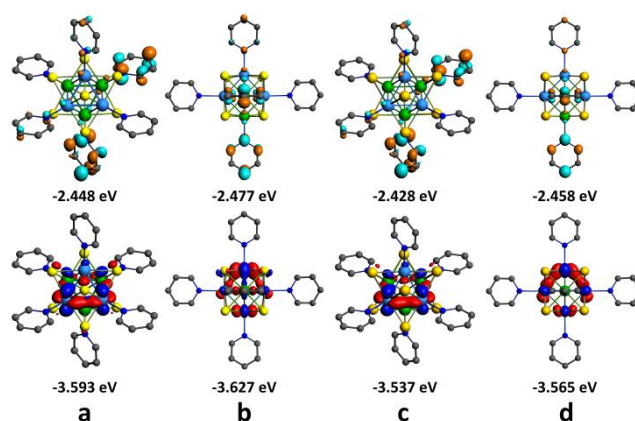


Figure 4. HOMO (bottom) and LUMO (top) orbitals of the different isomers of the $[\text{Re}_3\text{Mo}_3\text{Q}_8(\text{py})_6]$ ($\text{Q} = \text{S}, \text{Se}$) clusters. a – *fac*- $[\text{Re}_3\text{Mo}_3\text{S}_8(\text{py})_6]$, b – *mer*- $[\text{Re}_3\text{Mo}_3\text{S}_8(\text{py})_6]$, c – *fac*- $[\text{Re}_3\text{Mo}_3\text{Se}_8(\text{py})_6]$, d – *mer*- $[\text{Re}_3\text{Mo}_3\text{Se}_8(\text{py})_6]$.

Table 1. Composition of MOs in near frontier orbital region.

| | Mo | Re | Q | tpb |
|--|-----|-----|-----|-----|
| <i>fac</i> -[Re ₃ Mo ₃ S ₈ (py) ₆] | | | | |
| LUMO | 4% | 3% | 0% | 92% |
| HOMO | 56% | 19% | 24% | 0% |
| HOMO-1 | 58% | 22% | 20% | 0% |
| HOMO-2 | 59% | 21% | 19% | 0% |
| <i>fac</i> -[Re ₃ Mo ₃ Se ₈ (py) ₆] | | | | |
| LUMO | 4% | 3% | 0% | 93% |
| HOMO | 55% | 18% | 27% | 0% |
| HOMO-1 | 55% | 21% | 23% | 0% |
| HOMO-2 | 59% | 23% | 18% | 0% |

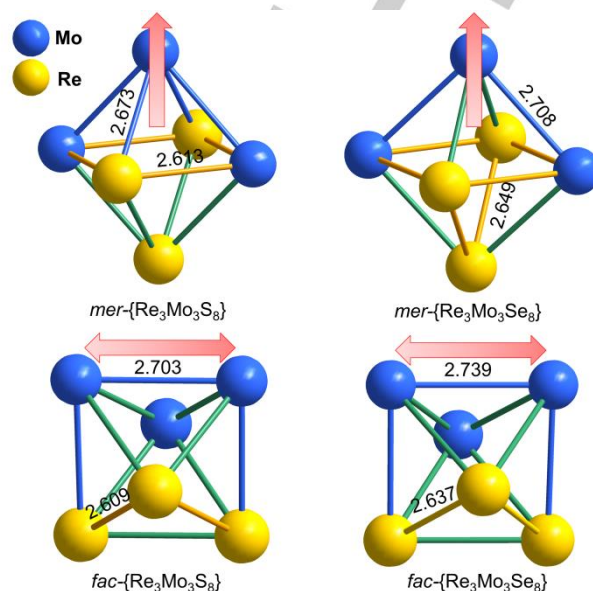
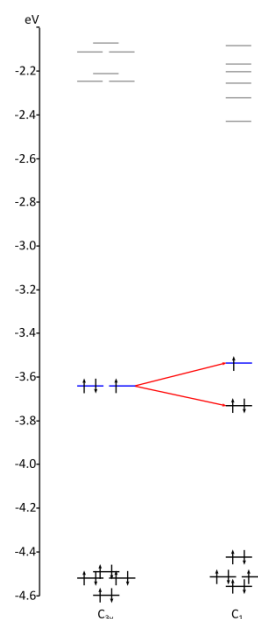
| | Mo | Re | Q | tpb |
|--|-----|-----|-----|-----|
| <i>mer</i> -[Re ₃ Mo ₃ S ₈ (py) ₆] | | | | |
| LUMO | 5% | 10% | 0% | 85% |
| HOMO | 51% | 26% | 23% | 0% |
| HOMO-1 | 38% | 41% | 21% | 0% |
| HOMO-2 | 74% | 2% | 24% | 0% |
| <i>mer</i> -[Re ₃ Mo ₃ Se ₈ (py) ₆] | | | | |
| LUMO | 4% | 9% | 0% | 87% |
| HOMO | 53% | 13% | 34% | 0% |
| HOMO-1 | 31% | 40% | 29% | 0% |
| HOMO-2 | 79% | 9% | 11% | 0% |

Optimized geometries for the *fac*-isomers calculated in C_1 symmetry (Figure 5) are far from possible C_{3v} symmetry showing large distortion of both [Re₃Mo₃Q₈(py)₆] clusters characterized by the one specific Mo–Mo distance (marked by red arrow in Figure 5), which is ~0.05 Å longer than the other metal-metal distances (Tables S1, S2).

Considering that the [Re₃Mo₃Q₈(TBP)₆] clusters have an odd number of electrons, the *fac*-isomers may undergo the Jahn-Teller (JT) effect. Previously, JT distortion was reported for 23 CVE [Re₆Q₈X₆]³⁻ (Q = S, Se; X = Cl, CN) clusters.^[16]

It is known that the character table for C_{3v} point group contains the **E** irreducible representation with doubly degenerate orbitals. Thus, energy levels diagram for the *fac*-isomer of the [Re₃Mo₃Se₈(py)₆] with C_{3v} symmetry was calculated in order to

verify possible JT effect. According to the calculations, it contains doubly degenerate orbitals occupied by three electrons, that results in the JT instability of *fac*-isomers and in geometry distortion with the split of degenerate orbitals (Figure 6).

**Figure 5.** Optimized geometries in *fac*- and *mer*-isomers of {Re₃Mo₃} of the [Re₃Mo₃Q₈(py)₆] clusters.**Figure 6.** Energy levels diagram in near frontier orbital region for *fac*- isomer of the [Re₃Mo₃Se₈(py)₆] cluster with C_{3v} (left) and C_1 (right) symmetries.

Conclusions

We demonstrate herein an efficient exchange reaction for the substitution of the terminal cyanide ligands in the octahedral heterometallic clusters $[\text{Re}_3\text{Mo}_3\text{Q}_8(\text{CN})_6]^{n-}$ ($\text{Q}=\text{S}, \text{Se}$) by 4-*tert*-butylpyridine. Two new compounds, namely $[\text{Re}_3\text{Mo}_3\text{S}_8(\text{TBP})_6]$ (**1**) and $[\text{Re}_3\text{Mo}_3\text{Se}_8(\text{TBP})_6]$ (**2**), were obtained and crystallized in the solvothermal conditions in high yields. It has been shown that the compounds **1** and **2** are paramagnetic with *g*-values of 2.245 and 2.299, respectively. The geometry of new compounds has been investigated using an X-Ray structural analysis, and their electronic structure has been analyzed using DFT calculations. The X-Ray structural analysis revealed that the cluster cores in both structures are based on the nearly perfect metal octahedron, while the DFT calculations showed that the optimized geometry is strongly distorted. This research opens the way for the ligand exchange chemistry applied to the heterometallic clusters with the $\{\text{Re}_3\text{Mo}_3\text{Q}_8\}$ cores and functional pyridine-based ligands.

Experimental Section

Materials and methods. The starting salts $\text{CaK}_4[\text{Re}_3\text{Mo}_3\text{S}_8(\text{CN})_6]\cdot 8\text{H}_2\text{O}$ and $\text{K}_5[\text{Re}_3\text{Mo}_3\text{Se}_8(\text{CN})_6]\cdot 11\text{H}_2\text{O}$ were prepared as described.^[5c,d] Other reagents and solvents were purchased from commercial sources and used without further purification.

EPR spectra at 77 K were registered using a Bruker EMX EPR-spectrometer. FT-IR spectra in KBr pellets were recorded on a Bruker Scimitar FTS 2000 spectrometer in the range 4000–375 cm^{-1} . Energy dispersive spectroscopy (EDS) was performed on a JEOL JSM-7100F scanning electron microscope equipped with an EDS detector SDD X-Max 50mm² Oxford Instruments AZtecEnergy. Elemental analysis was performed with a Thermo Electron Microanalyser Flash EA1112 CHNS/O. Cyclic voltammetry was carried out on a Metrohm Computrace 797 VA voltammetry analyzer using three-electrode scheme with GC working, Pt auxiliary and Ag/AgCl reference electrodes. The investigations were carried out for $2.5\cdot 10^{-3}$ M solution of cluster salts in 0.1 M solution of Bu_4NClO_4 in CH_2Cl_2 under Ar atmosphere.

The single crystals of compounds **1** and **2** for diffraction studies were selected directly from the reaction mixtures. Diffraction data for **1** were collected at 296 K using a Bruker Nonius X8 Apex CCD diffractometer (graphite monochromated Mo- K_α radiation, $\lambda = 0.71073$ Å). The ϕ - and ω -scan techniques were employed to measure intensities. Absorption corrections were applied using the SADABS program.^[17] The crystal structure was solved by direct methods and refined by the full-matrix least squares techniques with the use of the SHELX package^[18] and OLEX2 GUI.^[19] The structure was refined as 2-component twin with twin law (0 1 0 1 0 0 0 -1), BASF 0.20. All non-hydrogen atoms were refined anisotropically. Atomic coordinates and atomic displacement parameters for pairs of disordered Mo and Re atoms were fixed to be the same using EXYZ and EADP constraints. Two disordered *tert*-butyl groups were refined with SADI, SIMU and DELU restraints. Hydrogen atoms were located geometrically and refined in rigid body approximation. Diffraction data for **2** were collected using a D8 VENTURE Bruker AXS diffractometer equipped with a (CMOS) PHOTON 100 detector, Mo- K_α radiation ($\lambda = 0.71073$ Å, multilayer monochromator). The structure was solved by dual-space algorithm using the SHELXT program,^[18] and then refined with full-matrix least-

squares methods based on F^2 (SHELXL).^[20] The contribution of the disordered solvents to the calculated structure factors was estimated following the Bypass algorithm^[21] implemented as the SQUEEZE option in PLATON.^[22] Large solvent accessible void with the volume of 571 Å³ was located at (-0.002 0.000 0.000) and containing 190 e⁻ was removed. *R*-factor before SQUEEZE was 0.0537. A new data set, free of solvent contribution, was then used in the final refinement. All non-hydrogen atoms were refined with anisotropic atomic displacement parameters. H atoms were finally included in their calculated positions and treated as riding on their parent atom with constrained thermal parameters. The crystal data collection and structure refinement conditions for **1** and **2** are summarized in Table 2. Selected interatomic distances are shown in Table 3.

Table 2. Summary of single-crystal data collections and structure refinement conditions of **1** and **2**.

| Compound | 1 | 2 |
|---|--|---|
| Chemical formula | $\text{C}_{54}\text{H}_{78}\text{Mo}_3\text{N}_6\text{Re}_3\text{S}_8$ | $\text{C}_{56}\text{H}_{81}\text{Mo}_3\text{N}_7\text{Re}_3\text{Se}_8$ |
| Formula weight | 1914.12 | 2330.37 |
| Space group | $P4_2/n$ | $P-1$ |
| <i>a</i> [Å] | 26.7541(6) | 14.431(2) |
| <i>b</i> [Å] | 26.7541(6) | 15.681(2) |
| <i>c</i> [Å] | 9.3946(3) | 18.758(2) |
| α [°] | 90 | 105.580(5) |
| β [°] | 90 | 103.786(5) |
| γ [°] | 90 | 98.813(5) |
| <i>V</i> [Å ³] | 6724.5(4) | 3862.3(8) |
| <i>Z</i> | 4 | 2 |
| Crystal size | 0.25×0.07×0.07 | 0.60×0.19×0.17 |
| λ [Å] | 0.71073 | 0.71073 |
| <i>T</i> [K] | 296(2) | 150(2) |
| ρ_{calc} [g/cm ³] | 1.891 | 2.004 |
| μ [mm ⁻¹] | 6.207 | 8.959 |
| Θ range [°] | 0.761 – 25.701 | 2.930 – 27.483 |
| Index range | -32 ≤ <i>h</i> ≤ 32 -32 ≤ <i>k</i> ≤ 31 -11 ≤ <i>l</i> ≤ 11 | -18 ≤ <i>h</i> ≤ 18 -20 ≤ <i>k</i> ≤ 20 -24 ≤ <i>l</i> ≤ 24 |
| Reflections collected | 54716 | 70201 |
| Unique reflections | 6401 | 17687 |
| Reflections observed | 5615 | 12717 |
| (<i>I</i> > 2 σ (<i>I</i>)) | | |
| <i>R</i> _{int} | 0.0613 | 0.0652 |
| Parameters refined | 400 | 678 |
| Restraints | 126 | 8 |
| GoF | 1.144 | 1.037 |
| <i>R</i> (<i>I</i> > 2 σ (<i>I</i>)) | 0.0390 | 0.0503 |
| <i>R</i> _w (<i>I</i> > 2 σ (<i>I</i>)) | 0.0730 | 0.1126 |
| $\Delta\rho_{\text{max}}, \Delta\rho_{\text{min}}$ [e Å ⁻³] | 1.198, -1.046 | 2.857, -2.924 |

Table 3. Selected interatomic distances in Å (range <average>) in the structures **1** and **2**.

| | 1 | 2 |
|-----|----------------------------------|------------------------------------|
| M–M | 2.6078(6) – 2.6157(6) <2.612> | 2.6316(6) – 2.6561(7) <2.640> |
| M–Q | 2.419(2) – 2.440(2) <2.430> | 2.5356(10) – 2.5570(10) <2.547> |
| M–N | 2.236(8) – 2.252(7) <2.246> | 2.223(8) – 2.261(8) <2.245> |

Synthesis of $[Re_3Mo_3S_8(TBP)_6]$ (1**).** Hydrothermal reaction of $CaK_4[Re_3Mo_3S_8(CN)_6] \cdot 8H_2O$ (60 mg, 0.038 mmol) and 4-tert-butylpyridine (300 μ L, 2.222 mmol) in 2 ml of a mixture of H_2O and CH_3CN (1:3 v/v) at 160 °C for 96 hours produced black rod-shaped crystals of **1**. The crystals were separated from the reaction mixture, washed with water, acetonitrile and dried in air. Yield: 50 mg (70%). EDS: Re / Mo / S = 2.8 : 3.2 : 8.3. IR (cm^{-1}): [py] 3092m, 3062s, 1598s, 1479s, 1441s, 1348m, 1232w, 1213s, 1146m, 1067s, 1039m, 1009m, 938w, 870w, 757s, 688s, 633w; [t-Bu] 2982s, 2909w, 1348m, 568w. Elemental analysis of $C_{54}H_{78}Mo_3N_6Re_3S_8$: calcd. (mass %) C 33.88, H 4.11, N 4.39, S 13.40; found C 34.03, H 4.20, N 4.45, S 13.31.

Synthesis of $[Re_3Mo_3Se_8(TBP)_6]$ (2**).** Compound **2** was synthesized using similar procedure as for **1**, except the use of $K_5[Re_3Mo_3Se_8(CN)_6] \cdot 11H_2O$ (60 mg, 0.030 mmol) as the starting compound. Yield: 40 mg (59%). EDS: Re / Mo / Se = 3.1 : 2.9 : 8.3. IR (cm^{-1}): [py] 3068vw 3037sh 1611s 1494m 1274m 1200vw 1226m 1067m 1019w 847sh 825m 748vw 725vw [t-Bu] 2962s 2901w 2868w 1413m 1365m 567m. Elemental analysis of $C_{54}H_{78}Mo_3N_6Re_3Se_8$: calcd. (mass %) C 28.33, H 3.43, N 3.67; found C 27.17 H 3.21, N 3.56.

Computational details. To simplify the quantum chemical calculations, the pyridine analogs of $[Re_3Mo_3Q_8(TBP)_6]$ (Q= S, Se) cluster complexes were used as a relevant approximation. Density functional theory (DFT) calculations were carried out for the clusters in *fac*- and *mer*- forms in ADF2017 program suit.^[23] Geometric parameters for the clusters were optimized with PW92 for LDA part of exchange-correlation functional, PBE for correlation correction and revPBE for exchange correction of GGA part of exchange-correlation functional^[24] and all-electron TZ2P basis set.^[25] The zero order regular approximation (ZORA) was used in all calculations in this work to take into account of the scalar relativistic effects.^[26] Effects of dichloromethane environment were added with Conductor like Screening Model (COSMO).^[27] All optimized structures have no imaginary frequencies.

Supplementary data

Crystallographic data for the structures of the title compounds have been deposited at the Cambridge Crystallographic Data Center under reference numbers CCDC 1896770 for **1** and CCDC 1896176 for **2**. Copies of this information may be obtained free of charge from the CCDC, 12 Union Road, Cambridge CB2 1EZ, UK (fax: +44 1223 336033; <http://www.ccdc.cam.ac.uk/conts/retrieving.html>).

Acknowledgments

V. Muravieva thanks the French Embassy for providing the scholarship for the co-tutelle PhD program between France and Russia. The authors greatly acknowledge the International Associate Laboratory No 1144 CLUSPOM between France and Russia. The authors also thank the "Centre de Diffractométrie X" (CDIFX) of the Institute of Chemical Science of Rennes for their single-crystal X-ray diffraction facilities. The author collective are acknowledged to Thierry Guizouarn for EPR measurements.

Keywords: cluster • ligand exchange • rhenium • molybdenum • electronic structure

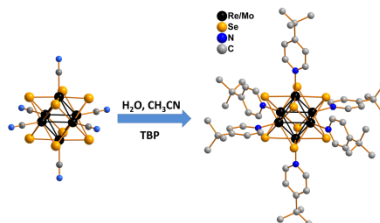
- a) S. Cordier, Y. Molard, K. A. Brylev, Y. V. Mironov, F. Grasset, B. Fabre, N. G. Naumov, *J. Clust. Sci.* **2014**, *26*, 53-81; b) S. Cordier, F. Grasset, Y. Molard, M. Amela-Cortes, R. Boukherroub, S. Ravaine, M. Mortier, N. Ohashi, N. Saito, H. Haneda, *J. Inorg. Organomet. Polym. Mater.* **2015**, *25*, 189; c) J.-C. P. Gabriel, K. Boubekeur, S. Uriel, P. Batail, *Chem. Rev.* **2001**, *101*, 2037-2066; d) A. A. Krasilnikova, M. A. Shestopalov, K. A. Brylev, I. A. Kirilova, O. P. Khripko, K. E. Zubareva, Y. I. Khripko, V. T. Podorognaya, L. V. Shestopalova, V. E. Fedorov, Y. V. Mironov, *J. Inorg. Biochem.* **2015**, *144*, 13-17.
- a) J. R. Long, L. S. McCarty, R. H. Holm, *J. Am. Chem. Soc.* **1996**, *118*, 4603-4616; b) J. R. Long, A. S. Williamson, R. H. Holm, *Angew. Chem., Int. Ed. Engl.* **1995**, *34*, 226-229; c) N. Prokopuk, D. F. Shriver, *Adv. Inorg. Chem.* **1999**, *46*, 1-49.
- a) Z. P. Zheng, J. R. Long, R. H. Holm, *J. Am. Chem. Soc.* **1997**, *119*, 2163-2171; b) P. J. Orto, G. S. Nichol, N. Okumura, D. H. Evans, R. Arratia-Perez, R. Ramirez-Tagle, R. Y. Wang, Z. P. Zheng, *Dalton Trans.* **2008**, 4247-4253; c) V. P. Fedin, A. A. Virovets, A. G. Sykes, *Inorg. Chim. Acta* **1998**, *271*, 228-230; d) Z. P. Zheng, X. Y. Tu, *CrystEngComm* **2009**, *11*, 707-719; e) M. N. Sokolov, M. A. Mihailov, E. V. Peresypkina, K. A. Brylev, N. Kitamura, V. P. Fedin, *Dalton Trans.* **2011**, *40*, 6375-6377; f) M. N. Sokolov, M. A. Mikhailov, K. A. Brylev, A. V. Virovets, C. Vicent, N. B. Kompankov, N. Kitamura, V. P. Fedin, *Inorg. Chem.* **2013**, *52*, 12477-12481.
- a) M. W. Willer, J. R. Long, C. C. McLauchlan, R. H. Holm, *Inorg. Chem.* **1998**, *37*, 328-333; b) Y. V. Mironov, K. A. Brylev, M. A. Shestopalov, S. S. Yarovoi, V. E. Fedorov, H. Spies, H. J. Pietzsch, H. Stephan, G. Geipel, G. Bernhard, W. Kraus, *Inorg. Chim. Acta* **2006**, *359*, 1129-1134; c) M. A. Shestopalov, Y. V. Mironov, K. A. Brylev, V. E. Fedorov, *Russ. Chem. Bull.* **2008**, *57*, 1644-1649; d) A. A. Ivanov, M. A. Shestopalov, K. A. Brylev, V. K. Khlestkin, Y. V. Mironov, *Polyhedron* **2014**, *81*, 634-638; e) M. A. Shestopalov, A. A. Ivanov, A. I. Smolentsev, Y. V. Mironov, *J. Struct. Chem. (Engl. Trans.)* **2014**, *55*, 139-141; f) M. A. Shestopalov, Y. V. Mironov, K. A. Brylev, S. G. Kozlova, V. E. Fedorov, H. Spies, H. J. Pietzsch, H. Stephan, G. Geipel, G. Bernhard, *J. Am. Chem. Soc.* **2007**, *129*, 3714-3721; g) L. F. Szczepura, D. L. Cedeno, D. B. Johnson, R. McDonald, S. A. Knott, K. M. Jeans, J. L. Durham, *Inorg. Chem.* **2010**, *49*, 11386-11394; h) T. Yoshimura, K. Umakoshi, Y. Sasaki, A. G. Sykes, *Inorg. Chem.* **1999**, *38*, 5557-5564.
- a) S. Cordier, N. Naumov, D. Salloum, F. Paul, C. Perrin, *Inorg. Chem.* **2004**, *43*, 219; b) N. G. Naumov, A. V. Virovets, V. E. Fedorov, *J. Struct. Chem. (Engl. Trans.)* **2000**, *41*, 499; c) V. K. Muravieva, Y. M. Gayfulin, M. R. Ryzhikov, I. N. Novozhilov, D. G. Samsonenko, D. A. Pirayez, V. Yanshole, N. G. Naumov, *Dalton Trans.* **2018**, *47*, 3366; d) Y. M. Gayfulin, N. G. Naumov, M. R. Ryzhikov, A. I. Smolentsev, V. A. Nadolnny, Y. V. Mironov, *Chem. Commun.* **2013**, *49*, 10019.

- [6] E. V. Alexandrov, A. V. Virovets, V. A. Blatov, E. V. Peresyphkina, *Chem. Rev.* **2015**, *115*, 12286-12319.
- [7] a) W. P. Fehlhammer, M. Fritz, *Chem. Rev.* **1993**, *93*, 1243-1280; b) C. Janiak, T. Dorn, H. Paulsen, B. Wrackmeyer, *Z. Anorg. Allg. Chem.* **2001**, *627*, 1663-1668; c) A. Žmikić, D. Cvrtić, D. Pavlović, I. Murati, W. Reynolds, S. Ašperger, *J. Chem. Soc., Dalton. Trans.* **1973**, 1284-1286; d) R. M. Naik, J. Sarkar, S. Prasad, *Microchem. J.* **2008**, *88*, 45-51; e) J. R. de Sousa, I. C. N. Diógenes, M. L. A. Temperini, F. A. M. Sales, S. d. O. Pinheiro, R. N. Costa Filho, J. S. de Andrade Júnior, Í. d. S. Moreira, *J. Organomet. Chem.* **2007**, *692*, 3691-3699; f) L. D. Slep, P. Alborés, L. M. Baraldo, J. A. Olabe, *Inorg. Chem.* **2002**, *41*, 114-120.
- [8] a) T. V. Larina, V. N. Ikorskii, N. T. Vasenin, V. F. Anufrienko, N. G. Naumov, E. V. Ostanina, V. E. Fedorov, *Russ. J. Coord. Chem.* **2002**, *28*, 554-556; b) C. Guilbaud, A. Deluzet, B. Domercq, P. Molinie, C. Coulon, K. Boubekeur, P. Batail, *Chem. Commun.* **1999**, 1867-1868.
- [9] C. Magliocchi, X. Xie, T. Hughbanks, *Inorg. Chem.* **2000**, *39*, 5000-5001.
- [10] N. G. Naumov, E. V. Ostanina, A. V. Virovets, M. Schmidtman, A. Müller, V. E. Fedorov, *Russ. Chem. Bull.* **2002**, *51*, 866-871.
- [11] F. Le Berre, O. Peña, C. Perrin, M. Sergent, R. Horyń, A. Wojakowski, *J. Solid State Chem.* **1998**, *136*, 151-159.
- [12] O. Peña, R. Horyn, M. Potel, J. Padiou, M. Sergent, *J. Less Common Met.* **1985**, *105*, 105-117.
- [13] a) F. Dorson, Y. Molard, S. Cordier, B. Fabre, O. Efremova, D. Rondeau, Y. Mironov, V. Cîrcu, N. Naumov, C. Perrin, *Dalton Trans.* **2009**, 1297-1299; b) Z. Zheng, T. G. Gray, R. H. Holm, *Inorg. Chem.* **1999**, *38*, 4888-4895; c) A. Y. Ledneva, N. G. Naumov, A. V. Virovets, S. Cordier, Y. Molard, *J. Struct. Chem. (Engl. Trans.)* **2012**, *53*, 132-137.
- [14] a) S. Jin, F. Popp, S. W. Boettcher, M. Yuan, C. M. Oertel, F. J. DiSalvo, *J. Chem. Soc., Dalton. Trans.* **2002**, 3096-3100; b) S. J. Hilsenbeck, V. G. Young, R. E. McCarley, *Inorg. Chem.* **1994**, *33*, 1822-1832.
- [15] T. Yoshimura, C. Suo, K. Tsuge, S. Ishizaka, K. Nozaki, Y. Sasaki, N. Kitamura, A. Shinohara, *Inorg. Chem.* **2010**, *49*, 531-540.
- [16] a) S.A. Baudron, A. Deluzet, K. Boubekeur, P. Batail, *Chem. Commun.* **2002**, 2124-2125; b) E. A. Deluzet, H. Duclaud, P. Sautet, S.A. Borshch, *Inorg. Chem.* **2002**, *41*, 2537-2542; c) T.G. Gray, C.M. Rudzinski, E.E. Meyer, D.G. Nocera, *J. Phys. Chem. A* **2004**, *108*, 3238-3243.
- [17] Bruker AXS Inc., APEX2 (Version 2.0), SAINT (Version 8.18c), and SADABS (Version 2.11), Bruker Advanced X-ray Solutions, Madison, Wisconsin, USA, 2000-2012.
- [18] G. M. Sheldrick, *Acta Crystallogr., Sect. A: Found. Adv.* **2015**, *71*, 3-8.
- [19] O. V. Dolomanov, L. J. Bourhis, R. J. Gildea, J. A. K. Howard, H. Puschmann, *J. Appl. Cryst.* **2009**, *42*, 339-341.
- [20] G. M. Sheldrick, *Acta Crystallogr., Sect. C: Struct. Chem.* **2015**, *71*, 3-8.
- [21] P. Vandersluijs, A. L. Spek, *Acta Crystallogr., Sect. A: Found. Crystallogr.* **1990**, *46*, 194-201.
- [22] A. L. Spek, *J. Appl. Cryst.* **2003**, *36*, 7-13.
- [23] a) ADF2012, SCM, Theoretical Chemistry, Vrije Universiteit, Amsterdam, The Netherlands, <http://www.scm.com>; b) G. te Velde, F. M. Bickelhaupt, E. J. Baerends, C. F. Guerra, S. J. A. Van Gisbergen, J. G. Snijders, T. Ziegler, *J. Comput. Chem.* **2001**, *22*, 931-967.
- [24] a) Y. K. Zhang, W. T. Yang, *Phys. Rev. Lett.* **1998**, *80*, 890-890; b) J. P. Perdew, K. Burke, M. Ernzerhof, *Phys. Rev. Lett.* **1996**, *77*, 3865-3868.
- [25] E. Van Lenthe, E. J. Baerends, *J. Comput. Chem.* **2003**, *24*, 1142-1156.
- [26] E. van Lenthe, A. Ehlers, E. J. Baerends, *J. Chem. Phys.* **1999**, *110*, 8943-8953.
- [27] C. C. Pye, T. Ziegler, *Theor. Chem. Acc.* **1999**, *101*, 396-408.

Entry for the Table of Contents (Please choose one layout)

FULL PAPER

Reaction of $[\text{Re}_3\text{Mo}_3\text{Q}_8(\text{CN})_6]^{n-}$ ($\text{Q} = \text{S}, n = 6$; $\text{Q} = \text{Se}, n = 5$) complexes with the 4-*tert*-butylpyridine (TBP) leads to complete substitution of coordinated cyano-ligands and formation of two new heterometallic complexes $[\text{Re}_3\text{Mo}_3\text{Q}_8(\text{TBP})_6]$ ($\text{Q} = \text{S}, \text{Se}$) obtained with high yields. DFT calculations shows a large distortion of M_6 metal cores in complexes.



Cluster Reactivity

Viktoria K. Muravieva, Yakov M. Gayfulin, Tatiana I. Lappi, Vincent Dorcet, Taisiya S. Sukhikh, Pierrick Lemoine, Maxim R. Ryzhikov, Yuri V. Mironov, Stéphane Cordier, Nikolay G. Naumov*

Page No. – Page No.

Apical cyanide ligands substitution
in heterometallic clusters
 $[\text{Re}_3\text{Mo}_3\text{Q}_8(\text{CN})_6]^{n-}$ ($\text{Q} = \text{S}, \text{Se}$)

**CRYSTAL STRUCTURE OF LAYERED CYANO-BRIDGED
COORDINATION POLYMERS $[M(NH_3)_6]_4[\{M(NH_3)_2\}\{Re_3Mo_3Se_8(CN)_6\}_2] \cdot 15H_2O$ ($M = Co, Ni$)**

V. K. Muravieva^{1,2}, P. Lemoine², S. Cordier²,
and N. G. Naumov^{1,3}

Two isostructural compounds of the composition $[M(NH_3)_6]_4[\{M(NH_3)_2\}\{Re_3Mo_3Se_8(CN)_6\}_2] \cdot 15H_2O$ ($M = Co, Ni$) are obtained by a reaction of a salt of heterometal cluster $[Re_3Mo_3Se_8(CN)_6]^{5-}$ anion with cobalt or nickel salts in an aqueous ammonia solution. The obtained compounds are structurally characterized. They correspond to the class of cyano-bridged coordination polymers. Two cyano groups of the octahedral cluster in the *trans* position form bridging bonds with Co(II) and Ni(II) cations. The obtained compounds are composed of highly charged polymeric $[\{M(NH_3)_2\}\{Re_3Mo_3Se_8(CN)_6\}_2]_{\infty}^{8-}$ layers formed by cluster anions and metal cations. The negative charge of the layers is compensated by $[M(NH_3)_6]^{2+}$ cationic complexes inside the polymeric layer and in the interstitial space of the structure.

DOI: 10.1134/S002247661901013X

Keywords: heterometal cluster, rhenium, molybdenum, coordination polymers, crystal structure.

Octahedral chalcogenide cluster complexes $[M_6Q_8(CN)_6]^{n-}$ ($M = Mo, Re$; $Q = S, Se, Te$) have been widely used as building blocks for designing various functional materials [1-4]. The ability of cyanide ligands to coordinate transition and post-transition metal cations provides the formation of poorly soluble polymeric solids with $M-CN-M'$ bridging coordination bonds. A large number of these coordination polymers with different structures have been obtained [5, 6]. Cluster $[M_6Q_8(CN)_6]^{n-}$ anions have the same topology and similar linear and volume characteristics, with the charge of the cluster anion depending on the nature of metal atoms in the metal cluster and the number of cluster skeletal electrons. The ratio of metal cation and cluster anion charges can appreciably affect the charge of obtained frameworks and the type of structure connectivity. Thus, a number of polymer structures based on the highly charged $[Mo_6Se_8(CN)_6]^{7-}$ anion and manganese(II) cations demonstrates a high negative charge of the framework, e.g. a three-dimensional $[\{Mn(H_2O)_2\}_3\{Mo_6Se_8(CN)_6\}_2]_{\infty}^{8-}$ network in the $(Me_4N)_8[\{Mn(H_2O)_2\}_3\{Mo_6Se_8(CN)_6\}_2] \cdot 4H_2O$ structure [7]. Rhenium cyanometalates $[Re_6Q_8(CN)_6]^{4-}$ ($Q = S, Se, Te$) have a lower charge, and generally, form low-charged or neutral polymer networks [8-11]. The heterometal cluster $[Re_3Mo_3Se_8(CN)_6]^{5-}$ obtained recently has the electronic structure and anion charge not typical of homometal analogues [12]. Unusual positively charged frameworks $[\{Cd(NH_3)_4\}_3\{Re_3Mo_3Se_8(CN)_6\}]X$ ($X = Cl, Br, I$) were obtained based on this anion and cadmium cations. These frameworks demonstrate a high thermal stability and promising redox properties [13].

¹Nikolaev Institute of Inorganic Chemistry, Siberian Branch, Russian Academy of Sciences, Novosibirsk, Russia; muravyeva@niic.nsc.ru. ²University of Rennes-1, Institute of Chemical Sciences, Rennes, France. ³Novosibirsk State University, Russia. Translated from *Zhurnal Strukturnoi Khimii*, Vol. 60, No. 1, pp. 106-113, January, 2019. Original article submitted August 16, 2018; revised August 27, 2018; accepted September 03, 2018.

Attempts to synthesize similar compounds from other transition metals resulted in the formation of compounds with another structure. In this work we report the synthesis of novel isostructural coordination polymers based on the heterometal $[\text{Re}_3\text{Mo}_3\text{Se}_8(\text{CN})_6]^{5-}$ cluster and Co(II) and Ni(II) cations. The obtained polymers are composed of highly charged layers of the composition $[\{\text{M}(\text{NH}_3)_2\}\{\text{Re}_3\text{Mo}_3\text{Se}_8(\text{CN})_6\}_2]_{\infty}^{8-}$. The negative charge is compensated by $[\text{M}(\text{NH}_3)_6]^{2+}$ cation complexes inside the polymer layer and in the interlayer space of the structure.

EXPERIMENTAL

Initial cluster salt $\text{K}_5[\text{Re}_3\text{Mo}_3\text{Se}_8(\text{CN})_6] \cdot 11\text{H}_2\text{O}$ was obtained by the previously reported procedure [12]. The other reagents were purchased from commercial sources and used without additional purification. The ratio of heavy elements in the obtained crystals was determined by energy dispersive X-ray analysis in the Hitachi TM-3000 electron microscope with a Bruker Nano EDS analyzer.

X-ray crystallographic analysis. Experimental data were obtained on a D8 VENTURE Bruker AXS diffractometer equipped with a (CMOS) PHOTON 100 detector, $\lambda = 0.71073 \text{ \AA}$ (MoK_α radiation). The structures were solved by a direct method using the SIR97 program [14] and refined by the full-matrix least squares technique in the anisotropic approximation using the SHELXL program package [15]. All non-hydrogen atoms were refined with anisotropic atomic displacement parameters. Hydrogen atoms of ammonia molecules were placed in geometrically calculated positions and refined in the riding model with dependent isotropic thermal parameters. Hydrogen atoms of water molecules were not localized. Crystallographic data and characteristics of diffraction experiments for compounds **1** and **2** are summarized in Table 1.

TABLE 1. Crystallographic Data and Characteristics of Diffraction Experiments for Compounds **1** and **2**

| Parameter | 1 | 2 |
|---|--|---|
| Chemical formula | $\text{C}_{12}\text{H}_{78}\text{Co}_3\text{Mo}_6\text{N}_{38}\text{Re}_6\text{Se}_{16}$ | $\text{C}_{12}\text{H}_{78}\text{Mo}_6\text{N}_{38}\text{Ni}_5\text{O}_{15}\text{Re}_6\text{Se}_{16}$ |
| Molecular weight, g/mol | 4005.97 | 4244.87 |
| Crystal symmetry, space group | Triclinic, $P\bar{1}$ | Triclinic, $P\bar{1}$ |
| Cell parameters ($a, b, c, \text{\AA}$; $\alpha, \beta, \gamma, \text{deg}$) | 14.5327(10), 14.5343(9), 14.9987(10); 115.259(3), 118.858(3), 92.755(3) | 14.5884(11), 14.6083(10), 14.9941(11); 115.186(3), 118.526(3), 92.364(3) |
| Volume, \AA^3 | 2376.8(3) | 2417.5(3) |
| Temperature, K | 150(2) | 150(2) |
| Z | 1 | 1 |
| Calculated density, g/cm^3 | 2.799 | 2.916 |
| Absorption coefficient, mm^{-1} | 15.371 | 15.248 |
| $F(000)$ | 1797 | 1922 |
| Crystal dimensions, mm | 0.095×0.065×0.035 | 0.080×0.050×0.030 |
| θ range, deg | 2.998–27.522 | 2.965–27.508 |
| Limiting Miller indices | $-18 \leq h \leq 18, -18 \leq k \leq 18,$ $-19 \leq l \leq 19$ | $-18 \leq h \leq 18, -18 \leq k \leq 18,$ $-19 \leq l \leq 19$ |
| Number of meas. / indep. reflections | 29256 / 10904 | 57212 / 11084 |
| $R(\text{int})$ | 0.0370 | 0.0502 |
| $GOOF$ | 1.036 | 1.036 |
| R for $I > 2\sigma(I)$ | $R_1 = 0.0389,$ $wR_2 = 0.0888$ | $R_1 = 0.0253$ $wR_2 = 0.0465$ |
| R for all reflections | $R_1 = 0.0572$ $wR_2 = 0.0974$ | $R_1 = 0.0412$ $wR_2 = 0.0508$ |
| Residual electron density max /min, e/\AA^3 | 1.661 / –2.912 | 1.799 / –0.946 |

Atomic coordinates and thermal parameters have been deposited with the Inorganic Crystal Structure Database (**1** CSD 434766, **2** CSD 434765) and can be received from Fachinformationszentrum Karlsruhe, 76344 Eggenstein-Leopoldshafen, Germany (fax: (+49)7247-808-666; e-mail: crysdata@fiz-karlsruhe.de, http://www.fiz-karlsruhe.de/request_for_deposited_data.html).

Preparation of $[\text{Co}(\text{NH}_3)_6]_4[\{\text{Co}(\text{NH}_3)_2\}\{\text{Re}_3\text{Mo}_3\text{Se}_8(\text{CN})_6\}_2]\cdot 15\text{H}_2\text{O}$ (1**).** 2 ml of an aqueous ammonia solution containing 7.0 mg of $\text{CoCl}_2\cdot 6\text{H}_2\text{O}$ (0.03 mmol) with an ammonia concentration of 12 wt.% was layered on 2 ml of an aqueous ammonia solution of $\text{K}_5[\text{Re}_3\text{Mo}_3\text{Se}_8(\text{CN})_6]\cdot 11\text{H}_2\text{O}$ (12.0 mg, 0.006 mmol) (6 wt.% of ammonia) in a thin glass tube with a constriction. The tube was tightly closed and left at room temperature for a week. During this time crystals of compound **1** grew on the tube walls. Crystals for the X-ray crystallographic studies were selected from the mother liquor directly before the measurement. According to the results of the energy dispersive analysis, the ratio of heavy elements for compound **1** was Co:Re:Mo:Se 2.6:3.1:2.9:8.3.

Preparation of $[\text{Ni}(\text{NH}_3)_6]_4[\{\text{Ni}(\text{NH}_3)_2\}\{\text{Re}_3\text{Mo}_3\text{Se}_8(\text{CN})_6\}_2]\cdot 15\text{H}_2\text{O}$ (2**).** Compound **2** with nickel was obtained similarly to **1** with the use of an aqueous ammonia solution containing 8.0 mg of $\text{NiCl}_2\cdot 6\text{H}_2\text{O}$ (0.03 mmol). Crystals for the X-ray crystallographic measurements were selected from the mother liquor directly before the measurement. According to the results of the energy dispersive analysis, the ratio of heavy elements for compound **2** was Ni:Re:Mo:Se 2.7:3.1:2.9:8.2.

RESULTS AND DISCUSSION

The first experiments on studying the preparation reactions of coordination polymers based on the heterometal $[\text{Re}_3\text{Mo}_3\text{Se}_8(\text{CN})_6]^{5-}$ cluster have shown that the mixing of aqueous solutions of the $\text{K}_5[\text{Re}_3\text{Mo}_3\text{Se}_8(\text{CN})_6]\cdot 11\text{H}_2\text{O}$ salt and transition metal salts resulted in a rapid formation of an amorphous precipitate even at very low concentration of reagents in the solutions used. This experimental fact seems to be due to the competition between water molecules in the metal coordination sphere of $[\text{M}(\text{H}_2\text{O})_6]^{n+}$ aqua complexes and the nitrogen atom of the cyano group of the cluster that occurs in favor of cyano groups, which leads to the formation of an insoluble amorphous precipitate containing a large number of bridging M–CN–M' bonds per anion.

The use of stable transition metal complexes $[\text{ML}_n]^{2+}$ (where L = NH_3 ; ethylenediamine (en); diethylenediamine (dien); 1,2S,3S,4-tetraaminobutane (threo-tab); *bis*(salicylidene) ethylenediamine (salen) and others) in these reactions enables the crystallization of a compound with a polymeric structure, and a decrease in the number of M–CN–M' bonds per metal atom generally results in the formation of low-dimensional structures (layered, chain, or discrete molecular structures) [16–19]. It is shown that the use of aqueous ammonia solutions of cadmium salts allows the preparation of first coordination polymers based on the cluster $[\text{Re}_3\text{Mo}_3\text{Se}_8(\text{CN})_6]^{5-}$ anion with the composition $[\{\text{Cd}(\text{NH}_3)_4\}_3\{\text{Re}_3\text{Mo}_3\text{Se}_8(\text{CN})_6\}]\text{X}$ (X = Cl, Br, I). The obtained polymeric frameworks were positively charged, with the structure containing halide anions (Cl^- , Br^- , I^-) forming hydrogen bonds with ammonia molecules [13].

The application of aqueous ammonia solutions of cobalt and nickel salts in reactions with the $\text{K}_5[\text{Re}_3\text{Mo}_3\text{Se}_8(\text{CN})_6]\cdot 11\text{H}_2\text{O}$ cluster anion salt under similar conditions did not yield compounds analogous to the previously obtained cadmium ones. Under the conditions described in EXPERIMENTAL two isostructural compounds with the composition $[\text{M}(\text{NH}_3)_6]_4[\{\text{M}(\text{NH}_3)_2\}\{\text{Re}_3\text{Mo}_3\text{Se}_8(\text{CN})_6\}_2]\cdot 15\text{H}_2\text{O}$ (M = Co (**1**), Ni (**2**)) were obtained. Compounds **1** and **2** have a layered structure. The structure of the obtained compounds is exemplified by compound **1**. The asymmetric unit of a cell of compound **1** contains atoms belonging to two crystallographically independent $[\text{Re}_3\text{Mo}_3\text{Se}_8(\text{CN})_6]^{5-}$ cluster anions. The $[\text{Re}_3\text{Mo}_3\text{Se}_8(\text{CN})_6]^{5-}$ anions have a structure typical of octahedral clusters $[\text{M}_6\text{Q}_8\text{L}_6]$ (Fig. 1). The metal core $\{\text{Re}_3\text{Mo}_3\}$ consisting of molybdenum and rhenium atoms has the shape of a distorted octahedron at which faces inner selenide ligands $\mu_3\text{-Se}$ are coordinated. Each metal atom is additionally coordinated by the apical CN ligand.

The obtained structures as well as all previously published with heterometal cluster cores $\{\text{Re}_3\text{Mo}_3\text{Q}_8\}$ (Q = S, Se) are characterized by disordering of metal atoms in the cluster core. In the obtained structures, rhenium and molybdenum

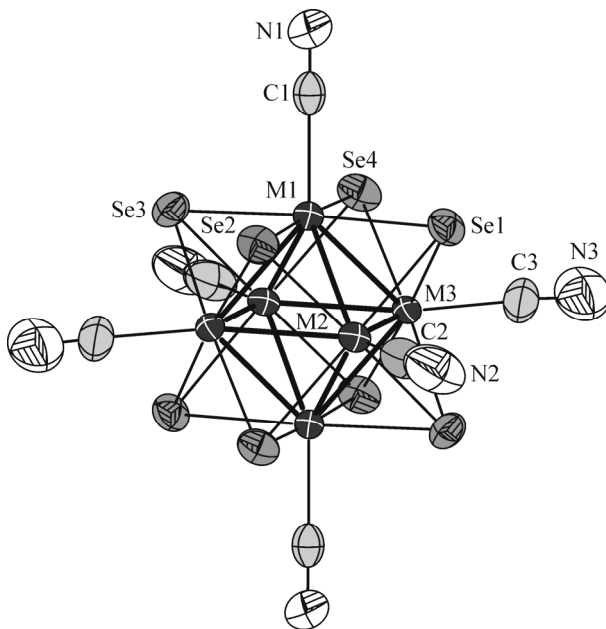


Fig. 1. Structure of the cluster $[\text{Re}_3\text{Mo}_3\text{Se}_8(\text{CN})_6]^{5-}$ anion in compound **1** in the model of ellipsoids with a 75% probability.

atoms share the same positions M1–M6. Occupancies of the obtained positions are close to 0.5; and total occupancies of metal positions result in the 1:1 ratio between rhenium and molybdenum in the cluster core. Metal positions M1–M3, four selenium atoms Se1–Se4, and three cyano groups formed by C1–C3, N1–N3 atoms belong to the first anion; and M4–M6, Se5–Se8, C4–C6, and N4–N6 atoms belong to the second anion respectively. All atoms forming cluster anions take general positions. The geometric centers of the anions coincide with the centers of inversion with coordinates (0 0 0) and (0.5 0.5 0). Thus, in the structure of **1** the cluster anions are located at the vertices and the center of the *C* face of the unit cell. The cationic part of the asymmetric unit is composed of five cobalt(II) atoms Co1–Co5 located at special positions with the $\bar{1}$ symmetry. The Co1 atom coordinates four cyano groups of the cluster through nitrogen atoms, forming square nodes $[\text{Co}(\text{NC})_4]$ determining the binding of the polymeric layer. Co1 is additionally coordinated by two ammonia molecules in the *trans* position. The coordination environment of the Co1 atom is a *trans*- $[\text{Co}(\text{NC})_4(\text{NH}_3)_2]$ octahedron (Fig. 2*a*). Cluster anions in the obtained structures serve as linear linkers being bonded to Co^{2+} cations via two cyano groups in the *trans*-position. Polymeric layers with the composition $[\{\text{Co}(\text{NH}_3)_2\}\{\text{Re}_3\text{Mo}_3\text{Se}_8(\text{CN})_6\}_2]_{\infty}^{8-}$ in compound **1** are distorted four-connected networks with the *sql* topology [20], which are formed by cluster anions and cobalt (Co1) cations (Fig. 3*a*). The cobalt atoms of the independent Co2–Co5 fragment are in the octahedral environment of ammonia molecules and form isolated $[\text{Co}(\text{NH}_3)_6]^{2+}$ cationic complexes (Fig. 2*b*) that compensate an excess negative charge of the polymeric layer. These complexes are located in the square network cavities and also in the interlayer space of the structure (Fig. 3*a, b*).

Interatomic distances in the structures of **1** and **2** are listed in Tables 2 and 3. In the cluster anions of structures **1** and **2** the M–M, M–Se, and M–C bond lengths are close to those found previously for the other compounds containing a heterometal $[\text{Re}_3\text{Mo}_3\text{Se}_8(\text{CN})_6]^n$ cluster anion (Table 2). The interatomic M–N_C distances obtained and bond angles of C–N–M bonds (M = Co, Ni, Table 3) are consistent with the literature data on polymeric compounds based on $[\text{Re}_6\text{Q}_8(\text{CN})_6]$ clusters and Co^{2+} and Ni^{2+} (2.16(1) Å and 168(1)° for $\text{Cs}_2\text{Co}[\text{Re}_6\text{Se}_8(\text{CN})_6]\cdot 2\text{H}_2\text{O}$ [21], 2.10(2) Å and 166(2)° for $(\text{Me}_4\text{N})_2[\{\text{Co}(\text{H}_2\text{O})_{1.5}\}_3\{\text{Re}_6\text{Se}_8(\text{CN})_6\}_2]\cdot \text{H}_2\text{O}$ [8]; 2.05(1) Å and 170(2)° for $(\text{Et}_4\text{N})_2[\{\text{Ni}(\text{H}_2\text{O})_2\}_3\{\text{Re}_6\text{S}_8(\text{CN})_6\}_2]\cdot 6.5\text{H}_2\text{O}$ [8]; 2.10(2) Å and 180° for $\text{Ni}_3[\text{Re}_6\text{Se}_8(\text{CN})_6]_2\cdot 33\text{H}_2\text{O}$ [11]). Isostructural compounds **1** and **2** contained cavities between the polymeric layers filled with water molecules. For compound **2** the quality of the crystal allowed us to localize water molecules in the cavities. Fifteen water molecules per unit cell were found. Water molecules in the cavities of compound **1**

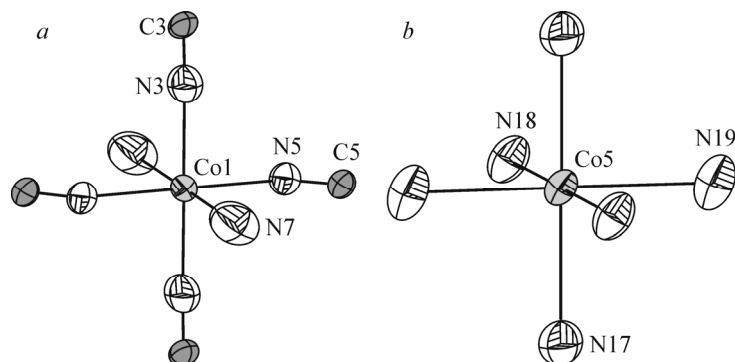


Fig. 2. Coordination environment of cobalt cations in the structure of **1** in the model of ellipsoids with a 50% probability. The cobalt atom of the polymeric layer $[\text{Co}(\text{NC})_4(\text{NH}_3)_2]$ (a), cationic complex $[\text{Co}(\text{NH}_3)_6]^{2+}$ (b), hydrogen atoms are omitted.

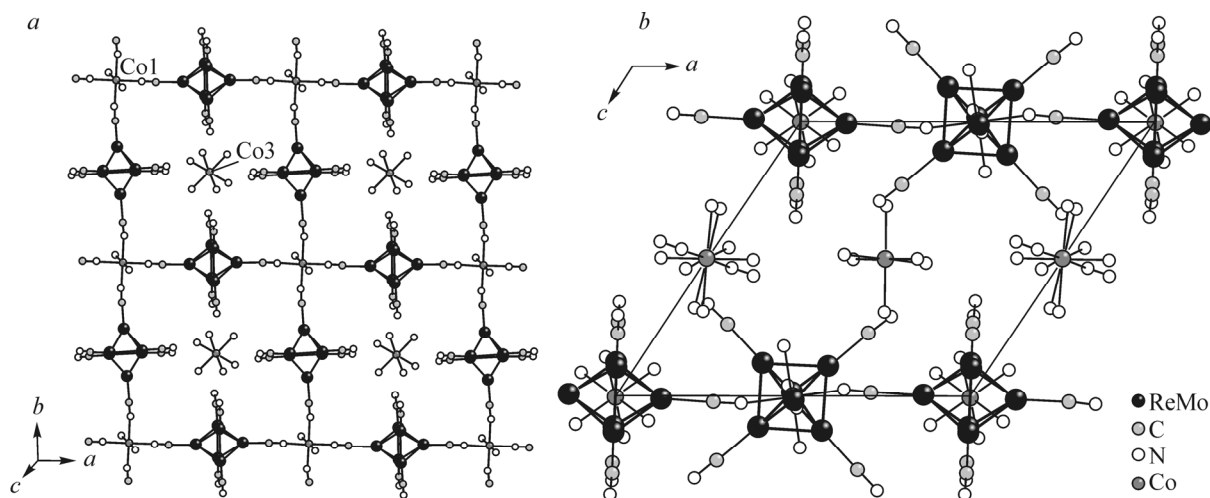


Fig. 3. Structure of compound **1**: topology of the polymeric layer in the structure of **1** (a), layer packing in the structure along the b axis (b). Selenium and hydrogen atoms and solvate water molecules are not shown.

turned out to be strongly disordered which made it impossible to localize them. The disordered electron density was removed from the cavities of structure **1** using the SQUEEZE procedure [22] of the PLATON program [23]. From the results of the SQUEEZE procedure cavities with a total volume of 436 \AA^3 and containing $159 e^-$ were found, which sufficiently well agrees with the number of solvate molecules in structure **2**. Before the removal of the disordered electron density the R -factor of structure **1** was 0.0433. Obtained coordination polymers **1** and **2** proved to be unstable in air. Partial loss of water and ammonia molecules caused the complete loss of crystallinity in the samples of compounds **1** and **2**.

Four-connected networks with the topology sql occur among mononuclear cyanometalate polymers, e.g., in $A[\text{Ag}_2\text{Cu}(\text{CN})_4]$, where $A = \text{K}, \text{Rb}, \text{Cs}$ [24]. For octahedral cluster cyanometalates this type of binding of polymeric networks is rare. The layer connectivity similar to that found for compounds **1** and **2** has been known for cluster coordination polymers with rare-earth metal cations $\text{Cs}_5[\{\text{Ln}(\text{H}_2\text{O})_4(\text{C}_2\text{H}_6\text{O})\}\{\text{Re}_6\text{Se}_8(\text{CN})_6\}_2] \cdot 2\text{H}_2\text{O}$ ($\text{Ln} = \text{La}, \text{Nd}$) [25]. However, in these structures the polymeric networks have a smaller charge as compared to those in **1** and **2**, which is due to a lower charge of the initial cluster anion.

Other layered compounds have been known among cluster cyanometalates. Thus, compounds with the composition $\text{Cs}_2\text{M}[\text{Re}_6\text{S}_8(\text{CN})_6] \cdot 2\text{H}_2\text{O}$ are formed by corrugated $[\{\text{Co}(\text{H}_2\text{O})_2\}\{\text{Re}_6\text{S}_8(\text{CN})_6\}]_{\infty}^{2-}$ layers where both cluster and metal cation form four-connected nodes of the square network [21]. The layered structure of the topology hcb was detected for the compound $[\{\text{Mn}(\text{H}_2\text{O})_3\}_2\{\text{Re}_6\text{Se}_8(\text{CN})_6\}] \cdot 3.3\text{H}_2\text{O}$, where two manganese cations form a node of the three-connected network

TABLE 2. Bond Lengths (min–max, ⟨average⟩) in Compounds **1** and **2** in Comparison with the Literature Data

| Compound | M*–M | M–Q | M–C | Reference |
|--|-------------------------------------|-------------------------------------|----------------------------------|-------------|
| CaK ₄ [Re ₃ Mo ₃ Se ₈ (CN) ₆] \cdot 8H ₂ O | 2.6273(8) | 2.439(2) | 2.173(13) | [29] |
| K ₅ [Re ₃ Mo ₃ Se ₈ (CN) ₆] \cdot 11H ₂ O | 2.6494(9) | 2.5464(9) | 2.14(2) | [12] |
| Cs ₅ [Re ₃ Mo ₃ Se ₈ (CN) ₆] \cdot H ₂ O | 2.6451(9)- 2.6459(9) ⟨2.645⟩ | 2.541(1)- 2.549(1) ⟨2.54⟩ | 2.157(11) | |
| (Ph ₄ P) ₄ [Re ₃ Mo ₃ Se ₈ (CN) ₆] \cdot 2CH ₃ CN | 2.6407(2)- 2.6619(2) ⟨2.654⟩ | 2.5197(3)- 2.5463(3) ⟨2.539⟩ | 2.164(3)- 2.171(3) ⟨2.17⟩ | |
| {[Cd(NH ₃) ₅] ₂ [Cd(NH ₃) ₄] ₃ [Re ₃ Mo ₃ Se ₈ (CN) ₆] ₂ } \cdot 5H ₂ O | 2.631(1)- 2.684(1) ⟨2.654⟩ | 2.527(2)- 2.564(2) ⟨2.547⟩ | 2.10(2)- 2.20(2) ⟨2.14⟩ | [13] |
| {[Cd(NH ₃) ₄] ₃ [Re ₃ Mo ₃ Se ₈ (CN) ₆]}Cl | 2.6465(5)- 2.6498(5) ⟨2.648⟩ | 2.5439(7)- 2.5475(9) ⟨2.545⟩ | 2.146(6) | |
| 1 | 2.6240(7)- 2.6802(7) ⟨2.6511⟩ | 2.5311(10)- 2.5629(9) ⟨2.549⟩ | 2.149(10)- 2.178(9) ⟨2.16⟩ | [This work] |
| 2 | 2.6224(4)- 2.6664(4) ⟨2.6465⟩ | 2.5308(6)- 2.5649(6) ⟨2.5495⟩ | 2.142(6)- 2.169(6) ⟨2.156⟩ | |

* M = Re, Mo.

TABLE 3. Bond Lengths (min–max, ⟨average⟩) and Bond Angles in the Complex Cations of Compounds **1** and **2**

| Bond | 1 | 2 |
|-------------------|----------------------------|----------------------------|
| | <i>d</i> , Å | |
| M*–N _C | 2.119(11)-2.144(9), ⟨2.13⟩ | 2.088(4)-2.109(4), ⟨2.098⟩ |
| M–N _{H3} | 2.127(10)-2.188(8), ⟨2.17⟩ | 2.094(5)-2.157(5), ⟨2.135⟩ |
| Angles | ω , deg | |
| C–N–M | 169.1(10), 169.3(10) | 168.2(5), 172.9(4) |

* M = Co, Ni.

with the composition $[\{Mn(H_2O)_3\}_4\{Re_6Se_8(CN)_6\}_3]$ [26]. Some compounds based on $[Re_6Se_8(CN)_6]^{4-}$ and $[SnMe_3]^+$ trimethyl tin cations also demonstrate layered structures. For instance, in $[(SnMe_2)_4(\mu_3-O)_2(\mu_2-OH)_2(H_2O)_2][\{SnMe_3\}_2\{Re_6Se_8(CN)_6\}]$ and $[(Me_3Sn)_3(OH)_2][\{Me_3Sn\}_3\{Re_6Se_8(CN)_6\}]_3$ compounds the cluster complex forms four-connected nodes of the polymeric layer [27, 28].

Thus, in this work, we obtained novel layered coordination polymers $[M(NH_3)_6]_4[\{M(NH_3)_2\}\{Re_3Mo_3Se_8(CN)_6\}_2]\cdot 15H_2O$ (M = Co (**1**), Ni (**2**)) based on heterometal cluster cyanometalate $[Re_3Mo_3Se_8(CN)_6]^{5-}$ and cobalt and nickel cations. The polymers obtained are composed of two-dimensional layers $[\{M(NH_3)_2\}\{Re_3Mo_3Se_8(CN)_6\}_2]_{\infty}^{8-}$ of the *sql* topology. These polymeric networks demonstrate a high negative charge compensated by complex $[M(NH_3)_6]^{2+}$ cations.

The authors are grateful to International Associate Laboratory N°1144 CLUSPOM between France and Russia and Centre de Diffractométrie X, Université de Rennes I for diffraction studies of single crystals.

V. Muravieva thanks the French Embassy for granting the scholarship for the co-tutelle PhD program between France and Russia.

The work was supported by RFBR (grant No. 17-53-16015).

REFERENCES

1. Y. Molard, A. Ledneva, M. Amela-Cortes, V. Circu, N. G. Naumov, C. Meriadec, F. Artzner, and S. Cordier. *Chem. Mater.*, **2011**, 23, 5122.
2. S. Cordier, Y. Molard, K. A. Brylev, Y. V. Mironov, F. Grasset, B. Fabre, and N. G. Naumov. *J. Clust. Sci.*, **2015**, 26, 53.
3. M. Shatruk, C. Avendano, and K. R. Dunbar. "Cyanide-Bridged Complexes of Transition Metals: A Molecular Magnetism Perspective". In: *Progress in Inorganic Chemistry*, **2009**, 56, 155-334.
4. L. G. Beauvais, M. P. Shores, and J. R. Long. *J. Am. Chem. Soc.*, **2000**, 122, 2763.
5. E. V. Alexandrov, A. V. Virovets, V. A. Blatov, and E. V. Peresypkina. *Chem. Rev.*, **2015**, 115, 12286.
6. V. E. Fedorov, N. G. Naumov, Yu. V. Mironov, A. V. Virovets, S. B. Artemkina, K. A. Brylev, S. S. Yarovoi, O. A. Efremova, and U. Kh. Pek. *J. Struct. Chem.*, **2002**, 43, 669.
7. K. A. Brylev, N. G. Naumov, A. V. Virovets, S. J. Kim, and V. E. Fedorov. *J. Clust. Sci.*, **2009**, 20, 165.
8. N. G. Naumov, A. V. Virovets, S. B. Artemkina, D. Y. Naumov, J. A. K. Howard, and V. E. Fedorov. *J. Solid State Chem.*, **2004**, 177, 1896.
9. N. G. Naumov, D. V. Soldatov, J. A. Ripmeester, S. B. Artemkina, and V. E. Fedorov. *Chem. Commun.*, **2001**, 571.
10. S. B. Artemkina, N. G. Naumov, A. V. Virovets, and V. E. Fedorov. *Eur. J. Inorg. Chem.*, **2005**, 142.
11. M. V. Bennett, L. G. Beauvais, M. P. Shores, and J. R. Long. *J. Am. Chem. Soc.*, **2001**, 123, 8022.
12. V. K. Muravieva, Y. M. Gayfulin, M. R. Ryzhikov, I. N. Novozhilov, D. G. Samsonenko, D. A. Piryazev, V. V. Yanshole, and N. G. Naumov. *Dalton Trans.*, **2018**, 47, 3366.
13. V. K. Muravieva, Y. M. Gayfulin, P. Lemoine, S. Cordier, and N. G. Naumov. *CrystEngComm*, **2018**, 20, 4164.
14. A. Altomare, M. C. Burla, M. Camalli, G. L. Cascarano, C. Giacovazzo, A. Guagliardi, A. G. G. Moliterni, G. Polidori, and R. Spagnac. *J. Appl. Crystallogr.*, **1999**, 32, 115.
15. G. M. Sheldrick. *Acta Crystallogr. C*, **2015**, 71, 3.
16. K. A. Brylev, G. Pilet, N. G. Naumov, A. Perrin, and V. E. Fedorov. *Eur. J. Inorg. Chem.*, **2005**, 461.
17. K. A. Brylev, N. G. Naumov, V. E. Fedorov, and J. A. Ibers. *J. Struct. Chem.*, **2005**, 46, S130.
18. Y. V. Mironov, N. G. Naumov, K. A. Brylev, O. A. Efremova, V. E. Fedorov, and K. Hegetschweiler. *Angew. Chem. Int. Ed.*, **2004**, 43, 1297.
19. Y. Kim, S. M. Park, and S. J. Kim. *Inorg. Chem. Commun.*, **2002**, 5, 592.
20. M. O'Keeffe, M. A. Peskov, S. J. Ramsden, and O. M. Yaghi. *Acc. Chem. Res.*, **2008**, 41, 1782.
21. N. G. Naumov, A. V. Virovets, Y. I. Mironov, S. B. Artemkina, and V. E. Fedorov. *Ukr. Khim. Zh.*, **1999**, 65, 21.
22. A. L. Spek. *Acta Crystallogr., Sect. C: Struct. Chem.*, **2015**, 71, 9.
23. A. L. Spek. *Acta Crystallogr., Sect. D: Biol. Crystallogr.*, **2009**, 65, 148.
24. A. M. Chippindale, S. M. Cheyne, and S. J. Hibble. *Angew. Chem. Int. Ed.*, **2005**, 44, 7942.
25. M. S. Tarasenko, N. G. Naumov, and N. V. Kuratieva. *J. Struct. Chem.*, **2015**, 56, 1143.
26. N. G. Naumov, S. B. Artemkina, A. V. Virovets, and V. E. Fedorov. *Russ. J. Coord. Chem.*, **2004**, 30, 792.
27. M. S. Tarasenko, A. Y. Ledneva, N. G. Naumov, D. Y. Naumov, and V. E. Fedorov. *J. Clust. Sci.*, **2005**, 16, 353.
28. M. S. Tarasenko, A. Yu. Ledneva, N. V. Kuratieva, D. Yu. Naumov, S. J. Kim, V. E. Fedorov, and N. G. Naumov. *Russ. J. Coord. Chem.*, **2007**, 33, 876.
29. Y. M. Gayfulin, N. G. Naumov, M. R. Ryzhikov, A. I. Smolentsev, V. A. Nadolnny, and Y. V. Mironov. *Chem. Commun.*, **2013**, 49, 10019.

References

1. Cotton F.A. Transition-metal compounds containing clusters of metal atoms // *Q. Rev., Chem. Soc.* – 1966. – V.20. – N.3. – P. 389-401.
2. Fedorov V.E., Mironov Y.V., Naumov N.G., Sokolov M.N., Fedin V.P. Chalcogenide clusters of Group 5–7 metals // *Russ. Chem. Rev.* – 2007. – V.76 – N.6. –P. 529-553.
3. Perrin A., Perrin C. The molybdenum and rhenium octahedral cluster chalcogenides in solid state chemistry: From condensed to discrete cluster units // *C. R. Chimie.* – 2012. – V.15. – N.9. – P. 815-836.
4. Sokolov M.N., Naumov N.G., Samoylov P.P., Fedin V.E. Clusters and cluster assemblies // *Comprehensive Inorganic Chemistry II (Second Edition)* ed. by Reedijk J. and Poeppelemeier K. – Amsterdam, 2013. – P. 271-310.
5. Chevrel R., Sergent M., Prigent J. Sur de nouvelles phases sulfurées ternaires du molybdène // *J. Solid State Chem.* – 1971. – V.3. – N.4. – P. 515-519.
6. Bronger W. Ternary sulfides - model compounds for the correlation of crystal-structure and magnetic-properties // *Angew. Chem.. Int. Ed.* – 1981. – V.20. – N.1. – P. 52-62.
7. Cordier S., Molard Y., Brylev K., Mironov Y., Grasset F., Fabre B., Naumov N. Advances in the engineering of near infrared emitting liquid crystals and copolymers, extended porous frameworks, theranostic tools and molecular junctions using tailored Re_6 cluster building blocks // *J. Clust. Sci.* – 2015. – V.2015. – P. 53-81.
8. Cordier S., Grasset F., Molard Y., Amela-Cortes M., Boukherroub R., Ravaine S., Mortier M., Ohashi N., Saito N., Haneda H. Inorganic molybdenum octahedral nanosized cluster units, versatile functional building block for nanoarchitectonics // *J. Inorg. Organomet. Polym. Mater.* – 2015. – V.25. – N.2. – P. 189-204.
9. Krasilnikova A.A., Shestopalov M.A., Brylev K.A., Kirilova I.A., Khripko O.P., Zubareva K.E., Khripko Y.I., Podorognaya V.T., Shestopalova L.V., Fedorov V.E., Mironov Y.V. Prospects of molybdenum and rhenium octahedral cluster complexes as X-ray contrast agents // *J. Inorg. Biochem.* – 2015. – V.144. – P. 13-17.

10. Kumar P., Kumar S., Cordier S., Paofai S., Boukherroub R., Jain S.L. Photoreduction of CO₂ to methanol with hexanuclear molybdenum [Mo₆Br₁₄]²⁻ cluster units under visible light irradiation // RSC Adv. – 2014. – V.4. – N.20. – P. 10420-10423.
11. Barras A., Cordier S., Boukherroub R. Fast photocatalytic degradation of rhodamine B over [Mo₆Br₈(N₃)₆]²⁻ cluster units under sun light irradiation // Appl. Catal., B. – 2012. – V.123-124. – P. 1-8.
12. Llusar R., Uriel S. Heterodimetallic chalcogen-bridged cubane-type clusters of molybdenum and tungsten containing first-row transition metals // Eur.J. Inorg. Chem. – 2003. – N.7. – P. 1271-1290.
13. Gushchin A.L., Laricheva Y.A., Sokolov M.N., Llusar R. Tri- and tetranuclear molybdenum and tungsten chalcogenide clusters: on the way to new materials and catalysts // Russ. Chem. Rev. – 2018. – V.87. – N.7. – P. 670-706.
14. Hernandez-Molina R., Sykes A.G. Chalcogenide-bridged cuboidal clusters with M₄Q₄ (M = Mo, W; Q = S, Se, Te) cores // J. Chem. Soc., Dalton Trans. – 1999. – N.18. – P. 3137-3148.
15. Perrin A., Sergent M., Fischer O. New compounds of the type Mo₂Re₄X₈ (M = S, Se) containing octahedral Mo₂Re₄ clusters // Mater. Res. Bull. – 1978. – V.13. – N.4. – P. 259-264.
16. Honle W., Flack H.D., Yvon K. Single-crystal x-ray study of Mo₆Se₈-type selenides containing partially substituted (Mo,Me)₆ clusters (Me = Ru,Re) // J. Solid State Chem. – 1983. – V.49. – N.2. – P. 157-165.
17. Berry F.J., Gibbs C.D. Synthesis of metal molybdenum tellurides of composition Mo_{6-x}M_xTe₈ (M = Ru or Rh) // Dalton Trans. – 1991. – N.1. – P. 57-59.
18. Berry F.J., Gibbs C.D., Greaves C. Structural-properties of the molybdenum ruthenium telluride of composition Mo_{4.5}Ru_{1.5}Te₈ // J. Solid State Chem. – 1991. – V.92. – N.1. – P. 148-153.
19. Perrin A., Chevrel R., Sergent M., Fischer O. Synthesis and electrical-properties of new chalcogenide compounds containing mixed (Mo,Me)₆ octahedral clusters (Me=Ru or Rh) // J. Solid State Chem. – 1980. – V.33. – N.1. – P. 43-47.
20. Neuhausen J., Finckh E.W., Tremel W. Nb_xRu_{6-x}Te₈, new chevrel-type clusters containing niobium and ruthenium // Inorg. Chem. – 1996. – V.35. – N.19. – P. 5622-5626.

21. Tulskey E.G., Long J.R. Heterometal substitution in the dimensional reduction of cluster frameworks: Synthesis of soluble $[\text{Re}_{6-n}\text{Os}_n\text{Se}_8\text{Cl}_6]^{(4-n)-}$ ($n=1-3$) cluster-containing solids // *Inorg. Chem.* – 2001. – V.40. – N.27. – P. 6990-7002.
22. Brylev K.A., Naumov N.G., Kozlova S.G., Ryzhikov M.R., Kim S.J., Kitamura N. Synthesis and structures of new octahedral heterometal rhenium-osmium cluster complexes // *Коорд. химия.* – 2012. – Т.38. – №.3. – С. 194-201.
23. Artemkina S.B., Naumov N.G., Kondrakov K.N., Virovets A.V., Kozlova S.G., Fedorov V.E. Cluster complexes with the novel heterometallic cluster core $\{\text{Mo}_5\text{NbI}_8\}$: synthesis, excision reactions, and crystal structures // *Z. Anorg. Allg. Chem.* – 2010. – V.636. – N.3-4. – P. 483-491.
24. Artemkina S.B., Tarasenko M.S., Virovets A.V., Naumov N.G. Heterometallic clusters with the $\{\text{Mo}_5\text{NbI}_8\}$ core: The synthesis and crystal structures of $(\text{Ph}_4\text{P})_2[\text{Mo}_5\text{NbI}_8\text{Cl}_6]$ and $(4\text{-MePyH})_5[\text{Mo}_5\text{NbI}_8\text{Cl}_6]\text{Cl}_2$ // *Russ. J. Coord. Chem.* – 2012. – V.38. – N.4. – P. 257-263.
25. Hodali H.A., Hung H.Y., Shriver D.F. Mass spectroscopic evidence for the formation of mixed-metal octahedral clusters $[\text{Mo}_n\text{W}_{6-n}\text{Cl}_{14}]^{2-}$ // *Inorg. Chim. Acta.* – 1992. – V.198. – P. 245-248.
26. Bruckner P., Peters G., Preetz W. Preparation of ^{19}F NMR spectroscopic evidence and study of the formation of metal-mixed cluster anions $(\text{Mo}_{6-n}\text{W}_n\text{Cl}_8^i\text{F}_6^a)^{2-}$, $n=0-6$ // *Z. Anorg. Allg. Chem.* – 1994. – V.620. – N.10. – P. 1669-1677.
27. Gayfulin Y.M., Naumov N.G., Ryzhikov M.R., Smolentsev A.I., Nadolinny V.A., Mironov Y.V. Heterometallic clusters with a new $\{\text{Re}_3\text{Mo}_3\text{S}_8\}$ core: direct synthesis, properties and DFT calculations // *Chem. Commun.* – 2013. – V.49. – N.85. – P. 10019.
28. Werner A. Neuere Anschauungen auf dem Gebiete der anorganischen Chemie: – F. Vieweg und sohn. – 1920. – 458 p.
29. Cotton F.A. High- and low-valence metal cluster compounds: a comparison // *Inorganic Chemistry: Toward the 21st Century* / ed. by Chisholm M.H. Washington D.C. – 1983. – P. 209-219.
30. Sokolov M.N., Abramov P.A. Chalcogenide clusters of Groups 8–10 noble metals // *Coord. Chem. Rev.* – 2012. – V.256. – N.17. – P. 1972-1991.
31. Schäfer H., Schnering H.G. Metall-Metall-Bindungen bei niederen Halogeniden, Oxyden und Oxydhalogeniden schwerer Übergangsmetalle

Thermochemische und strukturelle Prinzipien // Angew. Chem. – 1964. – V.76. – N.20. – P. 833-849.

32. Shibahara T., Yamasaki M., Watase T., Ichimura A. Syntheses and electrochemistry of sulfur-bridged incomplete cubane-type mixed-metal clusters of molybdenum(IV) and tungsten(IV). X-ray structures of $[\text{MoW}_2\text{S}_4(\text{H}_2\text{O})_9](\text{CH}_3\text{C}_6\text{H}_4\text{SO}_3) \cdot 4.9\text{H}_2\text{O}$, $[\text{Mo}_2\text{WS}_4(\text{H}_2\text{O})_9](\text{CH}_3\text{C}_6\text{H}_4\text{SO}_3) \cdot 4.9\text{H}_2\text{O}$, $\text{Na}_2[\text{MoW}_2\text{S}_4(\text{Hnta})_3] \cdot 5\text{H}_2\text{O}$, and $\text{Na}_2[\text{Mo}_2\text{WS}_4(\text{Hnta})_3] \cdot 5\text{H}_2\text{O}$ // Inorg. Chem. – 1994. – V.33. – N.2. – P. 292-301.
33. Kuwata S., Andou M., Hashizume K., Mizobe Y., Hidai M. Structures and reactivities of diruthenium dithiolene complexes and triruthenium sulfido clusters derived from a hydrosulfido-bridged diruthenium complex // Organometallics. – 1998. – V.17. – N.16. – P. 3429-3436.
34. Nishioka T., Isobe K. Syntheses and crystal-structures of triangular rhodium and iridium complexes with triply bridging sulfido ligands // Chem. Lett. – 1994. – N.9. – P. 1661-1664.
35. Hashizume K., Mizobe Y., Hidai M. Preparation of the hydrosulfido-bridged diruthenium complex $[(\eta^5\text{-C}_5\text{Me}_5)\text{RuCl}(\mu\text{-SH})_2\text{Ru}(\eta^5\text{-C}_5\text{Me}_5)\text{Cl}]$ and its transformation into a cubane-type tetraruthenium sulfido cluster or triangular heterometallic RhRu_2 sulfido cluster // Organometallics. – 1996. – V.15. – N.15. – P. 3303-3309.
36. Kajitani H., Seino H., Mizobe Y. Synthesis of a sulfido-capped trinuclear cluster $[(\eta^5\text{-C}_5\text{Me}_5)\text{Ir}]_2\{\text{Mo}(\text{CO})_3\}(\mu^3\text{-S})_2$ and its reactions at the molybdenum site forming a series of Ir_2MoS_2 clusters // Organometallics. – 2007. – V.26. – N.14. – P. 3499-3508.
37. Shibahara T. Cubane and incomplete cubane-type molybdenum and tungsten oxo sulfido clusters // Adv. Inorg. Chem. – 1991. – V.37. – P. 143-173.
38. Zhu N.Y., Zheng Y.F., Wu X.T. The designed synthesis and characterization of 2 novel heterometallic trinuclear incomplete cubane-like clusters $(\text{CH}_3\text{CH}_2)_4\text{N}(\text{M}_2\text{CuS}_4)(\text{S}_2\text{C}_2\text{H}_4)_2(\text{PPh}_3)$ ($\text{M} = \text{Mo}, \text{W}$) // Polyhedron. – 1991. – V.10. – N.23-24. – P. 2743-2755.
39. Jakob S., Strukturen, magnetismus und phasenumwandlungen der Mott-isolatoren $\text{Ga}(\text{M}_{4-x}\text{M}'_x)\text{Q}_8$ und $(\text{M}_{4-x}\text{M}'_x)\text{Q}_4\text{I}_4$ ($\text{M}, \text{M}' = \text{Mo}, \text{Nb}, \text{Ta}$; $\text{Q} = \text{S}, \text{Se}$; $x = 0 - 4$): Ph.D thesis. Ludwig-Maximilians-Universität, München, 2007.
40. Bichler D., Magnetismus und strukturelle Phasenumwandlungen von Verbindungen mit tetraedrischen Metallclustern: Ph.D thesis. Ludwig-Maximilians-Universität, München, 2010.

41. Powell A.V., McDowall A., Szkoda I., Knight K.S., Kennedy B.J., Vogt T. Cation substitution in defect thiospinels: Structural and magnetic properties of $\text{GaV}_{4-x}\text{Mo}_x\text{S}_8$ ($0 \leq x \leq 4$) // *Chem. Mater.* – 2007. – V.19. – N.20. – P. 5035-5044.
42. Bichler D., Johrendt D. Interplay of Magnetism and Bonding in $\text{GaV}_{4-x}\text{Cr}_x\text{Se}_8$ // *Chem. Mater.* – 2011. – V.23. – N.11. – P. 3014-3019.
43. Perrin C., Chevrel R., Sergent M. New molybdenum rhenium thio compounds with mixed tetrahedral cluster // *J. Solid State Chem.* – 1976. – V.19. – N.3. – P. 305-308.
44. Fedorov V.E., Mironov Y.V., Fedin V.P., Mironov Y.I. $\text{Re}_4\text{S}_4\text{Te}_4$ – A new mixed rhenium chalcogenide containing a tetrahedral Re_4 cluster // *Journal of Structural Chemistry.* – 1994. – V.35. – N.1. – P. 146-147
45. Khudorozhko G.F., Kravtsova E.A., Mazalov L.N., Fedorov V.E., Bulusheva L.G., Asanov I.P., Parygina G.K., Mironov Y.V. X-ray emission and X-ray photoelectron study of the electronic structure of polymeric cubanocluster compounds $\text{Re}_{4-x}\text{Mo}_x\text{S}_4\text{Te}_4$ // *Journal of Structural Chemistry.* – 1996. – V.37. – N.5. – P. 767-772.
46. Perrin C., Chevrel R., Sergent M. Sur un nouveau cluster tétraédrique de molybdène dans les chalcogénures MMo_4S_8 ($\text{M} = \text{Al}, \text{Ga}$), GaMo_4Se_8 et dans les thiochalcogénures MoS ($\text{X} = \text{Cl}, \text{Br}, \text{I}$) // *C. R. Seances Acad. Sci., Ser. C.* – 1975. – V.280. – P. 949.
47. Yaich H.B., Jegaden J.C., Potel M., Sergent M., Rastogi A.K., Tournier R. Nouveaux chalcogénures et chalcologénures à clusters tétraédriques Nb_4 ou Ta_4 // *J. Less-Common Met.* – 1984. – V.102. – N.1. – P. 9-22.
48. Ohki Y., Uchida K., Hara R., Kachi M., Fujisawa M., Tada M., Sakai Y., Sameera W.M.C. Cubane-type $\text{Mo}_3\text{S}_4\text{M}$ clusters with first-row groups 4-10 transition-metal halides supported by C_5Me_5 ligands on molybdenum // *Chem. Eur. J.* – 2018. – V.24. – N.64. – P. 17138-17147.
49. Herbst K., Monari M., Brorson M. Heterobimetallic, cubane-like $\text{Mo}_3\text{S}_4\text{M}'$ cluster cores containing the noble metals $\text{M}' = \text{Ru}, \text{Os}, \text{Rh}, \text{Ir}$. Unprecedented tri(μ -carbonyl) bridge between ruthenium atoms in $[(\eta^5\text{-Cp}')_3\text{Mo}_3\text{S}_4\text{Ru}]_2(\mu\text{-CO})_3]^{2+}$ // *Inorg. Chem.* – 2001. – V.40. – N.13. – P. 2979-2985.
50. Herbst K., Rink B., Dahlenburg L., Brorson M. Heterobimetallic cubane-like cluster compounds prepared as the homologous series $[(\eta^5\text{-Cp}')_3\text{Mo}_3\text{S}_4\text{M}'(\text{PPh}_3)]^+$ ($\text{M}' = \text{Ni}, \text{Pd}, \text{Pt}$). Crystal structures show that platinum

- is smaller than palladium // *Organometallics*. – 2001. – V.20. – N.17. – P. 3655-3660.
51. Herbst K., Zanello P., Corsini M., D'Amelio N., Dahlenburg L., Brorson M. A complete family of isostructural cluster compounds with cubane-like M_3S_4M' cores ($M = Mo, W$; $M' = Ni, Pd, Pt$): Comparative crystallography and electrochemistry // *Inorg. Chem.* – 2003. – V.42. – N.4. – P. 974-981.
 52. Sokolov M., Esparza P., Hernandez-Molina R., Platas J.G., Mederos A., Gavin J.A., Llusar R., Vicent C. Preparation and properties of the full series of cuboidal clusters $[Mo_xW_{4-x}Se_4(H_2O)_{12}]^{n+}$ ($n=4-6$) and their derivatives // *Inorg. Chem.* – 2005. – V.44. – N.4. – P. 1132-1141.
 53. Algarra A.G., Sokolov M.N., Gonzalez-Platas J., Fernandez-Trujillo M.J., Basallote M.G., Hernandez-Molina R. Synthesis, reactivity, and kinetics of substitution in W_3PdSe_4 cuboidal clusters. A reexamination of the kinetics of substitution of the related W_3S_4 cluster with thiocyanate // *Inorg. Chem.* – 2009. – V.48. – N.8. – P. 3639-3649.
 54. Llusar R., Uriel S., Vicent C. Transition metal incorporation into seleno-bridged cubane type clusters of molybdenum and tungsten. X-Ray crystal structures of the first Mo_3CuSe_4 derivatives // *J. Chem. Soc., Dalton Trans.* – 2001. – N.19. – P. 2813-2818.
 55. Hernandez-Molina R., Sykes A.G. Reactions of the heterometallic cuboidal clusters Mo_3MS_4 ($M = Co, Ni, Pd, Cu$) and Mo_3NiSe_4 with CO: electron counts and kinetic thermodynamic studies with $M = Ni, Pd$ // *Coord. Chem. Rev.* – 1999. – V.187. – P. 291-302.
 56. Hernandez-Molina R., Sokolov M.N., Clausen M., Clegg W. Synthesis and structure of nickel-containing cuboidal clusters derived from $[W_3Se_4(H_2O)_9]^{4+}$. Site-differentiated substitution at the nickel site in the series $[W_3NiQ_4(H_2O)_{10}]^{4+}$ ($Q = S, Se$) // *Inorg. Chem.* – 2006. – V.45. – N.26. – P. 10567-10575.
 57. Sokolov M.N., Dybtsev D.N., Virovets A.V., Hegetschweiler K., Fedin V. Synthesis and crystal structure of a supramolecular adduct of the cubane cluster $[ClPdMo_3Se_4(H_2O)_7Cl_2]^+$ with macrocyclic cavitand cucurbituril // *Russ. Chem. Bull.* – 2000. – V.49. – N.11. – P. 1877-1881.
 58. Sakai N., Saito T. Synthesis and structures of tetranuclear rhenium-cobalt mixed metal sulfide clusters $Re_3CoS_4Cl_6(PMe_2Ph)_4$ // *Polyhedron*. – 2004. – V.23. – N.17. – P. 2611-2614.
 59. Scott T.A., Holm R.H. VFe_3S_4 single and double cubane clusters: synthesis, structures, and dependence of redox potentials and electron distribution on

- ligation and heterometal // *Inorg. Chem.* – 2008. – V.47. – N.8. – P. 3426-3432.
60. Bechlars B., Issac I., Feuerhake R., Clerac R., Fuhr O., Fenske D. Syntheses, structures and magnetic properties of new chalcogen-bridged heterodimetallic cluster compounds with heterocubane structure // *Eur.J. Inorg. Chem.* – 2008. – N.10. – P. 1632-1644.
 61. Pasynskii A.A., Eremenko I.L., Orazsakhov B., Kalinnikov V.T., Aleksandrov G.G., Struchkov Y.T. Anti-ferromagnetic complexes with metal-metal bonds .6. Transformation of the anti-ferromagnetic metallacycle $(\text{Cp}_2\text{Cr}_2\text{SCMe}_3)(\mu^3\text{-S})_2\text{Co}(\text{CO})_2$ into the diamagnetic metallatetrahedron $\text{Cp}_3\text{Cr}_3(\mu^3\text{-S})_4\text{Co}(\text{CO})$ // *J. Organomet. Chem.* – 1981. – V.214. – N.3. – P. 367-372.
 62. Eremenko I.L., Pasynskii A.A., Orazsakhov B., Ellert O.G., Novotortsev V.M., Kalinnikov V.T., Poraikoshits M.A., Antsyshkina A.S., Dikareva L.M., Ostrikova V.N., Struchkov Y.T., Gerr R.G. Interaction of heteronuclear chromium-containing clusters with carboxylic acids - molecular-structure of the paramagnetic tetrahedral cluster $\text{CP}_3\text{Cr}_3(\mu^3\text{-S})_4\text{Fe}(\text{OOCMe}_3)$ // *Inorg. Chim. Acta.* – 1983. – V.73. – N.2. – P. 225-229.
 63. Rauchfuss T.B., Weatherill T.D., Wilson S.R., Zebrowski J.P. Stepwise assembly of heterometallic M_4S_4 clusters - the structure of $(\text{MeCp})_2\text{V}_2\text{Fe}_2(\text{NO})_2\text{S}_4$ -a 58e cubane // *J. Am. Chem. Soc.* – 1983. – V.105. – N.21. – P. 6508-6509.
 64. Rauchfuss T.B., Gammon S.D., Weatherill T.D., Wilson S.R. Localized structural effects in the heterometallic thiocubanes $(\text{MeCp})_2\text{V}_2\text{M}_2\text{S}_4(\text{NO})_2$ where $\text{M}_2=\text{Fe}_2, \text{Co}_2$, and Ni_2 // *New J. Chem.* – 1988. – V.12. – N.6-7. – P. 373-375.
 65. Lorenz A., Fenske D. Chalcogenoniobates as reagents for the synthesis of new heterobimetallic niobium coinage metal chalcogenide clusters // *Z. Anorg. Allg. Chem.* – 2001. – V.627. – N.9. – P. 2232-2248.
 66. McLean I.J., Hernandez-Molina R., Sokolov M.N., Seo M.S., Virovets A.V., Elsegood M.R.J., Clegg W., Sykes A.G. Preparation, structure and properties of three $[\text{Mo}_x\text{W}_{4-x}\text{S}_4(\text{H}_2\text{O})_{12}]^{5+}$ ($x = 1-3$) and $[\text{MoW}_3\text{Se}_4(\text{H}_2\text{O})_{12}]^{5+}$ cuboidal complexes alongside $\text{Mo}_4\text{S}_4(\text{H}_2\text{O})_{12}]^{5+}$ and $[\text{Mo}_4\text{Se}_4(\text{H}_2\text{O})_{12}]^{5+}$ // *J. Chem. Soc., Dalton Trans.* – 1998. – N.15. – P. 2557-2562.
 67. Eremenko I.L., Pasynskii A.A., Katugin A.S., Ellert O.G., Shklover V.E., Struchkov Y.T. Synthesis of the electron-deficient paramagnetic cluster $(\text{CH}_3\text{C}_5\text{H}_4)_4\text{V}_4\text{S}_4$ and its molecular-structure // *Bull. Acad. Sci. USSR D. Chem. Sci.* – 1984. – V.33. – N.7. – P. 1531-1532.

68. Pasynskii A.A., Eremenko I.L., Rakitin Y.V., Novotortsev V.M., Ellert O.G., Kalinnikov V.T., Shklover V.E., Struchkov Y.T., Lindeman S.V., Kurbanov T.K., Gasanov G.S. Anti-ferromagnetic complexes with metal metal bonds .9. Synthesis and molecular-structures of "methylcyclopentadienylchromium(III) sulfide diamagnetic tetramer and the anti-ferromagnetic copper(II) Bromide Adduct Of The Tetranuclear Cluster $(\text{MeC}_5\text{H}_4)_4\text{Cr}_4(\mu^3\text{-O})(\mu^3\text{-S})_3$ // J. Organomet. Chem. – 1983. – V.248. – N.3. – P. 309-320.
69. Fedin V.P., Samsonenko D.G., Virovets A.V., Kalinina I.V., Naumov D.Y. Synthesis, structures, and properties of molybdenum and tungsten chalcogenide cubane complexes $(\text{NH}_4)_6[\text{M}_4\text{Q}_4(\text{CN})_{12}]\cdot 6\text{H}_2\text{O}$ (M=Mo or W; Q=S or Se) // Russ. Chem. Bull. – 2000. – V.49. – N.1. – P. 19-25.
70. Fedin V.P., Elsegood M.R.J., Clegg W., Sykes A.G. High-yield synthesis of the cuboidal rhenium cluster $[\text{Re}_4\text{S}_4(\text{CN})_{12}]^{4+}$ by reaction of the triangular cluster $[\text{Re}_3\text{S}_7\text{Br}_6]^+$ with cyanide // Polyhedron. – 1996. – V.15. – N.3. – P. 485-488.
71. Sharp C.R., Duncan J.S., Lee S.C. $[\text{Fe}_4\text{S}_4]^q$ Cubane Clusters ($q = 4+, 3+, 2+$) with Terminal Amide Ligands // Inorg. Chem. – 2010. – V.49. – N.14. – P. 6697-6705.
72. Shibahara T., Sakane G., Naruse Y., Taya K., Akashi H., Ichimura A., Adachi H. Syntheses and characterization of cubane-type clusters with molybdenum-iron-sulfur (Mo_3FeS_4) or molybdenum-nickel-sulfur (Mo_3NiS_4) cores - X-ray structures of $\text{Mo}_3\text{FeS}_4(\text{H}_2\text{O})_{10}(\text{CH}_3\text{C}_6\text{H}_4\text{SO}_3)_4\cdot 7\text{H}_2\text{O}$ and $\text{Mo}_3\text{FeS}_4(\text{H}_2\text{O})(\text{NH}_3)_9\text{Cl}_4$, and discrete variational (DV)-X-alpha calculation of the electronic-structures of $[\text{Mo}_3\text{FeS}_4(\text{H}_2\text{O})_{10}]^{4+}$, $[\text{Mo}_3\text{FeS}_4(\text{H}_2\text{O})(\text{NH}_3)_9]^{4+}$, and $[\text{Mo}_3\text{NiS}_4(\text{H}_2\text{O})_{10}]^{4+}$ // Bull. Chem. Soc. Jpn. – 1995. – V.68. – N.10. – P. 2769-2782.
73. Curtis M.D., Riaz U., Curnow O.J., Kampf J.W., Rheingold A.L., Haggerty B.S. Molecular-structures of the bimetallic sulfide clusters $\text{Cp}'_2\text{Mo}_2\text{Co}_2\text{S}_4(\text{CO})_2$, $\text{Cp}'_2\text{Mo}_2\text{Co}_2\text{S}_3(\mu_3\text{-PPh})(\text{CO})_2$, $\text{Cp}'_3\text{Mo}_3\text{CoS}_4(\text{CO})$, and $\text{Cp}'_3\text{Mo}_3\text{FeS}_4(\text{SH})$ // Organometallics. – 1995. – V.14. – N.11. – P. 5337-5343.
74. Shibahara T., Yamasaki M., Akashi H., Katayama T. Cubane-type mixed-metal clusters with Mo_3NiS_4 cores - syntheses, characterization, and X-ray structures of $[\text{Mo}_3\text{NiS}_4(\text{H}_2\text{O})_{10}](\text{CH}_3\text{C}_6\text{H}_4\text{SO}_3)_4\cdot 7\text{H}_2\text{O}$ and $\text{Ca}_{2.5}\text{Mo}_3\text{NiS}_4(\text{Hnta})(\text{nta})_2\text{Cl}\cdot 14\text{H}_2\text{O}$ // Inorg. Chem. – 1991. – V.30. – N.12. – P. 2693-2699.
75. Feliz M., Garriga J.M., Llusar R., Uriel S., Humphrey M.G., Lucas N.T., Samoc M., Luther-Davies B. Synthesis, structure, and optical-limiting properties of heterobimetallic M_3CuS_4 cuboidal clusters (M = Mo or W) with

- terminal phosphine ligands // *Inorg. Chem.* – 2001. – V.40. – N.24. – P. 6132-6138.
76. Herbst K., Dahlenburg L., Brorson M. Methylcyclopentadienyl-substituted tungsten(IV) sulfide cluster $[(\eta^5\text{-Cp})_3\text{W}_3\text{S}_4]^+$ and its heterobimetallic derivative $[(\eta^5\text{-Cp})_3\text{W}_3\text{S}_4\text{Ni(PPh}_3)]^+$ // *Inorg. Chem.* – 2001. – V.40. – N.9. – P. 1989-1992.
 77. Zhang Y.P., Bashkin J.K., Holm R.H. phosphine cleavage of iron(III)-bridged double cubanes - a new route to MoFe_3S_4 single cubanes // *Inorg. Chem.* – 1987. – V.26. – N.5. – P. 694-702.
 78. Kawaguchi H., Yamada K., Ohnishi S., Tatsumi K. Construction of a cyclic tricubane cluster $[\text{Cp}^{*2}\text{Mo}_2\text{Fe}_2\text{S}_4]_3(\mu\text{-S}_4)_3$ from the $\text{Mo}_2\text{Fe}_2\text{S}_4$ single cubane component // *J. Am. Chem. Soc.* – 1997. – V.119. – N.44. – P. 10871-10872.
 79. Mansour M.A., Curtis M.D., Kampf J.W. Oxidative substitution of carbonyl groups by halogen or RS center dot on the cubane cluster $(\text{Cp}_2\text{Mo}_2\text{Co}_2\text{S}_4)\text{-Mo-Et(CO)}_2$: Preparation of 58-VSE electron-deficient clusters as models for an organometallic desulfurization material // *Organometallics.* – 1997. – V.16. – N.15. – P. 3363-3370.
 80. Mansour M.A., Curtis M.D., Kampf J.W. Synthesis and structural characterization of tetranuclear, bimetallic sulfide nitrosyl and carbonyl clusters of the type $\text{Cp}_2\text{M}_2\text{M}'_2\text{S}_{3,4}\text{L}_n$ ($\text{M}=\text{Mo}, \text{W}$; $\text{M}'=\text{Fe}, \text{Co}$; $\text{L}=\text{NO}, \text{CO}$) // *Organometallics.* – 1997. – V.16. – N.2. – P. 275-284.
 81. Shibahara T., Akashi H., Yamasaki M., Hashimoto K. Reaction of $[\text{Mo}_3\text{S}_4(\text{H}_2\text{O})_9]^{4+}$ with cobalt and mercury - syntheses and X-ray structures of double cubane-type cluster, $(\text{H}_2\text{O})_9\text{Mo}_3\text{S}_4\text{CoCoS}_4\text{Mo}_3(\text{H}_2\text{O})_9(\text{CH}_3\text{C}_6\text{H}_4\text{SO}_3)_8 \cdot 18\text{H}_2\text{O}$ and sandwich cubane-type cluster, $(\text{H}_2\text{O})_9\text{Mo}_3\text{S}_4\text{HgS}_4\text{Mo}_3(\text{H}_2\text{O})_9(\text{CH}_3\text{C}_6\text{H}_4\text{SO}_3)_8 \cdot 20\text{H}_2\text{O}$ // *Chem. Lett.* – 1991. – N.4. – P. 689-692.
 82. Shibahara T., Sakane G., Maeyama M., Kobashi H., Yamamoto T., Watase T. Uptake of ethylene by sulfur-bridged cubane-type molybdenum/tungsten-nickel clusters $[\text{M}_3\text{NiS}_4(\text{H}_2\text{O})_{10}]^{4+}$ ($\text{M}_3=\text{Mo}_3, \text{Mo}_2\text{W}, \text{MoW}_2, \text{W}_3$): syntheses, structures and H-1 NMR spectra // *Inorg. Chim. Acta.* – 1996. – V.251. – N.1-2. – P. 207-225.
 83. Fedin V.P., Seo M.S., Saysell D.M., Dybtsev D.N., Elsegood M.R.J., Clegg W., Sykes A.G. Formation (and properties) of palladium derivatives of $[\text{Mo}_3\text{Q}_4(\text{H}_2\text{O})_9]^{4+}$: absence of similar derivatives of $[\text{W}_3\text{Q}_4(\text{H}_2\text{O})_9]^{4+}$ ($\text{Q}=\text{S}, \text{Se}$) // *J. Chem. Soc., Dalton Trans.* – 2002. – N.2. – P. 138-143.

84. Shibahara T., Akashi H., Kuroya H. Preparation and X-ray structure of a mixed-metal double-cubane-type aqua ion, $[(\text{H}_2\text{O})_9\text{Mo}_3\text{S}_4\text{CuCuS}_4\text{Mo}_3(\text{H}_2\text{O})_9]^{8+}$ // J. Am. Chem. Soc. – 1988. – V.110. – N.10. – P. 3313-3314.
85. Sokolov M., Coichev N., Moya H., Hernandez-Molina R., D. Borman C., Geoffrey Sykes A. New procedures for the preparation of $[\text{Mo}_3\text{S}_4(\text{H}_2\text{O})_9]^{4+}$, $[\text{Mo}_4\text{S}_4(\text{H}_2\text{O})_{12}]^{5+}$ and $[\text{Mo}_7\text{S}_8(\text{H}_2\text{O})_{18}]^{8+}$ and their Se analogues: redox and substitution studies on the double cube $[\text{Mo}_7\text{S}_8(\text{H}_2\text{O})_{18}]^{8+}$ // J. Chem. Soc., Dalton Trans. – 1997. – P. 1863.
86. Yang Y., Liu Q.T., Huang L.G., Kang B.S., Lu J.X. Assembly of heterometallic $\text{V}_2\text{M}_2\text{S}_4$ cubane-like clusters - syntheses and structures of $\text{Et}_4\text{N}_2\text{V}_2\text{M}_2\text{S}_4(\text{OC}_4\text{H}_8\text{Dtc})_2(\text{SPh})_2$ (M = Cu, Ag, Dtc = dithiocarbamate) // J. Chem. Soc., Chem. Commun. – 1992. – N.20. – P. 1512-1514.
87. Curtis M.D., Williams P.D., Butler W.M. Preparation, structures, and electrochemistry of tetranuclear sulfido clusters $\text{Cp}_2\text{M}_2\text{M}'_2\text{S}_{2-4}$ (M = Mo, W; M' = Fe, CO, Ni) // Inorg. Chem. – 1988. – V.27. – N.16. – P. 2853-2862.
88. Brunner H., Grassl R., Wachter J., Nuber B., Ziegler M.L. Synthesis and structural characterization of transition-metal sulfide clusters with Cp^* -Mo- ($\text{Cp}^* = \text{C}_5\text{Me}_5$), CuCl and Fe(NO) building-blocks // J. Organomet. Chem. – 1990. – V.393. – N.1. – P. 119-129.
89. Wu J.H., Zhu N.Y., Du S.W., Wu X.T., Lu J.X. The synthesis and characterization of a novel cubane-like cluster $(\text{CH}_3\text{CH}_2)_4\text{N}_4(\text{W}_2\text{Cu}_2\text{S}_4)(\text{SCN})_8$ // Inorg. Chim. Acta. – 1991. – V.185. – N.2. – P. 181-185.
90. Bronger W., Koppe C., Loevenich M., Schmitz D., Schuster T. $\text{Cs}_3\text{Re}_5\text{OsS}_{11}$, a compound containing mixed rhenium osmium clusters // Z. Anorg. Allg. Chem. – 1997. – V.623. – N.5. – P. 695-698.
91. Preetz W., Peters G., Bublit D. Preparation and spectroscopic investigations of mixed octahedral complexes and clusters // Chem. Rev. – 1996. – V.96. – N.3. – P. 977-1025.
92. Superconductivity in ternary compounds I: structural, electronic, and lattice properties / ed. by Fischer O., Maple L. – Berlin: Springer Science & Business Media, 2012. – 277 p.
93. Belin S., Chevrel R., Sergent M. Structure of Mo_7S_8 : A new binary sulfide synthesized by self molybdenum intercalation // Mater. Res. Bull. – 1998. – V.33. – N.1. – P. 43-57.
94. Miller G.J., Smith M. Hexamolybdenum Octatelluride, Mo_6Te_8 // Acta Crystallogr., Sect. C. – 1998. – V.54. – N.6. – P. 709-710.

95. Damien D., de Novion C.H., Gal J. Superconductivity in the neptunium Chevrel phase $\text{Np}_{1+x}\text{Mo}_6\text{Se}_8$ // *Solid State Commun.* – 1981. – V.38. – N.5. – P. 437-440.
96. Caillat T., Fleurial J.P., Snyder G.J. Potential of Chevrel phases for thermoelectric applications // *Solid State Sci.* – 1999. – V.1. – N.7-8. – P. 535-544.
97. Peña O. Chevrel phases: Past, present and future // *Phys. C.* – 2015. – V.514. – P. 95-112.
98. Bronger W., Miessen H.J., Muller P., Neugroschel R. Synthesis and crystal-structure of $\text{Li}_4\text{Re}_6\text{S}_{11}$ // *J. Less-Common Met.* – 1985. – V.105. – N.2. – P. 303-310.
99. Meyer J.L., McCarley R.E. Chemistry of polynuclear metal-halides .13. Mixed-metal $\text{M}_6\text{X}_{12}\text{N}^+$ species containing both tantalum and molybdenum // *Inorg. Chem.* – 1978. – V.17. – N.7. – P. 1867-1872.
100. Preetz W., Harder K. Separation and characterization of mixed-metal clusters $[(\text{NbNTa}_{6-n})\text{Cl}_{12}]^{2+}$, $n = 0-6$ // *Z. Anorg. Allg. Chem.* – 1991. – V.597. – N.6. – P. 163-172.
101. Kirakci K., Cordier S., Perrin C. Synthesis and characterization of $\text{Cs}_2\text{Mo}_6\text{X}_{14}$ ($\text{X} = \text{Br}$ or I) hexamolybdenum cluster halides: Efficient Mo_6 cluster precursors for solution chemistry syntheses // *Z. Anorg. Allg. Chem.* – 2005. – V.631. – N.2-3. – P. 411-416.
102. Bruckner P., Preetz W., Punjer M. Synthesis, crystal structure, NMR, vibrational spectra, and normal coordinate analysis of the cluster anions $(\text{Mo}_6\text{I}_8^i)\text{Y}_6^a)^{2-}$, $\text{Y}^a = \text{F}, \text{Cl}, \text{Br}, \text{I}$ // *Z. Anorg. Allg. Chem.* – 1997. – V.623. – N.1. – P. 8-17.
103. Perrin A., Leduc L., Sergent M. Halogen bridged Re_6L_8 units in octahedral cluster rhenium chalcogenides // *Eur. J. Solid. State Inorg. Chem.* – 1991. – V.28. – N.5. – P. 919-931.
104. Long J.R., Williamson A.S., Holm R.H. Dimensional reduction of $\text{Re}_6\text{Se}_8\text{Cl}^{2-}$ sheets, chains, and discrete clusters composed of chloride-terminated $\text{Re}_6\text{Q}_8^{2+}$ ($\text{Q} = \text{S}, \text{Se}$) cores // *Angew. Chem. Int. Ed.* – 1995. – V.34. – N.2. – P. 226-229.
105. Zheng Z.P., Long J.R., Holm R.H. A basis set of Re_6Se_8 cluster building blocks and demonstration of their linking capability: directed synthesis of an $\text{Re}_{12}\text{Se}_{16}$ dicluster // *J. Am. Chem. Soc.* – 1997. – V.119. – N.9. – P. 2163-2171.

106. Tulskey E.G., Crawford N.R.M., Baudron S.A., Batail P., Long J.R. Cluster-to-metal magnetic coupling: Synthesis and characterization of 25-electron $[\text{Re}_{6-n}\text{Os}_n\text{Se}_8(\text{CN})_6]^{(5-n)-}$ ($n=1, 2$) clusters and $\{\text{Re}_{6-n}\text{Os}_n\text{Se}_8 \text{CNCu}(\text{Me}_6\text{tren})_6\}^{9+}$ ($n=0, 1, 2$) assemblies // *J. Am. Chem. Soc.* – 2003. – V.125. – N.50. – P. 15543-15553.
107. Fedin V.P., Kalinina I.V., Samsonenko D.G., Mironov Y.V., Sokolov M.N., Tkachev S.V., Virovets A.V., Podberezskaya N.V., Elsegood M.R.J., Clegg W., Sykes A.G. Synthesis, structure, and properties of molybdenum and tungsten cyano complexes with cuboidal $\text{M}_4(\mu^3\text{-E})_4$ ($\text{M} = \text{Mo}, \text{W}$; $\text{E} = \text{S}, \text{Se}, \text{Te}$) cores // *Inorg. Chem.* – 1999. – V.38. – N.9. – P. 1956-1965.
108. Fedin V.P., Kalinina I.V., Virovets A.V., Podberezskaya N.V., Neretin I.S., Slovokhotov Y.L. Synthesis and structure of a tetranuclear niobium telluride cuboidal cluster with a central $\mu_4\text{-O}$ ligand // *Chem. Commun.* – 1998. – N.23. – P. 2579-2580.
109. Fedin V.P., Kalinina I.V., Virovets A.V., Fenske D. Synthesis, structures, and properties of the niobium and tantalum telluride cubane clusters $[\text{M}_4(\mu_4\text{-O})(\mu_3\text{-Te})_4(\text{CN})_{12}]^{6-}$ ($\text{M} = \text{Nb}$ or Ta) // *Russ. Chem. Bull.* – 2001. – V.50. – N.6. – P. 930-934.
110. Magliocchi C., Xie X., Hughbanks T. A cyanide-bridged chain of Mo_6Se_8 Clusters: a product of cyanide-melt cluster synthesis // *Inorg. Chem.* – 2000. – V.39. – N.22. – P. 5000-5001.
111. Mironov Y.V., Virovets A.V., Naumov N.G., Ikorskii V.N., Fedorov V.E. Excision of the $\{\text{Mo}_6\text{Se}_8\}$ cluster core from a chevrel phase: synthesis and properties of the first molybdenum octahedral cluster selenocyanide anions $[\text{Mo}_6\text{Se}_8(\text{CN})_6]^{7-}$ and $[\text{Mo}_6\text{Se}_8(\text{CN})_6]^{6-}$ // *Chem. Eur. J.* – 2000. – V.6. – N.8. – P. 1361-1365.
112. Mironov Y.V., Fedorov V.E., McLauchlan C.C., Ibers J.A. Layered $\text{K}_4[\text{Re}_6\text{S}_{10}(\text{CN})_2]$ and chainlike $\text{K}_4[\text{Re}_6\text{Se}_{10}(\text{CN})_4]$: new types of chalcocyanide cluster compounds with bridging chalcogenide ligands // *Inorg. Chem.* – 2000. – V.39. – N.8. – P. 1809-1811.
113. Mironov Y.V., Naumov N.G., Kozlova S.G., Kim S.-J., Fedorov V.E. $[\text{Re}_{12}\text{CS}_{17}(\text{CN})_6]^{n-}$ ($n=6, 8$): a sulfido–cyanide rhenium cluster with an interstitial carbon atom // *Angew. Chem., Int. Ed.* – 2005. – V.44. – N.42. – P. 6867-6871.
114. Naumov N.G., Brylev K.A., Mironov Y.V., Virovets A.V., Fenske D., Fedorov V.E. Synthesis and structures of new octahedral water-soluble heterometal rhenium-molybdenum clusters // *Polyhedron.* – 2004. – V.23. – N.4. – P. 599-603.

115. Shibahara T., Yamasaki M., Sakane G., Minami K., Yabuki T., Ichimura A. Syntheses and electrochemistry of incomplete cubane-type clusters with M_3S_4 cores (M = molybdenum, tungsten). X-ray structures of $[W_3S_4(H_2O)_9](CH_3C_6H_4SO_3)_4 \cdot 9H_2O$, $Na_2[W_3S_4(Hnta)_3] \cdot 5H_2O$, and $(bpyH)_5[W_3S_4(NCS)_9] \cdot 3H_2O$ // *Inorg. Chem.* – 1992. – V.31. – N.4. – P. 640-647.
116. Martinez M., Ooi B.L., Sykes A.G. Reaction paths in the formation of triangular and cuboidal molybdenum/sulfur cluster complexes as aqua ions by reduction of molybdenum(V) dimers // *J. Am. Chem. Soc.* – 1987. – V.109. – N.15. – P. 4615-4619.
117. Keck H., Kruse A., Kuchen W., Mathow J., Wunderlich H. Vierkernige Molybdän-Schwefel-Cluster mit Dithiophosphinatoliganden // *Z. Naturforsch.* – 1987. – V.42. – P. 1373-1378.
118. Brunner H., Kauermann H., Wachter J. The reaction of the sulfur-rich compounds $(C_5Me_5)_2Mo_2S_4$ and $(C_5Me_5)_2Cr_2S_5$ with M-M double bonding of the complex $\eta^5-C_5R_5(CO)_2M'_2$ ($R=H, CH_3$ and $M'=Cr, Mo, W$) and 2-nuclear and 3-nuclear clusters with M_3S_4 and M_4S_4 structures // *J. Organomet. Chem.* – 1984. – V.265. – N.2. – P. 189-198.
119. Brunner H., Wachter J. Investigation of the formation of new bimetallic clusters of the type $(\eta-C_5Me_5)_2M_2M'_2(\mu^3-S)_4(CO)_2$ ($M=Cr, Mo$; $M'=Co$), containing the $M_2M'_2S_4$ core // *J. Organomet. Chem.* – 1982. – V.240. – N.2. – P. C41-C44.
120. Halbert T.R., Cohen S.A., Stiefel E.I. Construction of heterometallic thiocubanes from $M_2S_2(\mu-S)_2$ core complexes - synthesis of $Co_2Mo_2S_4(S_2CNEt_2)_2(CH_3CN)_2(CO)_2$, $Co_2W_2S_4(S_2CNEt_2)_2(CH_3CN)_2(CO)_2$ and structure of the $Co_2Mo_2(\mu^3-S)_4$ cluster // *Organometallics*. – 1985. – V.4. – N.9. – P. 1689-1690.
121. Cohen S.A., Stiefel E.I. Dinuclear tungsten(V) and molybdenum(V) compounds containing $[M_2S_2(\mu-S)_2]^{2+}$ cores - synthesis and reactivity of $[N(C_2H_5)_4]_2M_2S_{12}$ ($M = W$ or Mo) and the crystal-structure of $[N(C_2H_5)_4]_2W_2S_2(\mu-S)_2(S_4)_2$ // *Inorg. Chem.* – 1985. – V.24. – N.26. – P. 4657-4662.
122. Zhu N.Y., Zheng Y.F., Wu X.T. The synthesis and characterization of 2 novel cubane-like clusters $M_2Cu_2S_4(PPh_3)_2(SCH_2CH_2S)_2$ ($M = Mo$ and W) // *J. Chem. Soc., Chem. Commun.* – 1990. – N.10. – P. 780-781.
123. Shibahara T., Akashi H., Kuroya H. Cubane-type $[Mo_3FeS_4]^{4+}$ aqua ion and X-ray structure of $Mo_3FeS_4(NH_3)_9(H_2O)Cl_4$ // *J. Am. Chem. Soc.* – 1986. – V.108. – N.6. – P. 1342-1343.

124. Rink B., Brorson M., Scowen I.J. New heterometallic cubane-like clusters $\{(\eta^5\text{-Cp})\text{Mo}\}_3\text{S}_4\{\text{M}'(\text{CO})_3\}$ (pts) ($\text{M}' = \text{Cr}, \text{Mo}, \text{W}$; pts = p-toluenesulfonate) obtained by ligand substitution reactions and insertion of $\{\text{M}'(\text{CO})_3\}$ fragments // *Organometallics*. – 1999. – V.18. – N.12. – P. 2309-2313.
125. Wu X.T., Lu S.F., Zu L.Y., Wu Q.J., Lu J.X. The synthesis and crystal-structure of a novel cubane-like molybdenum copper sulfur cluster $\text{Mo}_3\text{CuS}_4[\text{S}_2\text{P}(\text{OC}_2\text{H}_5)_2]_3 \cdot \text{I} \cdot \text{CH}_3\text{COO} \cdot \text{HCON}(\text{CH}_3)_2$ // *Inorg. Chim. Acta*. – 1987. – V.133. – N.1. – P. 39-42.
126. Zhan H.Q., Zheng Y.F., Wu X.T., Lu J.X. The synthesis and crystal-structure of a cubane-like tungsten copper sulfur cluster $\text{W}_3\text{CuS}_4[\text{S}_2\text{P}(\text{OC}_2\text{H}_5)_2]_3 \cdot \text{I} (\mu^2\text{-CH}_3\text{COO} \cdot \text{C}_5\text{H}_5\text{N})$ // *Inorg. Chim. Acta*. – 1989. – V.156. – N.2. – P. 277-280.
127. Zheng Y.F., Zhan H.Q., Wu X.T., Lu J.X. The synthesis and crystal-structure of a cubane-like tungsten copper sulfur cluster, $\text{W}_3\text{CuS}_4(\text{S}_2\text{P}(\text{OEt})_2)_3\text{I}(\mu^2\text{-PhCO}_2)(\text{MeCN})$ // *Trans. Met. Chem.* – 1989. – V.14. – N.3. – P. 161-164.
128. Saito T., Yamamoto N., Yamagata T., Imoto H. Synthesis of $[\text{Mo}_6\text{S}_8(\text{PEt}_3)_6]$ by reductive dimerization of a trinuclear molybdenum chloro sulfido cluster complex coordinated with triethylphosphine and methanol: a molecular model for superconducting Chevrel phases // *J. Am. Chem. Soc.* – 1988. – V.110. – N.5. – P. 1646-1647.
129. Hernandez-Molina R., Sokolov M., G Sykes A. Behavioral patterns of heterometallic cuboidal derivatives of $[\text{M}_3\text{Q}_4(\text{H}_2\text{O})_9]^{4+}$ ($\text{M} = \text{Mo}, \text{W}$; $\text{Q} = \text{S}, \text{Se}$) // *Acc. Chem. Res.* – 2001. – V.34. – P. 223-30.
130. Varey J.E., Sykes A.G. Rate constants for thiocyanate substitution at mo and w on the trinuclear incomplete-cuboidal clusters $[\text{Mo}_2\text{WS}_4(\text{H}_2\text{O})_9]^{4+}$ and $[\text{MoW}_2\text{S}_4(\text{H}_2\text{O})_9]^{4+}$ // *J. Chem. Soc., Dalton Trans.* – 1993. – N.22. – P. 3293-3297.
131. Saysell D.M., Borman C.D., Kwak C.-H., Sykes A.G. Ligand substitution reactions at the nickel of $[\text{Mo}_3\text{NiS}_4(\text{H}_2\text{O})_{10}]^{4+}$ with two water soluble phosphines, CO, Br⁻, I⁻, and NCS⁻ and the inertness of the 1,4,7-triazacyclononane (L) Complex $[\text{Mo}_3(\text{NiL})\text{S}_4(\text{H}_2\text{O})_9]^{4+}$ // *Inorg. Chem.* – 1996. – V.35. – N.1. – P. 173-178.
132. Saysell D.M., Lamprecht G.J., Darkwa J., Sykes A.G. Aqueous solution chemistry of the Mo_3PdS_4 cube: substitution reactions and the double to single cube Interconversion induced by CO, Two Phosphines, Cl⁻, Br⁻, and NCS // *Inorg. Chem.* – 1996. – V.35. – N.19. – P. 5531-5535.

133. Nasreldin M., Li Y.-J., Mabbs F.E., Sykes A.G. Preparation and properties of the heterometallic cuboidal cluster $[\text{Mo}_3\text{CuS}_4(\text{H}_2\text{O})_{10}]^{5+}$ and comparisons with $[\text{Mo}_3\text{CuS}_4(\text{H}_2\text{O})_{10}]^{4+}$ // *Inorg. Chem.* – 1994. – V.33. – N.19. – P. 4283-4289.
134. Orto P.J., Nichol G.S., Okumura N., Evans D.H., Arratia-Perez R., Ramirez-Tagle R., Wang R.Y., Zheng Z.P. Cluster carbonyls of the $[\text{Re}_6(\square^3\text{-Se})_8]^{2+}$ core: synthesis, structural characterization, and computational analysis // *Dalton Trans.* – 2008. – N.32. – P. 4247-4253.
135. Fedin V.P., Virovets A.A., Sykes A.G. Synthesis of the first sulfido-bridged octahedral rhenium(III) aqua ion $[\text{Re}_6\text{S}_8(\text{H}_2\text{O})_6]^{2+}$ // *Inorg. Chim. Acta.* – 1998. – V.271. – N.1-2. – P. 228-230.
136. Zheng Z.P., Tu X.Y. Crystal engineering supported by the $[\text{Re}_6(\mu_3\text{-Se})_8]^{2+}$ core-containing clusters // *CrystEngComm.* – 2009. – V.11. – N.5. – P. 707-719.
137. Sokolov M.N., Mihailov M.A., Peresypkina E.V., Brylev K.A., Kitamura N., Fedin V.P. Highly luminescent complexes $[\text{Mo}_6\text{X}_8(\text{n-C}_3\text{F}_7\text{COO})_6]^{2-}$ (X = Br, I) // *Dalton Trans.* – 2011. – V.40. – N.24. – P. 6375-6377.
138. Sokolov M.N., Mikhailov M.A., Brylev K.A., Virovets A.V., Vicent C., Kompankov N.B., Kitamura N., Fedin V.P. Alkynyl complexes of high-valence clusters. Synthesis and luminescence properties of $[\text{Mo}_6\text{I}_8(\text{C-CC}(\text{O})\text{OMe})_6]^{2-}$, the first complex with exclusively organometallic outer ligands in the family of octahedral $\{\text{M}_6\text{X}_8\}$ Clusters // *Inorg. Chem.* – 2013. – V.52. – N.21. – P. 12477-12481.
139. Willer M.W., Long J.R., McLauchlan C.C., Holm R.H. Ligand substitution reactions of $[\text{Re}_6\text{S}_8\text{Br}_6]^{4-}$: A basis set of Re_6S_8 clusters for building multicluster assemblies // *Inorg. Chem.* – 1998. – V.37. – N.2. – P. 328-333.
140. Mironov Y.V., Brylev K.A., Shestopalov M.A., Yarovoi S.S., Fedorov V.E., Spies H., Pietzsch H.J., Stephan H., Geipel G., Bernhard G., Kraus W. Octahedral rhenium cluster complexes with organic ligands: synthesis, structure and properties of $\text{Re}_6\text{Q}_8(3,5\text{-Me}_2\text{PzH})_6\text{Br}_2 \cdot 2(3,5\text{-Me}_2\text{PzH})$ (Q=S, Se) // *Inorg. Chim. Acta.* – 2006. – V.359. – N.4. – P. 1129-1134.
141. Shestopalov M.A., Mironov Y.V., Brylev K.A., Fedorov V.E. First molecular octahedral rhenium cluster complexes with terminal As- and Sb-donor ligands // *Russ. Chem. Bull.* – 2008. – V.57. – N.8. – P. 1644-1649.
142. Ivanov A.A., Shestopalov M.A., Brylev K.A., Khlestkin V.K., Mironov Y.V. A family of octahedral rhenium cluster complexes $\text{trans-}\{\text{Re}_6\text{Q}_8\}(\text{PPh}_3)_4\text{X}^{2-}$ (Q = S or Se, X = Cl, Br or I): preparation and halide-dependent luminescence properties // *Polyhedron.* – 2014. – V.81. – P. 634-638.

143. Shestopalov M.A., Ivanov A.A., Smolentsev A.I., Mironov Y.V. Crystal structure of the octahedral cluster complex *trans*-[$\{\text{Re}_6\text{S}_8\}(\text{pyz})_4\text{I}_2\cdot 2\text{pyz}$] // J. Struct. Chem. – 2014. – V.55. – N.1. – P. 139-141.
144. Shestopalov M.A., Mironov Y.V., Brylev K.A., Kozlova S.G., Fedorov V.E., Spies H., Pietzsch H.J., Stephan H., Geipel G., Bernhard G. Cluster core controlled reactions of substitution of terminal bromide ligands by triphenylphosphine in octahedral rhenium chalcobromide complexes // J. Am. Chem. Soc. – 2007. – V.129. – N.12. – P. 3714-3721.
145. Szczepura L.F., Cedeno D.L., Johnson D.B., McDonald R., Knott S.A., Jeans K.M., Durham J.L. Substitution of the terminal chloride ligands of $[\text{Re}_6\text{S}_8\text{Cl}_6]^{4-}$ with triethylphosphine: photophysical and electrochemical properties of a new series of $\text{Re}_6\text{S}_8^{2+}$ based clusters // Inorg. Chem. – 2010. – V.49. – N.24. – P. 11386-11394.
146. Yoshimura T., Umakoshi K., Sasaki Y., Sykes A.G. Synthesis, structures, and redox properties of octa(μ^3 -sulfido)hexarhenium(III) complexes having terminal pyridine ligands // Inorg. Chem. – 1999. – V.38. – N.24. – P. 5557-5564.
147. Naumov N.G., Virovets A.V., Podberezskaya N.V., Fedorov V.E. Synthesis and crystal structure of $\text{K}_4[\text{Re}_6\text{Se}_8(\text{CN})_6]\cdot 3.5\text{H}_2\text{O}$ // J. Struct. Chem. – 1997. – V.38. – N.5. – P. 857-862.
148. Yarovoi S.S., Mironov Y.V., Naumov D.Y., Gatilov Y.V., Kozlova S.G., Kim S.-J., Fedorov V.E. Octahedral hexahydroxo rhenium cluster complexes $[\text{Re}_6\text{Q}_8(\text{OH})_6]^{4-}$ (Q = S, Se): synthesis, structure, and properties // Eur.J. Inorg. Chem. – 2005. – V.2005. – N.19. – P. 3945-3949.
149. Mironov Y., Brylev K., Kim S.-J., Kozlova S., Kitamura N., Fedorov V. Octahedral cyanohydroxo cluster complex *trans*- $[\text{Re}_6\text{Se}_8(\text{CN})_4(\text{OH})_2]^{4-}$: synthesis, crystal structure, and properties // Inorg. Chim. Acta. – 2011. – V.370. – P. 363-368.
150. Alexandrov E.V., Virovets A.V., Blatov V.A., Peresypkina E.V. Topological motifs in cyanometallates: from building units to three-periodic frameworks // Chem. Rev. – 2015. – V.115. – N.22. – P. 12286-12319.
151. Fedorov V.E., Naumov N.G., Mironov Y.V., Virovets A.V., Artemkina S.B., Brylev K.A., Yarovoi S.S., Efremova O.A., Peak U.H. Inorganic coordination polymers based on chalcocyanide cluster complexes // J. Struct. Chem. – 2002. – V.43. – N.4. – P. 669-684.

152. Efremova O., Mironov Y., Fedorov V. Design of cyano-bridged coordination polymers based on tetrahedral rhenium cluster cyanide complexes and 3d transition metals // *Ber. Dtsch. Chem. Ges.* – 2006. – V.2006. – P. 2533-2549.
153. Brylev K.A., Naumov N.G., Virovets A.V., Kim S.J., Fedorov V.E. Novel three-dimensional coordination polymers based on $[\text{Mo}_6\text{Se}_8(\text{CN})_6]^{7-}$ anions and Mn^{2+} Cations // *J. Clust. Sci.* – 2009. – V.20. – N.1. – P. 165-176.
154. Naumov N.G., Cordier S., Perrin C. An extended open framework based on disordered $[\text{Nb}_6\text{Cl}_9\text{O}_3(\text{CN})_6]^{5-}$ cluster units: Synthesis and crystal structure of $\text{Cs}_3\text{Mn}[\text{Nb}_6\text{Cl}_9\text{O}_3(\text{CN})_6]0.6\text{H}_2\text{O}$ // *Solid State Sci.* – 2005. – V.7. – N.12. – P. 1517-1521.
155. Zhang J.-J., Lachgar A. Octahedral metal clusters as building blocks of trimetallic superexpanded prussian blue analogues // *Inorg. Chem.* – 2015. – V.54. – N.3. – P. 1082-1090.
156. Bennett M.V., Beauvais L.G., Shores M.P., Long J.R. Expanded Prussian blue analogues incorporating $[\text{Re}_6\text{Se}_8(\text{CN})_6]^{3-/4-}$ clusters: adjusting porosity via charge balance // *J. Am. Chem. Soc.* – 2001. – V.123. – N.33. – P. 8022-8032.
157. Shores M.P., Beauvais L.G., Long J.R. Cluster-Expanded Prussian Blue Analogues // *J. Am. Chem. Soc.* – 1999. – V.121. – N.4. – P. 775-779.
158. Buser H.J., Schwarzenbach D., Petter W., Ludi A. The crystal structure of Prussian Blue: $\text{Fe}_4[\text{Fe}(\text{CN})_6]_3 \cdot x\text{H}_2\text{O}$ // *Inorg. Chem.* – 1977. – V.16. – N.11. – P. 2704-2710.
159. Naumov N.G., Virovets A.V., Mironov Y.I., Artemkina S.B., Fedorov V.E. Synthesis and crystal structure of new layered cluster cyanides $\text{Cs}_2\text{M}[\text{Re}_6\text{S}_8(\text{CN})_6] \cdot 2\text{H}_2\text{O}$ ($\text{M}=\text{Mn}^{2+}, \text{Fe}^{2+}, \text{Co}^{2+}, \text{Cd}^{2+}$): size control over framework dimension // *Ukr. Khim. Zh.* – 1999. – V.65. – N.5-6. – P. 21-27.
160. Naumov N.G., Artemkina S.B., Virovets A.V., Fedorov V.E. Facile transformation of isolated fragments to infinite chains in rhenium chalcocyanide clusters: synthesis and structure of $(\text{Pr}_4\text{N})_2\text{M}(\text{H}_2\text{O})_5[\text{Re}_6\text{X}_8(\text{CN})_6] \cdot \text{H}_2\text{O}$ and $(\text{Pr}_4\text{N})_2\text{M}(\text{H}_2\text{O})_4[\text{Re}_6\text{S}_8(\text{CN})_6]$ ($\text{X}=\text{S}, \text{Se}$; $\text{M}=\text{Mn}, \text{Ni}$) // *J. Solid State Chem.* – 2000. – V.153. – N.2. – P. 195-204.
161. Artemkina S., Naumov N., Virovets Alexander V., Oeckler O., Simon A., Erenburg S., Bausk Nikolai V., Fedorov V. Two molecular-type complexes of the octahedral Rhenium(III) cyanocluster anion $[\text{Re}_6\text{Se}_8(\text{CN})_6]^{4-}$ with M^{2+} ($\text{Mn}^{2+}, \text{Ni}^{2+}$) // *Eur.J. Inorg. Chem.* – 2002. – V.2002. – P. 1198-1202.
162. Virovets A.V., Gayfulin Y.M., Peresyphkina E.V., Mironov Y.V., Naumov N.G. Novel 'anti-Prussian blue' structure based on Zn^{2+} nodes and

- [Re₃Mo₃S₈(CN)₆]⁶⁻ heterometallic cluster spacers and its rearrangement to Prussian blue // *CrystEngComm*. – 2015. – V.17. – N.6. – P. 1477-1482.
163. Gayfulin Y.M., Piryazev D.A., Mironov Y.V., Naumov N.G. Framework coordination polymer based on the [Re₃Mo₃S₈(CN)₆]⁶⁻ heterometallic cluster anions and Cd²⁺ cations // *Russ. J. Coord. Chem.* – 2017. – V.43. – N.6. – P. 364-367.
 164. Mueller A., Jostes R., Eltzner W., Nie C., Diemann E., Boegge H., Zimmermann M., Dartmann M., Reinsch-Vogell U., Che S., Cyvin S.J., Cyvin B.N. Synthetic, spectroscopic, X-ray structural, and quantum-chemical studies of cyanothiomolybdates with Mo₂S₂, Mo₃S₄ and Mo₄S₄ cores: a remarkable class of species existing with different electron populations and having the same central units as the ferredoxins // *Inorg. Chem.* – 1985. – V.24. – N.19. – P. 2872-2884.
 165. Cotton F.A., Feng X. Electronic structure and bonding in trinuclear molybdenum and tungsten cluster compounds of M₃X₁₃ type // *Inorg. Chem.* – 1991. – V.30. – N.19. – P. 3666-3670.
 166. Harris S. Structure, bonding and electron counts in cubane-type clusters having M₄S₄, M₂M₂'S₄ and MM₃'S₄ cores // *Polyhedron*. – 1989. – V.8. – N.24. – P. 2843-2882.
 167. Bahn C.S., Tan A., Harris S. Bonding in Mo₃M'S₄ cubane-type clusters: variations in electronic structure when M' is a main Group or transition metal // *Inorg. Chem.* – 1998. – V.37. – N.11. – P. 2770-2778.
 168. Nebbache N., Belhocine Y., Meghezzi A. DFT analysis of electronic and bonding properties in face-bridged inorganic octahedral clusters M₆L₁₄ // *Res. J. Pharm., Biol. Chem. Sci.* – 2014. – V.5. – P. 902.
 169. Nebbache N., Fontaine B., Meyer H.J., Gautier R., Halet J.-F. Theoretical analysis of the structure and bonding in electron-rich edge-bridged octahedral tungsten chloride clusters // *Solid State Sci.* – 2013. – V.19. – P. 150-155.
 170. G.M. Sheldrick, *SADABS version 2014/5*, *SADABS Bruker AXS Inc., Madison, Wisconsin, USA*.
 171. Sheldrick G.M. Crystal structure refinement with SHELXL // *Acta Crystallogr., Sect. C: Struct. Chem.* – 2015. – V.71. – N.Pt 1. – P. 3-8.
 172. Spek A.L. Single-crystal structure validation with the program PLATON // *J. Appl. Cryst.* – 2003. – V.36. – P. 7-13.

173. Kraus W., Nolze G. Powder Cell - a program for the representation and manipulation of crystal structures and calculation of the resulting X-ray powder patterns // *J. Appl. Cryst.* – 1996. – V.29. – P. 301-303.
174. Briois V., Fonda E., Belin S., Barthe L., Rubbens M., Villain F., La Fontaine C. // *Proceedings of UVX 2010 - 10e Colloque sur les Sources Coherentes et Incoherentes UV, VUV et X; Applications et Developpements Recents, UVX 2010.* – 2011. – P. 41-47.
175. Pettifer R.F., Borowski M., Loeffen P.W. The physics of ionization chambers - or how to improve your signal-to-noise ratio for transmission EXAFS measurements // *J. Synchrotron Radiat.* – 1999. – V.6. – P. 217-219.
176. Ravel B., Newville M. Athena, Artemis, Hephaestus: data analysis for X-ray absorption spectroscopy using IFEFFIT // *J. Synchrotron Radiat.* – 2005. – V.12. – P. 537-541.
177. ADF2017, *SCM, Theoretical Chemistry, Vrije Universiteit, Amsterdam, The Netherlands.*
178. te Velde G., Bickelhaupt F.M., Baerends E.J., Fonseca Guerra C., van Gisbergen S.J.A., Snijders J.G., Ziegler T. Chemistry with ADF // *J. Comput. Chem.* – 2001. – V.22. – N.9. – P. 931-967.
179. Fonseca Guerra C., Snijders G.J., te Velde G., Baerends J.E. Towards an order-N DFT method // *Theor. Chem. Acc.* – 1998. – V.99. – N.6. – P. 391-403.
180. Perdew J.P., Burke K., Ernzerhof M. Generalized gradient approximation made simple // *Phys. Rev. Lett.* – 1996. – V.77. – N.18. – P. 3865-3868.
181. Perdew J.P., Wang Y. Accurate and simple analytic representation of the electron-gas correlation energy // *Phys. Rev. B.* – 1992. – V.45. – N.23. – P. 13244-13249.
182. Van Lenthe E., Ehlers A., Baerends E.-J. Geometry optimizations in the zero order regular approximation for relativistic effects // *J. Chem. Phys.* – 1999. – V.110. – N.18. – P. 8943-8953.
183. Van Lenthe E., Baerends E.J. Optimized Slater-type basis sets for the elements 1–118 // *J. Comput. Chem.* – 2003. – V.24. – N.9. – P. 1142-1156.
184. Pye C.C., Ziegler T. An implementation of the conductor-like screening model of solvation within the Amsterdam density functional package // *Theor. Chem. Acc.* – 1999. – V.101. – N.6. – P. 396-408.

185. Brotherton T.K., Lynn J.W. The synthesis and chemistry of cyanogen // *Chem. Rev.* – 1959. – V.59. – N.5. – P. 841-883.
186. Larina T.V., Ikorskii V.N., Vashenin N.T., Anufrienko V.F., Naumov N.G., Ostanina E.V., Fedorov V.E. Electronic state of rhenium complexes with octahedral chalcocyanide cluster anions $[\text{Re}_6\text{Q}_8(\text{CN})_6]^{3-}$ (Q = S, Se, Te). EPR and magnetic susceptibility studies // *Russ. J. Coord. Chem.* – 2002. – V.28. – N.8. – P. 554-556.
187. Guilbaud C., Deluzet A., Domercq B., Molinie P., Coulon C., Boubekour K., Batail P. $[(\text{NBu}^{n4+})_3[\text{Re}_6\text{S}_8\text{Cl}_6]]^{3-}$: synthesis and luminescence of the paramagnetic, open shell member of a hexanuclear chalcocyanide cluster redox system // *Chem. Commun.* – 1999. – N.18. – P. 1867-1868.
188. Naumov N.G., Ostanina E.V., Virovets A.V., Schmidtman M., Müller A., Fedorov V.E. 23-Electron Re_6 metal clusters: syntheses and crystal structures of $(\text{Ph}_4\text{P})_3[\text{Re}_6\text{S}_8(\text{CN})_6]$, $(\text{Ph}_4\text{P})_2(\text{H})[\text{Re}_6\text{Se}_8(\text{CN})_6]$, and $(\text{Et}_4\text{N})_2(\text{H})[\text{Re}_6\text{Te}_8(\text{CN})_6] \cdot 2\text{H}_2\text{O}$ // *Russ. Chem. Bull.* – 2002. – V.51. – N.5. – P. 866-871.
189. Perrin C., Ihmaine S., Sargent M. Ternary and quaternary chlorides with $(\text{Nb}_6\text{Cl}_{18})^{n-}$ units in low valence niobium chemistry // *New J. Chem.* – 1988. – V.12. – N.6-7. – P. 321-328.
190. Koningsberger D.C., Prins R. X-ray absorption: principles, applications, techniques of EXAFS, SEXAFS and XANES / – New York: Wiley. – 1987. – 673 p.
191. Rehr J.J., Albers R.C. Theoretical approaches to X-ray absorption fine structure // *Rev. Mod. Phys.* – 2000. – V.72. – N.3. – P. 621-654.
192. Muravieva V.K., Gayfulin Y.M., Ryzhikov M.R., Novozhilov I.N., Samsonenko D.G., Piryazev D.A., Yanshole V.V., Naumov N.G. Mixed-metal clusters with a $\{\text{Re}_3\text{Mo}_3\text{Se}_8\}$ core: from a polymeric solid to soluble species with multiple redox transitions // *Dalton Trans.* – 2018. – V.47. – N.10. – P. 3366-3377.
193. Magliocchi C., Xie X., Highbanks T. Cyanide-melt synthesis of reduced molybdenum selenide clusters // *Inorg. Chem.* – 2004. – V.43. – N.6. – P. 1902-1911.
194. Gabriel J.-C.P., Boubekour K., Uriel S., Batail P. Chemistry of hexanuclear rhenium chalcocyanide clusters // *Chem. Rev.* – 2001. – V.101. – N.7. – P. 2037-2066.
195. Kozlova S.G., Gabuda S.P., Brylev K.A., Mironov Y.V., Fedorov V.E. Electronic spectra and DFT calculations of hexanuclear chalcocyanide

- rhodium clusters // J. Phys. Chem. A. – 2004. – V.108. – N.47. – P. 10565-10567.
196. Naumov N.G., Artemkina S.B., Virovets A.V., Fedorov V.E. New layered polymer $[\{\text{Mn}(\text{H}_2\text{O})_3\}_2\{\text{Re}_6\text{Se}_8(\text{CN})_6\}]\cdot 3.3\text{H}_2\text{O}$: synthesis and properties // Russ. J. Coord. Chem. – 2004. – V.30. – N.11. – P. 792-799.
197. Tarasenko M.S., Ledneva A.Y., Naumov N.G., Naumov D.Y., Fedorov V.E. Novel low dimensional cluster compounds: syntheses and crystal structures of $\text{Cs} \{\text{Me}_3\text{Sn}\}_3\{\text{Re}_6\text{Se}_8(\text{CN})_6\}$, $\{\text{Me}_3\text{Sn}(\text{H}_2\text{O})\}_2\{\text{Me}_3\text{Sn}\}\{\text{Re}_6\text{Se}_8(\text{CN})_6\}\text{H}_2\text{O}$, and $(\text{Me}_3\text{Sn})_3(\text{OH})_2\{\text{Me}_3\text{Sn}\}_3\{\text{Re}_6\text{Se}_8(\text{CN})_6\}$. pH control of the structural dimensionality // J. Clust. Sci. – 2005. – V.16. – N.3. – P. 353-365.
198. Tarasenko M.S., Ledneva A.Y., Kurat'eva N.V., Naumov D.Y., Kim S.-J., Fedorov V.E., Naumov N.G. Synthesis and structure of novel coordination compounds based on $[\text{Re}_6\text{Q}_8(\text{CN})_6]^{4-}$ ($\text{Q} = \text{S}, \text{Se}$) and $(\text{SnMe}_3)^+$ // Russ. J. Coord. Chem. – 2007. – V.33. – N.12. – P. 876-885.
199. Steiner T. The hydrogen bond in the solid state // Angew. Chem. Int. Ed. – 2002. – V.41. – P. 48-76.
200. Shannon R. Revised effective ionic radii and systematic studies of interatomic distances in halides and chalcogenides // Acta Crystallogr., Sect. A – 1976. – V.32. – N.5. – P. 751-767.
201. Hoskins B.F., Robson R., Scarlett N.V.Y. Synthesis and structure of $\text{Rb}[\text{Cd}\{\text{Ag}(\text{CN})_2\}_3]$ containing three independent, interpenetrating α -polonium-related nets // J. Chem. Soc., Chem. Commun. – 1994. – N.18. – P. 2025-2026.
202. Ledneva A.Y., Virovets A.V., Naumov N.G. Interpenetrating frameworks in the structure of the $[(\text{SnMe}_3)_3\text{Re}_6\text{Se}_8(\text{CN})_6]$ cluster complex // J. Struct. Chem. – 2013. – V.54. – N.4. – P. 815-819.
203. Jin S., DiSalvo F.J. 3-D Coordination Network Structures Constructed from $[\text{W}_6\text{S}_8(\text{CN})_6]^{6-}$ Anions // Chem. Mater. – 2002. – V.14. – N.8. – P. 3448-3457.
204. Fehlhammer W.P., Fritz M. Emergence of a CNH and cyano complex based organometallic chemistry // Chem. Rev. – 1993. – V.93. – N.3. – P. 1243-1280.
205. Slep L.D., Alborés P., Baraldo L.M., Olabe J.A. Kinetics and mechanism of ligand interchange in pentacyano-L-osmate(II) complexes ($\text{L} = \text{H}_2\text{O}, \text{NH}_3, \text{N}$ -heterocyclic ligands) // Inorg. Chem. – 2002. – V.41. – N.1. – P. 114-120.

206. Naik R.M., Sarkar J., Prasad S. Kinetic determination of cysteine and thiosulphate by inhibition of Hg(II) catalyzed ligand substitution reaction // *Microchem. J.* – 2008. – V.88. – N.1. – P. 45-51.
207. Mironov Y.V., Cody J.A., Albrecht-Schmitt T.E., Ibers J.A. Cocrystallized mixtures and multiple geometries: Syntheses, structures, and NMR spectroscopy of the Re_6 clusters $[\text{NMe}_4]_4[\text{Re}_6(\text{Te}_{8-n}\text{Se}_n)(\text{CN})_6]$ ($n = 0-8$) // *J. Am. Chem. Soc.* – 1997. – V.119. – N.3. – P. 493-498.
208. Muravieva V.K., Gayfulin Y.M., Lemoine P., Cordier S., Naumov N.G. Stabilization of interpenetrating cluster-based frameworks promoted by N-H...X hydrogen bonds: synthesis, structures and properties of $\{[\text{Cd}(\text{NH}_3)_4]_3[\text{Re}_3\text{Mo}_3\text{Se}_8(\text{CN})_6]\}_X$ ($X = \text{Cl}, \text{Br}$ and I) // *CrystEngComm.* – 2018. – V.20. – P. 4164-4172
209. Muravieva V.K., Lemoine P., Cordier S., Naumov N.G. Crystal Structure of Layered Cyano-Bridged Coordination Polymers $[\text{M}(\text{NH}_3)_6]_4[\{\text{M}(\text{NH}_3)_2\}\{\text{Re}_3\text{Mo}_3\text{Se}_8(\text{CN})_6\}_2] \cdot 15\text{H}_2\text{O}$ ($\text{M} = \text{Co}, \text{Ni}$) // *J. Struct. Chem.* – 2019. – V.60. – N.1. – P. 99-105.
210. Zheng Z., Gray T.G., Holm R.H. Synthesis and structures of solvated monoclusters and bridged di- and triclusters based on the cubic building block $[\text{Re}_6(\mu_3\text{-Se})_8]^{2+}$ // *Inorg. Chem.* – 1999. – V.38. – N.21. – P. 4888-4895.
211. Mironov Y.V., Kozhomuratova Z.S., Naumov D.Y., Fedorov V.E. Synthesis and structure of a new molecular octahedral cluster complex $\text{Mo}_6\text{Se}_8(\text{Ph}_3\text{P})_6 \cdot 2\text{H}_2\text{O}$ // *J. Struct. Chem.* – 2007. – V.48. – N.2. – P. 383-387.
212. Jin S., Popp F., Boettcher S.W., Yuan M., Oertel C.M., DiSalvo F.J. Synthesis, characterization and properties of $\text{Mo}_6\text{S}_8(4\text{-tert-butylpyridine})_6$ and related $\text{M}_6\text{S}_8\text{L}_6$ cluster complexes ($\text{M} = \text{Mo}, \text{W}$) // *J. Chem. Soc., Dalton Trans.* – 2002. – N.16. – P. 3096-3100.
213. Muravieva V.K., Gayfulin Y.M., Lappi T.I., Dorcet V., Sukhikh T.S., Lemoine P., Ryzhikov M.R., Mironov Y.V., Cordier S., Naumov N.G. Apical cyanide ligands substitution in heterometallic clusters $[\text{Re}_3\text{Mo}_3\text{Q}_8(\text{CN})_6]^{n-}$ ($\text{Q} = \text{S}, \text{Se}$) // *Eur.J. Inorg. Chem.* – 2019. – P. 2685-2690.

Titre : Briques moléculaires à clusters hétérométalliques chalcogénées $\{\text{Re}_{6-x}\text{Mo}_x\text{Se}_8\}$ $x = 1-3$: cristallographie, structures électroniques et propriétés redox

Mots clés : clusters de métaux de transition, complexe hétérométallique, chimie redox, calculs DFT, polymères de coordination, EXAFS

Résumé : Les clusters octaédriques de molybdène (Mo) et de rhénium (Re) présentent un intérêt croissant pour des applications dans plusieurs domaines tels que la santé ou l'énergie. Ceci en raison de la richesse de leurs propriétés physico-chimiques et structurales (ex. : absorption/émission de lumière, oxydation réversibles et modulables). L'introduction d'un second métal dans la composition du cluster constitue un excellent moyen pour i) modifier et contrôler les propriétés physicochimiques du cluster et ii) générer de nouvelles propriétés. Avant cette étude, seuls quelques travaux consacrés principalement à la synthèse et aux études structurales de composés hétérométalliques octaédriques étaient rapportées dans la littérature.

La principale difficulté qui a limité le développement de ce champ de recherche était la formation simultanée et la co-cristallisation de plusieurs clusters

hétérométalliques avec des rapports Mo/Re différents ou bien pour un même rapport, de plusieurs isomères. Ce problème a été résolu dans ce travail en utilisant la séparation post-synthétique basée sur les différences des comportements redox et de solubilité des chalcogénures à clusters hétérométalliques. Cela nous a permis d'étudier individuellement la structure, les caractéristiques spectroscopiques et les propriétés redox de clusters bien définis de type $[\text{Re}_{6-x}\text{Mo}_x\text{Se}_8(\text{CN})_6]^{n-}$ ($x = 1, 2, 3$). Ces travaux fournissent une série de clusters Mo/Re capables de plusieurs transitions électrochimiques dans une fenêtre étroite de potentiels, accompagnés d'une modification de leur spectre optique. Ils pourront par exemple être utilisés pour la réalisation de capteurs.

Title : Molecular building blocks of chalcogenide heterometallic clusters $\{\text{Re}_{6-x}\text{Mo}_x\text{Se}_8\}$ $x = 1-3$: crystallography, electronic structures and redox properties

Keywords : transition metal cluster, heterometallic complex, redox chemistry, DFT calculations, coordination polymers, EXAFS

Abstract : Octahedral cluster compounds of molybdenum and rhenium are of growing interest due to the set of promising properties caused by intrinsic characteristics of the cluster core, such as photoluminescence, reversible redox transitions preserving the geometry of the cluster core, and magnetism. A change in the composition of the metal core with the formation of heterometallic cluster can serve as an excellent tool for controlled modification of the physicochemical properties of cluster and introducing new features non-typical for homometallic analogues. Prior to the start of this study, only a few works devoted mainly to the synthesis and study of the structure of octahedral heterometallic compounds were presented in the literature. The main difficulty hampering the further development of this field was the formation and co-crystallization of several heterometallic clusters of different metal ratio in the

same reaction conditions. This problem was successfully solved using the post-synthetic separation based on the deviations in the redox character and salts solubility of Re/Mo chalcogenide clusters of different metal ratio. It allowed us the individual study of the structure, spectroscopic characteristics, and redox properties of well-defined heterometallic cluster complexes $[\text{Re}_{6-x}\text{Mo}_x\text{Se}_8(\text{CN})_6]^{n-}$ ($x = 1, 2, 3$).

The present research provided a series of Re / Mo clusters capable of several electrochemical transitions in a narrow potential window, accompanied by a change in the optical spectrum of the cluster complex. Clusters with such reversible color-changing redox transitions are of interest in the field of electrochemically active materials and can be used to design sensors.